INFORMATION TO USERS

This manuscript has been reproduced from the microfilm master. UMI films the text directly from the original or copy submitted. Thus, some thesis and dissertation copies are in typewriter face, while others may be from any type of computer printer.

The quality of this reproduction is dependent upon the quality of the copy submitted. Broken or indistinct print, colored or poor quality illustrations and photographs, print bleedthrough, substandard margins, and improper alignment can adversely affect reproduction.

In the unlikely event that the author did not send UMI a complete manuscript and there are missing pages, these will be noted. Also, if unauthorized copyright material had to be removed, a note will indicate the deletion.

Oversize materials (e.g., maps, drawings, charts) are reproduced by sectioning the original, beginning at the upper left-hand corner and continuing from left to right in equal sections with small overlaps.

Photographs included in the original manuscript have been reproduced xerographically in this copy. Higher quality 6" x 9" black and white photographic prints are available for any photographs or illustrations appearing in this copy for an additional charge. Contact UMI directly to order.

ProQuest Information and Learning
300 North Zeeb Road, Ann Arbor, MI 48106-1346 USA
800-521-0600

ERUPTIVE STRATIGRAPHY AND THE TRANSPORT AND DEPOSITION OF PYROCLASTIC MATERIAL FROM THE CALDERA-FORMING ERUPTION OF VOLCÁN CEBORUCO, NAYARIT, MEXICO

A

THESIS

Presented to the Faculty
of the University of Alaska Fairbanks
in Partial Fulfillment of the Requirements
for the Degree of

MASTER OF SCIENCE

By
Brandon L. Browne, B.S.

Fairbanks, Alaska
August 2001

ERUPTIVE STRATIGRAPHY AND THE TRANSPORT AND DEPOSITION OF PYROCLASTIC MATERIAL FROM THE CALDERA-FORMING ERUPTION OF VOLCÁN CEBORUCO, NAYARIT, MEXICO

by

Brandon L. Browne

RECOMMENDED:

Advisory Committee Chair

Department Head

APPROVED:

Dean, College of Science, Engineering, and Mathematics

Dean of the Graduate School

6-18-01

Date

Abstract

The ~1000 A.D. eruption of Volcán Ceboruco produced 3-4 km^3 of rhyodacitic to dacitic magma erupted as the Jala Pumice, forming a 3.7-km-wide caldera. The tephra sequence consists of alternating Plinian fall and pyroclastic surge deposits, and a series of lithic-rich pyroclastic flow deposits. The latter are known as the Marquesado and North-Flank Pyroclastic Flow deposits. Stratigraphic evidence and results of a comprehensive analysis of accidental lithic and pumice populations constrain the timing of caldera collapse, and the emplacement of the pyroclastic flow deposits to the end of the Jala Pumice. Mass accumulation calculations of particles from fall layers display sedimentation patterns consistent with deposition from dilute and turbulent currents with low particle concentration. Pyroclastic flow and surge deposits likely resulted from density-stratified currents, with a basal region of relatively high particle concentration, and an upper dilute layer that transports particles in turbulent suspension.

Table of Contents

List of Figures

List of Tables

Acknowledgments

I would like to thank the following people for their insight, contributions, and generous assistance towards this thesis. Firstly, my advisor, Dr. James Gardner, was extremely committed and dedicated to my research. His inexhaustible willingness for repeated meetings and discussions benefited me greatly, and I am thankful for all that he taught me. Drs. Jessica Faust-Larsen and John Eichelberger acted on my committee and always supported my research with genuine interest and enthusiasm. The Alaska Volcano Observatory provided me with funding for travel to wonderful and pristine natural laboratories for volcanic research such as Katmai National Park and Okmok volcano, as well as important scientific conferences such as the Fall 2000, American Geophysical Union conference, in San Francisco, California. Dr. José-Luis Macías is a practiced authority in Trans-Mexican volcanology, and has kindly discussed a number of critical ideas and processes with me during this research. Ricardo Saucédo and José-Luis Arce assisted Dr. Gardner and myself with our fieldwork in Mexico, and I am grateful for their time and effort. Dr. Paul Layer generously allowed me to perform all of my sieve analysis in his geochronology laboratory in the Department of Geology and Geophysics at the University of Alaska Fairbanks, and Dr. James Begét granted me access to his laser-particle counter, in his Quaternary geology laboratory, also located in the Department of Geology and Geophysics at the University of Alaska Fairbanks. My parents, Dr. Peter and Anne Browne, have always encouraged me to explore and discover that which interests me the most, and I am truly grateful to them for that. Carrie Schoeppach has been a source of endless comfort and support throughout this thesis. She is the bravest person I know, and I love her for all that she does for me every single day of my life.

1. Introduction

The processes of transport and sedimentation in pyroclastic clouds and eruptive columns generated from volcanic eruptions remain poorly understood as a result of the complex fluid dynamics and thermodynamics of the clouds, the uncertain extent of interaction with topography, and the difficulty of direct observation. Because of this, modeling efforts aimed at predicting and explaining pyroclastic transport and deposition are based largely on the textural and granulometric characteristics of the resulting pyroclastic deposits (Walker, 1971, 1973, 1981; Sparks, 1976; 1986; Carey and Sigurdsson, 1985; 1989; Carey and Sparks, 1986; Cas and Wright, 1987; Sparks et al., 1991; Sparks et al. 1992; Wilson and Walker, 1982; Bursik et al., 1992b).

The mechanics of particle transport and deposition, and therefore depositional patterns, are predominantly a function of the particle concentration of the pyroclastic density current (Bursik et al., 1998). In the case of dilute and turbulent currents with low particle concentration (<0.1 vol.%), deposition results from suspended sedimentation (Figure 1) (Martin and Nokes, 1988; Sparks et al., 1991; Bursik et al., 1992b; Woods and Bursik, 1991). In the case of density currents with greater particle concentrations (0.1-10's vol.%), inertial and partially fluidized currents deposit material via *en masse* freezing (Figure 1) (Sparks, 1976; Wilson and Walker, 1982). Some workers have held that a complete transition occurs between these end members (Cas and Wright, 1987; Fisher 1983), whereas others believe that distinct gaps exist between specific flow-types (Wilson and Walker, 1982; Walker and McBroome, 1983). Recently described pyroclastic flow and surge deposits, such as those found at Mount St. Helens, 1980, and Mount Pele, 1902, cannot be easily differentiated as either type of density current and their interpretation remains controversial (Fisher and Heiken, 1982; Walker and McBroome, 1983).

Comprehensive studies that focus on describing and modeling pyroclastic fall deposits are widespread (Walker, 1973, 1981; Carey and Sigurdsson, 1985; Sparks, 1986;

Carey et al., 1988; Sparks et al., 1991; Woods and Bursik, 1991; Bursik et al., 1992b; Sparks et al., 1992; Ernst et al., 1996) and are fairly well accepted because of the agreement that exists between model predictions and direct observations (Carey et al., 1990). Field observations show that with increasing distance from the eruption vent, a pyroclastic fall deposit decreases in median grain size (Md_ϕ), and abundance in accidental lithic content, while also exhibiting an increase in sorting (σ_ϕ). In addition, fall deposits exponentially decrease in thickness with distance (Pyle, 1989; 1995). Some of the more successful modeling efforts that attempt to quantify how pyroclastic fall deposits form are based on the observations of Pyle (1989; 1995), and the presumption that the umbrella regions of volcanic plumes are sufficiently turbulent and dilute systems that travel with a constant volume flux (Carey and Sparks, 1986; Sparks et al., 1991; Bursik et al., 1992b; Sparks et al., 1992).

Models of the dispersal of tephra from volcanic plumes have been recently developed that have been shown to be consistent in observed fall-out sedimentation patterns (Carey and Sparks, 1986; Carey et al., 1990; Sparks et al., 1991; Bursik et al., 1992b; Sparks et al., 1992). The theoretical model is most thoroughly presented in Sparks et al. (1991) and Bursik et al. (1992b) and the principal results are summarized here. Sedimentation of tephra from volcanic plumes occurs from the margins of the vertically rising eruption column, and from the laterally spreading umbrella cloud (Figure 2). Particles of greatest density and size are deposited from along the plume margins and produce proximal deposits. Most particles, however, are transported to near the top of the eruption column by strong vertical flow (Woods, 1988; Woods and Bursik, 1991). Upon reaching a height where the plume is neutrally buoyant, the current spreads laterally and forms the umbrella region of the eruptive column (Sparks, 1986). The boundary between the vertically rising column and the horizontally spreading cloud is referred to as the column-corner, and deposits found beneath the column-corner are referred to as being at a distance, r_o, from the vent (Figure 2).

The volume flux of the umbrella region of an eruption cloud is modeled by Sparks et al. (1991) and Bursik et al. (1992b) as being dilute, turbulent, and moving at a constant volume flux. In a turbulent flow, the settling of particles is opposed by the turbulence itself, which encourages continued entrainment and mixing rather than deposition. A gradient of downward increasing particle concentration is established as a consequence of the opposing effects of settling and turbulent dispersion (Martin and Nokes, 1988; Sparks, 1991). When the settling velocity of a particle exceeds the spreading velocity of the plume, sedimentation occurs. Settling velocities of particles from the umbrella region of volcanic plumes, U_T, are calculated as:

$$U_T = C_D [(d g \sigma \beta)^{-1}]. \qquad (1)$$

where C_D is the drag coefficient, β is the bulk density of the plume, g is gravitational acceleration, and d and σ are the particle diameter and density, respectively (Carey and Sparks, 1986). The model of Sparks et al. (1991) and Bursik et al. (1992b) predicts the mass accumulation on the ground per unit area from suspended sedimentation, S, for a given size-fraction (i), particles will be a function of distance from the vent, r:

$$S = S_0 \exp [(-\pi \{r^2 - r_0^2\} v_i) / Q]. \qquad (2)$$

where S_0 is the mass accumulation per unit area at r_0, Q is the volumetric flow rate of the laterally moving umbrella cloud, and v_i is the settling velocity of the particles of a given grain diameter, d. Equation (2) is for sedimentation of particles of equal v_i, and not the sum accumulation of a bulk deposit. Equation (2) predicts that deposition of a particle of equal v_i should decrease exponentially with distance in dilute and turbulent currents, whereas, particles deposited *en masse* should remain relatively constant. Previous studies have shown how pumice clasts often vary in density, sometimes dramatically, with size

(Walker, 1971). As a result, only particles with constant densities (accidental lithics and crystals, and not pumice) are used in this study.

Pyroclastic flow deposits (PFD's) are often described as being massive, poorly sorted, ash-rich deposits that may exceed 1000 m in thickness and can be found 100's km from a source vent (Sparks, 1976; Fisher, 1979). Generation of PFD's are thought to occur from a variety of mechanisms during explosive eruptions, including column-collapse (Figure 2) (Sparks and Wilson, 1976; Bursik and Woods, 1991), gravitational collapse of a summit dome (Yamamoto et al., 1993), or low altitude fountain-feeding from the eruptive plume over the crater rim (Hoblitt, 1986). Simple models (Mohr-Coulomb, Hsü, 1975) envision the behavior of pyroclastic flows like that of avalanches. That is, as an *en masse* sliding block of some frictional strength that will move on ground slopes greater than some critical slope angle, θ, and reach a distance, L, that is a function of the height of the origin, H, and θ, such that:

$$L = H / \tan\theta \qquad (3)$$

The dispersal of many pyroclastic flow deposits is not, however, accurately predicted by this relationship, for there is no way to account for flow mass or turbulent stresses at high velocities (Wilson, 1980, 1984). Furthermore, a value for H is rarely known to any degree of certainty.

More recent interpretations have speculated that pyroclastic flow deposits formed from partially fluidized gas-particle mixtures with particle concentrations on order of ~ 10 vol. % (Sparks, 1976). In addition, it is suggested that the behavior of pyroclastic flows is a consequence of their gas content and volume. That is, small-volume, gas-poor pyroclastic flows behave like cold debris avalanches, that "flow" as a combination of laminar and plug flow and are deposited *en masse*, whereas large-volume, gas-rich pyroclastic flows initially flowed turbulently and deflated with distance into a laminar

flow regime (Sparks, 1976; Wilson, 1980). Wilson and Walker (1982) and Wilson (1984) extended that model by suggesting that pyroclastic flows represented a distinct form of pyroclastic density current whose structure consists of a head, body, and tail, with each region producing different deposits owing to the different flow regimes and conditions believed to exist in specific regions.

Fluidization is generally regarded as the dominant factor in the movement of pyroclastic flows (Sparks, 1976; Wilson and Walker, 1982; Wilson, 1985). The process of fluidization occurs as a bed of solid particles takes on the rheology of a fluid and is able to flow under the influence of gravity (Sparks, 1976; Wilson and Walker, 1982; Wilson, 1985). Total fluidization occurs only when air is passed through a bed of solid particles with a very narrow grain size (Sparks, 1976; Wilson, 1980). PFD's are typically very poorly sorted and enriched in fine material, making total fluidization impossible. Experimental analyses by Wilson (1980, 1984) indicate, however, that if the volume of fine-grained particles represent a sufficient proportion of the total grain size distribution, then a fluid-like matrix will develop, allowing the material to flow downslope under the influence of gravity.

Pyroclastic surge deposits are commonly distinguished from other pyroclastic deposits by having complex bed forms, such as cross bedding, dune structures, and laminar bedding (Sparks, 1976; Fisher, 1979; Allen, 1984). Surge deposits are typically better sorted (σ_ϕ) at a similar range in median diameters (Md_ϕ) compared to pyroclastic flow deposits (Walker, 1971; Sparks, 1976). Wohletz and Sheridan (1979) interpreted surge clouds as initially lean-phase fluidized systems, which deflate from the continual loss of gas, and thus transform from a viscous to an inertial current with increased distance. This interpretation was sparked by repeated field observations of systematic changes from sandwave bed forms at proximal distances, to massive beds at medial sites, to planar bedding at distal locations within basaltic phreatomagmatic base-surge deposits (Wohletz and Sheridan, 1979).

Further research on the dynamics of pyroclastic surges by Fisher (1979, 1983, 1990) and Valentine (1987) suggested that regional transport of particles and local deposition occurs in two distinctly different systems acting within the surge cloud. In this case, the overlying (or upper) transport system is dilute and turbulent, whereas the underlying (or lower) depositional system moves laminarly such as saltation and granular flow (Figure 1). The basal depositional system thus depends on both the local topographic controls (e.g. "blocking", See Figure 3), and the quantity of material supplied from the transport system. The most compelling example of this may be the pyroclastic blast-surge deposits from the 1980 eruption of Mount St. Helens (Fisher, 1990; Druitt, 1992).

Most recently, pyroclastic surges have been modeled as eruptive plumes traveling through the atmosphere, where particles are transported entirely in turbulent suspension (Woods et al., 1998; Bursik et al., 1998). In this model, sedimentation of material from pyroclastic surge clouds occurs straight from a dilute and turbulent "transport-system", without a basal "depositional-system". Models for eruptive plume sedimentation, this model predicts that particles are deposited systematically as an exponential function of distance from source location. Ironically, the most convincing study to support this model also comes from that of the 1980 Mount St. Helens blast-surge (Bursik et al., 1998).

This thesis seeks to model the transport and depositional mechanics of the pyroclastic fall, flow, and surge deposits through a systematic study of the deposits formed from the ~ 1000 A.D. caldera-forming eruption of Volcán Ceboruco. The complex eruption sequence of alternating pyroclastic fall, surge, and flow deposits offers an exceptional opportunity to further examine how pyroclastic material is transported and deposited from a wide range of pyroclastic density currents. In addition, our newly described proximal and distal deposits, and comprehensive analysis of variations of accidental lithic and pumice-types through the eruptive sequence, allows a re-description of the eruptive stratigraphy and discussion of the timing of caldera collapse.

The ~1000 A.D. eruption of Volcán Ceboruco, located in Nayarit, Mexico, emplaced 3-4 km^3 (DRE, Dense Rock Equivalent) of rhyodacite to dacite magma and resulted in the formation of a 3.7 km wide caldera. The tephra deposited from this eruption is referred to as the Jala Pumice and the Marquesado Pyroclastic Flow deposits. The Jala Pumice is a complex sequence of alternating Plinian fall deposits and pyroclastic surge and flow deposits, located to the north and northeast of Ceboruco. The Marquesado Pyroclastic Flow deposits consist of repeated units of massive-to-stratified, lithic-rich, matrix-supported layers, located predominantly to the south and southwest of the volcano. This study constrains the timing of the Marquesado pyroclastic flow deposits to the end of the Jala Pumice sequence through stratigraphic evidence.

2. Geologic Setting and Eruptive History

Volcán Ceboruco, a 2164 m high composite volcano located in the state of Nayarit, in western Mexico, is one the westernmost active volcanoes in the Trans-Mexican Volcanic Belt (Gunn and Mooser, 1971; Nelson, 1980; Moore et al., 1994). Ceboruco is truncated by two concentric calderas, the older of which measures 3.7 km in diameter and the younger is approximately 1.5 km in diameter (Figure 4). Volcán Ceboruco's structure is noticeably asymmetric with the north and northeast flanks being steeply dipping at 25°-35°, and the south flanks at ~15°.

Volcán Ceboruco rests in a down-dropped graben structure that comprises the Jala and Ahuacatlán valleys. A N60°W trending escarpment of the Sierra Madre Formation abruptly marks the northern margin of this basin (Figure 5). These cliffs rise in excess of 230 m above the valley floor and represent the front of a rugged and complex plateau that extends to the north (Figure 6). The Sierra Madre formation, composed of Tertiary rhyolitic ash-flow tuffs (Gunn and Mooser, 1971; Nelson, 1980), most likely underlies Ceboruco (Nelson, 1980; Moore et al., 1994). The concealed deeper levels beneath Ceboruco may also be composed in part of granitic material (Figure 7), because such

xenoliths are often found in the erupted products from cinder cones located immediately adjacent to the northwest and southeast of Ceboruco (Thorpe and Francis, 1975; Nelson, 1980), and in the erupted products of Volcán Ceboruco (this study).

The eruptive history of Volcán Ceboruco was described extensively by Nelson (1980), and will be summarized here. The eruptive sequence can be divided into three stages of predominantly effusive activity, separated by two episodes of caldera formation. The first stage includes extrusion of the most voluminous proportion of the volcano, with 60 km^3 of andesitic lava flows compared to only 7 km^3 of erupted material in the next two stages. This period was followed by an unspecified period of quiescence with the exception of the effusion of a rhyolitic and a rhyodacitic lava dome (Cerro Pedregoso and Cerro Pochetero, respectively). The first stage ended with the A.D. ~1000 eruption that resulted in the deposition of 3-4 km^3 (DRE) of magma as the Jala Pumice deposit to the north and northeast, and the Marquesado pyroclastic flow deposits to the south, along with the formation of the outer caldera, which remains open to the south. The second stage began with the emplacement of the Dos Equis dacite dome, which partially filled the caldera. Continued lava extrusions, ranging from basaltic andesite to dacite in composition, destabilized the dome, causing it to collapse and form the inner caldera.

The third stage of eruptive sequence consists of historical activity of Ceboruco, which is limited to an eruption in 1870-1872, where a dacite lava flow and pyroclastic deposits were emplaced on the western flanks of the cone (Ordoñez, 1897). Weak fumerolic activity from this eruption persists today. Earlier work by Williams (1950), Gunn and Mooser (1971), Thorpe and Francis (1975), and Nelson (1980) focused predominantly on the structural and compositional evolution of Volcán Ceboruco. Those studies showed that the principal rock types found at Ceboruco are basaltic andesite to andesite, with a significant amount of olivine-bearing basalt. Alkali basalt, dacite, and rhyolite are also found, but are not common. With the exception of recent work performed by Gardner and Tait (2000), which looked closely at the ~1000 A.D. caldera-

forming eruption by calculating mass eruption rates in the cases of the Plinian fall layers and the erupted volumes of individual layers in the eruptive sequence, a quantitative evaluation of the pyroclastic deposits at Volcán Ceboruco has remained undone.

3. Methods

3.1. Field Studies:

For this study, the Jala Pumice deposit was measured, described, and sampled at 55 sites, 19 of which were mapped by Gardner and Tait (2000). Moreover, 52 samples of pyroclastic surge deposits and 17 samples of pyroclastic flow deposits were acquired (a total of 118 samples underwent sieving and component analysis). Some pyroclastic surge deposits were sampled on the flanks of the volcano, but most were sampled atop the northern plateau (Figure 5). Pyroclastic flow deposits were sampled at localities to the southwest of Ceboruco and on the eastern and northern flanks. Each pyroclastic fall deposit was measured and described in terms of grain size, lithic content, and any apparent grading. Each pyroclastic surge and flow deposit was measured and described in terms of relative grain size, color, lithic content, and bedding structures.

3.2. Analytical and Component Studies:

Granulometric analysis for this study was performed in accordance with methods outlined by Walker (1971) and Sparks (1976). Every pyroclastic fall, surge, and flow deposit sample was wet-sieved in 0.5 phi (ϕ) increments from $-5.0\ \phi$ (32 mm) to $4.0\ \phi$ (1/16 mm). Following at least 12 hours in which the bulk sample was soaked in deionized water to disaggregate finer particles, all sieving was performed by hand to avoid breaking pumice clasts. The material remaining on each sieve was weighed to ± 0.01 g on a laboratory balance. Pyroclastic fall deposit samples collected and provided by Gardner and Tait (2000) also underwent granulometric and component analysis in this study (-2.0 to $4.0\ \phi$ only). Unfortunately, the sampling practices of Gardner and Tait (2000) involved

sieving, weighing, and counting particles that were coarser than -2.5 ϕ in the field at 1.0 ϕ intervals. The remaining material was "split" into a representative bulk sample, which was analyzed in this study. Therefore, granulometric and component analysis from all pyroclastic fall deposits coarser than −2.0 ϕ represent integrated estimates on a 0.5 ϕ interval. A Swift Automatic point counter (Hacker Instruments, Model E) was used for manual particle counting of all 0.5 interval phi sizes from −5.0 to 4.0 ϕ for component analysis, and a Spectrex 2000 Laser-particle analyzer with SuperCount version 8.13d for Windows was used to measure the grain-size distribution for particles finer than 4.0 ϕ (4.5, 5.0, 6.0, and 7.0 ϕ). Mass fractions of total particles in the 4.0 ϕ to 7.0 ϕ (individual component mass fractions were not determined), were calculated by multiplying the number of automated laser-particle counts of a grain size fraction to weight fractions using the commonly used proportional conversion of 0.65 per 1.0 ϕ (Cas and Wright, 1987), from the measured value of 4.0 ϕ particles. Specific results for all samples are found in Appendix I and II.

Analyses were plotted as cumulative frequency curves to determine the median diameter, Md_ϕ ($=\phi_{50}$), and the inclusive graphic standard deviation, σ_ϕ (IGSD= $\{[(\phi_{84} - \phi_{16})/4] + [(\phi_{95} - \phi_5)/6.6]\}$), which is a measure of sorting (Folk and Ward, 1957). A measure of "fines", F2 (total wt.% finer than 4.0 ϕ), has also been done for each sample. These parameters were chosen as they are relatively simple compared to other graphical statistics used in the literature and also because it enabled comparison with most other studies of pyroclastic deposits. An outline of the statistical formulae as defined by Folk and Ward (1957) used in this analysis are presented in Appendix I.

Components of each sample analyzed were divided into 6 main groups: White pumice, Gray pumice, Banded pumice, crystals, lithics, and glass shards. For sizes greater than 1.0 ϕ (0.5 mm), each component was separated by hand under a binocular microscope and then weighed on a laboratory balance. For grain sizes between 1.0 ϕ and

4.0 ϕ (0.5-0.063 mm), a minimum of 500 grains were counted (750 for PFD's) and the proportion of components were converted to weight fractions using a proportional conversion factor determined through repeated sample tests to calculate the correct weight percentage. Specific results for all samples in this thesis are presented in Appendix I and II. Histograms that show the component and granulometric diversity of analyzed samples display White pumice in white, Gray pumice in white with 10% stipples, Banded pumice in white with 30% stipples, Crystals in gray, Lithics in black, Glass in white with 60% stipples, and Non-component Analyzed (NA) in cross-hatching. All samples in this study represent bulk samples of the deposit at a given locality, unless otherwise indicated.

4. ~1000 A.D. Caldera-Forming Eruption

The ~1000 A.D. caldera-forming eruption of Volcán Ceboruco produced 3- 4 km^3 (DRE) of tephra, less than 0.3 km^3 of which is contained in pyroclastic surge and flow deposits, including the Marquesado flow deposits (Table 1) (Gardner and Tait, 2000). The Jala Pumice contains two different magma types. One is rhyodacitic in composition; the other is dacitic (herein referred to as White Pumice and Gray Pumice, respectfully). Banded pumices, consisting of intermingling streaks of the two magma compositions are quite abundant in specific levels in the Jala pumice sequence (Figure 8). Overall, Gray pumices comprise less than 15 wt.% of the erupted volume, but, in the uppermost layers of the Jala Pumice, they account for more than 90% of the juvenile material.

The petrology of the Jala Pumice was most performed by Nelson (1980) and Gardner and Tait (2000) and will be summarized here. Rhyodacite pumices are composed of highly vesicular rhyodacite glass and <1 vol.% plagioclase, with minor amounts of orthopyroxene, magnetite, and ilmenite. The dacitic pumices are microlite rich and composed of modestly vesicular glass and phenocrysts of plagioclase, clinopyroxene, orthopyroxene, hornblende, magnetite, ilmenite, and minor olivine. Both pumices are

relatively homogeneous. Gardner and Tait (2000) and Chertkoff and Gardner (2000) interpret the dacitic magma as the likely product of mixing between the rhyodacite and a more basic magma prior to eruption, as evidenced by zoned magnetite-ilmenite pairs that yield core temperature of ~1030°C and rim temperatures of ~865°C (Gardner and Tait, 2000), and the abundance of reaction-rims surrounding phenocrysts not seen in the rhyodacite magma, such as hornblende, clinopyroxene, and olivine (Chertkoff and Gardner, 2000).

The Jala Pumice is composed primarily of at least 7 pyroclastic fall layers (P0-P6), 6 of which are Plinian (P1-P6). The coarse, widely distributed P1 fall layer is the most voluminous, and accounts for ~70% of the total erupted volume (Table 1). The remaining stratigraphy consists of alternating pyroclastic fall, surge (S1, S2, and S3), and pyroclastic flow layers (North-Flank and Marquesado flow deposits), reflective of the fluctuating mass eruption rate of the eruption (Figure 9). The overall lithic content (lithic wt.%) steadily increases from less than 10 wt.% in the base to >90 wt.% in the uppermost lithic fall deposits. Isopach and isopleth maps of the pyroclastic fall layers of the Jala Pumice constructed by Gardner and Tait (2000) indicate that the eruptive vent was located on the north flank of Ceboruco, rather than atop the former summit (Figure 5), where caldera-collapse occurred.

Lithic subpopulations vary in the Jala Pumice eruptive sequence (Figure 10). In this paper, "Lithic" describes variably vesiculated non-juvenile rock fragments (vesicularity varies from 0 to ~70%) that were accidentally incorporated into the eruptive mass. Lithic types found in the Jala Pumice sequence are classified as either surficial lava fragments from near the eruptive vent, fragments of Sierra Madre basement rock, or "Granitic-clast" lithics. Surficial lava fragments include a wide assortment of scoria and dense lava clasts. Granitic clasts are described here as crystal masses of plagioclase and quartz, ± biotite, and have also been found in eruptive tephra from several of the local cinder cones that surround Volcán Ceboruco (Thorpe and Francis, 1975). Studies by

Thorpe and Francis (1975) and Nelson (1980) suggests that the granitic clasts are likely from concealed bedrock or possibly wall rock surrounding the Ceboruco magma chamber, probably existing beneath Sierra Madre basement rock (Figure 7).

5. Revised Eruptive Stratigraphy of the Jala Pumice

Previously published characteristics and stratigraphy of the ~1000 AD caldera-forming eruption of Volcán Ceboruco (Nelson, 1980; Gardner and Tait, 2000) are augmented with granulometric and component analyses, along with interpretations from newly described proximal, medial, and distal pyroclastic deposits. The greatest emphasis will be on the deposits that have not been previously described in detail, such as the surge layers (S1, S2, and S3) and flow deposits (Marquesado and North-Flank), but all relevant information from layers within the Jala Pumice will be presented. In this section, brief descriptions of the stratigraphic units will be combined with new findings of how the Md_ϕ, σ_ϕ, F2, lithic-type, and pumice-type populations vary through the eruptive sequence.

This study has subdivided the caldera-forming eruption into three phases based on eruptive style and component variation (Table 1). These phases represent a continuum of shifting eruptive styles that correlate with stratigraphic subunits of the pyroclastic fall, surge, and flow deposits (Figure 11). The four main sources of tephra that are recognized in this thesis are: (1; *P* and *L*) Plinian or non-Plinian lapilli (either pumice or lithic rich) deposited as fall-out from either the vertical column or the umbrella region of an eruptive plume, (2; *S*) material deposited from pyroclastic surges, (3; *M* and *F*) material deposited from pyroclastic flows, and (4; *c*1 and *c*2) fine ash and rare lapilli elutriated from pyroclastic flows and probably deposited as co-ignimbrite ash fall. The discrimination of pyroclastic material within the complex stratigraphy of the Jala Pumice as either pyroclastic fall, surge, or flow deposits is based on a combination of granulometric and component analysis, and direct field evidence of the deposits' dispersal characteristics, thickness variability, and internal stratigraphy, such as cross-bedding and planar bedding.

Subsequent numbers designate the relative order in the eruptive sequence, e.g., S1 refers to the first surge deposit in the Jala Pumice sequence.

The terms proximal, medial, and distal are used to characterize the distance of a deposit (with the exception of Marquesado deposits, see below) from the main eruption vent, indicated in Figure 5. Proximal refers to a deposit found within 3 km from vent, and includes all flank deposits. Medial refers to deposits located from 3 to 10 km from vent, and include nearly all deposits found on the northern plateau, and in the Jala and Ahuacatlan river valleys, including those found at Location 11. Distal refers to deposits found more than 10 km from vent, and includes the northernmost deposits on the plateau, some Marquesado deposits, and deposits found near the villages of Santa Fe, Rosa Blanca, and El Aguacate (Figure 5). Marquesado deposit distances were measured from the Ceboruco caldera center, and not from the main eruptive vent.

5.1. Phase I:

Deposits of Phase I include (1) the initial P0 fall deposit, and (2) the P1 fall deposit (Figure 12).

P0 fall layer:

The P0 fall layer marks the base of the Jala Pumice sequence, resting on a pre-eruption soil layer that commonly contains abundant lava blocks in a matrix of brownish-orange alluvium. P0 is restricted to a narrow lobe that extends to the north-northwest, and accounts for less than 0.3% of the total erupted volume of the Jala Pumice. The thickness of P0 ranges from 80 cm at its thickest exposure at medial locations to less than 10 mm at distal locations or at locations greater than ~2 km off the main dispersal axis. The clast-supported deposit, exhibits moderately well sorting (σ_ϕ: 1.33), a Md_ϕ of −1.6, no obvious grading, and contains ~10 wt.% lithic material and accretionary lapilli clasts in proximal localities. However, only one deposit was sampled (Locality 18). Juvenile material of the P0 unit is predominantly White pumice and tan colored accretionary lapilli, but rare Gray

and Banded pumice clasts can be found (Figure 13). Gardner and Tait (2000) estimate the total volume of P0 to be 0.01 km^3 (DRE), with a peak eruption rate of $<10^6$ kg/s.

P1 fall layer:

The P1 fall deposit is the most voluminous and widespread layer of the Jala Pumice, accounting for more that 75% of the total erupted volume (Table 1). Estimates of mass eruption rate from Gardner and Tait (2000) for the base of P1 are $4x10^7$ kg/s and back to $8x10^7$ kg/s for the coarsest-grained level located approximately 60% up from the deposit's base. Isopach and maximum lithic isopleth maps indicate that the dispersal axis of the P1 fall layer extends approximately N70°E from Ceboruco (Gardner and Tait, 2000). P1 decreases in thickness with distance from the eruptive vent (Gardner and Tait, 2000), and consists of well-sorted, clast-supported, sub-angular, White pumice lapilli that exhibit steady reverse grading in the lower 60% of the deposit, and rapid normal grading in the uppermost 5-10%. Gray and Banded pumice are rare (<3 wt.%), especially in distal deposits. Accidental lithic contents range from <5 wt.% in the lower portion of P1, to ~15 wt.% in the upper 10% of the deposit (Figure 14).

Every P1, as well as every other Jala Pumice fall, deposit Md_ϕ vs. σ_ϕ values plot within the "Pyroclastic Fall Deposit" zone defined by Walker (1971) (Figure 15). Granulometric analyses of P1 deposits from the top ~20 cm (bulk) and basal ~20 cm (bulk) was performed from 7 localities ranging from 4.5 to 25 km from the eruptive vent (Figure 16). The Md_ϕ, maximum pumice diameter, maximum lithic diameter, and bulk accidental lithic content from base and top of P1 all decrease systematically with increasing distance from the vent. In addition, both the top and bottom of the P1 deposit show an increase in overall crystal content, and only weak improvement in sorting (σ_ϕ) with distance.

Analyses of accidental lithic populations of the P1 fall deposit indicate that between 70-85 % are surficial lava fragments, between 15 and 30 % are Granitic-clast lithics, and less than 2% are Sierra Madre lithics (Figure 10).

The uppermost 1 to 4 cm of the P1 fall deposit represents the extreme end to the normal grading trend observed in the top 5-10% of the P1 layer (Figure 9). This portion is composed of a thin layer (<3 cm) of clast-supported, sub-rounded White pumice lapilli and ash. The pumice-rich layer at P1's top shows similar component make-up and dispersal characteristics as the rest of the P1 unit but exhibits similar granulometry (Md_ϕ: -0.2, σ_ϕ: 1.14) to the P0 fall layer.

5.2. Phase II:

The deposits of Phase II include (1) a thin and narrowly dispersed lithic-rich level atop P1, (2) the S1 surge deposit, (3) the P2 fall deposit, (4) the S2 surge deposit, (5) the P3 fall layer, (6) the S3 surge deposit, and (7) the P4 fall deposit (Figure 17).

Lithic-rich fall deposit:

On top of the pumice-rich layer of P1 lies a thin (<1 cm) well-sorted, clast-supported, lithic-rich layer of surficial andesitic lithic fragments that is depleted in juvenile material. The dispersal characteristics of this layer resemble P0, rather than P1, and thus are assumed to represent the beginning of Phase II (Figure 12).

S1 surge deposit:

The S1 surge layer represents the first pyroclastic surge in the Jala Pumice (Figure 18). Because of the limited aerial extent of the fine-grained lithic-rich layer atop P1, S1 is the first layer of the Phase II stratigraphy at most localities. S1 is found on the north, northeast, and eastern flanks of Ceboruco and atop the northern plateau (Figure 19). S1 is also present as a thin (0.5-2 cm) ash layer at localities west of Santa Fe, 25 km north of Ceboruco, and atop a 1620 m ridge immediately north of the village of Coapan (Figure 5). S1 was estimated to represent a volume of ~0.002 km^3 (DRE) by Gardner and Tait

(2000), however, this calculation was based on a total lithic content of ~30 wt.%. Granulometric analysis (Table 3) from this study indicates an average lithic content of ~55 wt.%, which suggests a volume of approximately 0.001 km^3 (DRE), accounting for <0.1 % of the total Jala Pumice volume (Table 1).

The Md_ϕ vs. σ_ϕ values for S1 deposit plot as an array across the "Pyroclastic Flow Deposit" zone and the "Pyroclastic Surge Deposit" zone as defined by Walker (1971) in Figure 15. Nonetheless, we define the S1 deposit as a surge deposit based on the abundance of accretionary and armored lapilli (Moore and Peck, 1967; Self and Sparks, 1978), moderate sorting, and massive, but thin (<15 cm) beds.

Proximally, the olive-gray-colored S1 deposit is predominately massive, moderately to poorly sorted, and contains abundant armored lapilli, and rare sub-rounded pumice clasts. No charred organic material is observed in the S1 deposit. Internal bedding structures in flank deposits were found at only one locality and include a massive bed at the base with faint laminations at the top 0.75 cm (Locality 5). The thickness of the S1 unit ranges from 1-2 mm to 5.5 cm on the flanks with the exception of one proximal deposit, which measures in excess of 3 m (Locality 6). This outcrop appears to reflect an exceptional instance where the S1 surge actively eroded and disrupted the underlying P1 fall deposit, as evidenced by its inflated, channel-filled, matrix-supported appearance (Figure 18).

Sampling of S1 was performed most extensively in medial locations atop the plateau to the north and northeast of Ceboruco along two transects, B-B' and C-C' (Figure 5). B-B' trends approximately N10°E from Ceboruco and represents the general flow direction of the S1 surge cloud, as evidenced by the linear trend of maximum bed thickness which parallels B-B'. The C-C' transect trends approximately N60°W along the upper crest of the Sierra Madre escarpment north of Ceboruco and represents a cross-section of the propagating current as it encountered the ~150 m cliff (Figure 20). At all sample localities on the northern plateau S1 is a massive, olive-gray-colored, moderately-

to-poorly sorted, armored-lapilli-bearing, ash-rich layer with faint laminations in the upper 20% of the deposit (Figure 21). S1 reaches a peak thickness of 15 cm at a site located 5 km from the vent atop the northern plateau, and then thins rapidly to <3 cm only 2 km downstream (Figure 20). S1 is found up to 25 km away from vent, where it displays intermittent pinch-and-swell geometries on ~1 m scale and is often observed as mantling fall deposit pumice clasts.

Along the B-B' (Figures 22 and 23) and C-C' (Figure 24) transects, the S1 layer displays variability in Md_ϕ, σ_ϕ, and F2 with distance. A linear relationship has been found to exist between thickness and Md_ϕ (and F2) along B-B', which shows that coarser grained deposits are up to 8 times thinner than the fines-enriched deposits, especially beyond 6 km (Figure 23). The thickest deposits contain the highest F2, the smallest Md_ϕ values, and a random distribution of sorting coefficients (σ_ϕ: 2.00-2.50). Along the crest of the Sierra Madre escarpment (C-C'), S1 is fines-rich (F2) and poorly sorted (σ_ϕ) compared to distal S1 deposits.

Distal S1 deposits range in thickness from 1- 2 cm, contain the coarsest Md_ϕ values, and display the most improved sorting (σ_ϕ: 2.04) observed atop the plateau (Figure 21). Distal S1 deposits also have the smallest F2 values (<5 wt.%).

Granulometric and component analysis of all S1 deposits are organized and presented in Appendix II. Analysis of accidental lithic populations of the S1 surge deposit indicate that 85-95% are surficial lava fragments with the remaining 5 to 15% being Granitic-clast lithics. Less than 1% of the accidental lithics are Sierra Madre fragments (Figure 10).

P2 fall layer:

Immediately above the S1 surge layer is the P2 fall deposit (Figure 25). The P2 layer has a volume of ~0.4 km^3 (DRE) and accounts for ~10% of the total erupted volume of the Jala Pumice (Table 1). Mass eruption rate estimates for P2 vary from ~$1x10^8$ kg/ s

for the basal layers, which is the most intense in the Jala Pumice stratigraphy, to $2x10^7$ kg/ s for the upper level (Gardner and Tait, 2000). The P2 fall layer has similar dispersal characteristics to the P1 fall layer with a dispersal axis of ~N50°E.

The internal stratigraphy of the P2 fall layer is distinct, and is therefore easily distinguished in both proximal and distal localities. Individual layers in the P2 stratigraphy are most easily recognized by local changes in grain size and overall pumice and lithic content. It is important to note, however, that although fluctuations in the overall lithic content are observed throughout the P2 fall deposit, the concentration of lithic fragments between grain sizes of 0 and 4.0 ϕ remain nearly constant (Figure 10). The base of P2 marks the dramatic increase of both lithic material and Gray and Banded pumices in the Jala Pumice stratigraphy, and is referred to here as the Lithic-Rich Base (LRB) (Table 2). The LRB is coarse-grained, clast-supported, and moderately sorted (Figure 26). Analyses of the LRB at proximal locations yield Md_ϕ values between –2.5 and -4.8 ϕ, σ_ϕ values between 1.15 and 1.26, and accidental lithic concentrations of 45-55 wt.%. Pumice populations in the P2 layer are composed of White pumice (>80 wt.%), Gray (<15 wt.%), and Banded pumice (<5 wt.%). Distally, the LRB layer has Md_ϕ values between –0.5 and –2.0 ϕ, σ_ϕ values between 0.8 and 1.1, and accidental lithic concentrations of 12-18 wt.% (Figure 26). Granulometric analysis of 7 LRB samples from sites ranging from 4 to 25 km away from the eruptive vent indicate that Md_ϕ, σ_ϕ, and wt.% lithics all decrease with distance (Figure 27). Total thickness also decreases with distance.

Above the LRB are a coarse-grained, pumice-rich level, a fine-grained level, and a coarse-grained, lithic-rich top (Figures 25 and 26). The coarse-grained (Mdϕ: -4.9 ϕ) pumice-rich level is clast-supported and moderately sorted (σϕ: ~1.50), and contains 25-30 wt.% lithics at proximal locations and <15 wt.% lithics at distal sites. The pumice population of this level is comprised of 65-75 wt.% White pumice, 15-25 wt.% Gray pumice, and 5-10 wt.% Banded pumice. The fine-grained (Md_ϕ: -2.4 ϕ) layer is

moderately sorted (σ_ϕ: 1.35) and contains ~40 wt.% lithics, and Gray and Banded pumice abundances of ~25 and ~10 wt.% respectively. This fine-grained region marks the point of highest Gray and Banded pumice abundance in Phase II (Figure 8). The upper half of the P2 fall deposit exhibits reverse grading from the fine-grained layer up to a coarse-grained (Mdϕ: -3.0 ϕ), clast-supported, moderately sorted ($\sigma\phi$: 1.44) level. Similar to the LRB, the top is enriched in lithics (~45 wt.%) and Gray and Banded pumice (>25 and ~5 wt.%, respectively). At proximal locations, it is common to see the top level of P2 eroded by the subsequently deposited S2 surge deposit.

Gray pumice clasts in P2 commonly have lithic-rich cores, and the Banded pumices often have intricate lithic clusters that result in the deformation of striations of the differing magma compositions. These textures are seen throughout Phase II and III, but not Phase I. Analyses of accidental lithic populations of the P2 fall deposit indicate that between 90-95 % are surficial lava fragments, between 4 and 8 % are Granitic-clast lithics, and approximately 3% are Sierra Madre lithics (Figure 10).

S2 surge deposit:

S2 surge deposits (Figure 28) are limited to the northeast, east, and southeast flanks of Ceboruco, and are distributed atop the plateau to the north (Figure 29). S2 is not found beyond 15 km from vent. Proximal sampling of the S2 layer was performed on the eastern and southeastern flanks of Ceboruco along the A-A' transect (Figure 30). S2 deposits at proximal sites are light gray and commonly exhibit internal stratifications, including cross bedding and planar bedding of mm to cm thick bands of alternating sandy ash-and-pumice layers with silty ash layers in the lower 60%, with faint laminations at the top 40% of the deposit. S2 was estimated to represent a volume of ~0.003 km^3 (DRE) by Gardner and Tait (2000), based on a total lithic content of ~30 wt.%. Granulometric analysis from this study (Table 3) indicates, however, an average lithic content of ~45 wt.%, which suggests a volume of approximately 0.002 km^3 (DRE), accounting for <0.15 % of the total Jala Pumice volume.

Like S1, Md_ϕ and σ_ϕ values for the S2 deposit plot across the intersection of the "Pyroclastic Flow Deposit" and "Pyroclastic Surge Deposit" fields of Walker (1971) (Figure 15). Nonetheless, we believe S2 is a surge deposit because of its abundance of internal stratigraphy, such as cross-bedding and planar bedding, moderate sorting, and abrupt changes in thickness (Figures 30 and 31) in response to topography (Fisher, 1979; Allen, 1984).

Deposits located along the eastern flank transect (A-A') display highly variable values of Md_ϕ, σ_ϕ, F2, and thickness as topography changes with distance (Figures 30 and 32). Almost all of the S2 deposits found along the eastern flank range from 4-10 cm thick and are moderately to poorly sorted ($\sigma\phi$: 2.50-3.75) (Figure 33). One S2 deposit on the A-A' profile located at the break in slope between the east flank of Ceboruco and the Jala valley floor (Locality 1) is nearly 25 cm thick, and displays anomalous Md_ϕ (4.3 ϕ), sorting (σ_ϕ: 1.03), and F2 values (F2: ~80 wt.%) (Figure 34).

Medial sampling of the S2 surge layer was performed along the B-B' transect, which is believed to parallel the general flow direction of the S2 surge cloud, based on the linear trend of S2 bed thickness that follows B-B'. With the exception of three localities located atop the crest of the Sierra Madre escarpment at the abrupt front of the northern plateau, S2 deposits on the plateau exhibit only massive internal structure with faint laminations in the top few centimeters. Medially, the S2 deposits are olive-gray in color, moderately to poorly sorted, and contain neither armored lapilli nor charred organic material.

Analyses of the medially located S2 surge deposit along the B-B' and C-C' transects are presented in Figures 35 and 36, respectively. Atop the northern plateau, despite the gradual decline in Md_ϕ with increasing distance, the S2 layer displays sudden and pronounced fluctuations in thickness and sorting in response to changing topography (Figure 31). No correlations exist between thickness and Md_ϕ or F2, and only a weak association is seen between thicknesses and sorting (Figure 35). S2 deposits along the C-

C' transect exhibit a very narrow range of Md_ϕ (3.6-4.2 ϕ) and sorting (σ_ϕ: 1.5-2.2), and display a unique correlation between proximity to the Sierra Madre cliff and the amount of fines enrichment (F2: 45-65 wt.%). Specifically, sample sites < 1 km from the escarpment ridge display F2 values >60 wt.% whereas deposits > 1 km downstream from the cliff face have F2 values <50 wt.%.

Only two sites atop the northern plateau include S2 deposits that exhibit internal stratigraphy (71 and 18) (Figure 37). Both are located within 7 km from the vent, where the B-B' and C-C' transects meet atop the northern plateau (Figure 5). Here, the S2 deposits range from 9 to 12 cm in thickness, and have intricate cross bedding in the basal 2-4 cm, massive bedding in the middle 3-5 cm, and planar bedding in the upper 2-4 cm. Cross-bedded samples are the finest grained (Md_ϕ: 2.0 ϕ) and best sorted (σ_ϕ: 1.5) (Figure 38). Massive layers are the coarsest-grained (Md_ϕ: 4.2 ϕ); display moderate sorting (σ_ϕ: 1.60), and contain the most amount of fine material (F2: >65 wt.%). The top, planar-bedded zone is the poorest sorted (σ_ϕ: 2.38), and has intermediate Md_ϕ and F2 values of 1.9 ϕ, and 21 wt.%, respectively.

Granulometric and component analysis of all S2 deposits are organized and presented in Appendix II. Analysis of accidental lithic populations of the S2 surge deposit yield abundances similar to those in the underlying P2 fall layer: 85-95 % surficial lava fragments, 4-10% Granitic-clast lithics, and less than 5% Sierra Madre lithics (Figure 10).

P3 and P4 fall layers (the P3/4 fall layer):

Immediately above the S2 deposit is the second fall layer of Phase II, the P3 fall layer (Figure 28). The P3 and subsequent P4 fall layers were often mapped as one unit because they can only be differentiated at proximal and some medial localities where the S3 surge layer exists between them. True thickness and accurate dispersal for the P3/4 layer is difficult to constrain because the top of the P3 layer is often eroded by the S3

surge deposit and the P4 fall layer is often partially eroded by either subsequently deposited pyroclastic flow deposits or soil development. Previous work by Gardner and Tait (2000) suggests that the dispersal of P3/4 are similar to P2, and that its combined volume accounts for ~8% of the total Jala Pumice volume (~0.5 km^3, DRE). Mass eruption rates during the deposition of the P3/4 fall layer are thought to have been between 1-4x10^7 kg/s (Gardner and Tait, 2000).

The base of the P3 fall layer consists of a coarse-grain, well sorted, clast-supported, pumice-lapilli layer, with pumice clasts up to 5 cm in diameter at proximal locations (Figure 39). The base consists of approximately 38 wt.% accidental lithics, with the remaining 62% being composed of 60-65% White pumice, 25-30% Gray pumice, and <8% Banded pumice. Md_ϕ and σ_ϕ for the base of P3 are -2.9 and 1.29, respectively. P3 exhibits normal grading, where the lithic content drops to approximately 25 wt.%, and the proportions of White, Gray, and Banded pumices are 60-65%, 30-35%, and <2%, respectively (Figure 8).

The lithic content at base of the P4 fall layer is similar to that of the top of P3, with approximately 30 wt.% lithics (Figure 39). The proportions of juvenile lapilli, however, are quite different. The abundance of White pumice at the base of P4 accounts for >95 % of the juvenile material, whereas Gray pumice accounts for <5 % of the total juvenile content. Less than 1 % of the juvenile material is Banded pumice (Figure 8). Md_ϕ and σ_ϕ for the base of P4 are -3.3 and 1.30, respectively (Locality 18). P4 is reversely graded, with the lithic content of the top nearly exceeding 60 wt.%, and are equivalent in size to the lithics found at the base of P3. It is important to note that although fluctuations in the overall lithic content are observed through the P3 and P4 fall deposit, the 0 to 4.0 ϕ grain size fraction of lithic content remains nearly constant. Therefore, observed increases in overall lithic wt.% correlate with an increase in coarse-grained lithics only. The top of P4 also marks a return of abundant Gray and Banded pumice clasts. Of the juvenile material at the top of P4, <50% is White, ~40% is Gray,

and >10% is Banded pumice (Figure 8). Md_ϕ and σ_ϕ for the top of P4 are –2.9 and 1.28 at Locality 18, respectively.

Similar to P2, Gray and Banded pumices contain either lithic-rich cores or masses of lithics that have deformed the banding textures. Lithics in the P3 and P4 fall layers are composed of between 80-85 % surficial lava fragments, 2-10 % Granitic-clast lithics, and 5-15 % Sierra Madre lithics. The P3 and P4 fall deposits mark the first significant increase in Sierra Madre lithics.

S3 surge deposit:

The third and final surge deposit in the Jala Pumice sequence is the S3 surge layer (Figure 40). The S3 layer is found only within 5 km of the vent on the northern, northeastern, and eastern flanks. The total volume of the S3 surge deposit is estimated to be <0.001 km^3 (DRE), accounting for <0.1 % of the total Jala Pumice volume (Table 1).

Md_ϕ and σ_ϕ values for S3 deposit plot across the "Pyroclastic Flow Deposit" and "Pyroclastic Surge Deposit" fields of Walker (1971) (Figure 15). Nonetheless, we believe S3 is a surge deposit based on the abundance of armored lapilli (Moore and Peck, 1967; Self and Sparks, 1978), complex planar bedding (Fisher, 1979; Allen, 1984), sub-rounded pumice clasts (Sigurdsson et al., 1987), and variations in thickness in response to changes in topography (Valentine, 1987; Fisher, 1990).

Proximal layers of S3 are pinkish-gray and display an intricate internal stratigraphy (Figure 40). The lower 30% of the bed is typically a massive, matrix supported, pumice-and-armored-lapilli-bearing layer. The middle 30% usually reversely grades upward into a section of repeated planar beds that contain coarse-grained pumice and accretionary lapilli (up to 1.1 cm in diameter). Pumice and lithic proportions are the same as those observed in the middle region of the P3/4 fall layer, with abundant Banded and Gray pumices. The upper 30% of S3 grades normally into a zone of repeated fine to very fine-grained laminations of alternating lithic and ashy layers.

At medial localities, the S3 surge deposit exists only as a 3-4 cm-thick, light-pinkish-gray coating of ash on pumice clasts in the middle of the P3/4 fall deposit (Figure 28). No indication of the S3 surge layer is observed in distal localities.

Owing to its limited distribution, only 4 samples of S3 were collected and analyzed, all of which lie along the A-A' transect. These samples exhibit a bimodal distribution of Mdϕ and F2, and a wide range of σϕ and thickness. Like the S2 surge layer, S3 at Locality 1, at the break in slope between the near-horizontal Jala valley floor and the eastern flank of Ceboruco, is anomalously fine-grained (Md_ϕ: 4.1 ϕ), well sorted (σ_ϕ: 2.0), and fines enriched (F2: >50 wt.%) (Figure 41). Also like the S2 layer, S3 at Locality 1 is anomalously thick (194 cm) (Figure 30).

5.3. Phase III:

The deposits of Phase III include (1) the Marquesado Pyroclastic Flow deposits, (2) the P5 and P6 fall deposits, (3) the North-Flank Pyroclastic Flow deposits, (4) the distally deposited *c1* and *c2* Co-Ignimbrite fall beds, and (5) the proximally deposited L1, L2, and L3 lithic-fall deposits, which cap the Jala Pumice eruptive sequence.

The Marquesado Pyroclastic Flow deposits:

The Marquesado Pyroclastic Flow sequence consists of relatively thick, valley-filling ash-flow deposits (1-10 m each) that are dispersed down the more gradually sloped southern flanks of Ceboruco onto the Ahuacatlan and Marquesado valley floors (Figure 5). Sampling of the Marquesado on the upper flanks is difficult because of the burial of the deposits by subsequently emplaced lava flows. However, sampling from this study indicates that Marquesado is present at the westernmost locality on the southern Ceboruco flank (Locality 52, see Figure 42).

Nelson (1980) and Gardner and Tait (2000) estimated the volume of the Marquesado deposits to be ~0.12 km^3 (DRE), which would account for <3 % of the total erupted volume of the Jala Pumice. We find that this approximation is an overestimate:

for the amount of accidental lithic fragments that were subtracted in the conversion from tephra to magma volume in the previous study was 20-40 wt.%. Component analysis of 13 Marquesado deposits from this study, yield an average lithic concentration in excess of 70 wt.%. Using a lithic concentration of ~70 wt.% yields a conservative magma volume of ~0.07 km^3 for the Marquesado deposits, which would account for <2% of the total Jala Pumice volume (Table 1).

Proximal deposits of the Marquesado flow deposits on the fringe of the southern edge of the outer caldera rim consist of at least 3 dark-pinkish-gray, matrix-supported, intricately stratified, ash-rich beds, typically 12-16 cm thick. The beds truncate Phase II layers (the P2 and P3/4 fall deposits, and the S3, S2, and very top of the S1 surge layers). The basal and middle layers are planar-bedded with beds composed of fine-grained lithic fragments and fine-grained, sub rounded White, Gray, and Banded pumice clasts interbedded with ash-rich layers (Figure 43). The upper layer is typically massive with thin and faint laminations rich in glass shards. The lithic populations are enriched in Sierra Madre (>10 vol.%) and depleted in Granitic-clast lithics (<1 vol.%), which match those of medial Marquesado deposits and contrasts with Phase I and II deposits. The proximal flank deposits are, however, significantly finer-grained (Md_ϕ of 2.1-4.2), better sorted (σ_ϕ: 1.50-2.31), and more fines enriched (F2: 55-65 wt.%), compared to the valley-fill deposits (Figure 44). At least 2 layers of equivalent thickness, color, and internal stratigraphy persist across the southern flank to the east, always remaining stratigraphically above the deposits of Phases I and II. No samples of those beds were collected, and so correlation is only tentative.

Near the village of Marquesado on the southwest side of Ceboruco, the Marquesado deposits consist of at least 3 graded units, typically 6-8 m thick each (Figure 45). Each flow unit is vertically and laterally graded from a basal, matrix-supported, lag breccia that commonly accounts for ~25 % of each unit's thickness, to a pinkish-gray, massive, poorly sorted, moderately ash-depleted zone (Figure 46). Blocks in the lag

breccia are primarily andesitic to dacitic lava fragments, similar to those found on Ceboruco. Volume estimates from point counting photographs indicate that 35-45 % of the deposit is matrix (Figure 47). Lag breccias extend as a lobe at the base of the Marquesado PFD's, and are found up to 9 km from Ceboruco. Lag breccia layers become thinner and become finer-grained with distance, and individual blocks become increasingly rounded (Figure 48). Medially, lithic blocks are angular to sub angular, account for ~90 wt.% in the breccia zone, and average ~9 cm in diameter, although blocks up to 180 cm in diameter are found. Smaller lithic fragments (<10 cm in diameter) are commonly sub-angular to sub-rounded. Pumice clasts are usually rounded, and average <2.5 cm in diameter, and are often segregated into oblong pumice lenses between 2 m and 15 cm long. Isolated pumice clasts are rare and are also rounded, averaging <0.5 cm in diameter. Pumices are composed of White (~75%), Gray (~20%), and Banded (~5%) types (Figure 8). Lithic populations of these deposits are composed of 80-90% surficial lava fragments, 7-12% Sierra Madre lithics, and less than 3% Granitic-clast lithics (Figure 10).

The flow body, located above their lag breccia counterpart is massive, poorly sorted, and medially contains lithic fragments <32 mm in diameter. Granulometric and component analysis of this upper layer indicates that it is identical to the matrix of the lag breccia in terms of Md_ϕ, σ_ϕ, F2, pumice and lithic content, and pumice and lithic populations (Figure 49).

Periphery Marquesado units observed at localities only 6.5 km from vent on the southern and eastern edge of exposed flow deposits exhibit no lag breccia (Figure 50). Here, the base of Marquesado deposits are composed of at least 3 massive, poorly sorted, moderately-ash-rich flow units, typically 3-4 m thick each. Lag-breccia-free deposits contain more juvenile pumice (up to 30 wt.%), and in general, pumice clasts are typically coarser-grained and more angular, compared to those in lag-breccia-bearing deposits. Lithic fragments average ~3 cm in diameter, and account for between 60 and 75 wt.% of

each flow deposit. The lowermost unit is light gray, whereas the upper two flow units are a darker grayish tan. Component analyses from each unit indicate, however, that there is no significant variation in lithic content, pumice content, or pumice population. A thin (<10 cm), nearly clast-supported, layer of medium-to-coarse-grained pumice lapilli exists between the first and second flow units (Figure 50). These pumice-rich beds maintain a relatively constant thickness in outcrop (~50 m), and do not contain sub-rounded or rounded pumice clasts, like the pumice lenses common to flow deposits. Pumice populations in this layer are composed of White pumice (~65%), Gray pumice (~25%), and Banded pumices (~10%), similar to the P5 and P6 fall layers of Phase III.

The North-Flank Pyroclastic Flow deposits:

Pyroclastic flow deposits that unconformably overlie the Phase II fall and surge deposits at the proximal north-flank exposures, and are found atop the P3/4 fall layers at medial localities atop the northern plateau, are referred to here as the North-Flank flow deposits (Figure 51). These deposits account for less than 0.1% of the total erupted Jala Pumice volume (Table 1).

The North-Flank pyroclastic flow deposits consist of at least 4 units (F1-F4) of increasing thickness (~30 cm to >2 m) and grain-size with height (Figure 52). Proximally, each layer is dark gray, predominantly massive, relatively coarse-grained (Md_ϕ: -2.9 to 0.2), poorly sorted (σ_ϕ: 2.90-3.55), and lithic rich (~70 wt.% lithics) (Figure 53). The upper 2 units (F3 and F4) are normally graded from a coarse-grained, lithic-rich breccia to a massive, poorly sorted bed which is very similar in composition and modal distribution to the lower two units (F1 and F2, see Figure 54). At many exposures, the F4 flow unit scours into the previously emplaced Phase I and II deposits (Figure 51).

Proximal North-Flank deposits typically contain lithic fragments <6 cm in diameter. Pumice clasts average 2.5 cm in diameter, but may range from 0.25 mm up to 5 cm in one deposit. Lithic populations are composed of between 83 and 88 % vent-derived surficial lava fragments, 8-15% Sierra Madre lithics, and <3% Granitic-clast lithics

(Figure 10). Pumice populations are equivalent to other Phase III deposits with White pumice accounting for up to 75%, and Gray and Banded pumices accounting for up to 20% and <10% respectively (Figure 8). Pumice clasts are typically sub-angular to sub-rounded, and are often segregated into oblong lenses 0.5 to 1 m in length.

Medial exposures of the North-Flank deposits atop the northern plateau (Localities 18, 71, and 82) are composed of one, dark gray, planar stratified, moderately sorted unit that ranges in thickness from 18 to 26 cm (Figure 17). Immediately above the unit is between 30 and 50 cm of pumice-bearing soil. It is not clear if the medial layer correlates to one or more of the one the 4 proximal deposits. Medial deposits consist of a basal layer that appears to have partially eroded the uppermost part of the P3/4 fall layer, with repeated (at least 3) planar bedded layers that start between 1 and 2 cm above the base. Each planar bed sequence is typically 6-8 cm thick, and is composed of layers of coarse-grained (2-8 mm diameter) pumice lapilli and lithic fragments alternating with massive, ash-rich beds. Flow deposits on the northern plateau are typically finer grained (Md_ϕ: -0.7 to 2.4), and are slightly better sorted (σ_ϕ: 2.4 to 2.9) than proximal deposits (Figure 53). F2 values from medially located samples range from 18 to 35 wt.%. Lithic content decreases slightly atop the plateau (29-60 wt.%), and the overall pumice content increases from <10 wt.% up to ~25 wt.% (Figure 54). Lithic and pumice populations found in the medial deposits are the same as those found on the northern flanks.

P5 and P6 fall layers:

The P5 and P6 fall deposits are rarely observed because of their limited distribution and erratic preservation. Proximally, North-flank pyroclastic flow deposits F3 and F4 are interbedded with P5 and P6. At distal locations, the two fall layers remain separated by a co-ignimbrite fall deposit (*c1*) (Figure 52). Gardner and Tait (2000) suggest that the combined P5/6 fall layer was dispersed more to the east than the P3/4 fall. Neither P5 nor P6 were sampled, but they appear finer grained and contain similar lithic concentrations to both the P2 and P3/4 fall deposits.

The distally located c1 and c2 co-ignimbrite fall layers:

There are at least two distally located co-ignimbrite fall layers, which are <10 mm thick and pinkish-tan in color (Figures 17 and 52). The layers are fine-grained (Md_ϕ: 0.4 to 3.2), and are predominantly composed of fine-grained lithic fragments, broken crystals, and glass shards. Deposits are moderately-to-well-sorted (σ_ϕ: 1.4 to 2.4), enriched in fine material (F2: 28-48 wt.%), and contain 70-85 wt.% lithics (Figure 55). The *c1* and *c2* layers are thickest near the town of El Aguacate, located approximately 25 km north-northeast of Ceboruco, where *c1* separates the P5 and P6 fall layers. Lithic populations of the *c1* and *c2* layers are composed of 80-85% lava fragments, 5-10% Sierra Madre lithics, and <1% Granitic-clast lithics (Figure 10). Pumice populations of the *c1* and *c2* layers are typically made up of 60-75% White pumice, 20-40% Gray pumice, and <10% Banded pumice (Figure 8).

The locally deposited L1, L2, and L3 Lithic fall layers:

The uppermost stratigraphy of Phase III and the Jala Pumice sequence is composed of at least 3 lithic-fall beds interbedded with at least 2 ash-rich beds, all of which are observed only in proximal locations (Figure 56). There may be more exposures of these deposits for they have only been observed, described, and correlated to the Jala Pumice recently because of newly exposed stratigraphic sections that have been uncovered through the construction of a highway that passes within 1 km of the northeast flank of Ceboruco. The L1, L2, and L3 deposits are erratically dispersed and are composed of non-graded, moderately-to-poorly sorted, clast-supported, coarse-grained, ash-depleted, lithic-rich fall deposits that range in thickness between 14 and 21 cm. The lithic content typically ranges from 60 to 80 wt.%, with one L3 sample containing more than 90 wt.% lithics (Figure 57). The lithics in L1, L2, and L3 are 80-90 wt.% lava fragments, 9-20 wt.% Sierra Madre lithics, and less than 1% Granitic-clast lithics. Pumice populations are less than 50% White pumice, 50-65% Gray pumice, and 4-5% Banded

pumice. Gray pumices greater than -1.5 ϕ in size often have lithic-rich cores, which may account for >30 % of their volume. Md_ϕ and σ_ϕ values for these deposits range from –1.1 to –3.2 ϕ, and 1.42 to 3.10 respectively (Figure 15).

The L1- L3 fall layers are interbedded with at least 2 ash-rich layers. These layers are typically gray to light gray, pumice-lapilli bearing, and cross-bedded, with thin (0.5- 1 cm) beds of lithic-rich and ashy alternating sequences at the base, and thin (<0.3 cm) laminated beds of alternating sandy, lithic-rich zones and ashy, lithic-poor zones at the top. The deposits are all fine grained (Md_ϕ: 1.9 to 2.85), moderately well sorted (σ_ϕ: 1.40 to 2.70), and are modestly enriched in fines (F2: 20 to 25 wt.%) (Figure 57). No accretionary lapilli are observed. The lithic content of these deposits typically range from 65-75 wt.%. The lithic population of the 2 ashy beds consist of between 80- 90 wt.% surficial lava fragments, 10-20 wt.% Sierra Madre lithics, and less than 1% Granitic-clast lithics. Pumice populations of the 2 ashy beds consist of less than 40% White pumice, 60-65% Gray pumice, and 4-5% Banded pumice.

6. The Transport and Deposition of Pyroclastic Material

The transport and deposition of particles from the fall, flow, and surge deposits of the Jala Pumice sequence are all modeled based on how mass accumulation of particles (lithics and crystals) in a given range of grain sizes vary with distance. Density currents that display an exponential decrease in mass accumulation, S (Equation 2), with distance indicate transport and deposition of material via turbulent suspension, whereas density currents that display relatively constant mass accumulation values, S, with distance indicate *en masse* transport and deposition (Figure 58).

6.1. The Transport and Deposition of the Jala Pumice Pyroclastic Fall Deposits

The presented model of transport and deposition of pyroclastic material in a volcanic plume fundamentally requires steady and constant volume flux (Sparks, 1991;

Bursik et al., 1992b). Deposits that display no grading or fluctuations in component abundance with distance suggest that they were deposited from a stable and relatively constant eruptive plume (Carey and Sparks, 1986). Therefore, layers that are modeled must not be extensively graded and must easily correlate with distal deposits to ensure accurate sampling. Few layers in the Jala Pumice meet these requirements. Nonetheless, the layers that were selected from the Jala Pumice for this model are (1) the basal ~10% of the P1 fall layer, (2) the upper ~10% of the P1 fall layer, and (3) the lithic-rich base (LRB) of the P2 fall layer because of their wide dispersal and distinct position in the Jala Pumice. All calculations used to model the mass accumulation, S, of particles at distance, r, from the fall layers utilize the mass accumulation of particles from Locality 18 as representing S_0, at distance, r_0, because of the approximation by Woods (1998):

$$r_0 \sim 0.25\ H_B, \qquad (4)$$

and Sparks et al. (1997):

$$(H_T - H_B) / H_T \sim 0.25, \qquad (5)$$

where H_T is the top of the umbrella region of the eruptive cloud and H_B is the base (Figure 2). Column height (H_T) was estimated from maximum lithic clast dispersal calculated by Gardner and Tait (2000), based on the model described by Carey and Sparks (1986), and then converting column height to mass eruption rate (Q) using the relationship, $H_T \sim Q^{1/4}$ (Sparks, 1986). Hence, for the majority of Phase I and II of the Jala Pumice eruption, r_0 is approximately 6 km.

Results from calculations of mass accumulation of particles with distance show distinctly different patterns for lithic and crystal particles in the base and top layers in P1 (Figure 59 and 60). Mass accumulation of coarse-grained lithics (-2.5, -2.0, -1.0 ϕ)

displays an exponential decrease in sedimentation with distance, whereas lithic clasts finer than −1.0 ϕ show a faint increase in sedimentation with distance, opposite to what is predicted. Mass accumulation of crystals with distance show significantly better agreement with model predictions for sedimentation via dilute and turbulent suspension.

Mass accumulation calculation results of lithics and crystals with distance show similar patterns for the LRB of the P2 fall layer (Figure 61). Similar to the mass accumulations of coarse-grained lithics (-2.5 and −2.0 ϕ) in P1 deposits, P2 lithic particles display an exponential decrease in sedimentation with distance, whereas lithic clasts finer that −2.0 ϕ show a faint increase, opposite to that which is predicted. Mass accumulation of crystals with distance show an exponential decrease in sedimentation for finer-grained crystals (2.0, 1.5, 1.0 ϕ), whereas crystals coarser than 0.0 ϕ slightly increase, also opposite to that which is predicted by the model.

This finding can be explained. In the model presented by Sparks (1991) and Bursik et al. (1992b), it is shown that the mass accumulation of particles with distance will exponentially decrease for all grain-sizes if sedimentation occurred from a dilute and turbulent current. Thus, it is required that the mass of particles of every grain-size be represented at each locality beyond the plume corner. The LRB of the P2 layer marks the peak in mass eruption rate in the Jala Pumice, implying a greater plume height. Woods (1988) showed that the distance from the plume axis to the plume corner, r_o, is a function of column height (Equation 4). Increasing the height of the eruptive plume may have extended the plume corner beyond the distance of Localities 18, 50, and 1, resulting in S_o values used in the accumulation calculations that are inadequate. Calculations show that r_o would be located approximately 5.25 km from vent during the deposition of P1, and 6 km from vent during the deposition of the LRB of P2 in response to the increased column height (H_T of P1 top ~ 28 km, H_T of LRB ~ 31 km). Such small increases in r_o are considered to be negligible considering the error in the method (Carey and Sparks, 1986; Carey et al., 1990). Nonetheless, the estimated r_o value range of 5.25-6 km indicates that

Localities 18, 50, and possibly 1 (3.4, 3.6, and 6.7 km respectively) would be located inside the plume corner. Deposition of material inside the plume corner may be chaotic and random, resulting from ballistic fallout of particles from the convective region of the plume, rather than the umbrella region (Pyle, 1989; Sparks 1991; Bonadonna et al., 1998). Removing Localities 18, 50, and 1 from the mass accumulation calculations for crystals in P2, and using Locality 29 as S_o displays an exponential decrease in sedimentation with distance (Figure 61 C and D). This indicates that crystals of the LRB of P2 were deposited from a dilute and turbulent current, at least beyond the plume corner, located at some point between Locality 1 and Locality 29.

A more general explanation for the nature of lithic mass accumulation with distance in all fall layers is that it may be a function of the diversity in lithic types in the Jala Pumice. Surficial lava fragments account for vast majority of the lithic content (>70% in P1, and >90% in P2). However, the vesicularity of surficial lithic fragments range from 0 to ~70% as a result of the Phase I and II lithic population primarily being composed of scoria, dense andesite, and poorly vesiculated lava fragments. Scoria dominates the fine-grained lithic populations (finer than 0.0 ϕ), whereas dense lava fragments account for the majority of the coarser-grained lithics (coarser than 0.0 ϕ). This inconsistency in lithic density with grain-size may have affected the accuracy of conversions of "lithic-counts" to lithic weight fractions, resulting in overestimates of particle mass for finer-grained scoria lithics.

Results from calculations of mass accumulation of crystals with distance show significantly better agreement with the model predictions from the base and top of P1, indicating that both layers were deposited from a dilute, turbulent particle-gas mixture. Crystals from the LRB of the P2 layer, however, do not display sedimentation patterns consistent with predictions from the model. One explanation for this deviation may be that the model of Sparks (1991) and Bursik et al. (1992b) requires deposition from a plume of constant flux. Although the Lithic-rich base is easily identified at all localities

and can be found >30 km from vent, the eruptive plume that deposited the Phase II stratigraphy was unstable and irregular in intensity as evidenced by the abundant grading, cyclic variation in overall lithic content, and changing pumice-types, especially in Gray pumice (Sigurdsson et al., 1985; Carey and Sparks, 1986; Sparks et al., 1991). This suggests the possibility that the deviation in mass accumulation trends for the LRB of P2 data from the model predictions may unfortunately result from sampling errors. Despite the ease in recognizing the P2 LRB proximally, it is less than 6 cm beyond 15 km and <2 cm at Locality 70, making the selective removal of loosely packed, clast-supported pumice and lithic clasts problematic.

In any case, particles of equal density from the layers in the most stable and uniform deposit of the Jala Pumice, P1, display an exponential decrease in sedimentation, S, with distance for each grain size. This can only be explained by deposition from turbulent suspension, because continual mixing accompanying deposition is the only process to result in an exponential decrease in particle concentration within a dilute current (Bursik et al., 1992a). This conclusion is in favor of turbulent transport and sedimentation from a dilute medium.

6.2. The Transport and Deposition of the Pyroclastic Flow Deposits

Pyroclastic flow deposits are thought to flow either as fluidized masses (Sparks, 1976; Wilson, 1980; Wilson and Walker, 1982), or as turbulent clouds (Fisher, 1979; Fisher and Heiken, 1982). To test if particle transport and deposition in Jala Pumice pyroclastic flows is dominated by fluidization or turbulent suspension, mass accumulation measurements were made on a series of 6 Marquesado flow deposits that extend to the west of Ceboruco from 6.5 to 12 km and modeled in the same way as the pyroclastic fall deposits as outlined above. Because pyroclastic flow clouds have no "corner" point where sedimentation begins, S_0 is assumed to equal the first profile in the sequence (Bursik et al., 1998). Mass accumulation calculations for Marquesado deposits

are from samples taken from the middle flow unit lag breccia and flow body, not the bulk flow deposit.

Results from the analysis of sedimentation from the middle Marquesado pyroclastic deposits display exponential trends for the coarsest lithic particles and horizontal trends for the remaining grain sizes of both lithics and crystals (Figure 62), suggesting that whereas the coarsest lithics appear to be deposited via dilute suspension, the majority of particles were emplaced via *en masse* freezing in each layer. Lateral extent of the North-Flank PFD's is limited, disallowing a meaningful modeling attempt to compare to Marquesado deposits.

6.3. The Transport and Deposition of the Pyroclastic Surge Deposits

Compared to pyroclastic flow deposits, surge deposits are often better sorted (σ_ϕ), display a more systematic decrease in Md_ϕ with distance, and display elaborate internal sedimentary structures that provide critical insight into the mechanisms by which particles are transported and deposited (Sparks, 1976; Wohletz and Sheridan, 1979; Fisher, 1986, 1992; Allen, 1984; Cole, 1991). Because of these observations, pyroclastic surges are considered to be low-concentration, turbulent currents (Fisher, 1979, 1992; Valentine, 1987).

Recent studies suggest that a key to resolving the dynamics of pyroclastic surges comes from careful analysis of deposits in regions of highly variable topography, because topography almost certainly exaggerates the development of density stratification within pyroclastic clouds (Kieffer, 1981; Walker, 1983; Fisher, 1990; Levine and Keiffer, 1991; Druitt, 1992; Woods et al., 1998; Bursik et al., 1998). To address this, we have performed a comprehensive study of the transport and depositional mechanics over the complex topography (150-240 m vertical relief) of the northern plateau (B-B') for S1 and S2, as well as the eastern flank (A-A') for S2 and S3.

Mass accumulation calculations of particles from S1 deposits along the B-B' transect are presented in Figure 63 (A and B). Except for the coarse-grain sizes, mass sedimentation of lithics in S1 does not decrease exponentially with distance, suggesting *en masse* deposition. Mass accumulations of crystals from S1 also display no systematic exponential decrease in sedimentation with distance. No systematic horizontal trend is observed, however, implying that transport and deposition was neither *en masse* nor from turbulent suspension. To see if this is the result of flow blocking and excess sedimentation downstream atop the plateau (Fisher, 1990; Woods et al., 1998), the first location (Locality 12) was removed from the calculations at the first site, r_0, along the traverse and replaced with Locality 18, which is located immediately atop the ridge crest (Figure 63 C and D). Although these results display an overall decline in mass accumulation with distance for each grain size with distance, the trends remain somewhat variable. This continued deviation of accumulating particles in the S1 surge deposits from the model outlined by Sparks et al (1991) and Bursik et al. (1992b; 1998) suggests that the S1 surge layer was not solely deposited from a dilute cloud.

Mass accumulation calculations of particles from the S2 surge deposit was performed along the A-A' eastern flank transect and the B-B' plateau transect. Along A-A', mass sedimentation trend lines of lithic and crystal particles decrease exponentially with distance, however, mass accumulation values for both particles are sporadic (Figure 64). This suggests that transport and deposition of material from S2 did not result via settling from turbulent suspension. Although mass accumulation values display an overall trend of decreasing deposition, it is not clear if sedimentation occurred via *en masse* freezing, however, because of the irregularity and random distribution of mass accumulation values for both lithic and crystals with distance. Furthermore, the occurrence of well-developed cross bedding and planar-bedding in the proximal S2 deposits makes *en masse* transport and deposition very unlikely (Fisher, 1986, 1990; Allen, 1984; Cole, 1991).

Along B-B', the mass accumulation of lithics and crystals from the S2 surge layer display an overall decline in sedimentation with distance, but the mass accumulation values are erratic in distribution (Figure 65, A and B). As with the S1 surge layer, the first location (Locality 12) was removed from the calculations as the first site, r_0, and replaced by Locality 18 to see if this results from flow blocking and excess accumulation on the upstream side of the northern escarpment compared to the accumulation atop the plateau (Figure 65, C and D). In this case, the mass accumulation of crystals with distance does appear to decrease exponentially as predicted by Equation (2). This exponential decrease in sedimentation with distance can be explained only by deposition from turbulent suspension, because continual mixing accompanying deposition is the only process to result in an exponential decrease in particle concentration within the transport medium (Sparks et al., 1991, Bursik et al., 1992b; 1998).

Mass accumulation calculations of particles from the S3 surge deposits were only performed along the A-A' eastern flank transect, owing to its limited distribution (Figure 66). Mass sedimentation of neither lithic nor crystal particles decrease exponentially with distance for any grain size. This suggests that transport and deposition of material did not result via settling out of turbulent suspension. It is not clear if sedimentation occurred via *en masse* freezing in place, however, because of the irregular and random distribution of mass accumulation values for both lithic and crystal particles with distance. Furthermore, sedimentation from the S3 surge appears to increase with distance, which is uncharacteristic of *en masse* freezing (Sparks, 1976; Wilson and Walker, 1982). The occurrence of well-developed planar bedforms in proximal S3 deposits makes *en masse* transport and deposition very unlikely (Fisher, 1986, 1990; Allen, 1984; Cole, 1991).

7. Discussion

Interpretations of the three phases of the ~1000 A.D. caldera-forming eruption are presented, and conceptual models for the transport and depositional mechanics of

pyroclastic material of the pyroclastic fall, flow, and surge deposits of the Jala Pumice are evaluated.

7.1. Interpretation of Phase I Deposits:

Phase I deposits are the consequence of material settling from a progressively intensifying and then suddenly stalling Plinian eruptive column. Following what appears to have been a short-lived, low energy vent clearing stage as evidenced by the small size of clasts enriched in vent derived lithics and the thin, elongated dispersal pattern of P0. Phase I deposits reversely grade for ~60% of the deposit thickness and then abruptly decrease in grain size at the top. Accidental lithic abundance parallels the gradual increase in overall grain size, yet never exceeds 15 wt.% of the deposit. This suggests a gradual rise of the eruptive plume as the magma output became more intense, followed by a period where the eruption seems to have briefly stalled, as evidenced by the thin, pumice-rich layer whose dispersal matches that of the rest of the P1 deposit. This pumice-rich layer represents the very end of Phase I.

Phase I deposits have a total lithic content of <30 wt.% in P0 and ~15 wt.% in P1. Compared to deposits of the following phases, Phase I layers contain an accidental lithic population, which is mainly vent-derived surficial lava fragments (70-80%), and the highest abundance of Granitic-clast lithics (15-30%), with few Sierra Madre lithics (<2%). Also, Phase I pumice populations contain the greatest amount of White pumice (>90%), with very minor amounts of Gray and Banded pumices (2-4% and 0.5-2% respectively).

Based on the subsurface stratigraphy of the area surrounding Volcán Ceboruco from Thorpe and Francis (1975), Nelson (1980), and Moore et al. (1994), the predominance of surficial lava fragment and Granitic-clast lithics suggests that during Phase I, lithic erosion and entrainment occurred mainly at magma chamber depths and at the vent (Figure 7). Alternatively, the least amount of erosion and entrainment of

accidental lithics into the eruptive column occurred at medial depths, because Phase I deposits have the least amount of Sierra Madre lithics compared to the other phases.

7.2. Interpretation of Phase II Deposits:

Gardner and Tait (2000) speculate that the lithic-rich fall layer immediately atop the fine-grained pumice bed of P1 represents the renewal of the briefly stalled eruption, and not the continuation of the waning P1 deposit. This study agrees with that, for it explains the similarities between the dispersal of the lithic-rich level to the initial layer of Phase I, P0, and the sudden abundance of accretionary lapilli, which is not present in P1. In addition, the lithic population of this layer is predominantly vent-derived surficial lava fragments (>95%), with few Granitic-clast and Sierra Madre lithics (<4% and <1%, respectively), unlike the P1 deposit. Gardner and Tait (2000) also suggest that this lithic-rich layer may represent the start of the caldera-forming eruption as evidenced by several other eruptions that display abrupt increases in lithic content. Sudden abundance of lithics and lack of juvenile material is commonly regarded as an indication of active cratering and subsequent vent erosion that commonly accompanies initial caldera collapse (Bacon, 1983; Druitt, 1985; Paladio-Melosantos et al., 1992; Feirstein and Hildreth, 1992; Rosi et al., 1993). This layer is, however, a thin, fine-grained, individual fall deposit that corresponds to a single and abrupt increase in lithic content, rather than a gradual increase throughout a deposit. This certainly suggests that the lithic-rich base of Phase II was deposited from a discrete explosion separate from P1, and was at least partially phreatomagmatic, that renewed this eruption and subsequently resulted in the emplacement of the S1 surge deposit. However, this study finds that the lithic-rich fall layer at that base of Phase II more likely reflects a reinitiating of the Jala Pumice eruption, whereas the P2 fall layer more likely directly correlates to the onset of caldera-collapse.

Phase II deposits above the lithic-rich fall layer are composed of a complex sequence of interbedded Plinian fall layers (P2, P3, and P4) and three pyroclastic surge deposits (S1, S2, and S3). Despite the similarities in fall deposit dispersal and eruption column heights (Gardner and Tait, 2000), Phase II fall layers display significant fluctuations in pumice types, lithic types, lithic content, and calculated mass eruption rates, compared to Phase I. This suggests that the fall deposits of Phase II were deposited from an eruptive column that became increasingly unstable with time as evidenced by the dramatic changes in grain-size and occurrence of repeated surge deposits (Sigurdsson et al., 1985; Carey and Sparks, 1986; Sigurdsson et al., 1987; Sigurdsson et al., 1990b). The large variation in pumice types between layers, especially marked by an abrupt influx of Banded pumice clasts, also suggests the active removal of different magma compositions was accompanied by conduit-flow mixing (Sigurdsson et al., 1985; Blake and Ivey, 1986; Freundt and Tait, 1986; Sigurdsson et al., 1990b). In addition, Gray and Banded pumices found in Phase II often contain cores of fine-grained lithics, suggesting an influx of lithic material into the erupting mass during withdrawal. Lastly, the coarse-grained lithic content observed in Phase II deposits are ~3 times greater compared to Phase I layers, signifying an abrupt flux of coarse lithic material into the Phase II eruptive column beginning at the base of the P2 fall layer, which likely marks the initial onset of caldera-collapse. Although the overall lithic content increases sharply from Phase I to Phase II, the increase in lithic fragments ranging from 0-4.0 ϕ in diameter remains relatively constant through the remainder of Phase II. This may be significant in understanding a mechanism of caldera-formation that has yet to be fully appreciated.

Phase II deposits exhibit different lithic populations than Phase I, suggesting a change in the region of most extreme accidental lithic erosion and entrainment. Phase II lithic populations show a large reduction in the distribution of Granitic-clast lithics (<6%), an increase in the abundance of surficial lava fragments (>88%), and a steady increase in the amount of Sierra Madre lithics (2-6%) compared to populations observed

in Phase I. This suggests that the majority of erosion and entrainment of accidental lithics occurred at the vent, with lesser amounts occurring around the magma chamber and at medial depths, possibly resulting from preliminary structural foundering near the surface (Suzuki-Kamata et al., 1993) (Figure 7).

Pyroclastic surge deposits occur throughout Phase II. The S1 layer rests atop a thin (<1 cm), lithic-rich, accretionary-lapilli-bearing, clast-supported fall layer whose dispersal mirrors that of the P0 deposit. This layer represents the onset of Phase II that subsequently deposited the S1 surge layer. S1 is an armored-and-accretionary-lapilli-bearing, ash-rich layer that is predominantly free of pumice lapilli, invariably massive, moderately to poorly sorted, and contains no charred organic material. This suggests a low temperature, phreatomagmatic origin for S1 (Waters and Fisher, 1971; Self and Sparks, 1978). Unlike S1, both S2 and S3 are moderately sorted, pumice-lapilli-bearing layers that vary strongly in Md_{ϕ}, σ_{ϕ}, and thickness with distance and local topographic changes. Armored lapilli are present in S3, but are absent in the S2 deposit. S2 and S3 surge layers exhibit internal stratigraphy in proximal localities and some medial sites (S2 only) that consists typically of cross bedding in the base, and planar bedding with thin laminations in the middle and top. This suggests S2 and S3 surges were more dilute and mobile than the S1 surge (Fisher, 1979; Allen, 1984; Sigurdsson et al., 1987; Sigurdsson et al., 1985; Carey, 1991). In addition, the S2 and S3 surge layers occur between Plinian fall deposits that display no signs of phreatomagmatic accompaniment at or near the contacts of the surge layers which imply that they are the result of intermittent partial column collapse of dense portions of the eruption column, and not of phreatomagmatic origin (Sparks and Wilson, 1976; Sigurdsson et al., 1985, Scott et al., 1992).

7.3. Phase III Interpretations:

Phase III deposits represent the final and cataclysmic stage of the caldera-forming eruption of Volcán Ceboruco. The deposits of Phase III mark the first and only

occurrence of several, small-volume, lithic-rich pyroclastic flow deposits, which are interbedded with relatively thin (<10 cm each) Plinian fall deposits, all of which is capped by a series of small-volume lithic falls and ash-rich deposits. Lithic types of Phase III consist of lava fragments (88-90%), the greatest amount of Sierra Madre lithics (5-12%) observed in the Jala Pumice stratigraphy, and the least amount of Granitic-clast lithics (<1%). Pumice types are composed of White (<75%), Gray (>20%), and Banded pumice (>5%). This suggests that the regions of erosion and entrainment of accidental lithic fragments in Phase III occurred at the vent and at medial depths, possibly from increased structural faulting and foundering (Suzuki-Kamata et al., 1993). Alternatively, significantly less erosion of lithic fragments occurred at magma chamber depth.

The broadly simultaneous emplacement of pyroclastic flow and non-graded pumice fall deposits imply that the activity of Phase III was dominated by continued gravitational collapse of dense portions of a weakening eruption column that was simultaneously depositing pumice and lithic fall deposits (Sparks and Wilson, 1976; Sigurdsson et al., 1985; Scott et al., 1992; Hildreth, 1983, 1991). Repeated gravitational collapse of the eruptive column was most likely induced by an intense and cyclic flux of accidental lithics, especially surficial lava fragments and Sierra Madre fragments from medial depth, into the lower convective region of the plume. Extensive loading of accidental lithics would greatly inhibit the convective potential of the eruptive plume, reducing its buoyancy and thus resulting in repeated syn-eruptive collapses (Sparks, 1986; Woods, 1988; Bursik and Woods, 1991). In addition, the stacked series of several (at least 7) pyroclastic flow deposits along the northeast, eastern, and southwest flanks suggest that they also accumulated gradually, although no definitive amount of time can be determined for the temporal relationship from the emplacement of one layer to another.

The presence of lithic-rich (65-90 wt.%) pyroclastic flow deposits on the northeast and southwest flanks suggests the existence of multiple, syn-eruptive vents

during Phase III. Isopach and isopleth maps from Gardner and Tait (2000) clearly indicate that the source vent for all of the Plinian fall layers existed on the northern flank, more than 100 m below the outer caldera rim, and more than 250 m below the extrapolated summit of Nelson (1980) prior to eruption-induced collapse of Ceboruco. In addition, the dispersal of every surge layer occurred almost exclusively to the north and northeast. Most of the pyroclastic flows were dispersed to the southwest. If the pyroclastic flows were the result of repeated gravitational collapse of dense regions within the eruption column on the northern flank, then the density currents would have had to flow initially uphill and over Ceboruco (~350 m), before heading down the southern flanks into the Ahuacatlan and Marquesado valleys. More likely, as caldera-collapse progressed, catastrophic structural foundering led to the eventual formation of an additional vent-region, possibly as a propagating ring fissure (Bacon, 1983), along the southwestern rim of the pre-collapsed summit. The lithic-rich nature of the flows, however, indicates that little magma utilized the ring faults. This resembles the lithic-rich flow deposits from the 1912 collapse of Mount Katmai, Alaska (Hildreth, 1991).

Marquesado and North-Flank pyroclastic flow deposits have equivalent lithic and pumice populations, and field observations suggest that interbedded pumice fall deposits within the North-Flank stratigraphy are identical to the thin pumice layers and lenses within the Marquesado deposits. Because of this, the North-Flank and Marquesado deposits are considered equivalent, although no definitive correlation of units can be made because of geographically isolated nature of the deposits.

At least 2 of the density currents that emplaced either the Marquesado or North-Flank flow deposits experienced convective removal of fine material and may have experienced a buoyant lift-off, generating co-ignimbrite plumes (Sparks and Walker, 1977; Woods, 1988). It is not possible to directly correlate the co-ignimbrite falls (*c1* and *c2*) with any flow unit because the lithic-types, pumice-types, and lithic content of the North-Flank and Marquesado deposits are virtually identical. Proximal stratigraphy with

increasing height is: F2, P5, F3, P6 and F4 (Figure 52). Distally, we find *c1* atop the P5 fall deposit and the *c2* layer immediately overlies the P6 fall layer, implying that the co-ignimbrite fall layers originated from the North-Flank pyroclastic flows F3 and F4 (Figure 52). Although Marquesado flow deposits at Locality 81 are interbedded with thin, nearly clast-supported, pumice-lapilli layers with corresponding pumice and lithic abundances to P5/6, there is unfortunately no exposure of any Marquesado unit that is clearly interbedded with either P5 or P6 fall deposits in the Ahuacatlan valley.

Finally, lithic fall deposits (L1, L2, and L3) cap the Phase III stratigraphy and represent the end of the eruption. On the basis of their very proximal distribution, moderate to poor sorting, and great abundance of lithics (up to 90 wt.%), these layers are interpreted as a compound fallout layer resulting from several explosions of varying energy and duration that produced alternating showers of blocks and ash. Similar deposits have been observed and described by Scott et al. (1992) and Rosi et al. (1993) from the caldera-forming eruptions of Mt. Pinatubo, Philippines, in 1991, and Vesuvius, Italy, in 1631.

The lithic content, especially the abundance of Sierra Madre lithic fragments, during Phase III is greater than at any other point in this eruption (Figure 10). Conversely, the abundances of White pumice and Granitic-clast lithics in Phase III are less than at any other point in the eruption. This suggests a significant shift in eruptive style from earlier phases to Phase III. It is interpreted that the late and culminating stages of caldera collapse occurred during Phase III. As collapse continued, erosion and entrainment of lithic material nearly stopped at magma chamber depths, and increased at surface vents (northeastern and southwestern), and medial depths, where Sierra Madre is believed to exist. In addition, the overwhelming abundance of Gray and Banded pumices in Phase III compared to White pumices is significant in terms of magma supply. It is not believed that the rhyodacite (White pumice) supply was exhausted in the chamber by this eruption, for the effusive eruption of the Dos Equis dome shortly following the Jala

Pumice eruption appears to be a hybrid mixture of the Jala rhyodacitic and more basic magma (Chertkoff and Gardner, 2000). Instead, with increased mass eruptive rate, more of the underlying dacitic (Gray pumice) magma was drawn-up preferentially to the rhyodacitic magma (Blake and Campbell, 1986; Sigurdsson et al., 1990a). As the dacitic magma ascended to the surface, actively eroded Sierra Madre lithic fragments and surficial lavas from caldera collapse became engulfed as evidenced by Gray and Banded pumices displaying cores and aggregates of lithic fragments.

Shifts in eruptive style, and lithic and pumice types during a caldera-forming eruption have been interpreted as indicating a change in the fragmentation level depth (Suzuki-Kamata et al., 1993). In the case of Ceboruco, the lithic content steadily increases from ~10 wt.% at the base of Phase I to >90 wt.% in the end of Phase III. The proportion of surficial lava fragments remains nearly constant (85-90%), suggesting relatively constant vent erosion compared to the lithic erosion and entrainment that occurred elsewhere. In addition, although the overall lithic content nearly increases by a factor of 10 through the eruption, there is very little change in lithic content for grain-sizes of 0-4.0 ϕ, suggesting that increases in lithic content occur mainly as a result of increases in coarse-grained surficial lava fragments at the vent induced by density segregation in the plume, not a mobile fragmentation level. The abundance of Sierra Madre and Granitic-clast lithics, however, vary substantially throughout the eruption. Phase I deposits are enriched in Granitic-clast lithics, whereas Phase II and III deposits show progressive depletion in Granitic-clasts and enrichment in Sierra Madre lithics. This implies that the fragmentation level may have decreased during the eruption because of the increased amount of accidental lithics from shallower depth (Figure 7).

7.4. Emplacement of Jala Pumice pyroclastic fall deposits

The Jala Pumice fall deposits appear to be produced by sedimentation from a dilute, low-concentration pyroclastic current, based on the observations that the fall

deposits are clast-supported and moderate to well sorted; fall deposits (P0-P6) thin exponentially with increasing distance from the eruptive vent (Gardner and Tait, 2000); all levels in the P1 and P2 fall layers display an overall decrease in Md_ϕ and lithic content with distance and an overall increase σ_ϕ, F2, and pumice content with distance; and, mass accumulation measurements of layers within fall deposits located beyond the estimated plume corner display an exponential decrease with distance.

7.5. Emplacement of the Jala Pumice pyroclastic flow deposits

A model for the transport and deposition of the Marquesado and North-Flank pyroclastic flow deposits must satisfy the following observations: (1) proximal deposits found high on the southwest flanks are thin (<20 cm), moderately well sorted, exhibit intricate planar bedding at the base and top, and are fines-rich (F2: 25-65 wt.%) and oxidized to a deep crimson color; (2) medial deposits have a basal lag breccia layer, and are poorly sorted, pinkish-gray in color, moderately fines-depleted (F2: <20 wt.%), and contain <8 wt.% pumice and >75 wt.% lithics; (3) granulometric analysis of the lag breccia matrix and non-lag breccia zones are identical, even though a clear planar boundary exists between them; (4) deposits found either distally or atop abrupt topographic obstacles in medial locations (Localities 18, 71, 77) are moderately-well sorted, enriched in rounded pumice clasts, and are intricately planar bedded; (5) mass accumulation variations for the Marquesado PFD's appear to support deposition via *en masse* freezing, except for the coarsest-grain sizes of lithics; (6) basal North-Flank PFD's (F3 and F4) are interbedded with Plinian fall layers P5 and P6 proximally; (7) distally, moderately-well sorted, ash-rich layers of equivalent component distribution to the Marquesado and North-Flank PFD's (*c1* and *c2*) are interbedded with Plinian fall layers P5 and P6; and, (8) Md_ϕ and σ_ϕ values for the Marquesado and North-Flank PFD's overlap the fields defined as "Pyroclastic Flow Deposit" and "Pyroclastic Surge Deposit"(Walker, 1971).

Phase III Jala Pumice PFD's are interpreted as resulting from gravitational collapse of an eruptive column (Figure 2) (Sparks and Wilson, 1976; Bursik and Woods, 1991), resulting from the excessive loading of cold lithic material into the lower convective zone of the eruptive plume, which accompanied the structural foundering of the caldera. In addition, the successive nature of the Marquesado and North-Flank PFD's up to 12 km from Ceboruco suggests that they were progressively emplaced as multiple flows.

Wilson (1980, 1984) and Wilson and Walker (1982) speculated that increased mobility of pyroclastic flow currents is largely a function of their gas content, and thus how fluidized they may become. Experimental results and field observations by Walker (1980, 1984) suggest that as air is entrained into a pyroclastic flow head, it is rapidly heated and expands. In addition, juvenile material, which is often the dominant component of PFD's (Sparks, 1976), is crushed as it is carried in the flow current, which results in intense expansion and uprising of large volumes of gas into the body of the flow. As the gas current passes through the moving flow, the current becomes fluidized, thus enabling the flow to move more energetically for greater distances in a laminar flow regime, rather than strictly *en masse* as suggested by Sparks (1976).

To produce pyroclastic flows capable of traveling 10's km's beyond the flanks of a volcano, the amount of gas and vapor retained after gravitational column collapse, or engulfment of surrounding air, must still be high enough to fluidize the debris to form a dispersed gas-particulate mixture (Wilson and Walker, 1982; Wilson, 1983, 1984). One of the most important characteristics of the Jala Pumice pyroclastic flows is their anomalously high lithic contents (65-90 wt.%), equally low pumice content, and modest F2 values. This is problematic when trying to explain how such low amounts of juvenile material could generate the appropriate quantity of hot gas, subsequently fluidizing the density current and allowing it to travel in excess of 12 km from vent along horizontal topography.

Interpretations from other lithic-rich flow deposits that bear resemblance to the Jala Pumice pyroclastic flow layers have been described as being fluidized despite the small abundance of juvenile material and influx of rising gas. Glicken (1991) reported that volcano-related landslides in Japan are unusually mobile, and are probably fluidized despite the low juvenile content (<10%) because of abundant clay material in the hydrothermally altered rock, which is a dominant constituent of the deposits. It was speculated that hydrothermally altered lithics contain large amounts of clays that would reduce the frictional resistance of colliding blocks, thus fluidizing the particles (Hsü, 1975, Glicken, 1991). In another example, a series of lithic-rich pyroclastic flow deposits (>80 wt.%) are described from Galeras volcano, Columbia, a volcano with similar elevation and morphology to Ceboruco. Calvache and Williams (1992) suggested that fluidization was achieved as a result of the abundant hydrothermally altered accidental lithics, instead of vertically expanding gas (Calvache and Williams, 1992). Galeras Hydrothermally altered lithics are absent, however, in the Jala Pumice PFD's. In addition, the Jala Pumice PFD's are found beyond 12 km from Ceboruco, which is more than 3 km further than the volcano-related landslide described by Glicken (1991), and more than double the extent of the Galeras pyroclastic flow deposits described by Calvache and Williams (1992).

Despite the minor juvenile component of the Jala Pumice pyroclastic flows, their flow behavior changed as a function of increased distance and underlying topography, based on the considerable diversity in granulometric and component character in the Marquesado and North-Flank PFD's around Ceboruco (Figure 50). The moderately well sorted, planar-bedded North-Flank deposits (Localities 18, 71, 77) that contain rounded pumice clasts atop the northern plateau cliff are suggestive of particle transport and deposition via saltation from a density current of low particle-concentration (Allen, 1984; Sigurdsson et al., 1987; Fisher, 1990; Cole, 1991; Druitt, 1992). Likewise, the sudden increases in σ_ϕ, F2, rounded pumice clasts, overall juvenile content (>35 wt.%), and

presence of internal planar bed forms at distal Marquesado deposits also suggests particle transport and deposition via saltation/ traction from a low particle-concentration density current. Thin, proximally located Marquesado deposits resemble pyroclastic veneer deposits (Wilson and Walker, 1982; Criswell, 1987; Fisher, 1990; Scott et al., 1991), because of their moderately well sorting, intricate layers of planar bedding, and genetic association with pyroclastic flow deposits. Wilson (1985) interpreted similar deposits from the Taupo Ignimbrite as representing a mass of particles that are jetted from the head of a fluidized flow in response to the violent expansion of ingested air. The proximal deposits at Ceboruco are, however, fines rich (F2: ~55 wt.%) relative to the valley-fill deposits (F2: <20 wt.%), as seen in other veneer layers, suggesting that the proximal Jala Pumice PFD's are not jetted from the flow head, but reflect veneer deposition.

In order to explain the observations listed above, a conceptual model for the transport and deposition of material in the Marquesado and North-Flank pyroclastic flow deposits has been developed, following that of Macias et al. (1998) (Figure 67). This study envisions a series of pyroclastic flows as being composed of two main density-stratified parts. The lower layer of the flow has a high particle concentration of coarse lithic blocks in a matrix of finer-grained particles, and an upper layer that has a lower particle concentration and transports material in turbulent suspension (Figure 67, A). This model conceives that the observed planar contacts between the lithic breccias and the associated flow units result from strong, and possibly sharp, density and velocity gradients between the two within the bottom layer of the flow (Burgisser et al., 2000).

Lag breccias are believed to develop in response to a hydraulic jump experienced at the incidence angle between the southwestern flank and the nearly horizontal valley floor (Figure 67, B) (Freundt and Schmincke, 1985; Hoblitt, 1986; Macias et al., 1998), whereby the basal layer of the flow essentially behaves as an avalanche of coarse lithic fragments and blocks as it approaches the flank base. Upon encountering the change in

slope, the speed of the flow is reduced drastically, resulting in the massive deposition of the coarse lithic bedload near the base of Ceboruco. The lateral extent of the breccias beyond the break in slope is interpreted to result from selective re-entrainment of deposited lithics by the upper region of the flow. As the lower portion of the flows propagates away from the volcano, transport and deposition occurs as sheets of material gradually decreasing in energy and particle-concentration only to be surpassed by later flow units (Figure 67, C).

Distally, finer grained lithic and pumice clasts were transported and deposited via rolling and saltation. Where topographic obstacles disallow the continued propagation of these flows, the basal layer experiences selective "blocking" (Valentine, 1987; Fisher, 1990; Bursik and Woods, 1996) and stop. The upper, low-concentration of the flow becomes decoupled, and continues downstream. Distal flow units will, therefore, be difficult to distinguish from one another, because the deposits will display a continuum of planar-bedded layers. Upon reaching a density less than the surrounding air because of loss of material, the flow may buoyantly lift off to form a co-ignimbrite cloud (Figure 67, D). This decoupling has been witnessed in recent eruptions of Mount St. Helens, Washington (Carey and Sigurdsson, 1985), Soufriere Hills, Montserrat, West Indies (Calder et, al., 1999), and Unzen volcano, Japan (Fujii and Nakata, 1999).

The conceptual model presented above allows for the extensive transport and deposition of lithic-rich pyroclastic material in agreement with the listed observations with little dependence upon expansion and subsequent fluidization. Instead, the effect of momentum would be critical. Applying the concept of the "energy line" from Sheridan (1979) and Hsü, (1975), which requires mass in motion to decelerate as a direct consequence of dissipation of kinetic energy by friction (e.g. topographic barriers), indicates that the Jala Pumice pyroclastic deposits are predicted to reach a run-out distance of 12 km if the original height of the flows were ~1900 m above the Ahuacatlan valley floor (~2700 m). This is in good agreement with the elevation of the modern-day

Ceboruco caldera rim, which is ~1650 m above the valley floor. Because there are only four locations where the Jala Pumice PFD's either succeeded or failed in overtopping a topographic obstacle, however, this suggestion should be regarded as an broad estimation.

7.6. Emplacement of Jala Pumice pyroclastic surge deposits

A model for the Jala Pumice surges has to account for a number of observed and numerically determined features: (1) S1, S2, and S3 are predominantly massive; (2) localities that display internal stratigraphy are limited to either the flanks of Volcán Ceboruco (S2 and S3) or atop the crest of the 150-240 m high Sierra Madre cliffs to the north (S1 and S2); (3) no charred organic material is found in any of the surge layers; (4) lateral granulometric variations occur from the proximal to the medial/ distal boundary in S1 and S2, and at the break in slope on the eastern flank; (5) dramatic variation in thickness, Md_ϕ, σ_ϕ, and F2 occur differentially from one surge to another in response to topographic change; (6) S1 and S3 contain abundant accretionary and armored lapilli, whereas S2 contains none; (7) dramatic fluctuations in grading, lithic-type, pumice-type, and overall lithic content in the fall deposits that lie immediately above and below S1 and S2 suggest significant modification in stability and conduit erosion of the eruptive column, whereas fall deposits above and below S3 have only minor component variability and little to no grading; and (8) the mass accumulated distribution of particles in S2 and S3 surges on the east flanks resemble modeled predictions for neither pure *en masse* nor turbulently suspended transport and deposition, whereas the mass accumulated distribution of particles from the S2 surge atop the plateau appear to support turbulent suspension and deposition. Transport and deposition from the S1 surge resemble neither pure *en masse* nor turbulent suspension.

Pyroclastic surges have been described as either an initially lean-phase fluidized flow (Wohletz and Sheridan, 1979) or as highly expanded gas-particle mixtures where

turbulence and saltation control particle transport and deposition (Fisher, 1983; Fisher and Valentine, 1986). Firstly, none of the Jala Pumice surge deposits display systematic facies variation with increased distance. A lean-phase fluidized model, therefore, cannot account for the behavior of the Jala Pumice surges. Secondly, the Jala Pumice surge deposits contain modest rounded pumice clasts, indicating that attrition of particles via saltation or inertial grain-flow at the base of the surge cloud may not have been abundant (Allen, 1984; Sigurdsson et al., 1987; Fisher, 1990; Cole, 1991; Druitt, 1992). The occurrence of internal bedding and high variability in deposit character with changing topography and increased distance suggest, however, that transport and deposition of material occurred at least partially in dilute and turbulent systems (Fisher, 1979; Allen, 1984; Valentine, 1987; Carey, 1991).

A conceptual model for the surges of this study envisions two main density stratified parts. The lower layer of the surge has a higher particle concentration that moves in laminar flow and an upper region that has a lower particle concentration that transport and deposits particles via dilute turbulence. Differences between the surge occur as a function of general flow conditions. That is, this study considers the surge deposits as representing transport and deposition from either Subcritical or Supercritical flow conditions (Bursik and Woods, 1996) (Figure 68). This model is presented in detail in Bursik and Woods (1996), and will be summarized here. As a dilute and expanded density current propagates forward, turbulent eddies may engulf and incorporate overlying air. The rate at which entrainment occurs depends on the ratio of the potential energy required to entrain the overlying buoyant fluid to the kinetic energy of the flow. This ratio is expressed by the Richardson number, R_i.

$$R_i = (\beta - \alpha)\, gh \quad \beta\mu^2, \qquad (6)$$

where β is the bulk density of the flow, α is the bulk density of the atmosphere, g is the gravitational acceleration, and h and μ are the flow thickness and velocity, respectively. Density currents that propagate with R_i values > 1 are Subcritical, and those with R_i values < 1 are Supercritical. Subcritical flows are relatively thick (1000-3000 m) and moving (10's m/ s), with relatively constant mass fluxes (Figure 68). Supercritical flows propagate as relatively thin (<1000 m), rapidly moving currents (100's m/ s) that entrain large amounts of air, which leads to shorter run-out distances. An empirical relationship between the entrainment coefficient, ε, and the Richardson number is described as, $\varepsilon \sim 0.003\ R_i^{-1}$ for Supercritical currents. For Subcritical currents, entrainment is negligible (Bursik and Woods, 1996). Therefore, sedimentation of material controls the evolution of Subcritical currents, which allows the surge cloud to travel a greater distance than if it were controlled by massive entrainment of air and subsequent inflation. On the other hand, the rampantly elutriating Supercritical flows deposit a smaller fraction of material from the surge cloud itself than in the Subcritical flow regime, the remainder being elutriated into an upper dilute portion of the current (Bursik and Woods, 1996).

Results from experimental modeling by Woods and Bursik (1998) on dilute and turbulent particle-laden density currents interacting with topographic obstacles indicate that as Subcritical flows surmount obstacles, numerous flow regimes may develop. Specifically, if the obstacle is small enough for the Subcritical flow to surmount *en masse*, the flow passes over it by increasing its velocity (μ) and lowering its bulk density (β) to conserve the total energy of the flow. Downstream from the topographic high, the entire flow may become Supercritical, as a result of the hydraulic jump in flow velocity experienced at the ridge front (Valentine, 1987; Woods and Bursik, 1998). Conversely, if the obstacle is too high for the Subcritical current to surmount *en masse*, then the upper fraction of the flow is reflected upstream (Woods and Bursik, 1998). Decoupling of the density current results in a hydraulic jump in the basal fraction of the flow, which may

then surpass the ridge as a Supercritical flow conditions (Valentine, 1987; Woods and Bursik, 1998).

The distribution of S1 deposits are widespread atop the northern plateau, extending for more than 20 km from vent, which is more than double the distribution of S2 and four times that of S3. Atop the plateau, however, S1 is only found at lower elevations (<180 m), at localities higher than that, such as those atop the 240 m ridge immediately north of the village of Coapan, only show S1 as a very thin ash layer (<5 mm). A velocity estimate of approximately 40 m/s can be made based on the occurrence of S1 deposits on the northern plateau topography, which is relatively slow moving compared to other surges described in the literature (Sigurdsson et al., 1985; Hoblitt, 1986; Sigurdsson et al., 1987; Macias et al., 1998; Bursik et al., 1998). S1 deposits reflect neither pure *en masse* nor turbulent suspension, based on mass accumulation with distance calculations on the northern plateau. S1 deposits are commonly massive with faint laminations in the upper 20% of the deposit. Granulometric analysis indicates that S1 at the front of the Sierra Madre escarpment are fines enriched (<60 wt.%) and moderately to poorly sorted (σ_ϕ: 2.05-2.80). Along the B-B' transect, the thickness of S1 deposit is predominantly thin (~5 cm), except at the front of the Sierra Madre cliff and atop the crest of the escarpment, where the thickness of S1 suddenly increases from 6-15 cm, and then abruptly falls to <2.5 cm. A positive correlation exists between Md_ϕ (and F2) and thickness, where thicker deposits have lower Md_ϕ values (fines rich) and thinner deposits have larger Md_ϕ values (fines depleted).

The S1 surge deposit reflects particle transport and deposition in Subcritical flow conditions (Bursik and Woods, 1996). That is, negligible entrainment of surrounding air, which results in a higher-particle concentration as the surge cloud slowly propagates away from the eruptive vent (Figure 69). Following what appears to have been a phreatomagmatic eruption, the low velocity of S1 impedes the completion of developing internal density stratification, and promotes massive deposition (Figure 69, A). Upon

encountering the northern plateau ridge, the basal, higher particle concentration region of S1 is partially blocked (Valentine, 1987; Fisher, 1990), resulting in massive deposition of moderately to poorly sorted bedload layers, possibly *en masse*. Rapid loss of material in the bedload of the surge allows for increased levels of particle supply from the upper dilute region of the surge as S1 steadily climbs the plateau front (Figure 69, B). This promotes fines deposition via dilute suspension in deposits adjacent to the Sierra Madre escarpment in thin laminations at the top of S1, and fines depletion in more distal deposits (Figure 69, C and D).

The S2 surge layer is consistently thicker than S1 and is only found within 10 km from vent. S2 deposits are found atop the 150 m plateau and high atop the 240 m ridge immediately north of the village of Coapan. A minimum velocity estimate for S2 is approximately 80 m/s, based on its ability to surmount topographic highs. There are no topographic obstacles that S2 did not flow over, however, and so this estimate must be considered to be conservative. Mass accumulation with distance calculations on the eastern flank (A-A') resemble neither pure *en masse* nor turbulent transport and deposition patterns, although S2 flank deposits do appear to reflect a flow modification at the break in slope and often have cross-bedding and planar-bedding, suggestive of saltation/ traction dilute and turbulent grain flow (Allen, 1984; Sigurdsson et al., 1987; Fisher, 1990; Cole, 1991; Druitt, 1992). Mass accumulation with distance calculations on the northern plateau (B-B') resemble that which is predicted from transport and deposition via turbulent suspension, especially if the first site in profile, Locality 12, is replaced by Locality 18, which is located on top of the plateau. With increased distance, S2 deposits decrease in Md_{ϕ}, improve in sorting (σ_{ϕ}), and increase in F2. Proximally, S2 deposits display intricate cross bedding and planar bedding immediately atop the plateau front cliff, and is massive beyond the escarpment front. In addition, S2 deposits in topographic lows are thicker and more poorly sorted, whereas S2 deposits in topographic highs are thinner and better sorted.

The S2 surge deposit reflects particle transport and deposition in Supercritical flow conditions (Figure 70) (Bursik and Woods, 1996). Following what appears to be partial column-collapse, the rapidly propagating surge is thin as it travels down the north and northeastern flanks, which facilitates early development of internal density stratification and deposition of material is dominated by saltation and granular flow (Figure 70, A). At the break in slope of the northern and northeastern flanks, the velocity of the flow abruptly decreases, resulting in massive unloading of material, and the formation of a weak elutriated cloud of fine particles (Figure 70, B). Upon encountering the Sierra Madre escarpment, the basal region of the S2 density current is blocked (Valentine, 1987; Fisher, 1990), resulting in a hydraulic jump in flow velocity, marked by the local change in surge deposit bed forms at the Sierra Madre cliff face. This also results in particle transport and deposition to be dominated largely by the upper dilute and turbulent transport system (Figure 70, C). Atop the plateau, however, the S2 surge rapidly reorganizes itself (Burgisser et al. 2000) into a density-stratified density current, as it continues to actively entrain air and deposition of material is topographically controlled. That is, topographic lows promote thicker, more poorly sorted deposits, and topographic highs result in thinner, better-sorted deposits. Continued entrainment of large amounts of air results in the volume of S2 to increase, thus a decrease in density, which eventually results in the abbreviated run-out of S2 with buoyant lift-off occurring at ~10 km distance (Figure 70, D).

Proximally, the S3 deposit ranges in thickness from 15-194 cm, thicker than either S1 or S2. More specifically, less than 2 km from the plateau, S3 is 3 times as thick as S2 and nearly 4 times as thick as S1. The S3 deposit is a distinct pink color, unlike either S1 or S2, and along the eastern flank transect (A-A'), S3 displays equivalent planar bedding, rounded pumices, subtle modifications in response to topography, and mass accumulation trends to the S2 layer. Beyond 3 km from the volcano, S3 exists only as a band of pink ash that coats the middle of the P3/ 4 fall layer. Despite the lack of evidence for either

phreatomagmatic accompaniment, significant change in lithic content, lithic types, or grading. S3 is enriched in armored and accretionary lapilli.

The S3 surge deposit reflects Supercritical flow conditions, probably at a higher velocity than S2 (Figure 71). Following what appears to have been a phreatomagmatic event, the density current is thin and rapidly travels down the northeastern flank, which facilitates early development of internal density stratification where saltation and attrition of particles seems to have been the principal means of particle transport and deposition in the basal surge levels (Figure 71, A). Between the break in slope of the northeastern flanks and the Sierra Madre escarpment, the S3 surge continued to entrain large amounts of surrounding air, resulting the coincident deposition of material and the rapid inflation of the density current, which subsequently formed an elutriated cloud of fine particles via buoyant lift-off (Figure 71, B). Fine-grained ash from the elutriated S3 surge cloud continued to drift in the direction of original flow direction, coating pumice lapilli clasts as they were deposited from the late P3 and early P4 fall layers locally atop the northern plateau (Figure 71, C).

The Subcritical vs. Supercritical flow conditions for the Jala Pumice surges are interpreted as function of particle concentration, rather than surge origin (phreatomagmatic versus purely magmatic). Surge origin is often proposed as having a significant control on flow dynamics because surges that are initiated by magma-water interactions are thought to have lower energy and a lower temperature (Moore, 1967; Moore and Peck, 1962; Fisher, 1971; Self and Sparks, 1978; Wohletz and Sheridan, 1979; Sigurdsson et al., 1987). Because both S1 and S3 have abundant armored lapilli, which indicate meteoric water interaction (Self and Sparks 1978; Wholetz and Sheridan, 1979), the S1 and S3 surges are likely to be at least somewhat phreatomagmatic in origin. Yet, S1 and S3 are very different. S3 contains rounded pumice clasts and abundant planar bedding, and is highly variable in thickness, whereas S1 contains no rounded pumices, is invariably massive, and displays little variation in thickness with topography. Also, S3 is

only found within 5 km from Ceboruco compared to S1, which is found beyond 20 km. It appears that the transport and depositional characteristics of S1 and S3 cannot solely result from their phreatomagmatic origin. Rather we believe that S1 had a greater particle-concentration than S3, and hence S1 travels as a Subcritical flow, whereas S3 flowed as a Supercritical flow.

Unlike S1 and S3, armored lapilli are absent in the S2 deposit. In addition, S2 and S3 occur between Plinian fall deposits that display no signs of phreatomagmatic accompaniment at or near the contacts of the surge layers, which implies that S2 resulted from partial collapse of dense portions of the eruption column (Self and Sparks, 1978; Sparks and Wilson, 1976; Sigurdsson et al., 1985, Scott et al., 1992). Both S2 and S3 have equivalent bed forms in proximal localities, however, even though S3 contains abundant armored lapilli, and is distinctly pinkish in color, compared to the olive-gray S2. It is therefore proposed that the transport and depositional characteristics of S2 and S3 are the direct result of a low-particle concentration density current engaged in a Supercritical flow regime, rather than their eruptive origin.

The Jala Pumice pyroclastic flow and surge deposits represent emplacement of material by density currents that cannot clearly be assigned as either "flow" or "surge" end member. Rather, a continuum exists between the Jala surge and the flow deposits as a function of particle concentration. This is significant to understanding and modeling of density currents in terms of flow conditions that is a direct function of particle concentration, which ultimately controls the transport and depositional mechanics of pyroclastic material.

7.7. Caldera formation

Gardner and Tait (2000) suggest that caldera collapse began at the transition from P1 to P2 (Phase I to Phase II), and possibly hadn't finalized until the very end of the Jala Pumice eruption sequence, based on the sudden influx of lithics and pumice diversity that

is observed in Phase II deposits compared to Phase I, and the highly variable nature of mass eruption rate throughout Phase II compared to the relatively steady conditions of Phase I. The speculation that caldera-formation could occur near the end of an eruption is contrary to traditional models for caldera formation (Druitt and Sparks, 1984) and to interpretations from different caldera-forming eruptions (Bond and Sparks, 1976; Smith, 1979; Bacon, 1983; Druitt and Francaviglia, 1992; Lipman, 1997). These models do not accurately explain the observations from the Jala Pumice (Gardner and Tait, 2000). In a model that assumes that magma is buoyant in the shallow crust and that no replenishment occurs during eruptive withdrawal (Tait et al., submitted), an eruption occurs when the magma chamber becomes "over-pressurized". This fractures the overlying rock, which propagates to the surface (Tait et al., 1989). As long as tension is maintained, the conduit remains open and the eruption is able to continue. Because of the relatively incompressible nature of magma (Blake, 1984; Tait et al., 1989), however, the "over-pressure" in the chamber diminishes quickly, and the tension required for an open conduit decreases, closing the conduit and stopping the eruption (Tait et al., 1989). Collapse will occur if the threshold of shear failure of the country rocks is attained before the conduit can close, stopping the eruption (Tait et al., submitted). Phase I deposits from the Jala Pumice reflect erosion of lithics at the vent, and the chamber walls as the initial "over-pressurized" phase progressed with an open conduit extending from the magma chamber to the surface.

The abrupt and simultaneous influx of Sierra Madre lithics and disappearance of Granitic-clast lithics that occurs late in Phase II and throughout Phase III reflect erosion of lithics at the vent and medial depths, but not the chamber walls (Figure 7). This may yield insight into important mechanisms that control "small-volume" (<10 km^3) caldera generation. Nelson (1980) and Moore et al. (1994) suggest that the basement rock of many volcanoes in the western portion of the Trans-Mexican Volcanic Belt is composed of the Tertiary aged Sierra Madre ignimbrite formation. In addition, the concealed deeper

layers around Ceboruco have been interpreted as being granitic in composition, because granitic-clast xenoliths are commonly found in the erupted products from several of the cinder cones located around Volcán Ceboruco (Thorpe and Francis, 1975; Nelson, 1980).

This differs to the late stage abundance of similar wall rock-lithics from the caldera-forming eruption of Mount Mazama (Crater Lake), as interpreted by Bacon (1983, 1992) and Suzuki-Kamata et al. (1993). From this eruption, the greatest abundance of "granitoids" occurs at the end of the eruption, rather than at the beginning like at Ceboruco. Bacon (1983) interprets the behavior of caldera-collapse at Mount Mazama following the model of Druitt and Sparks (1984). It therefore seems plausible that whereas, inward-dipping faults would essentially disrupt the uppermost Ceboruco composite structure and the Sierra Madre basement rock while sealing the magma chamber closed, outward-dipping faulting would disrupt the entire subsurface, especially the magma chamber. This would account for the simultaneously observed abrupt increase in surface and medial depth erosion (Surficial + Sierra Madre lithics) and the discontinued wall rock erosion (Granitic-clast lithics) seen in the Phase II and III deposits at Ceboruco. The caldera-forming eruption at Volcán Ceboruco appears, therefore, to suggest that critical mechanisms for large volume (100-1000 km^3) caldera-collapse, as outlined by Druitt and Sparks (1984), are not fundamental to smaller volume (<10 km^3) caldera formation.

8. Conclusions

The Jala Pumice eruptive stratigraphy is divided into three phases based on changes in eruptive style and eruptive products. The first phase (Phase I) of the eruption saw a sustained Plinian column (P1), during which 2.5-3 km^3 of magma erupted. This phase apparently ended abruptly (top of P1) and was followed by Phase II, which began with a thin, lithic-rich and accretionary-lapilli-bearing fall layer and continued as alternating Plinian columns and pyroclastic surge emplacement. Approximately 0.5 km^3

of magma erupted during Phase II. In addition, mass eruption rate, lithic type and content, and pumice types were varied highly, compared to the first phase. Phase III of the eruption consisted dominantly of repeated gravitational column collapse events, which resulted in the emplacement of a series of lithic-rich (65-85 wt.%) pyroclastic flow deposits (Marquesado and North-Flank), with at least two Plinian fall deposits (P5, P6). The second and third phases of the eruption also marked changes in the composition of erupted magma. During Phase I, rhyodacite (White pumice) was erupted, with very little dacite (Gray pumice) and mixed pumices (Banded pumice). Phase II marked large increases in both Gray and Banded pumices at the expense of White pumice, and by Phase III, Gray pumice accounted for more than 50 wt.% of the juvenile material erupted.

The overall lithic content increased from ~10 wt.% in Phase I to >90 wt.% in Phase III. Although the proportion of surficial lava fragments remained relatively constant throughout the eruption (85-90 wt.%), two other types of accidental lithics varied systematically through the eruption. In Phase I, granitic-clast wall rock lithics dominated, whereas in Phase III, Sierra Madre ignimbrite lithics were prominent. Phase II has intermediate proportions of each.

Caldera-collapse occurred at the finale of the eruption, unlike many other described caldera-forming eruptions (Bond and Sparks, 1976; Bacon, 1983; Hildreth, 1983; Druitt and Sparks, 1984), and is marked by a lithic rich facies (65-90 wt.% lithics) of pyroclastic flow and lithic fall deposits, which are identical in terms of lithic and pumice components, and abundances. Marquesado pyroclastic deposits are found southwest of Ceboruco and the North-Flank pyroclastic flow deposits are isolated to the northeast. The distinct separation of the two Phase III pyroclastic flow deposit sequences are the likely result of new vents opening on the southwest side of Ceboruco, possibly via ring-fault propagation (Bacon, 1983). The small abundance of wall rock and surficial lava fragments in Phase I compared to the large abundance of Sierra Madre basement rock and surficial lava fragments in Phases II and III suggest that collapse may have actually

jammed the eruption conduit, which sealed the magma chamber and suspended the eruption.

Field observations and modeling of three levels in the pyroclastic fall deposits (P1 base, P1 top, and P2 lithic-rich base) indicate that beyond the plume corner, they were produced by deposition of particles from a dilute and turbulent eruptive plume (Sparks, 1986; Carey et al., 1988; Sparks et al., 1991).

Deposits of the thick, massive, poorly sorted Marquesado and North-Flank pyroclastic flow deposits resulted from a series of poorly expanded density currents of gas and particles in a density stratified flow, with a basal, lithic-rich zone that transported large lithic blocks in a matrix-supported current, and an upper, more dilute layer that transported particles in suspension (Macias et al., 1998). The pyroclastic flows experienced a hydraulic jump at the break in slope between the 15-35° flanks and the nearly horizontal valley floors, which drastically reduced velocity, causing the dumping of the coarse-grained bedload, forming extensive lag breccia deposits. The transport and deposition of material beyond that break occurs via saltation in a traction grain-carpet system (Fisher, 1979, 1990) upon encountering topographic obstacles or sufficient run-out distance because of a decrease in bulk particle concentration.

Thin, cross-bedded-to-massive, moderately sorted Jala Pumice pyroclastic surge layers were produced from dilute density currents, which varied in their flow conditions and particle concentration (Fisher, 1979; Valentine, 1987; Fisher, 1990). The high susceptibility of topographically induced modification on pyroclastic currents suggests that density stratification and particle concentration play a essential role in the behavior of pyroclastic density currents, and that modeling the transport and deposition of material in pyroclastic flows and surges as occurring via pure dilute and turbulent suspension, is appropriate only where the basal region is sufficiently "blocked". The origin of the Jala Pumice surges (phreatomagmatic versus magmatic) appears to have little control on their flow dynamics. Results from this study, therefore, indicate that a continuum exists

between pyroclastic "flow" and "surge" end members, and may also exist between pyroclastic "surge" and "fall" deposits. In fact, the majority of the density currents generated during the ~1000 A.D. caldera-forming eruption of Volcán Ceboruco were transitional in nature.

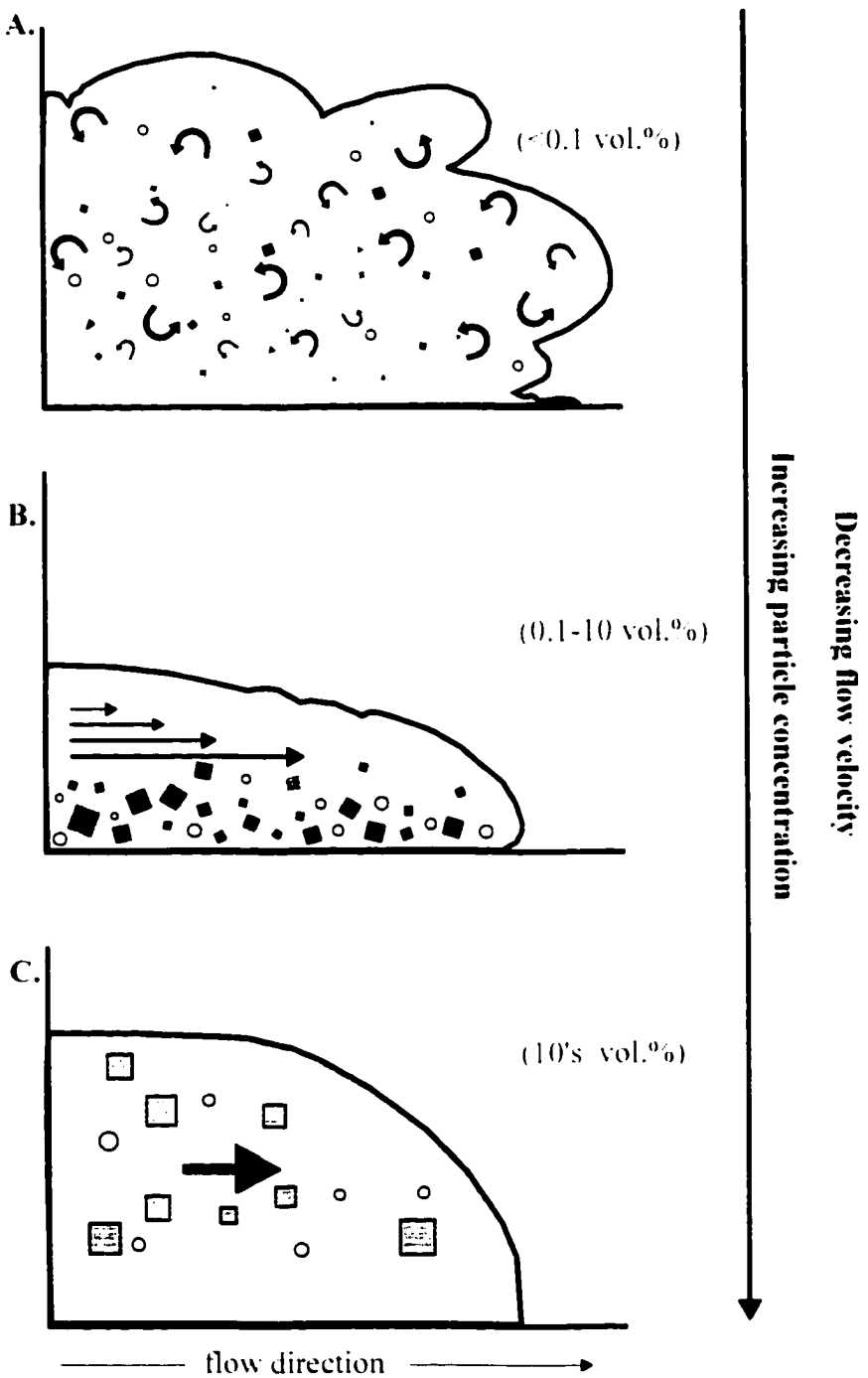

Figure 1. Schematic characteristics of turbulent (A. Sedimentation via dilute and turbulent suspension), laminar (B. Sedimentation via saltation/ traction and inertial grain-flow), and *en masse* (C. Sedimentation via freezing in place) flow regimes as a function of particle concentration and flow velocity.

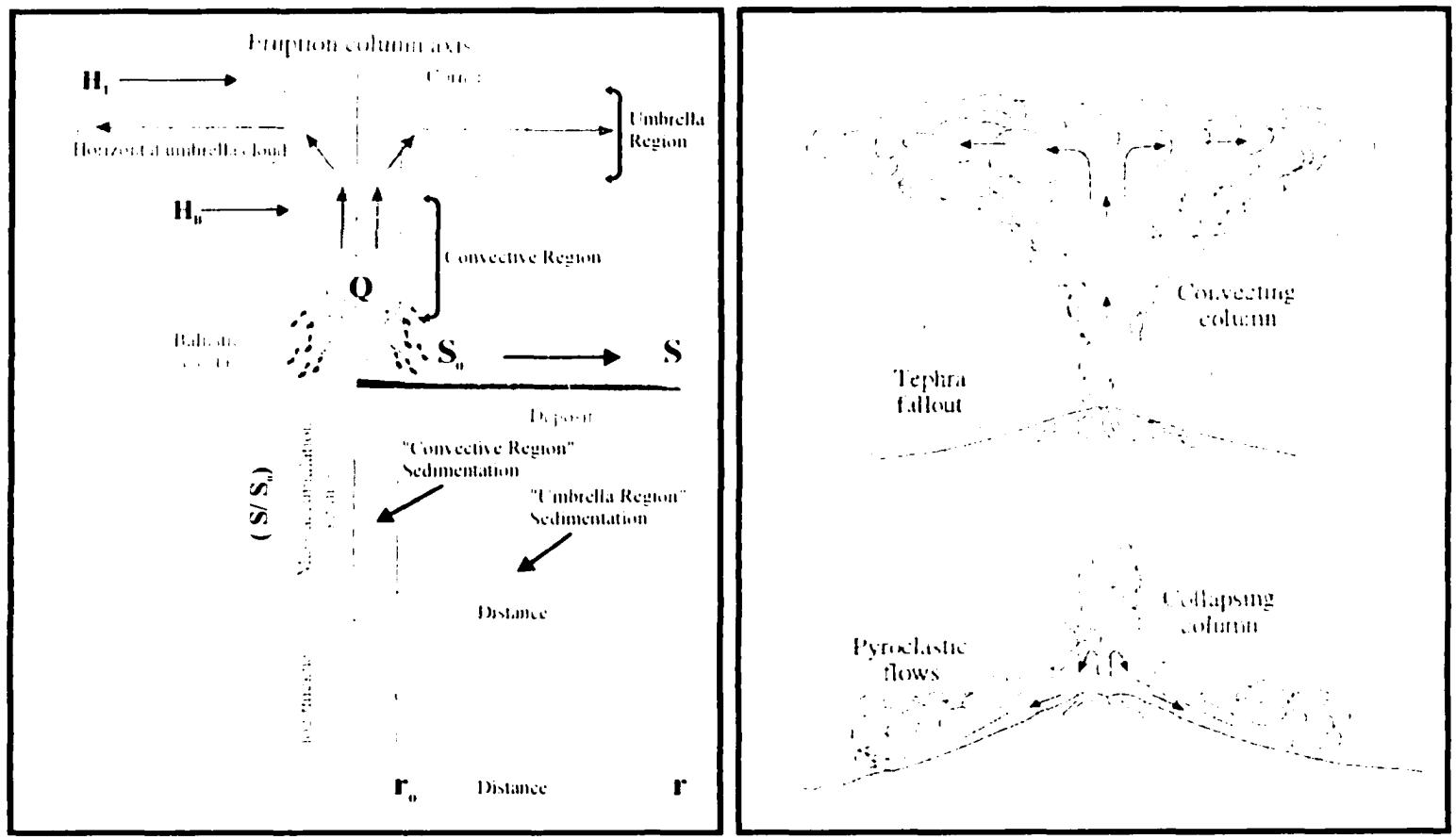

Figure 2. Schematic features of an eruptive plume, modified from Sparks et al. (1997). Right: the inner and outer regions of the plume, locations of the convective region and the umbrella region, position of the plume corner, and height of plume neutral buoyancy (H_n) with the surrounding atmosphere and the height of the plume top (H_1). The graphs show schematically the variation of mass of one grain size in mass per unit area (S/S_o) and per unit distance. Left: schematic differences of a "convecting" column and a "collapsing" eruptive column leading to the generation of pyroclastic flow deposits.

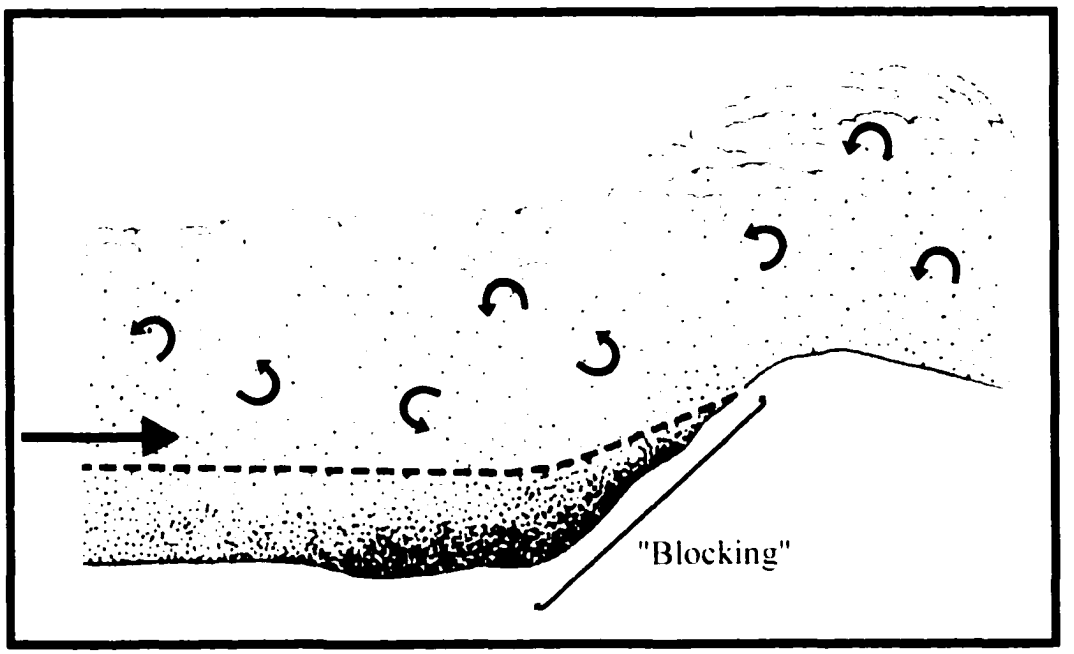

Figure 3. "Blocking" in a density stratified pyroclastic surge induced by a topographic obstacle, modified from Valentine, 1987. The dashed line indicates the position of the dividing streamline, which occurs at a height that is a function of the upstream kinetic energy, density gradient of the current, and the potential energy gained by overtopping the hill (Valentine, 1987). Below the dividing streamline, material is unable to flow over the obstacle and must either stop or flow around it. In a pyroclastic surge, this may result in the emplacement of thick, massive deposits adjacent to obstacles or topographic lows.

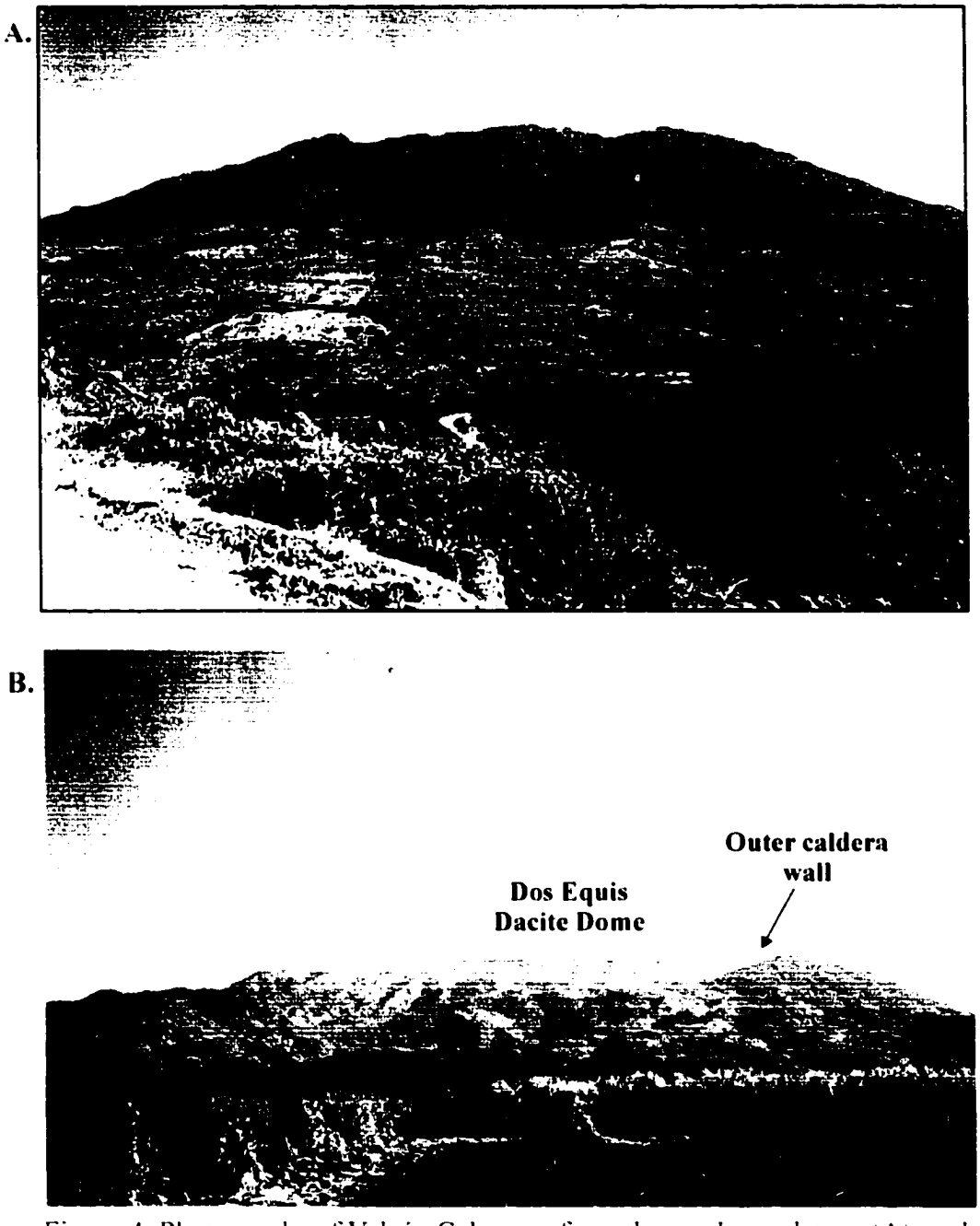

Figure 4. Photographs of Volcán Ceboruco from the northern plateau (A), and from the village Marquesado (B), located to the southwest.

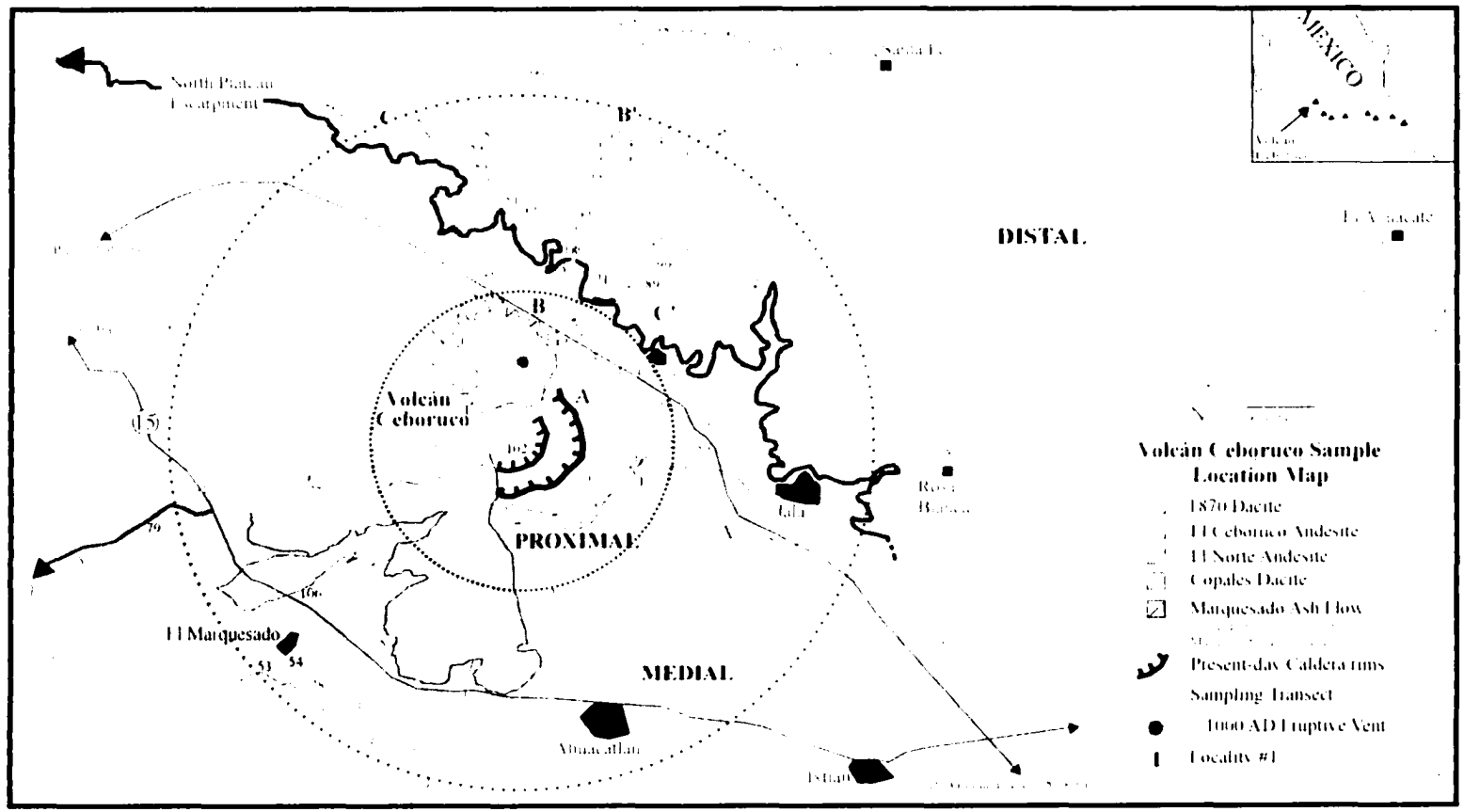

Figure 5. Location and geologic map of Volcán Ceboruco, modified from Nelson (1980).Present-day distributions of post-caldera andesites and dacites, outlines of inner and outer caldera walls, and ~1000 A.D. eruptive vent from Gardner and Tait (2000) are indicated. Transects A-A', B-B', and C-C" are shown, and the crest of the Sierra Madre escarpment to the north is illustrated in bold. Contour lines are provided atop the northern plateau to illustrate the complex topography of that region. Numbers refer to sample localities; and solid-shaded regions indicate the extent of the Marquesado pyroclastic flow deposits, modified from Nelson (1980), with the darker solid-shaded region signifying the extent of the basal lithic lag-breccia. Proximal, Medial, and Distal zones are indicated, and a general regional map is shown in the upper right.

Figure 6. Photograph of the Sierra Madre escarpment to the north of Ceboruco with contour intervals superimposed to clarify topography. In addition, the bold arrow shows the predominant flow direction of the three pyroclastic surge deposits.

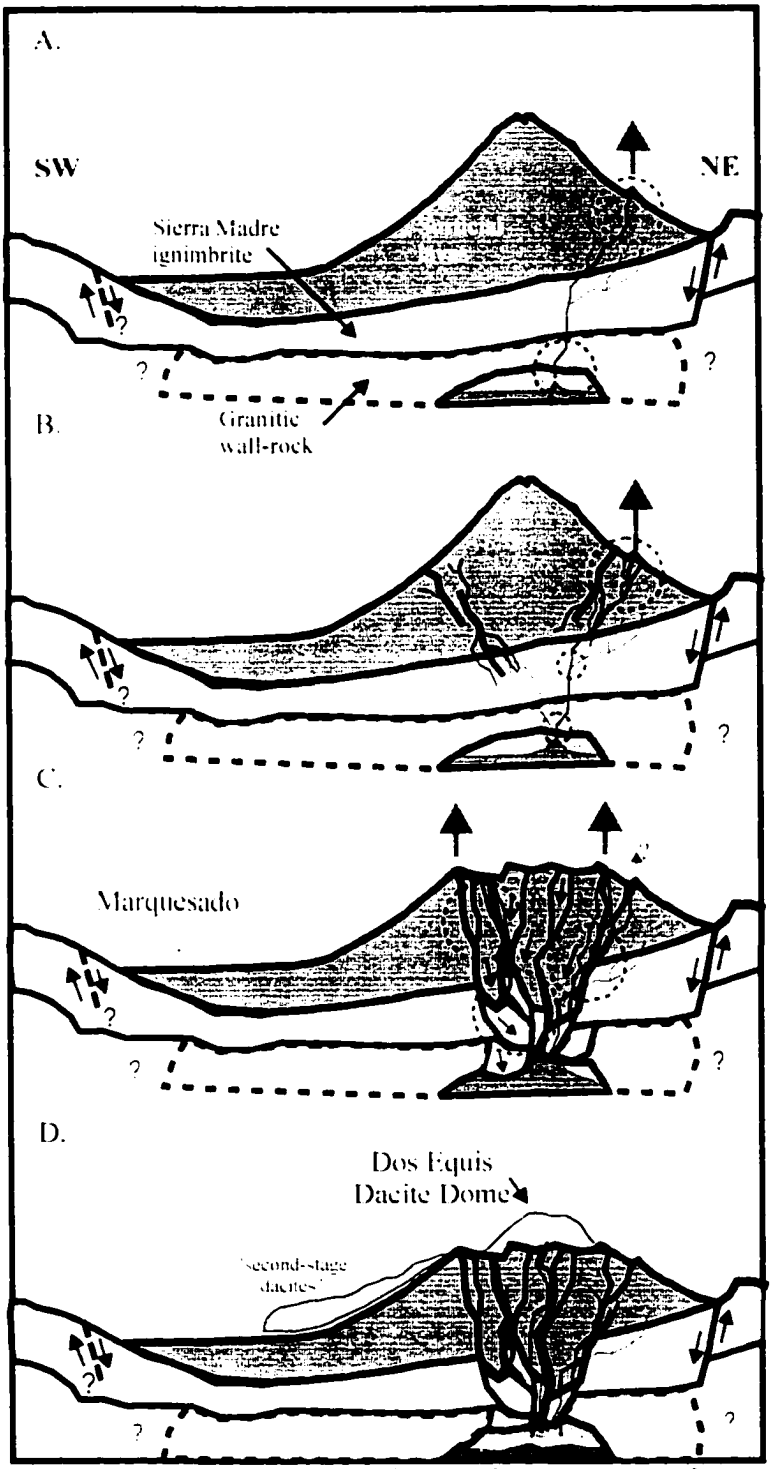

Figure 7. Schematic diagram illustrating sequence of ~1000 A.D. Jala Pumice eruption and subsurface stratigraphy inferred by Thorpe and Francis (1975), Nelson (1980), and Luhr et al. (1989).

Figure 7 continued. Sierra Madre ignimbrite basement rock and granitic country rock are noted, along with proposed location of normal faulting to the north and south of Ceboruco, suggested by Thorpe and Francis (1975). Arrows indicate primary location of eruption vent, whereas dashed circles indicate the predominant regions of accidental lithic incorporation during the different phases of the Jala Pumice eruption based on subpopulation abundances of lithic types observed in the Jala Pumice sequence. A. Initiation of Phase I of the Jala Pumice eruption from a vent on the north flank (Gardner and Tait, 2000). Erosion of lithic material occurred at the vent and from the granitic country rock surrounding the Ceboruco magma chamber. B. Following a brief stall in the eruption after Phase I, Phase II began with increased levels of eroded surficial lava fragments, and subequal levels of Sierra Madre and Granitic clasts marking the onset of preliminary caldera-collapse. Isopach information suggests that the eruptive vent remained on the north flank of Ceboruco at this time (Gardner and Tait, 2000). C. The emplacement of the lithic-rich Marquesado and North-Flank pyroclastic flow deposits represent the onset of Phase III, as caldera-collapse is finalized. Lithic types of the Phase III deposits indicate that erosion of accidental lithics occurred in the Sierra Madre basement rock and at the surface, but not from deeper granitic country rock. D.. Emplacement of the Dos Equis dome and subsequent dacite lava flows on Ceboruco's west and southwest flanks overflow and bury the majority of the SW flank Marquesado flow deposits. See text for additional discussion.

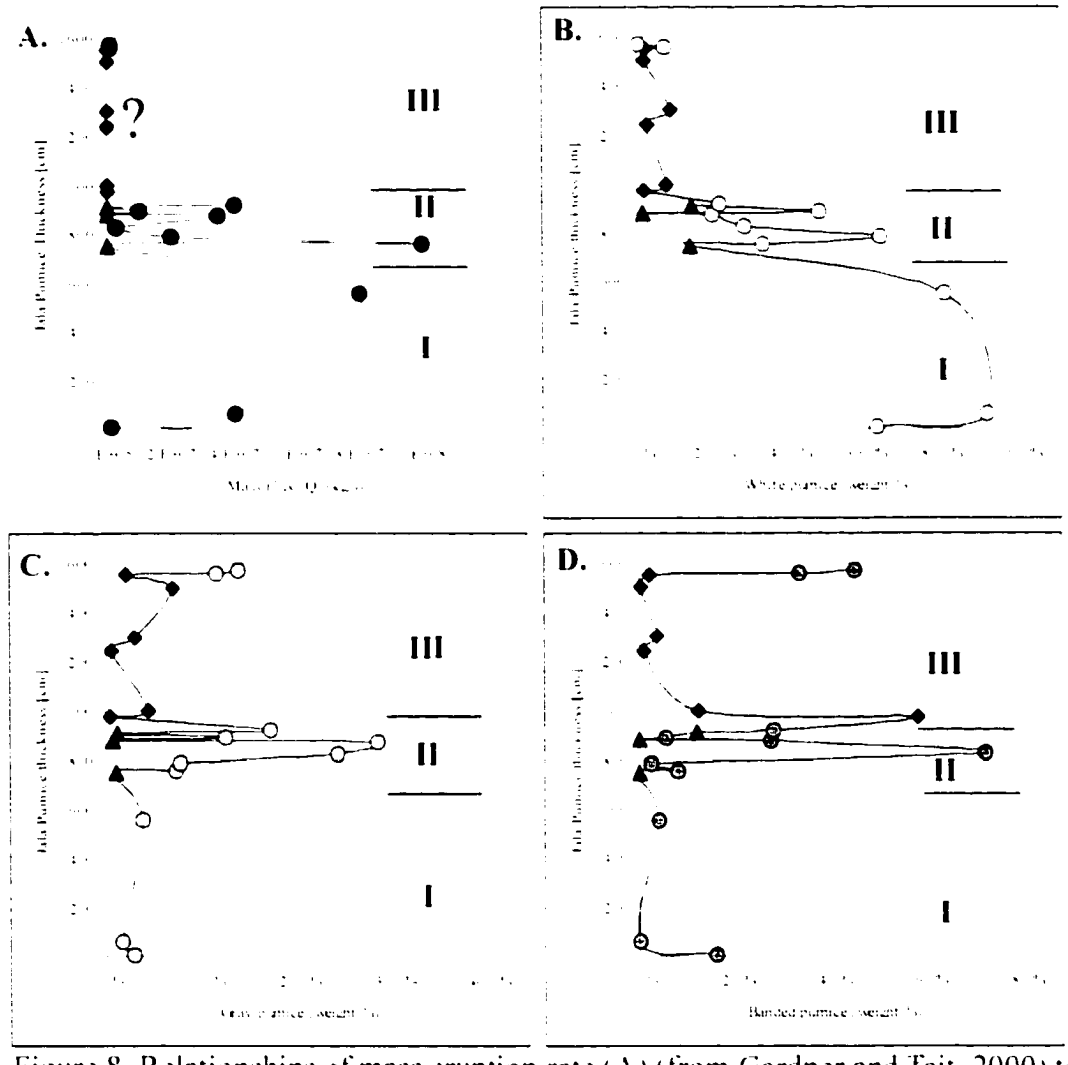

Figure 8. Relationships of mass eruption rate (A) (from Gardner and Tait, 2000) to fluctuations in White (B), Gray (C), and Banded pumice (D) abundance throughout the Jala Pumice stratigraphy at Localities 12 and 18.Solid triangles and diamonds indicate pyroclastic surge and flow deposits, respectively. Phase I, II, and III boundaries are also shown. Phase I and II stratigraphy from Locality 18. Phase III stratigraphy from Locality 12.

Figure 9. Relationships of mass eruption rate (A) (from Gardner and Tait, 2000) to fluctuations in Md (B) and Sorting(C), through the Jala Pumice stratigraphy at Localities 12 and 18.Solid triangles and diamonds indicate pyroclastic surge and flow deposits, respectively. Phase I, II, and III boundaries are also shown. Phase I and II stratigraphy from Locality 18, Phase III stratigraphy from Locality 12.

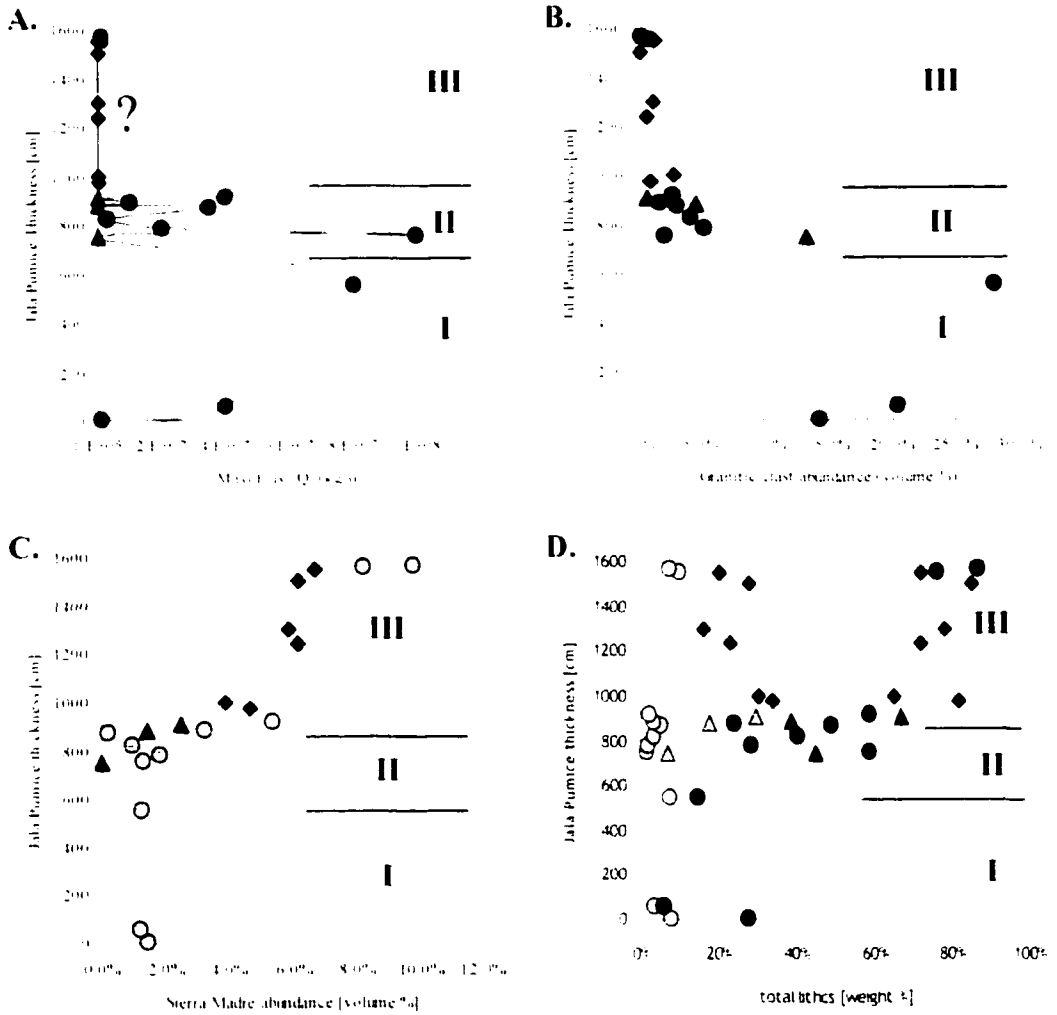

Figure 10. Relationships of mass eruption rate (A) (from Gardner and Tait, 2000) to fluctuations in Granitic-clast (B) and Sierra Madre (C) abundance, and the total lithic content (D) through the Jala Pumice eruptive stratigraphy at Localities 12 and 18. Solid triangles and diamonds indicate pyroclastic surge and flow deposits, respectively. Note that whereas the overall lithic content (black) fluctuates throughout Phase I and II of the eruption, the lithic content of lithics 0 to 4.0 (light gray) remains nearly constant, indicating that overall lithic content in Phase I and II is controlled by the amount of coarse-grained lithics (D). In addition, the inverse relationship of Granitic-clast lithic abundance compared to Sierra Madre lithics in Phase I and Phase III deposits is clear. Phase I and II stratigraphy from Locality 18, Phase III stratigraphy from Locality 12.

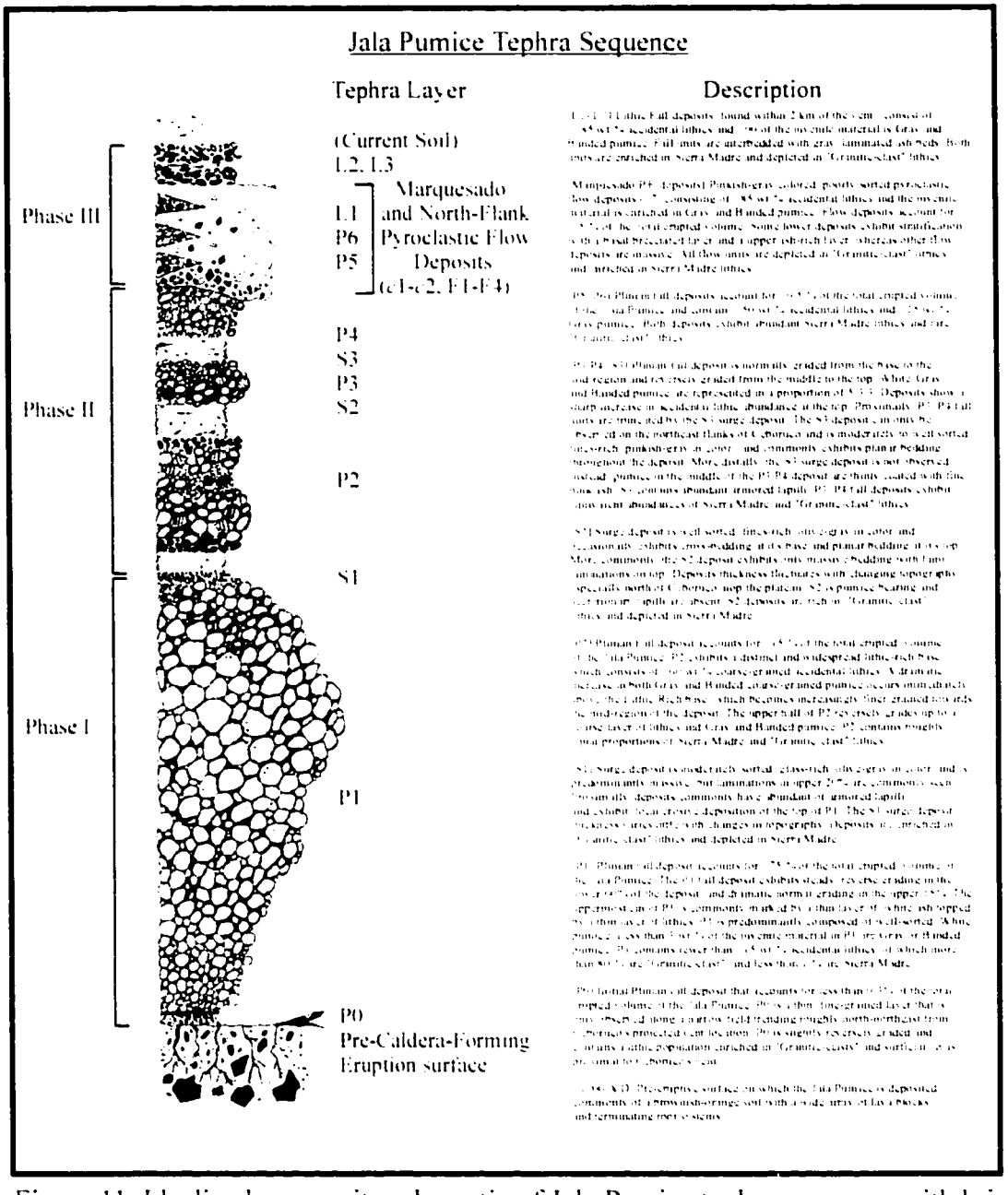

Figure 11. Idealized composite schematic of Jala Pumice tephra sequence with brief descriptions of each layer. Stratigraphy is based on field relations, lithic content, pumice populations, lithic types, and previous work performed by Gardner and Tait, 2000. Relative number of lithics (black), and White (white), Gray (gray), and Banded (striped) pumices reflect proportions observed in field deposits. Column is scaled to erupted volume, not true thickness or grain-size.

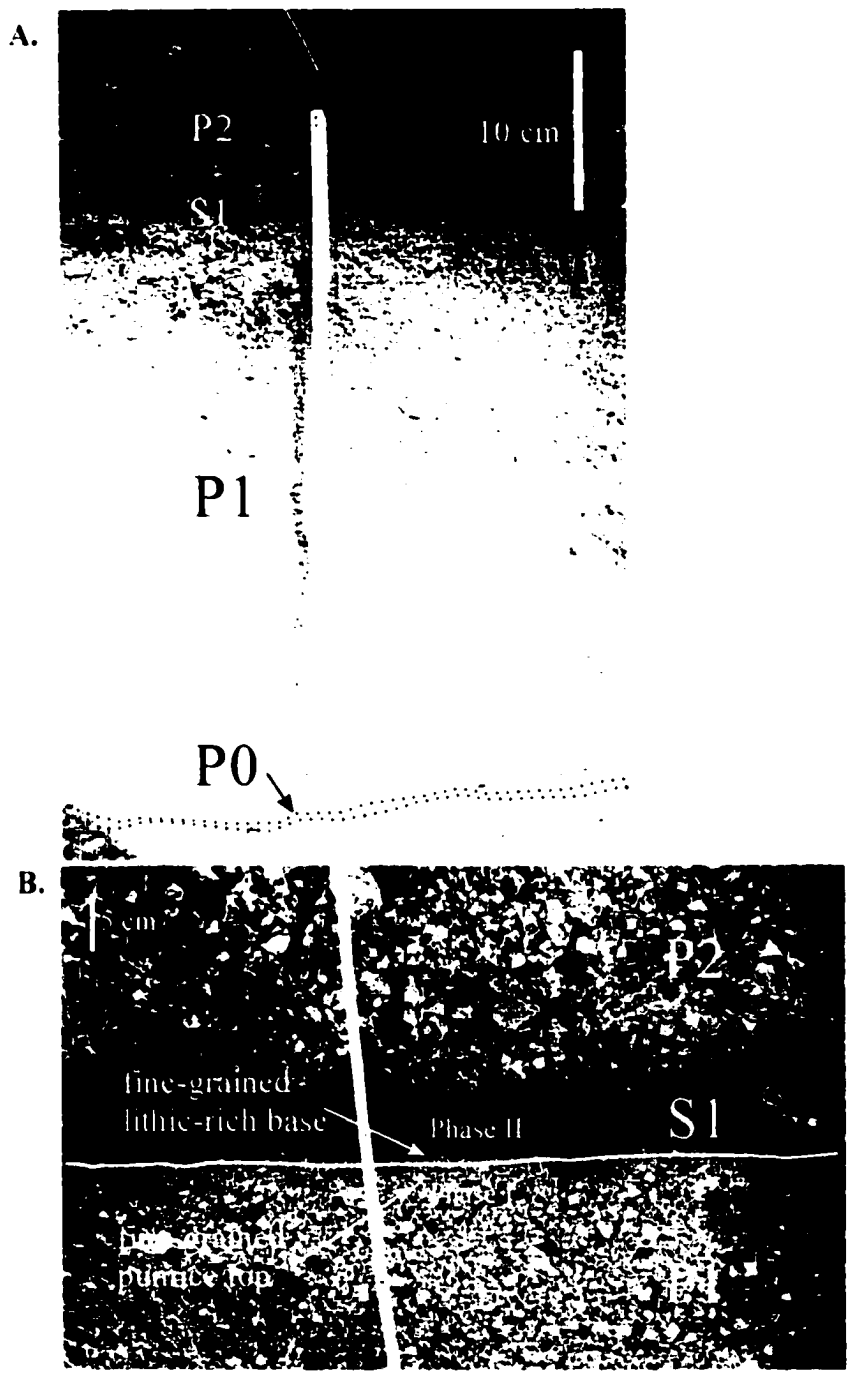

Figure 12. Photographs of Phase I deposits P0 and P1 fall layers from Locality 29 (A), and the position of the fine-grained pumice top of P1 and the fine-grained lithic-rich base of Phase II at Locality 18 (B). S1 and the base of P2 are also shown.

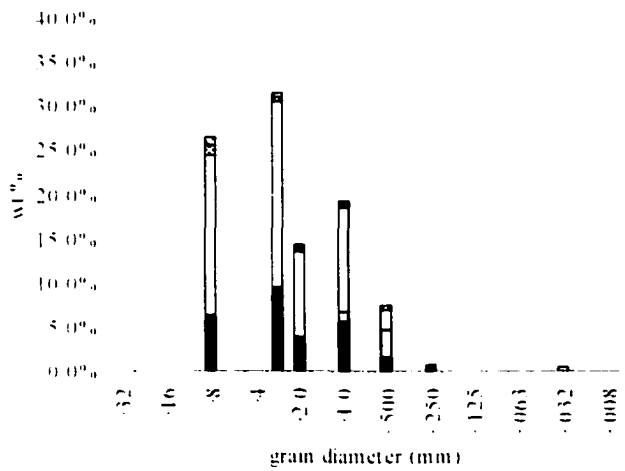

Figure 13. Modal and component analysis of the P0 fall layer from Locality 18.

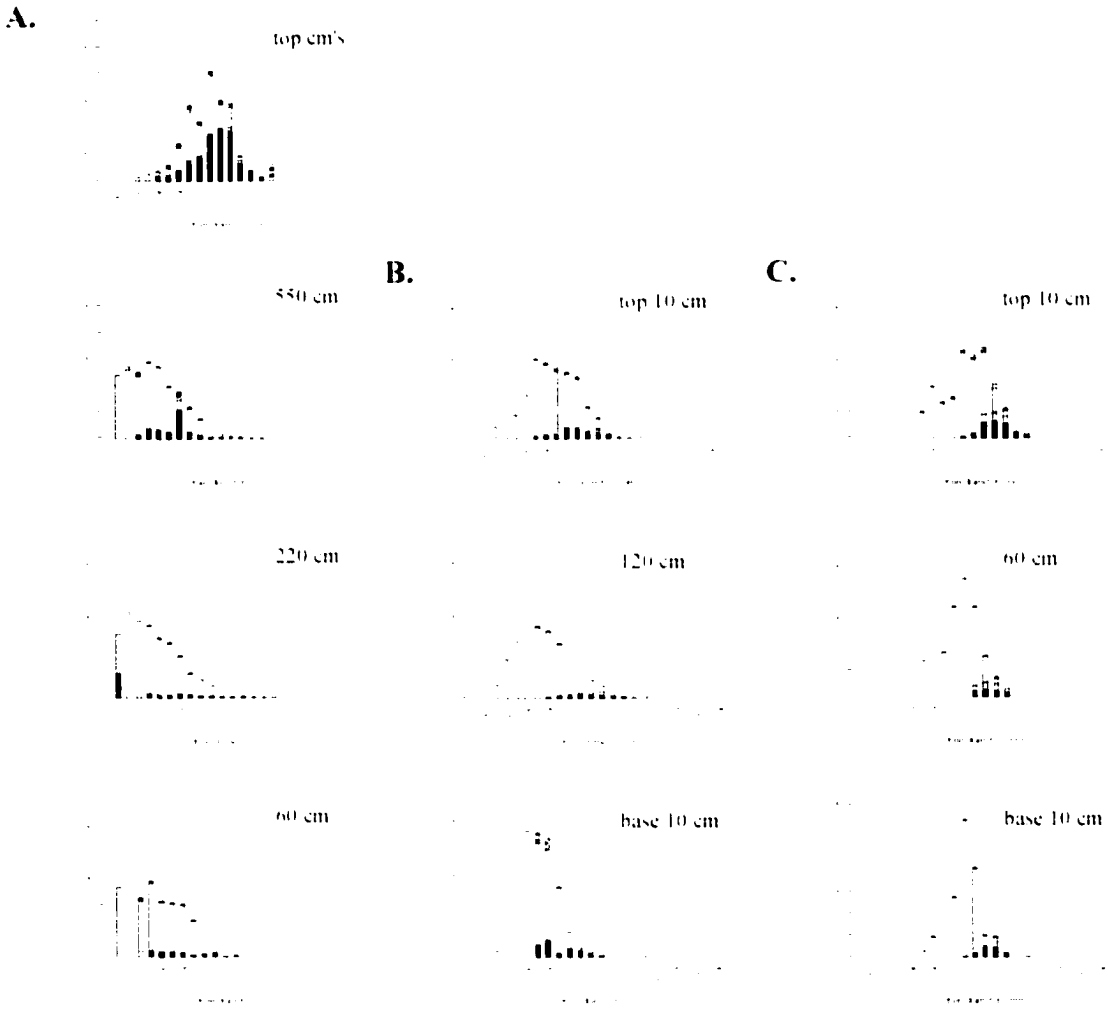

Figure14. Modal and component analyses of different heights through the P1 fall layer deposits with increasing distance at Locality 18 (A), Locality 29 (B), and Locality 69 (C).

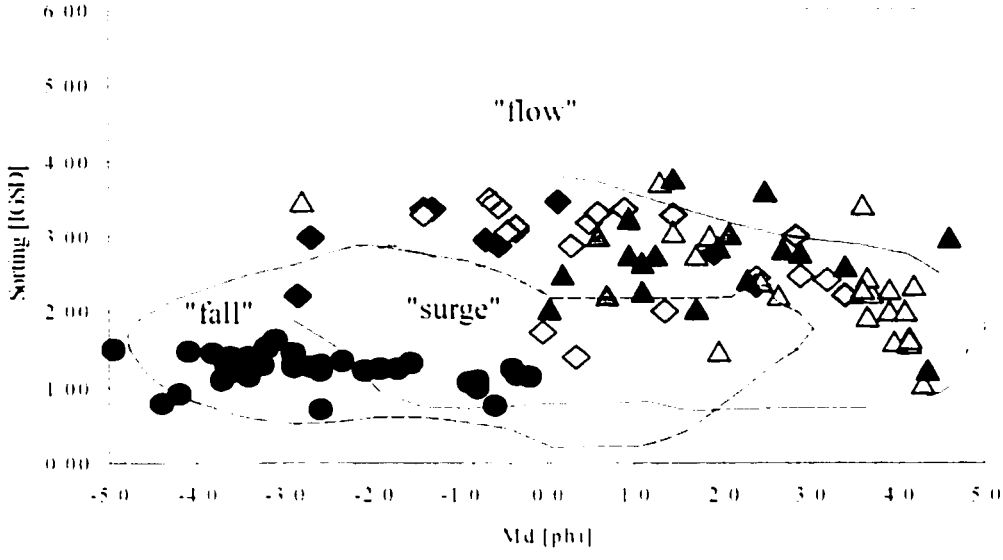

Figure 15. Fields for pyroclastic "Flow", "Surge", and "Fall" deposits based on Md and Sorting values (from Walker, 1971), with Md and Sorting values from Jala Pumice fall (solid circles), surge (triangles, S1: solid, S2: open, S3: gray), and flow deposits (diamonds, Marquesado: solid, North-Flank: gray, *c*1 and *c*2: open) from this study.

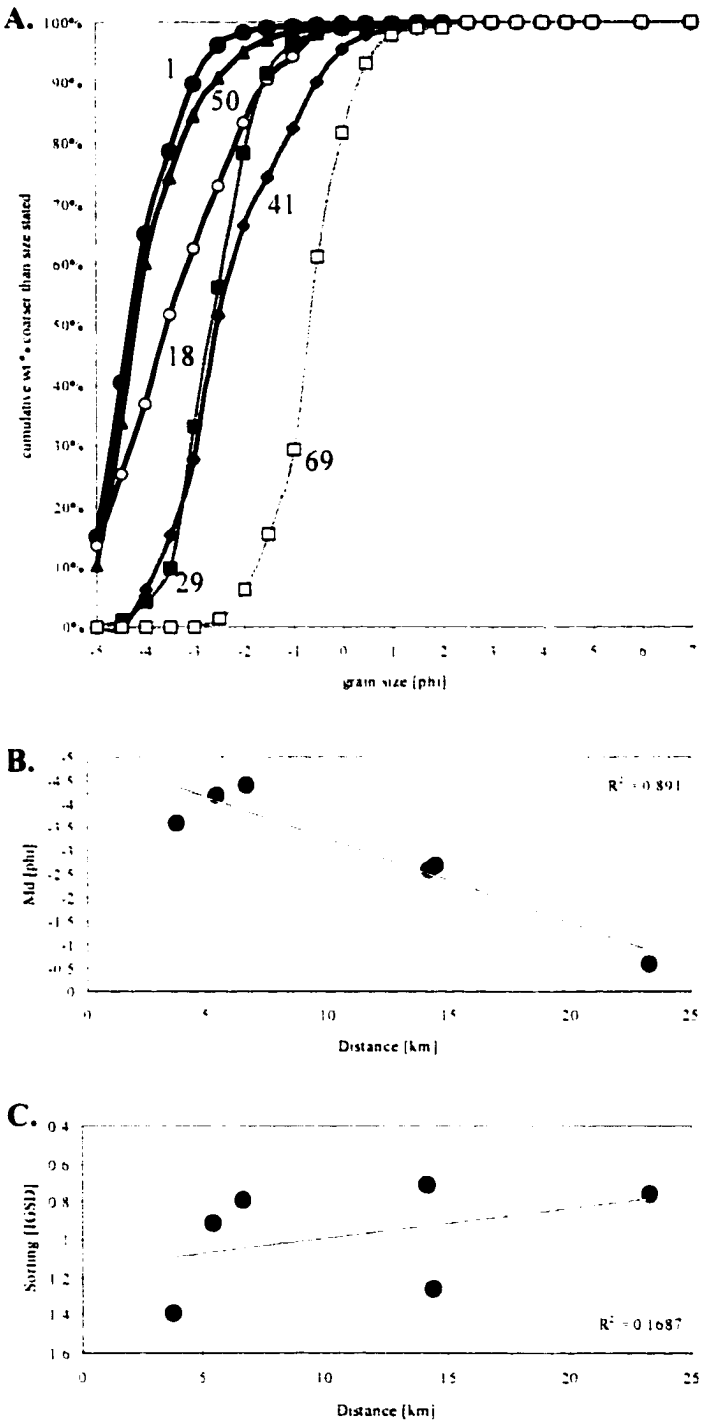

Figure 16. Cumulative curves (A). and changes in Md (B) and Sorting (C) with increasing distance for the base of the P1 fall layer. and Cumulative curves (D) and changes in Md (E) and Sorting (F) with increasing distance for the top of the P1 fall layer deposit. Sample localities are noted on cumulative curves for corresponding analysis.

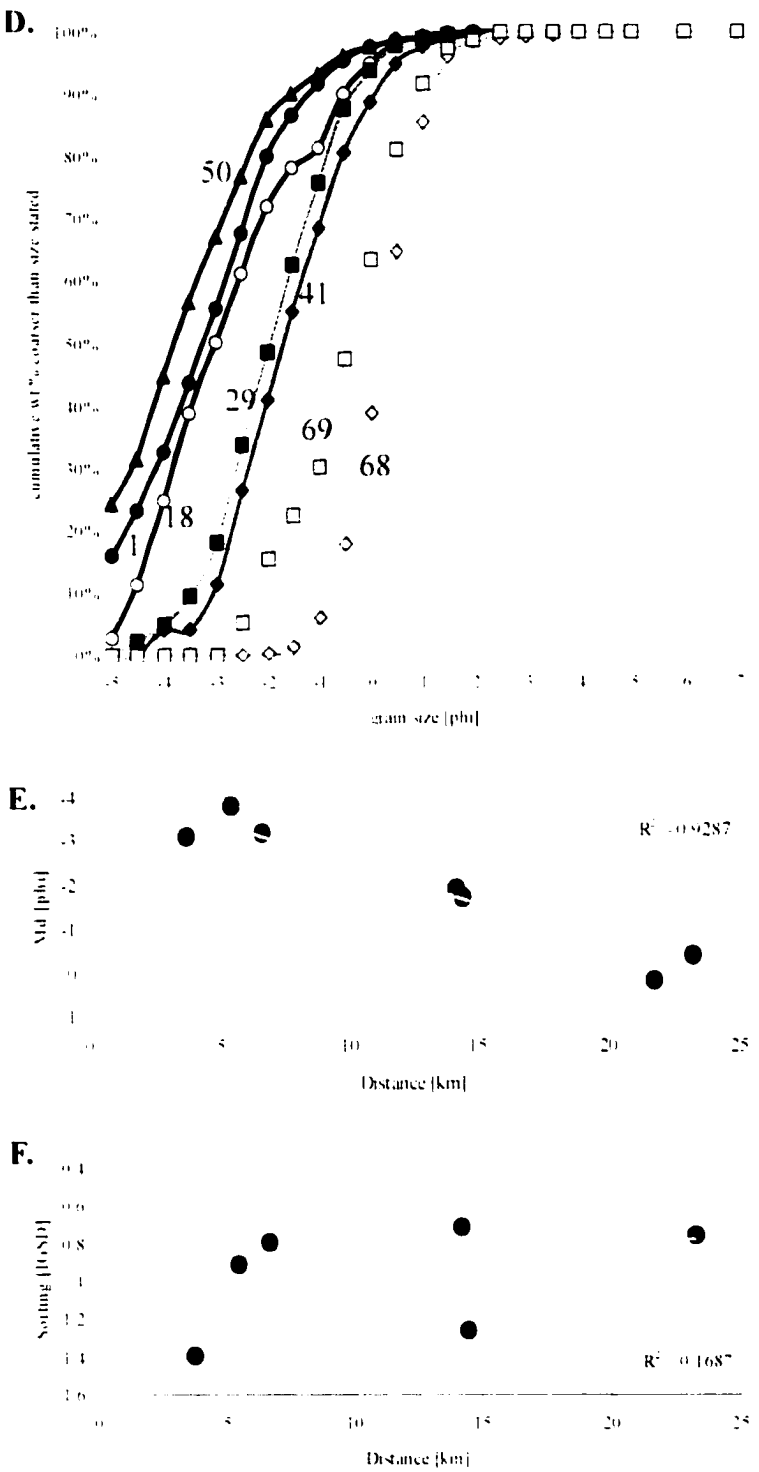

Figure 16 continued.

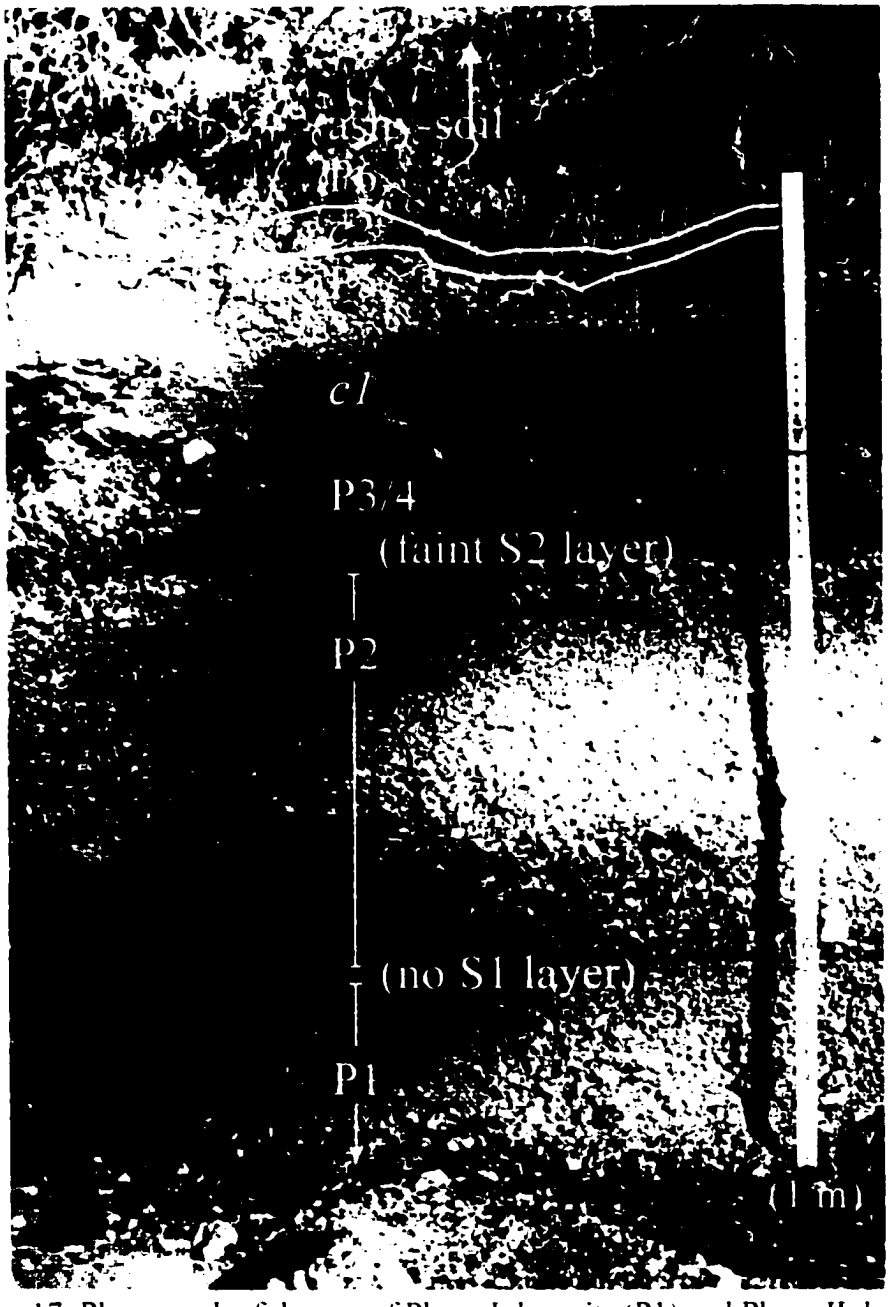

Figure 17. Photograph of the top of Phase I deposits (P1) and Phase II deposits, S1, P2, S2, P3/4, and the thinly stratified *c1* and *c2* co-ignimbrite fall layers and P5 and P6 fall layers of Phase III (Locality 33). A 1 m staff is provided for scale. Photo from J.E. Gardner

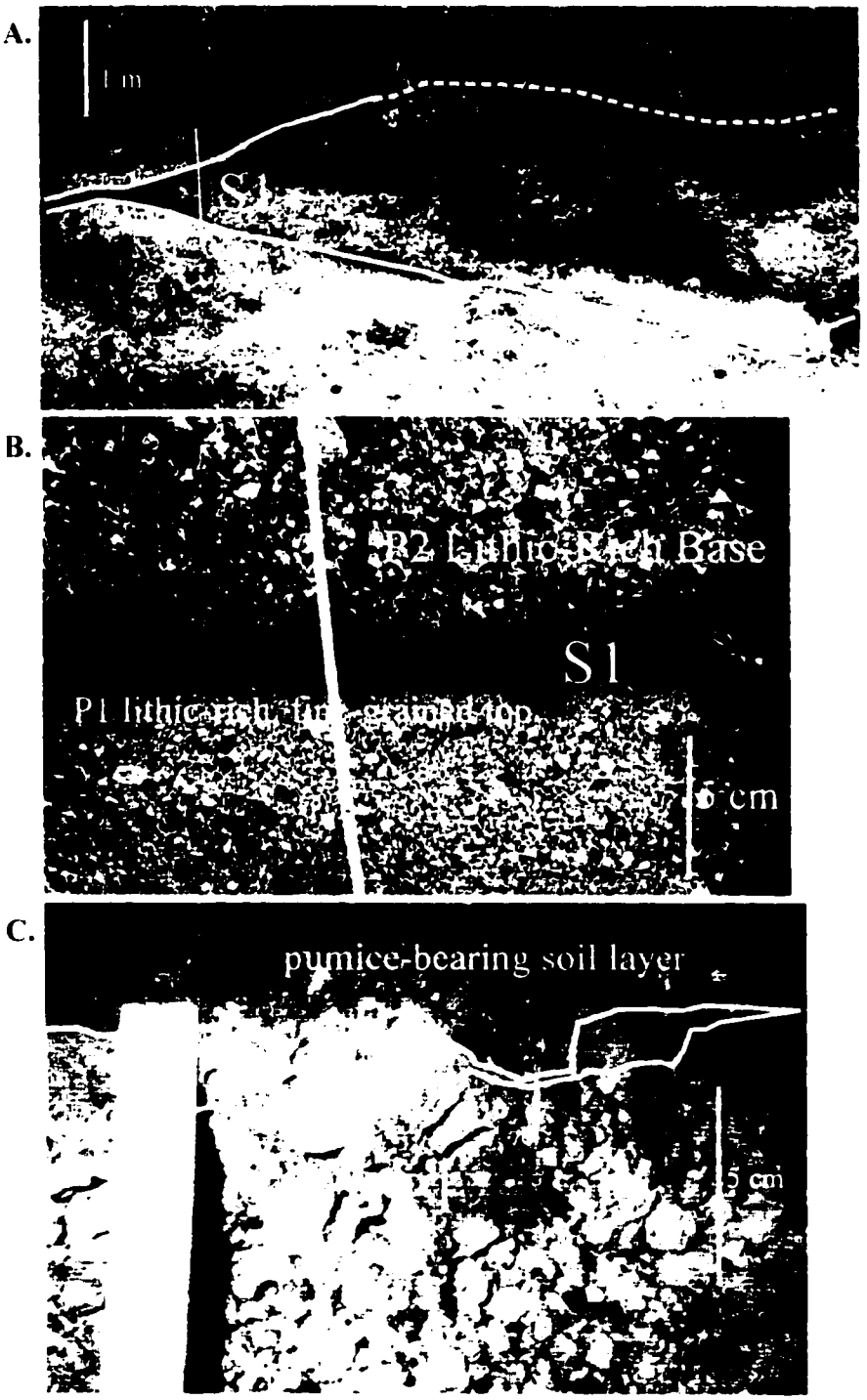

Figure 18. Photographs of the S1 surge layer proximally (A, Locality 6), medially (B, Locality 88), and distally (C, Locality 45). Note the dramatic inflation of S1 at Locality 6 to > 3 m, the massive S1 layer in medial localities, and distal deposits appear to drape over the top of pumice lapilli of the P1 fall layer. This texture may be the result of alteration from the soil layer above distal S1 layers.

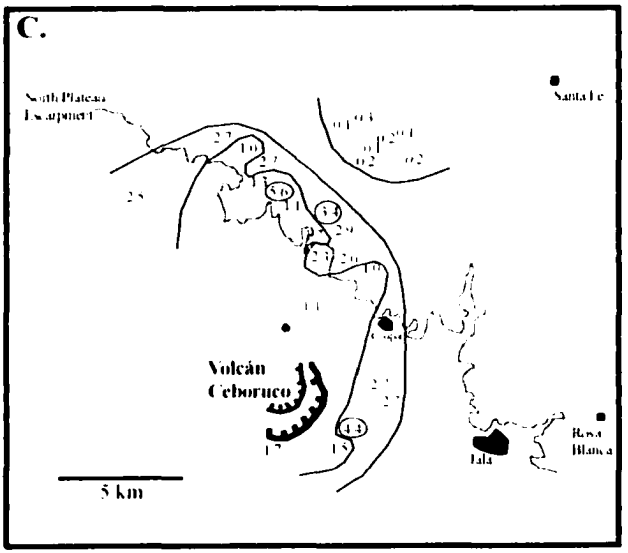

Figure 19. Isopach map (A), and Sorting (B) and *Md* (C) distribution maps for the S1 surge deposit.

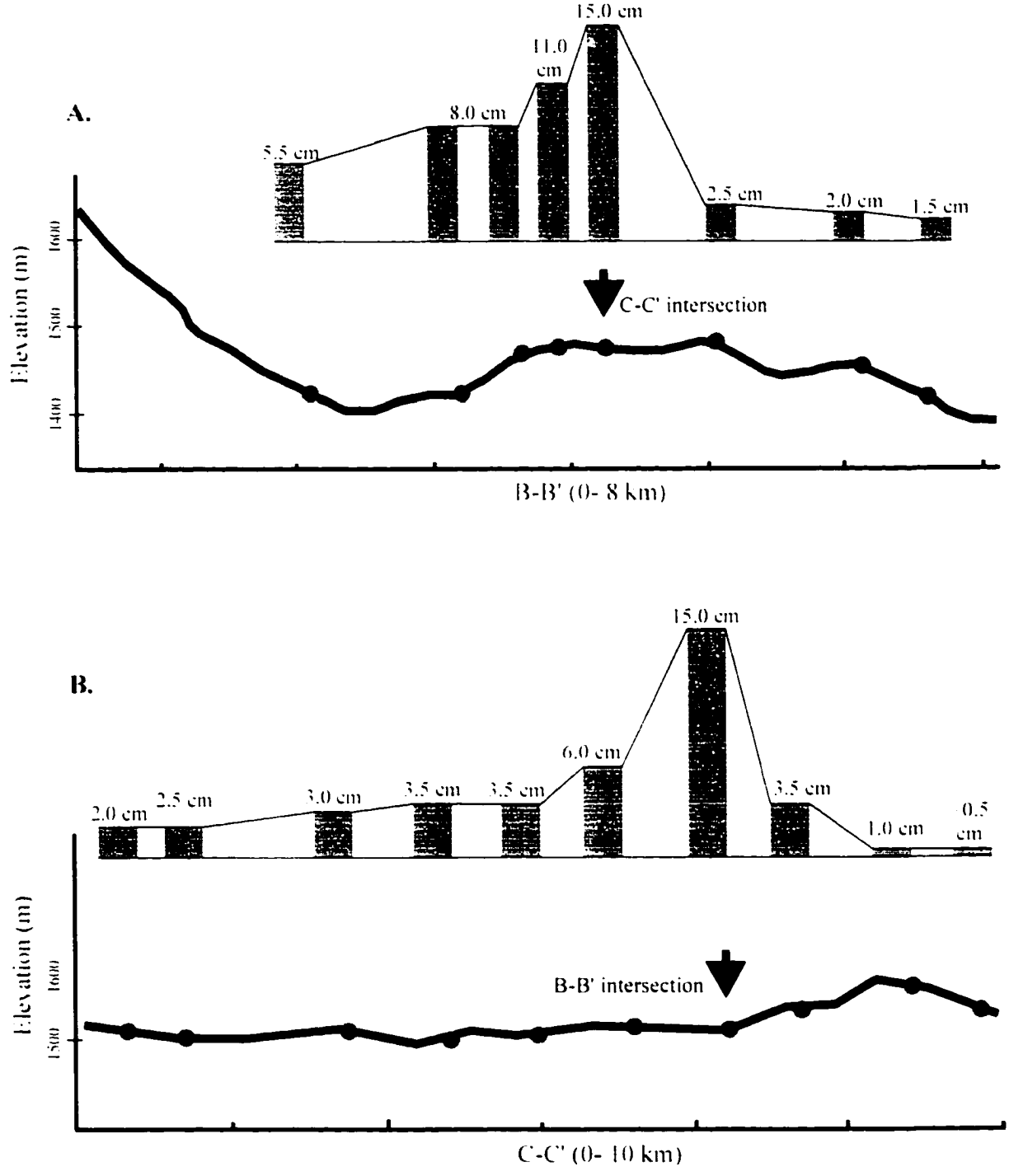

Figure 20. S1 deposit thickness along the B-B' (A) and C-C' (B) transects, with corresponding topography and location of where the two transects intersect.Note the abrupt decrease in S1 thickness atop the northern plateau and atop the high elevation ridgeline north of Coapan. See text for discussion.

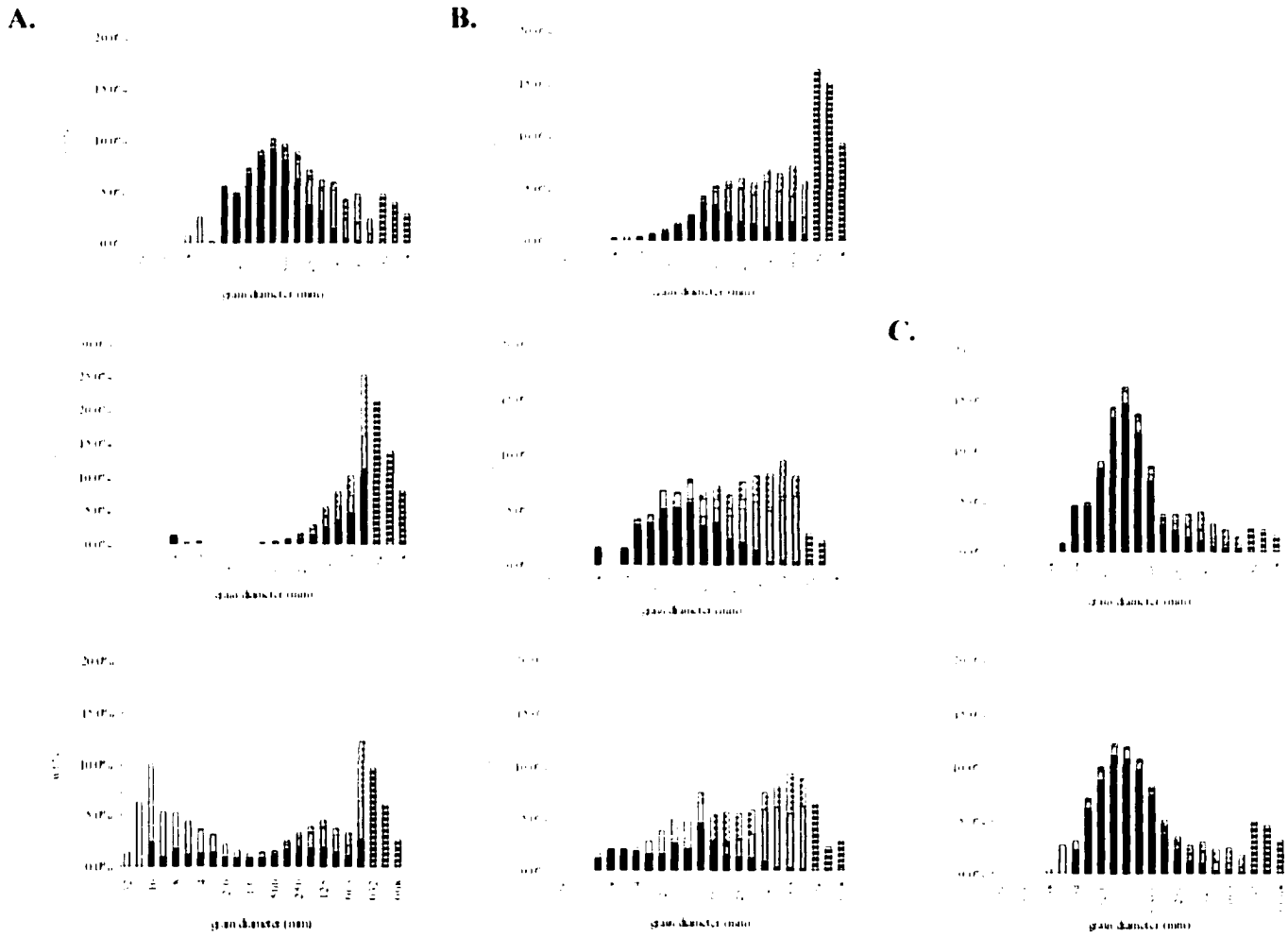

Figure 21. Modal and component analysis of proximal (A, from top: Locality 12 [B-B'], 6, and 5 [A-A']), medial (B, from top: Locality 88, 18, and 82 [B-B']), and nearly distal (C, from top: 45 and 44 [B-B']) S1 deposits. Note the high variability of sorting in proximal deposits (left), compared to medial deposits (middle and right). Also, the abrupt improvement in sorting and loss of fine material at Localities 44 and 45 are shown.

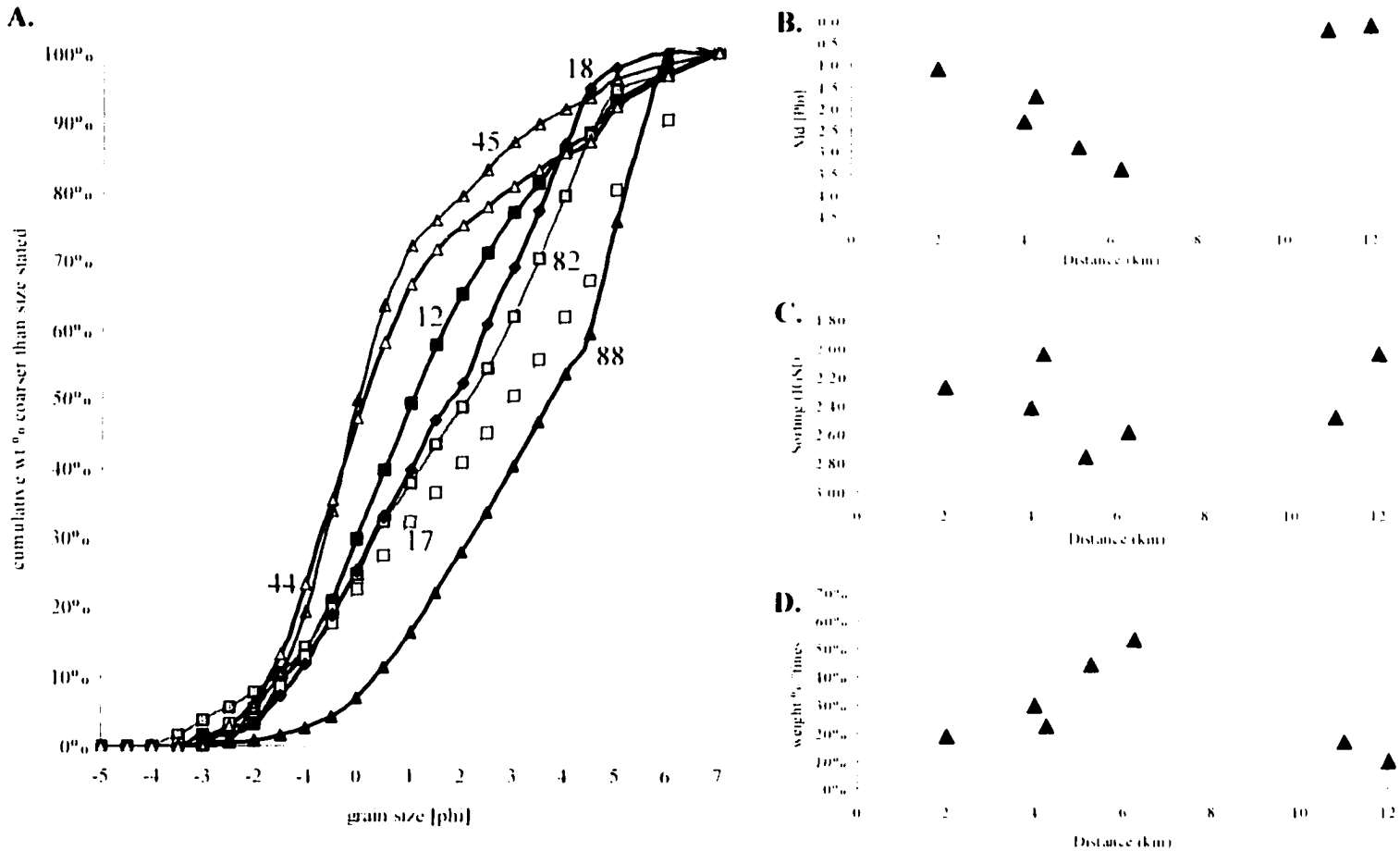

Figure 22. Granulometric analysis of S1 along the B-B' transect, including cumulative curves (A), and Md, Sorting, and F2 with distance (B, C, and D, respectively).Distal deposits have the highest Md values, lowest amount of fine material (F2), and are the best sorted compared to other S1 deposits on the plateau.

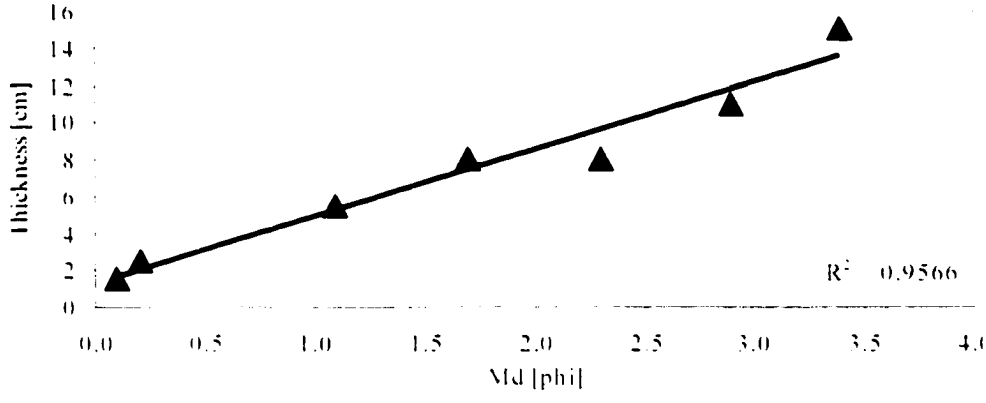

Figure 23. S1 deposit thickness versus Md values along the B-B' transect. This correlation shows that the thickest S1 deposits are fines enriched, whereas the thinnest S1 deposits are fines depleted.

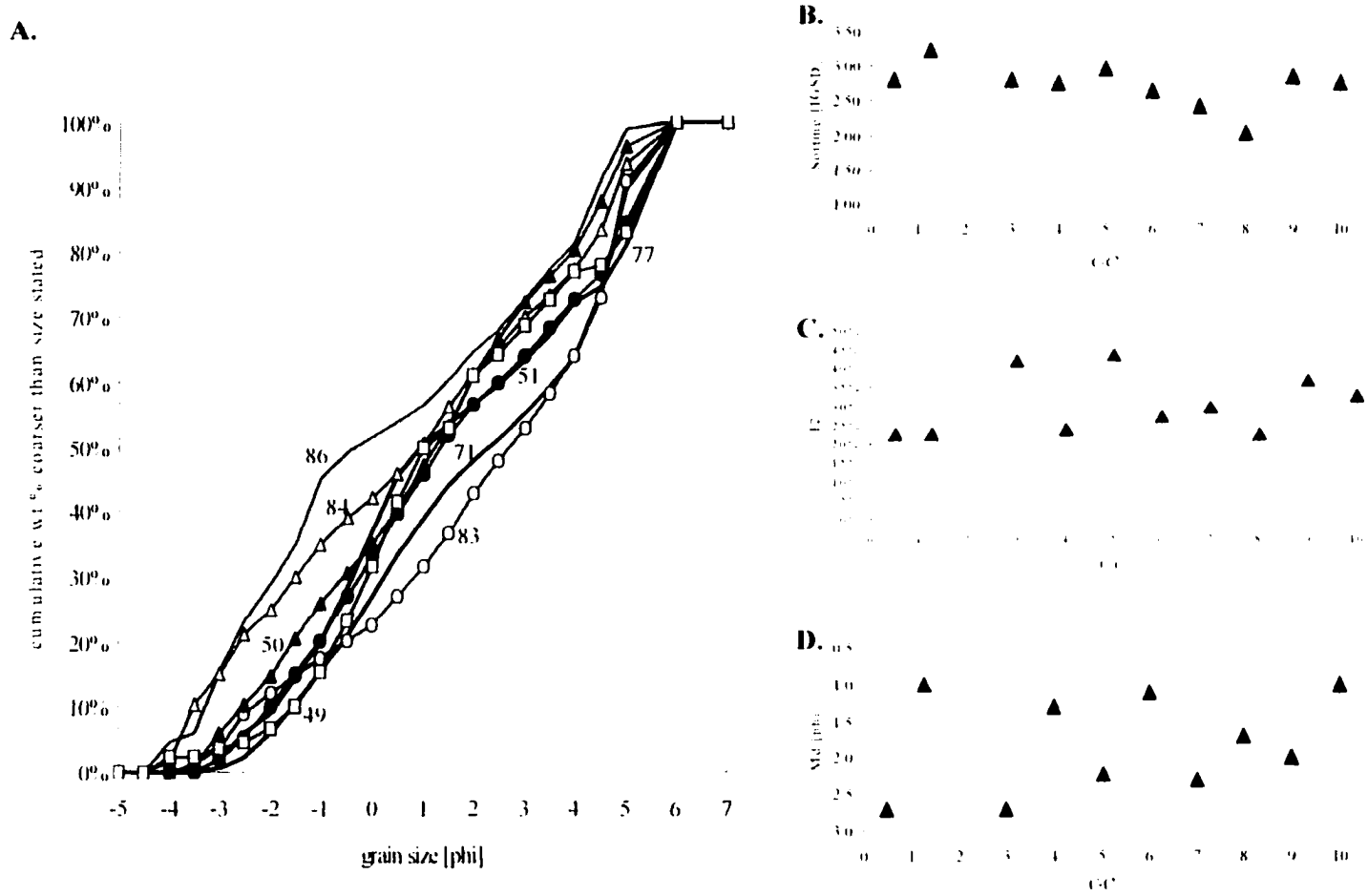

Figure 24. Granulometric analysis of S1 along the C-C" transect, including cumulative curves (A), and Sorting, F2, and Md with distance (B, C, and D, respectively). Sample localities for S1 samples are shown for specific cumulative curves (A). Despite the relatively constant sorting (ó) in S1 deposits, note the fluctuations in F2 and Md across the C-C" transect, which may result from the undulating front of the Sierra Madre plateau escarpment.

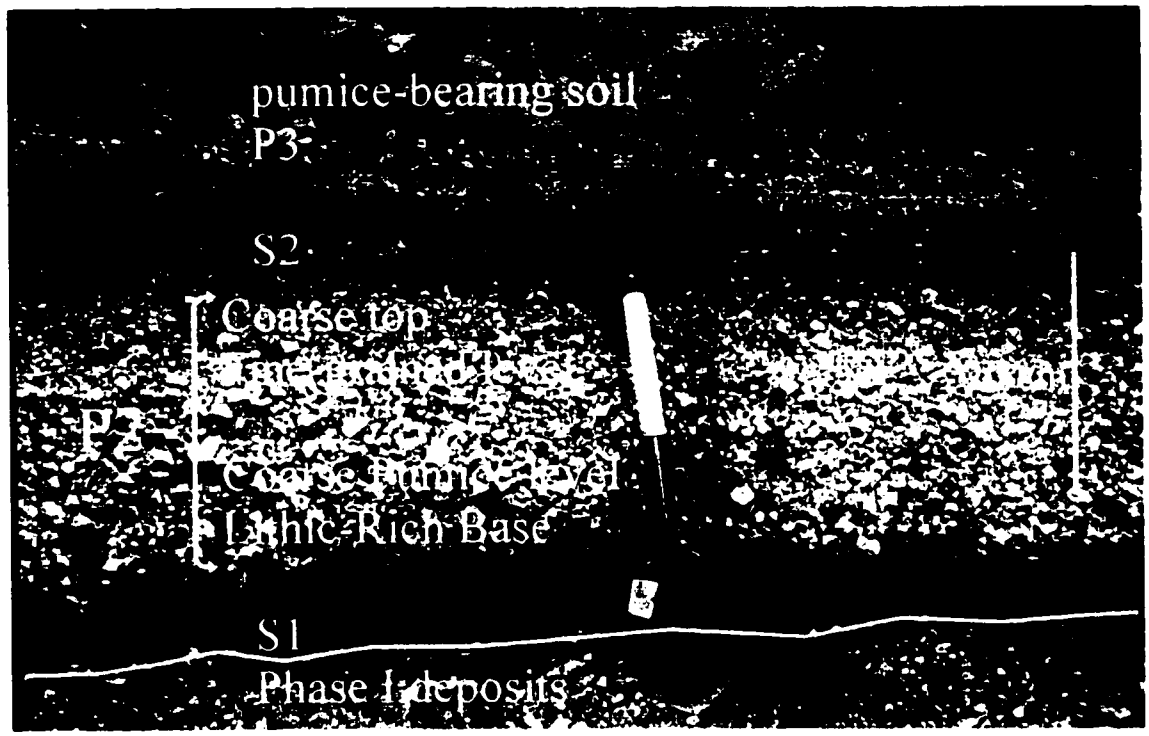

Figure 25. Photograph of the P2 fall layer, with S1 below and S2 above (from Locality 3).

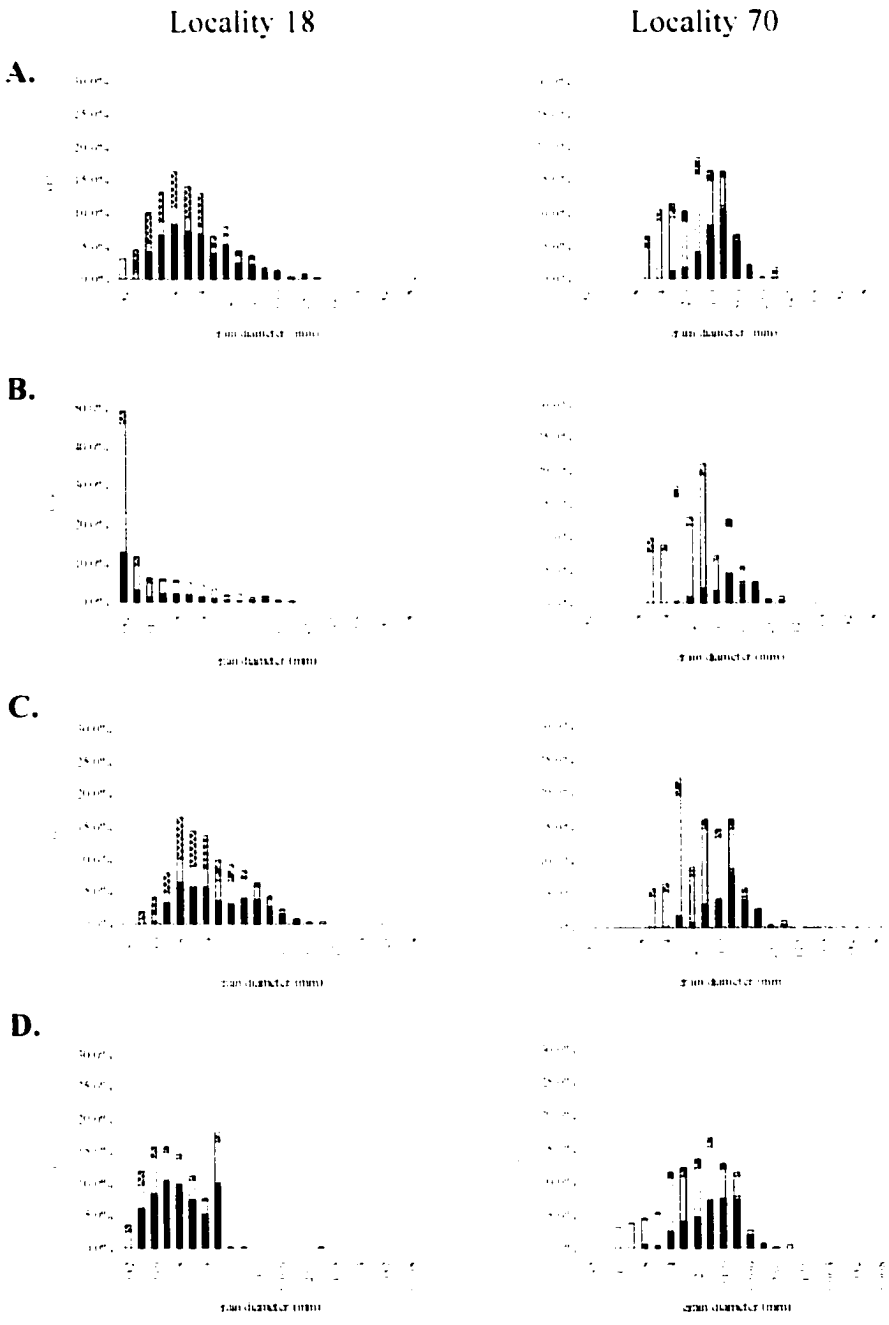

Figure 26. Modal and component analyses of different heights (A. Lithic-rich base; B. Coarse-pumice level; C. Fine-grained level; and D. Coarse top) through the P2 fall layer with increasing distance from Locality 18 to Locality 70. Locality 18 is ~3 km from vent, and Locality 70 is >20 km from vent. Note the reduction of dense phases such as lithics and Banded and Gray pumices with distance, as well as the reduction in Md. See text for discussion.

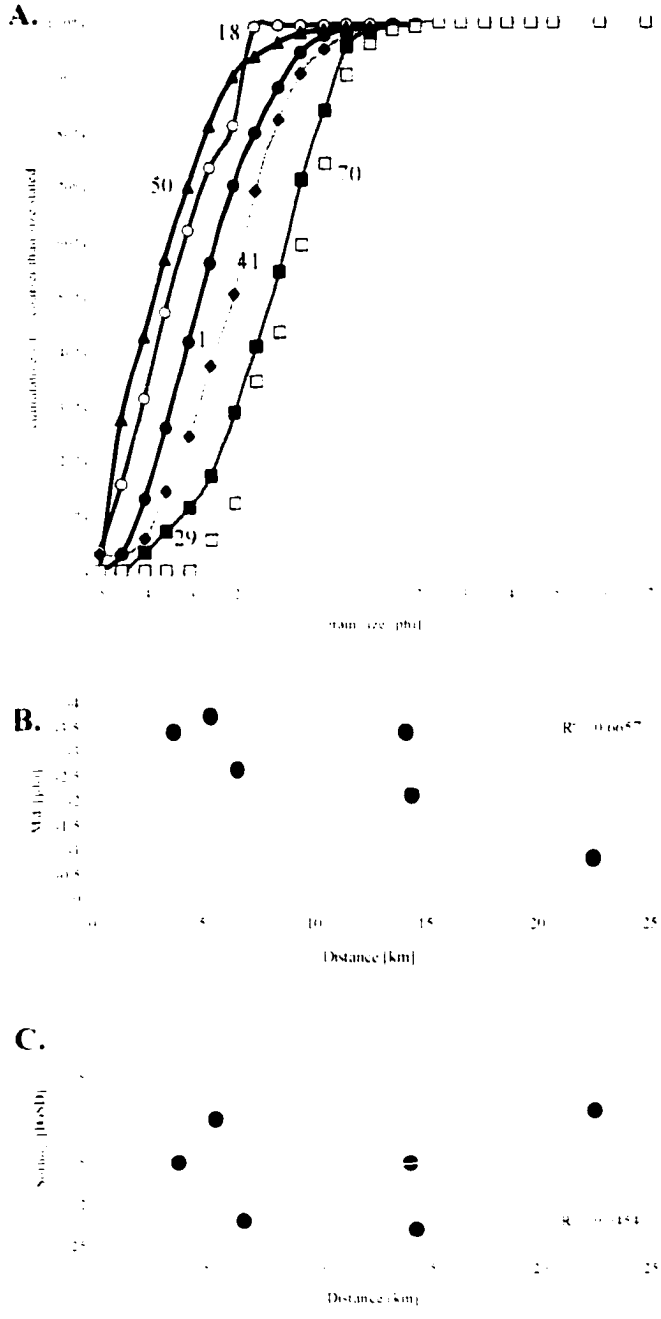

Figure 27. Cumulative Curves (A), and changes in Md (B) and Sorting (C) with increasing distance for the Lithic-rich base of the P2 fall layer. Analyses are from 6 localities (3- 27 km from vent), which are noted adjacent to the particular cumulative curve. Note that whereas the LRB of P2 exhibits a reduction in Md with distance, the Sorting values display little or no improvement with increased distance.

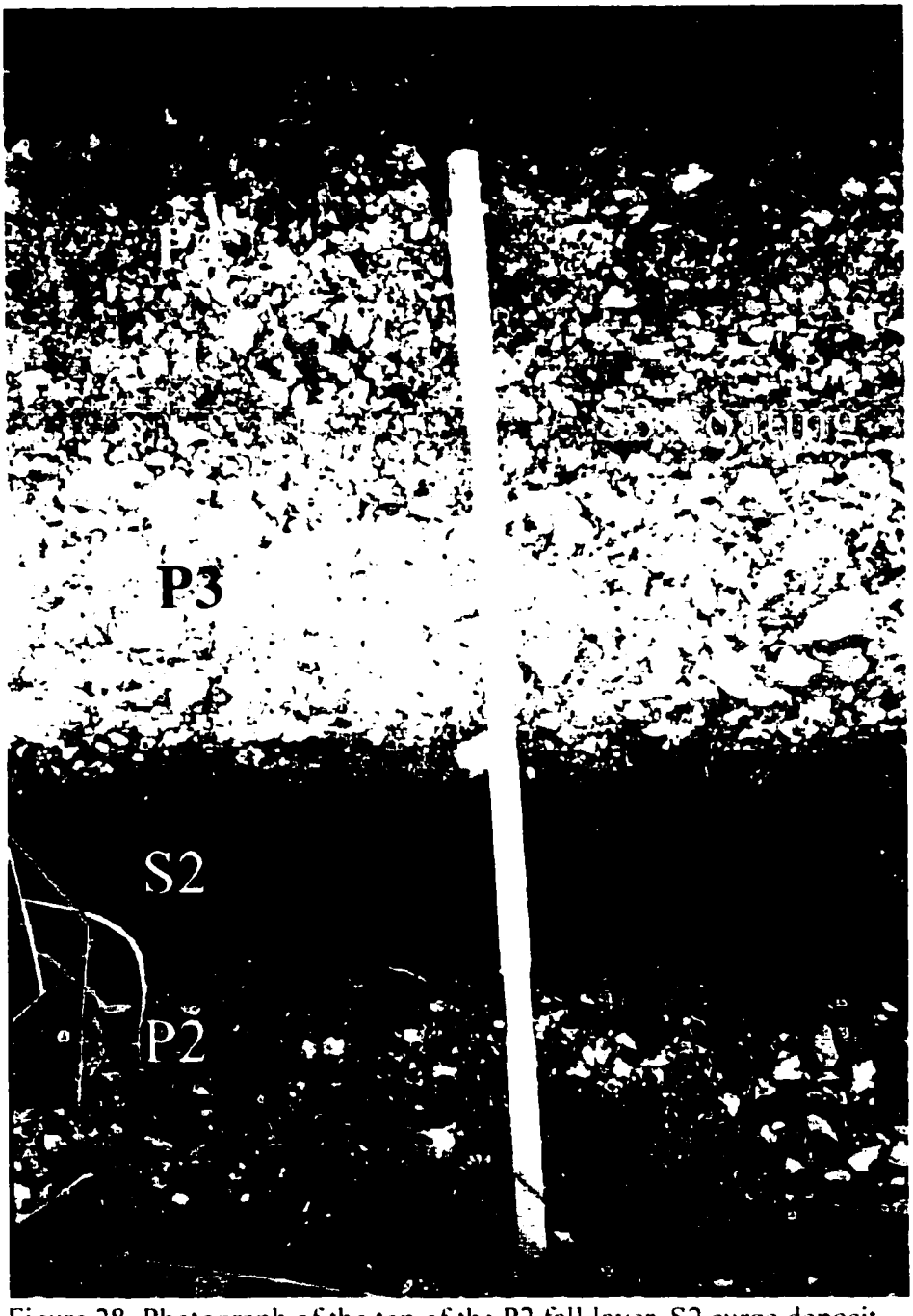

Figure 28. Photograph of the top of the P2 fall layer, S2 surge deposit, P3/4 fall layer, and the thinly coated pumices from the S3 surge (from Locality 18). A 60 cm staff is present for scale.

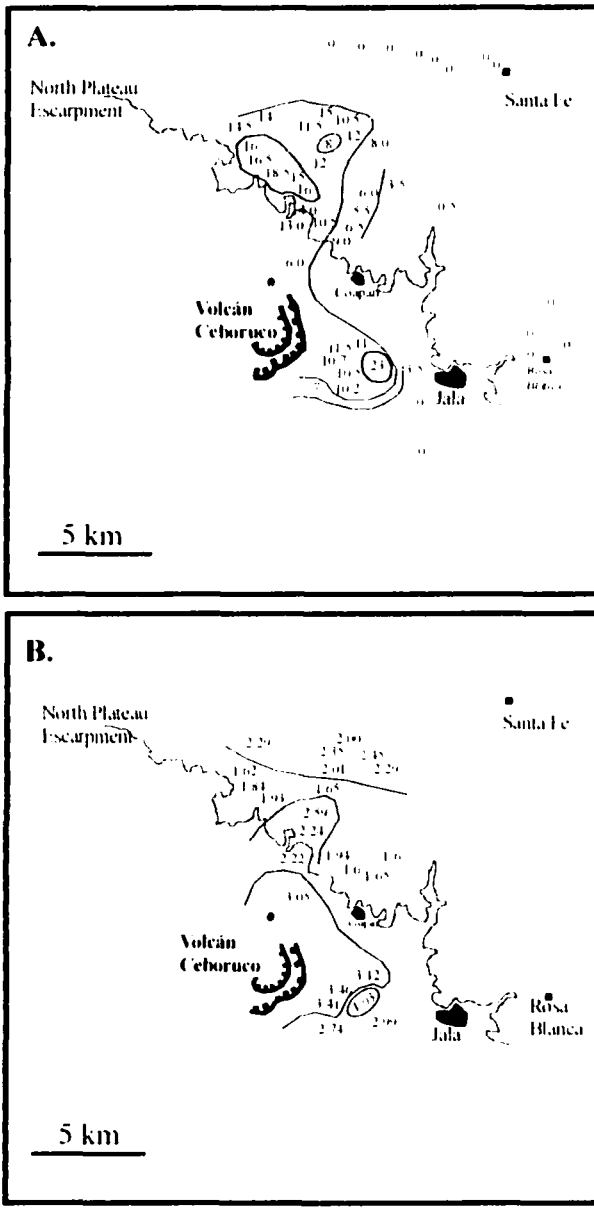

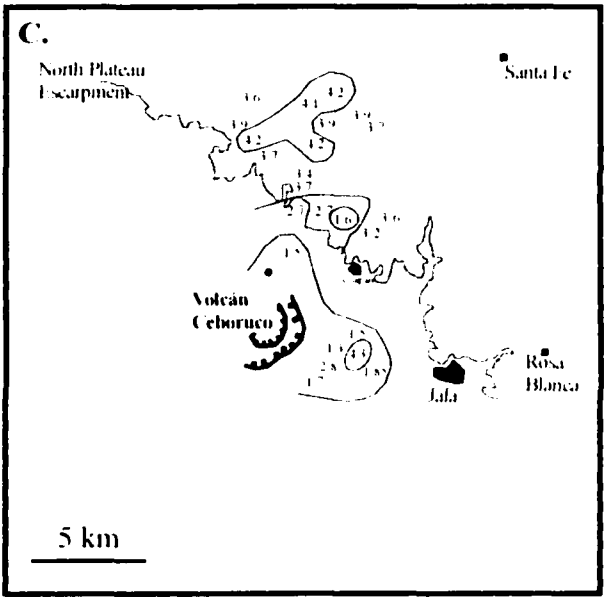

Figure 29. Isopach map (A), and Sorting (B) and Md (C) distribution maps for the S2 surge deposit.

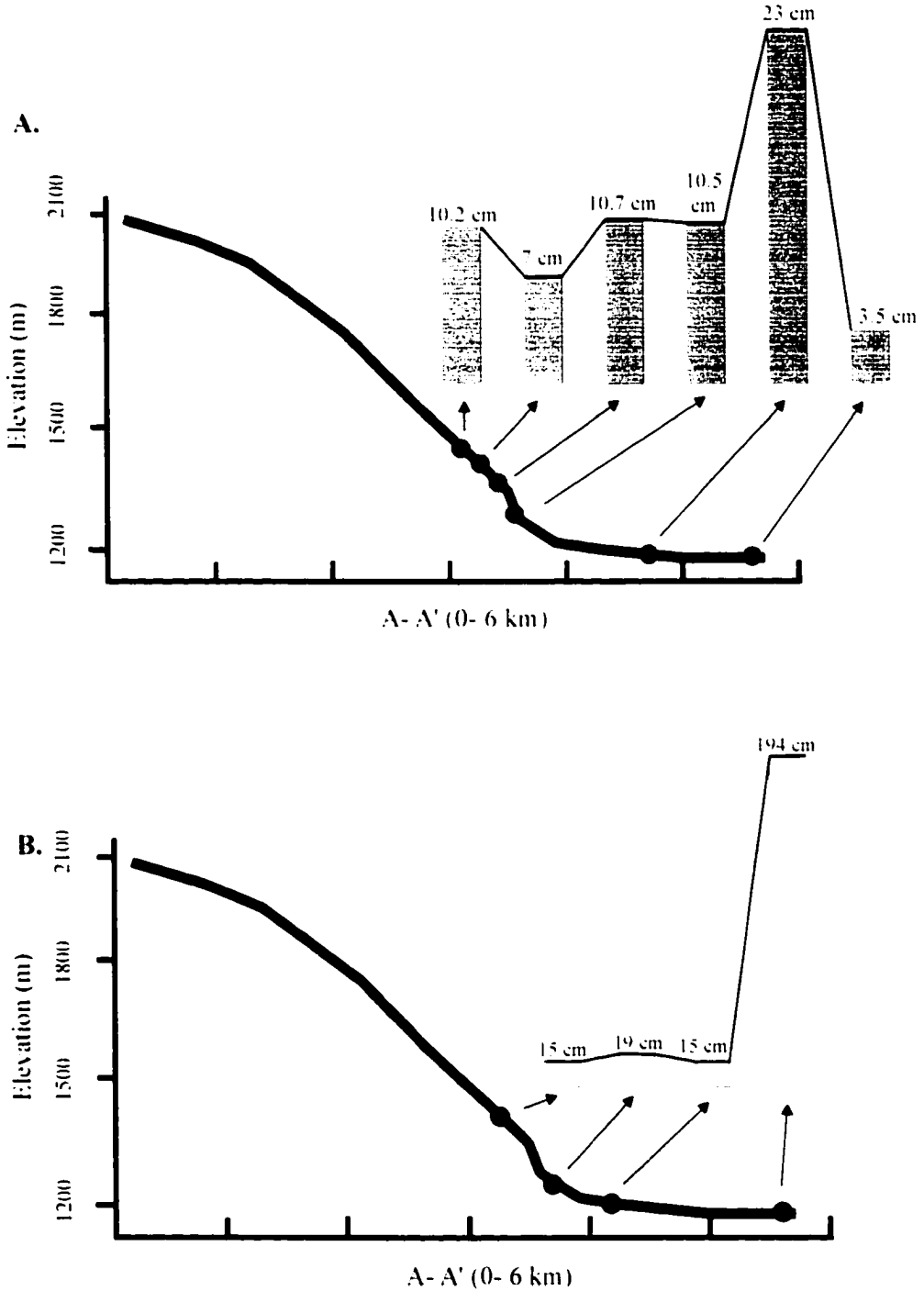

Figure 30. S2 (A) and S3 (B) deposit thickness along the A-A' transect, with corresponding topography. Shaded circles indicate sample localities. An abrupt increase in S2 and S3 thickness occurs at the break in slope.

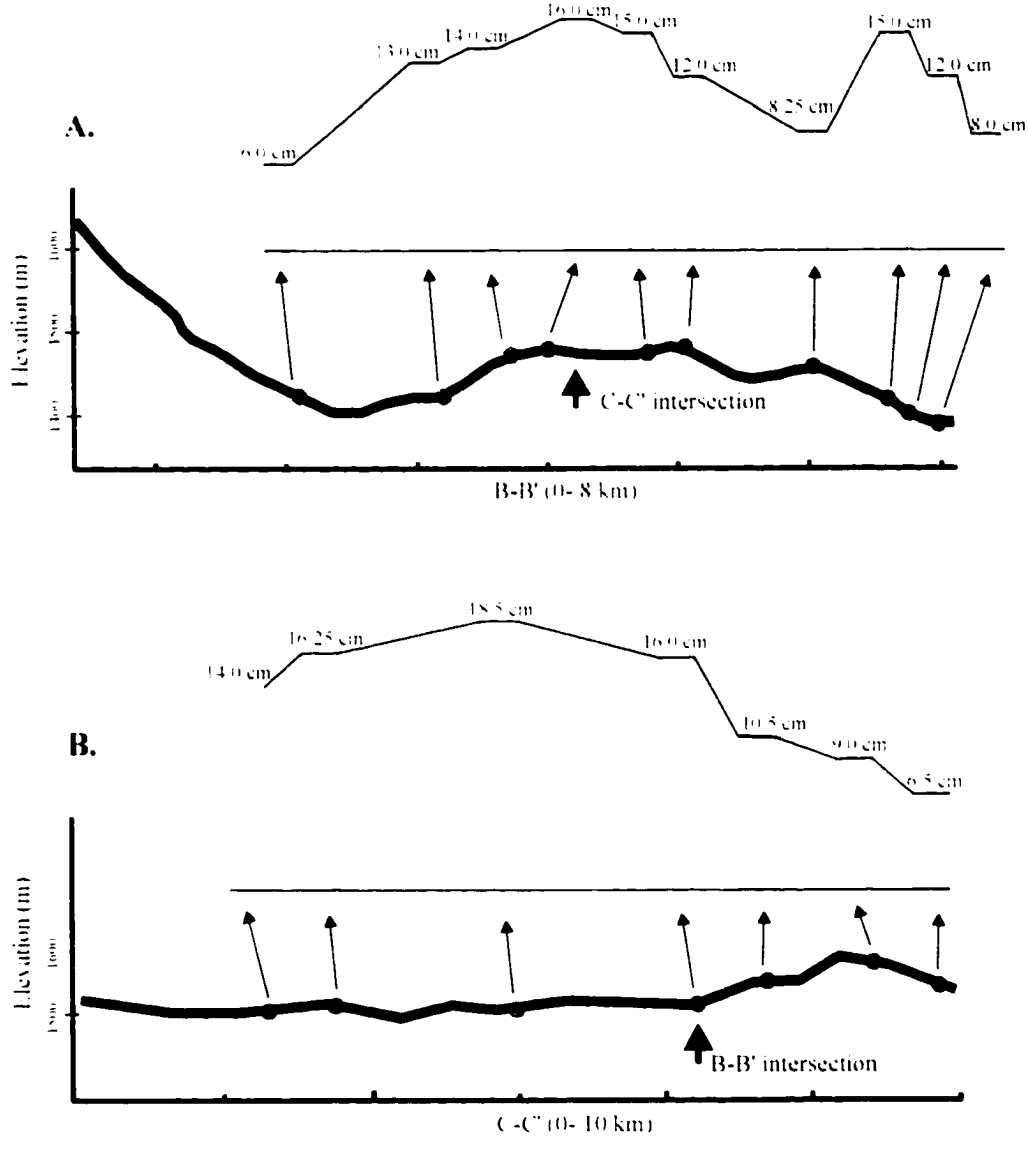

Figure 31. S2 deposit thickness along the B-B' (A) and C-C' (B) transects, with corresponding topography.Note the increased thickness of S2 atop the northern plateau in topographic lows and thinner deposits at topographic highs, and the considerably thicker nature of S2 atop the plateau in topographic lows compared to the higher elevation ridgeline north of Coapan. S2 deposits are more than 3 times as thick along this ridge compared to the S1 surge deposit.

C.

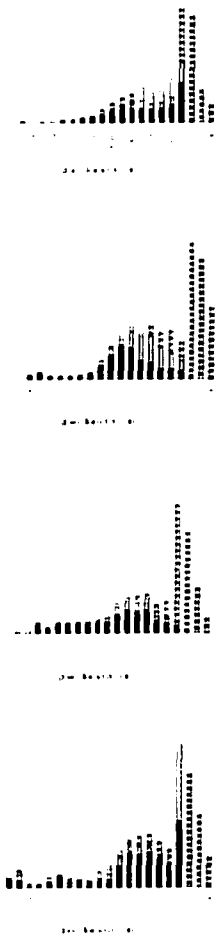

Figure 32. Modal and component analysis of proximal (A, from top: Locality 4, 6, 7, 5), medial (B, from top: 51, 88, 18, 82), and nearly distal (C, from top: 43, 44, 93, 46) S2 deposits.Considerable variability exists in the proximal S2 deposits, compared to the uniform nature of particle size distribution in the deposits found atop the plateau with increasing distance. Also, despite the nearly constant amount of fine material (< 0.032 mm), S2 samples from topographic lows (e.g. Localities 82, 46, 88, and 93) are more poorly sorted compared to samples from topographic highs (e.g. Localities18, 43, 51, and 44).

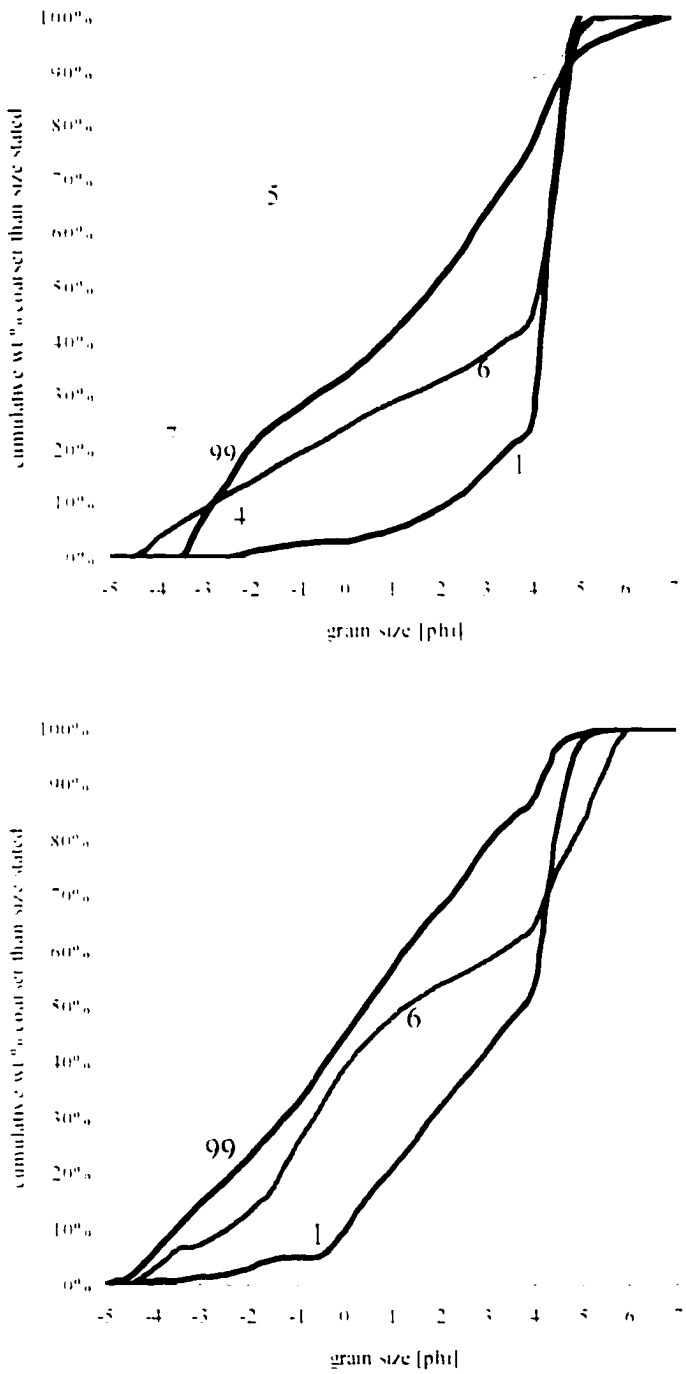

Figure 33. Cumulative curves for the S2 (top) and S3 (base) surge deposits along the A-A' transect. Sample localities are adjacent to their corresponding cumulative curves.

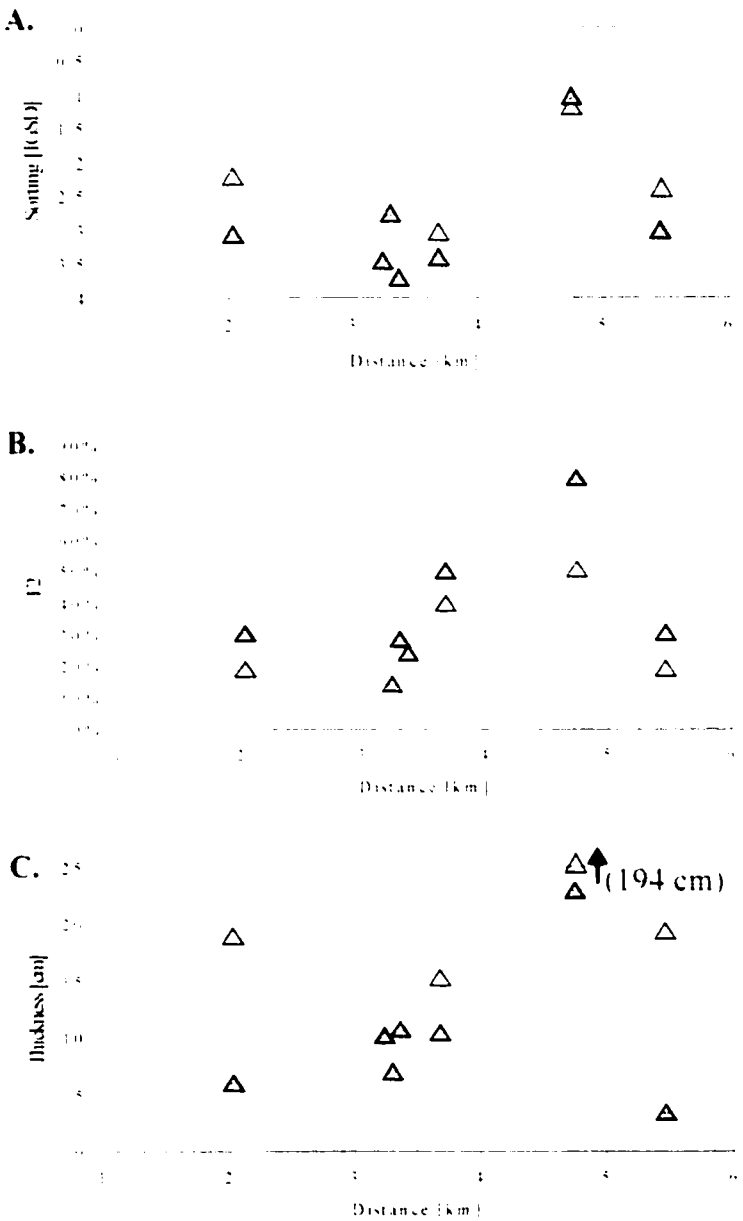

Figure 34. Granulometric analysis S2 (filled) and S3 (open) surge deposits along the A-A' transect, including sorting (A), F2 (B), and thickness (C) with distance. Note the drastic improvement in sorting, and increase in F2 and thickness in both S2 and S3 surge deposits at approximately 5 km from vent, corresponding to the location of the break in slope between the eastern flank and the valley floor.

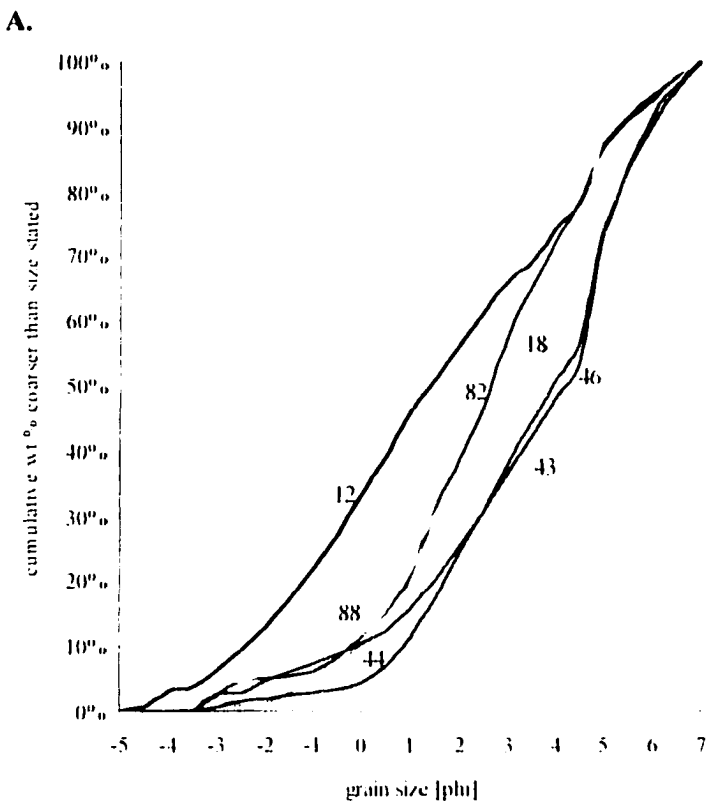

Figure 35. Granulometric analysis of S2 deposits along the B-B' transect, including cumulative curves (A), and Md, F2, sorting, and sorting vs. thickness correlation (B, C, D, and E, respectively) S2 deposits display a continual increase in fines, and an improvement in sorting, along with a steady decrease in Md with distance, similar to pyroclastic fall deposits. In addition, thinner S2 deposits are systematically better sorted than thicker S2 deposits.

Distance (km)

Distance (km)

Distance (km)

Sorting [ϕSD]

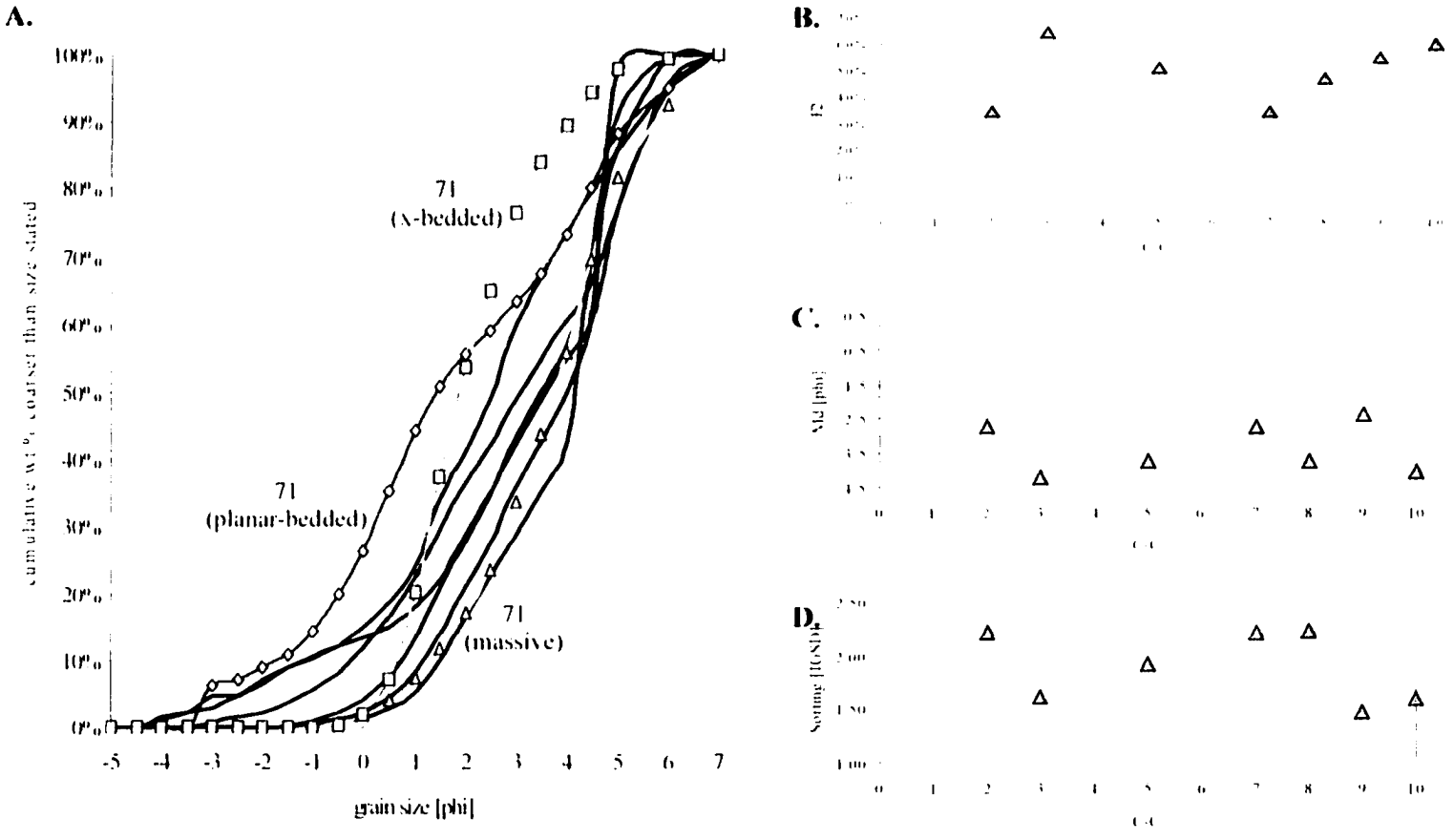

Figure 36. Granulometric analysis of S2 deposits along the C-C" transect, including cumulative curves (A), and F2, Md, and sorting with distance (B, C, and D, respectively). Specific internal bedforms from S2 at Locality 71 are placed adjacent to their corresponding cumulative curves, showing that the majority of S2 deposits along the C-C" transect reflect similar modal distribution to the massive and planar-bedded layers, rather than the cross-bedded layers.

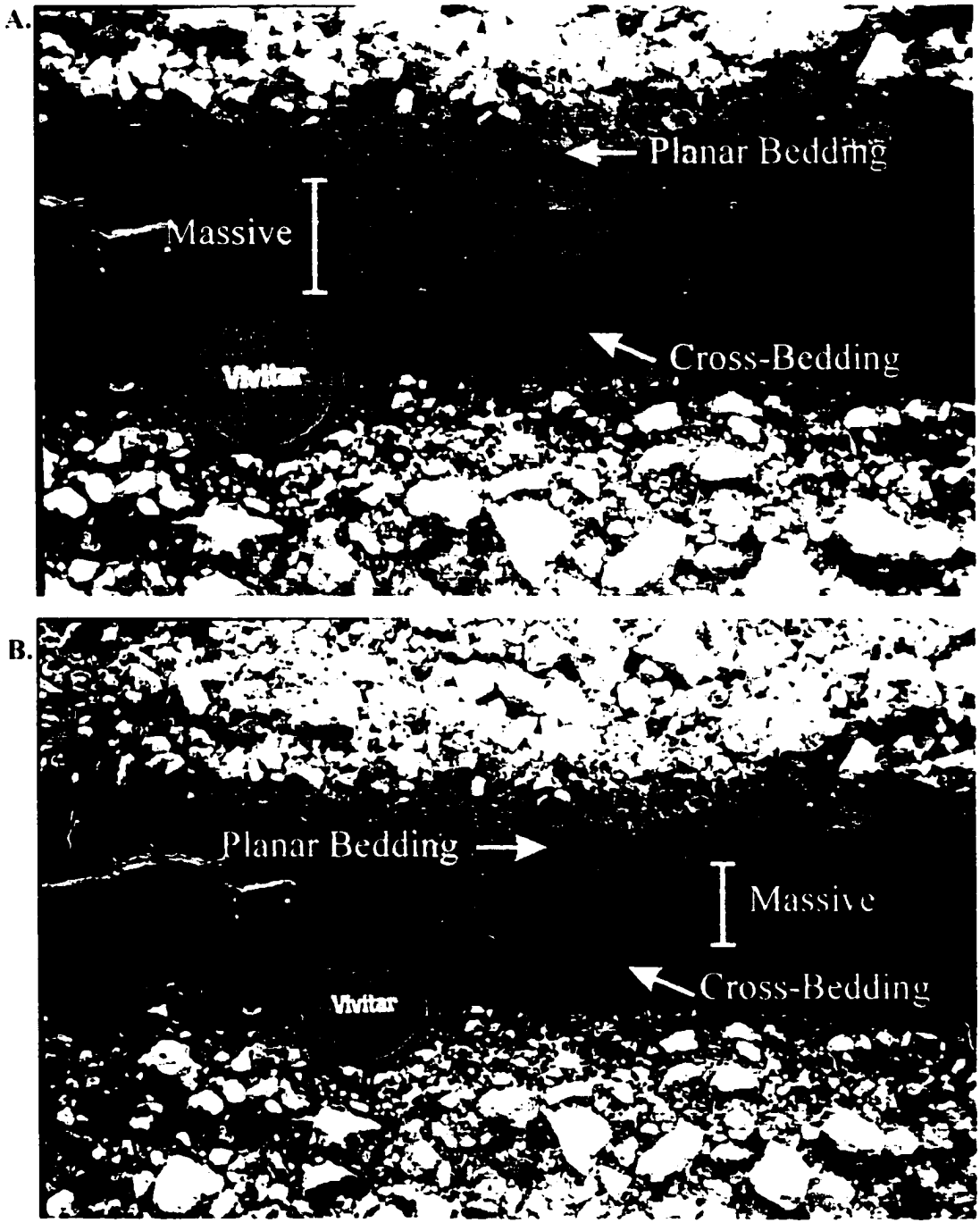

Figure 37. Photgraphs of the internal stratigraphy of the S2 surge deposit atop the northern plateau at Localities 71 (top) and 77 (base).

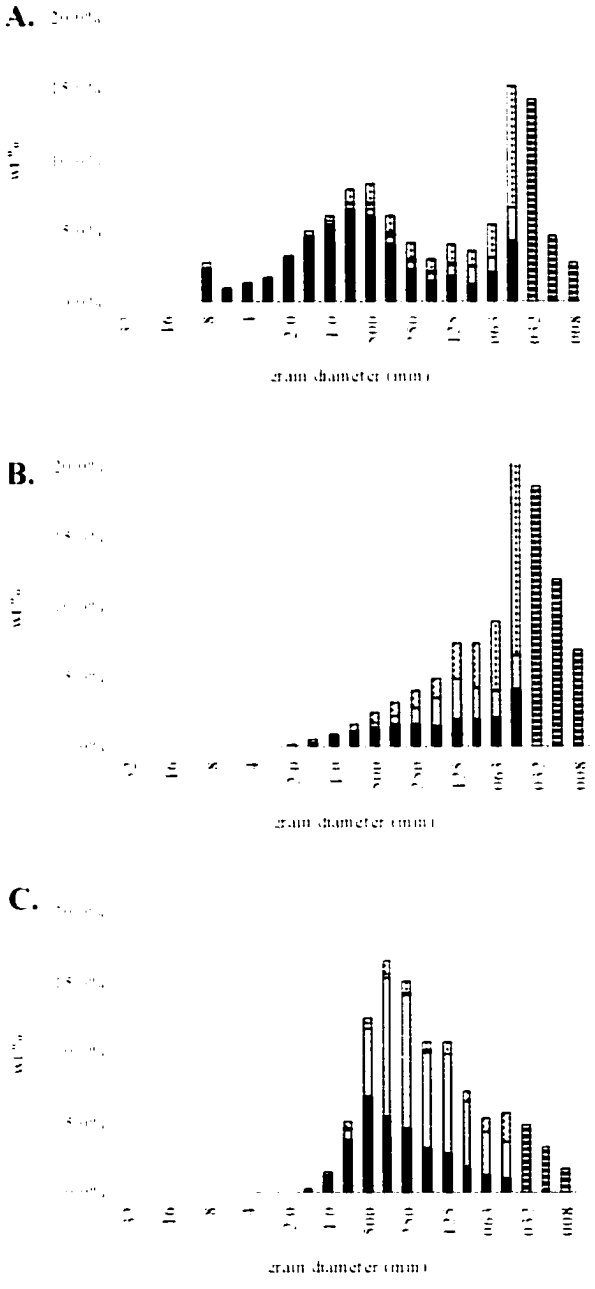

Figure 38. Modal and component analysis of the planar-bedded (A), massive (B), and cross-bedded (C), stratigraphy within the S2 surge deposit at Locality 71. The upper planar beds appear to display a bimodal distribution of fine and medium grained particles, whereas the middle massive bed is better sorted and enriched in fine-grained particles. Basal cross-bedded layers are fines depleted and well sorted.

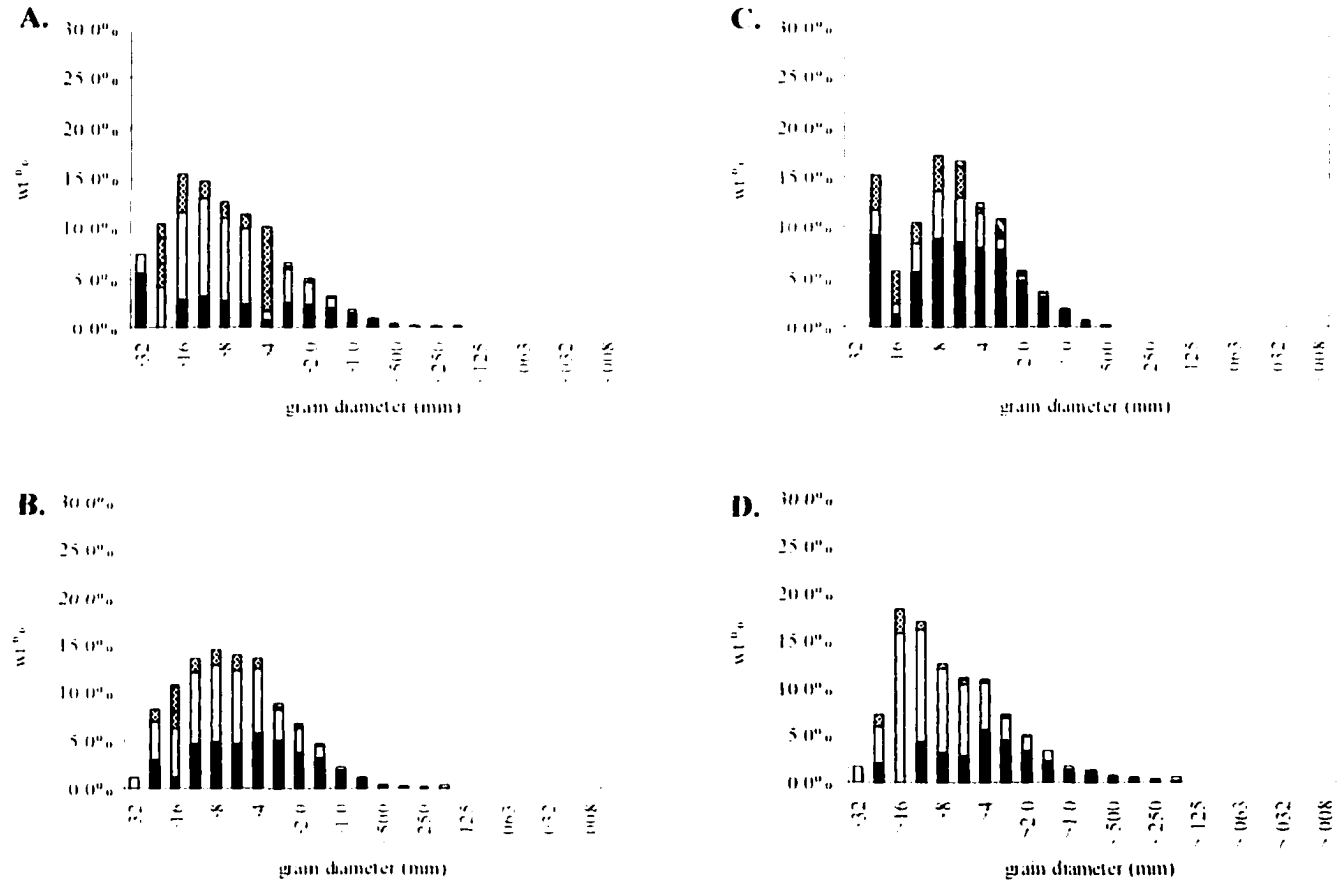

Figure 39. Modal and component analyses of the P3 (A, pumice-rich top; B, lithic-rich base), and the P4 (C, Lithic-rich top; D, pumice-rich base) fall layers at Locality 18.

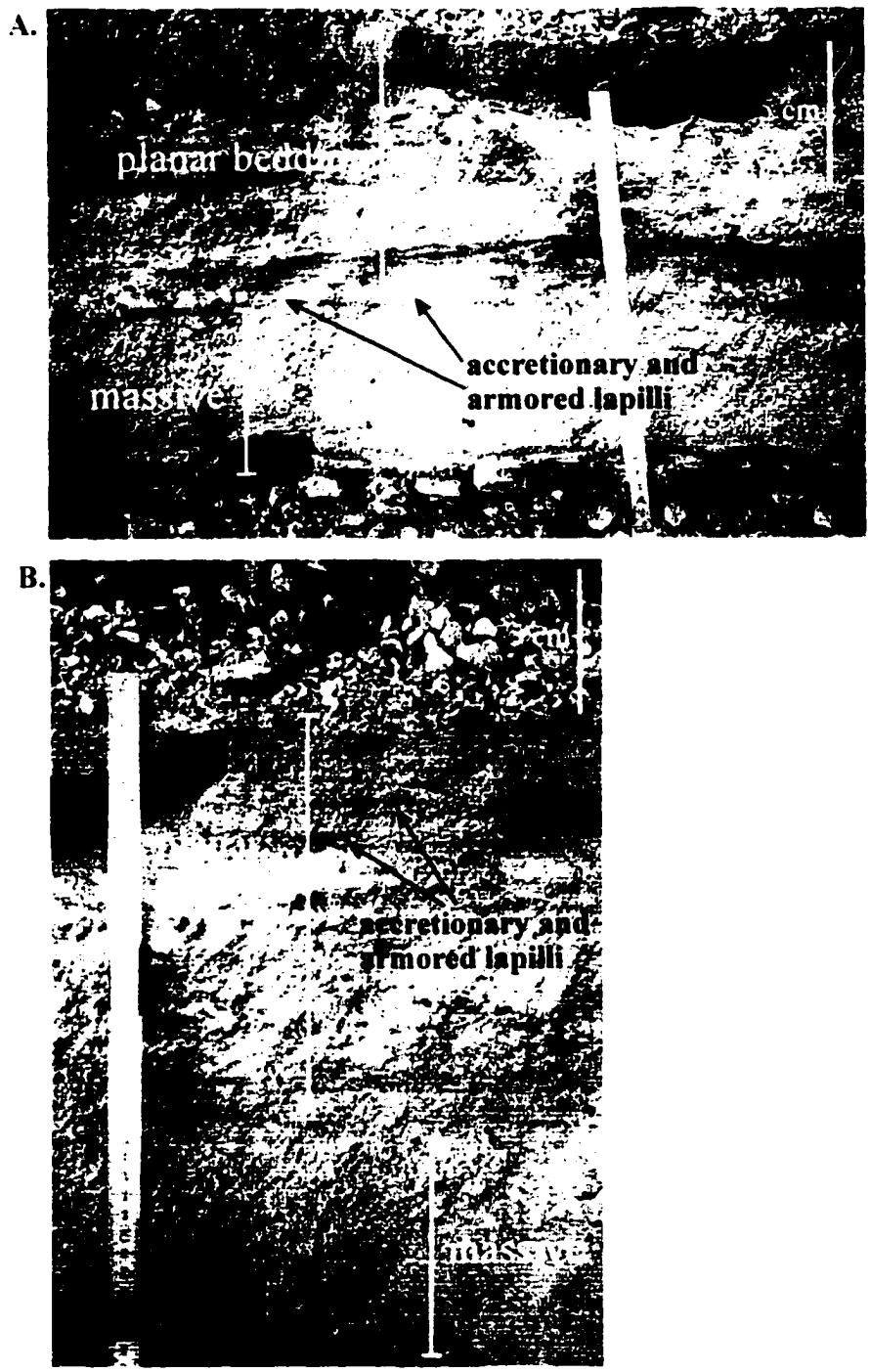

Figure 40. Photographs of the S3 surge deposit at Localities 6 (A) and 12 (B). Basal regions are commonly massive, whereas the upper zones display intricate planar bedding. Note the abundance of rolled accretionary and armored lapilli in the middle and upper planar beds.

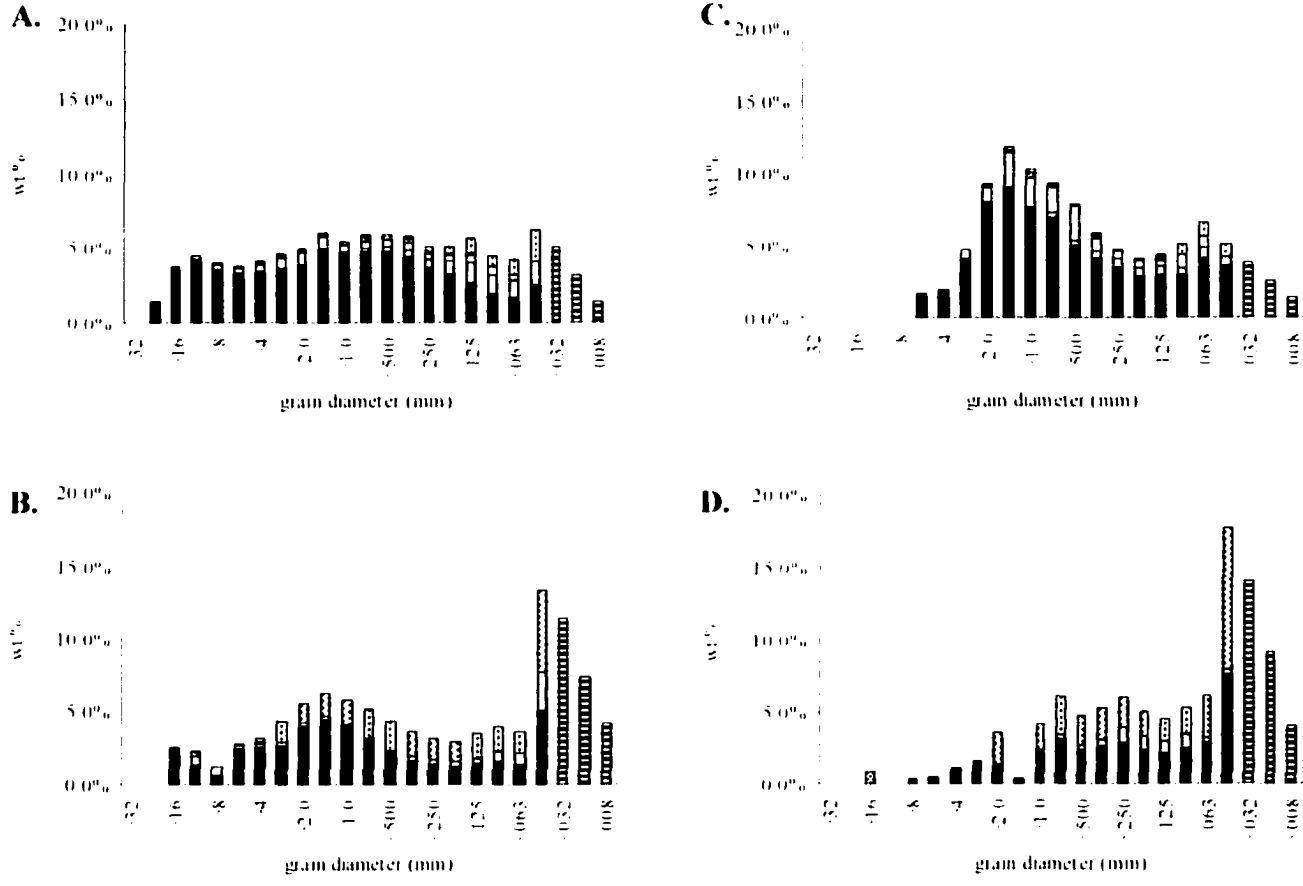

Figure 41. Modal and component analysis of the S3 surge deposit form Localities 99, 6, 12, and 1 (A, B, C, D, respectively).

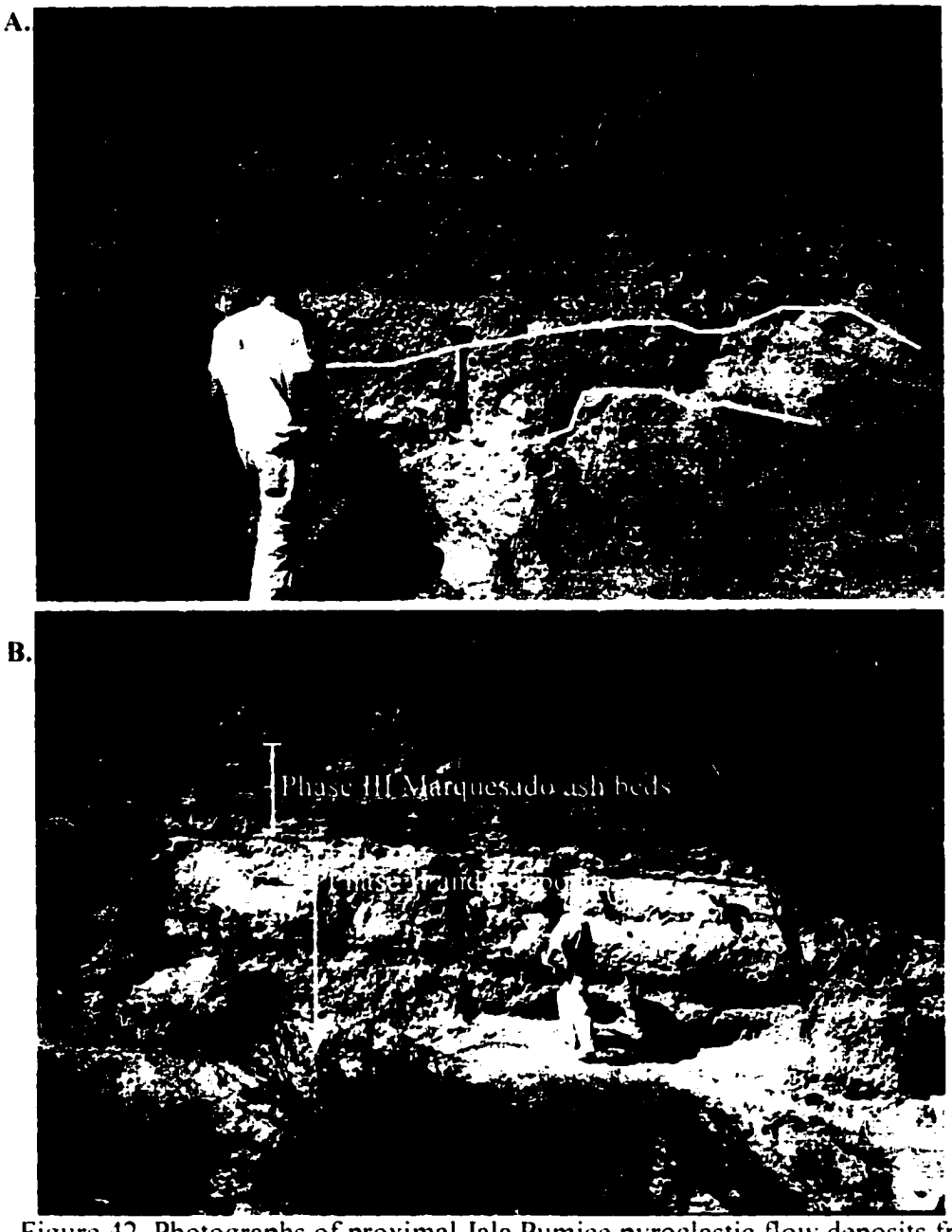

Figure 42. Photographs of proximal Jala Pumice pyroclastic flow deposits from Phase III at Localities 52 and 112 (A and B, respectively). Thinly bedded ash deposits on the southeast flanks resemble Marquesado and North-Flank PFD's in overall lithic content, Sierra Madre lithic content, pumice types, and stratigraphy. A. Proximal Marquesado ash beds at Locality 52; and B. the continuance of Phase III ash beds across the southern and eastern flanks of Ceboruco atop the Phase I and II stratigraphy. Note that these ash beds are also distinctly rust-color compared to the lighter-colored Phase I and II deposits.

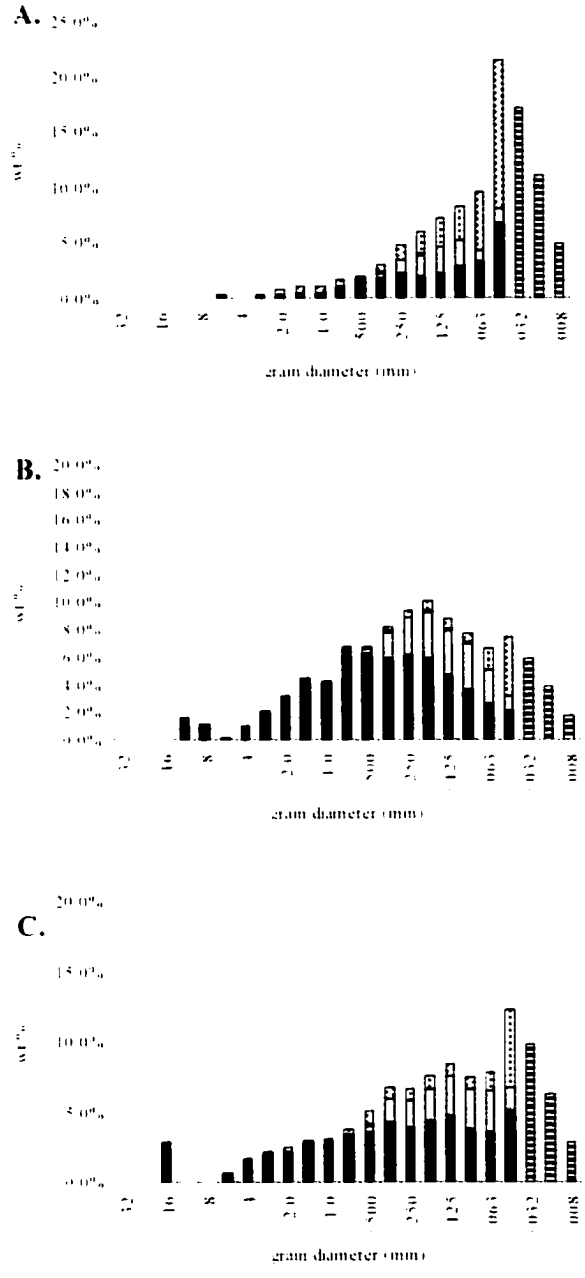

Figure 43. Modal and component analysis of the top massive (A), middle planar-bedded (B), and lower planar-bedded (C) units of proximal Marquesado pyroclastic flow deposits from Locality 52.

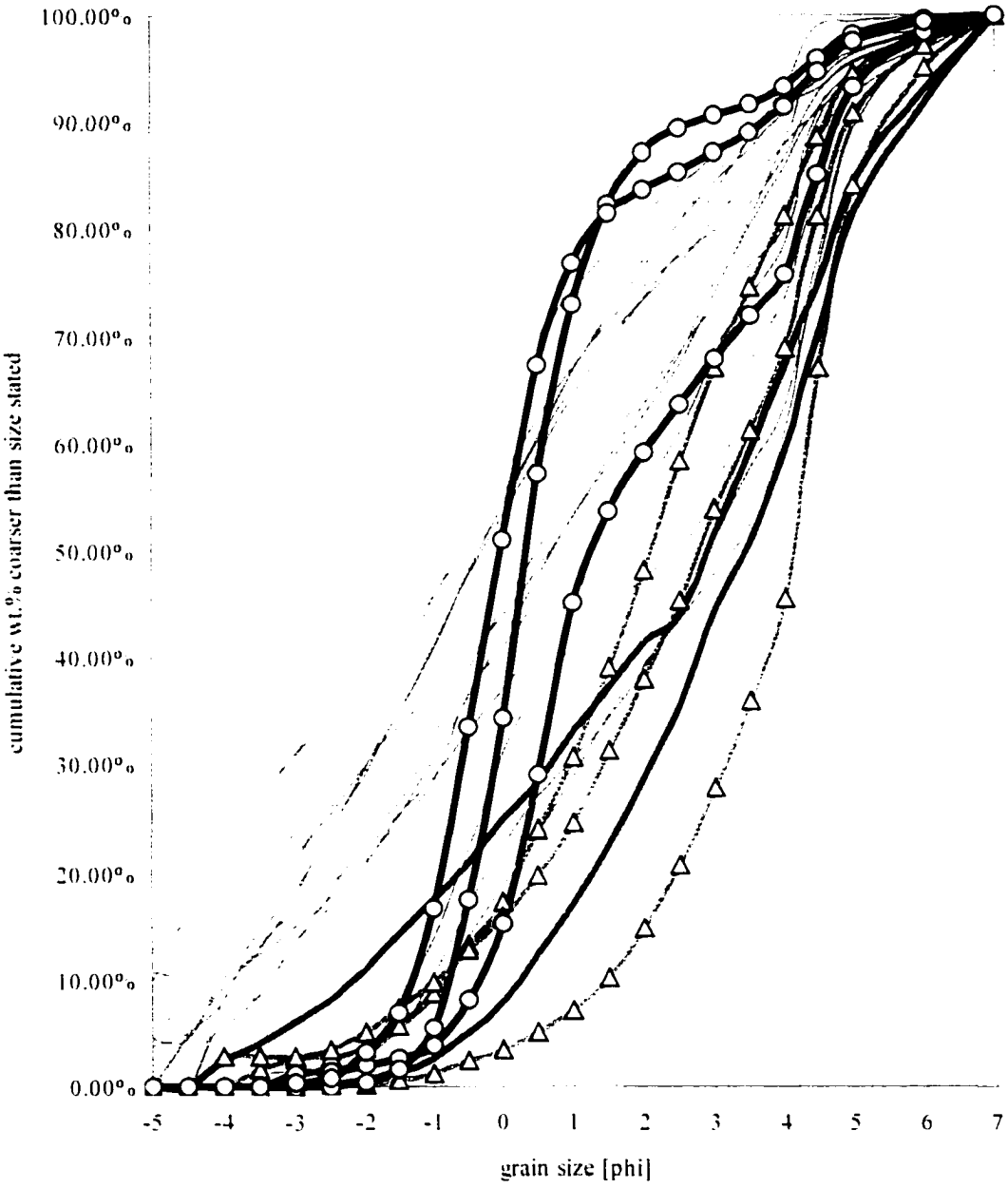

Figure 44. Cumulative curves of medial Marquesado flow and lag breccia deposits (solid thin), distal Marquesado flow deposits (solid bold), proximal Marquesado deposits (bold with open-triangle pattern), with superimposed distal co-ignimbrite fall layers (bold with open-circle pattern).

Figure 45. Photograph of the Marquesado pyroclastic flow cliffs with highlighted zones of basal lag breccia to the southwest of Ceboruco at Locality 53. Cliffs in this region are made up of at least three flow layers(1, 2, and 3), each between 7-10 m thick.

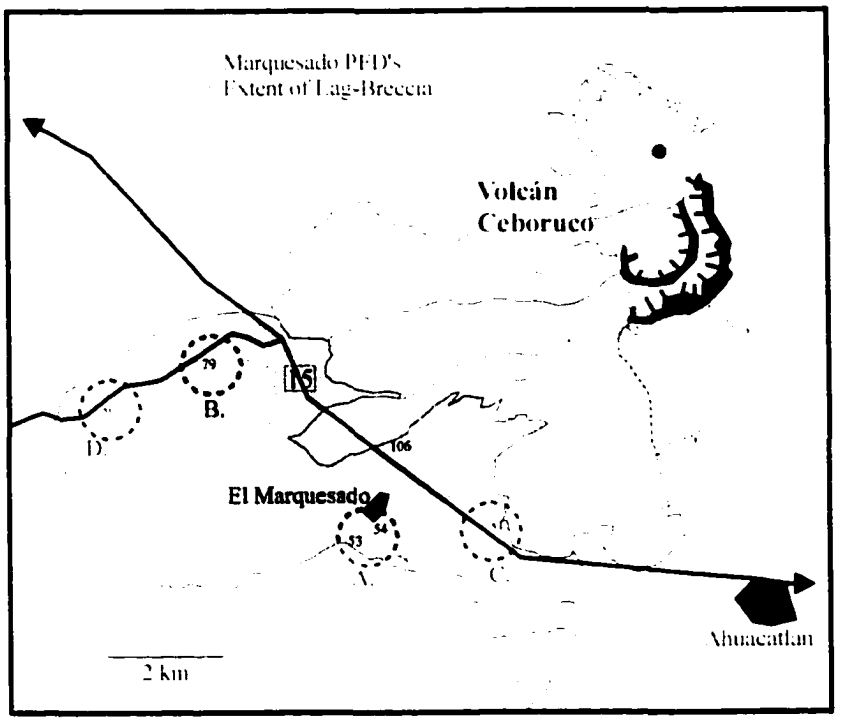

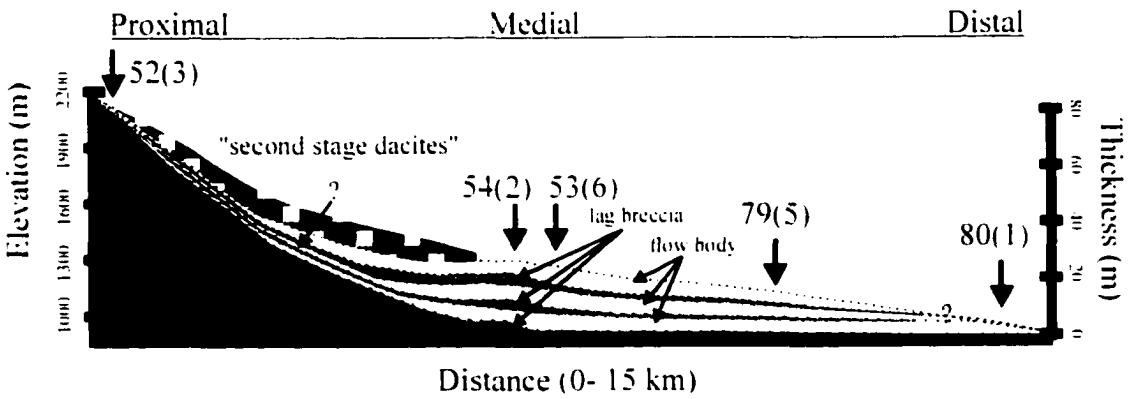

Figure 46. Modified from Nelson (1980), map of the Marquesado flow deposits, with extent of basal lag breccia (shaded) and locations of samples analyzed (dashed circles) (top), and generalized proximal-to-distal cross-section of Marquesado deposits (base). Arrows indicate Location number with the number of samples collected in parenthesis.

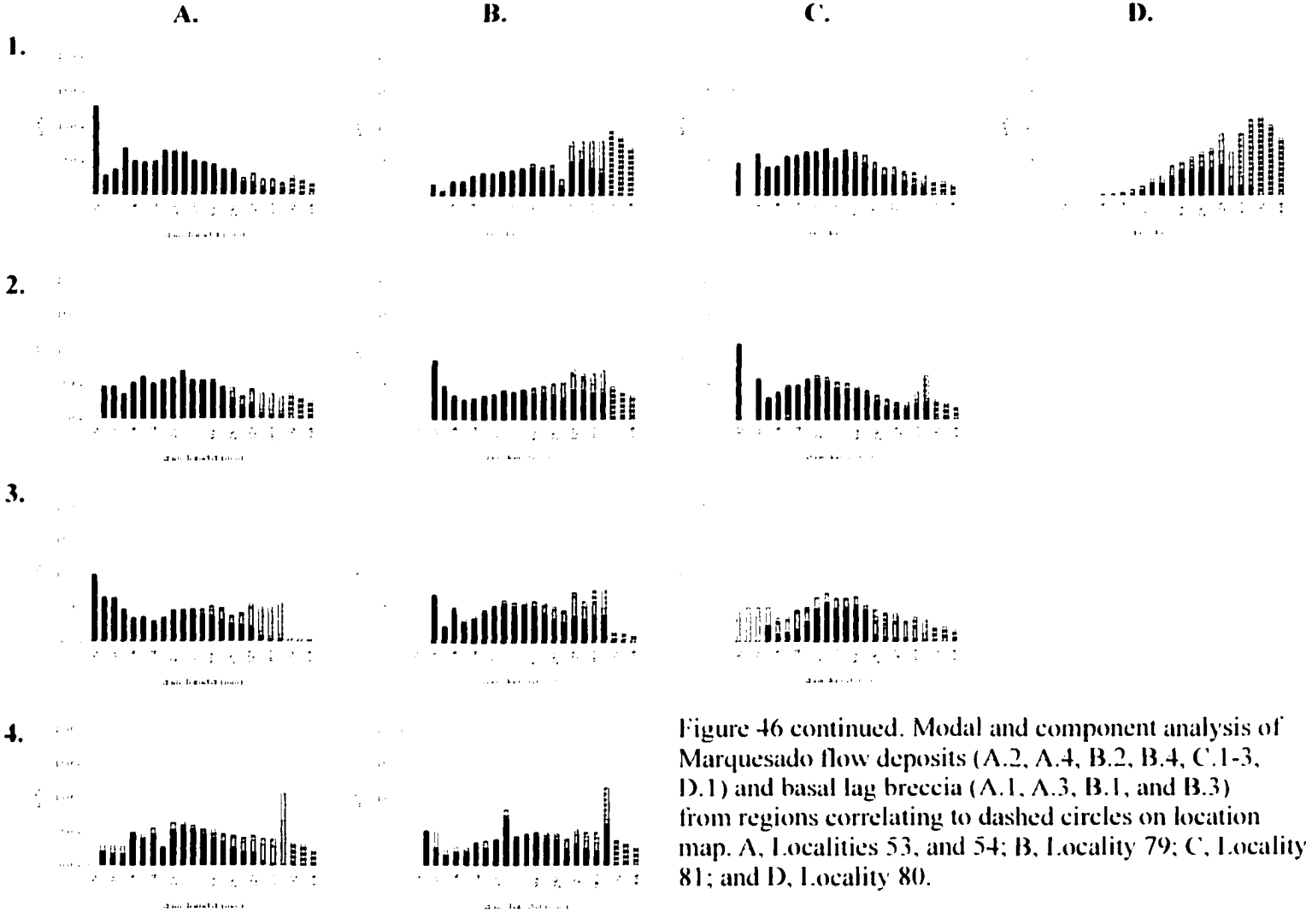

Figure 46 continued. Modal and component analysis of Marquesado flow deposits (A.2, A.4, B.2, B.4, C.1-3, D.1) and basal lag breccia (A.1, A.3, B.1, and B.3) from regions correlating to dashed circles on location map. A, Localities 53, and 54; B, Locality 79; C, Locality 81; and D, Locality 80.

Figure 47. Photograph of Marquesado basal lag breccia at Locality 54, with 1.5 m staff for scale in center. At this distance (~6 km), lag-breccia units are typically > 4 m thick, and lithic blocks in the breccia are non-graded, angular, and measure up to 180 cm in diameter. Modal analysis of lag breccia matrix indicates that it is identical to the upper portion of Marquesado deposits ("flow body" layer).

Figure 48. Composite photographs of the Marquesado flow and lag breccia sequence of deposits ~9 km from vent (Locality 79). Note that lag breccia deposits at this distance are normally graded, thinner (< 2 m), and contain smaller (< 20 cm), subrounded lithic clasts.

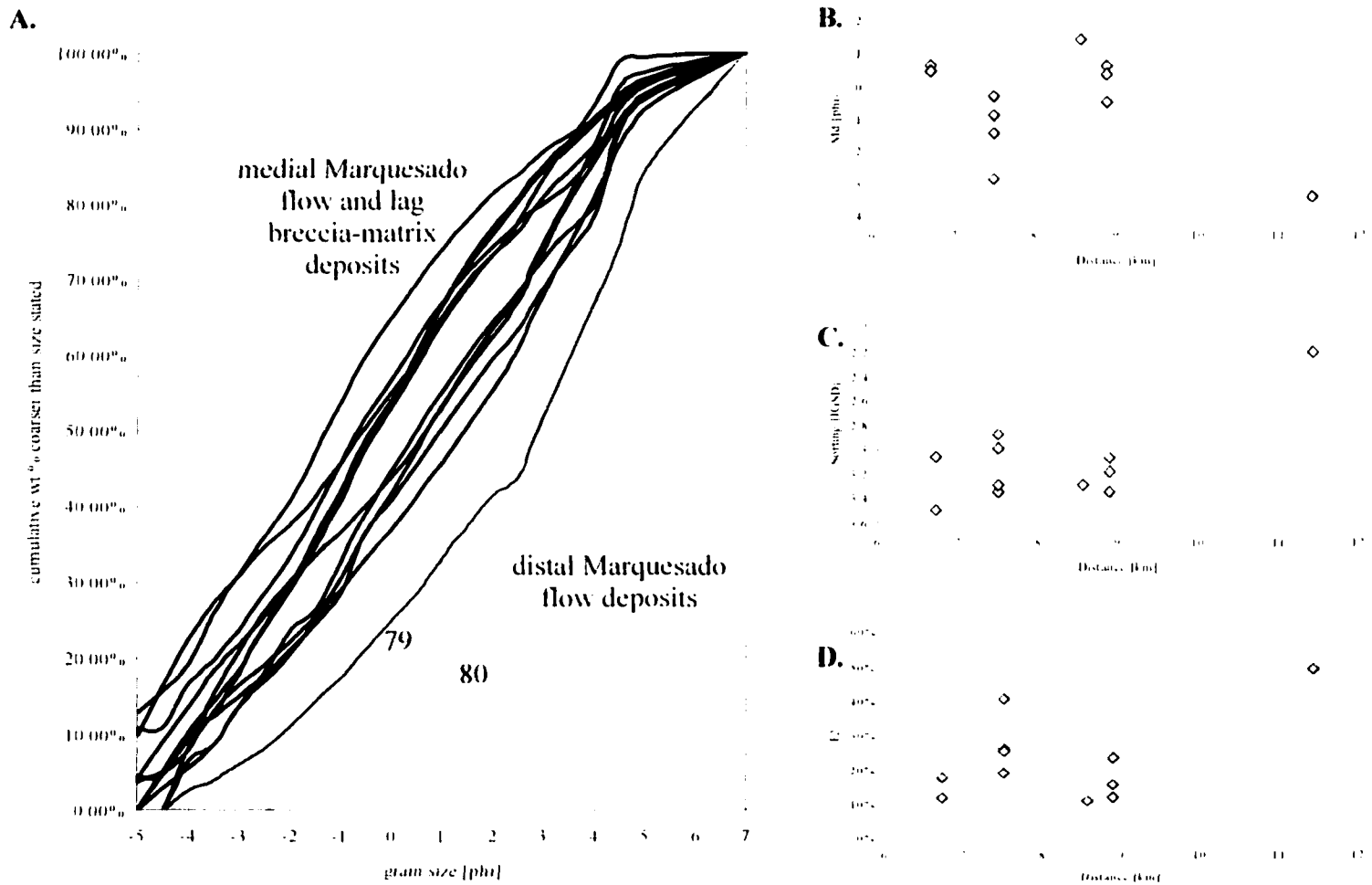

Figure 49. Granulometric analysis of medial and distal Marquesado flow deposits, including cumulative curves (A), and Md, sorting, and F2 with distance (B, C, and D, respectively). Medial deposits are poorly sorted, and relatively ash-poor for both lag breccia matrix and flow body samples. Distal deposits contain more fines and are better sorted.

Figure 50. Photograph of the peripheral Marquesado series of deposits where the basal lag breccia is absent with thin, nearly clast-supported beds of pumice lapilli in between flow 1 and 2, and 2 and 3 (from Locality 81). Component and modal analysis of these deposits are identical to samples of lag-breccia matrix and in samples above basal lag-breccia units (see Figure 46). Also, note that this Marquesado deposit sequence is the most eastern off all Marquesado PFD's observed, and that it contains 2 thin beds (< 10 cm) of clast supported pumice lapilli. Field inspection of these layers show strong resemblance to the P5 and P6 fall layers, however, definitive correlation to these Phase III fall layers is not possible.

Figure 51. Photograph of proximal North-Flank pyroclastic flow deposit sequence (F1, F2, F3, and F4) at Locality 12 (Note 2 m scale). North-Flank flow deposits steadily increase in thickness from F1 to F4, and progressively channel-fill previously emplaced deposits, especially for the largest flow unit, F4.

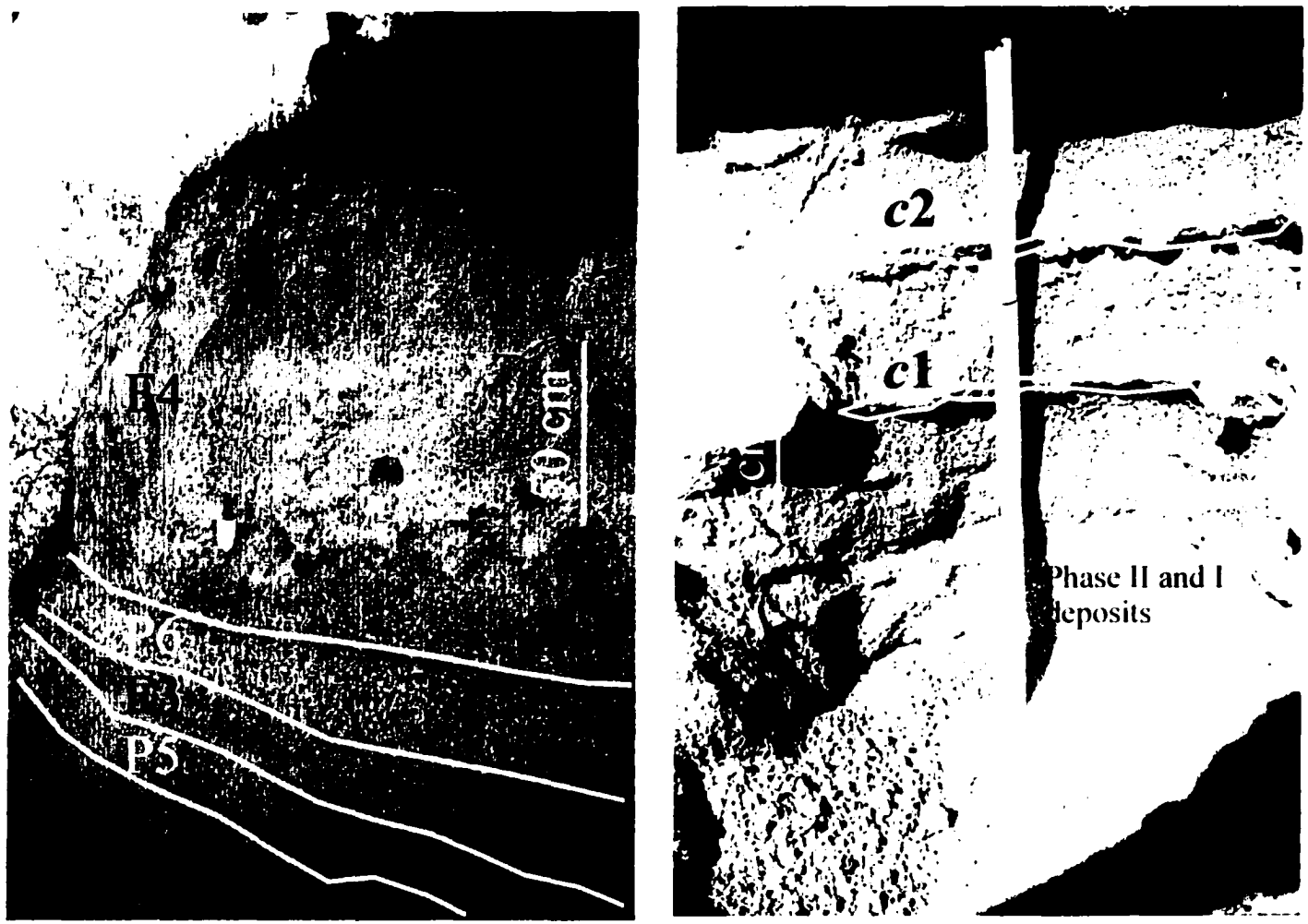

Figure 52. Photographs of of the proximal North-Flank flow deposits (F2, F3, and F4) interbedded with the P5 and P6 fall layers (left), and distally, the *c*1 and *c*2 co-ignimbrite fall layers interbedded with the P5 and P6 fall layers (right).

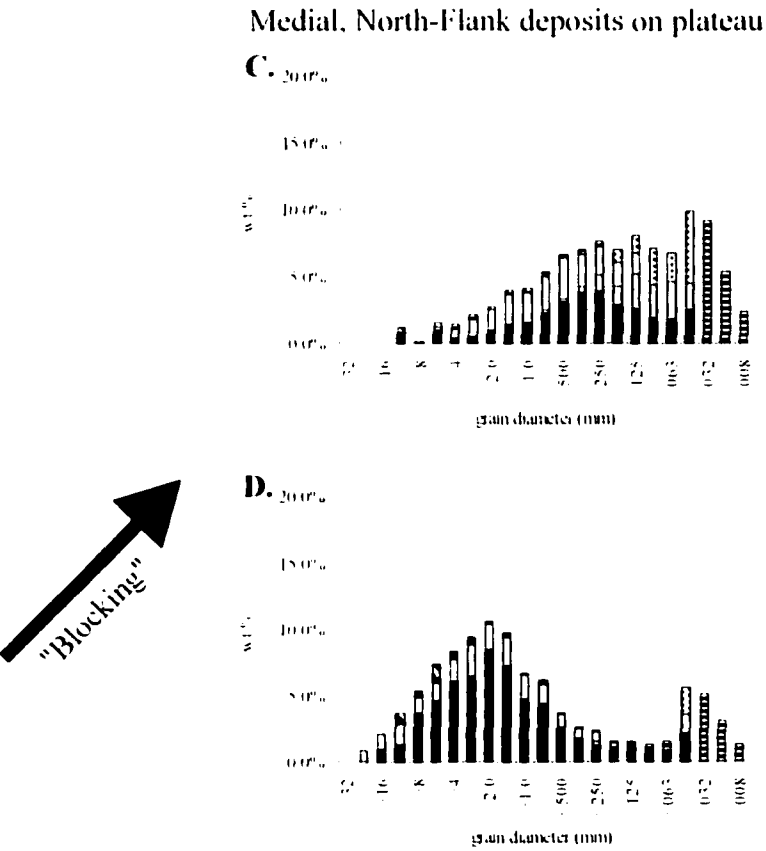

Figure 53. Modal and component analysis of North-Flank flow deposits, including flank, proximal (A and B) deposits, and plateau, medial (C and D) deposits. Note the dramatic improvement in sorting and pumice content in the deposits atop the plateau compared to proximal deposits, resulting from topographic blocking.

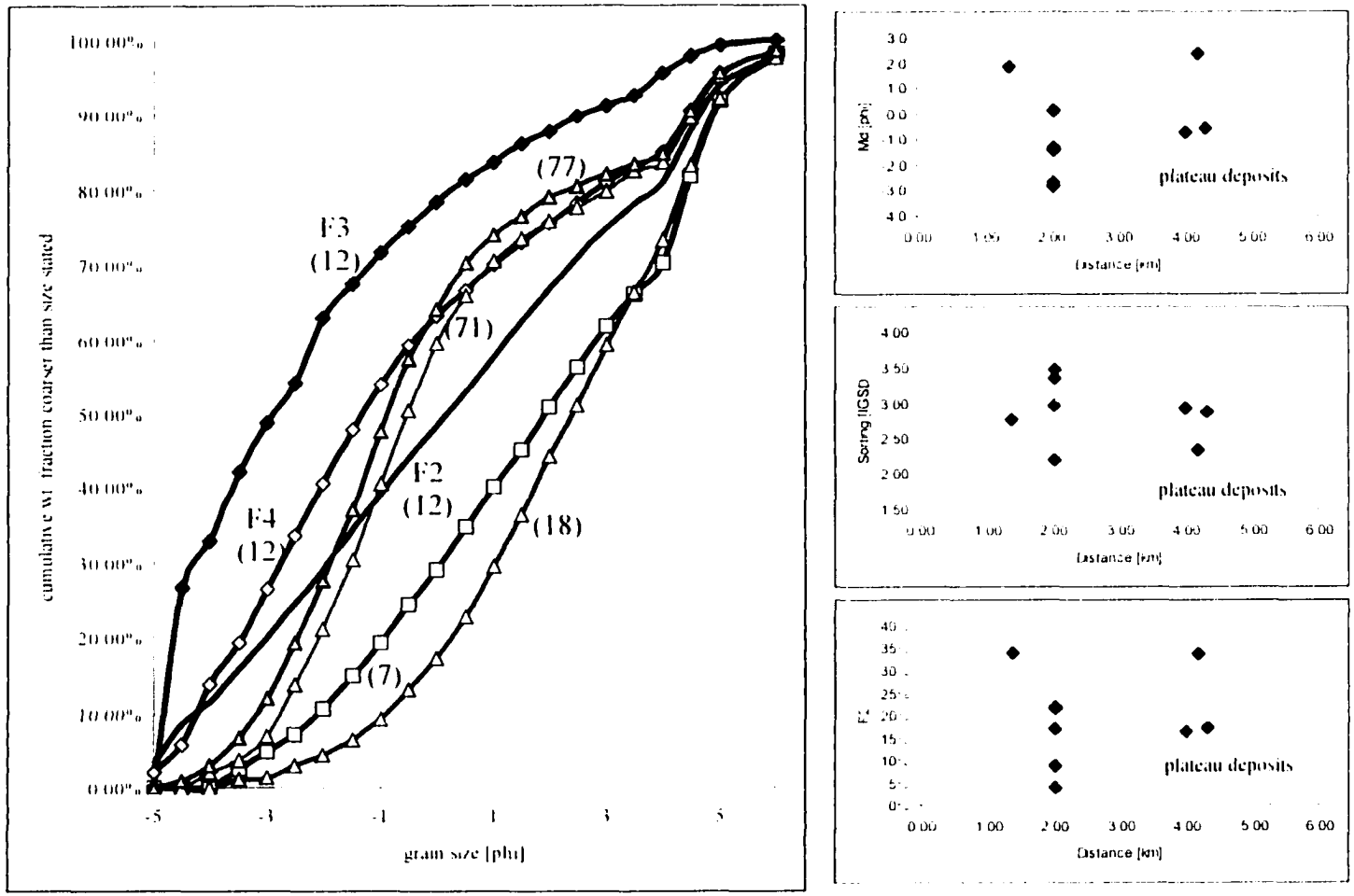

Figure 54. Granulometric analysis of proximal and medial North-Flank flow deposits, including cumulative curves (A), and Md, sorting, and F2 with distance (B, C, and D, respectively).

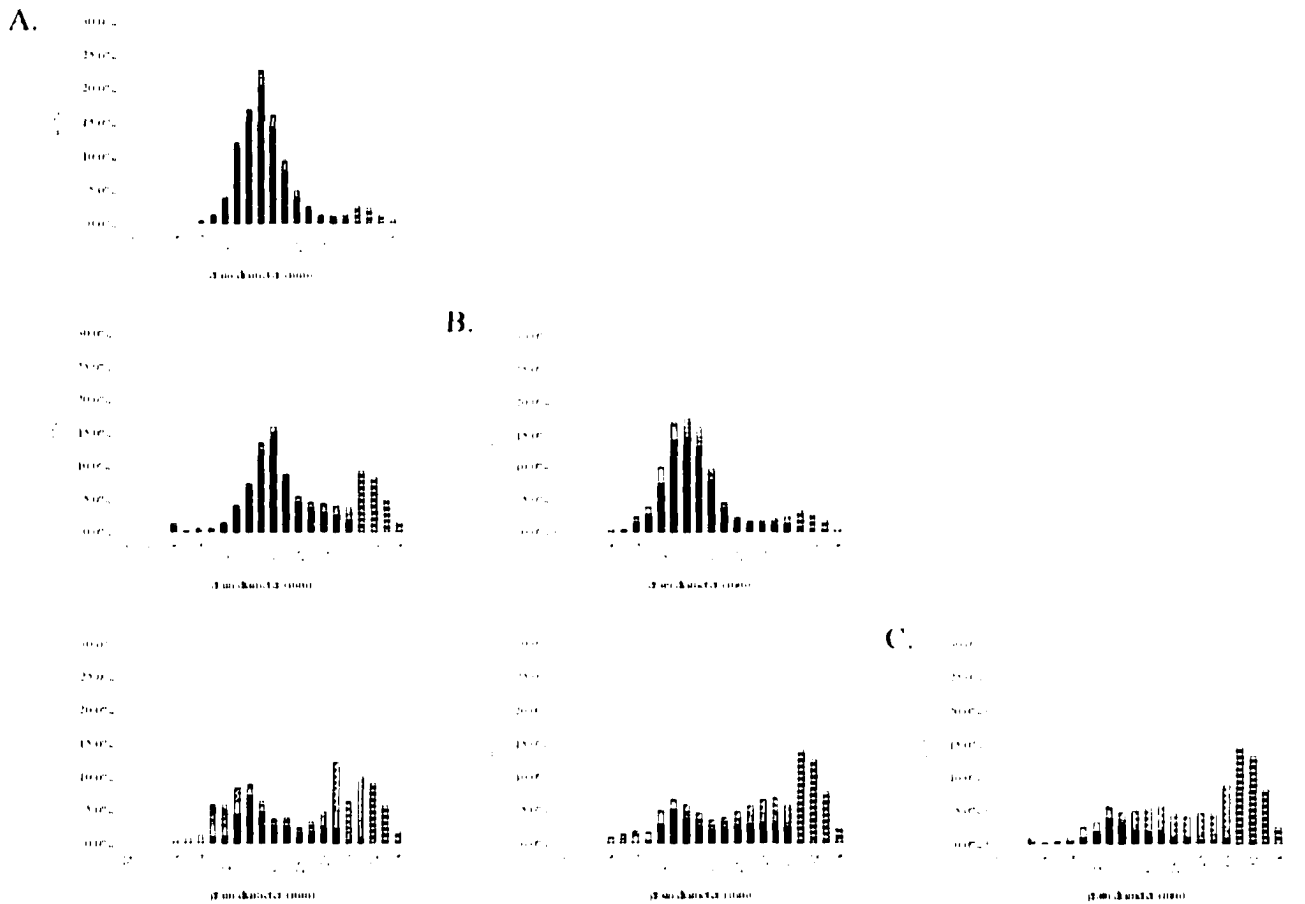

Figure 55. Modal and component analysis of the *c*1, and *c*2 co-ignimbrite fall layers from Localities 65 (A, from top: *c*3 ?, *c*2, and *c*1), 67 (B, from top: *c*2, *c*1), and 68 (C, *c*1). Note the consistently poorer sorted nature of the *c*1 fall unit, compared to the *c*2 and *c*3 units. The significance of the *c*3 layer remains unclear, for is only observed at Locality 65.

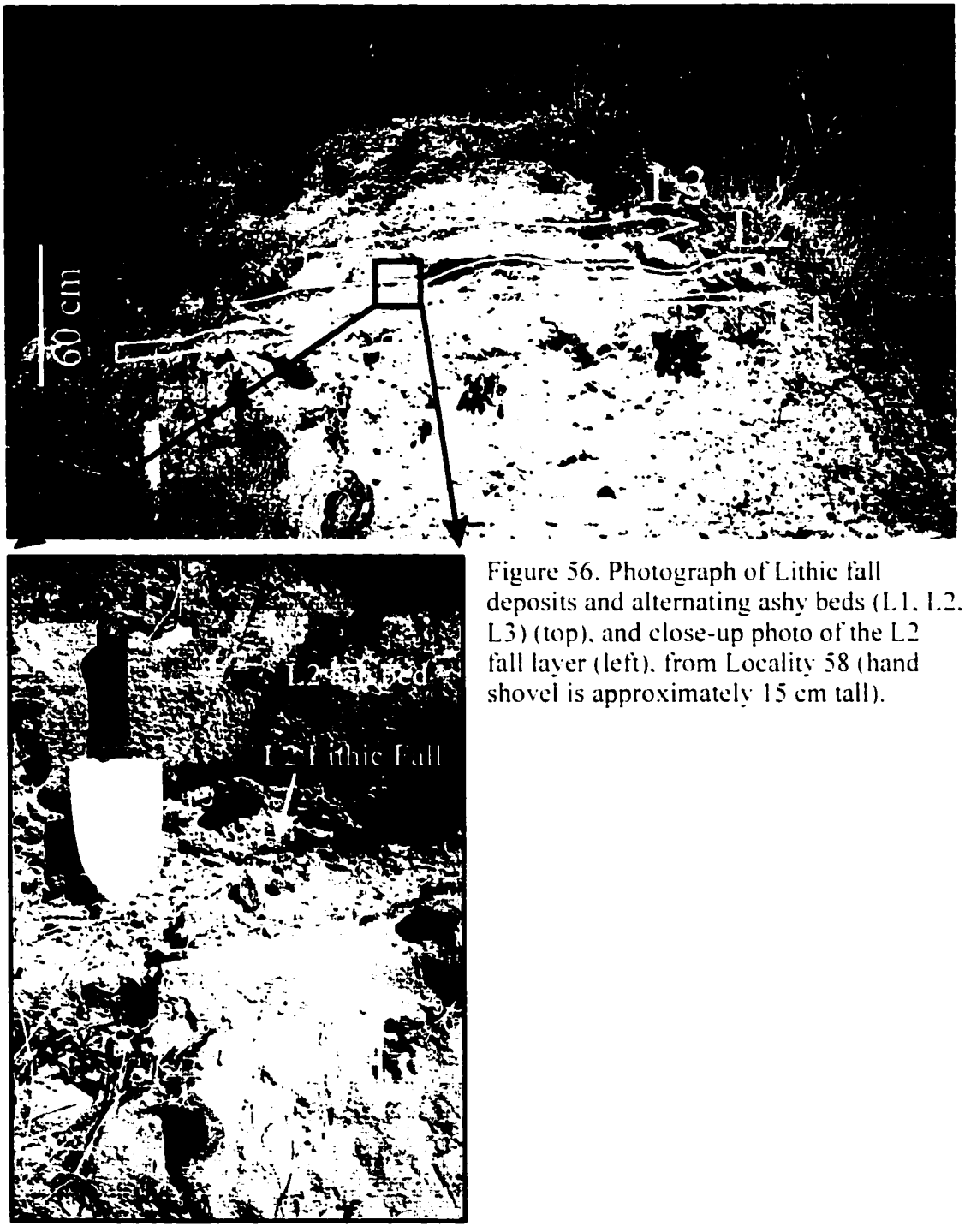

Figure 56. Photograph of Lithic fall deposits and alternating ashy beds (L1, L2, L3) (top), and close-up photo of the L2 fall layer (left), from Locality 58 (hand shovel is approximately 15 cm tall).

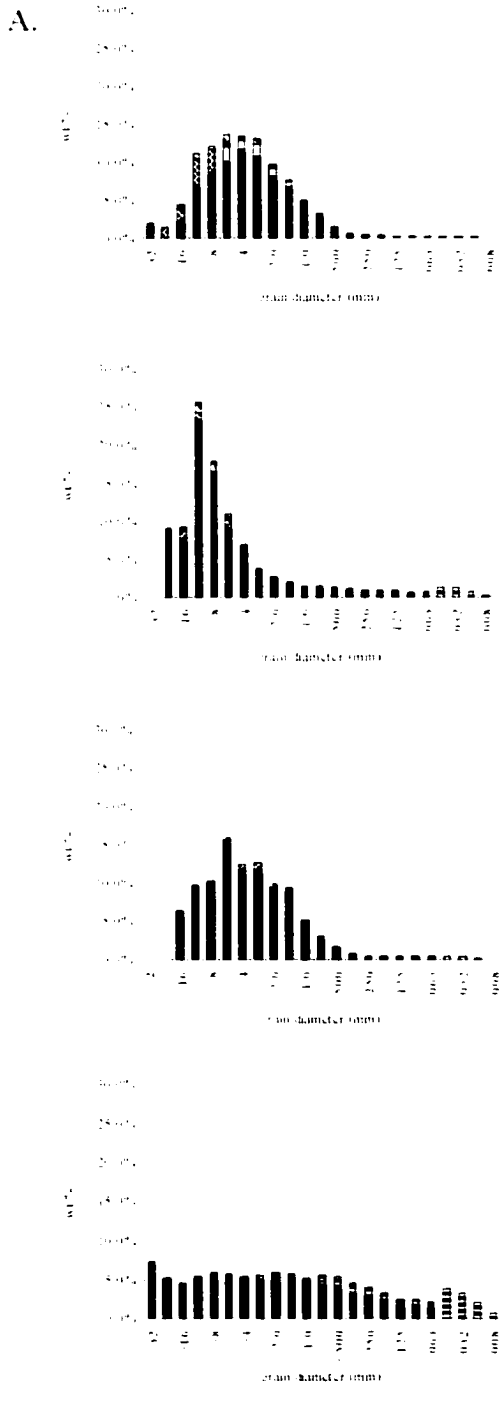

Figure 57. Modal and component analysis of the Lithic fall (A, from top: Localities 58, L3; 12, L2; 112, L2;and, 109, L1) and alternating ashy beds (B, from top :Localities 58 and 12). In addition to the anomalously high lithic content (> 85 wt.%), note the variability in sorting from one fall deposit to another, which suggests a ballistic source rather than sedimentation from an umbrella region of a plume.

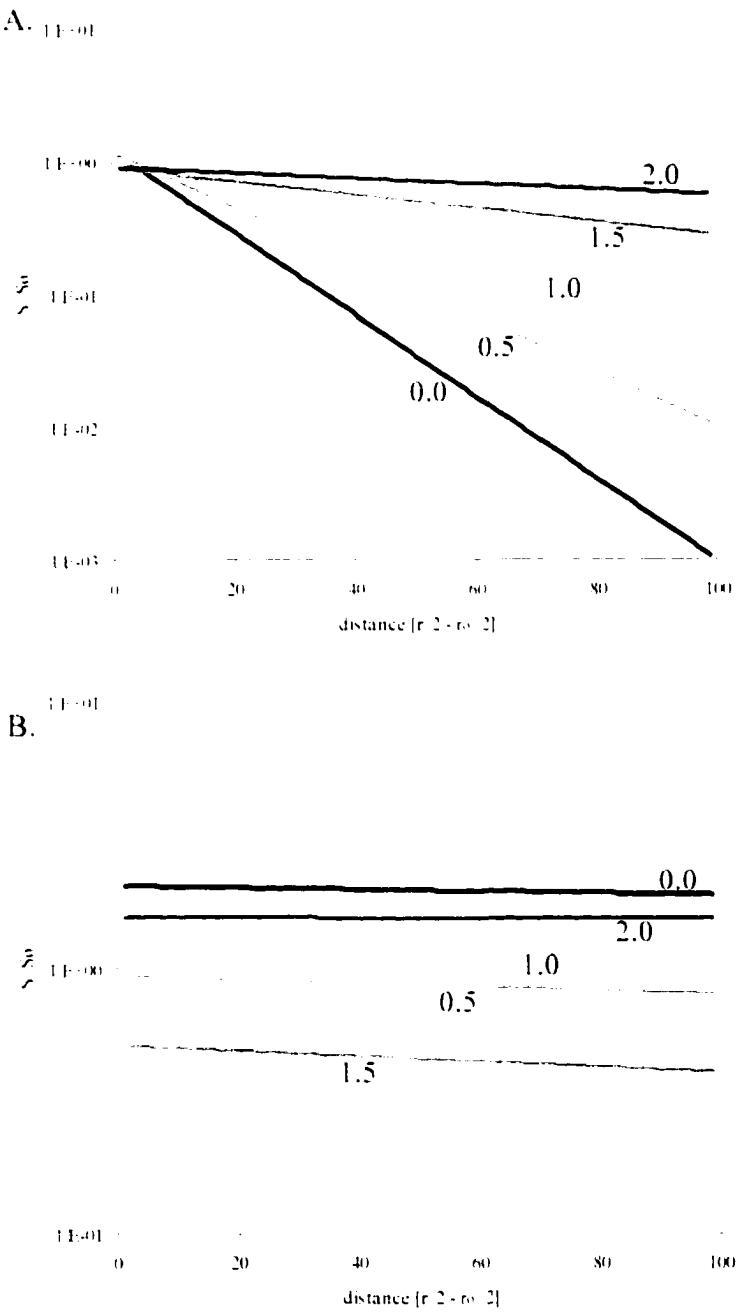

Figure 58. Idealized dilute (A) and *en masse* (B) sedimentation of particles (S/S_o) of different grain sizes with increasing distance from the plume corner (r_o) or from a point designated as the first in a lateral profile, described by the model of Sparks (1991) and Bursik et al. (1992a). Grain sizes 0.0 to 2.0 phi are indicated adjacent to corresponding mass accumulation trends.

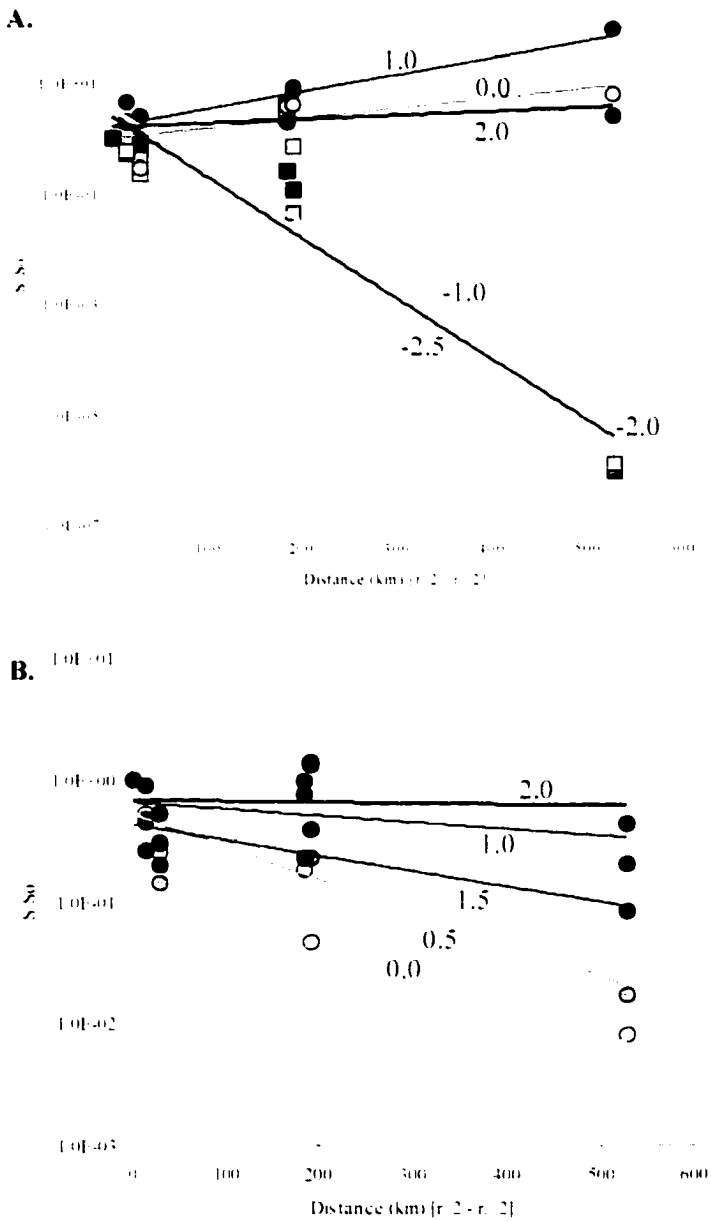

Figure 59. Mass accumulation values for lithic (A) and crystal (B) particles, with distance for the base of the P1 fall layer (S_0 = sample from Locality 18). Note that despite the exponential decrease in the coarsest-grained lithics, the general patterns for lithic sedimentation are somewhat erratic, whereas sedimentation of crystals exponentially decreases with distance. Thus, the distribution of crystal mass with distance reflects particle transport and deposition from a dilute and turbulent low-particle concentration density current. Grain sizes for lithic (-2.5 to 2.0) and crystal particles (0.0 to 2.0) are indicated adjacent to corresponding mass accumulation trends.

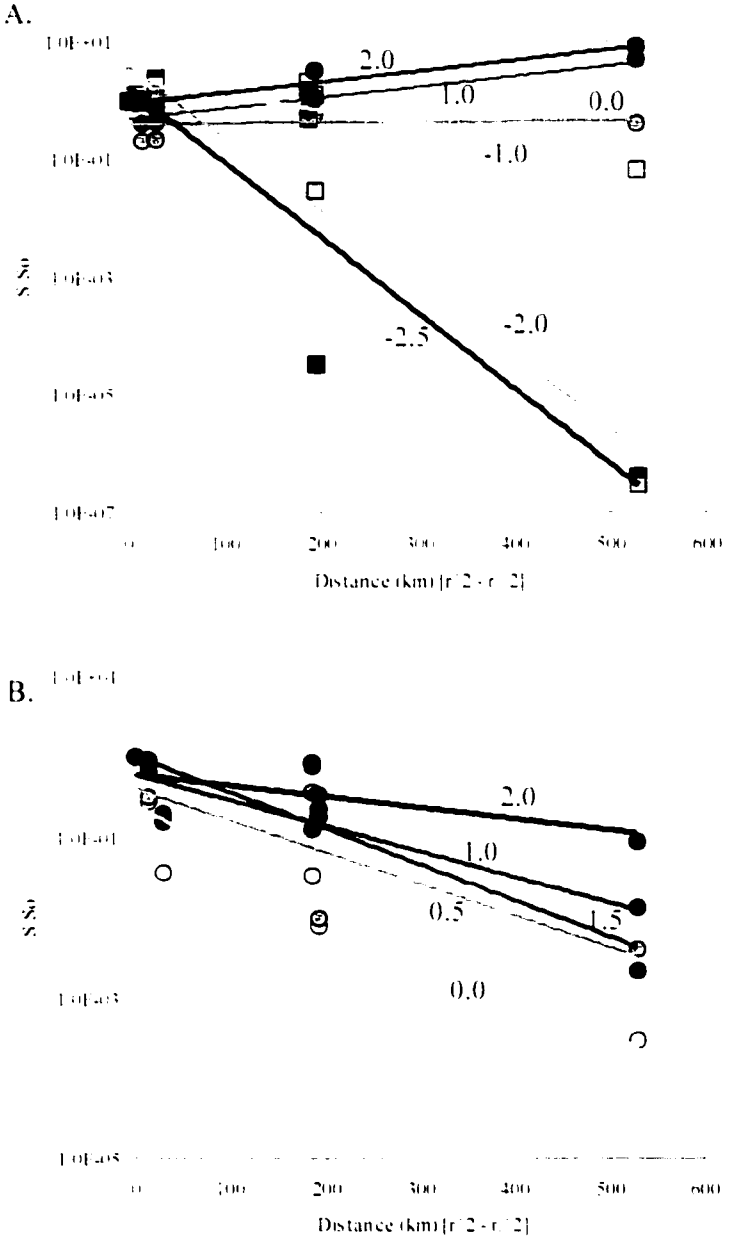

Figure 60. Mass accumulation values for lithic (A) and crystal (B) particles with distance for the top of the P1 fall layer (S_n = sample from Locality 18). Note that patterns for lithic sedimentation continue to be somewhat erratic, whereas sedimentation of crystals exponentially decreases with distance. Thus, the distribution of crystal mass with distance reflects particle transport and deposition from a dilute and turbulent low-particle concentration density current. Grain sizes for lithic (-2.5 to 2.0) and crystal particles (0.0 to 2.0) are indicated adjacent to corresponding mass accumulation trends.

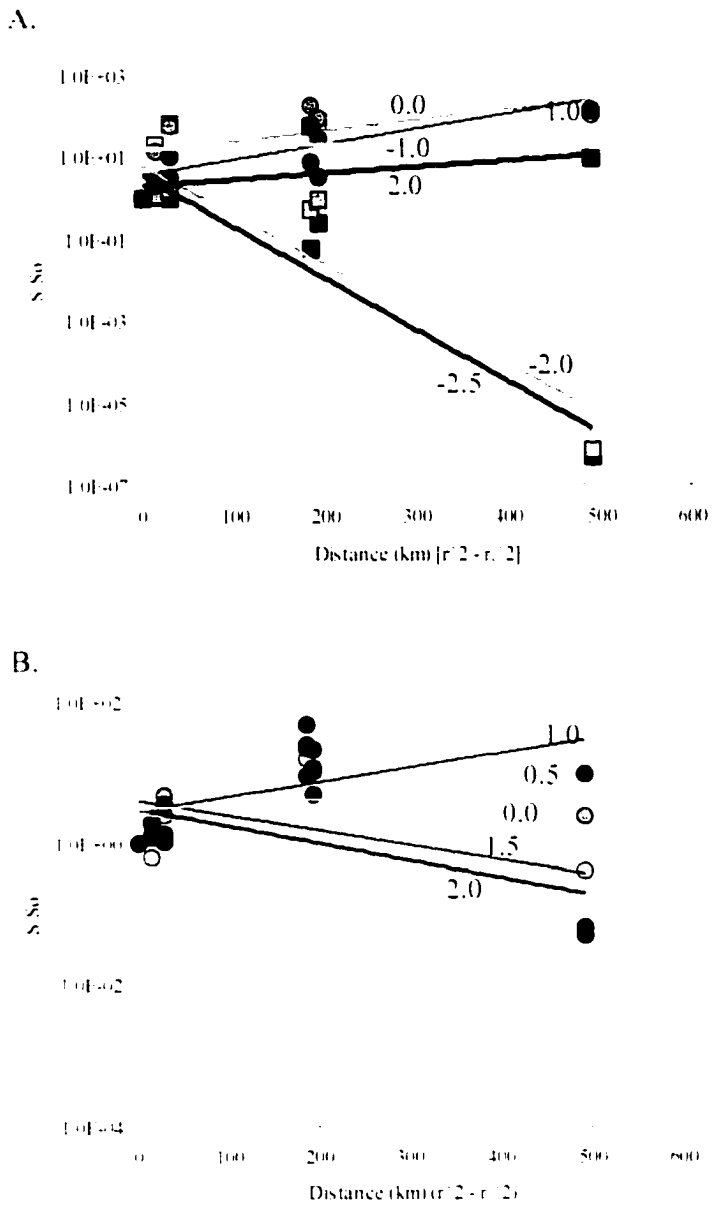

Figure 61. Mass accumulation values for lithic (A) and crystal (B) particles with distance from the lithic-rich base of the P2 fall layer (S_0 = P2 sample from Locality 18). Note that patterns for lithic and crystal sedimentation in this case are both erratic. However, if sample Localities 18, 50, and 1 are considered to reflect convective sedimentation, because they are located ~6 km or less from the eruptive vent, thus inside the plume corner, and are removed from the calculations, the sedimentation of lithic and crystal particles drastically improve (C and D).

C.

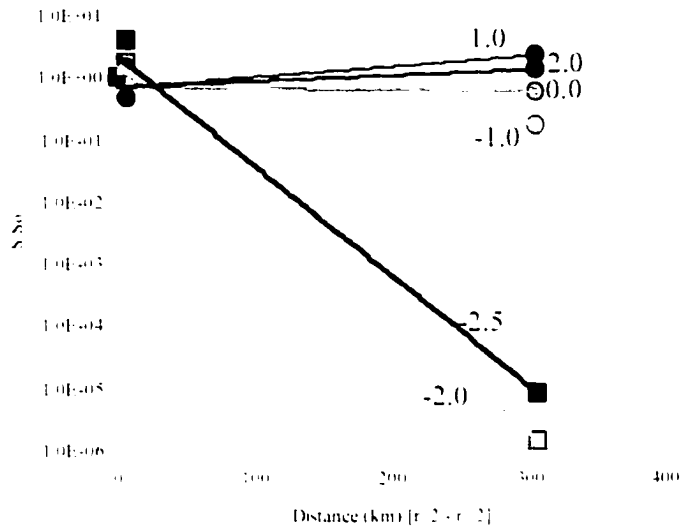

D.

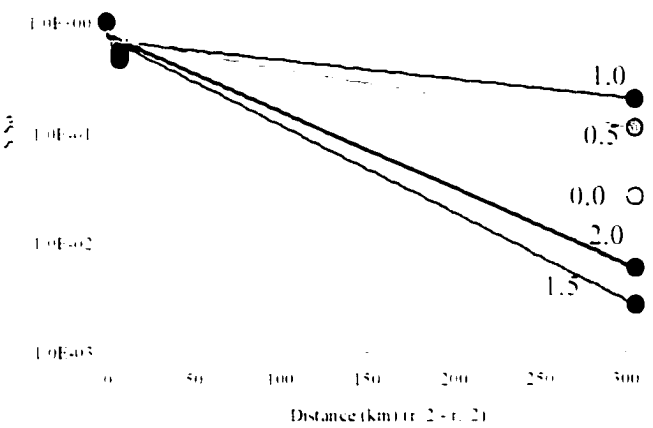

Figure 61 continued. From these localities, the distribution of crystal mass with distance reflects particle transport and deposition from a dilute and turbulent low-particle concentration density current. See text for additional discussion. Grain sizes for lithic (-2.5 to 2.0) and crystal particles (0.0 to 2.0) are indicated adjacent to corresponding mass accumulation trends.

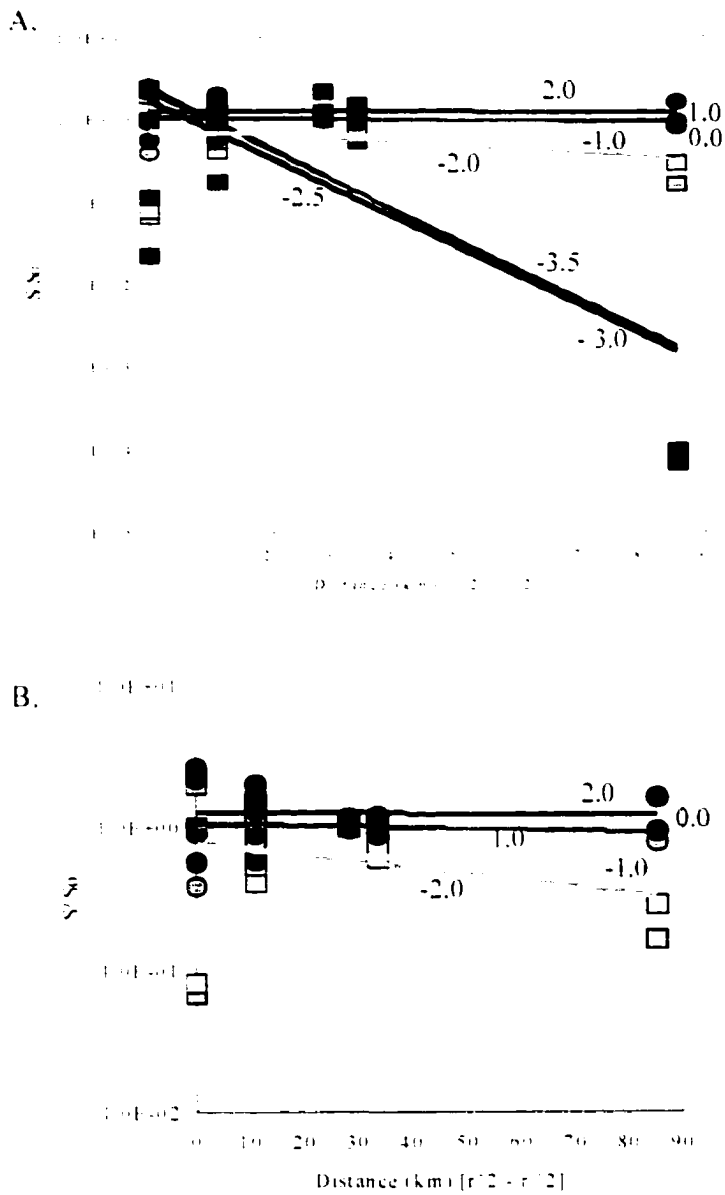

Figure 62. Mass accumulation values for lithic (A) and crystal (B) particles with distance from the Marquesado flow deposits. Whereas the coarsest lithic clasts do exhibit exponential sedimentation, the remaining lithic clasts and crystals display a somewhat random distribution in mass accumulation values. Best-fit curves for each grain-size is subhorizontal, which reflects *en masse* freezing from a high-particle concentration density current. The poor correlation of data points, however, suggests that transport and deposition of particles was not purely *en masse* (S_0 = Locality 54). Grain sizes for lithic (-3.5 to 2.0) and crystal particles (0.0 to 2.0) are indicated adjacent to corresponding mass accumulation trends.

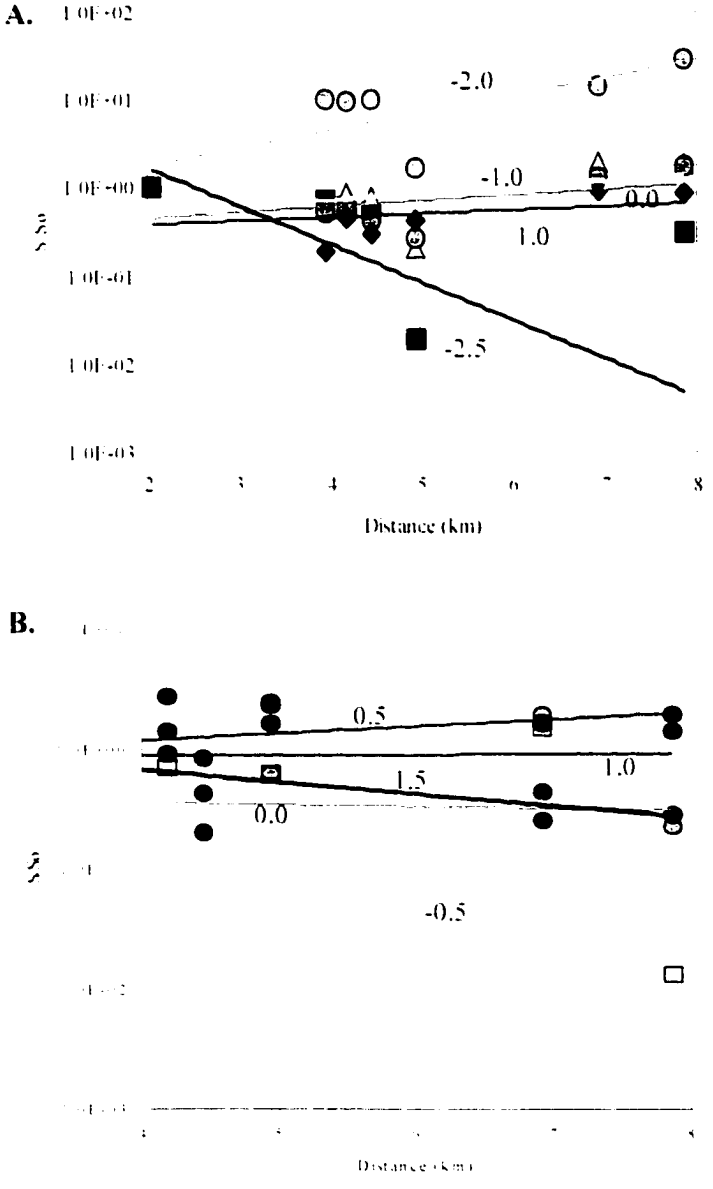

Figure 63. Mass accumulation of lithic (A) and crystal (B) particles from S1 deposits along the B-B' transect (S_0 = Locality 12). The erratic array of mass accumulation values for lithic and crystal particles in S1 suggest that the transport and deposition of material reflect neither perfect sedimentation from dilute and turbulent low-particle density currents, nor from *en masse* freezing from a high-particle concentration density current. To test if this may result from blocking at the plateau escarpment, S_0 values were replaced with the sample at Locality 18, which is on top of the plateau. Mass accumulation values for lithic and crystal particles from these calculations are shown in C and D, respectively.

C.

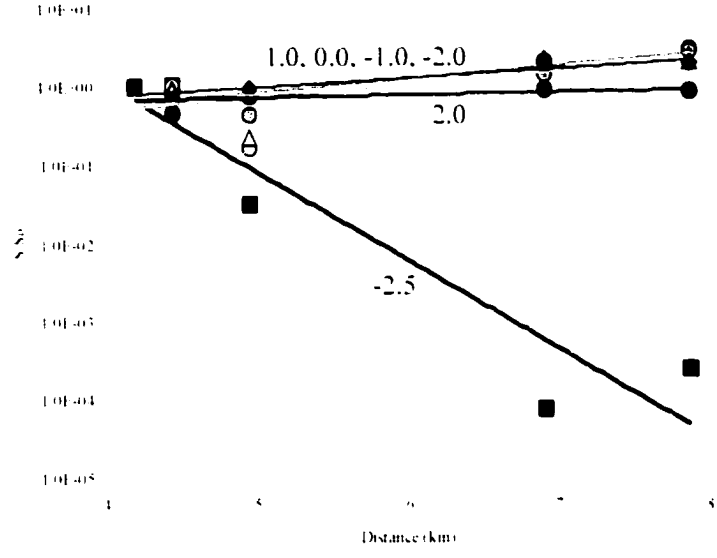

D.

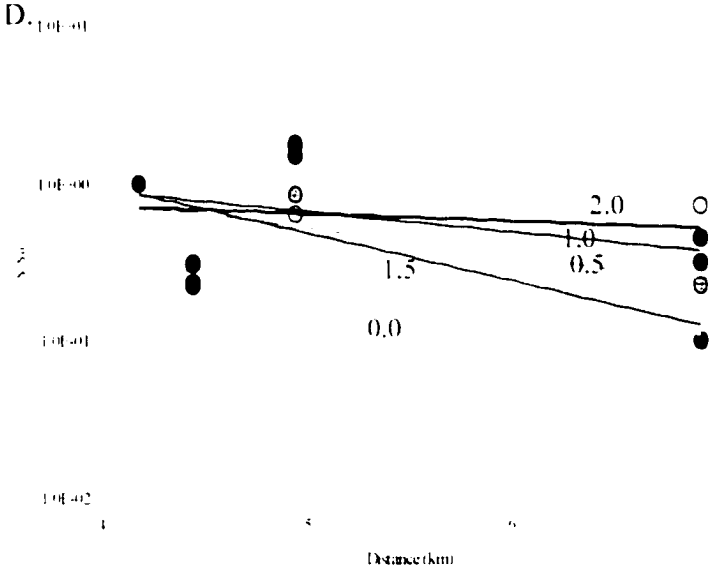

Figure 63 continued. Because mass accumulation values in these calculations remains erratic in nature, topographic blocking probably did not affect the transport and deposition of material in the S1 surge. Grain sizes for lithic (-2.5 to 2.0) and crystal particles (0.0 to 2.0) are indicated adjacent to corresponding mass accumulation trends.

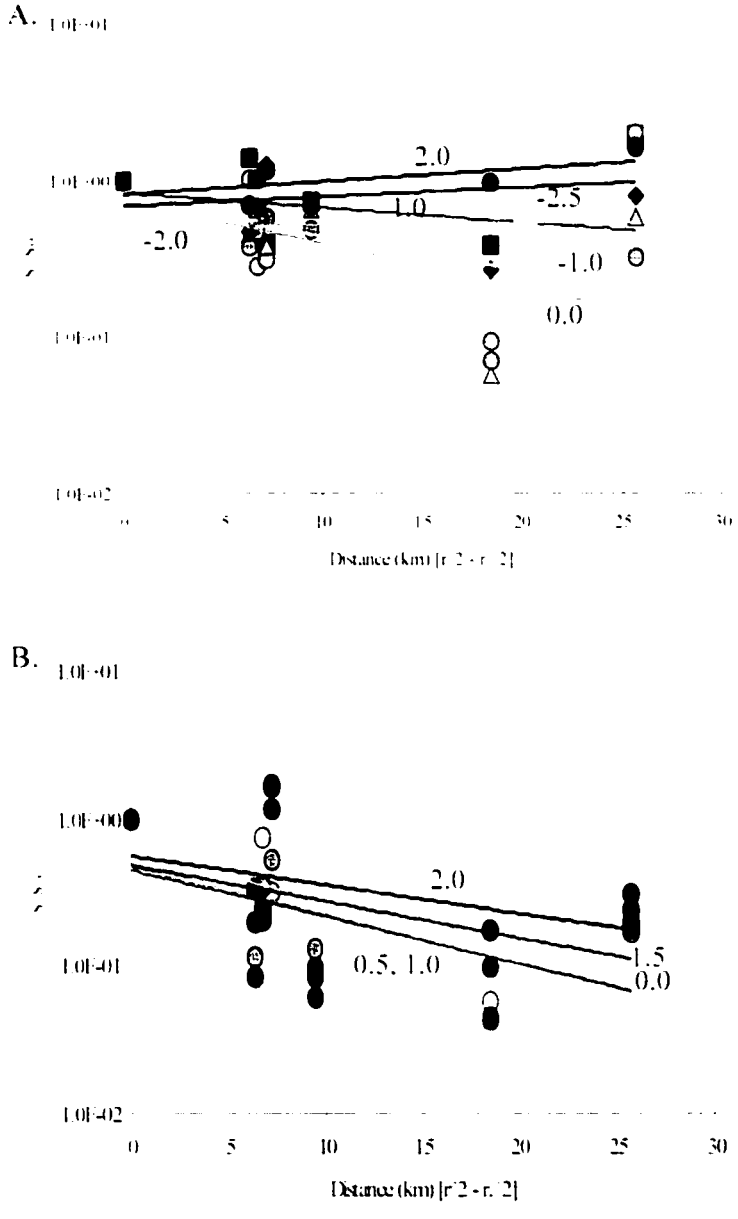

Figure 64. Mass accumulation values for lithic (A) and crystal (B) particles from S2 surge deposits along the A-A' transect (S_2 = S2 sample from Locality 7). In both cases, although the coarsest lithic clasts do exhibit exponential sedimentation, the majority of the lithic clasts and crystals display somewhat erratic mass accumulation patterns that appear to reflect neither *en masse* freezing from a high-particle concentration density current nor via turbulent suspension. Grain sizes for lithic (-2.5 to 2.0) and crystal particles (0.0 to 2.0) are indicated adjacent to corresponding mass accumulation trends.

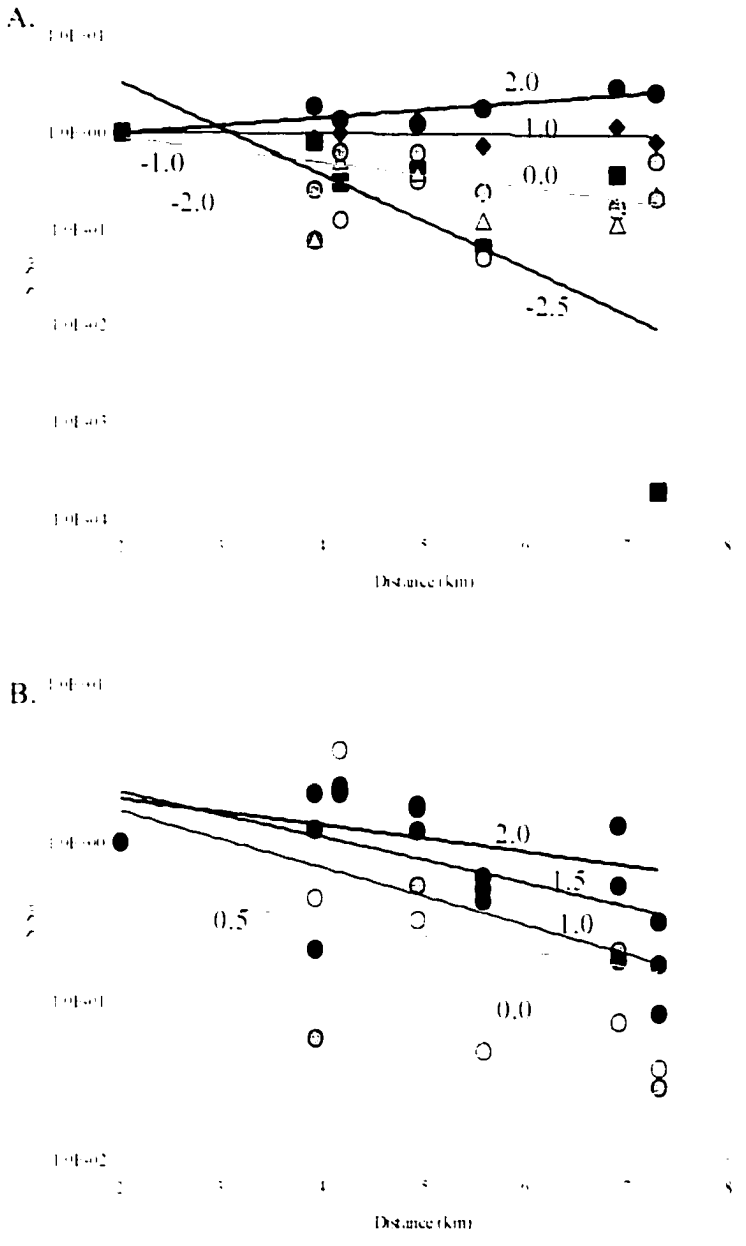

Figure 65. Mass accumulation values of lithic (A) and crystal (B) particles with distance for S2 surge deposits along the B-B' transect. To test whether the Sierra Madre cliff face may have had any affect on the S2 surge cloud (e.g. "blocking"). A and B present values for S2 particles with Locality 12 (on the northern flank) representing S_1, whereas figures C and D show S2 deposit values with Locality 18 (atop the plateau) representing S_2. Despite the erratic nature of the lithic particles in both calculations, the mass accumulation of crystals with distance improves dramatically when considering deposits at Locality 18 as representing S_2 rather than at Locality 12.

C.

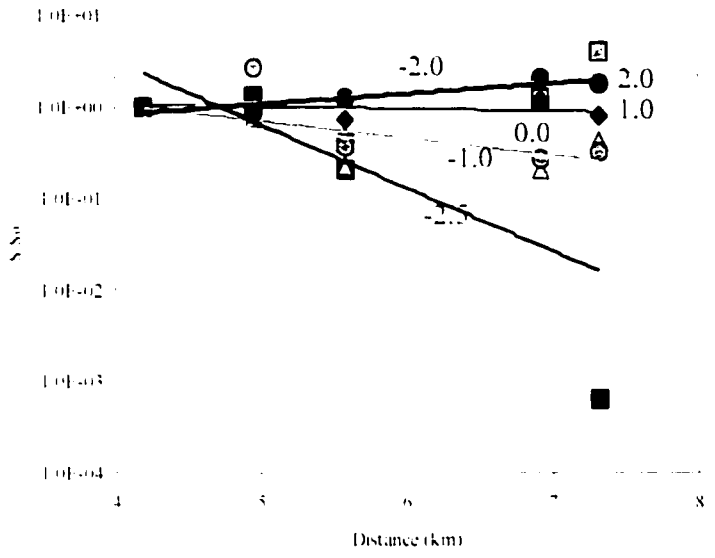

D.

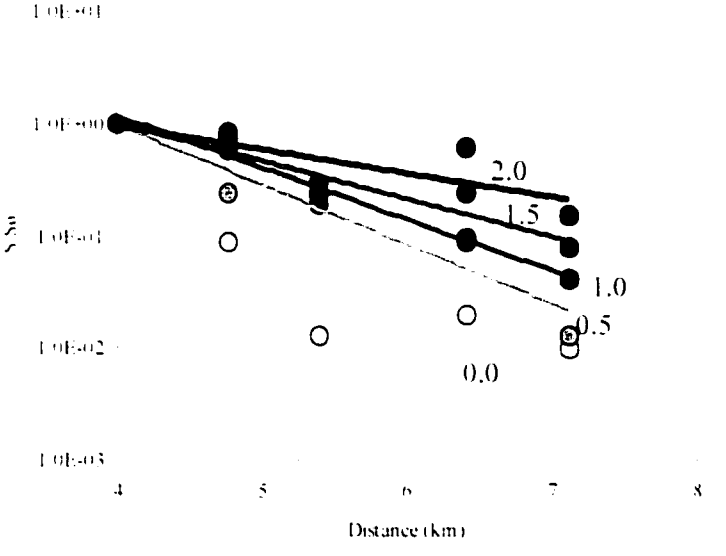

Figure 65 continued. This indicates that atop the plateau, sedimentation of particles from the S2 surge occurred predominantly via turbulent suspension. This is likely the result of topographic blocking of coarser-grained material that had accumulated at the base of the density current when S2 encountered the Sierra Madre escarpment. Grain sizes for lithic (-2.5 to 2.0) and crystal particles (0.0 to 2.0) are indicated adjacent to corresponding mass accumulation trends.

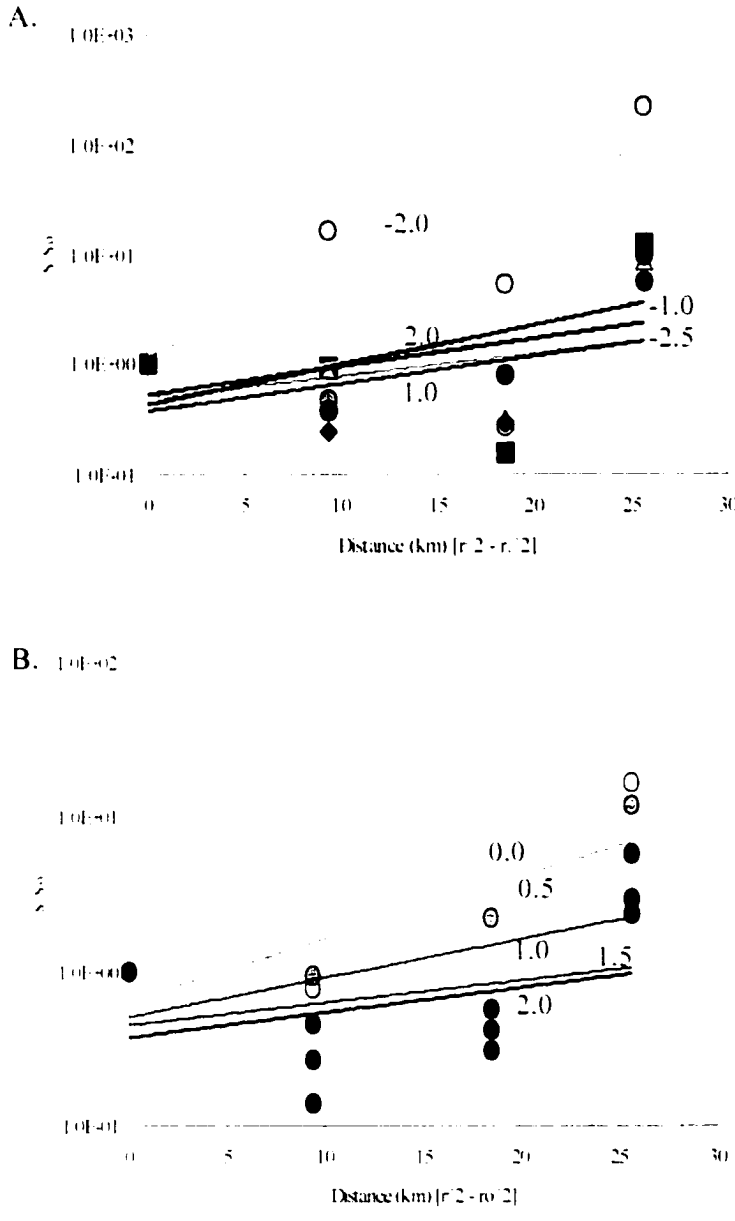

Figure 66. Mass accumulation values for lithic (A) and crystal (B) particles with distance for S3 surge deposits along the A-A' transect (S_3= Locality 6). Lithic and crystal clasts display erratic mass accumulation patterns that reflect *en masse* freezing rather than sedimentation via turbulent suspension. Also, a general increase in sedimentation with distance is observed, which is not predicted by *en masse* sedimentation. Internal planar bedding is abundant in S3, however, which suggests transport and deposition in a laminar flow regime. Grain sizes for lithic (-2.5 to 2.0) and crystal particles (0.0 to 2.0) are indicated..

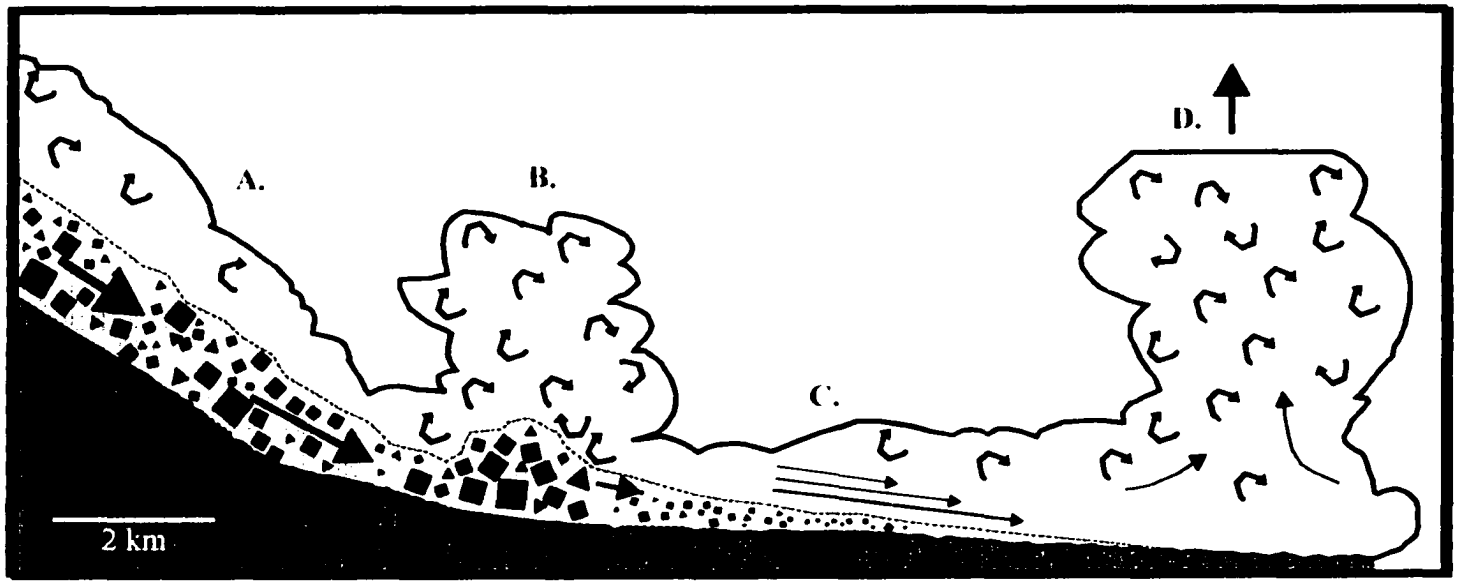

Figure 67. Conceptual model for the transport and deposition of material from the Marquesado flow deposits (after Macias at el., 1998). The flow is depicted as separated into two main parts, a basal dense zone rich in lithic clasts, and an upper dilute zone rich in finer-grained particles resulting from prolonged pulses of column-collapse. A, Following column-collapse, the density current flows down the southwestern flanks via momentum owning to the exceptionally high particle-concentration of the basal zone of the flow; B, Upon encountering the break in slope at the base of the SW flank, the velocity of the flow abruptly decreases, resulting in massive unloading of coarse blocks of lithics as a lag-breccia, and the formation of an elutriated cloud of fine particles owing to the hydraulic jump experienced at the flank base; C, Lithic clasts are re-entrained into the density current and deposited downstream as a function of their size and the settling velocity within the density current. The systematic decrease in lithic clast size and increase in subrounded lithics in basal lag-breccia deposits with distance suggests that attrition of particles via saltation and inertial-grain flow at the base of the density current was the predominant nature of particle transport and deposition in this region; D, With continued sedimentation of material, the density currents eventually reaches a bulk density less than that of the surrounding atmosphere, at this point the Marquesado flow buoyantly lifts off into a co-ignimbrite cloud.

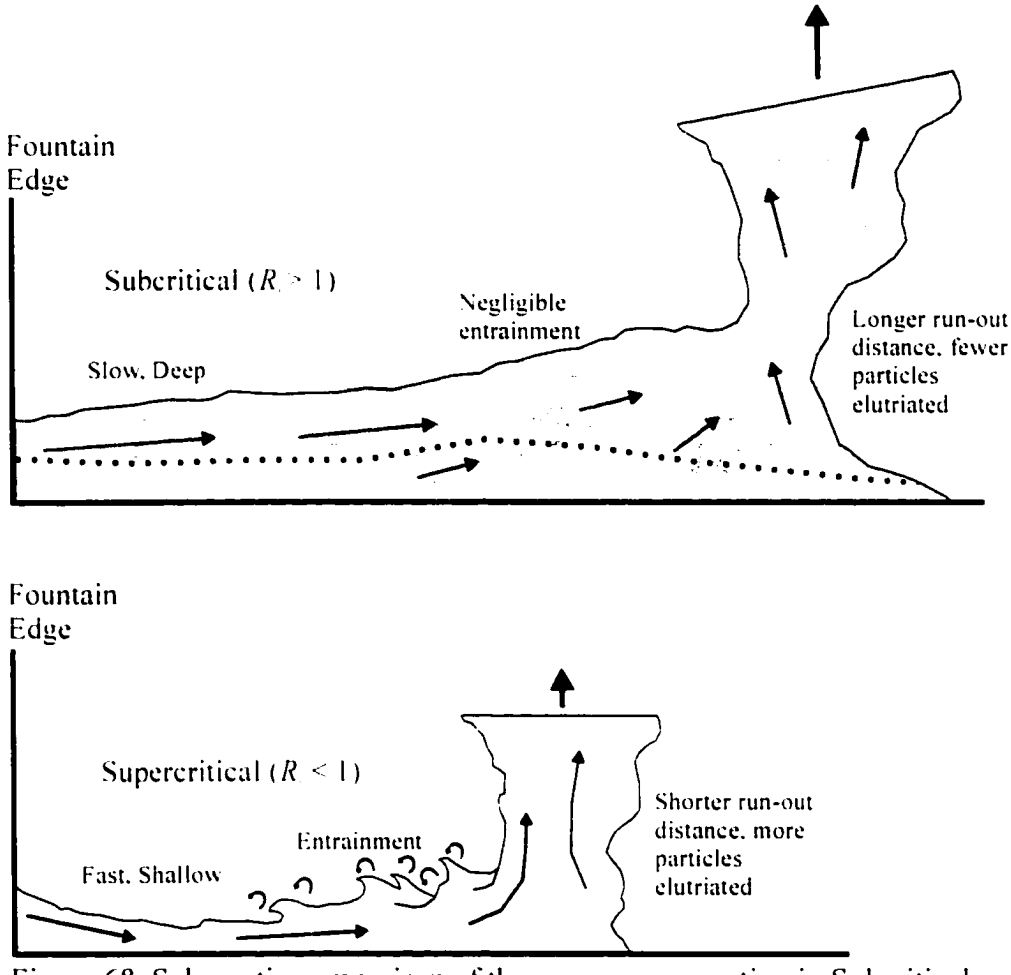

Figure 68. Schematic comparison of the processes operating in Subcritical (top) and Supercritical (base) flow regimes, modified from Bursik and Woods (1996). In this model, the run-out distance, and thus the capacity for the transport and deposition of material with distance is largely a function of the mass of air that is entrained into the "flow" body, and the "flow" velocity. The rate in which entrainment occurs is expressed by the Richardson number (R_i), which depends on the ratio of the potential energy required to entrain the overlying buoyant current to the kinetic energy of the flow (Equation 5). Subcritical density currents are thicker and slowly propagate with a nearly constant volume flux because entrainment of air is negligible, whereas Supercritical density currents are thinner and rapidly propagate, which facilitates the entrainment of large amounts of air and the subsequent inflation of the density current. Therefore, Subcritical "flows" will have longer run-out distances prior to buoyant lift-off compared to "flows" traveling in a Supercritical flow regime.

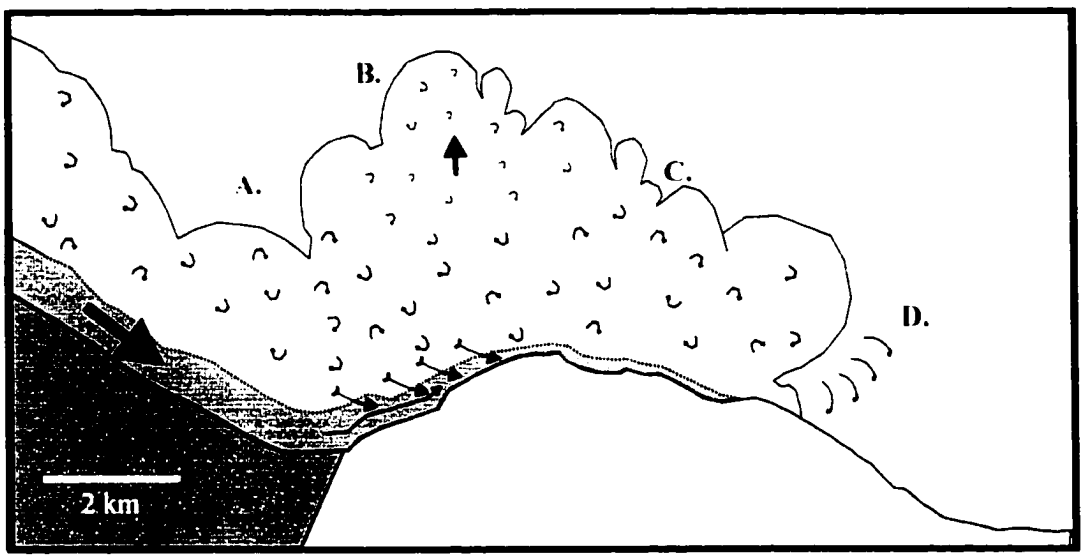

Figure 69. Conceptual model of transport and deposition of material from the S1 surge deposit to the north of Volcán Ceboruco. A. Following what was probably a phreatomagmatic eruption, the density current is thick and slowly travels down the northern flank of Ceboruco in a Subcritical flow regime, which impedes complete development of internal density stratification; B. As the density current propagates up and over the Sierra Madre escarpment, the velocity of the density current decreases, which results in the simultaneous deposition of material (largely *en masse*) and increased supply of fine particles from the transport system to the depositional system; C. Atop the plateau, the S1 surge progressively deposits material (largely *en masse*) in greater and greater amounts owing to the continual decrease in flow velocity. As the velocity of forward motion in the S1 surge cloud approaches zero, the upper and dilute portion buoyantly rises, which transports fine material vertically; D. Distally thin S1 deposits result from the sedimentation of fines-depleted material via turbulent suspension.

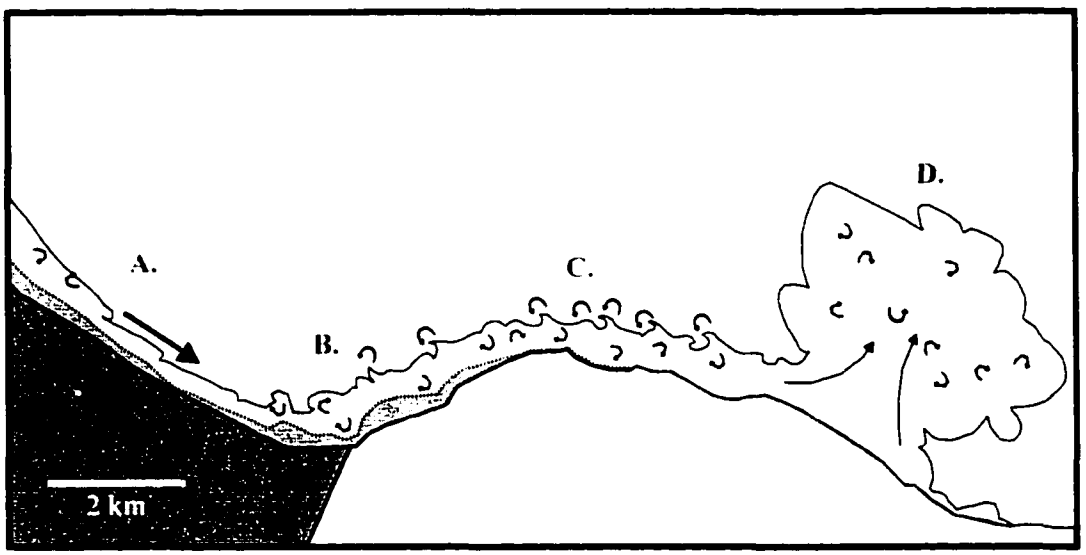

Figure 70. Conceptual model for the transport and deposition of material from the S2 surge deposit to the north of Volcán Ceboruco. A. Following a partial column-collapse event, the density current is thin and rapidly travels down the northern flank of Ceboruco in a Supercritical flow regime, which facilitates early development of internal density stratification; B. At the break in slope of the northern and northeastern flanks, the velocity of the flow abruptly decreases, resulting in massive unloading of material, and the formation of a weak elutriated cloud of fine particles. At the Sierra Madre escarpment, the basal region of the S2 density current is blocked, resulting in both a hydraulic jump in flow velocity, marked by the local change in surge deposit bedforms at the Sierra Madre cliff face, and for particle deposition to be largely dominated by the upper dilute and turbulent transport system once upon the plateau; C. Atop the plateau, the S2 surge current actively entrains surrounding air and deposits material as a function of topography, where topographic lows promote thicker, more poorly sorted deposits, and topographic highs result in thinner, better sorted deposits; D. Continued entrainment of large amounts of air results in the volume of S2 to increase, thus a decrease in density, which eventually results in the abbreviated run-out distance of the S2 surge with buoyant lift-off.

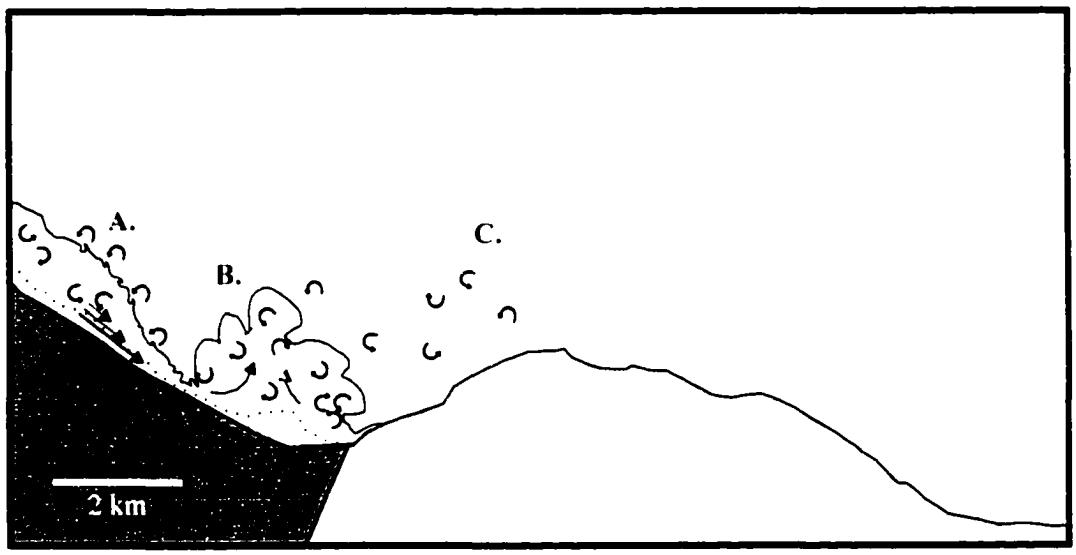

Figure 71. Conceptual model for the transport and deposition of material from the S3 surge deposits to the north of Volcán Ceboruco. A. Following what appears to have been a phreatomagmatic event, the density current is thin and rapidly travels down the northern flank of Ceboruco in a Supercritical flow regime, which facilitates early development of internal density stratification where saltation and attrition of particles seems to have been the principal means of particle transport and deposition in the basal surge levels as evidenced by the abundance of rounded and rolled material; B. Between the break in slope of the northern and northeastern flanks and the Sierra Madre escarpment, the S3 surge continued to entrain large amounts of surrounding air, resulting the coincident deposition of material and the rapid inflation of the density current, which subsequently formed an elutriated cloud of fine particles via buoyant lift-off; C. Fine-grained ash from the elutriated The S3 surge cloud continues to drift in the direction of original flow direction, coating pumice lapilli clasts as they were deposited from the late P3 and early P4 fall layers locally atop the northern plateau.

Table 1. Pyroclastic stratigraphy and eruptive style from the ~1000 A.D. Jala Pumice eruption ([a] and [b], from Gardner and Tait, 2000). Tephra volumes estimated from isopach maps. Magma volumes calculated assuming a deposit density of 900 kg/ m^3, a magma density of 2500 kg/ m^3, and subtracting lithic contents. Stratigraphic nomenclature based on Gardner and Tait, 2000. (--): not determined.

Eruptive Phase	Jala Pumice Tephra Layer	Volume (km^3)	Mass Eruption Rate (kg s^{-1})[b]	Eruption Style
Phase I	P0	0.01[a]	~ 10^6	Brief, initial, low energy vent clearing stage.
	P1	2.5- 2.85	8×10^7	Main eruptive deposit from a high-energy, steady Plinian eruption column from a single vent located on the north flank of Ceboruco.
Phase II	S1	0.001	--	Phreatomagmatic pyroclastic surge deposit found predominantly on the North Plateau
	P2	1.7[a]	1×10^7 to 2×10^7	Phase II Plinian fall layers (P2 and P3 4) represent deposition from an unstable and partially collapsing eruptive column. Initiation of caldera-collapse is interpreted to have begun here, although all Plinian fall layers continue to be erupted form the north flank vent.
	S2	0.002	--	Pyroclastic surge resulting from partial column collapse.
	P3 4	0.1- 0.3[a]	1 to 4×10^7	See above.
	S3	~ 0.001	--	Pyroclastic surge with armored lapilli abundance similar to S1, but internal stratigraphy similar to S2. Probable phreato-magmatic origin

Table 1 continued.

Phase III	F1, F2	n.a.	--	Phase III deposits are dominated by lithic-rich (~70 wt.%) pyroclastic flow sequences, and at least 2 Plinian fall deposits (P5, P6). The simultaneous deposition of Plinian fall deposits and pyroclastic flow deposits are the result of repeated gravitational column-collapse events.
	P5, P6	n.a.	--	Poorly exposed Plinian fall deposits
	F3, F4	n.a.	--	See above
	c1, c2	n.a.	--	Co-ignimbrite fall layers from the F3 and F4 North-Flank PFD's
	Marquesado	0.07	--	See above
	L1, L2, L3	n.a.	--	Final fall deposits resulting from several alternating showers of block and ash as caldera-collapse finalized.

Table 2. Location and granulometric analyses for the P1, P2, and P3/4 fall layers

Locality	Distance from vent (km)	Sample #	Mdφ	σφ	F2 (wt %)
1	6.67	P1 0-20 cm	-4.4	0.79	0
		P1 120-135 cm	-3.7	1.17	0
		P1 227-247 cm	-3.2	1.53	0
		P2 LRB	-2.6	1.22	0
18	3.73	P0	-1.6	1.33	0.56 %
		P1 50-70 cm	-3.6	1.39	0
		P1 200-220 cm	-3.7	1.31	0
		P1 540-560 cm	-3.6	1.29	0
		P1 -40 cm	-4.1	1.47	0
		P1 -20 cm	-3.1	1.63	0
		P1 fine-grain top	-0.2	1.14	0
		P2 LRB	-3.4	1.15	0
		P2 26-66 cm	-4.9	1.51	0
		P2 83-111 cm	-2.4	1.35	0.45
		P2 111-118 cm	-2.9	1.44	0.17
		P3 LRB	-2.9	1.29	0.44
		P3 upper pumice	-3.4	1.40	0.26
		P4 lower pumice	-3.3	1.30	0.52
		P4 lithic top	-2.9	1.28	0.05
29	14.17	P1 0-20 cm	-2.6	0.71	0
		P1 120-140 cm	-2.6	1.29	0
		P1 240-259 cm	-1.9	1.24	0
		P2 LRB	-3.4	1.15	0.58
41	14.42	P1 0-20 cm	-2.7	1.26	0
		P1 -10 cm	-1.7	1.25	0
		P2 LRB	-2.1	1.23	0
50	5.42	P1 0-15 cm	-4.2	0.91	0
		P1 -15 cm	-3.8	1.46	0.34
		P2 LRB	-3.7	1.10	0.54
69	23.25	P1 0-30 cm	-0.6	0.76	0.86
		P1 57-87 cm	-0.8	0.98	0.51
		P1 -10 cm	-0.4	1.24	1.34
70	22.5	P2 LRB	-0.8	1.09	0.87
		P2 CPL	-0.9	1.07	0.84
		P2 top	-0.4	1.16	1.63

Table 3. Location, thickness, and granulometric analyses for the S1, S2, and S3 surge deposits.

Locality	Distance (km)	Thickness (cm)	Sample #	Mdϕ	σϕ	F2 (wt %)
S1						
5	3.24	4.2	CBV-5-1	1.5	3.77	34.37
6	3.68	2.5	CBV-6-1	4.4	1.21	79.16
11	5.97	4.8	CBV-11-1	2.5	3.59	41.48
12	2.03	5.5	CBV-12-1	1.1	2.27	18.81
17	4.45	11	CBV-S-24	2.9	2.76	44.36
18	3.37	8	CBV-S-1	1.7	2.04	22.68
44	6.92	2	CBV-S-4	0.2	2.49	16.99
45	7.87	1	CBV-S-34	0.1	2.04	10.08
49	4.76	6	CBV-S-6	1.1	2.65	27.31
50	5.42	3.5	CBV-S-11	1.3	2.75	23.76
51	5.33	3.5	CBV-S-9	5.6	2.97	43.61
71	4.05	2	CBV-S-25	2.0	2.84	36.84
77	4.32	0.5	CBV-S-29	1.0	2.75	32.73
82	3.94	8	CBV-S-8	2.3	2.42	29.85
83	6.35	3	CBV-S-13	2.7	2.81	41.9
84	7.11	2	CBV-S-15	1.0	3.22	26.54
85	7.12	1.5	No sample	na	na	na
86	7.18	2.5	CBV-S-17	2.7	2.81	22.58
88	4.95	15	CBV-S-22	3.4	2.59	53.37
S2						
1	6.67	23	CBV-1-1	4.3	1.03	79.75
4	3.30	7	CBV-4-1	1.7	2.74	28.66
5	3.24	10.2	CBV-5-2	-2.8	3.46	14.14
6	3.68	10.5	CBV-6-4	3.6	3.41	50.21
7	3.37	10.7	CBV-7-1	1.3	3.70	23.96
12	2.03	6	CBV-12-6	1.5	3.05	30.73
18	3.37	14	CBV-S-2	3.7	2.24	47.21
43	5.59	15	CBV-S-21	4.2	1.65	61.53
44	6.92	12	CBV-S-5	3.9	2.01	55.41
46	8.2	12	CBV-S-33	3.7	2.45	51.34
51	5.33	18.5	CBV-S-10	3.7	1.93	51.26
71	4.05	5.5	CBV-S-26a	2.5	2.38	42.19
71	4.05	3.8	CBV-S-26b	4.2	1.57	68.06
71	4.05	1.3	CBV-S-26c	2	1.48	20.62
77	4.32	9	CBV-S-28	4	1.6	59.99
82	3.94	13	CBV-S-7	2.7	2.22	34.7
83	6.35	16	CBV-S-14	4.2	1.62	64.76
85	7.24	14	CBV-S-16	3.6	2.29	52.09
88	4.95	16	CBV-S-23	3.4	2.59	48.54
92	7.87	15	CBV-S-31	4.1	2	61.14
93	7.75	8	CBV-S-32	3.9	2.29	53.16
94	7.62	8.2	CBV-S-30	4.2	2.35	57.68
99	5.46	3.5	CBV-99-3	1.9	2.99	30.44
S3						
1	4.76	15	CBV-1-2	3.6	2.24	50.9
6	3.68	15.2	CBV-6-2	2.1	3.02	39.92
99	5.46	19.4	CBV-99-1	0.6	3.05	20.07
12	2.03	19	CBV-12-7b	0.7	2.21	19.38

Table 4. Location, thickness, and granulometric analyses for the North-Flank and Marquesado flow deposits, and the co-ignimbrite fall layers (*'s indicate lag breccia matrix samples).

Locality	Distance (km)	Thickness (cm)	Sample #	Mdϕ	σϕ	F2
North-Flank						
7	3.37	22	CBV-7-2	1.9	2.78	33.87
12	2.03	58	CBV-12-3 (F2)	0.2	3.47	22.15
12	2.03	195	CBV-12-4 (F3)	-2.9	2.2	4.07
12	2.03	205	CBV-12-5 (F3)	-2.7	2.98	8.81
12	2.03	550	CBV-12-8 (F4)	-1.4	3.35	17.1
12	2.03	485	CBV-12-9 (F4)	-1.3	3.35	21.82
18	3.73	25.2	CBV-S-3	2.4	2.34	33.6
29	14.17	6.5	CBV-29-2	2.4	2.34	39.77
71	4.05	13	CBV-F-1	-0.7	2.94	16.7
77	4.32	11.5	CBV-F-2	0.6	2.88	17.46
Marquesado						
53	8.89	750	*CBV-M-1	0.5	3.19	23.47
53	8.89	850	CBV-M-2	-0.6	3.39	11.73
53	8.89	650	CBV-M-3	-0.4	3.07	15.68
54	8.47	450	*CBV-M-5	-1.4	3.29	10.93
78	9.21	(pumice lens)	CBV-M-4	-0.4	3.13	12.64
79	9.75	85	*CBV-M-6	0.9	3.35	26.22
79	9.75	125	CBV-M-7	0.3	2.88	19.16
79	9.75	75	*CBV-M-8	1.5	3.29	25.36
79	9.75	150	CBV-M-9	2.9	2.99	40.55
80	11.45	65	CBV-M-10	3.4	2.2	49.28
81	6.73	500	CBV-M-13	-0.7	3.49	17.68
81	6.73	885	CBV-M-14	-0.5	3.06	11.75
81	6.73	260	CBV-M-16	0.6	3.31	19.78
52	1.6	14	CBV-52-2a	2.1	1.57	25.32
52	1.6	18	CBV-52-2b	2.8	2.33	38.79
52	1.6	22	CBV-52-2c	4.2	1.51	64.03
c1, c2, c3						
65	26.92	4.2	CBV-65-1 (c1)	2.4	2.43	32.71
65	26.92	3.1	CBV-65-2 (c2)	1.4	2.01	28.2
65	26.92	3.2	CBV-65-3 (c3)	0.4	1.41	8.32
67	22.61	4.5	CBV-67-1 (c1)	2.9	2.46	42.22
67	22.61	3.5	CBV-67-2 (c2)	-0.1	1.74	10.95
68	22.73	4.2	CBV-68-2 (c1)	3.2	2.41	47.47

References

Allen, JRL. 1984. Sedimentary structures: Their character and physical basis (Developments in Sedimentology, v. 30): Amsterdam, Elsevier

Bacon, CR. 1983. Eruptive history of Mount Mazama and Crater Lake caldera, Cascade Range, USA: Journal of volcanology and Geothermal Research, v. 18, p. 57- 115

Bacon, CR. 1992. Partially melted granodiorite and related rocks ejected from Crater Lake caldera, Oregon: Transactions of the Royal Society of Edinburgh, v. 83, p. 27- 47

Bacon, CR, Druitt, TH. 1989. Compositional evolution of the zoned calc-alkaline magma chamber of Mount Mazama, Crater Lake Oregon: Contributions to Mineralogy and Petrology, v. 98, p. 224- 256

Blake, S, Ivey, GN. 1986. Magma-mixing and the dynamics of withdrawal from stratified reservoirs: Journal of Volcanology and Geothermal Research, v. 27, p. 153- 178

Blake, S, Campbell, I. 1986. The dynamics of magma-mixing during flow in volcanic conduits: Contributions to Mineralogy and Petrology, v. 94, p. 72- 81

Bonadonna, C, Ernst, GGJ, Sparks, RSJ. 1998. Thickness variations and volume estimates of tephra fall deposits: the importance of particle Reynolds number: Journal of Volcanology and Geothermal Research, v. 81, p. 173- 187

Bond, A, Sparks, RSJ. 1976. The Minoan eruption of Santorini, Greece: Journal of the Geological Society of London, v. 312, p. 1- 16

Burgisser, A, Bergantz, G, Gardner, J. 2000. Implications of self-organization in pyroclastic density currents: AGU fall meeting, Eos, Transactions, American Geophysical Union, v. 81 (48)

Bursik, MI, Carey, SN, Sparks, RSJ. 1992a. A gravity model for the May 18, 1980, Mount St. Helens plume: Geophysical Research Letters, v. 19, p. 1663- 1666

Bursik, MI, Kurbatov, AV, Sheridan, MF, Woods, AW. 1998. Transport and deposition in the May 18, 1980, Mount St. Helens blast flow: Geology, v. 26, p. 155- 158

Bursik, MI, Sparks, RSJ, Gilbert, JS, Carey, SN. 1992b. Sedimentation of tephra by

volcanic plumes: I. Theory and its comparison with a study of the Fogo A Plinian deposit, Sao Miguel (Azores): Bulletin of Volcanology, v. 54, p. 329- 344

Bursik, MI, Woods, AW, 1991, Buoyant, Superbuoyant, and collapse eruption columns: Journal of Volcanology and Geothermal Research, v. 45, p. 347- 350

Bursik, MI, Woods, AW, 1996, The dynamics and thermodynamics of large ash flows: Bulletin of Volcanology, v. 58, p. 175- 193

Calder, ES, Cole, PD, Dade, WB, Druitt, TH, Hoblitt, RP, Huppert, HE, Ritchie, L, Sparks, RSJ, Young, SR, 1999, Mobility of pyroclastic flows and surges at the Soufriere Hills volcano, Montserrat: Geophysical Research Letters, v. 26, p. 537-540

Calvache, ML, Williams, SN, 1992, Lithic-dominated pyroclastic flows at Galeras volcano, Columbia- An unrecognized volcanic hazard: Geology, v. 20, p. 539-542

Carey, SN, 1991, Transport and deposition of tephra by pyroclastic flows and surges: Sedimentation in Volcanic Settings, SEPM Special Publication No. 45, p. 39- 57

Carey, SN, Sigurdsson, H, 1982, Influence of particle aggregation on deposition of distal tephra from the May 18, 1980 eruption of Mount St. Helens volcano: Journal of Geophysical Research, v. 87, p. 7061- 7072

Carey, SN, Sigurdsson, H, 1985, The May 18, 1980 eruption of Mount St. Helens II. Modeling of dynamics of the Plinian phase: Journal of Geophysical Research, v. 90, p. 2948- 2958

Carey, SN, Sigurdsson, H, Sparks, RSJ, 1988, Experimental studies of particle-laden plumes: Journal of Geophysical Research, v. 93, p. 15,314- 15,328

Carey, SN, Sigurdsson, H, 1989, The intensity of Plinian eruptions: Bulletin of Volcanology, v. 51, p. 28- 40

Carey, SN, Sigurdsson, H, Gardner, JE, Criswell, W, 1990, Variations in column height and magma discharge during the May 18, 1980 eruption of Mount St. Helens: Journal of Volcanology and Geothermal Research, v. 43, p. 99- 112

Carey, SN, Sparks, RSJ, 1986, Quantitative models of the fallout and dispersal of tephra

from volcanic eruption columns: Bulletin of Volcanology, v. 48, p. 109- 125

Cas RAF, Wright, JV, eds., 1987, Volcanic successions: Modern and ancient: Allen and Unwin, London

Chertkoff, D, Gardner, JE, 2000, Timing between mixing and the caldera-forming eruption of Volcán Ceboruco, Mexico: AGU fall meeting, Eos, Transactions, American Geophysical Union, v. 81 (48)

Cole, PD, 1991, Migration direction of sand-wave structures in pyroclastic surge deposits: Implications for depositional processes: Geology, v. 19, p. 1108- 1111

Criswell, CW, 1987, Chronology and pyroclastic stratigraphy of the May 18, 1980, eruption of Mount St. Helens, Washington: Journal of Geophysical Research, v. 92, p. 10.237- 10.266

Druitt, TH, 1985, Vent evolution and lag breccia formation during the Cape Riva eruption of Santorini, Greece: Journal of Volcanology and Geothermal Research, v. 93, p. 439- 454

Druitt, TH, 1992, Emplacement of the 18 May 1980 lateral blast deposit ENE of Mount St. Helens, Washington: Bulletin of Volcanology, v. 54, p. 554- 572

Druitt, TH, Sparks, RSJ, 1982, A proximal ignimbrite breccia facies on Santorini volcano, Greece: Journal of Volcanology and Geothermal Research, v. 13, p. 147-171

Druitt, TH, Sparks, RSJ, 1984, On the formation of calderas during ignimbrite formation: Nature, v. 310, p. 679-681

Druitt, TH, Francaviglia, 1992, Caldera formation on Santorini and the physiography of the islands in the late Bronze Age: Bulletin of Volcanology, v. 54, p. 484-493

Druitt, TH, 1998, Pyroclastic density currents: Geological Society of London Special Publication, v. 145, p. 145-182

Ernst, GGJ, Sparks, RSJ, Carey, SN, Bursik, MI, 1996, Sedimentation from turbulent jets and plumes: Journal of Geophysical Research, v. 101, p. 5575- 5589

Fierstein, J, Hilderth, W, 1992, The Plinian eruptions of 1912 at Novarupta, Katmai National Park, Alaska: Bulletin of Volcanology, v. 54, p. 646- 684

Fisher, RV, 1971, Features of coarse-grained, high-concentration fluids and their deposits: Journal of Sedimentary Petrology, v. 41, p. 916- 927

Fisher, RV, 1979, Models for pyroclastic surges and pyroclastic flows: Journal of Volcanology and Geothermal Research, v. 6, p. 305- 318

Fisher, RV, 1983, Flow transformations in sediment gravity flows: Geology, v. 11, p. 273- 274

Fisher, RV, 1990, Transport and deposition of a pyroclastic surge across an area of high relief: The 18 May 1980 eruption of Mount St. Helens, Washington: Geological Society of America Bulletin, v. 102, p. 1038- 1054

Fisher, RV, 1995, Decoupling of pyroclastic currents: hazard assessments: Journal of Volcanology and Geothermal Research, v. 66, p. 257- 263

Fisher, RV, Heiken GH, 1982, Mt Pelée, Martinique: May 8 and 20 pyroclastic flows and surges: Journal of Volcanology and Geothermal, v. 13, p. 339- 371

Fisher, RV, Heiken, GH, 1983, Mt Pelée, Martinique: May 8 and 20 pyroclastic flows and surges- Reply: Journal of Volcanology and Geothermal, v. 19, p. 180- 184

Folk, RL, Ward, WC, 1957, Brazos river bar: a study of the significance of grain size parameters: Journal of Sedimentary Petrology, v. 27, p. 3- 26

Freundt, A, Tait, S, 1986, The entrainment of high-viscosity magma into low-viscosity magma in eruption conduits: Bulletin of Volcanology, v. 48, p. 325- 339

Fujii, T, Nakada, S, 1999, The 15 September 1991 pyroclastic flows at Unzen Volcano (Japan): a flow model for associated ash-cloud surges: Journal of Volcanology and Geothermal Research, v. 89, p. 159- 172

Gardner, JE, Tait, S, 2000, The caldera-forming eruption of Volcán Ceboruco, Mexico: Bulletin of Volcanology, v. 62, p. 20- 33

Glicken, H, 1991, Sedimentary architecture of large volcanic-debris avalanches: Sedimentation in Volcanic Settings, SEPM Special Publication No. 45, p. 99- 106

Gunn, B, Mooser, F, 1971, Geochemistry of the volcanics of central Mexico: Bulletin Volcanologiques, v. 34, p. 577- 614

Hildreth, W, 1991, The timing of caldera collapse at Mount Katmai in response to

magma withdrawal toward Novarupta: Geophysical Research Letters, v. 18, p. 1541- 1544

Hildreth, W. 1983. The compositionally zoned eruption of 1912 in the Valley of Ten Thousand Smokes, Katmai National Park, Alaska: Journal of Volcanology and Geothermal Research, v. 18, p. 1- 56

Hoblitt, RP. 1986. Observations of the Eruption of July 22 and August 7, 1980, at Mount St. Helens, Washington: U.S. Geological Survey Professional Paper 1335, p. 38- 49

Hsü, K. 1975. Catastrophic debris stream (sturzstrome) generated by rock fall: Geological Society of America Bulletin, v. 86, p. 401- 140

Inman, DL. 1952. Measures for describing the size distribution of sediments: Journal of Sedimentary Petrology, v. 22, p. 125- 145

Keiffer, SW. 1981. Fluid dynamics of the May 18 directed blast at Mount St. Helens: U.S. Geological Survey Professional Paper 1250, p. 379- 400

Legros, F, Kelfoun, K. 2000. On the ability of pyroclastic flows to scale topographic obstacles: Journal of Volcanology and Geothermal Research, v. 98, p. 235- 241

Levine, AH, Kieffer, SW. 1991. Hydraulics of the August 7, 1980 pyroclastic flow at Mount St. Helens, Washington: Nature, v. 19, p. 1121- 1124

Lipman, P, Dungan, M, Bachman, O. 1997. Comagmatic granophyric granite in the Fish Canyon Tuff, Colorado: Implications for magma chamber processes during a large ash-flow eruption: Geology, v. 25, p. 915- 918

Luhr, JF, Allan, JF, Carmichael, ISE, Nelson, SA, Hasenaka, T. 1989. Primitive calc-alkaline and alkaline rock types from the western Mexican volcanic belt: Journal of Geophysical Research, v. 94, p. 4515- 4530

Luhr, JF. 2000. The geology and petrology of Volcán San Juan (Nayarit, Mexico) and the compositionally zoned Tepic Pumice: Journal of Volcanology and Geothermal Research, v. 95, p. 109- 156

Macias, JL, Sheridan, MF, Espindola, JM. 1997. Reappraisal of the 1982 eruptions of El

Chichón Volcano, Chiapas, Mexico: new data from proximal deposits: Bulletin of Volcanology, v. 58, p. 459- 471

Macias, JL, Espindola, JM, Bursik, MI, Sheridan, MF, 1998, Development of lithic-breccias in the 1982 pyroclastic flow deposits of El Chichón Volcano, Mexico: Journal of Volcanology and Geothermal Research, v. 83, p. 173- 196

Martin, D, Nokes, R, 1988, Crystal settling in a vigorously convective magma chamber: Nature, v. 332, p. 534- 536

Moore, JG, 1967, Base surge in recent volcanic eruptions: Bulletin of Volcanology, v. 30, p. 332- 363

Moore, JG, Peck, DL, 1962, Accretionary lapilli in volcanic rocks of the western United States: Journal of Geology, v. 70, p. 182- 193

Moore, G, Marone, C, Carmichael, ISE, Renne, P, 1994, Basaltic volcanism and extension near the intersection of the Sierra Madre volcanic province and the Mexican Volcanic Belt: Geological Society of America Bulletin, v. 106, p. 383-394

Nelson, SA, 1980, Geology and petrology of Volcán Ceboruco, Nayarit, Mexico: Geological Society of America Bulletin, v. 91, p. 2290- 2431

Ordoñez, E, 1897, Les volcans Colima et Ceboruco: Memorial Society of Science, Antonio Alzate 7, Mexico, v. 11, p. 329, 333

Paladino-Melosantos, MLO, Solidum, RR, Scott, WE, Quiambao, RB, Umbal, JV, Rodolfo, KS, Tubianosa, BS, Reyes, PJD, Alonso, RA, Ruelo, HB, eds., 1992, Tephra falls of the 1991 eruptions of Mount Pinatubo: "Fire and Mud: Eruptions and Lahars of Pinatubo volcano, Philippines", PHIVOLCS, Quezon City and University of Washington Press, Seattle

Paladino, DM, Valentine, GA, 1995, Coarse-tail vertical and lateral grading in pyroclastic flow deposits of the Latera Volcanic Complex (Vulsini, central Italy): origin and implications for flow dynamics: Journal of Volcanology and Geothermal Research, v. 69, p. 343- 364

Pyle, DM, 1989, The thickness, volume, and grain-size of tephra fall deposits: Bulletin of

Volcanology, v. 51, p. 1- 15

Pyle, DM, 1995, Assessment of the minimum volume of tephra fall deposits: Journal of Volcanology and Geothermal Research, v. 69, p. 379- 382

Rosi, M, Principe, C, Vecci, R, 1993, The 1631 Vesuvius eruption, A reconstruction based on historical and stratigraphical data: Journal of Volcanology and Geothermal Research, v. 58, p. 151- 182

Rosi, M, Vezzoli, L, Castelmenzano, A, Grieco, G, 1999, Plinian pumice fall deposit of the Campanian Ignimbrite eruption (Phlegraean Fields, Italy): Journal of Volcanology and Geothermal Research, v. 91, p. 179- 198

Sato, H, Fujii, T, Nakada, S, 1992, Crumbling of dacite dome lava and generation of pyroclastic flows at Unzen Volcano: Nature, v. 360, p. 664- 666

Schumacher, R, Schmincke, H, 1990, The lateral facies of ignimbrites at Laacher See volcano: Bulletin of Volcanology, v. 52, p. 271- 285

Scott, WE, Hoblitt, RP, Torres, RC, Self, S, Martinez, MML, Nillos Jr., T, eds.,1992, Pyroclastic flows of the June 15, 1991 climactic eruption of Mount Pinatubo: "Fire and Mud: Eruptions and Lahars of Pinatubo volcano, Philippines", PHIVOLCS, Quezon City and University of Washington Press, Seattle

Self, S, Sparks, RSJ, 1978, Characteristics of widespread pyroclastic deposits formed by the interaction of silicic magma and water: Bulletin of Volcanology, v. 41, p. 196- 212

Sigurdsson, H, Carey, SN, Cornell, W, Pescatore, T, 1985, The eruption of Vesuvius in A.D. 79: National Geographic Research, v. 1(3), p. 332- 387

Sigurdsson, H, Carey, SN, Fisher, RV, 1987, The 1982 eruptions of El Chichon volcano, Mexico (3): Physical properties of pyroclastic surges: Bulletin of Volcanology, v. 49, p. 467- 488

Sigurdsson, H, Cornell, W, Carey, SN, 1990a, Influence of magma withdrawal on compositional gradients during the AD 79 Vesuvius eruption: Nature, v. 345, p. 519- 521

Sigurdsson, H, Carey, SN, Palais, JM, Devine, J, 1990b, Pre-eruption compositional

gradients and mixing of andesite and dacite magma erupted from Nevado del Ruiz Volcano, Columbia in 1985: Journal of Volcanology and Geothermal Research, v. 41, p. 127- 151

Sheridan, MF, 1979, Emplacement of pyroclastic flows: A review: Geological Society of America Special Paper 180, p. 125- 136

Smith, RL, 1979, Ash-flow magmatism: Geological Society of America Special Paper, v. 180, p. 5- 27

Sohn, YK, Chough, SK, 1989, Depositional processes of the Suwolbong tuff ring, Cheju Island (Korea): Sedimentology, v. 36, p. 837- 855

Sparks, RSJ, 1976, Grain-size variations in ignimbrites and implications for the transport of pyroclastic flows: Sedimentology, v. 23, p. 147- 188

Sparks, RSJ, 1986, The dimensions and dynamics of volcanic eruption columns: Bulletin of Volcanology, v. 48, p. 3- 15

Sparks, RSJ, Wilson, CJH, 1976, A model for the formation of ignimbrite by gravitational column collapse: Journal of the Geological Society of London, v. 132, p. 441- 452

Sparks, RSJ, Walker, GPL, 1977, The significance of vitric-enriched air-fall ashes associated with crystal-enriched ignimbrites: Journal of Volcanology and Geothermal Research, V. 2, p. 329- 341

Sparks, RSJ, Carey, SN, Sigurdsson, H, 1991, Sedimentation from gravity currents generated by turbulent plumes: Sedimentology, v. 38, p. 839- 856

Sparks, RSJ, Bursik, MI, Ablay, GJ, Thomas, RME, Carey, SN, 1992, Sedimentation of tephra by volcanic plumes, Part II: Controls on thickness and grain-size variations of tephra fall deposits: Bulletin of Volcanology, v. 54, p. 685- 695

Sparks, RSJ, Bursik, MI, Carey, SN, Gilbert, JG, Glaze, LS, Sigurdsson, H, Woods, AW, eds., 1997, "Volcanic Plumes", Wiley, Chichester

Suzuki-Kamata, K, Kamata, H, Bacon, C, 1993, Evolution of the caldera-forming eruption at Crater Lake, Oregon, Indicated by component analysis of lithic fragments: Journal of Geophysical Research, v. 98, p. 14,059- 14,074

Tait, S. Gardner, JE. Russo, G. 2001. The formation of small calderas during explosive volcanic eruptions I. Observations and model descriptions: (Submitted) Earth and Planetary Science Letters

Thorpe, RS. Francis, PW. 1975. Volcán Ceboruco: A major composite volcano of the Mexican Volcanic Belt: Bulletin Volcanologique, v. 39, p. 201- 213

Valentine, GA. 1987. Stratified flow in pyroclastic surges: Bulletin of Volcanology, v. 49, p. 616- 630

Valentine, GA. 1998. Damage to structures by pyroclastic flows and surges, inferred from nuclear weapons effects: Journal of volcanology and Geothermal Research, v. 87, p. 117- 140

Valentine, GA. Fisher, RV. 1993. Glowing avalanches: new research on volcanic density currents: Science, 259, p. 1130- 1131

Walker, GPL. 1971. Grain-size characteristics of pyroclastic deposits: Journal of Geology, v. 79, p. 696- 714

Walker, GPL. 1973. Explosive volcanic eruptions- a new classification scheme: Geological Rundsch, v. 62, p. 431- 446

Walker, GPL. 1980. The Taupo Pumice: product of the most powerful known (Ultraplinian) eruption: Journal of Volcanology and Geothermal Research, v. 8, p. 69- 94

Walker, GPL. 1981. Plinian eruptions and their products: Bulletin of Volcanology, v. 44, p. 223- 240

Walker, GPL. 1983. Ignimbrite types and ignimbrite problems: Journal of Volcanology and Geothermal Research, v. 17, p. 65-88

Walker, GPL. 1985. Origin of coarse lithic breccias near ignimbrite source vents: Journal of Volcanology and Geothermal Research, v. 25, p. 157- 171

Walker, GPL. McBroome, LA. 1983. Mount St. Helens 1980 and Mount Pelée 1902- flow or surge?: Geology, v. 11, p. 571- 574

Waters, AC. Fisher, RV. 1971. Base surges and their deposits: Capelinhos and Taal volcanoes: Journal of Geophysical Research, v. 76, p. 5596- 5614

Williams, H. 1950. Volcanoes of the Paracutin region, Mexico: U.S. Geological Survey Bulletin, v. 965-B, p. 165 - 279

Wilson, CJH. 1980. The role of fluidization in emplacement of pyroclastic flows: An experimental approach: Journal of Volcanology and Geothermal Research, v. 8, p. 231- 249

Wilson, CJH. 1984. The role of fluidization in emplacement of pyroclastic flows II. Experimental results and their interpretations: Journal of Volcanology and Geothermal Research, v. 8, p. 55- 84

Wilson, CJH. 1985. The Taupo eruption, New Zealand: II. The Taupo ignimbrite: Philosophical Transactions of the Royal Society of London, v. 314, p. 229- 310

Wilson, CJH, Walker, GPL. 1982. Ignimbrite depositional facies: The anatomy of a pyroclastic flow: Journal of the Geological Society of London, v. 139, p. 581- 592

Wohletz KH, Sheridan, MF. 1979. A model of pyroclastic surge, *in* Chapin, CE, and Elston, OH, eds. Ash Flow Tuffs: Geological Society of America Special Paper 180, p. 177- 194

Wohletz KH, McGretchin, TR, Sanford, MT, Jones, E. 1984. Hydrodynamic aspects of caldera-forming eruptions: Journal of Geophysical Research, v. 89, p. 8269- 8286

Woods, AW. 1988. The fluid dynamics and thermodynamics of eruption columns: Bulletin of Volcanology, v. 50, p. 169- 193

Woods, AW, Bursik, MI. 1991. Particle fallout, thermal disequilibrium and volcanic plumes: Bulletin of Volcanology, v. 53, p. 559- 570

Woods, AW, Bursik, MI, Kurbatov, AV. 1998. The interaction of ash flows with ridges: Bulletin of Volcanology, v. 60, p. 38- 51

Yamamoto, T, Takarada, S, Suto, S. 1993. Pyroclastic flows from the 1991 eruption of Unzen Volcano, Japan: Bulletin of Volcanology, v. 55, p. 166- 175

Appendix 1.

Granulometric Analysis:

Formulae of used Inman (1952) parameters:

Median Diameter (Md_ϕ): ϕ_{50}.

Weight fraction "Fines" (F2): $\sum \phi$ 4.5, ϕ 5.0, ϕ 6.0, and ϕ 7.0

and from Folk and Ward (1957):

Inclusive Graphic Standard Deviation, a measure of sorting (σ_ϕ):

$[(\phi_{84} - \phi_{16})/4] + [(\phi_{95} - \phi_5)/6.6]$

Component Analysis:

The relative proportions of the different components in a pyroclastic deposit reflect its mode of formation, and provide insight into its mode of transport (Walker, 1971; Sparks, 1976). In this study, component analysis was performed in the following procedure:

1. For all grain sizes (-5.0 to 4.0 ϕ, at 0.5 ϕ intervals), components were discriminated as, White Pumice, Gray Pumice, Banded Pumice, Lithic, Crystal, or Glass if the juvenile material was nearly or totally vesicle free (<10%). Where noted, most lithic component counts in samples were distinguished further as, Proximal Lavas, Sierra Madre, of Granitic clasts.
2. With the exception of the pyroclastic fall deposits collected by Gardner and Tait (2000), which were sieved and weighed (-5.0 to –2.5 ϕ) in the field, all particles in the grain sizes between 31.5 mm and 5.6 mm (-5.0 to –2.5 ϕ) were counted and weighed as total weight at the University of Alaska Fairbanks.
3. For particles in the grain sizes between 4.0 mm and 0.5 mm (-2.0 to 1.0 Φ), random splits of particles were counted in groups of >500 with the aid of an automated point counter and a binocular microscope. As the counts were performed, each component would be separated and placed in their respective component group to the side. Once I had exceeded 500 counts, I would weigh

the respective amounts of each component and convert that split into the total weight for that grain size interval.

4. For particles in the grain sizes between 0.5 and 0.063 mm (2.0 to 4.0 ϕ), components were randomly point-counted under a binocular microscope in sets of >500 particles. These abundances were then converted into weight fraction by multiplying the respective abundance of the component by a conversion attained from an average of >1000 particles of that same component previously counted and weighed at the very beginning of this study. These averages were used for fall, surge, and flow samples alike.
5. For particles in the grain-sizes finer that 0.045 mm (4.5 to 7.0 ϕ), a Spectrex Model E laser particle counter was used in cooperation with the 2000 Win-Spec software. At least 1000 particles were laser counted, to assure the most reliable results recommended by the manufacturer. Precise identification of components could not accurately be done with these micro-particles, however, so only bulk weight fractions of grain size intervals of finer that 0.045 mm could be determined using an average density per grain-size fraction that was converted to mass as outlined in Appendix 2. The "Not Available" ("NA") abbreviation in the granulometric analysis histograms represents these finer grain size intervals.

Appendix 2.

A collection of sample locality descriptions is presented in this section along with the granulometric and component analysis results from each sample. All sample localities discussed in this thesis are presented in order of Locality number, and include the latitude and longitude location of the locality (* = if one was taken), measured stratigraphy, a brief description of important Jala Pumice tephra layers, and the correlating sample ID number (if one was taken).

In the granulometric and component analysis result pages, all the samples that were analyzed for this thesis are presented here, with the sample number being located in the upper left corner of each page for reference. Granulometric results from the Jala Pumice tephra is organized in accordance to the stratigraphic position of the tephra layer, with the P0 fall analysis being presented first, and the L1, L2, and L3 Lithic fall analyses being presented last (e.g. P0, P1, S1, P2, S2...). Sample ID names may include a reference to the height in the deposit from which it was taken, where positive intervals (e.g. 200-220 cm) refer to the height as measured from the deposits base and negative intervals (e.g. –20 to –40 cm) refer to the height as measured from the deposits top. All tables include the bulk weight of the sample, the weight fractions of each 0.5 ϕ interval, and the corresponding cumulative weight percentages. Most sample weights are in presented in milligrams to an 0.1 mg accuracy, however, all grain-sizes coarser than –2.0 ϕ in the P1, P2, P3, and P4 samples were measured to an accuracy of 1.0 g in the field by Gardner and Tait (2000). In addition, in all P1, P2, P3, and P4 samples, the weight fraction indicated at the 2.5 ϕ grain-size represents the bulk weight $\leq 2.5\phi$.

Granulometric analyses are presented in the upper right corner (Md_ϕ, σ_ϕ, and F2), and component analysis results are presented in the lower two tables. Abbreviations such as Wp, Gp, and Bp represent White, Gray, and Banded Pumice, respectively. Minor lithic population counts (Sierra Madre and Granitic clast lithics) were performed on samples in the –1.0 ϕ to 3.0 ϕ (2.0-0.125 mm) grain-size interval only.

All fields that display a numerical value (≥0) indicate that analysis of that sample was performed, whereas samples that were not analyzed for a given component display the n.a. (not analyzed) notation. Fields that display a "0.0+" notation indicate that the value for that field is greater than 0, but less than 0.0.

Conversion factors used for the different components in this thesis for the 2.0 ϕ to 4.0 ϕ (and the N.A. estimates for 4.5 ϕ to 7.0 ϕ) are presented below in mg:

ϕ	*mm*	Wp	Gp	Bp	Xtal	Lithic	Glass	N.A.
2.0	0.250	0.015	0.018	0.018	0.045	0.045	0.040	*
2.5	0.180	0.006	0.007	0.007	0.014	0.014	0.0013	*
3.0	0.125	0.0031	0.0031	0.0031	0.0058	0.0058	0.0053	*
3.5	0.090	*	*	*	0.0046	0.0046	0.0036	*
4.0	0.063	*	*	*	0.0029	0.0029	0.0023	*
4.5	0.045	*	*	*	0.0019	0.0019	0.0015	0.0017
5.0	0.032							0.0016
6.0	0.016							0.0011
7.0	0.008							0.0007

Locality #	Lat Long *	Tephra Layers (Top to Base)	Tephra Thickness	Notable Observations	Sample ID
1	n.a.	Pumice - soil	80 cm		
		North-Flank PFD veneer deposit	15 cm	Pinkish-gray. Stratified at base. Armored-lapilli at base	
		P4	12 cm		
		S3	15 cm	Pinkish-gray. Lower ½ is Stratified	CBV-1-2
		P3	6 cm		
		S2	23 cm	Top is olive-gray, base is Pinkish-gray. Intricately stratified with planar and cross bedding	CBV-1-1
		P2	28 cm		P2:LRB
		S1	4.5 cm	Olive-gray. massive	
		P1 top	2 cm	Accretionary-lapilli-bearing	CBV-1-3
		P1	247 cm		P1:227-247 cm. P1:120-135 cm. P1:0-20 cm

Locality #	Lat Long *	Tephra Layers (Top to Base)	Tephra Thickness	Notable Observations	Sample ID
5	n.a.	Pumice - soil	~70 cm		
		S2	14 cm	Olive-gray, Intricately stratified with planar and cross bedding	CBV-5-2
		P2	19 cm		
		S1	7 → ~300 cm	Olive-gray, massive, poorly sorted ash bed that laterally inflates into ~300 cm ~2 m away	CBV-5-1
		P1	~100 cm		

Locality #	Lat Long *	Tephra Layers (Top to Base)	Tephra Thickness	Notable Observations	Sample ID
6	n.a.	Pumice - Soil	~50 cm		
		Marquesado PFD veneer deposit	26 cm	Rust-Gray, Intricately planar bedded	CBV-6-3
		P4	6 cm		
		S3	12 cm	Pinkish-gray, Armored-and -accretionary lapilli-rich, planar bedded	CBV-6-2
		P3	3.5 cm		
		S2	10 cm	Olive-gray, planar bedded	
		P2	14 cm		
		S1	2.5 cm	Olive-gray, massive	CBV-6-1
		P1	~85 cm		

Locality #	Lat Long *	Tephra Layers (Top to Base)	Tephra Thickness	Notable Observations	Sample ID
7	N21° 6' 58.4" W104° 29' 0.2"	Pumice - Soil	~55 cm		
		P6	10 cm		
		North-Flank PFD (F3)	23 cm	Light-gray, massive	CBV-7-2
		P5	13 cm		
		North-Flank PFD (F2)	22 cm	Light-gray, massive	
		P4	15 cm		
		S3	17 cm	Pinkish-gray, cross bedded base, armored lapilli-rich	
		P3	35 cm		
		S2	107 cm	Olive-gray, cross bedded base, massive middle, laminated top	CBV-7-1
		P2	18 cm		
		S1	138 cm	Olive-gray, massive, pumice-bearing (~13 cm diameter)	
		P1	~300 cm		

Locality #	Lat Long *	Tephra Layers (Top to Base)	Tephra Thickness	Notable Observations	Sample ID
11	N21° 10' 46.3" W104° 32' 28.7"	Pumice - Soil	~30 cm		
		P2	~15 cm		
		S1	4.5-5 cm	Olive-gray, massive, pumice bearing	CBV-11-1
		P1	60 cm		

Locality #	Lat Long *	Tephra Layers (Top to Base)	Tephra Thickness	Notable Observations	Sample ID
12	N21° 8' 54.6" W104 29' 16.6"	Pumice - Soil	~100 cm		
		L2	45 cm	~90% lithic block fall interbedded with ashy bed	CBV-12e-2: Fall. CBV-12e-3: Ash bed
		L1	47 cm	~90% lithic block fall interbedded with ashy bed	
		North-Flank PFD (F4)	~400 cm	Dark-gray. Massive body accounts for ~70% of thickness. lithic blocks in lag breccia ~35 cm in diameter	CBV-12-8
		P6	14 cm		
		North-Flank PFD (F3)	210 cm	Dark-gray. massive. lag breccia at base is 20 cm thick	CBV-12-4: Pumice lens CBV-12-5: bulk
		P5	12 cm		
		North-Flank PFD (F2)	58 cm	Dark gray. massive. no lag breccia	CBV-12-3
		North-Flank PFD (F1)	9 cm	Dark gray. massive. no lag breccia	CBV-12-2
		P4	20 cm		
		S3	19 cm	Accretionary lapilli-rich. Intricately stratified with planar and cross bedding	CBV-12-7a: Planar beds CBV-12-7b: Massive beds
		P3	21 cm		
		S2	5 cm	Planar bedded in middle-top	CBV-12-6
		P2	31 cm		
		S1	5.5 cm	Massive with lithic-rich lenses in base	CBV-12-1
		P1	>150 cm		

Locality #	Lat Long *	Tephra Layers (Top to Base)	Tephra Thickness	Notable Observations	Sample ID
17	N21° 10' 20.8" W104° 29' 32.0"	Pumice - Soil	44 cm		
		P3-4	25 cm		
		S2	12 cm	Olive-gray, planar bedded	
		P2	101 cm		
		S1	10.5 cm	Pinkish-gray, basal 3 cm is cross bedded, massive otherwise	CBV-S-24
		P1	>700 cm		

Locality #	Lat Long *	Tephra Layers (Top to Base)	Tephra Thickness	Notable Observations	Sample ID
18	n.a.	Pumice - Soil	~100 cm		
		North-Flank PFD	25 cm	Dark gray. Planar beds defined by layers of massive beds and rounded pumice lapilli layers. Entrainment of P4 lithics and pumice at base	CBV-S-3
		S3 (coating)	2 cm		
		P3-4	28 cm		P4 Lithic-top. P4 Lower pumice. P3 Upper pumice. P3 LRB
		S2	14 cm	Olive-gray. cross bedded base. massive middle. and planar bedded top. rounded pumices abundant in top and base	CBV-S-2
		P2	118 cm		111-118cm. 83-111cm. 26-66cm. 0-26cm
		S1	7 cm	Olive-gray. massive. thin laminations in top 1.5 cm	CBV-S-1
		P1	748 cm	Thin bed of accretionary-lapilli - lithics at very top 1 cm	Upper cm's. -20cm. -40cm. 550-560 cm. 200-220 cm. 50-70 cm
		P0	35 cm	Accretionary-lapilli and lithic-rich	P0-18

Locality #	Lat Long *	Tephra Layers (Top to Base)	Tephra Thickness	Notable Observations	Sample ID
29	N21° 7' 55.2" W104° 22' 8.1"	Pumice + Soil	12 cm		
		P3	2.5 cm		
		S2	2 mm	Faint, thin olive-gray ash	
		P2	12.5 cm	Lower 3.5 cm is coarser-grained and lithic-rich	P2 LRB
		P1	259 cm	Thin bed of accretionary-lapilli + lithics at very top 1 cm	CBV-29-1: (Top 1 cm) 240-259 cm 120-140 cm 0-20 cm

Locality #	Lat Long *	Tephra Layers (Top to Base)	Tephra Thickness	Notable Observations	Sample ID
41	n.a.	Pumice + Soil	30 cm		
		P3	2 cm	Vertically grades into pumice-rich, ashy soil	
		P2	25 cm	Lower 7 cm is lithic-rich	LRB
		S1	1 cm	Light-gray, ash coating	
		P1	63 cm		-10 cm 0-20 cm

Locality #	Lat Long *	Tephra Layers (Top to Base)	Tephra Thickness	Notable Observations	Sample ID
43	N21° 11' 2.6" W104° 29' 23.8"	Pumice - Soil	~25 cm		
		S2	15 cm	Pinkish-gray, massive with thin planar bedding at top	CBV-S-21
		P2	47 cm		
		S1	3.5 cm	Olive-gray, massive with laminations at top 1 cm, armored-lapilli rich	CBV-S-20
		P1	443 cm		

Locality #	Lat Long *	Tephra Layers (Top to Base)	Tephra Thickness	Notable Observations	Sample ID
44	n.a.	Pumice - Soil	~30 cm		
		S2	12.5 cm	Pinkish-gray, faintly stratified with planar bedding	CBV-S-5
		P2	77 cm		
		S1	1.7-2.5 cm	Olive-gray, massive with laminations at top 1.2 cm, armored-lapilli rich, Lithic-rich lenses	CBV-S-4: Bulk sample CBV-S-4a: Lithic-rich lens
		P1	382 cm		

Locality #	Lat Long *	Tephra Layers (Top to Base)	Tephra Thickness	Notable Observations	Sample ID
45	N21° 12' 1.8" W104° 28' 45.6"	Pumice - Soil	·15 cm		
		S2	7.8-8.5 cm	Pinkish-gray, fluctuating thickness, massive	
		P2	87 cm		
		S1	1.5-2 cm	Light-gray, massive	CBV-S-34
		P1	363 cm		

Locality #	Lat Long *	Tephra Layers (Top to Base)	Tephra Thickness	Notable Observations	Sample ID
46	N21° 12' 4.4" W104° 28' 36.0"	Pumice - Soil	·30 cm		
		S2	12 cm	Pinkish-gray, massive with thin planar bedding at top, coarse-grained pumice - lithics in middle 5 cm	CBV-S-33
		P2	·80 cm		
		S1	1.5 cm	Olive-gray, massive with laminations at top 0.5 cm, basal cm drapes over P1 top	CBV-S-20
		P1	363 cm		

Locality #	Lat Long *	Tephra Layers (Top to Base)	Tephra Thickness	Notable Observations	Sample ID
49	n.a.	Pumice - Soil	·25 cm		
		P2	·30 cm	Vertically grades into pumice-rich, ashy soil	
		S1	5.5 cm	Olive-gray, massive, Armored-lapilli rich	CBV-S-6
		P1	332 cm		CBV-S-6a: P1 top cm
		P0	4.5 cm		

Locality #	Lat Long *	Tephra Layers (Top to Base)	Tephra Thickness	Notable Observations	Sample ID
50	N21° 11' 19.9" W104° 30' 55.6"	Pumice - Soil	22 cm		
		S2	17 cm	Pinkish-gray, massive with thin planar bedding at top	
		P2	41 cm		LRB
		S1	3.5 cm	Olive-gray, massive with laminations at top 1.75 cm	CBV-S-11
		P1	183 cm		CBV-S-12 (P1 top cm), -15 cm, 0-15 cm

Locality #	Lat Long *	Tephra Layers (Top to Base)	Tephra Thickness	Notable Observations	Sample ID
51	n.a.	Pumice - Soil	24 cm		
		S2	18.5 cm	Pinkish-gray, massive with thin planar bedding in upper 5 cm	CBV-S-10
		P2	52 cm		
		S1	3.5 cm	Olive-gray, massive with laminations at top 1 cm, armored-lapilli rich, top 2 cm inundated with lithics and pumices from P2 base	CBV-S-9
		P1	100 cm		

Locality #	Lat Long *	Tephra Layers (Top to Base)	Tephra Thickness	Notable Observations	Sample ID
52	n.a., (100 m east of where southern flank road from Jala enters outer caldera wall)	Pumice - ashy Soil	~55 cm		
		Marquesado-North-Flank PDF	83 cm	Pinkish-gray, massive top and middle, basal 18 cm is planar bedded with abundant rounded lithics and pumices	
		P5	5.5 cm	Pumice fall with abundant lithics (~30%) and gray pumice clasts	
		Marquesado-North-Flank PFD	61 cm	Deep rust colored, intricately stratified in lower and upper 20 cm. Uncomformibly erodes ~3 cm of S1 top	CBV-52-2a (top) CBV-52-2b (middle) CBV-52-2c (base)
		S1	4.5 cm	Olive-gray, planar bedded. Armored-lapilli rich	CBV-52-1
		P1	~60 cm		

Locality #	Lat Long *	Tephra Layers (Top to Base)	Tephra Thickness	Notable Observations	Sample ID
53	N21° 4' 47" W104° 35' 2"	Ashy Soil Marquesado PFD's	100 cm ~30 m	Series of at least 3 flow units, each unit is pinkish-gray in color with a massive, poorly sorted, ashy body with a lag breccia at it's base. Lag breccias are 10-30% of the thickness of each flow unit. Three flow units in this locality sum to ~30 m in relief	CBV-M-1: Lower flow body, CBV-M-2: Middle flow body, CBV-M-3: Upper flow breccia matrix

Locality #	Lat Long *	Tephra Layers (Top to Base)	Tephra Thickness	Notable Observations	Sample ID
54	n.a.	Ashy, blocky soil Marquesado PFD's	300 cm ~6 m	Upper flow lag breccia exposure. Blocks up to 180 m in diameter in a finer-grained matrix	CBV-M-5: Upper flow lag breccia matrix

Locality #	Lat Long *	Tephra Layers (Top to Base)	Tephra Thickness	Notable Observations	Sample ID
65	N21° 10' 17.9" W104° 15' 35.9"	Pumice - Soil	~15 cm		
		P8 (?)	10 cm	Pumice fall	
		P7 (?)	9 cm	Pumice fall	
		c3	3.75 cm	Pinkish-gray, fine ash	CBV-65-3
		P6	4.5 cm		
		c2	1.2 cm	Pinkish-gray, fine ash	CBV-65-2
		P5	3.5 cm		
		c1	2.75 cm	Pinkish-gray, fine ash	CBV-65-1
		P3-4	2 mm		
		S2	2 mm	Light gray ash layer	
		P2	4.7 cm		
		P1	~100 cm		

Locality #	Lat Long *	Tephra Layers (Top to Base)	Tephra Thickness	Notable Observations	Sample ID
67	N21° 9' 51.4" W104° 17' 50.6"	Pumice - Soil	~18 cm		
		c3	1.75 cm	Pinkish-gray, fine ash	CBV-67-2
		P6	5 cm		
		c2	7 mm	Pinkish-gray, fine ash	
		P5	3 cm		
		c1	5.5 cm	Pinkish-gray, fine ash	CBV-67-1
		P3-4	2.5 cm		
		P2	9.7 cm		
		P1	~100 cm		

Locality #	Lat Long *	Tephra Layers (Top to Base)	Tephra Thickness	Notable Observations	Sample ID
68	N21° 10' 26.5" W104° 17' 46.7"	Pumice - Soil	~10 cm		
		P5	5.5 cm		
		c1	5 cm	Pinkish-gray, fine ash	CBV-68-2
		P3-4	4.6 cm		
		S2	2 mm	Olive-gray, fine ash	
		P2	13.2 cm	3 mm lithic-rich base, reversely graded above that	CBV-68-1: P1 top cm
		P1	~100 cm		

Locality #	Lat Long *	Tephra Layers (Top to Base)	Tephra Thickness	Notable Observations	Sample ID
69	N21° 11' 29.7" W104° 17' 35.3"	Pumice - Soil	~10 cm		
		c3	2 cm	Pinkish-gray, fine ash	
		P6	4 cm		
		c2	3 cm	Pinkish-gray, fine ash	
		P5	2.6 cm		
		c1	5 cm	Pinkish-gray, fine ash	
		P3-4	2.2 cm		
		S2	2 mm	Olive-gray, fine ash	
		P2	12.5 cm		
		P1	~100 cm		~10 cm 57-87 cm 0-30 cm

Locality #	Lat Long *	Tephra Layers (Top to Base)	Tephra Thickness	Notable Observations	Sample ID
70	N21° 9' 47.4" W104° 16' 37.3"	Pumice + Soil	~10 cm		
		c3	2 cm	Pinkish-gray, fine ash	
		P6	4 cm		
		c2	3 cm	Pinkish-gray, fine ash	
		P5	2.6 cm		
		c1	5 cm	Pinkish-gray, fine ash	
		P3 4	2.6 cm		
		S2	2 mm	Olive-gray, fine ash	
		P2	5.5 cm		Top cm's, Middle level, and LRB
		P1	~100 cm		

Locality #	Lat Long *	Tephra Layers (Top to Base)	Tephra Thickness	Notable Observations	Sample ID
71	N21° 10' 4.9" W104° 29' 13.2"	Pumice - Soil	~50 cm		
		P5	10 cm	Rust-Gray.	
		North-Flank PFD	13 cm	Dark gray. Massive base that reversely grades into planar bedded middle and top, abundant rounded pumice clasts. Normally graded 3 cm from top	CBV-F-1
		P3-4	39 cm		
		S2	10.5 cm	Olive-gray. cross bedded base, massive middle, and planar bedded top composed of rounded pumices	CBV-S-26a: Planar beds. CBV-S-26b: Massive middle. CBV-S-26c: Cross bedded base
		P2	156 cm		
		S1	2.5-3 cm	Pinkish-gray. massive, thinning to north and east	CBV-S-25
		P1	~600 cm		CBV-S-27: P1 top cm

Locality #	Lat/Long *	Tephra Layers (Top to Base)	Tephra Thickness	Notable Observations	Sample ID
77	N21° 9' 43.4" W104° 29' 6.0"	Pumice - ashy soil	~30 cm		
		P5	13.5 cm	Rust-Gray.	
		North-Flank PFD	11 cm	Pinkish-gray. Massive base. planar bedded middle and top. abundant rounded pumice clasts	CBV-F-2
		P3-4	33 cm		
		S2	9 cm	Olive-gray. cross bedded base. massive middle and faint. thin laminations at top 3 cm	CBV-S-28
		P2	170 cm		
		S1	1.5-2.5 cm	Pinkish-gray. massive. thinning to north and east to ~1 cm where it coats P1 top	CBV-S-29
		P1	~600 cm		

Locality #	Lat Long *	Tephra Layers (Top to Base)	Tephra Thickness	Notable Observations	Sample ID
78	n.a.	Ashy Soil Marquesado PFD's	100 cm ~30 m	Series of at least 3 flow units, each unit is pinkish-gray in color with a massive, poorly sorted, ashy body with no lag breccia base. Three flow units in this locality sum to ~30 m in relief. Pumice lenses are commonly ~5 m in length and 0.2 m in height	CBV-M-4: Pumice lens in Flow 2

Locality #	Lat Long *	Tephra Layers (Top to Base)	Tephra Thickness	Notable Observations	Sample ID
79	N21° 06' 40" W104° 35' 60"	Ashy Soil Marquesado PFD's	100 cm ~15 m	Series of 2 flow units, each unit is pinkish-gray in color with a massive, poorly sorted, ashy body with a lag breccia at it's base. Lag breccias are 5-10% of the thickness of each flow unit. Three flow units in this locality sum to ~15 m in relief. Lag breccias are thinner than medially and are composed of sub-rounded to rounded lithic blocks up to 8 cm diameter	CBV-M-6: Lower flow breccia matrix. CBV-M-7: Middle flow body. CBV-M-8: Upper flow breccia matrix. CBV-M-9: Upper flow body

Locality #	Lat Long *	Tephra Layers (Top to Base)	Tephra Thickness	Notable Observations	Sample ID
80	N21° 5' 32" W104° 37' 23"	Ashy Soil Marquesado PFD's	100 cm ~1 m	1 flow unit. Pinkish-gray in color, planar bedded throughout with rounded coarse-grained pumices and finer-grained lithics. No lag breccia in deposits beyond Locality 79	CBV-M-10 CBV-M-11 CBV-M-12. Base, middle and top samples, respectively

Locality ¤	Lat Long *	Tephra Layers (Top to Base)	Tephra Thickness	Notable Observations	Sample ID
81	n.a.	Ashy Soil Marquesado PFD's	100 cm ~20 m	Series of 3 flow units, top two units are light-gray, basal unit is pinkish-gray. All units are massive, and poorly sorted ashy bodies with no lag breccia base. A nearly clast-supported, pumice lapilli rich (~30% lithics) layer exists between Flow 1 and 2, never exceeding 10 cm in thickness, pumice-rich layer is laterally continuous, not a pumice lens	CBV-M-13: Lower flow, CBV-M-14: Middle flow, CBV-M-16: Upper flow

Locality #	Lat Long *	Tephra Layers (Top to Base)	Tephra Thickness	Notable Observations	Sample ID
82	n.a.	Pumice - Soil	50 cm		
		S2	13 cm	Pinkish-gray, thin planar bedding at base and upper 5 cm, massive middle	CBV-S-7
		P2	110 cm		
		S1	8 cm	Olive-gray, massive with laminations at top 1.5 cm, armored-lapilli rich	CBV-S-8
		P1	700 cm		

Locality #	Lat Long *	Tephra Layers (Top to Base)	Tephra Thickness	Notable Observations	Sample ID
83	N21° 11' 36.8" W104° 31' 2.9"	Pumice - Soil	35 cm		
		S2	16 cm	Olive-gray, massive	CBV-S-14
		P2	48 cm		
		S1	3 cm	Olive-gray, massive	CBV-S-13
		P1	152 cm		

Locality #	Lat Long *	Tephra Layers (Top to Base)	Tephra Thickness	Notable Observations	Sample ID
84	N21° 11' 59.4" W104° 30' 55.4"	Pumice - Soil	24 cm		
		S1	2 cm	Olive-gray, draping over P1 top	CBV-S-15
		P1	153 cm	No lithic-rich, accretionary-lapilli top of P1	

Locality #	Lat Long *	Tephra Layers (Top to Base)	Tephra Thickness	Notable Observations	Sample ID
85	N21° 12' 1.7" W104° 30' 28"	Pumice - Soil	35 cm		
		S2	14 cm	Pinkish-gray, massive with planar bedding composed of medium-grained lithics in upper 5 cm	CBV-S-16
		P2	52 cm		
		S1	1.75 cm	Olive-gray, massive, fine-grained, drapes over P1 top	
		P1	>100 cm		CBV-S-18: P1 top cm

Locality #	Lat Long °	Tephra Layers (Top to Base)	Tephra Thickness	Notable Observations	Sample ID
86	N21° 12' 10.7" W104° 31' 24.9"	Pumice - Soil	24 cm		
		P2	65 cm	Vertically grades into pumice-rich soil	
		S1	2.5 cm	Olive-gray, massive with faint laminations at top 1 cm	CBV-S-17
		P1	100 cm		

Locality #	Lat Long °	Tephra Layers (Top to Base)	Tephra Thickness	Notable Observations	Sample ID
88	N21° 10' 41.9" W104° 29' 34.5"	Pumice - Soil	50 cm		
		S2	16 cm	Pinkish-gray, massive with thin planar bedding in upper 5 cm	CBV-S-23
		P2	90 cm		
		S1	14.5 cm	Olive-gray, massive base, cross bedded in middle with faint laminations in upper 3.5 cm	CBV-S-22
		P1	100 cm		

Locality #	Lat Long *	Tephra Layers (Top to Base)	Tephra Thickness	Notable Observations	Sample ID
92	N21° 12' 10.0" W104° 29' 5.5"	Pumice - Soil	~35 cm		
		S2	15-16 cm	Pinkish-gray, massive with thin planar bedding in upper 3 cm	CBV-S-31
		P2	55 cm		
		S1	~1 cm	Olive-gray, massive fine ash drapes over P1 top	
		P1	~500 cm		

Locality #	Lat Long *	Tephra Layers (Top to Base)	Tephra Thickness	Notable Observations	Sample ID
93	N21° 12' 4.4" W104° 28' 17.1"	Pumice - Soil	~60 cm		
		S2	8 cm	Pinkish-gray, massive with thin planar bedding in upper 3 cm and fine laminations in top 1 cm	CBV-S-32
		P2	50 cm		
		S1	~1 cm	Olive-gray, massive fine ash drapes over P1 top	
		P1	~100 cm		

Locality #	Lat Long *	Tephra Layers (Top to Base)	Tephra Thickness	Notable Observations	Sample ID
94	N21° 11' 59.2" W104° 29' 11.7"	Pumice - Soil	~75 cm		
		S2	12 cm	Pinkish-gray, massive with fine-grained laminations in top 0.5 cm	CBV-S-32
		P2	45 cm		
		S1	1 cm	Olive-gray, massive fine ash drapes over P1 top	
		P1	~100 cm		

Locality #	Lat Long *	Tephra Layers (Top to Base)	Tephra Thickness	Notable Observations	Sample ID
99	N21° 7' 50.6" W104° 28' 9.6"	Pumice - Soil	60 cm		
		P4	5 cm	Vertically grades into pumice-rich soil	
		S3	194 cm	Pinkish-gray, contains rounded pumice lenses, accretionary-lapilli, and is lithic poor	CBV-99-1
		P3	5 cm		
		S2	3.5	Light-gray, upper 1.5 cm is planar bedded	CBV-99-3
		P2	37 cm		
		S1	6 cm	Olive-gray, massive fine ash drapes over P1 top	CBV-99-2
		P1	700 cm	No lithic-rich, accretionary-lapilli top to P1	

Locality #	Lat Long *	Tephra Layers (Top to Base)	Tephra Thickness	Notable Observations	Sample ID
93	N21° 12' 4.4" W104° 28' 17.1"	Pumice - Soil	~60 cm		
		S2	8 cm	Pinkish-gray, massive with thin planar bedding in upper 3 cm and fine laminations in top 1 cm	CBV-S-32
		P2	50 cm		
		S1	~ 1 cm	Olive-gray, massive fine ash drapes over P1 top	
		P1	~100 cm		

P0 at Locality 18 [P0-18] [Total sample weight: 292943.6 mg]

Grain diameter		Weight fractions:		Granulometric Analysis						
ϕ	mm	weight [mg]	Cumulative weight %	ϕ_{05}	ϕ_{25}	ϕ_{50}	ϕ_{75}	Md_ϕ	σ_ϕ	F2
-5.0	31.5	0	0	0.8	-0.2	-3.1	-3.2	-1.6	1.33	0.56%
-4.5	22.4	0	0							
-4.0	16.0	0	0							
-3.5	11.2	0	0							
-3.0	8.0	77709.6	26.53							
-2.5	5.6									
-2.0	4.0									
-1.5	2.8	92071.7	57.96							
-1.0	2.0	41400.3	72.09							
-0.5	1.4									
0.0	1.0	56016.4	91.21							
0.5	0.710									
1.0	0.500	21971.4	98.71							
1.5	0.355									
2.0	0.250	1913.6	99.36							
2.5	0.180									
3.0	0.125	231.8	99.44							
3.5	0.088									
4.0	0.063									
4.5	0.045	302.9	99.55							
5.0	0.032	1325	100.00							
6.0	0.017									
7.0	0.008									

	Minor Lithic Counts		Abundance [volume %]	
	SML	GCL	SML	GCL
	0	0	0	0
	4	3	2.5	1.9
	9	10	5.1	5.6
	7	46	2.3	14.9
	0	0	0	0

Counts:

ϕ	Wp	Gp	Bp	Xtal	Lithic	Glass	NA	total counts
-5.0	0	0	n.a.	0	0	0	0	0
-4.5	0	0	n.a.	0	0	0	0	0
-4.0	0	0	n.a.	0	0	0	0	0
-3.5	0	0	n.a.	0	0	0	0	0
-3.0	189	11	10	0	21	0	0	231
-2.5							0	
-2.0							0	
-1.5	767	15	10	0	196	0	0	988
-1.0	1066	31	6	0	203	0	0	1306
-0.5							0	
0.0	536	18	2	31	158	5	0	750
0.5							0	
1.0	367	44	0	412	178	19	0	1020
1.5							0	
2.0	105	19	0	292	309	25	0	750
2.5							0	
3.0	19	3	0	405	182	141	0	750
3.5							0	
4.0							0	
4.5	29	0	0	78	51	342	0	500
5.0	7	0	0	74	68	351	0	500
6.0	0	0	0	0	0	0	*	*
7.0	0	0	0	0	0	0	0	0

Bulk Weight Percentages:

Wp	Gp	Bp	Xtal	Lithic	Glass	NA
0	0	n.a.	0	0	0	0
0	0	n.a.	0	0	0	0
0	0	n.a.	0	0	0	0
0	0	n.a.	0	0	0	0
18.07	1.11	0.96	0	6.32	0	0
						0
						0
20.82	0.56	0.45	0	9.59	0	0
9.69	0.41	0.08	0	3.95	0	0
						0
11.71	0.45	0.05	1.07	5.67	0.16	0
						0
2.25	0.30	0	3.32	1.49	0.14	0
						0
0.03	0.01	0	0.29	0.30	0.02	0
						0
0.0+	0.0+	0	0.04	0.02	0.01	0
						0
						0
0.0+	0	0	0.02	0.01	0.07	0
0.0+	0	0	0.02	0.01	0.08	0
*	*	*	*	*	*	0.45
*	*	*	*	*	*	0
62.57	**2.84**	**1.54**	**4.76**	**27.36**	**0.48**	**0.45**

P1 at Locality 1 [0-20 cm from base] [Total sample weight: 2126300 mg]

Grain diameter		Weight Fractions		Granulometric Analysis						
ϕ	mm	weight [mg]	Cumulative weight %	ϕ_{05}	ϕ_{84}	ϕ_{16}	ϕ_{95}	Md_ϕ	σ_ϕ	Fl
-5.0	31.5	319000	15.00	-2.6	-3.3	-4.9	-5.2	-4.4	0.79	0.00%
-4.5	22.4	545000	40.63							
-4.0	16.0	516000	64.90							
-3.5	11.2	293000	78.68							
-3.0	8.0	235000	89.73							
-2.5	5.6	140000	96.32							
-2.0	4.0	43300	98.35							
-1.5	2.8	15931.9	99.10							
-1.0	2.0	6100.7	99.39							
-0.5	1.4	3546.0	99.56							
0.0	1.0	2413.9	99.67							
0.5	0.710	2005.5	99.76							
1.0	0.500	1834.8	99.85							
1.5	0.355	1141.3	99.90							
2.0	0.250	580.8	99.93							
2.5	0.180	1445.1	100.00							
3.0	0.125	0								
3.5	0.088	0								
4.0	0.063	0								
4.5	0.045	0								
5.0	0.032	0								
6.0	0.017	0								
7.0	0.008	0								

Minor Lithic Counts		Abundance [volume %]	
SMI	GCI	SMI	GCI
0	2	0	1.6
0	11	0	4.9
0	8	0	6.3
0	4	0	1.8
0	0	0	0
0	0	0	0
0	0	0	0
0	0	0	0

Counts:

ϕ	Wp	Gp	Bp	Xtal	Lithic	Glass	NA	total counts
-5.0	51	0	n.a.	0	1	0	0	52
-4.5	128	0	n.a.	0	2	0	0	130
-4.0	179	0	n.a.	0	1	0	0	180
-3.5	149	5	n.a.	0	8	0	0	162
-3.0	309	9	n.a.	0	19	0	0	637
-2.5	1129	14	n.a.	0	33	0	0	1176
-2.0	691	43	n.a.	0	63	0	0	797
-1.5	354	0	0	0	83	0	0	437
-1.0	262	0	1	0	128	0	0	391
-0.5	272	0	0	3	225	0	0	500
0.0	358	0	0	15	127	0	0	500
0.5	260	0	0	21	219	0	0	500
1.0	151	0	0	25	319	3	0	498
1.5	96	0	0	68	317	19	0	500
2.0	61	0	0	95	321	23	0	500
2.5	0	0	0	0	0	0	*	*
3.0	0	0	0	0	0	0	0	0
3.5	0	0	0	0	0	0	0	0
4.0	0	0	0	0	0	0	0	0
4.5	0	0	0	0	0	0	0	0
5.0	0	0	0	0	0	0	0	0
6.0	0	0	0	0	0	0	0	0
7.0	0	0	0	0	0	0	0	0

Bulk Weight Percentages:

Wp	Gp	Bp	Xtal	Lithic	Glass	NA
11.89	0	n.a.	0	3.11	0	0
23.78	0	n.a.	0	1.85	0	0
23.86	0	n.a.	0	0.40	0	0
12.39	0.20	n.a.	0	1.19	0	0
9.91	0.15	n.a.	0	0.98	0	0
5.91	0.10	n.a.	0	0.58	0	0
1.55	0.14	n.a.	0	0.35	0	0
0.53	0	0	0	0.22	0	0
0.14	0	0.0+	0	0.15	0	0
0.07	0	0	0.0+	0.10	0	0
0.07	0	0	0.0+	0.04	0	0
0.04	0	0	0.0+	0.05	0	0
0.02	0	0	0.0+	0.06	0.0+	0
0.01	0	0	0.01	0.04	0.0+	0
0.0+	0	0	0.01	0.02	0.0+	0
0	0	0	0	0	0	0.07
0	0	0	0	0	0	0
0	0	0	0	0	0	0
0	0	0	0	0	0	0
0	0	0	0	0	0	0
0	0	0	0	0	0	0
0	0	0	0	0	0	0
90.18	**0.59**	**0.0+**	**0.02**	**9.14**	**0.0+**	**0.07**

P1 at Locality 1 [120-135 cm from base] [Total sample weight: 1274700 mg]

Grain diameter		Weight Fractions:		Granulometric Analysis						
ϕ	mm	weight [mg]	Cumulative weight %	ϕ_{05}	ϕ_{84}	ϕ_{10}	ϕ_{50}	Md_ϕ	σ_ϕ	F2
-5.0	31.5	77000	6.04	-1.2	-2.4	-4.7	-5.1	-3.7	1.17	0.00%
-4.5	22.4	225000	23.69							
-4.0	16.0	190000	38.60							
-3.5	11.2	195000	53.90							
-3.0	8.0	185000	68.41							
-2.5	5.6	155000	80.57							
-2.0	4.0	108700	89.10							
-1.5	2.8	50551.9	93.06							
-1.0	2.0	38023.8	96.04							
-0.5	1.4	24297.5	97.95							
0.0	1.0	10894.1	98.80							
0.5	0.710	5666.7	99.25							
1.0	0.500	2624.6	99.46							
1.5	0.355	1176.7	99.55							
2.0	0.250	917.4	99.62							
2.5	0.180	4847.4	100.00							
3.0	0.125	0								
3.5	0.088	0								
4.0	0.063	0								
4.5	0.045	0								
5.0	0.032	0								
6.0	0.017	0								
7.0	0.008	0								

Minor Lithic Counts		Abundance [volume %]	
SML	GCL	SML	GCL
0	0	0	0
0	0	0	0
0	0	0	0
0	6	0	3.8
0	10	0	3.9
0	0	0	0
0	0	0	0
0	0	0	0

Counts:

ϕ	Wp	Gp	Bp	Xtal	Lithic	Glass	NA	total counts
-5.0	15	0	n.a.	0	0	0	0	15
-4.5	57	0	n.a.	0	0	0	0	57
-4.0	64	0	n.a.	0	0	0	0	64
-3.5	104	9	n.a.	0	3	0	0	116
-3.0	181	19	n.a.	0	10	0	0	210
-2.5	405	39	n.a.	0	25	0	0	469
-2.0	2071	31	n.a.	0	72	0	0	2174
-1.5	433	2	10	0	55	0	0	500
-1.0	429	2	6	0	53	0	0	490
-0.5	426	0	5	4	65	0	0	500
0.0	347	0	4	58	91	0	0	500
0.5	208	0	4	125	160	3	0	500
1.0	135	0	0	104	259	2	0	500
1.5	204	0	0	51	229	16	0	500
2.0	245	0	0	30	202	23	0	500
2.5	0	0	0	0	0	0	*	*
3.0	0	0	0	0	0	0	0	0
3.5	0	0	0	0	0	0	0	0
4.0	0	0	0	0	0	0	0	0
4.5	0	0	0	0	0	0	0	0
5.0	0	0	0	0	0	0	0	0
6.0	0	0	0	0	0	0	0	0
7.0	0	0	0	0	0	0	0	0

Bulk Weight Percentages:

Wp	Gp	Bp	Xtal	Lithic	Glass	NA
6.04	0	n.a.	0	0	0	0
17.65	0	n.a.	0	0	0	0
14.91	0	n.a.	0	0	0	0
14.00	0.57	n.a.	0	0.73	0	0
11.28	1.25	n.a.	0	1.98	0	0
9.11	1.16	n.a.	0	1.89	0	0
7.70	0.16	n.a.	0	0.66	0	0
3.11	0.02	0.12	0	0.71	0	0
2.31	0.02	0.05	0	0.61	0	0
1.48	0	0.02	0.02	0.39	0	0
0.50	0	0.01	0.13	0.22	0	0
0.18	0	0.0+	0.11	0.15	0.01	0
0.04	0	0	0.04	0.12	0.0+	0
0.04	0	0	0.01	0.05	0.0+	0
0.01	0	0	0.01	0.04	0.0+	0
0	0	0	0	0	0	0.38
0	0	0	0	0	0	0
0	0	0	0	0	0	0
0	0	0	0	0	0	0
0	0	0	0	0	0	0
0	0	0	0	0	0	0
0	0	0	0	0	0	0
0	0	0	0	0	0	0
88.36	**3.18**	**0.20**	**0.32**	**7.55**	**0.01**	**0.38**

P1 at Locality 1 [227-247 cm from base] [Total sample weight: 2047300 mg]

Grain diameter		Weight Fractions:		Granulometric Analysis:						
ϕ	mm	weight [mg]	Cumulative weight %	ϕ_{05}	ϕ_{25}	ϕ_{16}	ϕ_{50}	Md_ϕ	σ_ϕ	F2
-5.0	31.5	325000	15.87	-0.6	-1.7	-4.9	-5.2	-3.2	1.53	0.00%
-4.5	22.4	148000	23.10							
-4.0	16.0	192000	32.48							
-3.5	11.2	230000	43.72							
-3.0	8.0	240000	55.44							
-2.5	5.6	251000	67.70							
-2.0	4.0	250300	79.92							
-1.5	2.8	133019.4	86.42							
-1.0	2.0	106301.9	91.61							
-0.5	1.4	78304.1	95.44							
0.0	1.0	45127.4	97.64							
0.5	0.710	23140.9	98.77							
1.0	0.500	10389.3	99.28							
1.5	0.355	3694.9	99.46							
2.0	0.250	1905.9	99.55							
2.5	0.180	911.6.1	100.00							
3.0	0.125	0								
3.5	0.088	0								
4.0	0.063	0								
4.5	0.045	0								
5.0	0.032	0								
6.0	0.017	0								
7.0	0.008	0								

Minor Lithic Counts		Abundance [volume %]	
SML	GCL	SML	GCL
n.a.	n.a.	n.a.	n.a.

Counts:

ϕ	Wp	Gp	Bp	Xtal	Lithic	Glass	NA	total counts
-5.0	66	0	n.a.	0	0	0	0	66
-4.5	38	0	n.a.	0	0	0	0	38
-4.0	66	0	n.a.	0	1	0	0	67
-3.5	102	1	n.a.	0	15	0	0	118
-3.0	542	3	n.a.	0	47	0	0	592
-2.5	1703	7	n.a.	0	139	0	0	1849
-2.0	4109	201	n.a.	0	341	0	0	4651
-1.5	359	4	14	0	123	0	0	500
-1.0	364	7	12	0	117	0	0	500
-0.5	381	7	7	0	105	0	0	500
0.0	396	8	3	9	78	6	0	500
0.5	280	5	2	38	168	7	0	500
1.0	125	6	0	94	263	12	0	500
1.5	153	4	0	62	261	20	0	500
2.0	195	2	0	28	250	24	0	500
2.5	0	0	0	0	0	0	0	0
3.0	0	0	0	0	0	0	0	0
3.5	0	0	0	0	0	0	0	0
4.0	0	0	0	0	0	0	0	0
4.5	0	0	0	0	0	0	0	0
5.0	0	0	0	0	0	0	0	0
6.0	0	0	0	0	0	0	0	0
7.0	0	0	0	0	0	0	0	0

Bulk Weight Percentages:

Wp	Gp	Bp	Xtal	Lithic	Glass	NA
16.34	0	n.a.	0	0	0	0
7.23	0	n.a.	0	0	0	0
9.10	0	n.a.	0	0.27	0	0
8.85	0.04	n.a.	0	2.34	0	0
9.15	0.05	n.a.	0	2.52	0	0
9.58	0.05	n.a.	0	0.63	0	0
9.60	0.66	n.a.	0	1.96	0	0
5.36	0.06	0.25	0	2.36	0	0
2.94	0.08	0.14	0	2.03	0	0
2.53	0.05	0.05	0	1.20	0	0
1.56	0.04	0.01	0.06	0.50	0.04	0
0.58	0.02	0.0+	0.09	0.42	0.02	0
0.10	0.01	0	0.10	0.29	0.01	0
0.03	0	0	0.03	0.11	0.01	0
0.02	0	0	0.01	0.06	0.01	0
0	0	0	0	0	0	0.45
0	0	0	0	0	0	0
0	0	0	0	0	0	0
0	0	0	0	0	0	0
0	0	0	0	0	0	0
0	0	0	0	0	0	0
0	0	0	0	0	0	0
0	0	0	0	0	0	0
82.97	**1.06**	**0.45**	**0.29**	**14.69**	**0.09**	**0.45**

P1 at Locality 18 [50-70 cm from base] [Total sample weight: 1539980 mg]

Grain diameter		Weight Fractions:		Granulometric Analysis:						
ϕ	mm	weight [mg]	Cumulative weight %	ϕ_{05}	ϕ_{84}	ϕ_{16}	$\phi_{\bar{x}}$	Md_ϕ	σ_ϕ	F2
-5.0	31.5	208000	13.51	-0.9	-1.9	-4.9	-5.2	-3.6	1.39	0.00%
-4.5	22.4	184000	25.45							
-4.0	16.0	176000	36.88							
-3.5	11.2	226000	51.56							
-3.0	8.0	168000	62.47							
-2.5	5.6	163000	73.05							
-2.0	4.0	159000	83.38							
-1.5	2.8	109190	90.47							
-1.0	2.0	60580	94.40							
-0.5	1.4	59090	98.24							
0.0	1.0	10590	98.93							
0.5	0.710	6140	99.33							
1.0	0.500	3360	99.54							
1.5	0.355	1330	99.63							
2.0	0.250	530	99.66							
2.5	0.180	5170	100.00							
3.0	0.125	0								
3.5	0.088	0								
4.0	0.063	0								
4.5	0.045	0								
5.0	0.032	0								
6.0	0.017	0								
7.0	0.008	0								

Minor Lithic Counts		Abundance [volume %]	
SMI.	GCI.	SMI.	GCI.
0	0	0	0
0	0	0	0
9	81	4.0	36.3
5	233	1.3	61.0
2	105	1.6	82.7
29	0	9.6	0
18	0	5.2	0
0	0	0	0
0	0	0	0

Counts:

ϕ	Wp	Gp	Bp	Xtal	Lithic	Glass	NA	total counts
-5.0	42	0	n.a.	0	0	0	0	42
-4.5	47	0	n.a.	0	0	0	0	47
-4.0	59	3	n.a.	0	0	0	0	62
-3.5	116	5	n.a.	0	6	0	0	127
-3.0	436	8	n.a.	0	13	0	0	457
-2.5	1324	20	n.a.	0	38	0	0	1382
-2.0	2944	79	n.a.	0	103	0	0	3126
-1.5	1244	4	0	0	29	0	0	1277
-1.0	1516	10	0	0	143	0	0	1669
-0.5	2561	13	0	4	341	0	0	2919
0.0	1390	8	0	62	223	0	0	1683
0.5	1048	9	0	207	382	0	0	1646
1.0	1265	11	0	96	127	0	0	1499
1.5	113	1	0	332	302	2	0	750
2.0	159	0	0	229	346	16	0	750
2.5	0	0	0	0	0	0	0	0
3.0	0	0	0	0	0	0	0	0
3.5	0	0	0	0	0	0	0	0
4.0	0	0	0	0	0	0	0	0
4.5	0	0	0	0	0	0	0	0
5.0	0	0	0	0	0	0	0	0
6.0	0	0	0	0	0	0	0	0
7.0	0	0	0	0	0	0	0	0

Bulk Weight Percentages:

Wp	Gp	Bp	Xtal	Lithic	Glass	NA
13.48	0	n.a.	0	0	0	0
11.95	0	n.a.	0	0	0	0
10.86	0.57	n.a.	0	0	0	0
13.18	0.27	n.a.	0	1.22	0	0
9.79	0.19	n.a.	0	0.93	0	0
9.48	0.19	n.a.	0	0.91	0	0
9.18	0.35	n.a.	0	0.79	0	0
6.78	0.03	0	0	0.28	0	0
3.25	0.03	0	0	0.66	0	0
3.10	0.02	0	0.01	0.71	0	0
0.51	0.0+	0	0.04	0.14	0	0
0.23	0.0+	0	0.06	0.11	0	0
0.17	0.0+	0	0.02	0.02	0	0
0.01	0.0+	0	0.04	0.04	0.0+	0
0.01	0	0	0.01	0.03	0.0+	0
0	0	0	0	0	0	0.34
0	0	0	0	0	0	0
0	0	0	0	0	0	0
0	0	0	0	0	0	0
0	0	0	0	0	0	0
0	0	0	0	0	0	0
0	0	0	0	0	0	0
0	0	0	0	0	0	0
0	0	0	0	0	0	0
91.98	**1.65**	**0**	**0.18**	**5.84**	**0.01**	**0.34**

P1 at Locality 18 [200-220 cm from base] [Total sample weight: 1622500 mg]

Grain diameter		Weight Fractions		Granulometric Analysis						
ϕ	mm	weight [mg]	Cumulative weight %	ϕ_{05}	ϕ_{84}	ϕ_{16}	ϕ_{50}	Md$_\phi$	σ_ϕ	F2
-5.0	31.5	196000	12.08	-4.9	-2.2	-4.9	-5.2	-3.7	1.31	0.00%
-4.5	22.4	262000	28.23							
-4.0	16.0	235000	42.71							
-3.5	11.2	222500	56.43							
-3.0	8.0	183000	67.70							
-2.5	5.6	168000	78.06							
-2.0	4.0	131000	86.13							
-1.5	2.8	76802.1	90.87							
-1.0	2.0	57338.4	94.40							
-0.5	1.4	38561.8	96.78							
0.0	1.0	18985.8	97.95							
0.5	0.710	10975.7	98.62							
1.0	0.500	5443.2	98.96							
1.5	0.355	3058.4	99.15							
2.0	0.250	2243.7	99.29							
2.5	0.180	11591	100.00							
3.0	0.125	0								
3.5	0.088	0								
4.0	0.063	0								
4.5	0.045	0								
5.0	0.032	0								
6.0	0.017	0								
7.0	0.008	0								

Minor Lithic Counts		Abundance [volume %]	
SML	GCL	SML	GCL
n.a.	n.a.	n.a.	n.a.

Counts:

ϕ	Wp	Gp	Bp	Xtal	Lithic	Glass	NA	total counts
-5.0	22	0	n.a.	0	1	0	0	23
-4.5	66	0	n.a.	0	0	0	0	66
-4.0	83	0	n.a.	0	0	0	0	83
-3.5	118	4	n.a.	0	4	0	0	126
-3.0	490	8	n.a.	0	9	0	0	507
-2.5	1396	18	n.a.	0	26	0	0	1440
-2.0	2461	45	n.a.	0	95	0	0	2601
-1.5	669	2	21	0	58	0	0	750
-1.0	699	2	7	0	42	0	0	750
-0.5	686	1	9	0	54	0	0	750
0.0	679	2	7	23	39	0	0	750
0.5	537	3	5	78	126	1	0	750
1.0	381	0	1	114	253	1	0	750
1.5	321	0	0	123	290	16	0	750
2.0	265	0	2	138	309	36	0	750
2.5	0	0	0	0	0	0	*	*
3.0	0	0	0	0	0	0	0	0
3.5	0	0	0	0	0	0	0	0
4.0	0	0	0	0	0	0	0	0
4.5	0	0	0	0	0	0	0	0
5.0	0	0	0	0	0	0	0	0
6.0	0	0	0	0	0	0	0	0
7.0	0	0	0	0	0	0	0	0

Bulk Weight Percentages:

Wp	Gp	Bp	Xtal	Lithic	Glass	NA
7.52	0	n.a.	0	4.56	0	0
16.15	0	n.a.	0	0	0	0
14.48	0	n.a.	0	0	0	0
12.73	0.20	n.a.	0	0.78	0	0
10.49	0.18	n.a.	0	0.61	0	0
9.59	0.16	n.a.	0	0.60	0	0
7.20	0.19	n.a.	0	0.69	0	0
3.90	0.02	0.21	0	0.61	0	0
3.08	0.01	0.04	0	0.40	0	0
2.07	0.0+	0.03	0	0.28	0	0
1.01	0.0+	0.01	0.05	0.09	0	0
0.44	0.0+	0.0+	0.08	0.14	0.0+	0
0.15	0	0.0+	0.06	0.13	0.0+	0
0.05	0	0	0.04	0.10	0.01	0
0.02	0	0.0+	0.03	0.08	0.01	0
0	0	0	0	0	0	0.71
0	0	0	0	0	0	0
0	0	0	0	0	0	0
0	0	0	0	0	0	0
0	0	0	0	0	0	0
0	0	0	0	0	0	0
0	0	0	0	0	0	0
0	0	0	0	0	0	0
88.88	**0.76**	**0.29**	**0.26**	**9.07**	**0.03**	**0.71**

P1 at Locality 18 [550-560 cm from base] [Total sample weight 1359000 mg]

Grain diameter		Weight Fractions		Granulometric Analysis						
ϕ	mm	weight [mg]	Cumulative weight %	ϕ_{95}	ϕ_{84}	ϕ_{16}	ϕ_5	Md$_\phi$	σ_ϕ	F5
-5.0	31.5	163000	11.99	-1.2	-2.2	-4.9	-5.2	-3.6	1.29	0.00%
-4.5	22.4	186000	25.68							
-4.0	16.0	172000	38.34							
-3.5	11.2	200000	53.05							
-3.0	8.0	187000	66.81							
-2.5	5.6	136000	76.82							
-2.0	4.0	123000	85.87							
-1.5	2.8	80883.3	91.82							
-1.0	2.0	52137.9	95.66							
-0.5	1.4	28235.6	97.74							
0.0	1.0	12908.6	98.69							
0.5	0.710	7699.3	99.25							
1.0	0.500	4273.4	99.57							
1.5	0.355	2723.3	99.77							
2.0	0.250	1966.5	99.91							
2.5	0.180	1172.2	100.00							
3.0	0.125	0								
3.5	0.088	0								
4.0	0.063	0								
4.5	0.045	0								
5.0	0.032	0								
6.0	0.017	0								
7.0	0.008	0								

Minor Lithic Counts		Abundance [volume %]	
SML	GCL	SML	GCL
4	0	4.8	0
5	0	6.5	0
3	33	2.6	28.2
3	207	1.1	73.7
4	341	1.1	93.2
4	0	0.9	0
0	0	0	0
0	0	0	0
0	0	0	0

Counts:

ϕ	Wp	Gp	Bp	Xtal	Lithic	Glass	NA	total counts
-5.0	33	0	n.a.	0	0	0	0	33
-4.5	45	2	n.a.	0	0	0	0	47
-4.0	53	4	n.a.	0	2	0	0	59
-3.5	98	3	n.a.	0	8	0	0	109
-3.0	465	6	n.a.	0	21	0	0	492
-2.5	1059	11	n.a.	0	47	0	0	1117
-2.0	109	75	n.a.	0	139	0	0	323
-1.5	618	4	21	0	107	0	0	750
-1.0	649	2	16	0	83	0	0	750
-0.5	662	1	10	0	77	0	0	750
0.0	568	2	11	52	117	0	0	750
0.5	310	4	6	139	281	0	0	750
1.0	281	0	2	98	366	3	0	750
1.5	240	0	0	64	442	4	0	750
2.0	255	0	0	92	391	12	0	750
2.5	0	0	0	0	0	0	*	*
3.0	0	0	0	0	0	0	0	0
3.5	0	0	0	0	0	0	0	0
4.0	0	0	0	0	0	0	0	0
4.5	0	0	0	0	0	0	0	0
5.0	0	0	0	0	0	0	0	0
6.0	0	0	0	0	0	0	0	0
7.0	0	0	0	0	0	0	0	0

Bulk Weight Percentages:

Wp	Gp	Bp	Xtal	Lithic	Glass	NA
11.99	0	n.a.	0	0	0	0
13.10	0.58	n.a.	0	0	0	0
10.98	0.86	n.a.	0	0.82	0	0
12.68	0.18	n.a.	0	1.86	0	0
11.89	0.16	n.a.	0	1.71	0	0
8.61	0.12	n.a.	0	1.28	0	0
1.77	1.72	n.a.	0	5.56	0	0
4.32	0.04	0.25	0	1.35	0	0
2.92	0.01	0.10	0	0.80	0	0
1.71	0.0+	0.03	0	0.34	0	0
0.63	0.0+	0.01	0.09	0.21	0	0
0.25	0.0+	0.0+	0.10	0.21	0	0
0.10	0.0+	0.0+	0.04	0.17	0.0+	0
0.04	0	0	0.02	0.14	0.0+	0
0.02	0	0	0.02	0.11	0.0+	0
0	0	0	0	0	0	0.09
0	0	0	0	0	0	0
0	0	0	0	0	0	0
0	0	0	0	0	0	0
0	0	0	0	0	0	0
0	0	0	0	0	0	0
0	0	0	0	0	0	0
0	0	0	0	0	0	0
0	0	0	0	0	0	0
81.01	**3.67**	**0.39**	**0.27**	**14.56**	**0.01**	**0.09**

P1 at Locality 18 [20–40 cm from top] [Total sample weight: 2147000 mg]

Grain diameter		Weight Fractions:		Granulometric Analysis:						
ϕ	mm	weight [mg]	Cumulative weight %	ϕ_{05}	ϕ_{25}	ϕ_{50}	ϕ_{75}	Md_ϕ	σ_ϕ	F2
-5.0	31.5	705000	32.84	-0.8	-2.2	-5.2	-5.5	-4.1	1.47	0.00%
-4.5	22.4	220000	43.08							
-4.0	16.0	175000	51.23							
-3.5	11.2	185000	59.85							
-3.0	8.0	215000	69.86							
-2.5	5.6	185000	78.48							
-2.0	4.0	173000	86.54							
-1.5	2.8	70312.9	89.81							
-1.0	2.0	79092.8	93.50							
-0.5	1.4	66695.9	96.60							
0.0	1.0	37997.5	98.37							
0.5	0.710	20761.8	99.34							
1.0	0.500	8692.4	99.75							
1.5	0.355	2480.8	99.86							
2.0	0.250	776.8	99.90							
2.5	0.180	2190	100.00							
3.0	0.125	0								
3.5	0.088	0								
4.0	0.063	0								
4.5	0.045	0								
5.0	0.032	0								
6.0	0.017	0								
7.0	0.008	0								

Minor Lithic Counts:		Abundance: [volume %]	
SML	GCL	SML	GCL
0	2	0	3.3
0	3	0	1.9
0	5	0	2.0
0	5	0	1.7
0	3	0	0.9
0	1	0	0.2
0	8	0	1.8
0	0	0	0
0	0	0	0

Counts:

ϕ	Wp	Gp	Bp	Xtal	Lithic	Glass	NA	total counts
-5.0	141	0	n.a.	0	0	0	0	141
-4.5	56	0	n.a.	0	0	0	0	56
-4.0	57	3	n.a.	0	1	0	0	61
-3.5	89	5	n.a.	0	7	0	0	101
-3.0	526	13	n.a.	0	26	0	0	565
-2.5	1412	28	n.a.	0	67	0	0	1507
-2.0	3026	113	n.a.	0	177	0	0	3316
-1.5	605	7	73	0	65	0	0	750
-1.0	647	5	38	0	60	0	0	750
-0.5	531	14	26	19	160	0	0	750
0.0	435	18	20	31	246	0	0	750
0.5	307	25	19	106	290	3	0	750
1.0	252	14	4	138	333	9	0	750
1.5	110	0	0	173	456	11	0	750
2.0	53	0	0	214	445	38	0	750
2.5	0	0	0	0	0	0	0	0
3.0	0	0	0	0	0	0	0	0
3.5	0	0	0	0	0	0	0	0
4.0	0	0	0	0	0	0	0	0
4.5	0	0	0	0	0	0	0	0
5.0	0	0	0	0	0	0	0	0
6.0	0	0	0	0	0	0	0	0
7.0	0	0	0	0	0	0	0	0

Bulk Weight Percentages:

Wp	Gp	Bp	Xtal	Lithic	Glass	NA
32.84	0	n.a.	0	0	0	0
10.25	0	n.a.	0	0	0	0
7.48	0.40	n.a.	0	0.26	0	0
7.38	0.20	n.a.	0	1.04	0	0
8.46	0.22	n.a.	0	1.33	0	0
7.27	0.19	n.a.	0	1.16	0	0
6.73	0.36	n.a.	0	0.97	0	0
2.32	0.04	0.47	0	0.45	0	0
2.85	0.03	0.24	0	0.57	0	0
1.88	0.05	0.09	0.11	0.97	0	0
0.83	0.04	0.04	0.09	0.77	0	0
0.35	0.04	0.02	0.14	0.41	0.0-	0
0.11	0.01	0.0-	0.08	0.20	0.0-	0
0.01	0	0	0.03	0.08	0.0-	0
0.0-	0	0	0.01	0.02	0.0-	0
0	0	0	0	0	0	0.10
0	0	0	0	0	0	0
0	0	0	0	0	0	0
0	0	0	0	0	0	0
0	0	0	0	0	0	0
0	0	0	0	0	0	0
0	0	0	0	0	0	0
0	0	0	0	0	0	0
88.76	**1.58**	**0.86**	**0.46**	**8.23**	**0.01**	**0.10**

PI at Locality 18 [bulk 20 cm from top] [Total sample weight 1997268 mg]

Grain diameter		Weight Fractions:		Granulometric Analysis						
ϕ	mm	weight [mg]	Cumulative weight %	$\phi_{5\%}$	ϕ_{95}	ϕ_{16}	ϕ_{50}	Md_ϕ	σ_ϕ	Fl
-5.0	31.5	54000	2.70	0.1	-0.8	-4.4	-4.7	-3.1	1.63	0.00%
-4.5	22.4	173000	11.37							
-4.0	16.0	271000	24.93							
-3.5	11.2	275000	38.70							
-3.0	8.0	230000	50.22							
-2.5	5.6	220000	61.23							
-2.0	4.0	213000	71.90							
-1.5	2.8	127720	78.29							
-1.0	2.0	60820	81.34							
-0.5	1.4	172820	89.99							
0.0	1.0	95770	94.79							
0.5	0.710	67420	98.16							
1.0	0.500	22550	99.29							
1.5	0.355	9790	99.78							
2.0	0.250	2740	99.92							
2.5	0.180	1640	100.00							
3.0	0.125	0								
3.5	0.088	0								
4.0	0.063	0								
4.5	0.045	0								
5.0	0.032	0								
6.0	0.017	0								
7.0	0.008	0								

	Minor Lithic Counts		Abundance [volume %]	
	SML	GCL	SML	GCL
-1.0	0	0	0	0
-0.5	0	0	0	0
0.0	0	6	0	2.2
0.5	0	9	0	2.8
1.0	0	1	0	0.2
1.5	0	6	0	1.6
2.0	0	3	0	0.7
2.5	0	0	0	0
3.0	0	0	0	0

Counts:

ϕ	Wp	Gp	Bp	Xtal	Lithic	Glass	NA	total counts
-5.0	11	0	n.a.	0	0	0	0	11
-4.5	36	0	n.a.	0	1	0	0	37
-4.0	92	1	n.a.	0	1	0	0	94
-3.5	71	9	n.a.	0	9	0	0	89
-3.0	577	18	n.a.	0	21	0	0	616
-2.5	1726	43	n.a.	0	60	0	0	1829
-2.0	3604	161	n.a.	0	252	0	0	4017
-1.5	493	12	26	0	98	0	0	629
-1.0	449	18	17	0	116	0	0	600
-0.5	505	14	11	0	136	0	0	666
0.0	427	15	8	24	276	0	0	750
0.5	295	13	5	116	321	0	0	750
1.0	132	5	1	197	415	0	0	750
1.5	152	8	0	209	380	1	0	750
2.0	120	1	0	220	405	4	0	750
2.5	0	0	0	0	0	0	*	*
3.0	0	0	0	0	0	0	0	0
3.5	0	0	0	0	0	0	0	0
4.0	0	0	0	0	0	0	0	0
4.5	0	0	0	0	0	0	0	0
5.0	0	0	0	0	0	0	0	0
6.0	0	0	0	0	0	0	0	0
7.0	0	0	0	0	0	0	0	0

Bulk Weight Percentages:

ϕ	Wp	Gp	Bp	Xtal	Lithic	Glass	NA
-5.0	2.75	0	n.a.	0	0	0	0
-4.5	7.61	0	n.a.	0	1.05	0	0
-4.0	13.14	0.15	n.a.	0	0.28	0	0
-3.5	10.69	0.64	n.a.	0	2.43	0	0
-3.0	10.03	0.33	n.a.	0	1.16	0	0
-2.5	9.58	0.32	n.a.	0	1.12	0	0
-2.0	8.63	0.55	n.a.	0	1.49	0	0
-1.5	4.32	0.14	0.38	0	1.55	0	0
-1.0	1.83	0.11	0.10	0	1.01	0	0
-0.5	5.72	0.16	0.13	0	2.65	0	0
0.0	2.17	0.09	0.05	0.19	2.30	0	0
0.5	1.19	0.08	0.01	0.54	1.55	0	0
1.0	0.15	0.01	0.0+	0.30	0.66	0	0
1.5	0.05	0.01	0	0.15	0.28	0.0+	0
2.0	0.01	0.0+	0	0.05	0.02	0.0+	0
2.5	0	0	0	0	0	0	0.08
3.0	0	0	0	0	0	0	0
3.5	0	0	0	0	0	0	0
4.0	0	0	0	0	0	0	0
4.5	0	0	0	0	0	0	0
5.0	0	0	0	0	0	0	0
6.0	0	0	0	0	0	0	0
7.0	0	0	0	0	0	0	0
	77.87	**2.59**	**0.67**	**1.23**	**17.55**	**0.01**	**0.08**

P1 at Locality 18 [top cm's] [Total sample weight: 93166 mg]

Grain diameter		Weight Fractions:		Granulometric Analysis						
ϕ	mm	weight [mg]	Cumulative weight %	$\phi_{5\%}$	ϕ_{25}	ϕ_{75}	ϕ_{95}	Md_ϕ	σ_ϕ	F2
-5.0	31.5	0	0	1.2	0.4	-1.8	-2.7	-0.2	1.14	0.00%
-4.5	22.4	0	0							
-4.0	16.0	632.5	0.68							
-3.5	11.2	1114.8	1.88							
-3.0	8.0	1755.3	3.76							
-2.5	5.6	2815.4	6.78							
-2.0	4.0	6538.5	13.80							
-1.5	2.8	13370.9	28.15							
-1.0	2.0	10492.9	39.41							
-0.5	1.4	19131.3	59.95							
0.0	1.0	14129.3	75.11							
0.5	0.710	13575.1	89.68							
1.0	0.500	4342.8	94.35							
1.5	0.355	1776.3	96.25							
2.0	0.250	626.3	96.92							
2.5	0.180	286.5	100.00							
3.0	0.125	0								
3.5	0.088	0								
4.0	0.063	0								
4.5	0.045	0								
5.0	0.032	0								
6.0	0.017	0								
7.0	0.008	0								

Minor Lithic Counts		Abundance [volume %]	
SML	GCL	SML	GCL
0	0	0	0
0	0	0	0
4	53	1.0	13.2
4	84	0.9	18.8
0	147	0	29.9
0	0	0	0
0	0	0	0
0	0	0	0
0	0	0	0

Counts:

ϕ	Wp	Gp	Bp	Xtal	Lithic	Glass	NA	total counts
-5.0	0	0	0	0	0	0	0	0
-4.5	0	0	0	0	0	0	0	0
-4.0	1	0	0	0	0	0	0	1
-3.5	2	0	0	0	0	0	0	2
-3.0	3	0	1	0	1	0	0	5
-2.5	16	1	2	0	4	0	0	23
-2.0	97	3	9	0	17	0	0	126
-1.5	545	23	27	0	127	0	0	722
-1.0	610	17	27	0	220	0	0	874
-0.5	483	13	19	2	230	3	0	750
0.0	308	15	10	5	402	10	0	750
0.5	239	12	8	32	447	12	0	750
1.0	164	6	1	73	491	15	0	750
1.5	176	9	0	128	419	18	0	750
2.0	207	11	0	170	343	19	0	750
2.5	0	0	0	0	0	0	0	0
3.0	0	0	0	0	0	0	0	0
3.5	0	0	0	0	0	0	0	0
4.0	0	0	0	0	0	0	0	0
4.5	0	0	0	0	0	0	0	0
5.0	0	0	0	0	0	0	0	0
6.0	0	0	0	0	0	0	0	0
7.0	0	0	0	0	0	0	0	0

Bulk Weight Percentages:

Wp	Gp	Bp	Xtal	Lithic	Glass	NA
0	0	0	0	0	0	0
0	0	0	0	0	0	0
0.68	0	0	0	0	0	0
1.20	0	0	0	0	0	0
0.79	0	0.26	0	0.83	0	0
1.23	0.10	0.65	0	1.04	0	0
4.41	0.19	0.50	0	1.91	0	0
9.20	0.53	0.76	0	3.86	0	0
6.00	0.24	0.38	0	4.64	0	0
10.80	0.30	0.44	0.07	8.84	0.09	0
4.58	0.26	0.17	0.12	9.82	0.22	0
3.78	0.32	0.10	0.65	9.48	0.23	0
0.80	0.03	0.01	0.47	3.27	0.09	0
0.23	0.04	0	0.36	1.23	0.05	0
0.08	0.03	0	0.19	0.38	0.02	0
0	0	0	0	0	0	3.08
0	0	0	0	0	0	0
0	0	0	0	0	0	0
0	0	0	0	0	0	0
0	0	0	0	0	0	0
0	0	0	0	0	0	0
0	0	0	0	0	0	0
0	0	0	0	0	0	0
43.78	**2.01**	**3.27**	**1.86**	**45.30**	**0.70**	**3.08**

P1 at Locality 29 [0-20 cm from base] [Total sample weight: 638890 mg]

Grain diameter		Weight Fractions:		Granulometric Analysis						
ϕ	mm	weight [mg]	Cumulative weight %	$\phi_{5\%}$	ϕ_{25}	ϕ_{75}	ϕ_{95}	Md_ϕ	σ_ϕ	F2
-5.0	31.5	0	0	-1.3	-2.3	-3.5	-3.9	-2.6	0.71	0.00%
-4.5	22.4	8000	1.25							
-4.0	16.0	19000	4.23							
-3.5	11.2	34420	9.61							
-3.0	8.0	150000	33.09							
-2.5	5.6	148000	56.26							
-2.0	4.0	141470	78.40							
-1.5	2.8	83563.3	91.48							
-1.0	2.0	30211.1	96.20							
-0.5	1.4	12033.8	98.09							
0.0	1.0	6419.2	99.09							
0.5	0.710	3611.3	99.66							
1.0	0.500	469.1	99.73							
1.5	0.355	343.9	99.78							
2.0	0.250	315.4	99.83							
2.5	0.180	1060	100.00							
3.0	0.125	0								
3.5	0.088	0								
4.0	0.063	0								
4.5	0.045	0								
5.0	0.032	0								
6.0	0.017	0								
7.0	0.008	0								

Minor Lithic Counts		Abundance [volume %]	
SML	GCL	SML	GCL
n.a.	n.a.	n.a.	n.a.

Counts:

ϕ	Wp	Gp	Bp	Xtal	Lithic	Glass	NA	total counts
-5.0	0	0	n.a.	0	0	0	0	0
-4.5	2	0	n.a.	0	0	0	0	2
-4.0	7	0	n.a.	0	0	0	0	7
-3.5	19	0	n.a.	0	0	0	0	19
-3.0	43	0	n.a.	0	0	0	0	43
-2.5	134	11	n.a.	0	5	0	0	150
-2.0	287	26	n.a.	0	23	0	0	336
-1.5	480	4	0	0	16	0	0	500
-1.0	391	5	0	1	103	0	0	500
-0.5	249	6	0	16	229	0	0	500
0.0	138	5	0	131	226	0	0	500
0.5	44	3	1	225	227	0	0	500
1.0	103	0	0	88	309	0	0	500
1.5	104	0	0	79	312	5	0	500
2.0	101	0	0	73	316	10	0	500
2.5	0	0	0	0	0	0	*	*
3.0	0	0	0	0	0	0	0	0
3.5	0	0	0	0	0	0	0	0
4.0	0	0	0	0	0	0	0	0
4.5	0	0	0	0	0	0	0	0
5.0	0	0	0	0	0	0	0	0
6.0	0	0	0	0	0	0	0	0
7.0	0	0	0	0	0	0	0	0

Bulk Weight Percentages:

Wp	Gp	Bp	Xtal	Lithic	Glass	NA
0	0	n.a.	0	0	0	0
1.25	0	n.a.	0	0	0	0
2.97	0	n.a.	0	0	0	0
5.39	0	n.a.	0	0	0	0
23.48	0	n.a.	0	0	0	0
18.77	2.04	n.a.	0	2.35	0	0
16.70	2.14	n.a.	0	3.30	0	0
12.20	0.14	0	0	0.73	0	0
2.98	0.06	0	0.01	1.68	0	0
0.69	0.02	0	0.07	1.10	0	0
0.19	0.01	0	0.29	0.52	0	0
0.09	0.0+	0.0+	0.23	0.24	0	0
0.01	0	0	0.01	0.05	0	0
0.01	0	0	0.01	0.04	0.0+	0
0.0+	0	0	0.01	0.04	0.0+	0
0	0	0	0	0	0	0.17
0	0	0	0	0	0	0
0	0	0	0	0	0	0
0	0	0	0	0	0	0
0	0	0	0	0	0	0
0	0	0	0	0	0	0
0	0	0	0	0	0	0
0	0	0	0	0	0	0
84.74	**4.41**	**0.0+**	**0.63**	**10.05**	**0.0+**	**0.17**

P1 at Locality 29 [120-140 cm from base] [Total sample weight 402550 mg]

Grain diameter		Weight Fractions		Granulometric Analysis						
φ	mm	weight [mg]	Cumulative weight %	ϕ_{05}	ϕ_{25}	ϕ_{16}	ϕ_{5}	Md$_{\phi}$	σ_{ϕ}	Fl
-5.0	31.5	0	0	-0.1	-1.1	-3.7	-4.4	-2.6	1.29	0.00%
-4.5	22.4	10000	2.48							
-4.0	16.0	30000	9.94							
-3.5	11.2	43480	20.74							
-3.0	8.0	70000	38.13							
-2.5	5.6	55000	51.79							
-2.0	4.0	51070	64.48							
-1.5	2.8	41496.5	74.78							
-1.0	2.0	39735.6	84.66							
-0.5	1.4	31837.0	92.56							
0.0	1.0	13929.6	96.02							
0.5	0.710	9253.0	98.32							
1.0	0.500	2916.9	99.05							
1.5	0.355	1250.4	99.36							
2.0	0.250	572.5	99.50							
2.5	0.180	2010	100.00							
3.0	0.125	0								
3.5	0.088	0								
4.0	0.063	0								
4.5	0.045	0								
5.0	0.032	0								
6.0	0.017	0								
7.0	0.008	0								

Minor Lithic Counts		Abundance [volume %]	
SML	GCL	SML	GCL
n.a.	n.a.	n.a.	n.a.

Counts:

φ	Wp	Gp	Bp	Xtal	Lithic	Glass	NA	total counts
-5.0	0	0	n.a.	0	0	0	0	0
-4.5	2	0	n.a.	0	0	0	0	2
-4.0	11	0	n.a.	0	0	0	0	11
-3.5	25	0	n.a.	0	0	0	0	25
-3.0	203	0	n.a.	0	0	0	0	203
-2.5	651	8	n.a.	0	1	0	0	660
-2.0	1151	5	n.a.	0	6	0	0	1162
-1.5	480	0	4	0	16	0	0	500
-1.0	482	1	0	0	17	0	0	500
-0.5	466	2	0	1	31	0	0	500
0.0	412	4	0	37	47	0	0	500
0.5	173	3	0	211	112	1	0	500
1.0	52	2	0	245	200	1	0	500
1.5	73	2	0	168	239	18	0	500
2.0	108	0	0	87	277	28	0	500
2.5	0	0	0	0	0	0	0	0
3.0	0	0	0	0	0	0	0	0
3.5	0	0	0	0	0	0	0	0
4.0	0	0	0	0	0	0	0	0
4.5	0	0	0	0	0	0	0	0
5.0	0	0	0	0	0	0	0	0
6.0	0	0	0	0	0	0	0	0
7.0	0	0	0	0	0	0	0	0

Bulk Weight Percentages:

Wp	Gp	Bp	Xtal	Lithic	Glass	NA
0	0	n.a.	0	0	0	0
2.48	0	n.a.	0	0	0	0
7.45	0	n.a.	0	0	0	0
10.80	0	n.a.	0	0	0	0
17.39	0	n.a.	0	0	0	0
13.38	0.22	n.a.	0	0.07	0	0
12.45	0.08	n.a.	0	0.16	0	0
9.60	0	0.13	0	0.58	0	0
9.15	0.03	0	0	0.69	0	0
7.05	0.03	0	0.02	0.81	0	0
2.58	0.03	0	0.37	0.48	0	0
0.98	0.02	0	0.84	0.46	0.0+	0
0.06	0.0+	0	0.36	0.30	0.0+	0
0.02	0.0+	0	0.11	0.16	0.01	0
0.01	0	0	0.03	0.09	0.01	0
0	0	0	0	0	0	0.50
0	0	0	0	0	0	0
0	0	0	0	0	0	0
0	0	0	0	0	0	0
0	0	0	0	0	0	0
0	0	0	0	0	0	0
0	0	0	0	0	0	0
0	0	0	0	0	0	0
0	0	0	0	0		0
0	0	0	0	0		0
93.40	**0.14**	**0.13**	**1.73**	**3.80**	**0.03**	**0.50**

P1 at Locality 29 [240-259 cm from base (~15 cm from top)] [Total sample weight 461960 mg]

Grain diameter		Weight Fractions		Granulometric Analysis						
ϕ	mm	weight [mg]	Cumulative weight %	ϕ_{05}	ϕ_{84}	ϕ_{16}	ϕ_{50}	Md_ϕ	σ	F2
-5.0	31.5	0	0	0.1	-0.7	-3.2	-3.9	-1.9	1.24	0.00%
-4.5	22.4	10000	2.16							
-4.0	16.0	12000	4.76							
-3.5	11.2	21433	9.40							
-3.0	8.0	40000	18.06							
-2.5	5.6	72000	33.65							
-2.0	4.0	68530	48.48							
-1.5	2.8	65389.8	62.64							
-1.0	2.0	60051.1	75.63							
-0.5	1.4	55620.8	87.67							
0.0	1.0	28449.5	93.83							
0.5	0.710	18773.3	97.90							
1.0	0.500	4672.5	98.91							
1.5	0.355	2126.7	99.37							
2.0	0.250	712.9	99.52							
2.5	0.180	2200	100.00							
3.0	0.125									
3.5	0.088	0								
4.0	0.063	0								
4.5	0.045	0								
5.0	0.032	0								
6.0	0.017	0								
7.0	0.008	0								

Minor Lithic Counts		Abundance [volume %]	
SML	GCL	SML	GCL
n.a.	n.a.	n.a.	n.a.

Counts:

ϕ	Wp	Gp	Bp	Xtal	Lithic	Glass	NA	total counts
-5.0	0	0	n.a.	0	0	0	0	0
-4.5	2	0	n.a.	0	0	0	0	2
-4.0	4	0	n.a.	0	0	0	0	4
-3.5	12	0	n.a.	0	0	0	0	12
-3.0	116	0	n.a.	0	0	0	0	116
-2.5	651	5	n.a.	0	*	0	0	663
-2.0	1321	26	n.a.	0	32	0	0	1379
-1.5	455	10	15	0	20	0	0	500
-1.0	488	4	7	0	41	0	0	500
-0.5	429	5	10	1	55	0	0	500
0.0	411	4	5	16	64	0	0	500
0.5	2983	6	3	71	127	0	0	500
1.0	154	10	0	118	213	5	0	500
1.5	96	6	0	117	272	9	0	500
2.0	51	1	0	114	321	13	0	500
2.5	0	0	0	0	0	0	*	*
3.0	0	0	0	0	0	0	0	0
3.5	0	0	0	0	0	0	0	0
4.0	0	0	0	0	0	0	0	0
4.5	0	0	0	0	0	0	0	0
5.0	0	0	0	0	0	0	0	0
6.0	0	0	0	0	0	0	0	0
7.0	0	0	0	0	0	0	0	0

Bulk Weight Percentages:

Wp	Gp	Bp	Xtal	Lithic	Glass	NA
0	0	n.a.	0	0	0	0
2.16	0	n.a.	0	0	0	0
2.60	0	n.a.	0	0	0	0
4.64	0	n.a.	0	0	0	0
8.66	0	n.a.	0	0	0	0
14.90	0.15	n.a.	0	0.51	0	0
13.64	0.38	n.a.	0	0.81	0	0
12.16	0.37	0.67	0	0.96	0	0
10.55	0.14	0.24	0	2.07	0	0
9.55	0.11	0.23	0.04	2.11	0	0
4.59	0.05	0.06	0.28	1.17	0	0
2.19	0.07	0.02	0.63	1.17	0	0
0.25	0.02	0	0.25	0.48	0.0*	0
0.05	0.01	0	0.12	0.28	0.01	0
0.01	0.0*	0	0.04	0.11	0.01	0
0	0	0	0	0	0	0.48
0	0	0	0	0	0	0
0	0	0	0	0	0	0
0	0	0	0	0	0	0
0	0	0	0	0	0	0
0	0	0	0	0	0	0
0	0	0	0	0	0	0
0	0	0	0	0	0	0
85.95	**1.30**	**1.22**	**1.36**	**9.67**	**0.02**	**0.48**

P1 at Locality 41 [0-10 cm from base] [Total sample weight: 338880 mg]

Grain diameter		Weight Fractions:		Granulometric Analysis:						
ϕ	mm	weight [mg]	Cumulative weight %	ϕ_{05}	ϕ_{25}	ϕ_{16}	ϕ_{5}	Md$_\phi$	σ_ϕ	Fl
-5.0	31.5	0	0	-0.1	-0.8	-3.4	-4.1	-2.7	1.26	0.00%
-4.5	22.4	0	0							
-4.0	16.0	21000	6.20							
-3.5	11.2	30000	15.05							
-3.0	8.0	42930	27.72							
-2.5	5.6	80000	51.32							
-2.0	4.0	50900	66.34							
-1.5	2.8	27268.3	74.39							
-1.0	2.0	27049.1	82.37							
-0.5	1.4	26072.5	90.07							
0.0	1.0	18072.5	95.40							
0.5	0.710	8118.7	97.80							
1.0	0.500	2667.0	98.58							
1.5	0.355	1158.5	98.92							
2.0	0.250	1258.6	99.30							
2.5	0.180	2385	100.00							
3.0	0.125	0								
3.5	0.088	0								
4.0	0.063	0								
4.5	0.045	0								
5.0	0.032	0								
6.0	0.017	0								
7.0	0.008	0								

Minor Lithic Counts		Abundance: [volume %]	
SMI.	GCI.	SMI.	GCI.
n.a.	n.a.	n.a.	n.a.

Counts:

ϕ	Wp	Gp	Bp	Xtal	Lithic	Glass	NA	total counts
-5.0	0	0	n.a.	0	0	0	0	0
-4.5	0	0	n.a.	0	0	0	0	0
-4.0	7	0	n.a.	0	0	0	0	7
-3.5	17	1	n.a.	0	0	0	0	18
-3.0	124	2	n.a.	0	0	0	0	126
-2.5	719	2	n.a.	0	1	0	0	722
-2.0	1048	11	n.a.	0	1	0	0	1060
-1.5	493	0	2	0	5	0	0	500
-1.0	483	0	3	0	14	0	0	500
-0.5	468	0	5	0	27	0	0	500
0.0	448	1	4	14	33	0	0	500
0.5	294	0	6	121	85	0	0	500
1.0	258	0	0	129	113	0	0	500
1.5	253	2	0	112	117	16	0	500
2.0	255	0	0	101	124	20	0	500
2.5	0	0	0	0	0	0	*	*
3.0	0	0	0	0	0	0	0	0
3.5	0	0	0	0	0	0	0	0
4.0	0	0	0	0	0	0	0	0
4.5	0	0	0	0	0	0	0	0
5.0	0	0	0	0	0	0	0	0
6.0	0	0	0	0	0	0	0	0
7.0	0	0	0	0	0	0	0	0

Bulk Weight Percentages:

Wp	Gp	Bp	Xtal	Lithic	Glass	NA
0	0	n.a.	0	0	0	0
0	0	n.a.	0	0	0	0
6.21	0	n.a.	0	0	0	0
8.61	0.24	n.a.	0	0	0	0
12.46	0.21	n.a.	0	0	0	0
23.41	0.09	n.a.	0	0.11	0	0
14.77	0.22	n.a.	0	0.03	0	0
7.85	0	0.05	0	0.14	0	0
7.45	0	0.07	0	0.46	0	0
6.93	0	0.08	0	0.69	0	0
4.51	0.01	0.05	0.22	0.55	0	0
1.35	0	0	0.60	0.44	0	0
0.35	0	0	0.23	0.21	0	0
0.11	0.04	0	0.10	0.11	0.01	0
0.10	0	0	0.11	0.14	0.02	0
0	0	0	0	0	0	0.70
0	0	0	0	0	0	0
0	0	0	0	0	0	0
0	0	0	0	0	0	0
0	0	0	0	0	0	0
0	0	0	0	0	0	0
0	0	0	0	0	0	0
0	0	0	0	0	0	0
0	0	0	0	0	0	0
94.20	**0.77**	**0.25**	**1.26**	**2.88**	**0.03**	**0.70**

P1 at Locality 41 [top 10 cm] [Total sample weight: 274590 mg]

Grain diameter		Weight Fractions		Granulometric Analysis						
ϕ	mm	weight [mg]	Cumulative weight %	$\phi_{5\%}$	ϕ_{84}	ϕ_{16}	ϕ_{5}	Md$_{\phi}$	σ_{ϕ}	Fl
-5.0	31.5	0	0	0.6	-0.3	-2.9	-3.4	-1.7	1.25	0.00%
-4.5	22.4	0	0							
-4.0	16.0	11000	4.01							
-3.5	11.2	0	4.01							
-3.0	8.0	20000	11.29							
-2.5	5.6	41590	26.44							
-2.0	4.0	40000	41.00							
-1.5	2.8	38418.9	54.99							
-1.0	2.0	37200.2	68.54							
-0.5	1.4	33435.2	80.72							
0.0	1.0	21614.7	88.59							
0.5	0.710	17390.9	94.92							
1.0	0.500	7362.1	97.60							
1.5	0.355	3397.9	98.84							
2.0	0.250	1339.3	99.33							
2.5	0.180	1840	100.00							
3.0	0.125	0								
3.5	0.088	0								
4.0	0.063	0								
4.5	0.045	0								
5.0	0.032	0								
6.0	0.017	0								
7.0	0.008	0								

Minor Lithic Counts		Abundance [volume %]	
SMI.	GCI.	SMI.	GCI.
n.a	n.a	n.a	n.a

Counts:

ϕ	Wp	Gp	Bp	Xtal	Lithic	Glass	NA	total counts
-5.0	0	0	0	0	0	0	0	0
-4.5	0	0	0	0	0	0	0	0
-4.0	4	0	0	0	0	0	0	4
-3.5	11	1	0	0	0	0	0	11
-3.0	57	0	0	0	0	0	0	57
-2.5	373	0	0	0	0	0	0	373
-2.0	817	5	0	0	1	0	0	823
-1.5	468	5	11	0	16	0	0	500
-1.0	451	6	20	0	23	0	0	500
-0.5	440	8	17	0	35	0	0	500
0.0	414	12	2	13	59	0	0	500
0.5	367	7	3	47	76	0	0	500
1.0	297	5	2	85	111	0	0	500
1.5	213	4	0	103	178	2	0	500
2.0	117	2	0	138	227	16	6	500
2.5	0	0	0	0	0	0	0	0
3.0	0	0	0	0	0	0	0	0
3.5	0	0	0	0	0	0	0	0
4.0	0	0	0	0	0	0	0	0
4.5	0	0	0	0	0	0	0	0
5.0	0	0	0	0	0	0	0	0
6.0	0	0	0	0	0	0	0	0
7.0	0	0	0	0	0	0	0	0

Bulk Weight Percentages:

Wp	Gp	Bp	Xtal	Lithic	Glass	NA
0	0	0	0	0	0	0
0	0	0	0	0	0	0
4.01	0	0	0	0	0	0
0	0.0-	0	0	0	0	0
7.28	0	0	0	0	0	0
15.15	0	0	0	0	0	0
14.40	0.12	0	0	0.04	0	0
12.54	0.18	0.49	0	0.77	0	0
11.36	0.22	0.73	0	1.24	0	0
10.19	0.19	0.41	0	1.39	0	0
5.95	0.20	0.03	0.30	1.39	0	0
4.09	0.15	0.03	0.77	1.30	0	0
1.40	0.03	0.01	0.53	0.72	0	0
0.31	0.02	0	0.32	0.58	0.01	0
0.04	0	0	0.16	0.93	0.02	0
0	0	0	0	0	0	0
0	0	0	0	0	0	0
0	0	0	0	0	0	0
0	0	0	0	0	0	0
0	0	0	0	0	0	0
0	0	0	0	0	0	0
0	0	0	0	0	0	0
0	0	0	0	0	0	0
86.72	**1.11**	**1.70**	**2.08**	**8.36**	**0.03**	**0**

P1 at Locality 50 [0-15 cm from base] [Total sample weight 1392210 mg]

Grain diameter		Weight Fractions		Granulometric Analysis						
ϕ	mm	weight [mg]	Cumulative weight %	ϕ_{05}	ϕ_{01}	ϕ_{10}	ϕ_{50}	Md_ϕ	σ_ϕ	F2
-5.0	31.5	143000	10.27	-2.1	-3.1	-4.9	-5.1	-4.2	0.91	0.00%
-4.5	22.4	328000	33.83							
-4.0	16.0	366000	60.12							
-3.5	11.2	200000	74.49							
-3.0	8.0	140000	84.54							
-2.5	5.6	85000	90.65							
-2.0	4.0	62100	95.12							
-1.5	2.8	27036.4	97.06							
-1.0	2.0	16861.3	98.27							
-0.5	1.4	10848.2	99.05							
0.0	1.0	4951.8	99.40							
0.5	0.710	3323.6	99.64							
1.0	0.500	1462.4	99.75							
1.5	0.355	870.6	99.81							
2.0	0.250	598.8	99.85							
2.5	0.180	2047	100.00							
3.0	0.125	0								
3.5	0.088	0								
4.0	0.063	0								
4.5	0.045	0								
5.0	0.032	0								
6.0	0.017	0								
7.0	0.008	0								

Minor Lithic Counts		Abundance [volume %]	
SML	GCL	SML	GCL
n.a.	n.a.	n.a.	n.a.

Counts:

ϕ	Wp	Gp	Bp	Xtal	Lithic	Glass	NA	total counts
-5.0	29	0	n.a.	0	0	0	0	29
-4.5	83	0	n.a.	0	0	0	0	83
-4.0	116	0	n.a.	0	6	0	0	122
-3.5	104	0	n.a.	0	6	0	0	110
-3.0	371	0	n.a.	0	11	0	0	382
-2.5	705	0	n.a.	0	18	0	0	723
-2.0	1112	16	n.a.	0	69	0	0	1197
-1.5	431	0	6	0	63	0	0	500
-1.0	396	0	5	0	99	0	0	500
-0.5	375	0	2	4	119	0	0	500
0.0	299	2	2	37	160	0	0	500
0.5	244	1	0	52	203	0	0	500
1.0	186	0	0	68	246	0	0	500
1.5	168	0	0	71	261	0	0	500
2.0	126	0	0	84	289	1	0	500
2.5	0	0	0	0	0	0	*	*
3.0	0	0	0	0	0	0	0	0
3.5	0	0	0	0	0	0	0	0
4.0	0	0	0	0	0	0	0	0
4.5	0	0	0	0	0	0	0	0
5.0	0	0	0	0	0	0	0	0
6.0	0	0	0	0	0	0	0	0
7.0	0	0	0	0	0	0	0	0

Bulk Weight Percentages:

Wp	Gp	Bp	Xtal	Lithic	Glass	NA
10.27	0	n.a.	0	0	0	0
23.56	0	n.a.	0	0	0	0
23.84	0	n.a.	0	2.45	0	0
13.02	0	n.a.	0	1.35	0	0
9.19	0	n.a.	0	0.87	0	0
5.62	0	n.a.	0	0.48	0	0
3.81	0.08	n.a.	0	0.58	0	0
1.51	0	0.04	0	0.40	0	0
0.78	0	0.01	0	0.42	0	0
0.50	0	0.0+	0.01	0.27	0	0
0.17	0.0+	0.0+	0.03	0.15	0	0
0.10	0.0+	0	0.03	0.11	0	0
0.03	0	0	0.02	0.06	0	0
0.01	0	0	0.01	0.04	0	0
0.0+	0	0	0.01	0.02	0.0+	0
0	0	0	0	0	0	0.15
0	0	0	0	0	0	0
0	0	0	0	0	0	0
0	0	0	0	0	0	0
0	0	0	0	0	0	0
0	0	0	0	0	0	0
0	0	0	0	0	0	0
0	0	0	0	0	0	0
92.41	**0.08**	**0.05**	**0.11**	**7.20**	**0.0+**	**0.15**

P1 at Locality 50 [top 15 cm] [Total sample weight: 1131360 mg]

Grain diameter		Weight Fractions		Granulometric Analysis						
ϕ	mm	weight [mg]	Cumulative weight %	ϕ_{05}	ϕ_{25}	ϕ_{10}	ϕ_{50}	Md_ϕ	σ_ϕ	F2
-5.0	31.5	275000	24.31	-0.6	-2.1	-5.1	-5.3	-3.8	1.46	0.00%
-4.5	22.4	83000	31.64							
-4.0	16.0	147000	44.64							
-3.5	11.2	135000	56.57							
-3.0	8.0	120000	67.18							
-2.5	5.6	110000	76.90							
-2.0	4.0	101360	85.86							
-1.5	2.8	47060.3	90.02							

Minor Lithic Counts		Abundance [volume %]	
SMI.	GCI.	SMI.	GCI.
n.a.	n.a.	n.a.	n.a.

-1.0	2.0	37005.5	93.29
-0.5	1.4	32086.3	96.12
0.0	1.0	17126.8	97.64
0.5	0.710	11314.7	98.64
1.0	0.500	6344.3	99.20
1.5	0.355	3663.1	99.52
2.0	0.250	1549.7	99.66
2.5	0.180	3849.3	100.00
3.0	0.125	0	
3.5	0.088	0	
4.0	0.063	0	
4.5	0.045	0	
5.0	0.032	0	
6.0	0.017	0	
7.0	0.008	0	

Counts:

ϕ	Wp	Gp	Bp	Xtal	Lithic	Glass	NA	total counts
-5.0	55	0	n.a.	0	0	0	0	55
-4.5	21	0	n.a.	0	0	0	0	21
-4.0	46	0	n.a.	0	3	0	0	49
-3.5	66	0	n.a.	0	5	0	0	71
-3.0	301	0	n.a.	0	13	0	0	314
-2.5	856	27	n.a.	0	38	0	0	921
-2.0	1718	61	n.a.	0	132	0	0	1911
-1.5	392	2	16	0	90	0	0	500
-1.0	366	5	13	0	116	0	0	500
-0.5	341	6	11	2	140	0	0	500
0.0	355	18	2	13	112	0	0	500
0.5	279	11	3	36	171	0	0	500
1.0	230	9	3	52	206	0	0	500
1.5	193	7	0	66	229	5	0	500
2.0	116	5	0	114	249	16	0	500
2.5	0	0	0	0	0	0	*	*
3.0	0	0	0	0	0	0	0	0
3.5	0	0	0	0	0	0	0	0
4.0	0	0	0	0	0	0	0	0
4.5	0	0	0	0	0	0	0	0
5.0	0	0	0	0	0	0	0	0
6.0	0	0	0	0	0	0	0	0
7.0	0	0	0	0	0	0	0	0

Bulk Weight Percentages:

Wp	Gp	Bp	Xtal	Lithic	Glass	NA
24.31	0	n.a.	0	0	0	0
7.34	0	n.a.	0	0	0	0
11.51	0	n.a.	0	1.49	0	0
10.50	0	n.a.	0	1.43	0	0
9.33	0	n.a.	0	1.28	0	0
8.16	0.34	n.a.	0	1.22	0	0
7.23	0.36	n.a.	0	1.37	0	0
2.79	0.02	0.19	0	1.16	0	0
1.87	0.04	0.10	0	1.27	0	0
1.61	0.03	0.05	0.02	1.13	0	0
0.92	0.05	0.01	0.05	0.48	0	0
0.48	0.03	0.0+	0.08	0.40	0	0
0.22	0.01	0.0+	0.06	0.27	0	0
0.07	0.01	0	0.05	0.19	0.0+	0
0.02	0.0+	0	0.01	0.09	0.0+	0
0	0	0	0	0	0	0.34
0	0	0	0	0	0	0
0	0	0	0	0	0	0
0	0	0	0	0	0	0
0	0	0	0	0	0	0
0	0	0	0	0	0	0
0	0	0	0	0	0	0
0	0	0	0	0	0	0
86.36	**0.89**	**0.35**	**0.28**	**11.78**	**0.0+**	**0.34**

P1 at Locality 68 [top 10 cm, CBV-68-2] [Total sample weight 13343.7 mg]

Grain diameter		Weight Fractions:		Granulometric Analysis:						
ϕ	mm	weight [mg]	Cumulative weight %	ϕ_{05}	ϕ_{84}	ϕ_{16}	ϕ_{5}	Md$_\phi$	σ_ϕ	F2
-5.0	31.5	0	0	1.3	0.4	-0.6	-1.1	0.2	0.61	0.52%
-4.5	22.4	0	0							
-4.0	16.0	0	0							
-3.5	11.2	0	0							
-3.0	8.0	0	0							
-2.5	5.6	0	0							
-2.0	4.0	34.5	0.26							
-1.5	2.8	155.3	1.42							

		Minor Lithic Counts		Abundance [volume %]	
		SML	GCL	SML	GCL
-1.0	2.0	607.3	5.97	0	0	0	0
-0.5	1.4	1593.7	17.92	0	0	0	0
0.0	1.0	2798.1	38.89	0	0	0	0
0.5	0.710	3430.2	64.59	0	3	4.5	4.7
1.0	0.500	2789.6	85.50	7	6	1.4	3.9
1.5	0.355	1405.1	96.03	2	24	1.5	17.3
2.0	0.250	317.1	98.41	2	38	0	28.6
2.5	0.180	83.5	99.03	0	0	0	0
3.0	0.125	37.5	99.31	0	0	0	0
3.5	0.088	22.0	99.48				
4.0	0.063	53.0	99.87				
4.5	0.045	16.8	100.00				
5.0	0.032	0					
6.0	0.017	0					
7.0	0.008	0					

Counts:

ϕ	Wp	Gp	Bp	Xtal	Lithic	Glass	NA	total counts
-5.0	0	0	n.a.	0	0	0	0	0
-4.5	0	0	n.a.	0	0	0	0	0
-4.0	0	0	n.a.	0	0	0	0	0
-3.5	0	0	n.a.	0	0	0	0	0
-3.0	0	0	n.a.	0	0	0	0	0
-2.5	0	0	n.a.	0	0	0	0	0
-2.0	1	0	n.a.	0	0	0	0	1
-1.5	12	0	0	0	0	0	0	12
-1.0	121	2	9	0	0	0	0	132
-0.5	478	8	13	0	1	0	0	500
0.0	367	30	17	1	8	6	0	500
0.5	273	19	9	14	64	27	0	500
1.0	225	2	0	31	155	39	0	500
1.5	143	1	0	59	139	76	0	500
2.0	0	0	0	115	133	109	0	500
2.5	0	0	0	0	0	*	0	121
3.0	0	0	0	0	0	*	0	249
3.5	0	0	0	0	0	*	0	251
4.0	0	0	0	0	0	*	0	1015
4.5	0	0	0	0	0	*	0	998
5.0	0	0	0	0	0	0	0	0
6.0	0	0	0	0	0	0	0	0
7.0	0	0	0	0	0	0	0	0

Bulk Weight Percentages:

Wp	Gp	Bp	Xtal	Lithic	Glass	NA
0	0	n.a.	0	0	0	0
0	0	n.a.	0	0	0	0
0	0	n.a.	0	0	0	0
0	0	n.a.	0	0	0	0
0	0	n.a.	0	0	0	0
0	0	n.a.	0	0	0	0
0.26	0	n.a.	0	0	0	0
1.16	0	0	0	0	0	0
4.02	0.10	0.43	0	0	0	0
11.39	0.20	0.32	0	0.04	0	0
17.50	1.40	0.79	0.06	0.53	0.37	0
16.93	1.59	0.36	0.90	4.27	1.66	0
9.92	0.08	0	1.48	7.71	1.72	0
2.95	0.04	0	1.66	4.01	1.87	0
0.29	0.04	0	0.70	0.81	0.59	0
0	0	0	0	0	0	0.63
0	0	0	0	0	0	0.28
0	0	0	0	0	0	0.16
0	0	0	0	0	0	0.40
0	0	0	0	0	0	0.13
0	0	0	0	0	0	0
0	0	0	0	0	0	0
0	0	0	0	0	0	0
64.72	**3.41**	**1.90**	**4.80**	**17.73**	**6.21**	**1.60**

P1 at Locality 69 [0-30 cm from base] [Total sample weight: 1206500 mg]

Grain diameter		Weight Fractions		Granulometric Analysis						
ϕ	mm	weight [mg]	Cumulative weight %	ϕ_{95}	ϕ_{84}	ϕ_{16}	ϕ_{5}	Md$_\phi$	σ_ϕ	F2
-5.0	31.5	0	0	0.7	0.2	-1.4	-1.7	-0.6	0.76	0.00%
-4.5	22.4	0	0							
-4.0	16.0	0	0							
-3.5	11.2	0	0							
-3.0	8.0	0	0							
-2.5	5.6	18000	1.49							
-2.0	4.0	57500	6.26							
-1.5	2.8	110362.6	15.41							
-1.0	2.0	168384.3	29.36							
-0.5	1.4	383017.7	61.11							
0.0	1.0	249071.7	81.75							
0.5	0.710	136110.9	93.03							
1.0	0.500	58583.2	97.89							
1.5	0.355	14051.8	99.05							
2.0	0.250	1012.8	99.14							
2.5	0.180	10400	100.00							
3.0	0.125	0								
3.5	0.088	0								
4.0	0.063	0								
4.5	0.045	0								
5.0	0.032	0								
6.0	0.017	0								
7.0	0.008	0								

Minor Lithic Counts		Abundance [volume %]	
SML	GCL	SML	GCL
0	0	0	0
0	0	0	0
0	0	0	0
0	5	0	4.6
0	9	0	4.1
0	11	0	4.7
0	7	0	2.8
0	0	0	0
0	0	0	0

Counts:

ϕ	Wp	Gp	Bp	Xtal	Lithic	Glass	NA	total counts
-5.0	0	0	n.a.	0	0	0	0	0
-4.5	0	0	n.a.	0	0	0	0	0
-4.0	0	0	n.a.	0	0	0	0	0
-3.5	0	0	n.a.	0	0	0	0	0
-3.0	0	0	n.a.	0	0	0	0	0
-2.5	164	0	n.a.	0	0	0	0	164
-2.0	1193	1	n.a.	0	0	0	0	1194
-1.5	498	0	2	0	0	0	0	500
-1.0	497	0	3	0	0	0	0	500
-0.5	493	1	4	0	2	0	0	500
0.0	479	2	4	2	13	0	0	500
0.5	261	0	3	127	109	0	0	500
1.0	25	0	0	253	222	0	0	500
1.5	57	0	0	192	232	19	0	500
2.0	84	0	0	87	294	35	0	500
2.5	0	0	0	0	0	0	*	*
3.0	0	0	0	0	0	0	0	0
3.5	0	0	0	0	0	0	0	0
4.0	0	0	0	0	0	0	0	0
4.5	0	0	0	0	0	0	0	0
5.0	0	0	0	0	0	0	0	0
6.0	0	0	0	0	0	0	0	0
7.0	0	0	0	0	0	0	0	0

Bulk Weight Percentages:

Wp	Gp	Bp	Xtal	Lithic	Glass	NA
0	0	n.a.	0	0	0	0
0	0	n.a.	0	0	0	0
0	0	n.a.	0	0	0	0
0	0	n.a.	0	0	0	0
0	0	n.a.	0	0	0	0
1.49	0	n.a.	0	0	0	0
4.76	0	n.a.	0	0	0	0
9.09	0.01	0.06	0	0	0	0
13.84	0.0+	0.12	0	0	0	0
31.31	0.0+	0.26	0	0.22	0	0
19.37	0.0+	0.19	0.13	0.86	0	0
6.13	0.0+	0.04	2.70	2.41	0	0
0.18	0	0	2.44	2.23	0	0
0.07	0	0	0.47	0.59	0.04	0
0.04	0	0	0.02	0.05	0.01	0
0	0	0	0	0	0	0.86
0	0	0	0	0	0	0
0	0	0	0	0	0	0
0	0	0	0	0	0	0
0	0	0	0	0	0	0
0	0	0	0	0	0	0
0	0	0	0	0	0	0
0	0	0	0	0	0	0
0	0	0	0	0	0	0
86.28	**0.02**	**0.67**	**5.76**	**6.36**	**0.05**	**0.86**

P1 at Locality 69 [57-87 cm from base] [Total sample weight: 1222518 mg]

Grain diameter		Weight Fractions		Granulometric Analysis						
ϕ	mm	weight [mg]	Cumulative weight %	ϕ_{05}	ϕ_{84}	ϕ_{16}	$\phi_{\sim}$	Md_{ϕ}	σ_{ϕ}	Fz
-5.0	31.5	0	0	0.6	-0.1	-2.1	-2.6	-0.8	0.98	0.00%
-4.5	22.4	0	0							
-4.0	16.0	0	0							
-3.5	11.2	0	0							
-3.0	8.0	0	0							
-2.5	5.6	87000	7.12							
-2.0	4.0	144500	18.94							
-1.5	2.8	107135.1	27.70							

Minor Lithic Counts		Abundance [volume %]	
SML	GCL	SML	GCL
n.a.	n.a.	n.a.	n.a.

-1.0	2.0	214460.7	45.24
-0.5	1.4	280760.9	68.21
0.0	1.0	215064.5	85.80
0.5	0.710	98475.3	93.86
1.0	0.500	46752.0	97.68
1.5	0.355	21274.4	99.42
2.0	0.250	908.2	99.49
2.5	0.180	6185	100.00
3.0	0.125	0	
3.5	0.088	0	
4.0	0.063	0	
4.5	0.045	0	
5.0	0.032	0	
6.0	0.017	0	
7.0	0.008	0	

Counts:

ϕ	Wp	Gp	Bp	Xtal	Lithic	Glass	NA	total counts
-5.0	0	0	n.a.	0	0	0	0	0
-4.5	0	0	n.a.	0	0	0	0	0
-4.0	0	0	n.a.	0	0	0	0	0
-3.5	0	0	n.a.	0	0	0	0	0
-3.0	0	0	n.a.	0	0	0	0	0
-2.5	787	0	n.a.	0	0	0	0	787
-2.0	2992	2	n.a.	0	0	0	0	2994
-1.5	494	0	4	0	2	0	0	500
-1.0	493	0	6	0	1	0	0	500
-0.5	495	0	4	0	1	0	0	500
0.0	452	1	6	19	22	0	0	500
0.5	339	4	9	81	67	0	0	500
1.0	159	1	4	179	122	35	0	500
1.5	29	1	1	225	216	28	0	500
2.0	12	0	0	236	221	31	0	500
2.5	0	0	0	0	0	0	*	*
3.0	0	0	0	0	0	0	0	0
3.5	0	0	0	0	0	0	0	0
4.0	0	0	0	0	0	0	0	0
4.5	0	0	0	0	0	0	0	0
5.0	0	0	0	0	0	0	0	0
6.0	0	0	0	0	0	0	0	0
7.0	0	0	0	0	0	0	0	0

Bulk Weight Percentages:

Wp	Gp	Bp	Xtal	Lithic	Glass	NA
0	0	n.a.	0	0	0	0
0	0	n.a.	0	0	0	0
0	0	n.a.	0	0	0	0
0	0	n.a.	0	0	0	0
0	0	n.a.	0	0	0	0
7.12	0	n.a.	0	0	0	0
11.81	0.01	n.a.	0	0	0	0
8.58	0	0.12	0	0.06	0	0
17.17	0	0.30	0	0.07	0	0
22.70	0	0.19	0	0.08	0	0
15.11	0.04	0.23	1.01	1.21	0	0
5.06	0.10	0.10	1.50	1.29	0	0
1.00	0.01	0.03	1.48	1.05	0.27	0
0.05	0.0+	0.0+	0.80	0.79	0.09	0
0.0+	0	0	0.04	0.02	0.0+	0
0	0	0	0	0	0	0.51
0	0	0	0	0	0	0
0	0	0	0	0	0	0
0	0	0	0	0	0	0
0	0	0	0	0	0	0
0	0	0	0	0	0	0
0	0	0	0	0	0	0
0	0	0	0	0	0	0
88.60	**0.16**	**0.97**	**4.83**	**4.57**	**0.36**	**0.51**

P1 at Locality 69 [115-145 cm from base (top 10 cm)] [Total sample weight 2250500 mg]

Grain diameter		Weight Fractions		Granulometric Analysis						
ϕ	mm	weight [mg]	Cumulative weight %	ϕ_{05}	ϕ_{25}	ϕ_{50}	ϕ_{75}	Md$_\phi$	σ_ϕ	F2
-5.0	31.5	0	0	1.3	0.7	-1.9	-2.6	-0.4	1.24	0.00%
-4.5	22.4	0	0							
-4.0	16.0	0	0							
-3.5	11.2	0	0							
-3.0	8.0	0	0							
-2.5	5.6	117000	5.20							
-2.0	4.0	225500	15.22							
-1.5	2.8	158589.7	22.27							
-1.0	2.0	179985.5	30.26							
-0.5	1.4	387558.5	47.48							
0.0	1.0	359236.6	63.45							
0.5	0.710	395359.4	81.01							
1.0	0.500	237277.1	91.56							
1.5	0.355	131826.8	97.42							
2.0	0.250	28097.0	98.66							
2.5	0.180	30070	100.00							
3.0	0.125	0								
3.5	0.088	0								
4.0	0.063	0								
4.5	0.045	0								
5.0	0.032	0								
6.0	0.017	0								
7.0	0.008	0								

Minor Lithic Counts		Abundance [volume %]	
SML	GCL	SML	GCL
n.a.	n.a.	n.a.	n.a.

Counts:

ϕ	Wp	Gp	Bp	Xtal	Lithic	Glass	NA	total counts
-5.0	0	0	n.a.	0	0	0	0	0
-4.5	0	0	n.a.	0	0	0	0	0
-4.0	0	0	n.a.	0	0	0	0	0
-3.5	0	0	n.a.	0	0	0	0	0
-3.0	0	0	n.a.	0	0	0	0	0
-2.5	1041	13	n.a.	0	0	0	0	1054
-2.0	4648	45	n.a.	0	0	0	0	4693
-1.5	485	3	12	0	0	0	0	500
-1.0	481	6	11	0	2	0	0	500
-0.5	474	6	13	0	7	0	0	500
0.0	461	6	14	1	18	0	0	500
0.5	363	7	17	41	67	5	0	500
1.0	255	2	22	71	135	15	0	500
1.5	143	0	13	109	205	30	0	500
2.0	57	0	0	141	247	55	0	500
2.5	0	0	0	0	0	0	0	0
3.0	0	0	0	0	0	0	0	0
3.5	0	0	0	0	0	0	0	0
4.0	0	0	0	0	0	0	0	0
4.5	0	0	0	0	0	0	0	0
5.0	0	0	0	0	0	0	0	0
6.0	0	0	0	0	0	0	0	0
7.0	0	0	0	0	0	0	0	0

Bulk Weight Percentages:

Wp	Gp	Bp	Xtal	Lithic	Glass	NA
0	0	n.a.	0	0	0	0
0	0	n.a.	0	0	0	0
0	0	n.a.	0	0	0	0
0	0	n.a.	0	0	0	0
0	0	n.a.	0	0	0	0
5.11	0.08	n.a.	0	0	0	0
9.88	0.14	n.a.	0	0	0	0
6.71	0.06	0.28	0	0	0	0
12.90	0.14	0.25	0	0.07	0	0
16.14	0.21	0.46	0	0.41	0	0
14.29	0.21	0.50	0.05	0.92	0	0
11.82	0.39	0.45	1.74	2.97	0.20	0
4.65	0.04	0.44	1.70	3.37	0.33	0
0.91	0	0.25	1.48	2.86	0.36	0
0.05	0	0	0.39	0.68	0.13	0
0	0	0	0	0	0	1.34
0	0	0	0	0	0	0
0	0	0	0	0	0	0
0	0	0	0	0	0	0
0	0	0	0	0	0	0
0	0	0	0	0	0	0
0	0	0	0	0	0	0
0	0	0	0	0	0	0
0	0	0	0	0	0	0
82.46	**1.27**	**2.63**	**5.36**	**11.28**	**1.02**	**1.34**

S1 at Locality 5 [CBV-5-1]. [Total sample weight: 971612 mg]

Grain diameter		Weight Fractions		Granulometric Analysis						
ϕ	mm	weight [mg]	Cumulative weight %	ϕ_{5}	ϕ_{25}	ϕ_{50}	ϕ_{75}	Md_{ϕ}	σ_{ϕ}	F2
-5.0	31.5	13200	1.36	5.6	4.7	-4.2	-4.7	1.5	3.77	34.4%
-4.5	22.4	62400	7.78							
-4.0	16.0	97600	17.83							
-3.5	11.2	52300	23.21							
-3.0	8.0	50900	28.45							
-2.5	5.6	43700	32.95							
-2.0	4.0	35200	36.57							
-1.5	2.8	31400	39.80							
-1.0	2.0	21600	42.02							
-0.5	1.4	15500	43.62							
0.0	1.0	12200	44.87							
0.5	0.710	12900	46.20							
1.0	0.500	13900	47.63							
1.5	0.355	24600	50.16							
2.0	0.250	32100	53.47							
2.5	0.180	37200	57.30							
3.0	0.125	44300	61.86							
3.5	0.088	36700	65.63							
4.0	0.063	32200	68.95							
4.5	0.045	118875	81.18							
5.0	0.032	94738	90.93							
6.0	0.017	60946	97.21							
7.0	0.008	27154	100.00							

Minor Lithic Counts		Abundance [volume %]	
SML	GCL	SML	GCL
n.a	n.a	n.a	n.a

Counts:

ϕ	Wp	Op	Bp	Xtal	Lithic	Glass	NA	total counts
-5.0	1	0	0	0	0	0	0	1
-4.5	9	0	0	0	0	0	0	9
-4.0	35	0	0	0	2	0	0	37
-3.5	53	0	0	0	3	0	0	56
-3.0	107	0	0	0	17	0	0	124
-2.5	260	0	0	0	32	0	0	292
-2.0	412	7	3	0	78	0	0	500
-1.5	389	13	2	0	96	0	0	500
-1.0	369	8	0	0	123	0	0	500
-0.5	316	3	0	3	178	0	0	500
0.0	265	0	0	17	218	0	0	500
0.5	150	2	0	28	291	29	0	500
1.0	92	3	0	46	346	13	0	500
1.5	91	2	0	81	283	43	0	500
2.0	87	2	0	119	236	56	0	500
2.5	49	2	0	174	212	63	0	500
3.0	22	1	0	206	193	78	0	500
3.5	11	0	0	209	175	105	0	500
4.0	5	0	0	141	134	220	0	500
4.5	0	0	0	136	101	263	0	500
5.0	*	*	*	*	*	*	320	320
6.0	*	*	*	*	*	*	310	310
7.0	*	*	*	*	*	*	210	210

Bulk Weight Percentages:

Wp	Op	Bp	Xtal	Lithic	Glass	NA
1.36	0	0	0	0	0	0
6.42	0	0	0	0	0	0
7.67	0	0	0	3.06	0	0
4.52	0	0	0	0.86	0	0
3.57	0	0	0	1.67	0	0
3.34	0	0	0	1.16	0	0
2.23	0.08	0.03	0	1.27	0	0
1.78	0.10	0.03	0	1.33	0	0
1.27	0.04	0	0	0.91	0	0
0.86	0.01	0	0.01	0.77	0	0
0.51	0	0	0.05	0.69	0	0
0.41	0.01	0	0.07	0.77	0.07	0
0.20	0.01	0	0.13	1.05	0.03	0
0.24	0.02	0	0.45	1.62	0.21	0
0.22	0.01	0	0.90	1.79	0.38	0
0.17	0.01	0	1.43	1.74	0.48	0
0.11	0.01	0	1.95	1.82	0.67	0
0.07	0	0	1.66	1.39	0.65	0
0.03	0	0	1.03	0.98	1.28	0
0.00	0	0	3.74	2.78	5.71	0
*	*	*	*	*	*	9.75
*	*	*	*	*	*	6.27
*	*	*	*	*	*	2.79
34.92	**0.30**	**0.06**	**11.42**	**25.66**	**8.83**	**18.81**

S1 at Locality 6 [CBV-6-1]. [Total sample weight: 196239.2 mg]

Grain diameter		Weight Fractions		Granulometric Analysis:						
ϕ	mm	weight [mg]	Cumulative weight %	ϕ_{05}	ϕ_{84}	ϕ_{16}	ϕ_{5}	Md_{ϕ}	σ_{ϕ}	F2
-5.0	31.5	0	0	6.4	5.6	3.3	2.2	4.4	1.21	79.16%
-4.5	22.4	0	0							
-4.0	16.0	0	0							
-3.5	11.2	0	0							
-3.0	8.0	2558.7	1.3							
-2.5	5.6	432.6	1.52							
-2.0	4.0	600.8	1.83							
-1.5	2.8	146.1	1.9							

				Minor Lithic Counts		Abundance [volume %]	
				SML	GCL	SML	GCL
-1.0	2.0	88.5	1.95	0	0	0	0
-0.5	1.4	106.3	2.00	0	0	0	0
0.0	1.0	132.3	2.07	0	0	0	0
0.5	0.710	278.9	2.21	0	0	0	0
1.0	0.500	522.6	2.48	2	4	28.6	57.1
1.5	0.355	1217.7	3.10	4	12	1	3.1
2.0	0.250	2945.2	4.60	15	18	6.9	8.3
2.5	0.180	5524.3	7.42	4	13	1.4	4.5
3.0	0.125	10927.9	12.99	1	6	0.4	2.7
3.5	0.088	15411.9	20.84				
4.0	0.063	20092.4	31.08				
4.5	0.045	49637.9	56.37				
5.0	0.032	42469.4	78.01				
6.0	0.017	27321.1	91.94				
7.0	0.008	15824.6	100.00				

Counts:

ϕ	Wp	Gp	Bp	Xtal	Lithic	Glass	NA	total counts
-5.0	0	0	0	0	0	0	0	1
-4.5	0	0	0	0	0	0	0	9
-4.0	0	0	0	0	0	0	0	37
-3.5	0	0	2	0	0	0	0	56
-3.0	0	0	1	0	2	0	0	124
-2.5	0	0	0	0	1	0	0	292
-2.0	0	0	0	0	5	0	0	500
-1.5	0	0	0	0	3	0	0	500
-1.0	5	0	0	0	3	0	0	500
-0.5	21	0	0	0	8	0	0	500
0.0	68	0	0	0	7	8	0	500
0.5	84	0	0	9	385	22	0	500
1.0	195	0	0	20	218	67	0	500
1.5	79	0	0	49	289	83	0	500
2.0	33	0	0	130	223	114	0	500
2.5	21	0	0	139	218	122	0	500
3.0	13	0	0	134	218	135	0	500
3.5	0	0	0	124	205	171	0	500
4.0	0	0	0	119	205	176	0	500
4.5	0	0	0	91	201	208	0	500
5.0	*	*	*	*	*	*	*2438*	*320*
6.0	*	*	*	*	*	*	*2272*	*310*
7.0	*	*	*	*	*	*	*2143*	*210*

Bulk Weight Percentages:

ϕ	Wp	Gp	Bp	Xtal	Lithic	Glass	NA
-5.0	0	0	0	0	0	0	0
-4.5	0	0	0	0	0	0	0
-4.0	0	0	0	0	0	0	0
-3.5	0	0	0	0	0	0	0
-3.0	0	0	0	0	1.30	0	0
-2.5	0	0	0	0	0.22	0	0
-2.0	0	0	0	0	0.31	0	0
-1.5	0	0	0	0	0.07	0	0
-1.0	0.02	0	0	0	0.03	0	0
-0.5	0.03	0	0	0	0.02	0	0
0.0	0.05	0	0	0	0.01	0.01	0
0.5	0.01	0	0	0	0.12	0.01	0
1.0	0.09	0	0	0.01	0.13	0.04	0
1.5	0.05	0	0	0.07	0.40	0.10	0
2.0	0.04	0	0	0.42	0.72	0.33	0
2.5	0.05	0	0	0.82	1.28	0.67	0
3.0	0.08	0	0	1.55	2.52	1.42	0
3.5	0	0	0	2.10	3.48	2.27	0
4.0	0	0	0	2.63	4.53	3.08	0
4.5	0	0	0	5.05	11.14	9.10	0
5.0	*	*	*	*	*	*	21.64
6.0	*	*	*	*	*	*	13.92
7.0	*	*	*	*	*	*	8.06
	0.42	**0**	**0**	**12.65**	**26.28**	**17.03**	**43.62**

S1 at Locality 11 [CBV-11-1]. [Total sample weight: 226100.9 mg]

Grain diameter		Weight Fractions		Granulometric Analysis						
ϕ	mm	weight [mg]	Cumulative weight %	ϕ_{05}	ϕ_{50}	ϕ_{95}	ϕ_{σ}	Md$_{\phi}$	σ	F2
-5.0	31.5	0	0	5.8	4.7	-3.3	-4.8	2.5	3.59	41.48%
-4.5	22.4	0	0							
-4.0	16.0	17950.1	7.94							
-3.5	11.2	13824.3	14.05							
-3.0	8.0	12138.1	19.42							
-2.5	5.6	10694.4	24.15							
-2.0	4.0	6226.7	26.91							
-1.5	2.8	7385.0	30.17							
-1.0	2.0	4864.9	32.32							
-0.5	1.4	6445.6	33.85							
0.0	1.0	2691.4	35.04							
0.5	0.710	4911.8	37.21							
1.0	0.500	7371.4	40.47							
1.5	0.355	8364.8	44.17							
2.0	0.250	6656.9	47.11							
2.5	0.180	6853.6	50.15							
3.0	0.125	9392.1	54.30							
3.5	0.088	9540.6	58.52							
4.0	0.063	12601.4	64.09							
4.5	0.045	32184.0	78.33							
5.0	0.032	25392	89.56							
6.0	0.017	16335	96.78							
7.0	0.008	7278	100.00							

Minor Lithic Counts		Abundance [volume %]	
SML	GCL	SML	GCL
0	6	0	4.3
0	19	0	6.7
0	40	0	18.8
0	62	0	21.6
0	87	0	24.9
0	71	0	24.0
0	59	0	24.8
0	44	0	16.9
0	41	0	15.0

Counts:

ϕ	Wp	Gp	Bp	Xtal	Lithic	Glass	NA	total counts
-5.0	0	0	0	0	0	0	0	1
-4.5	0	0	0	0	0	0	0	9
-4.0	2	0	0	0	1	0	0	37
-3.5	4	0	0	0	3	0	0	56
-3.0	6	2	0	0	10	0	0	124
-2.5	10	14	0	0	19	0	0	292
-2.0	26	3	0	0	25	0	0	500
-1.5	74	2	0	0	86	4	0	500
-1.0	126	15	0	2	140	12	0	500
-0.5	171	9	0	4	282	34	0	500
0.0	209	1	0	7	213	70	0	500
0.5	127	2	0	10	287	74	0	500
1.0	63	3	0	11	350	73	0	500
1.5	53	2	0	21	296	128	0	500
2.0	48	0	0	38	238	176	0	500
2.5	31	0	0	41	260	168	0	500
3.0	22	0	0	53	274	151	0	500
3.5	0	0	0	62	289	149	0	500
4.0	0	0	0	29	242	229	0	500
4.5	0	0	0	15	211	274	0	500
5.0	•	•	•	•	•	•	*32375*	*32375*
6.0	•	•	•	•	•	•	*30273*	*30273*
7.0	•	•	•	•	•	•	*21286*	*21286*

Bulk Weight Percentages:

Wp	Gp	Bp	Xtal	Lithic	Glass	NA
0	0	0	0	0	0	0
0	0	0	0	0	0	0
3.99	0	0	0	3.95	0	0
4.16	0	0	0	1.95	0	0
0.74	0	0	0	4.63	0	0
0.53	0.79	0	0	3.41	0	0
0.78	0.11	0	0	1.86	0	0
1.01	0.04	0	0	2.11	0.11	0
0.57	0.10	0	0.02	1.37	0.09	0
0.36	0.02	0	0.01	1.03	0.10	0
0.37	0	0	0.02	0.62	0.18	0
0.54	0.01	0	0.04	1.28	0.30	0
0.32	0.02	0	0.07	2.41	0.44	0
0.20	0.02	0	0.17	2.42	0.89	0
0.11	0	0	0.25	1.56	1.03	0
0.09	0	0	0.26	1.68	1.01	0
0.10	0	0	0.46	2.39	1.20	0
0	0	0	0.56	2.61	1.05	0
0	0	0	0.36	2.98	2.24	0
0	0	0	0.48	6.79	6.96	0
•	•	•	•	•	•	11.23
•	•	•	•	•	•	7.22
•	•	•	•	•	•	3.22
13.87	**1.11**	**0**	**2.70**	**45.05**	**15.60**	**21.67**

S1 at Locality 12 [CBV-12-1]. [Total sample weight 80378.1 mg]

Grain diameter		Weight Fractions		Granulometric Analysis						
ϕ	mm	weight [mg]	Cumulative weight %	ϕ_{05}	ϕ_{84}	ϕ_{16}	ϕ_{50}	Md_ϕ	σ_ϕ	F2
-5.0	31.5	0	0	5.5	3.9	-0.8	-1.8	1.1	2.27	18.81%
-4.5	22.4	0	0							
-4.0	16.0	0	0							
-3.5	11.2	0	0							
-3.0	8.0	502.7	0.63							
-2.5	5.6	1958.5	3.06							
-2.0	4.0	1247	3.22							
-1.5	2.8	4472.2	8.78							

Minor Lithic Counts		Abundance [volume %]	
SMI.	GCI.	SMI.	GCI.
n.a.	n.a.	n.a.	n.a.

-1.0	2.0	3869	13.59
-0.5	1.4	5835	20.85
0.0	1.0	7159	29.76
0.5	0.710	8075	39.81
1.0	0.500	7585	49.24
1.5	0.355	7057	58.02
2.0	0.250	5646	65.05
2.5	0.180	4912	71.16
3.0	0.125	4682	76.98
3.5	0.088	3378	81.19
4.0	0.063	3841	85.97
4.5	0.045	1919	88.35
5.0	0.032	3857	93.15
6.0	0.017	3192	97.12
7.0	0.008	2313	100.00

Counts:

ϕ	Wp	Gp	Bp	Xtal	Lithic	Glass	NA	total counts
-5.0	0	0	0	0	0	0	*0*	0
-4.5	1	0	0	0	0	0	*0*	1
-4.0	1	0	0	0	0	0	*0*	1
-3.5	1	0	0	0	0	0	*0*	1
-3.0	1	0	0	0	4	0	*0*	5
-2.5	1	0	0	0	0	0	*0*	1
-2.0	1	0	0	0	17	0	*0*	18
-1.5	18	15	0	0	76	0	*0*	109
-1.0	21	16	0	1	236	0	*0*	274
-0.5	66	39	0	3	642	0	*0*	750
0.0	51	20	0	5	673	0	*0*	750
0.5	47	30	0	10	653	9	*0*	750
1.0	38	34	1	45	608	25	*0*	750
1.5	63	14	1	122	497	54	*0*	750
2.0	79	13	0	240	352	66	*0*	750
2.5	78	6	0	238	345	90	*0*	757
3.0	48	0	0	460	175	67	*0*	750
3.5	16	0	0	376	54	352	*0*	698
4.0	8	0	0	165	27	349	*0*	549
4.5	0	0	0	183	20	398	*0*	601
5.0	*	*	*	*	*	*	*25750*	25750
6.0	*	*	*	*	*	*	*31000*	31000
7.0	*	*	*	*	*	*	*35286*	35286

Bulk Weight Percentages:

ϕ	Wp	Gp	Bp	Xtal	Lithic	Glass	NA
-5.0	0	0	0	0	0	0	0
-4.5	0	0	0	0	0	0	0
-4.0	0	0	0	0	0	0	0
-3.5	0	0	0	0	0	0	0
-3.0	0.63	0	0	0	0	0	0
-2.5	2.44	0	0	0	0	0	0
-2.0	0	0	0	0	0.15	0	0
-1.5	18	0.02	0	0	5.54	0	0
-1.0	0.18	0.20	0	0.02	4.41	0	0
-0.5	0.39	0.24	0	0.03	6.59	0	0
0.0	0.38	0.17	0.01	0.06	8.29	0	0
0.5	0.40	0.51	0.01	0.13	8.88	0.11	0
1.0	0.36	0.36	0	0.56	7.87	0.29	0
1.5	0.35	0.24	0	1.47	6.15	0.57	0
2.0	0.27	0.05	0	2.47	3.62	0.60	0
2.5	0.29	0.03	0	2.07	3.00	0.73	0
3.0	0.21	0	0	3.71	1.41	0.49	0
3.5	0.09	0	0	1.88	0.37	1.87	0
4.0	0.06	0	0	1.66	0.27	2.78	0
4.5	0	0	0	0.84	0.09	1.48	0
5.0	*	*	*	*	*	*	4.80
6.0	*	*	*	*	*	*	3.97
7.0	*	*	*	*	*	*	2.88
	6.05	**1.82**	**0.02**	**14.90**	**56.64**	**8.92**	**11.65**

S1 at Locality 17 [CBV-S-24]. [Total sample weight: 359692.8 mg]

Grain diameter		Weight Fractions:		Granulometric Analysis						
ϕ	mm	weight [mg]	Cumulative weight %	ϕ_{05}	ϕ_{25}	ϕ_{10}	ϕ_{5}	Md_{ϕ}	σ_{ϕ}	F2
-5.0	31.5	0	0	6.2	5.4	-0.6	-2.1	2.9	2.76	44.36%
-4.5	22.4	0	0							
-4.0	16.0	0	0							
-3.5	11.2	1168.7	0.32							
-3.0	8.0	4600.6	1.6							
-2.5	5.6	5703.6	3.19							
-2.0	4.0	7740.7	5.34							
-1.5	2.8	12056.9	8.69							
-1.0	2.0	15204.1	12.87							
-0.5	1.4	17626.0	17.77							
0.0	1.0	17066.3	22.52							
0.5	0.710	17718.2	27.44							
1.0	0.500	17054.4	32.18							
1.5	0.355	15674.7	36.54							
2.0	0.250	15143.8	40.75							
2.5	0.180	15362.5	45.02							
3.0	0.125	19591.5	50.47							
3.5	0.088	18605.5	55.64							
4.0	0.063	22246.7	61.83							
4.5	0.045	18523.7	66.98							
5.0	0.032	51760	81.37							
6.0	0.017	44520	93.75							
7.0	0.008	22500	100.00							

Minor Lithic Counts		Abundance [volume %]	
SML	GCL	SML	GCL
n.a.	n.a.	n.a.	n.a.

Counts:

ϕ	Wp	Gp	Bp	Xtal	Lithic	Glass	NA	total counts
-5.0	0	0	0	0	0	0	0	0
-4.5	0	0	0	0	0	0	0	0
-4.0	0	0	0	0	0	0	0	0
-3.5	1	1	0	0	0	0	0	2
-3.0	0	0	0	0	4	0	0	4
-2.5	3	3	0	0	12	0	0	18
-2.0	33	11	0	0	36	0	0	80
-1.5	72	28	0	0	159	0	0	259
-1.0	75	13	0	0	212	0	0	300
-0.5	92	14	0	0	278	12	0	396
0.0	114	16	0	0	338	30	0	498
0.5	78	12	0	11	286	113	0	500
1.0	55	0	0	24	228	192	0	499
1.5	29	0	0	31	179	261	0	500
2.0	0	0	0	54	122	324	0	500
2.5	0	0	0	68	117	315	0	500
3.0	0	0	0	89	113	298	0	500
3.5	0	0	0	115	97	287	0	499
4.0	0	0	0	188	85	240	0	513
4.5	0	0	0	146	74	264	0	484
5.0	*	*	*	*	*	*	*27250*	27250
6.0	*	*	*	*	*	*	*34091*	34091
7.0	*	*	*	*	*	*	*27000*	2700

Bulk Weight Percentages:

ϕ	Wp	Gp	Bp	Xtal	Lithic	Glass	NA
-5.0	0	0	0	0	0	0	0
-4.5	0	0	0	0	0	0	0
-4.0	0	0	0	0	0	0	0
-3.5	0.13	0.19	0	0	0	0	0
-3.0	0	0	0	0	1.28	0	0
-2.5	0.09	0.09	0	0	1.40	0	0
-2.0	0.46	0	0.14	0	1.55	0	0
-1.5	0.71	0.04	0	0	2.6	0	0
-1.0	0.57	0.14	0	0	3.46	0	0
-0.5	0.75	0.12	0	0	3.90	0.13	0
0.0	0.74	0.12	0	0	3.60	0.29	0
0.5	0.68	0.15	0	0.11	2.93	1.06	0
1.0	0.41	0	0	0.24	2.34	1.75	0
1.5	0.13	0	0	0.30	1.75	2.18	0
2.0	0	0	0	0.49	1.11	2.61	0
2.5	0	0	0	0.61	1.05	2.62	0
3.0	0	0	0	1.02	1.30	3.13	0
3.5	0	0	0	1.36	1.15	2.66	0
4.0	0	0	0	2.51	1.13	2.54	0
4.5	0	0	0	1.76	0.89	2.51	0
5.0	*	*	*	*	*	*	14.39
6.0	*	*	*	*	*	*	12.38
7.0	*	*	*	*	*	*	6.25
	4.67	**0.85**	**0.14**	**8.40**	**31.44**	**21.48**	**33.02**

S1 at Locality 18 [CBV-S-1]. [Total sample weight: 264930.8 mg]

Grain diameter		Weight Fractions		Granulometric Analysis						
ϕ	mm	weight [mg]	Cumulative weight %	ϕ_{5}	ϕ_{25}	ϕ_{50}	ϕ_{75}	Md$_\phi$	σ_ϕ	F2
-5.0	31.5	0	0	4.3	3.8	1.7	-0.7	1.7	2.04	22.68%
-4.5	22.4	0	0							
-4.0	16.0	0	0							
-3.5	11.2	0	0							
-3.0	8.0	4201	1.59							
-2.5	5.6	0	1.59							
-2.0	4.0	10910	3.12							
-1.5	2.8	12160	7.24							
-1.0	2.0	18150	11.83							
-0.5	1.4	17570	25.31							
0.0	1.0	20540	33.06							
0.5	0.710	19040	39.69							
1.0	0.500	17570	46.88							
1.5	0.355	19040	53.62							
2.0	0.250	17050	60.88							
2.5	0.180	20050	69.01							
3.0	0.125	21530	77.32							
3.5	0.088	22020	86.76							
4.0	0.063	25010	94.89							
4.5	0.045	21533	97.78							
5.0	0.032	7645	97.78							
6.0	0.017	5890	100							
7.0	0.008	0	100							

Minor Lithic Counts		Abundance [volume %]	
SMI	GCI	SMI	GCI
0	0	0	0
0	0	0	0
0	0	0	0
0	0	0	0
10	36	2	7.1
5	43	1.1	9.1
11	41	3.1	11.5
0	0	0	0
0	0	0	0

Counts:

ϕ	Wp	Gp	Bp	Xtal	Lithic	Glass	NA	total counts
-5.0	0	0	0	0	0	0	*0*	0
-4.5	0	0	0	0	0	0	*0*	0
-4.0	0	0	0	0	0	0	*0*	0
-3.5	0	0	0	0	0	0	*0*	0
-3.0	0	0	0	0	3	0	*0*	3
-2.5	0	0	0	0	0	0	*0*	0
-2.0	3	0	0	0	44	0	*0*	47
-1.5	34	14	0	0	159	0	*0*	207
-1.0	192	22	0	1	535	0	*0*	750
-0.5	256	27	0	2	465	0	*0*	750
0.0	219	17	0	6	508	0	*0*	750
0.5	221	13	0	31	474	10	*0*	749
1.0	221	6	0	83	357	76	*0*	743
1.5	149	0	0	123	341	131	*0*	744
2.0	177	0	0	201	229	143	*0*	750
2.5	158	0	0	266	174	152	*0*	750
3.0	107	0	0	375	109	159	*0*	750
3.5	29	0	0	266	13	223	*0*	531
4.0	18	0	0	296	16	21	*0*	551
4.5	0	0	0	469	15	186	*0*	670
5.0	*	*	*	*	*	*	*35312*	35312
6.0	*	*	*	*	*	*	*39545*	39545
7.0	*	*	*	*	*	*	*0*	0

Bulk Weight Percentages:

Wp	Gp	Bp	Xtal	Lithic	Glass	NA
0	0	0	0	0	0	0
0	0	0	0	0	0	0
0	0	0	0	0	0	0
0	0	0	0	0	0	0
0	0	0	0	1.59	0	0
0	0	0	0	0	0	0
0.03	0	0	0	1.50	0	0
0.4	0.15	0	0	3.57	0	0
0.64	0.11	0	0.01	3.83	0	0
1.61	0.18	0	0.02	5.04	0	0
1.34	0.12	0	0.06	5.11	0	0
1.50	0.19	0	0.35	5.60	0.11	0
1.60	0.05	0	0.70	3.53	0.67	0
0.76	0	0	1.34	3.83	1.26	0
0.62	0	0	2.10	2.39	1.33	0
0.79	0	0	3.10	2.03	1.65	0
0.68	0	0	4.44	1.29	1.72	0
0.40	0	0	4.64	0.23	3.05	0
0.27	0	0	5.57	0.30	3.3	0
0	0	0	6.04	0.17	1.89	0
*	*	*	*	*	*	2.89
*	*	*	*	*	*	2.22
*	*	*	*	*	*	0
10.64	**0.80**	**0**	**28.46**	**40.01**	**14.98**	**5.11**

S1 at Locality 44 [CBV-S-4]. [Total sample weight: 82481.3 mg]

Grain diameter		Weight Fractions		Granulometric Analysis						
ϕ	mm	weight [mg]	Cumulative weight %	$\phi_{5\%}$	ϕ_{84}	ϕ_{16}	ϕ_{50}	Md_ϕ	σ_ϕ	F2
-5.0	31.5	0	0	5.8	3.7	-1.4	-2.2	0.2	2.49	16.99%
-4.5	22.4	0	0							
-4.0	16.0	0	0							
-3.5	11.2	0	0							
-3.0	8.0	286.8	0.35							
-2.5	5.6	2207.9	3.02							
-2.0	4.0	2559.2	6.13							
-1.5	2.8	5874.1	13.25							
-1.0	2.0	8237.3	23.24							
-0.5	1.4	10068.9	35.44							
0.0	1.0	9779.6	47.3							
0.5	0.710	8863.4	58.05							
1.0	0.500	6926.1	66.44							
1.5	0.355	4152.3	71.48							
2.0	0.250	2945.3	75.05							
2.5	0.180	2204.0	77.72							
3.0	0.125	2445.8	80.69							
3.5	0.088	1918.7	83.01							
4.0	0.063	1990.4	85.43							
4.5	0.045	1446.5	87.18							
5.0	0.032	4210	92.28							
6.0	0.017	3745	96.82							
7.0	0.008	2625	100.00							

Minor Lithic Counts		Abundance [volume %]	
SMI	GCI	SMI	GCI
n.a.	n.a.	n.a.	n.a.

Counts:

ϕ	Wp	Gp	Bp	Xtal	Lithic	Glass	NA	total counts
-5.0	0	0	0	0	0	0	0	0
-4.5	0	0	0	0	0	0	0	0
-4.0	0	0	0	0	0	0	0	0
-3.5	0	0	0	0	0	0	0	0
-3.0	1	0	0	0	0	0	0	1
-2.5	0	0	0	0	1	0	0	1
-2.0	12	0	0	0	16	0	0	28
-1.5	25	6	2	0	103	0	0	136
-1.0	68	28	0	0	391	0	0	487
-0.5	53	26	0	2	486	0	0	567
0.0	84	16	3	7	638	2	0	750
0.5	59	15	0	15	658	3	0	750
1.0	46	18	0	22	627	37	0	750
1.5	59	16	0	54	508	113	0	750
2.0	36	3	0	111	431	169	0	750
2.5	68	0	2	190	280	212	0	752
3.0	72	0	0	264	196	218	0	750
3.5	0	0	0	237	61	388	0	686
4.0	0	0	0	135	58	359	0	552
4.5	0	0	0	87	36	382	0	505
5.0	*	*	*	*	*	*	24875	24875
6.0	*	*	*	*	*	*	32182	32182
7.0	*	*	*	*	*	*	35429	35429

Bulk Weight Percentages:

ϕ	Wp	Gp	Bp	Xtal	Lithic	Glass	NA
-5.0	0	0	0	0	0	0	0
-4.5	0	0	0	0	0	0	0
-4.0	0	0	0	0	0	0	0
-3.5	0	0	0	0	0	0	0
-3.0	0.35	0	0	0	0	0	0
-2.5	2.68	0	0	0	0	0	0
-2.0	0.94	0	0	0	2.17	0	0
-1.5	0.72	0.19	0.11	0	6.10	0	0
-1.0	0.72	0.43	0	0	8.84	0	0
-0.5	0.70	0.36	0	0.04	11.10	0	0
0.0	0.85	0.19	0.03	0.11	10.64	0.03	0
0.5	0.70	0.27	0	0.21	9.52	0.04	0
1.0	0.39	0.17	0	0.24	7.22	0.38	0
1.5	0.19	0.16	0	0.37	3.62	0.69	0
2.0	0.06	0.01	0	0.56	2.18	0.76	0
2.5	0.11	0	0	0.73	1.07	0.75	0
3.0	0.16	0	0	1.12	0.83	0.85	0
3.5	0	0	0	0.92	0.24	1.17	0
4.0	0	0	0	0.68	0.29	1.44	0
4.5	0	0	0	0.36	0.17	1.25	0
5.0	*	*	*	*	*	*	5.10
6.0	*	*	*	*	*	*	4.54
7.0	*	*	*	*	*	*	3.18
	8.57	**1.78**	**0.14**	**5.34**	**63.99**	**7.36**	**12.82**

S1 at Locality 45 [CBV-S-34]. [Total sample weight: 25656.7 mg]

Grain diameter		Weight Fractions:		Granulometric Analysis:						
ϕ	mm	weight [mg]	Cumulative weight %	ϕ_{05}	ϕ_{25}	ϕ_{10}	$\phi_{<}$	Md_{ϕ}	σ_{ϕ}	F2
-5.0	31.5	0	0	4.8	2.7	-1.2	-2.2	0.1	2.04	10.08%
-4.5	22.4	0	0							
-4.0	16.0	0	0							
-3.5	11.2	0	0							
-3.0	8.0	0	0							
-2.5	5.6	216.1	0.84							
-2.0	4.0	1205.5	5.54							
-1.5	2.8	1254.6	10.43							

Minor Lithic Counts		Abundance [volume %]	
SML	GCL	SML	GCL
n.a.	n.a.	n.a.	n.a.

-1.0	2.0	2289.5	19.35
-0.5	1.4	3676.3	33.68
0.0	1.0	4162.1	49.91
0.5	0.710	3498.9	63.54
1.0	0.500	2192.3	72.09
1.5	0.355	944.3	75.77
2.0	0.250	940	79.43
2.5	0.180	947.1	83.12
3.0	0.125	1012.8	87.07
3.5	0.088	730.4	89.92
4.0	0.063	557.9	92.09
4.5	0.045	401.9	93.66
5.0	0.032	645	96.18
6.0	0.017	575	98.43
7.0	0.008	405	100.00

Counts:

ϕ	Wp	Gp	Bp	Xtal	Lithic	Glass	NA	total counts
-5.0	0	0	0	0	0	0	*0*	0
-4.5	0	0	0	0	0	0	*0*	0
-4.0	0	0	0	0	0	0	*0*	0
-3.5	0	0	0	0	0	0	*0*	0
-3.0	0	0	0	0	0	0	*0*	0
-2.5	0	0	0	0	1	0	*0*	1
-2.0	1	0	0	0	10	0	*0*	11
-1.5	4	1	0	0	25	0	*0*	30
-1.0	23	0	0	0	123	0	*0*	146
-0.5	60	14	0	0	535	0	*0*	609
0.0	90	22	0	6	632	0	*0*	750
0.5	76	30	0	14	630	0	*0*	750
1.0	57	21	0	69	590	13	*0*	750
1.5	64	12	0	83	511	80	*0*	750
2.0	112	10	0	124	382	122	*0*	750
2.5	62	0	2	215	256	215	*0*	750
3.0	40	0	0	182	186	342	*0*	750
3.5	89	0	0	106	89	418	*0*	702
4.0	99	0	0	138	99	525	*0*	861
4.5	45	0	0	51	45	452	*0*	593
5.0	*	*	*	*	*	*	*24875*	24875
6.0	*	*	*	*	*	*	*32782*	32782
7.0	*	*	*	*	*	*	*35429*	35429

Bulk Weight Perventages:

Wp	Gp	Bp	Xtal	Lithic	Glass	NA
0	0	0	0	0	0	0
0	0	0	0	0	0	0
0	0	0	0	0	0	0
0	0	0	0	0	0	0
0	0	0	0	0	0	0
0	0	0	0	0.84	0	0
0.11	0	0	0	4.59	0	0
0.23	0.1	0	0	4.56	0	0
0.72	0	0	0	8.21	0	0
0.86	0.21	0	0	13.26	0	0
1.25	0.35	0	0.13	14.48	0	0
0.97	0.70	0	0.25	11.72	0	0
0.49	0.20	0	0.78	6.94	0.14	0
0.15	0.09	0	0.42	2.67	0.36	0
0.21	0.02	0	0.69	2.13	0.61	0
0.14	0	0.01	1.14	1.35	1.06	0
0.12	0	0	1.02	1.05	1.76	0
0.34	0	0	0.51	0.43	1.57	0
0.23	0	0	0.41	0.29	1.24	0
0	0	0	0.18	0.16	1.22	0
*	*	*	*	*	*	2.52
*	*	*	*	*	*	2.24
*	*	*	*	*	*	1.57
5.82	**1.67**	**0.01**	**5.53**	**72.68**	**7.96**	**6.33**

S1 at Locality 49 [CBV-S-6]. [Total sample weight: 227140.8 mg]

Grain diameter		Weight Fractions		Granulometric Analysis						
ϕ	mm	weight [mg]	Cumulative weight %	ϕ_{05}	ϕ_{84}	ϕ_{16}	ϕ_s	Md_ϕ	σ_ϕ	F2
-5.0	31.5	0	0	5.5	4.9	-0.9	-2.4	1.1	2.65	27.31%
-4.5	22.4	0	0							
-4.0	16.0	56622.1	2.48							
-3.5	11.2	0	2.48							
-3.0	8.0	2582.1	3.61							
-2.5	5.6	2193.8	4.58							
-2.0	4.0	5035.8	6.79							
-1.5	2.8	7853.8	10.25							
-1.0	2.0	11568.9	15.35							
-0.5	1.4	17873.5	23.21							
0.0	1.0	19000.9	31.58							
0.5	0.710	22104.2	41.31							
1.0	0.500	19200.4	49.76							
1.5	0.355	14641.7	56.21							
2.0	0.250	10625.1	60.89							
2.5	0.180	7730.5	64.29							
3.0	0.125	10135.1	68.75							
3.5	0.088	8945.1	72.69							
4.0	0.063	9576.2	76.91							
4.5	0.045	20792.6	86.06							
5.0	0.032	16400	93.28							
6.0	0.017	10550	97.93							
7.0	0.008	4700	100.00							

	Minor Lithic Counts		Abundance [volume %]	
	SMI.	GCI.	SMI	GCI.
	3	19	1.1	6.7
	0	16	0	4.4
	0	12	0	3.7
	0	11	0	3.5
	1	8	0.3	2.8
	0	6	0	2.3
	0	5	0	2.9
	0	5	0	3.3
	0	6	0	3.8

Counts:

ϕ	Wp	Gp	Bp	Xtal	Lithic	Glass	NA	total counts
-5.0	0	0	0	0	0	0	*0*	0
-4.5	0	0	0	0	0	0	*0*	0
-4.0	0	0	0	0	1	0	*0*	1
-3.5	0	0	0	0	0	0	*0*	0
-3.0	0	0	0	0	2	0	*0*	2
-2.5	6	0	0	0	4	0	*0*	10
-2.0	25	3	0	0	24	1	*0*	53
-1.5	81	2	0	0	108	9	*0*	200
-1.0	11	2	0	0	283	16	*0*	312
-0.5	96	3	0	3	366	32	*0*	500
0.0	90	2	0	10	328	70	*0*	500
0.5	71	3	0	18	316	92	*0*	500
1.0	63	5	0	29	288	115	*0*	500
1.5	61	2	0	42	263	132	*0*	500
2.0	57	2	0	101	172	168	*0*	500
2.5	43	0	0	116	152	189	*0*	500
3.0	28	0	0	109	158	205	*0*	500
3.5	0	0	0	91	142	267	*0*	500
4.0	0	0	0	85	126	289	*0*	500
4.5	0	0	0	62	91	347	*0*	500
5.0	*	*	*	*	*	*	*1026*	1026
6.0	*	*	*	*	*	*	*951*	951
7.0	*	*	*	*	*	*	*676*	676

Bulk Weight Percentages:

Wp	Gp	Bp	Xtal	Lithic	Glass	NA
0	0	0	0	0	0	0
0	0	0	0	0	0	0
0	0	0	0	2.48	0	0
0	0	0	0	0	0	0
0	0	0	0	1.14	0	0
0.30	0	0	0	0.67	0	0
0.59	0.09	0	0	1.40	0.14	0
0.95	0.03	0	0	2.27	0.21	0
0.09	0.02	0	0	4.77	0.22	0
0.97	0.03	0	0.05	6.38	0.44	0
1.00	0.03	0	0.18	6.00	1.17	0
1.07	0.08	0	0.36	6.49	1.74	0
0.83	0.07	0	0.50	5.21	1.84	0
0.40	0.04	0	0.59	3.79	1.63	0
0.20	0.01	0	1.07	1.82	1.58	0
0.14	0	0	0.85	1.12	1.29	0
0.14	0	0	1.04	1.50	1.78	0
0	0	0	0.81	1.27	1.86	0
0	0	0	0.81	1.21	2.20	0
0	0	0	1.33	1.90	5.87	0
*	*	*	*	*	*	7.22
*	*	*	*	*	*	4.65
*	*	*	*	*	*	2.07
6.68	**0.4**	**0**	**7.59**	**49.42**	**21.97**	**13.94**

S1 at Locality 50 [CBV-S-11]. [Total sample weight: 159792.8 mg]

Grain diameter		Weight Fractions		Granulometric Analysis						
ϕ	mm	weight [mg]	Cumulative weight %	ϕ_{05}	ϕ_{25}	ϕ_{10}	ϕ_{50}	Md$_\phi$	σ_ϕ	F2
-5.0	31.5	0	0	5.2	4.3	-1.7	-3.1	1.3	2.75	23.76%
-4.5	22.4	0	0							
-4.0	16.0	0	2.48							
-3.5	11.2	1570.3	2.48							
-3.0	8.0	8321.9	3.61							
-2.5	5.6	6836.1	4.58							
-2.0	4.0	7087	6.79							
-1.5	2.8	9070	10.25							
-1.0	2.0	8428.4	15.35							
-0.5	1.4	7605.3	23.21							
0.0	1.0	6825.5	31.58							
0.5	0.710	9017.3	41.31							
1.0	0.500	10342.1	49.76							
1.5	0.355	9762.8	56.21							
2.0	0.250	12649.2	60.89							
2.5	0.180	9084.1	64.29							
3.0	0.125	8786.2	68.75							
3.5	0.088	6445.4	72.69							
4.0	0.063	6767.8	76.91							
4.5	0.045	12365.5	86.06							
5.0	0.032	9750	93.28							
6.0	0.017	6275	97.93							
7.0	0.008	2790	100.00							

Minor Lithic Counts		Abundance [volume %]	
SML	GCL	SML	GCL
4	2	1.5	0.8
0	3	0	1.1
0	1	0	0.4
0	2	0	0.9
0	2	0	1.0
0	0	0	0
0	0	0	0
0	0	0	0
0	3	0	2.7

Counts:

ϕ	Wp	Gp	Bp	Xtal	Lithic	Glass	NA	total counts
-5.0	0	0	0	0	0	0	*0*	0
-4.5	0	0	0	0	0	0	*0*	0
-4.0	0	0	0	0	0	0	*0*	0
-3.5	0	1	0	0	1	0	*0*	2
-3.0	2	2	0	0	6	0	*0*	10
-2.5	6	5	0	0	16	0	*0*	27
-2.0	28	1	0	0	36	0	*0*	65
-1.5	59	11	0	0	112	6	*0*	188
-1.0	172	3	0	1	259	15	*0*	450
-0.5	168	0	0	4	266	62	*0*	500
0.0	152	0	0	10	229	109	*0*	500
0.5	108	0	0	23	221	148	*0*	500
1.0	72	0	0	43	195	190	*0*	500
1.5	78	0	0	66	142	214	*0*	500
2.0	86	0	0	89	87	238	*0*	500
2.5	79	0	0	103	97	221	*0*	500
3.0	63	0	0	106	112	219	*0*	500
3.5	0	0	0	115	91	294	*0*	500
4.0	0	0	0	91	74	335	*0*	500
4.5	0	0	0	54	51	388	*0*	500
5.0	*	*	*	*	*	*	*609*	609
6.0	*	*	*	*	*	*	*570*	570
7.0	*	*	*	*	*	*	*398*	398

Bulk Weight Percentages:

ϕ	Wp	Gp	Bp	Xtal	Lithic	Glass	NA
-5.0	0	0	0	0	0	0	0
-4.5	0	0	0	0	0	0	0
-4.0	0	0	0	0	0	0	0
-3.5	0	0.43	0	0	0.55	0	0
-3.0	0.42	0	0	0	4.78	0	0
-2.5	0.39	0.35	0	0	3.54	0	0
-2.0	1.05	0.05	0	0	3.34	0	0
-1.5	1.16	0.30	0	0	3.98	0.23	0
-1.0	1.20	0.03	0	0.01	3.86	0.18	0
-0.5	1.12	0	0	0.04	3.04	0.56	0
0.0	0.92	0	0	0.10	2.27	0.99	0
0.5	1.06	0	0	0.27	2.67	1.65	0
1.0	0.75	0	0	0.59	2.76	2.38	0
1.5	0.51	0	0	0.92	2.04	2.63	0
2.0	0.55	0	0	1.69	1.65	4.02	0
2.5	0.44	0	0	1.33	1.26	2.66	0
3.0	0.41	0	0	1.29	1.36	2.44	0
3.5	0	0	0	1.06	0.84	2.13	0
4.0	0	0	0	0.89	0.73	2.61	0
4.5	0	0	0	1.00	1.07	5.66	0
5.0	*	*	*	*	*	*	6.11
6.0	*	*	*	*	*	*	3.93
7.0	*	*	*	*	*	*	1.75
	9.98	**1.16**	**0**	**9.19**	**39.74**	**28.14**	**11.79**

S1 at Locality 51 [CBV-S-9]. [Total sample weight: 205172.8 mg]

Grain diameter		Weight Fractions		Granulometric Analysis						
ϕ	mm	weight [mg]	Cumulative weight %	ϕ_{05}	ϕ_{84}	ϕ_{16}	ϕ_{50}	Md$_\phi$	σ_ϕ	F2
-5.0	31.5	0	0	6.4	5.5	-1.1	-2.3	5.6	2.97	43.61%
-4.5	22.4	0	0							
-4.0	16.0	0	0							
-3.5	11.2	0	0							
-3.0	8.0	3305.9	1.61							
-2.5	5.6	6094.6	4.58							
-2.0	4.0	7544.2	8.26							
-1.5	2.8	8563.1	12.43							

Minor Lithic Counts		Abundance [volume %]	
SML	GCL	SML	GCL
n.a.	n.a.	n.a.	n.a.

-1.0	2.0	9012	16.82
-0.5	1.4	10960.4	22.17
0.0	1.0	10715.9	27.39
0.5	0.710	11115.9	32.81
1.0	0.500	10109.8	37.73
1.5	0.355	10516.4	42.86
2.0	0.250	7838.6	46.68
2.5	0.180	6084.8	49.65
3.0	0.125	6794.6	52.96
3.5	0.088	7033.2	56.39
4.0	0.063	7851	60.21
4.5	0.045	6596.3	63.43
5.0	0.032	29860	77.98
6.0	0.017	28215	91.73
7.0	0.008	16960	100.00

Counts:

ϕ	Wp	Gp	Bp	Xtal	Lithic	Glass	NA	total counts
-5.0	0	0	0	0	0	0	0	0
-4.5	0	0	0	0	0	0	0	0
-4.0	0	0	0	0	0	0	0	0
-3.5	0	0	0	0	0	0	0	0
-3.0	0	5	0	0	1	0	0	6
-2.5	5	1	0	0	12	0	0	18
-2.0	4	3	0	0	44	0	0	51
-1.5	27	12	0	0	127	0	0	166
-1.0	64	76	0	0	466	0	0	606
-0.5	68	40	0	1	391	0	0	500
0.0	78	19	0	10	383	10	0	500
0.5	71	12	0	19	361	37	0	500
1.0	63	8	0	67	303	59	0	500
1.5	71	4	0	109	243	73	0	500
2.0	77	0	0	157	183	83	0	500
2.5	51	0	0	227	146	76	0	500
3.0	29	0	0	305	109	57	0	500
3.5	0	0	0	259	180	61	0	500
4.0	0	0	0	216	161	123	0	500
4.5	0	0	0	98	116	286	0	500
5.0	*	*	*	*	*	*	187	187
6.0	*	*	*	*	*	*	254	254
7.0	*	*	*	*	*	*	242	242

Bulk Weight Percentages:

Wp	Gp	Bp	Xtal	Lithic	Glass	NA
0	0	0	0	0	0	0
0	0	0	0	0	0	0
0	0	0	0	0	0	0
0	0	0	0	0	0	0
0	0.75	0	0	0.86	0	0
0.32	0.07	0	0	2.58	0	0
0.13	0.12	0	0	3.43	0	0
0.41	0.25	0	0	3.51	0	0
0.28	0.41	0	0	3.74	0	0
0.15	0.28	0	0.01	4.59	0	0
0.17	0.15	0	0.11	5.67	0.10	0
0.07	0.17	0	0.21	4.13	0.39	0
0.06	0.07	0	0.67	3.16	0.54	0
0	0.06	0	1.21	2.77	0.71	0
0	0	0	1.36	1.59	0.64	0
0	0	0	1.45	0.93	0.45	0
0	0	0	2.10	0.75	0.36	0
0	0	0	1.82	1.27	0.34	0
0	0	0	1.74	1.30	0.79	0
0	0	0	0.72	0.85	1.65	0
*	*	*	*	*	*	14.56
*	*	*	*	*	*	13.75
*	*	*	*	*	*	8.27
1.59	**2.33**	**0**	**11.4**	**42.13**	**5.97**	**36.58**

S1 at Locality 71 [CBV-S-25]. [Total Sample weight: 265171.5 mg]

Grain diameter		Weight Fractions		Granulometric Analysis						
ϕ	mm	weight [mg]	Cumulative weight %	ϕ_{05}	ϕ_{84}	ϕ_{16}	ϕ_{50}	Md_ϕ	σ_ϕ	F2
-5.0	31.5	0	0	6.2	5.2	-1.1	-2.2	2.0	2.84	36.84%
-4.5	22.4	0	0							
-4.0	16.0	0	0							
-3.5	11.2	0	0							
-3.0	8.0	1915	0.72							
-2.5	5.6	5185.7	2.28							
-2.0	4.0	10064.5	6.47							
-1.5	2.8	13211.2	11.46							

		Minor Lithic Counts		Abundance [volume %]	
		SML	GCL	SML	GCL
-1.0	2.0	13900.8	16.70	8	10	2.2	2.7
-0.5	1.4	15765.7	22.64	7	10	1.9	3.4
0.0	1.0	17651.2	29.3	9	12	2.6	5.1
0.5	0.710	15508.9	35.15	6	17	1.8	6.7
1.0	0.500	16710.7	41.45	4	21	1.3	6.7
1.5	0.355	13933.8	46.7	5	18	1.9	5.2
2.0	0.250	10582.3	50.7	4	11	1.9	4.5
2.5	0.180	9798	54.39	2	9	1	3.0
3.0	0.125	12268.7	59.02	0	6	0	0
3.5	0.088	10976.9	63.16				
4.0	0.063	12746.5	67.96				
4.5	0.045	9915.5	71.70				
5.0	0.032	29865	82.97				
6.0	0.017	28215	93.6				
7.0	0.008	16960	100.00				

Counts:

ϕ	Wp	Gp	Bp	Xtal	Lithic	Glass	NA	total counts
-5.0	0	0	0	0	0	0	0	0
-4.5	0	0	0	0	0	0	0	0
-4.0	0	0	0	0	0	0	0	0
-3.5	0	0	0	0	0	0	0	0
-3.0	1	0	0	0	2	0	0	3
-2.5	1	0	0	0	15	0	0	16
-2.0	9	0	0	0	56	0	0	65
-1.5	11	0	0	0	117	0	0	128
-1.0	48	11	0	1	360	26	0	446
-0.5	43	10	0	9	372	66	0	500
0.0	37	7	0	15	349	92	0	500
0.5	31	6	0	27	333	103	0	500
1.0	20	1	0	46	314	119	0	500
1.5	18	0	0	91	270	121	0	500
2.0	12	0	0	152	210	126	0	500
2.5	11	0	0	158	200	131	0	500
3.0	9	0	0	165	198	128	0	500
3.5	0	0	0	171	181	148	0	500
4.0	0	0	0	143	158	199	0	500
4.5	0	0	0	101	103	296	0	500
5.0	*	*	*	*	*	*	*1867*	1867
6.0	*	*	*	*	*	*	*2565*	2565
7.0	*	*	*	*	*	*	*2422*	2422

Bulk Weight Percentages:

	Wp	Gp	Bp	Xtal	Lithic	Glass	NA
	0	0	0	0	0	0	0
	0	0	0	0	0	0	0
	0	0	0	0	0	0	0
	0	0	0	0	0	0	0
	0.08	0	0	0	0.64	0	0
	0.04	0	0	0	1.92	0	0
	0.23	0	0	0	3.56	0	0
	0.25	0	0	0	4.74	0	0
	0.29	0.09	0	0.01	4.58	0.27	0
	0.32	0.08	0	0.11	4.77	0.66	0
	0.32	0.07	0	0.20	4.89	1.18	0
	0.26	0.09	0	0.31	4.03	1.15	0
	0.19	0.01	0	0.58	4.13	1.39	0
	0.09	0	0	0.99	3.02	1.16	0
	0.03	0	0	1.27	1.75	0.94	0
	0.04	0	0	1.21	1.53	0.93	0
	0.05	0	0	1.57	1.89	1.12	0
	0	0	0	1.51	1.60	1.02	0
	0	0	0	1.50	1.66	1.65	0
	0	0	0	0.86	0.88	2.00	0
	*	*	*	*	*	*	11.26
	*	*	*	*	*	*	10.64
	*	*	*	*	*	*	6.40
	2.19	**0.34**	**0**	**10.11**	**45.59**	**13.47**	**28.3**

S1 at Locality 77 [CBV-S-29] [Total sample weight: 182047.3 mg]

Grain diameter		Weight Fractions:		Granulometric Analysis						
ϕ	mm	weight [mg]	Cumulative weight %	ϕ_{05}	ϕ_{25}	ϕ_{16}	ϕ_{5}	Md_{ϕ}	σ_{ϕ}	F2
-5.0	31.5	0	0	5.6	4.6	-1.4	-2.7	1.0	2.75	32.73%
-4.5	22.4	0	0							
-4.0	16.0	0	0							
-3.5	11.2	0	0							
-3.0	8.0	3533.1	1.94							
-2.5	5.6	7357.9	5.98							
-2.0	4.0	5847.3	9.19							
-1.5	2.8	9326.6	14.32							
-1.0	2.0	10375.3	20.02							
-0.5	1.4	14977.8	28.24							
0.0	1.0	15730.5	36.89							
0.5	0.710	15699.2	45.51							
1.0	0.500	8849.7	50.37							
1.5	0.355	6063.1	53.70							
2.0	0.250	5213.4	56.56							
2.5	0.180	5323.9	59.49							
3.0	0.125	7093.3	63.39							
3.5	0.088	7064.4	67.27							
4.0	0.063	9366.8	72.41							
4.5	0.045	19788.7	83.28							
5.0	0.032	15770	91.94							
6.0	0.017	10145	97.52							
7.0	0.008	4520	100.00							

Minor Lithic Counts		Abundance [volume %]	
SMI.	GCI.	SMI	GCI.
0	0	0	0
0	0	0	0
0	0	0	0
0	0	0	0
0	0	0	0
3	6	0.9	1.8
4	2	1.7	0.9
5	6	2.3	2.7
3	8	1.4	3.7

Counts:

ϕ	Wp	Gp	Bp	Xtal	Lithic	Glass	NA	total counts
-5.0	0	0	0	0	0	0	0	0
-4.5	0	0	0	0	0	0	0	0
-4.0	0	0	0	0	0	0	0	0
-3.5	0	0	0	0	0	0	0	0
-3.0	4	0	0	0	2	0	0	6
-2.5	3	2	0	0	16	0	0	21
-2.0	6	7	0	0	42	0	0	55
-1.5	64	12	0	0	142	0	0	218
-1.0	49	23	0	0	533	0	0	605
-0.5	49	25	0	1	425	0	0	500
0.0	57	21	0	0	422	0	0	500
0.5	61	29	0	4	406	0	0	500
1.0	62	24	0	15	379	20	0	500
1.5	53	21	0	39	328	59	0	500
2.0	49	3	0	103	231	114	0	500
2.5	38	0	0	114	220	128	0	500
3.0	31	0	0	119	219	131	0	500
3.5	0	0	0	121	209	170	0	500
4.0	0	0	0	97	204	199	0	500
4.5	0	0	0	54	191	255	0	500
5.0	*	*	*	*	*	*	986	986
6.0	*	*	*	*	*	*	922	922
7.0	*	*	*	*	*	*	657	657

Bulk Weight Percentages:

Wp	Gp	Bp	Xtal	Lithic	Glass	NA
0	0	0	0	0	0	0
0	0	0	0	0	0	0
0	0	0	0	0	0	0
0	0	0	0	0	0	0
0.75	0	0	0	1.19	0	0
0.21	0.14	0	0	3.69	0	0
0.16	0.23	0	0	2.82	0	0
0.94	0.20	0	0	3.99	0	0
0.23	0.15	0	0	5.32	0	0
0.50	0.26	0	0.02	7.45	0	0
0.64	0.27	0	0	7.74	0	0
0.59	0.65	0	0.07	7.31	0	0
0.46	0.20	0	0.15	3.87	0.18	0
0.17	0.20	0	0.27	2.33	0.36	0
0.10	0.01	0	0.65	1.46	0.64	0
0.10	0	0	0.72	1.37	0.74	0
0.14	0	0	0.98	1.80	0.98	0
0	0	0	1.01	1.75	1.11	0
0	0	0	1.09	2.29	1.77	0
0	0	0	1.32	4.65	4.90	0
*	*	*	*	*	*	8.66
*	*	*	*	*	*	5.57
*	*	*	*	*	*	2.48
4.99	**2.31**	**0**	**6.28**	**59.03**	**10.68**	**16.71**

S1 at Locality 82 [CBV-S-8] [Total sample weight: 151534.3 g]

Grain diameter		Weight Fractions		Granulometric Analysis						
ϕ	mm	weight [mg]	Cumulative weight %	ϕ_{05}	ϕ_{50}	ϕ_{95}	ϕ_z	Md_ϕ	σ_ϕ	F2
-5.0	31.5	0	0	5.1	4.3	-0.7	-2.6	2.3	2.42	29.85%
-4.5	22.4	0	0							
-4.0	16.0	0	0							
-3.5	11.2	2484.3	1.64							
-3.0	8.0	3052.4	3.65							
-2.5	5.6	3077.9	5.68							
-2.0	4.0	3179.7	7.78							
-1.5	2.8	4150.9	10.52							
-1.0	2.0	5790	14.34							
-0.5	1.4	8230	19.77							
0.0	1.0	7570	24.77							
0.5	0.710	11390	32.29							
1.0	0.500	8190	37.69							
1.5	0.355	8500	43.3							
2.0	0.250	8230	48.73							
2.5	0.180	8720	54.49							
3.0	0.125	11390	62.00							
3.5	0.088	12340	70.15							
4.0	0.063	13990	79.38							
4.5	0.045	13375	88.20							
5.0	0.032	9940	94.76							
6.0	0.017	3450	97.04							
7.0	0.008	4490	100.00							

Minor Lithic Counts		Abundance [volume %]	
SML	GCL	SML	GCL
n.a.	n.a.	n.a.	n.a.

Counts:

ϕ	Wp	Gp	Bp	Xtal	Lithic	Glass	NA	total counts
-5.0	0	0	0	0	0	0	*0*	0
-4.5	0	0	0	0	0	0	*0*	0
-4.0	0	0	0	0	0	0	*0*	0
-3.5	1	0	0	0	0	0	*0*	1
-3.0	1	0	0	0	6	0	*0*	7
-2.5	1	0	0	0	0	0	*0*	1
-2.0	23	0	0	0	20	0	*0*	43
-1.5	440	0	0	0	64	0	*0*	504
-1.0	445	0	0	0	278	0	*0*	723
-0.5	501	0	0	0	292	0	*0*	793
0.0	269	0	0	4	243	0	*0*	516
0.5	16	1	0	5	348	127	*0*	497
1.0	13	0	0	32	289	412	*0*	746
1.5	9	4	0	117	185	431	*0*	746
2.0	0	3	0	217	165	356	*0*	741
2.5	0	0	0	294	156	310	*0*	750
3.0	0	0	0	488	75	187	*0*	750
3.5	0	0	0	354	12	158	*0*	524
4.0	0	0	0	271	14	251	*0*	536
4.5	0	0	0	540	13	299	*0*	852
5.0	*	*	*	*	*	*	*34750*	34750
6.0	*	*	*	*	*	*	*17545*	17545
7.0	*	*	*	*	*	*	*35875*	35875

Bulk Weight Percentages:

Wp	Gp	Bp	Xtal	Lithic	Glass	NA
0	0	0	0	0	0	0
0	0	0	0	0	0	0
0	0	0	0	0	0	0
0.55	0	0	0	1.09	0	0
0.04	0	0	0	1.97	0	0
0.17	0	0	0	1.83	0	0
0.31	0	0	0	1.79	0	0
1.15	0	0	0	1.59	0	0
2.24	0	0	0	1.58	0	0
2.87	0	0	0	2.57	0	0
2.94	0	0	0.10	1.95	0	0
1.98	0.01	0	0.06	4.41	1.06	0
0.10	0	0	0.26	2.41	2.64	0
0.05	0.20	0	0.91	1.48	2.95	0
0.02	0.01	0	1.68	1.28	2.45	0
0	0	0	2.33	1.15	2.28	0
0	0	0	4.99	0.78	1.75	0
0	0	0	5.89	0.20	2.06	0
0	0	0	5.17	0.27	3.80	0
0	0	0	6.04	0.15	2.64	0
*	*	*	*	*	*	6.56
*	*	*	*	*	*	2.28
*	*	*	*	*	*	2.96
12.42	**0.22**	**0**	**27.43**	**26.50**	**21.63**	**11.80**

S1 at Locality 83 [CBV-S-13] [Total sample weight: 151477.5 g]

Grain diameter		Weight Fractions		Granulometric Analysis						
ϕ	mm	weight [mg]	Cumulative weight %	ϕ_{05}	ϕ_{84}	ϕ_{16}	ϕ_{σ}	Md_{ϕ}	σ_{ϕ}	F2
-5.0	31.5	0	0	5.8	4.8	-1.3	-2.7	2.7	2.81	41.90%
-4.5	22.4	0	0							
-4.0	16.0	0	0							
-3.5	11.2	2271.7	1.5							
-3.0	8.0	3239.5	3.64							
-2.5	5.6	8440.6	9.21							
-2.0	4.0	4477.6	12.17							
-1.5	2.8	4167.6	14.92							

	Minor Lithic Counts		Abundance [volume %]	
	SMI	GCI	SMI	GCI
-1.0	2.0	3883.6	17.48	0	4	0	3
-0.5	1.4	4184.6	20.24	0	5	0	2
0.0	1.0	3688.7	22.68	0	5	0	2.4
0.5	0.710	6406.5	26.91	0	4	0	2
1.0	0.500	7174.4	31.64	0	1	0	0.5
1.5	0.355	7629.5	36.68	0	2	0	1.5
2.0	0.250	8942.3	42.58	0	1	0	1
2.5	0.180	7753.1	47.70	0	0	0	0
3.0	0.125	7868	52.90	0	0	0	0
3.5	0.088	7877.9	58.10				
4.0	0.063	8868.3	63.95				
4.5	0.045	21645.7	78.24				
5.0	0.032	17075	89.52				
6.0	0.017	10985	96.77				
7.0	0.008	4895	100.00				

Counts:

ϕ	Wp	Gp	Bp	Xtal	Lithic	Glass	NA	total counts
-5.0	0	0	0	0	0	0	0	0
-4.5	0	0	0	0	0	0	0	0
-4.0	1	0	0	0	0	0	0	0
-3.5	1	1	0	0	0	0	0	2
-3.0	10	1	0	0	2	0	0	4
-2.5	11	0	0	0	18	0	0	28
-2.0	33	0	0	0	27	0	0	38
-1.5	86	0	0	0	58	0	0	91
-1.0	187	0	0	0	135	4	0	225
-0.5	183	0	0	0	251	62	0	500
0.0	120	0	0	8	209	100	0	500
0.5	68	1	0	38	203	139	0	500
1.0	97	0	0	46	190	196	0	500
1.5	72	4	0	53	132	218	0	500
2.0	66	3	0	71	101	256	0	500
2.5	51	0	0	91	88	255	0	500
3.0	0	0	0	96	94	259	0	500
3.5	0	0	0	103	81	316	0	500
4.0	0	0	0	81	62	357	0	500
4.5	0	0	0	53	49	398	0	500
5.0	*	*	*	*	*	*	*1067*	1067
6.0	*	*	*	*	*	*	*998*	998
7.0	*	*	*	*	*	*	*699*	699

Bulk Weight Percentages:

Wp	Gp	Bp	Xtal	Lithic	Glass	NA
0	0	0	0	0	0	0
0	0	0	0	0	0	0
0	0	0	0	0	0	0
1.01	0.49	0	0	0	0	0
0.22	0.23	0	0	1.69	0	0
0.79	0	0	0	4.78	0	0
0.42	0	0	0	2.54	0	0
0.66	0	0	0	2.09	0	0
0.58	0	0	0	1.94	0.05	0
0.74	0	0	0	1.48	0.33	0
0.65	0	0	0.04	1.21	0.53	0
0.95	0	0	0.33	1.81	1.14	0
0.51	0	0	0.46	1.97	1.80	0
0.54	0	0	0.63	1.61	2.27	0
0.33	0	0	0.99	1.41	3.37	0
0.33	0	0	1.05	1.01	2.73	0
0.31	0	0	1.10	1.08	2.71	0
0	0	0	1.24	0.98	2.98	0
0	0	0	1.11	0.85	3.89	0
0	0	0	1.82	1.68	10.79	0
*	*	*	*	*	*	11.27
*	*	*	*	*	*	7.25
*	*	*	*	*	*	3.23
8.04	**0.72**	**0**	**8.77**	**28.13**	**32.59**	**21.75**

S1 at Locality 86 [CBV-S-17] [Total sample weight: 140834.4 mg]

Grain diameter		Weight Fractions		Granulometric Analysis						
ϕ	mm	weight [mg]	Cumulative weight %	ϕ_{05}	ϕ_{84}	ϕ_{16}	$\phi_{\sim}$	Md$_\phi$	σ_ϕ	Fz
-5.0	31.5	0	0	5.2	4.3	-2.8	-3.6	-4.0 1	2.81	22.58%
-4.5	22.4	0	0							
-4.0	16.0	6653.8	4.72							
-3.5	11.2	1734.9	5.96							
-3.0	8.0	13287.3	13.39							
-2.5	5.6	10806.1	23.06							
-2.0	4.0	8395.5	29.03							
-1.5	2.8	8199.6	34.85							
-1.0	2.0	14213.9	44.94							
-0.5	1.4	6077.1	49.26							
0.0	1.0	3270.5	51.58							
0.5	0.710	3311.4	53.93							
1.0	0.500	3483.1	56.40							
1.5	0.355	5512.4	60.32							
2.0	0.250	6181.8	64.71							
2.5	0.180	4813.1	68.12							
3.0	0.125	6354.3	72.63							
3.5	0.088	6736.9	77.42							
4.0	0.063	5675.6	81.45							
4.5	0.045	10357.2	88.80							
5.0	0.032	8170	94.6							
6.0	0.017	5255	98.34							
7.0	0.008	2340	100.00							

Minor Lithic Counts		Abundance [volume %]	
SML	GCL	SML	GCL
n.a.	n.a.	n.a.	n.a.

Counts:

ϕ	Wp	Gp	Bp	Xtal	Lithic	Glass	NA	total counts
-5.0	0	0	0	0	0	0	*0*	0
-4.5	0	0	0	0	0	0	*0*	0
-4.0	0	0	0	0	1	0	*0*	1
-3.5	0	0	0	0	1	0	*0*	1
-3.0	5	6	0	0	6	0	*0*	17
-2.5	3	13	0	0	21	0	*0*	37
-2.0	16	11	0	0	27	0	*0*	54
-1.5	64	0	0	0	111	0	*0*	175
-1.0	138	0	0	0	243	119	*0*	500
-0.5	87	0	0	3	255	155	*0*	500
0.0	68	0	0	4	238	190	*0*	500
0.5	53	0	0	1	162	284	*0*	500
1.0	54	0	0	16	259	171	*0*	500
1.5	50	0	0	24	241	185	*0*	500
2.0	52	0	0	57	261	130	*0*	500
2.5	54	0	0	134	172	140	*0*	500
3.0	49	0	0	120	168	163	*0*	500
3.5	22	0	0	112	194	172	*0*	500
4.0	11	0	0	103	108	278	*0*	500
4.5	0	0	0	51	64	385	*0*	500
5.0	*	*	*	*	*	*	*32438*	32438
6.0	*	*	*	*	*	*	*30091*	30091
7.0	*	*	*	*	*	*	*21284*	21284

Bulk Weight Percentages:

Wp	Gp	Bp	Xtal	Lithic	Glass	NA
0	0	0	0	0	0	0
0	0	0	0	0	0	0
0	0	0	0	4.72	0	0
0	0	0	0	1.23	0	0
1.40	1.71	0	0	6.32	0	0
0.26	1.20	0	0	6.20	0	0
0.99	0.84	0	0	4.13	0	0
1.41	0	0	0	4.41	0	0
1.61	0	0	0	6.08	2.40	0
0.51	0	0	0.03	2.56	1.22	0
0.21	0	0	0.02	1.21	0.88	0
0.20	0	0	0	0.82	1.33	0
0.21	0	0	0.08	1.38	0.80	0
0.20	0	0	0.21	2.12	1.39	0
0.17	0	0	0.55	2.54	1.12	0
0.17	0	0	1.00	1.28	0.97	0
0.26	0	0	1.17	1.64	1.45	0
0.18	0	0	1.17	2.93	1.41	0
0.08	0	0	0.94	0.99	2.02	0
0	0	0	0.92	1.12	5.34	0
*	*	*	*	*	*	5.80
*	*	*	*	*	*	3.73
*	*	*	*	*	*	1.66
7.86	**3.75**	**0.00**	**6.09**	**50.78**	**20.33**	**11.19**

S1 at Locality 88[CBV-S-22] [Total sample weight: 242544.8 mg]

Grain diameter		Weight Fractions		Granulometric Analysis						
ϕ	mm	weight [mg]	Cumulative weight %	$\phi_{0.5}$	$\phi_{0.1}$	Φ_1	ϕ_x	Md$_\phi$	σ_ϕ	F2
-5.0	31.5	0	0	6.5	5.8	1.0	-0.3	3.7		53.37%
-4.5	22.4	0	0							
-4.0	16.0	0	0							
-3.5	11.2	0	0							
-3.0	8.0	484.4	0.20							
-2.5	5.6	802.5	0.53							
-2.0	4.0	872.1	0.89							
-1.5	2.8	1702.4	1.59							

Minor Lithic Counts		Abundance [volume %]	
SMI.	GCI.	SMI.	GCI.
n.a.	n.a.	n.a.	n.a.

-1.0	2.0	2679.5	2.70
-0.5	1.4	4130.1	4.40
0.0	1.0	6061.9	6.90
0.5	0.710	10270.9	11.13
1.0	0.500	12579.5	16.32
1.5	0.355	13745.0	21.99
2.0	0.250	14224.1	27.85
2.5	0.180	13570.2	33.45
3.0	0.125	16542.8	40.27
3.5	0.088	15436.9	46.63
4.0	0.063	17230.9	53.74
4.5	0.045	13745.2	59.40
5.0	0.032	39525	75.70
6.0	0.017	26555	90.77
7.0	0.008	22390	100.00

Counts:

ϕ	Wp	Gp	Bp	Xtal	Lithic	Glass	NA	total counts
-5.0	0	0	0	0	0	0	*0*	0
-4.5	0	0	0	0	0	0	*0*	0
-4.0	0	0	0	0	0	0	*0*	0
-3.5	0	0	0	0	0	0	*0*	0
-3.0	1	0	2	0	0	0	*0*	3
-2.5	0	0	0	0	1	0	*0*	1
-2.0	14	0	0	0	25	0	*0*	43
-1.5	36	3	0	0	69	0	*0*	108
-1.0	95	10	0	0	233	0	*0*	338
-0.5	138	17	0	0	451	0	*0*	606
0.0	69	21	0	11	649	0	*0*	750
0.5	52	17	0	54	627	0	*0*	750
1.0	63	14	0	196	465	12	*0*	750
1.5	39	4	0	302	338	67	*0*	750
2.0	23	3	0	384	222	118	*0*	750
2.5	14	0	0	363	198	175	*0*	750
3.0	0	0	0	473	133	143	*0*	749
3.5	0	0	0	260	147	187	*0*	594
4.0	0	0	0	168	115	240	*0*	523
4.5	0	0	0	128	44	328	*0*	500
5.0	*	*	*	*	*	*	*25063*	25063
6.0	*	*	*	*	*	*	*33727*	33727
7.0	*	*	*	*	*	*	*32429*	32429

Bulk Weight Percentages:

ϕ	Wp	Gp	Bp	Xtal	Lithic	Glass	NA
-5.0	0	0	0	0	0	0	0
-4.5	0	0	0	0	0	0	0
-4.0	0	0	0	0	0	0	0
-3.5	0	0	0	0	0	0	0
-3.0	0.02	0	0.13	0	0.05	0	0
-2.5	0.33	0	0	0	0	0	0
-2.0	0.07	0	0.04	0	0.26	0	0
-1.5	0.10	0.01	0	0	0.59	0	0
-1.0	0.17	0.03	0	0	0.91	0	0
-0.5	0.25	0.03	0	0	1.42	0	0
0.0	0.15	0.05	0	0.04	2.26	0	0
0.5	0.23	0.12	0	0.30	3.59	0	0
1.0	0.33	0.08	0	1.35	3.34	0.08	0
1.5	0.14	0.04	0	2.34	2.69	0.46	0
2.0	0.06	0.01	0	3.13	1.81	0.85	0
2.5	0.05	0	0	2.78	1.52	1.25	0
3.0	0	0	0	4.38	1.23	1.21	0
3.5	0	0	0	2.99	1.69	1.68	0
4.0	0	0	0	2.52	1.73	2.86	0
4.5	0	0	0	1.68	0.56	3.41	0
5.0	*	*	*	*	*	*	16.30
6.0	*	*	*	*	*	*	15.07
7.0	*	*	*	*	*	*	9.23
	1.90	**0.37**	**0.17**	**21.51**	**23.65**	**11.80**	**40.60**

P2 at Locality 1 [Lithic-rich base] [Total sample weight: 1039900 mg]

Grain diameter		Weight Fractions		Granulometric Analysis						
ϕ	mm	weight [mg]	Cumulative weight %	ϕ_{05}	ϕ_{84}	ϕ_{16}	ϕ_z	Md_ϕ	σ_ϕ	F2
-5.0	31.5	0	0	-0.4	-1.2	-3.7	-4.4	-2.6	1.22	0.00%
-4.5	22.4	33000	3.17							
-4.0	16.0	105000	13.27							
-3.5	11.2	132000	25.96							
-3.0	8.0	165000	41.83							
-2.5	5.6	150000	56.26							
-2.0	4.0	145900	70.29							
-1.5	2.8	99553	79.86							
-1.0	2.0	87027.8	88.23							
-0.5	1.4	65198.0	94.50							
0.0	1.0	34072.3	97.77							
0.5	0.710	13423.5	99.06							
1.0	0.500	4081.2	99.46							
1.5	0.355	1390.9	99.59							
2.0	0.250	1133.9	99.70							
2.5	0.180	3120.1	100.00							
3.0	0.125	0								
3.5	0.088	0								
4.0	0.063	0								
4.5	0.045	0								
5.0	0.032	0								
6.0	0.017	0								
7.0	0.008	0								

Minor Lithic Counts		Abundance [volume %]	
SML	GCL	SML	GCL
n.a.	n.a.	n.a.	n.a.

Counts:

ϕ	Wp	Gp	Bp	Xtal	Lithic	Glass	NA	total counts
-5.0	0	0	n.a.	0	0	0	0	0
-4.5	9	0	n.a.	0	0	0	0	9
-4.0	29	0	n.a.	0	4	0	0	33
-3.5	38	0	n.a.	0	20	0	0	58
-3.0	243	0	n.a.	0	71	0	0	314
-2.5	691	34	n.a.	0	212	0	0	937
-2.0	1071	201	n.a.	0	691	0	0	1963
-1.5	122	16	9	0	353	0	0	500
-1.0	195	14	18	0	273	0	0	500
-0.5	258	11	29	0	202	0	0	500
0.0	165	6	16	4	309	0	0	500
0.5	70	1	4	27	398	0	0	500
1.0	81	5	2	26	383	3	0	500
1.5	111	5	2	26	351	5	0	500
2.0	157	3	0	27	304	9	0	500
2.5	0	0	0	0	0	0	0	0
3.0	0	0	0	0	0	0	0	0
3.5	0	0	0	0	0	0	0	0
4.0	0	0	0	0	0	0	0	0
4.5	0	0	0	0	0	0	0	0
5.0	0	0	0	0	0	0	0	0
6.0	0	0	0	0	0	0	0	0
7.0	0	0	0	0	0	0	0	0

Bulk Weight Percentages:

Wp	Gp	Bp	Xtal	Lithic	Glass	NA
0	0	n.a.	0	0	0	0
3.17	0	n.a.	0	0	0	0
7.93	0	n.a.	0	2.17	0	0
6.53	0	n.a.	0	6.17	0	0
8.51	0	n.a.	0	7.64	0	0
6.88	0.45	n.a.	0	7.09	0	0
4.91	1.31	n.a.	0	7.81	0	0
1.47	0.26	0.18	0	7.66	0	0
1.98	0.21	0.26	0	5.92	0	0
2.50	0.11	0.09	0	3.37	0	0
0.77	0.03	0.01	0.03	2.36	0	0
0.24	0.0+	0.0+	0.06	0.98	0	0
0.05	0.0+	0.0+	0.02	0.32	0.0+	0
0.02	0.0+	0.0+	0.01	0.11	0.0+	0
0.01	0.0+	0	0.01	0.08	0.0+	0
0	0	0	0	0	0	0.30
0	0	0	0	0	0	0
0	0	0	0	0	0	0
0	0	0	0	0	0	0
0	0	0	0	0	0	0
0	0	0	0	0	0	0
0	0	0	0	0	0	0
0	0	0	0	0	0	0
44.97	**2.37**	**0.54**	**0.13**	**51.68**	**0.01**	**0.30**

P2 at Locality 18 [0-26 cm from base (Lithic-rich base)] [Total sample weight: 2569000 mg]

Grain diameter		Weight fractions		Granulometric Analysis						
ϕ	mm	weight [mg]	Cumulative weight %	ϕ_{05}	ϕ_{84}	ϕ_{16}	$\phi_{\bar{x}}$	Md_{ϕ}	σ_{ϕ}	F2
-5.0	31.5	92000	3.58	-1.6	-1.8	-4.4	-4.9	-3.4	1.15	0.00%
-4.5	22.4	312000	15.73							
-4.0	16.0	405000	31.49							
-3.5	11.2	406000	47.29							
-3.0	8.0	380000	62.09							
-2.5	5.6	290000	73.37							
-2.0	4.0	200000	81.16							
-1.5	2.8	465349.4	99.27							

				Minor Lithic Counts		Abundance [volume %]	
				SML	GCL	SML	GCL
-1.0	2.0	3672.4	99.42	1	0	10.0	0
-0.5	1.4	2765.3	99.52	0	0	0	0
0.0	1.0	1702.2	99.59	3	8	10.3	27.6
0.5	0.710	1286.5	99.64	4	16	6.3	25.4
1.0	0.500	1087.7	99.68	2	31	1.2	18.3
1.5	0.355	949.7	99.72	4	0	1.2	0
2.0	0.250	1025.3	99.76	13	0	3.0	0
2.5	0.180	6160	100.00	0	0	0	0
3.0	0.125	0		0	0	0	0
3.5	0.088	0					
4.0	0.063	0					
4.5	0.045	0					
5.0	0.032	0					
6.0	0.017	0					
7.0	0.008	0					

Counts:

ϕ	Wp	Gp	Bp	Xtal	Lithic	Glass	NA	total counts
-5.0	13	5	n.a.	0	0	0	0	18
-4.5	25	13	n.a.	0	8	0	0	46
-4.0	53	12	n.a.	0	39	0	0	104
-3.5	65	23	n.a.	0	86	0	0	174
-3.0	307	51	n.a.	0	232	0	0	590
-2.5	734	95	n.a.	0	526	0	0	1355
-2.0	349	25	n.a.	0	342	0	0	716
-1.5	275	17	19	0	236	0	0	547
-1.0	9	2	0	0	10	0	0	21
-0.5	11	5	1	0	14	0	0	31
0.0	14	1	0	9	29	0	0	53
0.5	18	2	0	28	63	0	0	111
1.0	39	2	0	34	169	3	0	247
1.5	32	1	0	67	341	8	0	449
2.0	155	2	0	116	437	40	0	750
2.5	0	0	0	0	0	0	*	*
3.0	0	0		0	0	0	0	0
3.5	0	0		0	0	0	0	0
4.0	0	0		0	0	0	0	0
4.5	0	0		0	0	0	0	0
5.0	0	0		0	0	0	0	0
6.0	0	0		0	0	0	0	0
7.0	0	0		0	0	0	0	0

Bulk Weight %'s:

ϕ	Wp	Gp	Bp	Xtal	Lithic	Glass	NA
-5.0	2.58	1.00	n.a.	0	0	0	0
-4.5	3.87	2.10	n.a.	0	6.17	0	0
-4.0	5.85	1.37	n.a.	0	8.54	0	0
-3.5	4.46	0.74	n.a.	0	10.60	0	0
-3.0	4.13	0.72	n.a.	0	9.94	0	0
-2.5	3.15	0.54	n.a.	0	7.59	0	0
-2.0	2.21	0.22	n.a.	0	5.35	0	0
-1.5	6.59	0.56	1.93	0	10.20	0	0
-1.0	0.40	0.01	0.26	0	0.09	0	0
-0.5	0.30	0.01	0.09	0	0.06	0	0
0.0	0.10	0.0+	0.01	0.01	0.04	0	0
0.5	0.0+	0.0+	0.0+	0.01	0.03	0	0
1.0	0.01	0.0+	0.0+	0.01	0.03	0.0+	0
1.5	0.0+	0.0+	0.0+	0.01	0.03	0.0+	0
2.0	0.0+	0.0+	0	0.01	0.03	0.0+	0
2.5	0	0	0	0	0	0	0.24
3.0	0	0	0	0	0	0	0
3.5	0	0	0	0	0	0	0
4.0	0	0	0	0	0	0	0
4.5	0	0	0	0	0	0	0
5.0	0	0	0	0	0	0	0
6.0	0	0	0	0	0	0	0
7.0	0	0	0	0	0	0	0
	31.43	**7.28**	**2.47**	**0.05**	**58.70**	**0.01**	**0.24**

P2 at Locality 18 [26-66 cm from base] [Total sample weight: 4285000 mg]

Grain diameter		Weight Fractions:		Granulometric Analysis:						
ϕ	mm	weight [mg]	Cumulative weight %	ϕ_{05}	ϕ_{84}	ϕ_{10}	ϕ_{5}	Md_{ϕ}	σ_{ϕ}	F2
-5.0	31.5	2117000	49.40	-0.8	-2.6	-5.0	-5.0	-4.9	1.51	0.00%
-4.5	22.4	514000	61.40							
-4.0	16.0	262000	67.51							
-3.5	11.2	258000	73.54							
-3.0	8.0	238000	79.09							
-2.5	5.6	238000	84.22							
-2.0	4.0	220000	88.75							
-1.5	2.8	194000	92.30							
-1.0	2.0	151909.8	94.02							
-0.5	1.4	73872.7	96.19							
0.0	1.0	93012.4	97.59							
0.5	0.710	60119.8	99.00							
1.0	0.500	60448.3	99.60							
1.5	0.355	11723.4	99.87							
2.0	0.250	3090.5	99.95							
2.5	0.180	2290	100.00							
3.0	0.125	0								
3.5	0.088	0								
4.0	0.063	0								
4.5	0.045	0								
5.0	0.032	0								
6.0	0.017	0								
7.0	0.008	0								

Minor Lithic Counts:		Abundance [volume %]	
SML	GCL	SML	GCL
2	0	1.6	0
1	0	1.8	0
3	20	1.3	8.7
2	75	0.6	22.6
8	31	2.4	9.5
15	0	4.1	0
12	0	3.8	0
0	0	0	0
0	0	0	0

Counts:

ϕ	Wp	Gp	Bp	Xtal	Lithic	Glass	NA	total counts
-5.0	284	26	n.a.	0	8	0	0	318
-4.5	72	25	n.a.	0	7	0	0	104
-4.0	57	14	n.a.	0	10	0	0	81
-3.5	86	14	n.a.	0	31	0	0	131
-3.0	402	31	n.a.	0	80	0	0	513
-2.5	1159	69	n.a.	0	220	0	0	1448
-2.0	854	36	n.a.	0	164	0	0	1054
-1.5	603	18	15	0	114	0	0	750
-1.0	590	17	16	2	125	0	0	750
-0.5	646	26	19	3	56	0	0	750
0.0	482	20	10	8	230	0	0	750
0.5	366	21	10	21	332	0	0	750
1.0	330	21	0	71	328	0	0	750
1.5	250	4	1	4	368	9	0	750
2.0	118	8	0	8	314	12	0	750
2.5	0	0	0	0	0	0	*	*
3.0	0	0	0	0	0	0	0	0
3.5	0	0	0	0	0	0	0	0
4.0	0	0	0	0	0	0	0	0
4.5	0	0	0	0	0	0	0	0
5.0	0	0	0	0	0	0	0	0
6.0	0	0	0	0	0	0	0	0
7.0	0	0	0	0	0	0	0	0

Bulk Weight %'s:

Wp	Gp	Bp	Xtal	Lithic	Glass	NA
33.65	3.05	n.a.	0	12.67	0	0
6.50	2.35	n.a.	0	3.15	0	0
3.82	0.97	n.a.	0	1.33	0	0
3.49	0.27	n.a.	0	2.26	0	0
3.24	0.26	n.a.	0	2.05	0	0
2.99	0.24	n.a.	0	1.91	0	0
2.95	0.18	n.a.	0	1.40	0	0
2.49	0.10	0.10	0	0.85	0	0
1.12	0.05	0.04	0.01	0.51	0	0
1.77	0.07	0.05	0.01	0.26	0	0
0.75	0.04	0.02	0.02	0.58	0	0
0.59	0.06	0.01	0.04	0.71	0	0
0.22	0.02	0.00	0.06	0.30	0	0
0.05	0.0+	0.0+	0.05	0.16	0.0+	0
0.0+	0.0+	0	0.03	0.03	0.0+	0
0	0	0	0	0	0	0.05
0	0	0	0	0	0	0
0	0	0	0	0	0	0
0	0	0	0	0	0	0
0	0	0	0	0	0	0
0	0	0	0	0	0	0
0	0	0	0	0	0	0
0	0	0	0	0	0	0
63.63	**7.72**	**0.22**	**0.20**	**28.17**	**0.01**	**0.05**

P2 at Locality 18 [83-111 cm from base] [Total sample weight 1271990 mg]

Grain diameter		Weight Fractions		Granulometric Analysis						
ϕ	mm	weight [mg]	Cumulative weight %	ϕ_{05}	ϕ_{25}	ϕ_{10}	ϕ_{50}	Md_ϕ	σ_ϕ	F2
-5.0	31.5	0	0	0.4	-0.6	-3.4	-3.9	-2.4	1.35	0.00%
-4.5	22.4	23000	1.81							
-4.0	16.0	52000	5.90							
-3.5	11.2	100000	13.76							
-3.0	8.0	210000	30.27							
-2.5	5.6	184000	44.73							
-2.0	4.0	175000	58.49							
-1.5	2.8	125623.8	68.37							
-1.0	2.0	116017.1	77.49							
-0.5	1.4	105376.0	85.77							
0.0	1.0	81748.5	92.20							
0.5	0.710	54181.4	96.46							
1.0	0.500	28015.4	98.66							
1.5	0.355	9188.7	99.38							
2.0	0.250	2148.5	99.55							
2.5	0.180	5690	100.00							
3.0	0.125	0								
3.5	0.088	0								
4.0	0.063	0								
4.5	0.045	0								
5.0	0.032	0								
6.0	0.017	0								
7.0	0.008	0								

Minor Lithic Counts		Abundance [volume %]	
SML	GCL	SML	GCL
0	0	0	0
3	0	1.2	0
4	0	1.2	0
4	0	1.0	0
6	0	1.4	0
8	0	1.8	0
9	0	1.9	0
0	0	0	0
0	0	0	0

Counts:

ϕ	Wp	Gp	Bp	Xtal	Lithic	Glass	NA	total counts
-5.0	0	0	n.a.	0	0	0	0	0
-4.5	2	3	n.a.	0	0	0	0	5
-4.0	5	12	n.a.	0	1	0	0	18
-3.5	13	46	n.a.	0	13	0	0	72
-3.0	138	219	n.a.	0	74	0	0	431
-2.5	376	476	n.a.	0	194	0	0	1046
-2.0	824	961	n.a.	0	613	0	0	2398
-1.5	333	2	199	0	216	0	0	750
-1.0	410	3	178	0	159	0	0	750
-0.5	368	10	114	0	258	0	0	750
0.0	330	17	60	0	343	0	0	750
0.5	281	18	37	21	391	2	0	750
1.0	222	19	21	52	431	5	0	750
1.5	162	14	16	91	449	18	0	750
2.0	121	9	12	118	467	23	0	750
2.5	0	0	0	0	0	0	*	*
3.0	0	0	0	0	0	0	0	0
3.5	0	0	0	0	0	0	0	0
4.0	0	0	0	0	0	0	0	0
4.5	0	0	0	0	0	0	0	0
5.0	0	0	0	0	0	0	0	0
6.0	0	0	0	0	0	0	0	0
7.0	0	0	0	0	0	0	0	0

Bulk Weight Percentages:

Wp	Gp	Bp	Xtal	Lithic	Glass	NA
0	0	n.a.	0	0	0	0
0.71	1.10	n.a.	0	0	0	0
1.05	2.62	n.a.	0	0.42	0	0
1.76	2.94	n.a.	0	3.16	0	0
3.77	6.30	n.a.	0	6.44	0	0
3.28	5.50	n.a.	0	5.69	0	0
3.07	5.07	n.a.	0	5.62	0	0
3.11	0.03	3.11	0	3.63	0	0
3.69	0.04	2.32	0	3.07	0	0
3.25	0.09	1.01	0	3.91	0	0
2.16	0.13	0.45	0	3.69	0	0
1.25	0.15	0.14	0.13	2.57	0.01	0
0.53	0.05	0.05	0.16	1.40	0.01	0
0.08	0.02	0.02	0.10	0.49	0.02	0
0.01	0.0+	0.0+	0.03	0.12	0.02	0
0	0	0	0	0	0	0.45
0	0	0	0	0	0	0
0	0	0	0	0	0	0
0	0	0	0	0	0	0
0	0	0	0	0	0	0
0	0	0	0	0	0	0
0	0	0	0	0	0	0
0	0	0	0	0	0	0
0	0	0	0	0	0	0
27.72	**24.04**	**7.10**	**0.42**	**40.21**	**0.06**	**0.45**

P2 at Locality 18 [111-118 cm from base (top level)] [Total sample weight 916932 mg]

Grain diameter		Weight Fractions		Granulometric Analysis						
ϕ	mm	weight [mg]	Cumulative weight %	ϕ_{05}	ϕ_{84}	ϕ_{16}	ϕ_{50}	Md_ϕ	σ_ϕ	F2
-5.0	31.5	29000	3.16	-0.1	-1.3	-4.2	-4.8	-2.9	1.44	0.00%
-4.5	22.4	41000	7.63							
-4.0	16.0	92000	17.67							
-3.5	11.2	120000	30.75							
-3.0	8.0	150000	47.11							
-2.5	5.6	128000	61.07							
-2.0	4.0	119000	74.05							
-1.5	2.8	58691.7	80.45							
-1.0	2.0	72632.8	88.37							
-0.5	1.4	38587.4	92.58							
0.0	1.0	31153.6	95.98							
0.5	0.710	14672.4	97.58							
1.0	0.500	11086.8	98.79							
1.5	0.355	3554.4	99.18							
2.0	0.250	59.62.4	99.83							
2.5	0.180	1590	100.00							
3.0	0.125									
3.5	0.088	0								
4.0	0.063	0								
4.5	0.045	0								
5.0	0.032	0								
6.0	0.017	0								
7.0	0.008	0								

Minor Lithic Counts		Abundance [volume %]	
SML	GCL	SML	GCL
0	0	0	0
0	0	0	0
2	23	0.5	5.7
2	53	0.4	10.5
4	65	0.7	11.8
0	0	0	0
0	0	0	0
0	0	0	0
0	0	0	0

Counts:

ϕ	Wp	Gp	Bp	Xtal	Lithic	Glass	NA	total counts
-5.0	6	0	n.a.	0	0	0	0	6
-4.5	3	8	n.a.	0	0	0	0	11
-4.0	4	13	n.a.	0	6	0	0	23
-3.5	11	48	n.a.	0	19	0	0	78
-3.0	72	135	n.a.	0	69	0	0	276
-2.5	192	286	n.a.	0	176	0	0	654
-2.0	252	665	n.a.	0	526	0	0	1443
-1.5	220	39	116	0	375	0	0	750
-1.0	222	17	131	0	380	0	0	750
-0.5	320	72	46	0	312	0	0	750
0.0	244	61	31	9	401	4	0	750
0.5	156	45	23	13	503	10	0	750
1.0	109	32	19	28	551	11	0	750
1.5	50	27	15	52	592	14	0	750
2.0	29	18	10	109	562	22	0	750
2.5	0	0	0	0	0	0	*	*
3.0	0	0	0	0	0	0	0	0
3.5	0	0	0	0	0	0	0	0
4.0	0	0	0	0	0	0	0	0
4.5	0	0	0	0	0	0	0	0
5.0	0	0	0	0	0	0	0	0
6.0	0	0	0	0	0	0	0	0
7.0	0	0	0	0	0	0	0	0

Bulk Weight Percentages:

Wp	Gp	Bp	Xtal	Lithic	Glass	NA
3.16	0	n.a.	0	0	0	0
1.18	3.29	n.a.	0	0	0	0
1.37	4.60	n.a.	0	4.07	0	0
2.12	4.37	n.a.	0	6.59	0	0
2.72	5.36	n.a.	0	8.28	0	0
2.31	4.55	n.a.	0	7.10	0	0
1.31	4.91	n.a.	0	6.76	0	0
1.23	0.30	1.09	0	3.78	0	0
1.41	0.16	1.20	0	5.16	0	0
1.38	0.32	0.20	0	2.31	0	0
0.81	0.23	0.12	0.05	2.18	0.02	0
0.31	0.12	0.03	0.03	1.09	0.02	0
0.14	0.04	0.03	0.05	0.94	0.02	0
0.01	0.02	0.01	0.03	0.31	0.01	0
0.01	0.01	0.0+	0.10	0.51	0.02	0
0	0	0	0	0	0	0.17
0	0	0	0	0	0	0
0	0	0	0	0	0	0
0	0	0	0	0	0	0
0	0	0	0	0	0	0
0	0	0	0	0	0	0
0	0	0	0	0	0	0
0	0	0	0	0	0	0
19.56	**28.28**	**2.68**	**0.26**	**48.96**	**0.09**	**0.17**

P2 at Locality 29 [Lithic-rich base] [Total sample weight: 332660 mg]

Grain diameter		Weight Fractions:		Granulometric Analysis						
ϕ	mm	weight [mg]	Cumulative weight %	ϕ_{95}	ϕ_{84}	ϕ_{16}	ϕ_{5}	Md_{ϕ}	σ_{ϕ}	F:
-5.0	31.5	0	0	0.4	-0.1	-2.6	-3.8	-1.2	1.27	0.00%
-4.5	22.4	0	0							
-4.0	16.0	11000	3.31							
-3.5	11.2	13000	7.21							
-3.0	8.0	15000	11.72							
-2.5	5.6	18200	17.19							
-2.0	4.0	38460	28.76							
-1.5	2.8	40500	40.93							
-1.0	2.0	45071.3	54.48							
-0.5	1.4	55990.5	71.31							
0.0	1.0	42589.9	84.11							
0.5	0.710	38310.8	95.63							
1.0	0.500	9132.9	98.38							
1.5	0.355	2557.3	99.14							
2.0	0.250	912.1	99.42							
2.5	0.180	1935	100.00							
3.0	0.125	0								
3.5	0.088	0								
4.0	0.063	0								
4.5	0.045	0								
5.0	0.032	0								
6.0	0.017	0								
7.0	0.008	0								

Minor Lithic Counts:		Abundance [volume %]	
SML	GCL	SML	GCL
n.a.	n.a.	n.a.	n.a.

Counts:

ϕ	Wp	Gp	Bp	Xtal	Lithic	Glass	NA	total counts
-5.0	0	0	n.a.	0	0	0	0	0
-4.5	0	0	n.a.	0	0	0	0	0
-4.0	4	0	n.a.	0	0	0	0	4
-3.5	6	0	n.a.	0	0	0	0	6
-3.0	39	2	n.a.	0	2	0	0	43
-2.5	146	3	n.a.	0	4	0	0	153
-2.0	568	41	n.a.	0	74	0	0	683
-1.5	347	37	3	0	113	0	0	500
-1.0	353	36	6	0	105	0	0	500
-0.5	302	34	11	1	152	0	0	500
0.0	238	24	8	6	224	0	0	500
0.5	128	15	3	30	324	0	0	500
1.0	131	12	0	47	304	6	0	500
1.5	75	9	0	83	319	14	0	500
2.0	35	0	0	108	323	34	0	500
2.5	0	0	0	0	0	0	*	*
3.0	0	0	0	0	0	0	0	0
3.5	0	0	0	0	0	0	0	0
4.0	0	0	0	0	0	0	0	0
4.5	0	0	0	0	0	0	0	0
5.0	0	0	0	0	0	0	0	0
6.0	0	0	0	0	0	0	0	0
7.0	0		0	0	0	0	0	0

Bulk Weight Percentages:

Wp	Gp	Bp	Xtal	Lithic	Glass	NA
0	0	n.a.	0	0	0	0
0	0	n.a.	0	0	0	0
3.31	0	n.a.	0	0	0	0
3.91	0	n.a.	0	0	0	0
3.70	0.20	n.a.	0	0.60	0	0
4.89	0.13	n.a.	0	0.45	0	0
8.12	0.83	n.a.	0	2.61	0	0
6.97	1.02	0.10	0	4.09	0	0
7.49	1.10	0.18	0	4.77	0	0
8.31	0.97	0.31	0.05	7.19	0	0
4.67	0.54	0.18	0.19	7.23	0	0
3.10	0.42	0.04	0.65	7.30	0	0
0.57	0.06	0	0.27	1.81	0.03	0
0.06	0.02	0	0.14	0.54	0.02	0
0.01	0	0	0.06	0.19	0.02	0
0	0	0	0	0	0	0.58
0	0	0	0	0	0	0
0	0	0	0	0	0	0
0	0	0	0	0	0	0
0	0	0	0	0	0	0
0	0	0	0	0	0	0
0	0	0	0	0	0	0
0	0	0	0	0	0	0
0	0	0	0	0	0	0
55.11	**5.29**	**0.81**	**1.36**	**36.78**	**0.07**	**0.58**

P2 at Locality 41 [Lithic-rich base] [Total sample weight: 536870 mg]

Grain diameter		Weight Fractions:		Granulometric Analysis						
ϕ	mm	weight [mg]	Cumulative weight %	ϕ_{05}	ϕ_{84}	ϕ_{16}	ϕ_5	Md_ϕ	σ_ϕ	F2
-5.0	31.5	17000	3.17	-0.1	-0.9	-3.4	-3.9	-2.1	1.23	0.00%
-4.5	22.4	0	3.17							
-4.0	16.0	15000	5.96							
-3.5	11.2	45000	14.34							
-3.0	8.0	55000	24.59							
-2.5	5.6	68400	37.33							
-2.0	4.0	71290	50.61							
-1.5	2.8	100568.3	69.34							
-1.0	2.0	69537.7	82.29							
-0.5	1.4	45485.4	90.76							
0.0	1.0	23527.8	95.15							
0.5	0.710	13391.4	97.64							
1.0	0.500	6809.4	98.91							
1.5	0.355	2638.8	99.40							
2.0	0.250	715.0	99.53							
2.5	0.180	2505	100.00							
3.0	0.125	0								
3.5	0.088	0								
4.0	0.063	0								
4.5	0.045	0								
5.0	0.032	0								
6.0	0.017	0								
7.0	0.008	0								

Minor Lithic Counts		Abundance [volume %]	
SML	GCL	SML	GCL
n.a.	n.a.	n.a.	n.a.

Counts:

ϕ	Wp	Gp	Bp	Xtal	Lithic	Glass	NA	total counts
-5.0	3	0	n.a.	0	0	0	0	3
-4.5	0	0	n.a.	0	0	0	0	0
-4.0	5	0	n.a.	0	0	0	0	5
-3.5	21	2	n.a.	0	2	0	0	25
-3.0	130	6	n.a.	0	7	0	0	143
-2.5	508	18	n.a.	0	26	0	0	552
-2.0	926	36	n.a.	0	211	0	0	1173
-1.5	285	31	27	0	157	0	0	500
-1.0	262	42	23	0	173	0	0	500
-0.5	228	54	19	0	199	0	0	500
0.0	120	12	7	13	348	0	0	500
0.5	139	9	5	21	326	0	0	500
1.0	163	6	0	32	299	0	0	500
1.5	156	5	0	56	283	0	0	500
2.0	130	0	0	87	277	0	0	500
2.5	0	0	0	0	0	0	*	*
3.0	0	0	0	0	0	0	0	0
3.5	0	0	0	0	0	0	0	0
4.0	0	0	0	0	0	0	0	0
4.5	0	0	0	0	0	0	0	0
5.0	0	0	0	0	0	0	0	0
6.0	0	0	0	0	0	0	0	0
7.0	0	0	0	0	0	0	0	0

Bulk Weight Percentages:

Wp	Gp	Bp	Xtal	Lithic	Glass	NA
3.17	0	n.a.	0	0	0	0
0	0	n.a.	0	0	0	0
2.79	0	n.a.	0	0	0	0
6.89	0.31	n.a.	0	1.18	0	0
8.40	0.41	n.a.	0	1.44	0	0
10.45	0.49	n.a.	0	1.80	0	0
8.21	0.45	n.a.	0	4.61	0	0
8.14	1.21	1.29	0	8.09	0	0
4.67	1.08	0.59	0	6.61	0	0
2.99	0.73	0.26	0	4.49	0	0
0.72	0.08	0.05	0.12	3.41	0	0
0.40	0.07	0.03	0.12	1.89	0	0
0.33	0.01	0	0.09	0.84	0	0
0.08	0.01	0	0.06	0.34	0	0
0.01	0	0	0.03	0.09	0	0
0	0	0	0	0	0	0.47
0	0	0	0	0	0	0
0	0	0	0	0	0	0
0	0	0	0	0	0	0
0	0	0	0	0	0	0
0	0	0	0	0	0	0
0	0	0	0	0	0	0
0	0	0	0	0	0	0
0	0	0	0	0	0	0
57.25	**4.85**	**2.22**	**0.42**	**34.79**	**0**	**0.47**

P2 at Locality 50 [Lithic-rich base] [Total sample weight: 833064 mg]

Grain diameter		Weight Fractions		Granulometric Analysis						
ϕ	mm	weight [mg]	Cumulative weight %	ϕ_{16}	ϕ_{84}	ϕ_{10}	ϕ_{90}	Md_ϕ	σ_ϕ	F2
-5.0	31.5	0	0	-1.4	-2.3	-4.6	-4.8	-3.7	1.10	0.00%
-4.5	22.4	230000	27.61							
-4.0	16.0	127000	42.85							
-3.5	11.2	118000	57.02							
-3.0	8.0	110000	70.22							
-2.5	5.6	92000	81.27							
-2.0	4.0	73710.0	90.11							
-1.5	2.8	31050.6	93.84							
-1.0	2.0	21108.6	96.38							
-0.5	1.4	14276.7	98.09							
0.0	1.0	5982.6	98.81							
0.5	0.710	3082.6	99.18							
1.0	0.500	932.6	99.29							
1.5	0.355	731.6	99.38							
2.0	0.250	690.2	99.46							
2.5	0.180	4500	100.00							
3.0	0.125	0								
3.5	0.088	0								
4.0	0.063	0								
4.5	0.045	0								
5.0	0.032	0								
6.0	0.017	0								
7.0	0.008	0								

Minor Lithic Counts:		Abundance [volume %]	
SML	GCL	SML	GCL
n.a.	n.a.	n.a.	n.a.

Counts:

ϕ	Wp	Gp	Bp	Xtal	Lithic	Glass	NA	total counts
-5.0	0	0	n.a.	0	0	0	0	0
-4.5	5	2	n.a.	0	10	0	0	17
-4.0	9	2	n.a.	0	17	0	0	28
-3.5	18	2	n.a.	0	27	0	0	47
-3.0	86	5	n.a.	0	71	0	0	162
-2.5	223	9	n.a.	0	177	0	0	409
-2.0	398	79	n.a.	0	419	0	0	896
-1.5	212	20	16	0	252	0	0	500
-1.0	196	22	14	0	268	0	0	500
-0.5	196	21	11	0	272	0	0	500
0.0	123	18	0	5	354	0	0	500
0.5	124	6	0	21	349	0	0	500
1.0	120	3	0	31	346	0	0	500
1.5	109	3	0	54	334	0	0	500
2.0	98	4	0	77	317	4	0	500
2.5	0	0	0	0	0	0	*	*
3.0	0	0	0	0	0	0	0	0
3.5	0	0	0	0	0	0	0	0
4.0	0	0	0	0	0	0	0	0
4.5	0	0	0	0	0	0	0	0
5.0	0	0	0	0	0	0	0	0
6.0	0	0	0	0	0	0	0	0
7.0	0	0	0	0	0	0	0	0

Bulk Weight Percentages:

Wp	Gp	Bp	Xtal	Lithic	Glass	NA
0	0	n.a.	0	0	0	0
2.43	1.01	n.a.	0	24.17	0	0
3.06	0.70	n.a.	0	11.48	0	0
3.78	0.20	n.a.	0	10.19	0	0
3.58	0.22	n.a.	0	9.41	0	0
2.97	0.16	n.a.	0	7.92	0	0
2.28	0.64	n.a.	0	5.92	0	0
1.10	0.14	0.14	0	2.35	0	0
0.60	0.10	0.06	0	1.77	0	0
0.48	0.05	0.02	0	1.15	0	0
0.12	0.02	0	0.01	0.57	0	0
0.06	0.01	0	0.02	0.29	0	0
0.02	0	0	0.01	0.08	0	0
0.01	0	0	0.01	0.07	0	0
0.01	0	0	0.01	0.06	0.0+	0
0	0	0	0	0	0	0.54
0	0	0	0	0	0	0
0	0	0	0	0	0	0
0	0	0	0	0	0	0
0	0	0	0	0	0	0
0	0	0	0	0	0	0
0	0	0	0	0	0	0
0	0	0	0	0	0	0
0	0	0	0	0	0	0
20.50	**3.25**	**0.22**	**0.06**	**75.43**	**0.0+**	**0.54**

P2 at Locality 70 [Lithic-rich base] [Total sample weight: 277000 mg]

Grain diameter		Weight Fractions:		Granulometric Analysis						
ϕ	mm	weight [mg]	Cumulative weight %	ϕ_{05}	ϕ_{84}	ϕ_{16}	$\phi_{\bar{x}}$	Md_{ϕ}	σ_{ϕ}	F2
-5.0	31.5	0	0	0.9	0.4	-1.9	-2.6	-0.8	1.09	0.00%
-4.5	22.4	0	0							
-4.0	16.0	0	0							
-3.5	11.2	0	0							
-3.0	8.0	0	0							
-2.5	5.6	16000	5.78							
-2.0	4.0	18000	12.27							
-1.5	2.8	61550.7	34.49							
-1.0	2.0	24958.0	43.50							
-0.5	1.4	44582.1	59.60							
0.0	1.0	40489.0	74.22							
0.5	0.710	44693.5	90.35							
1.0	0.500	15074.4	96.12							
1.5	0.355	7369.3	98.78							
2.0	0.250	972.7	99.13							
2.5	0.180	2400	100.00							
3.0	0.125	0								
3.5	0.088	0								
4.0	0.063	0								
4.5	0.045	0								
5.0	0.032	0								
6.0	0.017	0								
7.0	0.008	0								

Minor Lithic Counts		Abundance [volume %]	
SML	GCL	SML	GCL
0	0	0	0
0	0	0	0
0	0	0	0
10	0	3.5	0
12	0	3.8	0
0	0	0	0
0	0	0	0
0	0	0	0
0	0	0	0

Counts:

ϕ	Wp	Gp	Bp	Xtal	Lithic	Glass	NA	total counts
-5.0	0	0	n.a.	0	0	0	0	0
-4.5	0	0	n.a.	0	0	0	0	0
-4.0	0	0	n.a.	0	0	0	0	0
-3.5	0	0	n.a.	0	0	0	0	0
-3.0	0	0	n.a.	0	0	0	0	0
-2.5	119	20	n.a.	0	0	0	0	139
-2.0	315	43	n.a.	0	0	0	0	358
-1.5	436	19	22	0	23	0	0	500
-1.0	424	29	24	0	23	0	0	500
-0.5	390	30	13	0	67	0	0	500
0.0	369	30	5	1	95	0	0	500
0.5	155	23	10	16	284	12	0	500
1.0	80	26	0	45	319	30	0	500
1.5	61	11	0	48	321	59	0	500
2.0	41	1	1	72	318	67	0	500
2.5	0	0	0	0	0	0	*	*
3.0	0	0	0	0	0	0	0	0
3.5	0	0	0	0	0	0	0	0
4.0	0	0	0	0	0	0	0	0
4.5	0	0	0	0	0	0	0	0
5.0	0	0	0	0	0	0	0	0
6.0	0	0	0	0	0	0	0	0
7.0	0	0	0	0	0	0	0	0

Bulk Weight Percentages:

ϕ	Wp	Gp	Bp	Xtal	Lithic	Glass	NA
-5.0	0	0	n.a.	0	0	0	0
-4.5	0	0	n.a.	0	0	0	0
-4.0	0	0	n.a.	0	0	0	0
-3.5	0	0	n.a.	0	0	0	0
-3.0	0	0	n.a.	0	0	0	0
-2.5	4.72	1.05	n.a.	0	0	0	0
-2.0	5.45	1.05	n.a.	0	0	0	0
-1.5	17.93	1.07	1.51	0	1.71	0	0
-1.0	7.48	0.69	0.57	0	0.81	0	0
-0.5	11.42	0.91	0.39	0	3.37	0	0
0.0	9.52	0.89	0.15	0.04	4.03	0	0
0.5	6.17	0.83	0.17	0.44	8.20	0.32	0
1.0	0.72	0.26	0	0.53	3.39	0.33	0
1.5	0.16	0.09	0	0.27	1.85	0.29	0
2.0	0.01	0.0+	0.0+	0.05	0.24	0.05	0
2.5	0	0	0	0	0	0	0.87
3.0	0	0	0	0	0	0	0
3.5	0	0	0	0	0	0	0
4.0	0	0	0	0	0	0	0
4.5	0	0	0	0	0	0	0
5.0	0	0	0	0	0	0	0
6.0	0	0	0	0	0	0	0
7.0	0	0	0	0	0	0	0
	63.58	**6.84**	**2.79**	**1.33**	**23.60**	**0.99**	**0.87**

P2 at Locality 70 [Coarse-pumice level] [Total sample weight, 367500 mg]

Grain diameter		Weight Fractions		Granulometric Analysis						
ϕ	mm	weight [mg]	Cumulative weight %	ϕ_{05}	ϕ_{84}	ϕ_{16}	$\phi_{\sim}$	Md.	σ_{ϕ}	F2
-5.0	31.5	0	0	0.5	0.4	-2.1	-2.6	-0.9	1.01	0.00%
-4.5	22.4	0	0							
-4.0	16.0	0	0							
-3.5	11.2	0	0							
-3.0	8.0	0	0							
-2.5	5.6	36000	9.80							
-2.0	4.0	32500	18.64							
-1.5	2.8	64377.9	36.16							

		Minor Lithic Counts		Abundance [volume %]	
		SML	GCL	SML	GCL
-1.0	2.0	47810.5	49.17	0	0	0	0
-0.5	1.4	77523.2	70.26	0	0	0	0
0.0	1.0	25998.2	77.34	0	0	0	0
0.5	0.710	46341.4	89.95	2	0	1.6	0
1.0	0.500	20003.8	95.39	3	0	1.4	0
1.5	0.355	11669.4	98.56	3	0	1.1	0
2.0	0.250	2190.0	99.16	3	0	0.9	0
2.5	0.180	3085	100.00	0	0	0	0
3.0	0.125	0		0	0	0	0
3.5	0.088	0					
4.0	0.063	0					
4.5	0.045	0					
5.0	0.032	0					
6.0	0.017	0					
7.0	0.008	0					

Counts:

ϕ	Wp	Gp	Bp	Xtal	Lithic	Glass	NA	total counts
-5.0	0	0	n.a.	0	0	0	0	0
-4.5	0	0	n.a.	0	0	0	0	0
-4.0	0	0	n.a.	0	0	0	0	0
-3.5	0	0	n.a.	0	0	0	0	0
-3.0	0	0	n.a.	0	0	0	0	0
-2.5	264	49	n.a.	0	0	0	0	313
-2.0	607	44	n.a.	0	0	0	0	651
-1.5	472	2	24	0	2	0	0	500
-1.0	448	2	32	0	18	0	0	500
-0.5	428	0	41	0	31	0	0	500
0.0	380	3	32	2	83	0	0	500
0.5	328	9	21	10	127	5	0	500
1.0	223	7	10	34	211	15	0	500
1.5	121	5	6	52	278	38	0	500
2.0	9	1	2	96	336	56	0	500
2.5	0	0	0	0	0	0	*	*
3.0	0	0	0	0	0	0	0	0
3.5	0	0	0	0	0	0	0	0
4.0	0	0	0	0	0	0	0	0
4.5	0	0	0	0	0	0	0	0
5.0	0	0	0	0	0	0	0	0
6.0	0	0	0	0	0	0	0	0
7.0	0	0	0	0	0	0	0	0

Bulk Weight Percentages:

Wp	Gp	Bp	Xtal	Lithic	Glass	NA
0	0	n.a.	0	0	0	0
0	0	n.a.	0	0	0	0
0	0	n.a.	0	0	0	0
0	0	n.a.	0	0	0	0
0	0	n.a.	0	0	0	0
7.86	1.93	n.a.	0	0	0	0
8.02	0.82	n.a.	0	0	0	0
15.95	0.09	1.36	0	0.12	0	0
10.88	0.07	1.12	0	0.94	0	0
17.24	0	1.70	0	2.15	0	0
4.80	0.04	0.46	0.04	1.72	0	0
7.21	0.37	0.41	0.31	4.16	0.15	0
2.05	0.07	0.10	0.41	2.65	0.17	0
0.41	0.05	0.06	0.37	2.05	0.24	0
0.0+	0.0+	0.0+	0.14	0.41	0.06	0
0	0	0	0	0	0	0.84
0	0	0	0	0	0	0
0	0	0	0	0	0	0
0	0	0	0	0	0	0
0	0	0	0	0	0	0
0	0	0	0	0	0	0
0	0	0	0	0	0	0
0	0	0	0	0	0	0
74.42	**3.44**	**5.21**	**1.27**	**14.20**	**0.62**	**0.84**

P2 at Locality 70 [top level] [Total sample weight: 204500 mg]

Grain diameter		Weight Fractions:		Granulometric Analysis						
ϕ	mm	weight [mg]	Cumulative weight %	ϕ_{05}	ϕ_{25}	ϕ_{10}	ϕ_{5}	Md_{ϕ}	σ_{ϕ}	F2
-5.0	31.5	0	0	0.9	0.4	-2.1	-2.6	-0.4	1.16	0.00%
-4.5	22.4	0	0							
-4.0	16.0	0	0							
-3.5	11.2	0	0							
-3.0	8.0	0	0							
-2.5	5.6	13000	6.36							
-2.0	4.0	21500	16.87							
-1.5	2.8	23400.1	28.31							

	Minor Lithic Counts		Abundance [volume %]	
	SML	GCL	SML	GCL
-1.0	2.0	21049.3	39.61	0	0	0	0
-0.5	1.4	37584.3	56.98	0	0	0	0
0.0	1.0	33331.4	73.28	0	0	0	0
0.5	0.710	33274.1	89.55	2	0	0.6	0
1.0	0.500	13706.7	96.26	2	0	0.5	0
1.5	0.355	4029.0	98.23	6	0	1.7	0
2.0	0.250	289.0	98.37	1	0	0.4	0
2.5	0.180	3335	100.00	0	0	0	0
3.0	0.125			0	0	0	0
3.5	0.088	0					
4.0	0.063	0					
4.5	0.045	0					
5.0	0.032	0					
6.0	0.017	0					
7.0	0.008	0					

Counts:

ϕ	Wp	Gp	Bp	Xtal	Lithic	Glass	NA	total counts
-5.0	0	0	n.a.	0	0	0	0	0
-4.5	0	0	n.a.	0	0	0	0	0
-4.0	0	0	n.a.	0	0	0	0	0
-3.5	0	0	n.a.	0	0	0	0	0
-3.0	0	0	n.a.	0	0	0	0	0
-2.5	91	21	n.a.	0	0	0	0	313
-2.0	379	43	n.a.	0	0	0	0	651
-1.5	409	5	58	0	28	0	0	500
-1.0	399	17	41	0	43	0	0	500
-0.5	360	33	36	0	71	0	0	500
0.0	266	21	21	8	181	3	0	500
0.5	95	12	10	17	361	5	0	500
1.0	34	5	4	49	395	13	0	500
1.5	38	2	0	89	350	21	0	500
2.0	39	1	0	107	237	116	0	500
2.5	0	0	0	0	0	0	*	*
3.0	0	0	0	0	0	0	0	0
3.5	0	0	0	0	0	0	0	0
4.0	0	0	0	0	0	0	0	0
4.5	0	0	0	0	0	0	0	0
5.0	0	0	0	0	0	0	0	0
6.0	0	0	0	0	0	0	0	0
7.0	0	0	0	0	0	0	0	0

Bulk Weight Percentages:

Wp	Gp	Bp	Xtal	Lithic	Glass	NA
0	0	n.a.	0	0	0	0
0	0	n.a.	0	0	0	0
0	0	n.a.	0	0	0	0
0	0	n.a.	0	0	0	0
0	0	n.a.	0	0	0	0
4.87	1.49	n.a.	0	0	0	0
9.06	1.46	n.a.	0	0	0	0
8.31	0.14	1.97	0	1.03	0	0
7.14	0.44	1.06	0	1.65	0	0
11.35	1.13	1.23	0	4.05	0	0
6.90	0.62	0.62	0.33	7.71	0.12	0
4.50	0.44	0.17	0.48	10.55	0.13	0
0.34	0.06	0.04	0.65	5.45	0.16	0
0.07	0.01	0	0.36	1.45	0.07	0
0.0+	0.0+	0	0.03	0.70	0.03	0
0	0	0	0	0	0	1.63
0	0	0	0	0	0	0
0	0	0	0	0	0	0
0	0	0	0	0	0	0
0	0	0	0	0	0	0
0	0	0	0	0	0	0
0	0	0	0	0	0	0
0	0	0	0	0	0	0
52.54	**5.79**	**5.09**	**1.85**	**32.59**	**0.51**	**1.63**

S2 at Locality 1[CBV-1-1] [Total sample weight: 206803.1 mg]

Grain diameter		Weight Fractions:		Granulometric Analysis						
ϕ	mm	weight [mg]	Cumulative weight %	ϕ_{05}	ϕ_{84}	ϕ_{16}	ϕ_{x}	Md_{x}	σ_{x}	F2
-5.0	31.5	0	0	6.2	5.3	2.9	0.9	4.5	1.40	79.36%
-4.5	22.4	0	0							
-4.0	16.0	0	0							
-3.5	11.2	0	0							
-3.0	8.0	0	0							
-2.5	5.6	0	0							
-2.0	4.0	1880.9	0.91							
-1.5	2.8	1874.7	1.82							

Minor Lithic Counts		Abundance [volume %]	
SML	GCL	SML	GCL
n.a.	n.a.	n.a.	n.a.

-1.0	2.0	1095.1	2.35
-0.5	1.4	1299.5	2.97
0.0	1.0	1113.9	3.51
0.5	0.710	1868.5	4.42
1.0	0.500	2295.4	5.53
1.5	0.355	3519.4	7.23
2.0	0.250	4537.7	9.42
2.5	0.180	6254.8	12.45
3.0	0.125	8347.6	16.48
3.5	0.088	8596.7	20.64
4.0	0.063	10737.5	25.83
4.5	0.045	60432.3	55.05
5.0	0.032	48160	78.34
6.0	0.017	30980	93.32
7.0	0.008	13805	100.00

Counts:

ϕ	Wp	Gp	Bp	Xtal	Lithic	Glass	NA	total counts
-5.0	0	0	0	0	0	0	*0*	0
-4.5	0	0	0	0	0	0	*0*	0
-4.0	0	0	0	0	0	0	*0*	0
-3.5	0	0	0	0	0	0	*0*	0
-3.0	0	0	0	0	0	0	*0*	0
-2.5	0	0	0	0	0	0	*0*	0
-2.0	7	0	0	0	1	0	*0*	8
-1.5	49	0	0	0	12	0	*0*	61
-1.0	82	0	0	0	24	0	*0*	106
-0.5	305	2	0	0	192	1	*0*	500
0.0	249	5	0	6	237	3	*0*	500
0.5	194	6	0	13	281	6	*0*	500
1.0	130	8	0	24	326	12	*0*	500
1.5	153	6	0	34	291	16	*0*	500
2.0	198	6	0	51	236	9	*0*	500
2.5	186	0	0	69	224	21	*0*	500
3.0	74	0	0	78	324	24	*0*	500
3.5	0	0	0	91	371	38	*0*	500
4.0	0	0	0	94	347	59	*0*	500
4.5	0	0	0	29	390	81	*0*	500
5.0	*	*	*	*	*	*	*3010*	3010
6.0	*	*	*	*	*	*	*2817*	2817
7.0	*	*	*	*	*	*	*1972*	1972

Bulk Weight Percentages:

Wp	Gp	Bp	Xtal	Lithic	Glass	NA
0	0	0	0	0	0	0
0	0	0	0	0	0	0
0	0	0	0	0	0	0
0	0	0	0	0	0	0
0	0	0	0	0	0	0
0	0	0	0	0	0	0
0.63	0	0	0	0.28	0	0
0.66	0	0	0	0.25	0	0
0.33	0	0	0	0.20	0	0
0.30	0	0	0	0.32	0	0
0.20	0	0	0.01	0.32	0	0
0.29	0.02	0	0.03	0.56	0.01	0
0.23	0.02	0	0.06	0.78	0.03	0
0.28	0.03	0	0.14	1.19	0.06	0
0.40	0.02	0	0.31	1.42	0.05	0
0.61	0	0	0.53	1.73	0.15	0
0.34	0	0	0.68	2.82	0.19	0
0	0	0	0.77	3.14	0.25	0
0	0	0	1.00	3.69	0.50	0
0	0	0	1.75	23.60	3.87	0
*	*	*	*	*	*	23.29
*	*	*	*	*	*	14.98
*	*	*	*	*	*	6.68
4.27	**0.09**	**0.00**	**5.28**	**40.30**	**5.11**	**44.95**

S2 at Locality 4[CBV-4-1] [Total sample weight: 171937.1 mg]

Grain diameter		Weight Fractions		Granulometric Analysis						
ϕ	mm	weight [mg]	Cumulative weight %	ϕ_{05}	ϕ_{25}	ϕ_{50}	ϕ_{75}	Md_ϕ	σ_ϕ	F2
-5.0	31.5	0	0	5.2	4.2	-1.6	-3.3	1.7	2.74	28.66%
-4.5	22.4	0	0							
-4.0	16.0	0	0							
-3.5	11.2	3782.9	2.20							
-3.0	8.0	8544.5	7.17							
-2.5	5.6	4062.9	9.53							
-2.0	4.0	1744.3	10.55							
-1.5	2.8	12361.0	17.74							
-1.0	2.0	7491.5	22.09							
-0.5	1.4	8768.0	27.19							
0.0	1.0	9186.2	32.54							
0.5	0.710	7123.8	36.68							
1.0	0.500	9519.7	42.22							
1.5	0.355	8056.8	46.91							
2.0	0.250	8828.4	52.04							
2.5	0.180	8786.6	57.15							
3.0	0.125	11656.2	63.93							
3.5	0.088	12740.7	71.34							
4.0	0.063	17204.3	81.35							
4.5	0.045	12636.9	88.70							
5.0	0.032	10070	94.55							
6.0	0.017	6480	98.32							
7.0	0.008	2885	100.00							

Minor Lithic Counts		Abundance [volume %]	
SMI	GCI	SMI	GCI
0	0	0	0
0	2	0	1.0
3	3	1.6	1.6
0	4	0	2.3
0	3	0	1.9
0	3	0	1.9
0	2	0	1.5
0	2	0	1.7
0	1	0	1.0

Counts:

ϕ	Wp	Gp	Bp	Xtal	Lithic	Glass	NA	total counts
-5.0	0	0	0	0	0	0	0	0
-4.5	0	0	0	0	0	0	0	0
-4.0	0	0	0	0	0	0	0	0
-3.5	1	0	0	0	1	0	0	2
-3.0	1	0	0	0	8	0	0	9
-2.5	8	0	0	0	9	0	0	17
-2.0	5	0	0	0	8	0	0	13
-1.5	80	3	0	0	109	104	0	296
-1.0	77	1	0	0	202	174	0	454
-0.5	79	0	0	2	198	221	0	500
0.0	31	0	0	9	188	272	0	500
0.5	24	0	0	24	171	281	0	500
1.0	14	0	0	27	162	297	0	500
1.5	9	0	0	28	154	309	0	500
2.0	7	0	0	35	137	321	0	500
2.5	4	0	0	41	119	336	0	500
3.0	2	0	0	49	104	345	0	500
3.5	0	0	0	52	9	354	0	500
4.0	0	0	0	46	49	405	0	500
4.5	0	0	0	31	21	448	0	500
5.0	*	*	*	*	*	*	629	629
6.0	*	*	*	*	*	*	584	584
7.0	*	*	*	*	*	*	412	412

Bulk Weight Percentages:

Wp	Gp	Bp	Xtal	Lithic	Glass	NA
0	0	0	0	0	0	0
0	0	0	0	0	0	0
0	0	0	0	0	0	0
1.04	0	0	0	1.16	0	0
0.21	0	0	0	4.76	0	0
0.53	0	0	0	1.83	0	0
0.17	0	0	0	0.84	0	0
1.41	0.06	0	0	3.55	2.17	0
0.41	0.01	0	0	2.32	1.61	0
0.56	0	0	0.02	2.41	2.11	0
0.22	0	0	0.10	2.17	2.86	0
0.16	0	0	0.20	1.51	2.28	0
0.12	0	0	0.31	1.95	3.16	0
0.04	0	0	0.28	1.61	2.75	0
0.03	0	0	0.39	1.53	3.19	0
0.02	0	0	0.44	1.28	3.37	0
0.02	0	0	0.71	1.50	4.55	0
0	0	0	0.91	1.65	4.85	0
0	0	0	1.11	1.18	7.72	0
0	0	0	0.56	0.37	6.41	0
*	*	*	*	*	*	5.86
*	*	*	*	*	*	3.77
*	*	*	*	*	*	1.68
4.94	**0.07**	**0.00**	**5.03**	**31.62**	**47.03**	**11.30**

S2 at Locality 5[CBV-5-2] [Total sample weight: 1134821 mg]

Grain diameter		Weight Fractions		Granulometric Analysis						
ϕ	mm	weight [mg]	Cumulative weight %	ϕ_{05}	ϕ_{84}	ϕ_{16}	ϕ_{50}	Md_ϕ	σ_ϕ	F2
-5.0	31.5	77105.0	6.79	4.7	3.3	-4.6	-5.1	-2.8	3.46	14.14%
-4.5	22.4	184600.0	23.06							
-4.0	16.0	154600.0	36.68							
-3.5	11.2	72000.0	43.03							
-3.0	8.0	57370.0	48.08							
-2.5	5.6	61300.0	53.49							
-2.0	4.0	53400.0	58.19							
-1.5	2.8	43300.0	62.01							
-1.0	2.0	35200.0	65.11							
-0.5	1.4	31700.0	67.90							
0.0	1.0	28400.0	70.41							
0.5	0.710	28300.0	72.90							
1.0	0.500	22200.0	74.86							
1.5	0.355	23500.0	76.93							
2.0	0.250	25800.0	79.20							
2.5	0.180	25100.0	81.41							
3.0	0.125	26200.0	83.72							
3.5	0.088	24300.0	85.86							
4.0	0.063	2880.00	88.40							
4.5	0.045	21868.5	92.97							
5.0	0.032	41335	96.91							
6.0	0.017	26580	98.96							
7.0	0.008	11850	100.00							

Minor Lithic Counts		Abundance [volume %]	
SML	GCL	SML	GCL
3	0	1.7	0
2	0	0.8	0
6	0	2.0	0
4	0	1.2	0
2	0	0.6	0
4	0	1.5	0
3	0	1.7	0
4	0	2.5	0
0	0	0	0

Counts:

ϕ	Wp	Gp	Bp	Xtal	Lithic	Glass	NA	total counts
-5.0	1	0	0	0	1	0	*0*	2
-4.5	0	0	0	0	6	0	*0*	6
-4.0	3	0	0	0	13	0	*0*	16
-3.5	8	0	2	0	22	0	*0*	21
-3.0	32	9	7	0	43	0	*0*	91
-2.5	131	20	14	0	99	0	*0*	264
-2.0	283	22	20	0	175	0	*0*	500
-1.5	278	10	16	0	196	0	*0*	500
-1.0	297	6	21	0	176	0	*0*	500
-0.5	231	10	15	0	244	0	*0*	500
0.0	174	12	13	8	293	0	*0*	500
0.5	128	8	12	13	326	13	*0*	500
1.0	133	6	15	26	320	0	*0*	500
1.5	137	7	10	58	274	14	*0*	500
2.0	140	9	7	99	176	69	*0*	500
2.5	12	8	7	*105*	159	209	*0*	*500*
3.0	0	9	5	74	140	272	*0*	500
3.5	0	0	0	66	137	297	*0*	500
4.0	0	0	0	61	121	318	*0*	500
4.5	0	0	0	54	89	357	*0*	500
5.0	*	*	*	*	*	*	*3241*	3241
6.0	*	*	*	*	*	*	*2416*	2416
7.0	*	*	*	*	*	*	*1693*	1693

Bulk Weight %'s:

ϕ	Wp	Gp	Bp	Xtal	Lithic	Glass	NA
-5.0	1.11	0	0	0	5.68	0	0
-4.5	0	0	0	0	16.27	0	0
-4.0	0.73	0	0	0	12.67	0	0
-3.5	0.47	0	0	0	5.88	0	0
-3.0	0.81	0.34	0	0	3.91	0	0
-2.5	1.22	0.35	0	0	3.83	0	0
-2.0	1.38	0.10	0.17	0	3.05	0	0
-1.5	1.11	0.04	0.52	0	2.14	0	0
-1.0	1.29	0.04	0.13	0	1.61	0	0
-0.5	0.95	0.04	0.06	0	1.73	0	0
0.0	0.62	0.05	0.05	0.05	1.73	0	0
0.5	0.54	0.05	0.04	0.07	1.74	0.06	0
1.0	0.41	0.02	0.05	0.11	1.36	0	0
1.5	0.30	0.05	0.07	0.27	1.33	0.06	0
2.0	0.27	0.02	0.02	0.58	1.03	0.36	0
2.5	0.02	0.02	0.02	0.49	0.75	0.91	0
3.0	0	0.02	0.01	0.36	0.69	1.22	0
3.5	0	0	0	0.32	0.67	1.14	0
4.0	0	0	0	0.36	0.71	1.74	0
4.5	0	0	0	0.58	0.96	3.03	0
5.0	*	*	*	*	*	*	3.64
6.0	*	*	*	*	*	*	2.34
7.0	*	*	*	*	*	*	1.04
	11.23	**1.16**	**1.14**	**3.19**	**67.74**	**8.52**	**7.02**

S2 at Locality 6 [CBV-6-4] [Total sample weight: 145438.3 mg]

Grain diameter		Weight Fractions		Granulometric Analysis						
ϕ	mm	weight [mg]	Cumulative weight %	ϕ_{05}	ϕ_{25}	ϕ_{16}	ϕ_{5}	Md$_{\phi}$	σ_{ϕ}	F2
-5.0	31.5	0	0	6.3	5.4	-2.1	-3.9	3.6	3.41	50.12%
-4.5	22.4	0	0							
-4.0	16.0	6092.1	4.19							
-3.5	11.2	5173.3	7.75							
-3.0	8.0	4114.1	10.57							
-2.5	5.6	5120.7	14.10							
-2.0	4.0	4009.2	16.85							
-1.5	2.8	4856.2	20.19							
-1.0	2.0	4366.6	23.19							
-0.5	1.4	4257.4	26.12							
0.0	1.0	4364.2	29.12							
0.5	0.710	4249.6	32.04							
1.0	0.500	4889.3	35.41							
1.5	0.355	3172.1	37.59							
2.0	0.250	3779.8	40.19							
2.5	0.180	3745.1	42.76							
3.0	0.125	4519.4	45.87							
3.5	0.088	5711.1	49.79							
4.0	0.063	7420.2	54.90							
4.5	0.045	3682.5	57.43							
5.0	0.032	30710	78.55							
6.0	0.017	19760	92.13							
7.0	0.008	11445	100.00							

Minor Lithic Counts		Abundance [volume %]	
SMI	GCI	SMI	GCI
n.a.	n.a.	n.a.	n.a.

Counts:

ϕ	Wp	Gp	Bp	Xtal	Lithic	Glass	NA	total counts
-5.0	0	0	0	0	0	0	*0*	0
-4.5	0	0	0	0	0	0	*0*	0
-4.0	3	0	0	0	0	0	*0*	3
-3.5	5	0	0	0	1	0	*0*	6
-3.0	3	0	0	0	3	0	*0*	6
-2.5	8	0	0	0	12	0	*0*	20
-2.0	21	0	0	0	23	0	*0*	44
-1.5	54	0	0	0	68	0	*0*	122
-1.0	112	0	0	0	177	0	*0*	289
-0.5	139	0	0	0	361	0	*0*	500
0.0	170	0	0	2	314	11	*0*	497
0.5	119	0	0	13	297	71	*0*	500
1.0	85	0	0	15	264	136	*0*	500
1.5	42	0	0	18	237	203	*0*	500
2.0	18	0	0	28	193	261	*0*	500
2.5	9	0	0	34	172	285	*0*	500
3.0	2	0	0	52	140	306	*0*	500
3.5	0	0	0	41	139	320	*0*	500
4.0	0	0	0	36	124	340	*0*	500
4.5	0	0	0	14	101	385	*0*	500
5.0	*	*	*	*	*	*	*1919*	1919
6.0	*	*	*	*	*	*	*1796*	1796
7.0	*	*	*	*	*	*	*1634*	1634

Bulk Weight Percentages:

Wp	Gp	Bp	Xtal	Lithic	Glass	NA
0	0	0	0	0	0	0
0	0	0	0	0	0	0
4.19	0	0	0	0	0	0
3.56	0	0	0	0	0	0
2.83	0	0	0	0	0	0
1.51	0	0	0	2.02	0	0
0.63	0	0	0	2.13	0	0
0.96	0	0	0	2.38	0	0
0.68	0	0	0	2.32	0	0
0.54	0	0	0	2.39	0	0
0.72	0	0	0.01	2.19	0.07	0
0.61	0	0	0.08	1.83	0.40	0
0.45	0	0	0.11	1.93	0.88	0
0.09	0	0	0.09	1.16	0.85	0
0.03	0	0	0.16	1.09	1.31	0
0.02	0	0	0.18	0.93	1.44	0
0.01	0	0	0.34	0.92	1.84	0
0	0	0	0.37	1.27	2.28	0
0	0	0	0.43	1.47	3.20	0
0	0	0	0.08	0.61	1.83	0
*	*	*	*	*	*	21.12
*	*	*	*	*	*	13.59
*	*	*	*	*	*	7.87
16.83	**0**	**0**	**1.85**	**24.64**	**14.10**	**42.58**

S2 at Locality 7 [CBV-7-1] [Total sample weight: 729617 mg]

Grain diameter		Weight Fractions:		Granulometric Analysis						
ϕ	mm	weight [mg]	Cumulative weight %	ϕ_{5}	ϕ_{5}	ϕ_{16}	ϕ_{5}	Md_{ϕ}	σ_{ϕ}	F2
-5.0	31.5	59400	8.14	5.6	4.7	-4.2	-4.7	1.5	3.77	23.96%
-4.5	22.4	35900	13.06							
-4.0	16.0	39300	18.45							
-3.5	11.2	16500	20.71							
-3.0	8.0	16900	23.03							
-2.5	5.6	21400	25.96							
-2.0	4.0	21800	28.95							
-1.5	2.8	21500	31.89							
-1.0	2.0	18800	34.47							
-0.5	1.4	18500	37.01							
0.0	1.0	21800	39.99							
0.5	0.710	25300	43.46							
1.0	0.500	34700	48.22							
1.5	0.355	38200	53.45							
2.0	0.250	43600	59.43							
2.5	0.180	38700	64.73							
3.0	0.125	44900	70.89							
3.5	0.088	37600	76.04							
4.0	0.063	41300	81.70							
4.5	0.045	52600	88.91							
5.0	0.032	41925	94.66							
6.0	0.017	26970	98.35							
7.0	0.008	12015	100.00							

Minor Lithic Counts		Abundance [volume %]	
SML	GCL	SML	GCL
0	3	0	1.8
2	9	1.0	4.7
0	12	0	4.9
0	6	0	2.6
0	4	0	1.7
0	6	0	2.5
0	7	0	3.2
0	6	0	2.9
0	0	0	0

Counts:

ϕ	Wp	Gp	Bp	Xtal	Lithic	Glass	NA	total counts
-5.0	0	0	0	0	1	0	*0*	1
-4.5	0	0	0	0	1	0	*0*	1
-4.0	0	0	0	0	4	0	*0*	4
-3.5	1	0	0	0	5	0	*0*	6
-3.0	19	2	5	0	10	0	*0*	36
-2.5	55	2	12	0	34	0	*0*	103
-2.0	154	8	29	0	86	0	*0*	277
-1.5	327	10	26	0	137	0	*0*	500
-1.0	311	12	14	0	163	0	*0*	500
-0.5	265	10	17	0	191	17	*0*	500
0.0	197	12	21	3	243	24	*0*	500
0.5	201	10	16	11	234	25	*0*	500
1.0	212	9	3	19	239	18	*0*	500
1.5	208	8	2	22	242	18	*0*	500
2.0	202	2	0	43	217	36	*0*	500
2.5	176	0	0	62	201	58	*0*	500
3.0	152	0	0	75	201	72	*0*	500
3.5	141	0	0	91	189	79	*0*	500
4.0	89	0	0	93	173	145	*0*	500
4.5	0	0	0	68	154	278	*0*	500
5.0	*	*	*	*	*	*	*2620*	2620
6.0	*	*	*	*	*	*	*2452*	2452
7.0	*	*	*	*	*	*	*1717*	1717

Bulk Weight Percentages:

Wp	Gp	Bp	Xtal	Lithic	Glass	NA
0	0	0	0	8.14	0	0
0	0	0	0	4.92	0	0
0	0	0	0	5.39	0	0
0.19	0	0	0	2.07	0	0
0.82	0	0	0	1.49	0	0
0.79	0.03	0.18	0	1.93	0	0
0.97	0.12	0.22	0	1.67	0	0
1.07	0.09	0.11	0	1.68	0	0
1.15	0.06	0.07	0	1.29	0	0
1.04	0.04	0.07	0	1.29	0.09	0
0.87	0.06	0.11	0.02	1.77	0.16	0
0.98	0.11	0.08	0.09	2.01	0.2	0
1.68	0.08	0.03	0.20	2.6	0.17	0
1.28	0.15	0.04	0.29	3.27	0.21	0
1.12	0.01	0	0.71	3.6	0.53	0
1.01	0	0	0.83	2.74	0.72	0
1.18	0	0	1.09	2.92	0.96	0
1.28	0	0	1.04	2.15	0.7	0
0.88	0	0	1.17	2.17	1.44	0
0	0	0	1.11	2.52	3.58	0
*	*	*	*	*	*	5.75
*	*	*	*	*	*	3.70
*	*	*	*	*	*	1.65
16.31	**0.75**	**0.91**	**6.55**	**55.62**	**8.76**	**11.10**

S2 at Locality 12 [CBV-12-6] [Total sample weight 299704.1 mg]

Grain diameter		Weight Fractions		Granulometric Analysis						
ϕ	mm	weight [mg]	Cumulative weight %	ϕ_{16}	ϕ_{84}	ϕ_{50}	ϕ_x	Md_ϕ	σ_ϕ	F2
-5.0	31.5	0	0	6.2	4.9	-1.7	-3.2	1.5	3.05	30.73%
-4.5	22.4	2231.8	0.74							
-4.0	16.0	7409.1	3.22							
-3.5	11.2	1604.4	3.75							
-3.0	8.0	7801.8	3.36							
-2.5	5.6	9174.8	9.42							
-2.0	4.0	10686.4	12.98							
-1.5	2.8	12062.8	17.01							
-1.0	2.0	13745	21.59							
-0.5	1.4	16303	27.03							
0.0	1.0	18485	33.20							
0.5	0.710	17463	39.03							
1.0	0.500	20382	45.83							
1.5	0.355	15278	50.93							
2.0	0.250	15948	56.25							
2.5	0.180	14742	61.17							
3.0	0.125	14827	66.11							
3.5	0.088	9468	69.27							
4.0	0.063	15574	74.47							
4.5	0.045	11364	78.26							
5.0	0.032	26845	87.22							
6.0	0.017	20460	94.04							
7.0	0.008	17855	100.00							

Minor Lithic Counts		Abundance [volume %]	
SML	GCL	SML	GCL
n.a.	n.a.	n.a.	n.a.

Counts:

ϕ	Wp	Gp	Bp	Xtal	Lithic	Glass	NA	total counts
-5.0	0	0	0	0	0	0	*0*	0
-4.5	1	0	0	0	0	0	*0*	1
-4.0	1	0	0	0	0	0	*0*	1
-3.5	1	0	0	0	0	0	*0*	1
-3.0	1	0	0	0	0	0	*0*	1
-2.5	1	0	0	0	0	0	*0*	1
-2.0	1	0	0	0	0	0	*0*	1
-1.5	103	17	0	0	147	0	*0*	275
-1.0	83	34	0	0	517	114	*0*	750
-0.5	60	16	0	0	601	73	*0*	750
0.0	85	21	0	16	519	109	*0*	750
0.5	37	3	0	77	298	335	*0*	750
1.0	22	2	0	136	301	289	*0*	750
1.5	40	3	0	193	244	270	*0*	750
2.0	21	1	0	231	193	301	*0*	750
2.5	6	0	0	299	124	321	*0*	750
3.0	2	0	0	349	82	317	*0*	750
3.5	0	0	0	179	18	395	*0*	592
4.0	0	0	0	73	8	420	*0*	501
4.5	0	0	0	191	14	305	*0*	510
5.0	*	*	*	*	*	*	*1677*	1677
6.0	*	*	*	*	*	*	*1859*	1859
7.0	*	*	*	*	*	*	*2551*	2511

Bulk Weight Percentages:

ϕ	Wp	Gp	Bp	Xtal	Lithic	Glass	NA
-5.0	0	0	0	0	0	0	0
-4.5	0.74	0	0	0	0	0	0
-4.0	1.65	0	0	0	0.82	0	0
-3.5	0.27	0	0	0	0.27	0	0
-3.0	0.54	0	0	0	1.86	0	0
-2.5	0.28	0	0	0	2.76	0	0
-2.0	0.53	0	0	0	3.01	0	0
-1.5	1.19	0.19	0	0	2.55	0	0
-1.0	0.84	0.16	0	0	3.53	0.63	0
-0.5	0.27	0.07	0	0	4.65	0.44	0
0.0	0.46	0.13	0	0.14	4.57	0.88	0
0.5	0.39	0.03	0	0.59	2.37	2.45	0
1.0	0.16	0.02	0	1.26	2.90	2.47	0
1.5	0.14	0.03	0	1.40	1.82	1.72	0
2.0	0.05	0	0	1.75	1.49	2.03	0
2.5	0.05	0	0	2.03	0.84	2.03	0
3.0	0.01	0	0	2.09	0.56	1.99	0
3.5	0	0	0	1.12	0.11	1.93	0
4.0	0	0	0	0.92	0.10	4.18	0
4.5	0	0	0	1.62	0.12	2.05	0
5.0	*	*	*	*	*	*	8.96
6.0	*	*	*	*	*	*	6.83
7.0	*	*	*	*	*	*	5.96
	7.57	**0.63**	**0**	**12.92**	**34.33**	**22.80**	**21.75**

S2 at Locality 18 [CBV-S-2] [Total sample weight: 368637.7 mg]

Grain diameter		Weight Fractions		Granulometric Analysis						
ϕ	mm	weight [mg]	Cumulative weight %	ϕ_{05}	ϕ_{16}	ϕ_{50}	ϕ_{84}	Mdφ	σ_ϕ	F2
-5.0	31.5	0	0	6.2	5.4	0.7	-0.9	3.7	2.24	47.21%
-4.5	22.4	0	0							
-4.0	16.0	0	0							
-3.5	11.2	0	0							
-3.0	8.0	2124.3	0.58							
-2.5	5.6	972.1	0.84							
-2.0	4.0	1979.1	1.38							
-1.5	2.8	4832.8	2.69							

				Minor Lithic Counts		Abundance [volume %]	
				SML	GCL	SML	GCL
-1.0	2.0	7233.5	4.65	0	0	0	0
-0.5	1.4	8783.5	7.03	0	0	0	0
0.0	1.0	13187.2	10.61	18	49	3.2	8.8
0.5	0.710	17473.9	15.35	17	74	3.8	16.3
1.0	0.500	22253.6	21.39	14	34	4.3	10.5
1.5	0.355	25494.8	28.30	0	0	0	0
2.0	0.250	25183.9	35.13	0	0	0	0
2.5	0.180	20838.2	40.79	0	0	0	0
3.0	0.125	23985.8	47.29	0	0	0	0
3.5	0.088	20244.6	52.79				
4.0	0.063	22289.5	58.83				
4.5	0.045	19529.9	64.13				
5.0	0.032	55405	79.16				
6.0	0.017	48530	92.32				
7.0	0.008	28300	100.00				

Counts:

ϕ	Wp	Gp	Bp	Xtal	Lithic	Glass	NA	total counts
-5.0	0	0	0	0	0	0	*0*	0
-4.5	0	0	0	0	0	0	*0*	0
-4.0	0	0	0	0	0	0	*0*	0
-3.5	0	0	0	0	0	0	*0*	0
-3.0	0	0	0	0	3	0	*0*	3
-2.5	3	0	0	0	2	0	*0*	5
-2.0	8	10	0	0	16	0	*0*	34
-1.5	16	0	0	0	89	0	*0*	105
-1.0	53	16	0	1	355	0	*0*	425
-0.5	56	31	0	105	558	0	*0*	750
0.0	44	30	0	106	556	14	*0*	750
0.5	40	32	0	209	453	21	*0*	755
1.0	44	18	0	313	325	50	*0*	750
1.5	16	4	0	333	327	70	*0*	750
2.0	21	0	0	379	206	129	*0*	735
2.5	30	0	0	394	168	158	*0*	750
3.0	28	0	0	406	139	267	*0*	840
3.5	19	0	0	279	94	297	*0*	689
4.0	11	0	0	218	61	314	*0*	604
4.5	0	0	0	209	31	319	*0*	559
5.0	*	*	*	*	*	*	*346*	346
6.0	*	*	*	*	*	*	*441*	441
7.0	*	*	*	*	*	*	*404*	404

Bulk Weight Percentages:

Wp	Gp	Bp	Xtal	Lithic	Glass	NA
0	0	0	0	0	0	0
0	0	0	0	0	0	0
0	0	0	0	0	0	0
0	0	0	0	0	0	0
0.19	0	0	0	0.58	0	0
0.05	0	0	0	0.23	0	0
0.02	0.08	0	0	0.36	0	0
0.39	0	0	0	1.22	0	0
0.97	0.05	0	0	1.78	0	0
0	0.60	0	0.34	1.87	0	0
0	0.10	0	0.51	2.77	0.06	0
0	0.26	0	1.29	2.91	0.12	0
0	0.12	0	2.53	2.74	0.37	0
0	0.05	0	3.10	3.13	0.57	0
0	0	0	3.66	1.99	1.11	0
0	0	0	3.09	1.32	1.15	0
0	0	0	3.29	1.12	1.97	0
0	0	0	2.47	0.29	2.06	0
0	0	0	2.46	0.69	2.81	0
0	0	0	2.25	0.33	2.71	0
*	*	*	*	*	*	15.03
*	*	*	*	*	*	13.16
*	*	*	*	*	*	7.68
1.62	**1.26**	**0**	**24.99**	**23.33**	**12.93**	**35.87**

S2 at Locality 43 [CBV-S-21] [Total sample weight 207819.4 mg]

Grain diameter		Weight Fractions		Granulometric Analysis						
ϕ	mm	weight [mg]	Cumulative weight %	ϕ_{05}	ϕ_{25}	ϕ_{10}	ϕ_{x}	Md_{ϕ}	σ_{ϕ}	F2
-5.0	31.5	0	0	5.8	4.9	1.6	0.3	4.2	1.65	61.53%
-4.5	22.4	0	0							
-4.0	16.0	0	0							
-3.5	11.2	597.8	0.29							
-3.0	8.0	0	0.29							
-2.5	5.6	350.1	0.46							
-2.0	4.0	364.2	0.63							
-1.5	2.8	980.3	1.10							

Minor Lithic Counts		Abundance [volume %]	
SML	GCL	SML	GCL
n.a.	n.a.	n.a.	n.a.

-1.0	2.0	1381.1	1.77
-0.5	1.4	2177.4	2.82
0.0	1.0	3028.2	4.27
0.5	0.710	5205.3	6.78
1.0	0.500	7461.4	10.37
1.5	0.355	9682.8	15.03
2.0	0.250	11208.6	20.42
2.5	0.180	13427.8	26.88
3.0	0.125	11749.5	32.54
3.5	0.088	12325.1	38.47
4.0	0.063	16973.8	46.63
4.5	0.045	45692.4	68.62
5.0	0.032	42920	89.27
6.0	0.017	13975	96.00
7.0	0.008	8320	100.00

Counts:

ϕ	Wp	Gp	Bp	Xtal	Lithic	Glass	NA	total counts
-5.0	0	0	0	0	0	0	0	0
-4.5	0	0	0	0	0	0	0	0
-4.0	0	0	0	0	0	0	0	0
-3.5	1	0	0	0	0	0	0	1
-3.0	0	0	0	0	0	0	0	0
-2.5	0	0	0	0	1	0	0	1
-2.0	1	0	0	0	2	0	0	3
-1.5	15	0	0	0	13	1	0	29
-1.0	56	0	0	0	46	3	0	105
-0.5	210	2	0	0	274	4	0	490
0.0	155	8	0	2	310	25	0	500
0.5	124	2	0	11	287	76	0	500
1.0	70	0	0	16	261	153	0	500
1.5	42	0	0	59	221	178	0	500
2.0	15	0	0	77	215	193	0	500
2.5	11	0	0	102	193	194	0	500
3.0	9	0	0	91	196	204	0	500
3.5	0	0	0	84	187	229	0	500
4.0	0	0	0	81	174	245	0	500
4.5	0	0	0	76	149	275	0	500
5.0	*	*	*	*	*	*	*2682*	2682
6.0	*	*	*	*	*	*	*1270*	1270
7.0	*	*	*	*	*	*	*1188*	1180

Bulk Weight Percentages:

Wp	Gp	Bp	Xtal	Lithic	Glass	NA
0	0	0	0	0	0	0
0	0	0	0	0	0	0
0	0	0	0	0	0	0
0.29	0	0	0	0	0	0
0	0	0	0	0	0	0
0	0	0	0	0.17	0	0
0.03	0	0	0	0.14	0	0
0.17	0	0	0	0.30	0.01	0
0.23	0	0	0	0.41	0.02	0
0.32	0	0	0	0.72	0.01	0
0.32	0.02	0	0.01	1.04	0.08	0
0.49	0.01	0	0.06	1.56	0.38	0
0.40	0	0	0.12	2.02	1.05	0
0.20	0	0	0.59	2.29	1.58	0
0.06	0	0	0.89	2.47	1.97	0
0.06	0	0	1.37	2.60	2.43	0
0.06	0	0	1.08	2.32	2.20	0
0	0	0	1.11	2.46	2.36	0
0	0	0	1.47	3.16	3.53	0
0	0	0	3.78	7.41	10.80	0
*	*	*	*	*	*	20.65
*	*	*	*	*	*	6.72
*	*	*	*	*	*	4.00
2.63	**0.03**	**0.0**	**10.48**	**29.07**	**26.42**	**31.37**

S2 at Locality 44 [CBV-S-5] [Total sample weight 235003.3 mg]

Grain diameter		Weight Fractions		Granulometric Analysis						
ϕ	mm	weight [mg]	Cumulative weight %	ϕ_{5}	ϕ_{5}	$\phi_{}$	$\phi_{}$	Md$_{\phi}$	σ_{ϕ}	F2
-5.0	31.5	0	0	6.4	5.7	1.4	0.2	3.9	2.01	55.41%
-4.5	22.4	0	0							
-4.0	16.0	0	0							
-3.5	11.2	0	0							
-3.0	8.0	1309.1	0.56							
-2.5	5.6	224.2	1.50							
-2.0	4.0	119.8	1.98							
-1.5	2.8	1230.5	2.50							
-1.0	2.0	1041.2	2.95							
-0.5	1.4	1377.5	3.53							
0.0	1.0	2243.7	4.49							
0.5	0.710	5882.3	6.99							
1.0	0.500	10082.1	11.28							
1.5	0.355	13781.3	17.15							
2.0	0.250	17152.0	24.44							
2.5	0.180	14735.1	30.71							
3.0	0.125	17252.8	38.06							
3.5	0.088	15360.0	44.59							
4.0	0.063	15977.3	51.39							
4.5	0.045	12319.4	56.63							
5.0	0.032	41990	74.50							
6.0	0.017	37100	90.29							
7.0	0.008	22830	100.00							

Minor Lithic Counts		Abundance [volume %]	
SML	GCL	SML	GCL
n.a.	n.a.	n.a.	n.a.

Counts:

ϕ	Wp	Gp	Bp	Xtal	Lithic	Glass	NA	total counts
-5.0	0	0	0	0	0	0	0	0
-4.5	0	0	0	0	0	0	0	0
-4.0	0	0	0	0	0	0	0	0
-3.5	0	0	0	0	0	0	0	0
-3.0	0	0	0	0	1	0	0	1
-2.5	0	0	0	0	5	0	0	5
-2.0	2	0	0	0	12	0	0	14
-1.5	6	3	0	0	15	0	0	24
-1.0	14	5	0	0	52	0	0	71
-0.5	79	16	0	0	190	0	0	285
0.0	205	23	0	7	515	0	0	750
0.5	179	54	0	35	481	1	0	750
1.0	168	38	0	23	504	17	0	750
1.5	101	1	0	88	523	37	0	750
2.0	105	2	0	205	377	61	0	750
2.5	65	0	0	352	279	54	0	750
3.0	29	0	0	331	216	174	0	750
3.5	0	0	0	213	105	234	0	552
4.0	0	0	0	145	90	311	0	546
4.5	0	0	0	146	118	400	0	664
5.0	*	*	*	*	*	*	2624	2624
6.0	*	*	*	*	*	*	3372	3372
7.0	*	*	*	*	*	*	3261	3261

Bulk Weight Percentages:

ϕ	Wp	Gp	Bp	Xtal	Lithic	Glass	NA
-5.0	0	0	0	0	0	0	0
-4.5	0	0	0	0	0	0	0
-4.0	0	0	0	0	0	0	0
-3.5	0	0	0	0	0	0	0
-3.0	0	0	0	0	0.56	0	0
-2.5	0	0	0	0	0.95	0	0
-2.0	0.03	0	0	0	0.45	0	0
-1.5	0.05	0.03	0	0	0.44	0	0
-1.0	0.05	0.02	0	0	0.37	0	0
-0.5	0.11	0.02	0	0	0.45	0	0
0.0	0.18	0.02	0	0.01	0.74	0	0
0.5	0.42	0.24	0	0.12	1.72	0	0
1.0	0.76	0.19	0	0.14	3.11	0.09	0
1.5	0.39	0.01	0	0.73	4.46	0.27	0
2.0	0.38	0.01	0	2.23	4.09	0.59	0
2.5	0.25	0	0	3.11	2.20	0.44	0
3.0	0.16	0	0	3.37	2.20	1.62	0
3.5	0	0	0	2.78	1.37	2.39	0
4.0	0	0	0	2.05	1.27	3.48	0
4.5	0	0	0	1.32	1.07	2.86	0
5.0	*	*	*	*	*	*	17.87
6.0	*	*	*	*	*	*	15.79
7.0	*	*	*	*	*	*	9.71
	2.78	**0.80**	**0**	**15.86**	**25.45**	**11.74**	**43.37**

S2 at Locality 46 [CBV-S-33] [Total sample weight: 372367.8 mg]

Grain diameter		Weight Fractions		Granulometric Analysis						
ϕ	mm	weight [mg]	Cumulative weight %	ϕ_{5}	ϕ_{25}	ϕ_{10}	ϕ_{50}	Md$_\phi$	σ_ϕ	F2
-5.0	31.5	0	0	5.6	4.9	0.5	-2.9	3.7	2.45	51.34%
-4.5	22.4	0	0							
-4.0	16.0	8077.1	2.17							
-3.5	11.2	8274.0	4.39							
-3.0	8.0	2110.5	4.96							
-2.5	5.6	2088.7	5.52							
-2.0	4.0	4758.4	6.80							
-1.5	2.8	6172.5	8.45							
-1.0	2.0	6743.4	10.27							
-0.5	1.4	7180.6	12.19							
0.0	1.0	6408.1	13.91							
0.5	0.710	7636.4	15.97							
1.0	0.500	10700.3	18.84							
1.5	0.355	17425.8	23.52							
2.0	0.250	23712.4	29.89							
2.5	0.180	24043.3	36.34							
3.0	0.125	24732.1	42.99							
3.5	0.088	21122.5	48.66							
4.0	0.063	17650.6	53.40							
4.5	0.045	68371.3	71.76							
5.0	0.032	54490	86.39							
6.0	0.017	35050	95.81							
7.0	0.008	15620	100.00							

Minor Lithic Counts		Abundance [volume %]	
SML	GCL	SML	GCL
n.a.	n.a.	n.a.	n.a.

Counts:

ϕ	Wp	Gp	Bp	Xtal	Lithic	Glass	NA	total counts
-5.0	0	0	0	0	0	0	0	0
-4.5	0	0	0	0	0	0	0	0
-4.0	1	0	0	0	1	0	0	2
-3.5	2	2	0	0	1	0	0	5
-3.0	2	0	0	0	2	0	0	4
-2.5	6	0	0	0	4	0	0	10
-2.0	39	6	0	0	21	0	0	66
-1.5	101	8	0	0	77	0	0	186
-1.0	292	11	0	0	197	0	0	500
-0.5	303	8	0	0	184	5	0	500
0.0	324	0	0	3	173	0	0	500
0.5	245	0	0	61	162	32	0	500
1.0	122	0	0	128	142	108	0	500
1.5	43	0	0	104	262	91	0	500
2.0	32	0	0	91	317	46	0	500
2.5	29	0	0	74	301	93	0	500
3.0	0	0	0	51	308	112	0	500
3.5	0	0	0	32	286	182	0	500
4.0	0	0	0	19	244	237	0	500
4.5	0	0	0	2	195	303	0	500
5.0	*	*	*	*	*	*	341	341
6.0	*	*	*	*	*	*	318	318
7.0	*	*	*	*	*	*	223	223

Bulk Weight Percentages:

ϕ	Wp	Gp	Bp	Xtal	Lithic	Glass	NA
-5.0	0	0	0	0	0	0	0
-4.5	0	0	0	0	0	0	0
-4.0	0.92	0	0	0	1.25	0	0
-3.5	0.55	0.67	0	0	1.02	0	0
-3.0	0.23	0	0	0	0.33	0	0
-2.5	0.21	0	0	0	0.35	0	0
-2.0	0.51	0.10	0	0	0.67	0	0
-1.5	0.03	0.09	0	0	1.53	0	0
-1.0	0.72	0.04	0	0	1.05	0	0
-0.5	0.92	0.03	0	0	0.96	0.02	0
0.0	0.91	0	0	0.01	0.80	0	0
0.5	0.88	0	0	0.27	0.76	0.14	0
1.0	0.57	0	0	0.79	0.91	0.61	0
1.5	0.20	0	0	1.03	2.66	0.79	0
2.0	0.21	0	0	1.25	4.35	0.56	0
2.5	0.19	0	0	1.01	4.09	1.17	0
3.0	0.22	0	0	0.71	4.29	1.43	0
3.5	0	0	0	0.39	3.52	1.75	0
4.0	0	0	0	0.20	2.56	1.98	0
4.5	0	0	0	0.08	8.21	10.07	0
5.0	*	*	*	*	*	*	14.63
6.0	*	*	*	*	*	*	9.41
7.0	*	*	*	*	*	*	4.19
	7.27	**0.93**	**0.0**	**5.74**	**39.31**	**18.52**	**28.23**

S2 at Locality 51 [CBV-S-10] [Total sample weight: 223046.9 mg]

Grain diameter		Weight Fractions:		Granulometric Analysis:						
ϕ	mm	weight [mg]	Cumulative weight %	ϕ_{05}	ϕ_{25}	ϕ_{10}	ϕ_{x}	Md_{ϕ}	σ_{ϕ}	F2
-5.0	31.5	0	0	6.4	5.2	1.2	0.2	3.65	1.93	51.26%
-4.5	22.4	0	0							
-4.0	16.0	0	0							
-3.5	11.2	0	0							
-3.0	8.0	0	0							
-2.5	5.6	0	0							
-2.0	4.0	0	0							
-1.5	2.8	925.7	0.42							

Minor Lithic Counts:		Abundance [volume %]	
SML	GCL	SML	GCL
0	6	0	40.0
0	19	0	8.0
0	40	0	16.9
0	62	0	23.6
0	87	0	36.3
0	71	0	32.3
0	59	0	28.5
0	44	0	21.4
0	41	0	21.0

-1.0	2.0	1396.9	1.04
-0.5	1.4	2806.5	2.3
0.0	1.0	4068.1	4.2
0.5	0.710	7304.4	7.4
1.0	0.500	13560.8	13.48
1.5	0.355	16136	20.71
2.0	0.250	16380	28.06
2.5	0.180	14849.6	34.71
3.0	0.125	17230.1	42.44
3.5	0.088	14060.2	48.74
4.0	0.063	13895.5	54.97
4.5	0.045	11983.3	60.34
5.0	0.032	35200	76.13
6.0	0.017	33260	91.04
7.0	0.008	19990	100.00

Counts:

ϕ	Wp	Gp	Bp	Xtal	Lithic	Glass	NA	total counts
-5.0	0	0	0	0	0	0	*0*	0
-4.5	0	0	0	0	0	0	*0*	0
-4.0	0	0	0	0	0	0	*0*	0
-3.5	0	0	0	0	0	0	*0*	0
-3.0	0	0	0	0	0	0	*0*	0
-2.5	0	0	0	0	0	0	*0*	0
-2.0	0	0	0	0	0	0	*0*	0
-1.5	2	0	0	0	0	0	*0*	2
-1.0	28	0	0	0	15	0	*0*	43
-0.5	121	4	0	0	237	0	*0*	362
0.0	257	1	0	3	236	3	*0*	500
0.5	265	0	0	4	233	8	*0*	510
1.0	234	1	0	14	240	11	*0*	500
1.5	191	0	0	58	220	31	*0*	500
2.0	154	0	0	91	207	48	*0*	500
2.5	116	0	0	104	206	74	*0*	500
3.0	65	0	0	121	195	119	*0*	500
3.5	46	0	0	112	193	149	*0*	500
4.0	0	0	0	74	184	242	*0*	500
4.5	0	0	0	42	146	312	*0*	500
5.0	*	*	*	*	*	*	*2208*	2208
6.0	*	*	*	*	*	*	*3023*	3023
7.0	*	*	*	*	*	*	*2856*	2856

Bulk Weight Percentages:

ϕ	Wp	Gp	Bp	Xtal	Lithic	Glass	NA
-5.0	0	0	0	0	0	0	0
-4.5	0	0	0	0	0	0	0
-4.0	0	0	0	0	0	0	0
-3.5	0	0	0	0	0	0	0
-3.0	0	0	0	0	0	0	0
-2.5	0	0	0	0	0	0	0
-2.0	0	0	0	0	0	0	0
-1.5	0.42	0	0	0	0	0	0
-1.0	0.29	0	0	0	0.33	0	0
-0.5	0.29	0.02	0	0	0.96	0	0
0.0	0.72	0.01	0	0.01	1.08	0.01	0
0.5	1.24	0	0	0.03	1.94	0.06	0
1.0	2.39	0.01	0	0.19	3.35	0.14	0
1.5	1.61	0	0	1.05	4.08	0.49	0
2.0	0.96	0	0	1.69	3.88	0.80	0
2.5	0.77	0	0	1.62	3.20	1.07	0
3.0	0.58	0	0	2.03	3.28	1.83	0
3.5	0.50	0	0	1.54	2.66	1.61	0
4.0	0	0	0	1.02	2.55	2.66	0
4.5	0	0	0	0.52	1.81	3.05	0
5.0	*	*	*	*	*	*	15.78
6.0	*	*	*	*	*	*	14.91
7.0	*	*	*	*	*	*	8.96
	9.77	**0.04**	**0**	**9.70**	**29.12**	**11.72**	**39.65**

S2 at Locality 71 [CBV-S-26a] [Total sample weight: 97400 mg]

Grain diameter		Weight Fractions:		Granulometric Analysis						
ϕ	mm	weight [mg]	Cumulative weight %	ϕ_{05}	ϕ_{25}	ϕ_{75}	ϕ_{95}	Md_ϕ	σ_ϕ	F2
-5.0	31.5	0	0	5.5	4.7	-0.4	-1.9	2.5	2.38	42.19%
-4.5	22.4	0	0							
-4.0	16.0	0	0							
-3.5	11.2	0	0							
-3.0	8.0	2654.4	2.73							
-2.5	5.6	899.3	3.65							
-2.0	4.0	1240.1	4.92							
-1.5	2.8	1655.4	6.62							

Minor Lithic Counts		Abundance [volume %]	
SML	GCL	SML	GCL
0	0	0	0
0	0	0	0
0	0	0	0
0	0	0	0
0	0	0	0
0	0	0	0
0	6	0	2.5
0	9	0	4.0
0	8	0	3.9

-1.0	2.0	3158.8	9.86
-0.5	1.4	4790.3	14.78
0.0	1.0	5904.5	20.84
0.5	0.710	7712.1	28.76
1.0	0.500	8047.6	37.03
1.5	0.355	5900.9	43.08
2.0	0.250	4052.8	47.24
2.5	0.180	2917.9	50.24
3.0	0.125	3956.3	54.30
3.5	0.088	3417.3	57.81
4.0	0.063	5308.9	63.26
4.5	0.045	14742.8	78.40
5.0	0.032	13850	92.62
6.0	0.017	4510	97.24
7.0	0.008	2680	100.00

Counts:

ϕ	Wp	Gp	Bp	Xtal	Lithic	Glass	NA	total counts
-5.0	0	0	0	0	0	0	*0*	0
-4.5	0	0	0	0	0	0	*0*	0
-4.0	0	0	0	0	0	0	*0*	0
-3.5	0	0	0	0	0	0	*0*	0
-3.0	1	0	0	0	2	0	*0*	3
-2.5	1	0	0	0	2	0	*0*	3
-2.0	1	0	0	0	8	0	*0*	9
-1.5	6	0	0	0	33	0	*0*	39
-1.0	19	0	0	0	155	0	*0*	174
-0.5	41	0	0	0	429	0	*0*	470
0.0	39	1	0	0	431	29	*0*	500
0.5	38	4	0	11	386	61	*0*	500
1.0	34	5	0	25	349	84	*0*	497
1.5	35	2	0	39	312	112	*0*	500
2.0	33	0	0	71	244	146	*0*	494
2.5	28	0	0	93	226	153	*0*	500
3.0	12	0	0	106	206	176	*0*	500
3.5	5	0	0	196	184	194	*0*	578
4.0	0	0	0	91	164	245	*0*	500
4.5	0	0	0	71	121	308	*0*	500
5.0	*	*	*	*	*	*	*865*	865
6.0	*	*	*	*	*	*	*409*	409
7.0	*	*	*	*	*	*	*383*	383

Bulk Weight Percentages:

Wp	Gp	Bp	Xtal	Lithic	Glass	NA
0	0	0	0	0	0	0
0	0	0	0	0	0	0
0	0	0	0	0	0	0
0	0	0	0	0	0	0
0.38	0	0	0	2.35	0	0
0.12	0	0	0	0.80	0	0
0.06	0	0	0	1.21	0	0
0.12	0	0	0	1.56	0	0
0.18	0	0	0	3.07	0	0
0.26	0	0	0	4.66	0	0
0.30	0.01	0	0	5.42	0.33	0
0.37	0.08	0	0.17	6.36	0.93	0
0.43	0.07	0	0.42	6.06	1.29	0
0.21	0.04	0	0.50	4.07	1.25	0
0.10	0	0	0.65	2.23	1.18	0
0.08	0	0	0.59	1.43	0.90	0
0.05	0	0	0.90	1.75	1.36	0
0.02	0	0	1.28	1.21	0.99	0
0	0	0	1.10	1.99	2.36	0
0	0	0	2.47	4.21	8.46	0
*	*	*	*	*	*	14.22
*	*	*	*	*	*	4.63
*	*	*	*	*	*	2.76
2.68	**0.20**	**0**	**8.08**	**48.38**	**19.05**	**21.61**

S2 at Locality 71 [CBV-S-26b] [Total sample weight: 56072.2 mg]

Grain diameter		Weight Fractions		Granulometric Analysis						
ϕ	mm	weight [mg]	Cumulative weight %	ϕ_{05}	ϕ_{25}	ϕ_{10}	ϕ_{50}	Md$_\phi$	σ_ϕ	F2
-5.0	31.5	0	0	6.2	5.3	2.4	0.6	4.2	1.57	68.06%
-4.5	22.4	0	0							
-4.0	16.0	0	0							
-3.5	11.2	0	0							
-3.0	8.0	0	0							
-2.5	5.6	0	0							
-2.0	4.0	0	0							
-1.5	2.8	0	0							
-1.0	2.0	39.3	0.07							
-0.5	1.4	247.4	0.51							
0.0	1.0	468.3	1.35							
0.5	0.710	881.1	2.92							
1.0	0.500	1363.6	5.35							
1.5	0.355	1758.3	8.49							
2.0	0.250	2237.8	12.48							
2.5	0.180	2673.8	17.24							
3.0	0.125	4139.3	24.63							
3.5	0.088	4102.2	31.91							
4.0	0.063	5001.5	40.86							
4.5	0.045	12169.8	62.57							
5.0	0.032	10410	81.13							
6.0	0.017	6700	93.08							
7.0	0.008	3880	100.00							

Minor Lithic Counts		Abundance [volume %]	
SML	GCL	SML	GCL
n.a.	n.a.	n.a.	n.a.

Counts:

ϕ	Wp	Gp	Bp	Xtal	Lithic	Glass	NA	total counts
-5.0	0	0	0	0	0	0	0	0
-4.5	0	0	0	0	0	0	0	0
-4.0	0	0	0	0	0	0	0	0
-3.5	0	0	0	0	0	0	0	0
-3.0	0	0	0	0	0	0	0	0
-2.5	0	0	0	0	0	0	0	0
-2.0	0	0	0	0	0	0	0	0
-1.5	0	0	0	0	0	0	0	0
-1.0	0	0	0	0	3	0	0	3
-0.5	21	0	0	0	23	0	0	44
0.0	24	4	0	7	152	48	0	235
0.5	29	1	0	76	368	188	0	662
1.0	0	0	0	121	366	234	0	721
1.5	0	0	0	140	362	248	0	750
2.0	0	0	0	219	286	245	0	750
2.5	0	0	0	298	231	221	0	750
3.0	0	0	0	282	189	279	0	750
3.5	0	0	0	211	175	364	0	750
4.0	0	0	0	138	151	461	0	750
4.5	0	0	0	71	118	561	0	750
5.0	*	*	*	*	*	*	657	657
6.0	*	*	*	*	*	*	609	609
7.0	*	*	*	*	*	*	557	557

Bulk Weight Percentages:

Wp	Gp	Bp	Xtal	Lithic	Glass	NA
0	0	0	0	0	0	0
0	0	0	0	0	0	0
0	0	0	0	0	0	0
0	0	0	0	0	0	0
0	0	0	0	0	0	0
0	0	0	0	0	0	0
0	0	0	0	0	0	0
0	0	0	0	0	0	0
0	0	0	0	0.07	0	0
0.15	0	0	0	0.29	0	0
0.06	0.01	0	0.03	0.58	0.17	0
0.03	0	0	0.18	0.92	0.43	0
0	0	0	0.41	1.29	0.73	0
0	0	0	0.60	1.60	0.94	0
0	0	0	1.21	1.58	1.20	0
0	0	0	1.94	1.50	1.33	0
0	0	0	2.87	1.92	2.59	0
0	0	0	2.30	1.91	3.11	0
0	0	0	1.88	2.06	4.98	0
0	0	0	2.44	4.04	15.21	0
*	*	*	*	*	*	18.57
*	*	*	*	*	*	11.95
*	*	*	*	*	*	6.92
0.24	**0.01**	**0**	**13.86**	**17.76**	**30.69**	**37.44**

S2 at Locality 71 [CBV-S-26c] [Total sample weight: 32435 mg]

Grain diameter		Weight Fractions		Granulometric Analysis						
ϕ	mm	weight [mg]	Cumulative weight %	ϕ_{05}	ϕ_{25}	ϕ_{16}	ϕ_{S}	Md_{ϕ}	σ_{ϕ}	F2
-5.0	31.5	0	0	4.9	3.9	0.8	0.4	1.9	1.48	20.62%
-4.5	22.4	0	0							
-4.0	16.0	0	0							
-3.5	11.2	0	0							
-3.0	8.0	0	0							
-2.5	5.6	0	0							
-2.0	4.0	0	0							
-1.5	2.8	0	0							
-1.0	2.0	0	0							
-0.5	1.4	59.7	0.18							
0.0	1.0	463.8	1.61							
0.5	0.710	1651.2	6.70							
1.0	0.500	4040.8	19.16							
1.5	0.355	5350.4	35.66							
2.0	0.250	4874.9	50.69							
2.5	0.180	3479.1	61.41							
3.0	0.125	3492.1	72.18							
3.5	0.088	2336.7	79.38							
4.0	0.063	1714.5	84.67							
4.5	0.045	1824.8	90.30							
5.0	0.032	1560	95.11							
6.0	0.017	1055	98.36							
7.0	0.008	530	100.00							

Minor Lithic Counts		Abundance [volume %]	
SML	GCL	SML	GCL
n.a.	n.a.	n.a.	n.a.

Counts:

ϕ	Wp	Gp	Bp	Xtal	Lithic	Glass	NA	total counts
-5.0	0	0	0	0	0	0	0	0
-4.5	0	0	0	0	0	0	0	0
-4.0	0	0	0	0	0	0	0	0
-3.5	0	0	0	0	0	0	0	0
-3.0	0	0	0	0	0	0	0	0
-2.5	0	0	0	0	0	0	0	0
-2.0	0	0	0	0	0	0	0	0
-1.5	0	0	0	0	0	0	0	0
-1.0	1	0	0	0	0	0	0	1
-0.5	7	0	0	0	7	0	0	14
0.0	25	4	0	7	171	46	0	253
0.5	46	1	0	116	516	71	0	750
1.0	31	0	0	293	398	28	0	750
1.5	29	0	0	439	236	46	0	750
2.0	16	0	0	468	221	45	0	750
2.5	7	0	0	482	213	48	0	750
3.0	3	0	0	488	191	68	0	750
3.5	0	0	0	467	189	94	0	750
4.0	0	0	0	431	158	161	0	750
4.5	0	0	0	318	118	314	0	750
5.0	*	*	*	*	*	*	975	975
6.0	*	*	*	*	*	*	958	958
7.0	*	*	*	*	*	*	760	760

Bulk Weight Percentages:

Wp	Gp	Bp	Xtal	Lithic	Glass	NA
0	0	0	0	0	0	0
0	0	0	0	0	0	0
0	0	0	0	0	0	0
0	0	0	0	0	0	0
0	0	0	0	0	0	0
0	0	0	0	0	0	0
0	0	0	0	0	0	0
0	0	0	0	0	0	0
0.07	0	0	0	0	0	0
0.09	0	0	0	0.12	0	0
0.10	0.02	0	0.04	1.03	0.25	0
0.39	0	0	0.80	3.71	0.47	0
0.30	0	0	4.83	6.82	0.42	0
0.11	0	0	9.84	5.44	0.91	0
0.04	0	0	9.58	4.52	0.82	0
0.03	0	0	6.96	3.08	0.64	0
0	0	0	7.07	2.77	0.90	0
0	0	0	4.61	1.87	0.73	0
0	0	0	3.18	1.17	0.94	0
0	0	0	2.62	0.97	2.04	0
*	*	*	*	*	*	4.81
*	*	*	*	*	*	3.25
*	*	*	*	*	*	1.64
1.13	**0.02**	**0**	**49.53**	**31.50**	**8.12**	**9.70**

S2 at Locality 77 [CBV-S-28] [Total sample weight: 166840 mg]

Grain diameter		Weight Fractions:		Granulometric Analysis						
ϕ	mm	weight [mg]	Cumulative weight %	$\phi_{5.6}$	ϕ_{84}	ϕ_{16}	ϕ_{5}	Md_{ϕ}	σ_{ϕ}	F2
-5.0	31.5	0	0	5.9	4.9	1.7	0.7	3.9	1.6	56.99%
-4.5	22.4	0	0							
-4.0	16.0	0	0							
-3.5	11.2	0	0							
-3.0	8.0	0	0							
-2.5	5.6	0	0							
-2.0	4.0	68.1	0.04							
-1.5	2.8	638.1	0.42							
-1.0	2.0	517.2	0.73							
-0.5	1.4	986.8	1.32							
0.0	1.0	1730.7	2.36							
0.5	0.710	3910.8	4.71							
1.0	0.500	6850.5	8.81							
1.5	0.355	9316.6	14.40							
2.0	0.250	11751.2	21.44							
2.5	0.180	11118.5	28.10							
3.0	0.125	13575.1	36.24							
3.5	0.088	11288.9	43.01							
4.0	0.063	12226.3	50.33							
4.5	0.045	32647.3	69.90							
5.0	0.032	26015	85.50							
6.0	0.017	16740	95.53							
7.0	0.008	7455	100.00							

Minor Lithic Counts		Abundance [volume %]	
SML	GCL	SML	GCL
0	6	0	46.2
0	19	0	15.3
0	40	0	19.8
0	62	0	21.3
0	87	0	24.0
0	71	0	23.5
0	59	0	27.4
0	44	0	20.6
0	41	0	20.3

Counts:

ϕ	Wp	Gp	Bp	Xtal	Lithic	Glass	NA	total counts
-5.0	0	0	0	0	0	0	*0*	0
-4.5	0	0	0	0	0	0	*0*	0
-4.0	0	0	0	0	0	0	*0*	0
-3.5	0	0	0	0	0	0	*0*	0
-3.0	0	0	0	0	0	0	*0*	0
-2.5	0	0	0	0	0	0	*0*	0
-2.0	1	0	0	0	0	0	*0*	1
-1.5	15	4	0	0	3	0	*0*	22
-1.0	26	5	0	0	13	0	*0*	44
-0.5	148	6	0	0	124	0	*0*	278
0.0	291	5	0	3	202	1	*0*	500
0.5	187	3	0	12	291	7	*0*	500
1.0	76	3	0	44	362	18	*0*	500
1.5	48	0	0	112	302	38	*0*	500
2.0	31	0	0	169	215	85	*0*	500
2.5	24	0	0	161	214	101	*0*	500
3.0	24	0	0	156	202	118	*0*	500
3.5	0	0	0	141	186	173	*0*	500
4.0	0	0	0	125	152	223	*0*	500
4.5	0	0	0	98	119	283	*0*	500
5.0	*	*	*	*	*	*	*1626*	1626
6.0	*	*	*	*	*	*	*1522*	1522
7.0	*	*	*	*	*	*	*1065*	1065

Bulk Weight Percentages:

Wp	Gp	Bp	Xtal	Lithic	Glass	NA
0	0	0	0	0	0	0
0	0	0	0	0	0	0
0	0	0	0	0	0	0
0	0	0	0	0	0	0
0	0	0	0	0	0	0
0	0	0	0	0	0	0
0.04	0	0	0	0	0	0
0.10	0.15	0	0	0.14	0	0
0.13	0.04	0	0	0.14	0	0
0.24	0.01	0	0	0.34	0	0
0.48	0.01	0	0.01	0.54	0.01	0
0.82	0.02	0	0.06	1.42	0.03	0
0.48	0	0	0.37	3.12	0.14	0
0.26	0	0	1.31	3.62	0.39	0
0.15	0	0	2.53	3.22	1.13	0
0.14	0	0	2.24	2.98	1.30	0
0.23	0	0	2.65	3.43	1.83	0
0	0	0	2.06	2.72	1.98	0
0	0	0	2.02	2.45	2.86	0
0	0	0	4.35	5.29	9.93	0
*	*	*	*	*	*	15.59
*	*	*	*	*	*	10.03
*	*	*	*	*	*	4.47
3.07	**0.21**	**0**	**17.60**	**29.41**	**19.60**	**30.09**

S2 at Locality 82 [CBV-S-7] [Total sample weight: 173169.8 mg]

Grain diameter		Weight Fractions		Granulometric Analysis						
ϕ	mm	weight [mg]	Cumulative weight %	ϕ_{05}	ϕ_{84}	ϕ_{16}	ϕ_{κ}	Md_{ϕ}	σ_{ϕ}	F2
-5.0	31.5	0	0	6.2	4.9	0.6	-2.0	2.7		34.70%
-4.5	22.4	0	0							
-4.0	16.0	0	0							
-3.5	11.2	0	0							
-3.0	8.0	4201	2.43							
-2.5	5.6	4070	4.78							
-2.0	4.0	4691	5.05							
-1.5	2.8	6907	5.45							

Minor Lithic Counts		Abundance [volume %]	
SMI	GCL	SMI	GCL
n.a.	n.a.	n.a.	n.a.

-1.0	2.0	1158	6.11
-0.5	1.4	3826	8.32
0.0	1.0	5044	11.24
0.5	0.710	6635	15.07
1.0	0.500	9684	20.66
1.5	0.355	18041	31.08
2.0	0.250	13414	38.82
2.5	0.180	13948	46.88
3.0	0.125	19263	58.00
3.5	0.088	12641	65.30
4.0	0.063	12540	72.54
4.5	0.045	10289	78.49
5.0	0.032	15575	87.48
6.0	0.017	12220	94.54
7.0	0.008	9465	100.00

Counts:

ϕ	Wp	Gp	Bp	Xtal	Lithic	Glass	NA	total counts
-5.0	0	0	0	0	0	0	*0*	0
-4.5	0	0	0	0	0	0	*0*	0
-4.0	1	0	0	0	0	0	*0*	1
-3.5	1	0	0	0	0	0	*0*	1
-3.0	0	0	0	0	1	0	*0*	1
-2.5	1	0	0	0	1	0	*0*	2
-2.0	2	0	0	0	4	0	*0*	6
-1.5	3	6	0	0	15	0	*0*	24
-1.0	25	8	0	0	67	0	*0*	100
-0.5	83	15	0	1	314	0	*0*	413
0.0	197	2	0	4	547	0	*0*	750
0.5	120	0	0	32	598	0	*0*	750
1.0	44	1	0	130	538	37	*0*	750
1.5	26	*0*	*0*	250	379	95	*0*	750
2.0	4	0	0	467	184	95	*0*	750
2.5	9	0	0	495	153	93	*0*	750
3.0	3	0	0	540	120	87	*0*	750
3.5	0	0	0	256	50	248	*0*	554
4.0	0	0	0	245	43	233	*0*	521
4.5	0	0	0	255	26	452	*0*	733
5.0	*	*	*	*	*	*	*973*	973
6.0	*	*	*	*	*	*	*1140*	1140
7.0	*	*	*	*	*	*	*1351*	1351

Bulk Weight Percentages:

Wp	Gp	Bp	Xtal	Lithic	Glass	NA
0	0	0	0	0	0	0
0	0	0	0	0	0	0
0	0	0	0	0	0	0
0	0	0	0	0	0	0
0	0	0	0	2.43	0	0
0.19	0	0	0	2.16	0	0
0.05	0	0	0	0.22	0	0
0.02	0.11	0	0	0.27	0	0
0.39	0.01	0	0	0.27	0	0
1.15	0.03	0	0	1.03	0	0
1.71	0.01	0	0.06	1.14	0	0
0.79	0	0	0.03	2.42	0.58	0
0.10	0.01	0	0.27	2.49	2.73	0
0.09	0.40	0	1.69	2.75	5.48	0
0.05	0.02	0	3.57	2.72	1.39	0
0.06	0	0	4.47	2.21	1.31	0
0.03	0	0	8.42	1.31	1.37	0
0	0	0	3.74	0.73	2.83	0
0	0	0	3.75	0.66	2.83	0
0	0	0	2.38	0.24	3.32	0
*	*	*	*	*	*	8.99
*	*	*	*	*	*	7.06
*	*	*	*	*	*	5.46
4.63	**0.59**	**0**	**28.38**	**23.05**	**21.84**	**21.51**

S2 at Locality 83 [CBV-S-14] [Total sample weight: 251243.7 mg]

Grain diameter		Weight Fractions:		Granulometric Analysis						
ϕ	mm	weight [mg]	Cumulative weight %	$\phi_{5\%}$	ϕ_{25}	ϕ_{10}	ϕ_{50}	Md_ϕ	σ_ϕ	F2
-5.0	31.5	0	0	6.2	5.2	1.9	0.9	4.2	1.62	64.76%
-4.5	22.4	0	0							
-4.0	16.0	0	0							
-3.5	11.2	0	0							
-3.0	8.0	0	0							
-2.5	5.6	0	0							
-2.0	4.0	0	0							
-1.5	2.8	270.2	0.11							
-1.0	2.0	530.5	0.32							
-0.5	1.4	927.0	0.69							
0.0	1.0	1405.7	1.25							
0.5	0.710	4309.9	2.96							
1.0	0.500	6066.8	5.38							
1.5	0.355	11174.3	9.82							
2.0	0.250	16780.5	16.50							
2.5	0.180	15620.3	22.72							
3.0	0.125	15627.6	28.94							
3.5	0.088	15814.4	35.24							
4.0	0.063	18861.6	42.74							
4.5	0.045	56678.8	65.30							
5.0	0.032	45170	83.28							
6.0	0.017	29060	94.85							
7.0	0.008	12945	100.00							

	Minor Lithic Counts		Abundance [volume %]	
	SML	GCL	SML	GCL
-1.0	0	2	0	33.3
-0.5	0	2	0	2.1
0.0	0	3	0	1.8
0.5	0	2	0	1.2
1.0	0	0	0	0
1.5	0	0	0	0
2.0	0	0	0	0
2.5	0	0	0	0
3.0	0	0	0	0

Counts:

ϕ	Wp	Gp	Bp	Xtal	Lithic	Glass	NA	total counts
-5.0	0	0	0	0	0	0	*0*	0
-4.5	0	0	0	0	0	0	*0*	0
-4.0	0	0	0	0	0	0	*0*	0
-3.5	0	0	0	0	0	0	*0*	0
-3.0	0	0	0	0	0	0	*0*	0
-2.5	0	0	0	0	0	0	*0*	0
-2.0	0	0	0	0	0	0	*0*	0
-1.5	3	2	0	0	0	0	*0*	5
-1.0	15	6	0	0	6	0	*0*	27
-0.5	31	23	0	0	94	0	*0*	148
0.0	160	0	0	4	167	169	*0*	500
0.5	94	0	0	19	166	221	*0*	500
1.0	30	0	0	33	161	276	*0*	500
1.5	32	0	0	39	155	274	*0*	500
2.0	37	0	0	54	131	278	*0*	500
2.5	33	0	0	71	127	269	*0*	500
3.0	21	0	0	68	119	292	*0*	500
3.5	0	0	0	51	102	347	*0*	500
4.0	0	0	0	32	84	384	*0*	500
4.5	0	0	0	19	62	419	*0*	500
5.0	*	*	*	*	*	*	*2823*	2823
6.0	*	*	*	*	*	*	*2642*	1642
7.0	*	*	*	*	*	*	*1849*	1849

Bulk Weight Percentages:

ϕ	Wp	Gp	Bp	Xtal	Lithic	Glass	NA
-5.0	0	0	0	0	0	0	0
-4.5	0	0	0	0	0	0	0
-4.0	0	0	0	0	0	0	0
-3.5	0	0	0	0	0	0	0
-3.0	0	0	0	0	0	0	0
-2.5	0	0	0	0	0	0	0
-2.0	0	0	0	0	0	0	0
-1.5	0.06	0.05	0	0	0	0	0
-1.0	0.09	0.05	0	0	0.07	0	0
-0.5	0.05	0.04	0	0	0.28	0	0
0.0	0.13	0	0	0.01	0.22	0.20	0
0.5	0.33	0	0	0.07	0.59	0.73	0
1.0	0.12	0	0	0.17	0.85	1.28	0
1.5	0.15	0	0	0.38	1.56	2.36	0
2.0	0.19	0	0	0.81	1.97	3.71	0
2.5	0.19	0	0	0.96	1.71	3.36	0
3.0	0.14	0	0	0.91	1.59	3.57	0
3.5	0	0	0	0.76	1.51	4.03	0
4.0	0	0	0	0.57	1.50	5.44	0
4.5	0	0	0	1.02	3.40	18.12	0
5.0	*	*	*	*	*	*	17.98
6.0	*	*	*	*	*	*	11.57
7.0	*	*	*	*	*	*	5.15
	1.45	**0.14**	**0**	**5.66**	**15.25**	**42.80**	**34.70**

S2 at Locality 85 [CBV-S-16] [Total sample weight 196369.9 mg]

Grain diameter		Weight Fractions		Granulometric Analysis						
ϕ	mm	weight [mg]	Cumulative weight %	ϕ_{05}	ϕ_{25}	ϕ_{16}	ϕ_{5}	Md$_\phi$	σ_ϕ	F2
-5.0	31.5	0	0	6.0	4.9	0.8	-2.3	3.6	2.29	52.09%
-4.5	22.4	0	0							
-4.0	16.0	3001.4	1.53							
-3.5	11.2	877.5	1.98							
-3.0	8.0	1672.5	2.83							
-2.5	5.6	3049.5	4.38							
-2.0	4.0	4690.9	6.77							
-1.5	2.8	3371.5	8.49							

	Minor Lithic Counts		Abundance [volume %]	
	SML	GCL	SML	GCL
-1.0	2.0	3453.0	10.24	0	6	0	12.2
-0.5	1.4	2602.1	11.57	0	19	0	10.4
0.0	1.0	2192.1	12.69	0	40	0	26.5
0.5	0.710	3280.6	14.36	0	62	0	31.3
1.0	0.500	5590.6	17.20	0	87	0	39.2
1.5	0.355	7781.6	21.17	0	71	0	30.6
2.0	0.250	12468.3	27.52	0	59	0	21.9
2.5	0.180	12230.2	33.74	0	44	0	19.1
3.0	0.125	15305.5	41.54	0	41	0	18.1
3.5	0.088	12518.7	47.91				
4.0	0.063	12995.3	54.53				
4.5	0.045	35179.7	72.45				
5.0	0.032	28035	86.72				
6.0	0.017	18035	95.91				
7.0	0.008	8035	100.00				

Counts:

ϕ	Wp	Gp	Bp	Xtal	Lithic	Glass	NA	total counts
-5.0	0	0	0	0	0	0	*0*	0
-4.5	0	0	0	0	0	0	*0*	0
-4.0	0	0	0	0	1	0	*0*	1
-3.5	1	0	0	0	0	0	*0*	1
-3.0	3	0	0	0	0	0	*0*	3
-2.5	13	0	0	0	3	0	*0*	16
-2.0	42	3	0	0	13	0	*0*	58
-1.5	75	10	0	0	19	0	*0*	104
-1.0	206	8	0	0	49	0	*0*	263
-0.5	309	9	0	0	182	0	*0*	500
0.0	343	6	0	0	151	0	*0*	500
0.5	293	5	0	4	198	0	*0*	500
1.0	247	0	0	20	222	11	*0*	500
1.5	198	4	0	51	232	15	*0*	500
2.0	154	2	0	58	269	17	*0*	500
2.5	109	0	0	121	230	40	*0*	500
3.0	70	1	0	160	227	42	*0*	500
3.5	48	0	0	191	153	105	*0*	500
4.0	0	0	0	68	104	328	*0*	500
4.5	0	0	0	22	56	422	*0*	500
5.0	*	*	*	*	*	*	*1752*	1752
6.0	*	*	*	*	*	*	*1369*	1369
7.0	*	*	*	*	*	*	*1148*	1148

Bulk Weight Percentages:

Wp	Gp	Bp	Xtal	Lithic	Glass	NA
0	0	0	0	0	0	0
0	0	0	0	0	0	0
0	0	0	0	1.53	0	0
0.45	0	0	0	0	0	0
0.85	0	0	0	0	0	0
0.96	0	0	0	0.59	0	0
1.29	0.11	0	0	0.98	0	0
0.13	0.45	0	0	1.13	0	0
1.12	0.06	0	0	0.57	0	0
0.65	0.02	0	0	0.66	0	0
0.64	0.01	0	0	0.46	0	0
0.82	0.03	0	0.02	0.81	0	0
1.19	0	0	0.13	1.46	0.06	0
0.91	0.06	0	0.50	2.36	0.13	0
0.83	0.01	0	0.93	4.33	0.24	0
0.67	0	0	1.73	3.29	0.53	0
0.63	0.01	0	2.69	3.82	0.65	0
0.51	0	0	2.61	2.13	1.17	0
0	0	0	1.04	1.59	3.98	0
0	0	0	0.96	2.44	14.52	0
*	*	*	*	*	*	14.28
*	*	*	*	*	*	9.18
*	*	*	*	*	*	4.09
11.65	**0.76**	**0**	**10.61**	**28.15**	**21.28**	**27.55**

S2 at Locality 88 [CBV-S-23] [Total sample weight: 304558.7 mg]

Grain diameter		Weight Fractions:		Granulometric Analysis						
ϕ	mm	weight [mg]	Cumulative weight %	ϕ_{05}	ϕ_{25}	ϕ_{10}	$\phi_{<}$	Md_{ϕ}	σ_{ϕ}	F2
-5.0	31.5	0	0	6.3	5.4	0.3	-2.4	3.4	2.59	48.54
-4.5	22.4	0	0							
-4.0	16.0	0	0							
-3.5	11.2	0	0							
-3.0	8.0	13007	4.27							
-2.5	5.6	1244.2	4.68							
-2.0	4.0	3985.3	5.99							
-1.5	2.8	4310.1	7.40							

Minor Lithic Counts		Abundance [volume %]	
SML	GCL	SML	GCL
n.a.	n.a.	n.a.	n.a.

-1.0	2.0	4985.3	9.04
-0.5	1.4	7807.9	11.60
0.0	1.0	8968.3	14.55
0.5	0.710	13350.4	18.93
1.0	0.500	17304.4	24.61
1.5	0.355	16855.2	30.15
2.0	0.250	16862.5	35.68
2.5	0.180	14686.3	40.51
3.0	0.125	17043.0	46.10
3.5	0.088	16311.4	51.46
4.0	0.063	17672.9	57.26
4.5	0.045	15182.5	62.25
5.0	0.032	54340	80.09
6.0	0.017	37255	92.32
7.0	0.008	23390	100.00

Counts:

ϕ	Wp	Gp	Bp	Xtal	Lithic	Glass	NA	total counts
-5.0	0	0	0	0	0	0	*0*	0
-4.5	0	0	0	0	0	0	*0*	0
-4.0	0	0	0	0	0	0	*0*	0
-3.5	0	0	0	0	0	0	*0*	0
-3.0	1	0	2	0	0	0	*0*	3
-2.5	0	0	0	0	1	0	*0*	1
-2.0	14	0	4	0	25	0	*0*	43
-1.5	36	3	0	0	69	0	*0*	108
-1.0	95	10	0	0	233	0	*0*	338
-0.5	138	17	0	0	451	0	*0*	606
0.0	69	21	0	11	649	0	*0*	7750
0.5	52	17	0	54	627	0	*0*	750
1.0	63	14	*0*	196	465	12	*0*	750
1.5	39	4	0	302	338	67	*0*	750
2.0	23	3	0	384	222	118	*0*	750
2.5	14	0	0	363	198	175	*0*	750
3.0	0	0	0	473	133	143	*0*	749
3.5	0	0	0	260	147	187	*0*	594
4.0	0	0	0	168	115	240	*0*	523
4.5	0	0	0	128	44	328	*0*	500
5.0	*	*	*	*	*	*	*339*	339
6.0	*	*	*	*	*	*	*338*	338
7.0	*	*	*	*	*	*	*334*	334

Bulk Weight Percentages:

Wp	Gp	Bp	Xtal	Lithic	Glass	NA
0	0	0	0	0	0	0
0	0	0	0	0	0	0
0	0	0	0	0	0	0
0	0	0	0	0	0	0
0.45	0	2.75	0	0	0	0
0	0	0	0	1.07	0	0
0.24	0	0.13	0	0.51	0	0
0.20	0.03	0	0	0.94	0	0
0.26	0.04	0	0	1.18	0	0
0.38	0.05	0	0	1.34	0	0
0.17	0.06	0	0.04	2.14	0	0
0.24	0.13	0	0.31	2.67	0	0
0.36	0.09	0	1.48	3.71	0.08	0
0.14	0.04	0	2.28	3.66	0.44	0
0.06	0.01	0	2.95	2.63	0.81	0
0.04	0	0	2.40	1.71	1.07	0
0	0	0	3.59	1.31	0.99	0
0	0	0	2.52	1.01	1.42	0
0	0	0	2.06	1.42	2.33	0
0	0	0	1.48	1.41	3.42	0
*	*	*	*	*	*	17.84
*	*	*	*	*	*	12.23
*	*	*	*	*	*	7.68
2.54	**0.45**	**2.88**	**19.11**	**26.71**	**10.56**	**37.75**

S2 at Locality 93 [CBV-S-32] [Total sample weight 205753 mg]

Grain diameter		Weight Fractions		Granulometric Analysis						
ϕ	mm	weight [mg]	Cumulative weight %	ϕ_{5}	ϕ_{84}	ϕ_{16}	ϕ_{c}	Md_{ϕ}	σ_{ϕ}	F2
-5.0	31.5	0	0	5.7	4.9	0.4	-2.1	3.9	2.29	53.16%
-4.5	22.4	0	0							
-4.0	16.0	0	0							
-3.5	11.2	652.1	0.32							
-3.0	8.0	4585.4	2.55							
-2.5	5.6	3588.3	4.29							
-2.0	4.0	2027.1	5.27							
-1.5	2.8	3050.1	7.19							

Minor Lithic Counts		Abundance [volume %]	
SML	GCL	SML	GCL
n.a	n.a	n.a	n.a

-1.0	2.0	4507.4	9.30
-0.5	1.4	4787.4	11.71
0.0	1.0	4671.9	13.98
0.5	0.710	5345.6	16.58
1.0	0.500	5828.7	19.41
1.5	0.355	9825.0	24.19
2.0	0.250	11678.6	29.86
2.5	0.180	12249.8	35.82
3.0	0.125	13118.7	42.19
3.5	0.088	9556.2	46.84
4.0	0.063	10601.6	51.99
4.5	0.045	42672.4	72.73
5.0	0.032	34375	89.44
6.0	0.017	15800	97.12
7.0	0.008	5925	100.00

Counts:

ϕ	Wp	Gp	Bp	Xtal	Lithic	Glass	NA	total counts
-5.0	0	0	0	0	0	0	*0*	0
-4.5	0	0	0	0	0	0	*0*	0
-4.0	0	0	0	0	0	0	*0*	0
-3.5	1	0	0	0	0	0	*0*	1
-3.0	8	0	0	0	0	0	*0*	8
-2.5	5	0	0	0	0	0	*0*	5
-2.0	9	3	0	0	16	0	*0*	28
-1.5	42	6	0	2	57	0	*0*	107
-1.0	129	11	0	2	166	0	*0*	308
-0.5	151	10	0	24	251	0	*0*	436
0.0	172	0	0	31	315	0	*0*	518
0.5	152	0	0	79	319	0	*0*	550
1.0	136	0	0	102	318	11	*0*	567
1.5	112	0	0	116	288	12	*0*	528
2.0	83	0	0	95	255	15	*0*	448
2.5	79	0	0	71	211	41	*0*	402
3.0	64	0	0	62	201	60	*0*	387
3.5	36	0	0	38	98	94	*0*	266
4.0	36	0	0	28	61	140	*0*	247
4.5	18	0	0	13	21	466	*0*	500
5.0	*	*	*	*	*	*	*2148*	2148
6.0	*	*	*	*	*	*	*1438*	1438
7.0	*	*	*	*	*	*	*847*	847

Bulk Weight Percentages:

Wp	Gp	Bp	Xtal	Lithic	Glass	NA
0	0	0	0	0	0	0
0	0	0	0	0	0	0
0	0	0	0	0	0	0
0.32	0	0	0	0	0	0
2.23	0	0	0	0	0	0
0.18	0.04	0	0	1.53	0	0
0.14	0.06	0	0	0.78	0	0
0.36	0.06	0	0.01	1.49	0	0
0.56	0.07	0	0.02	1.54	0	0
0.56	0.04	0	0.15	1.59	0	0
0.53	0	0	0.15	1.59	0	0
0.52	0	0	0.40	1.68	0	0
0.54	0	0	0.53	1.72	0.05	0
0.53	0	0	1.17	2.98	0.11	0
0.82	0	0	1.38	3.70	0.19	0
0.57	0	0	1.19	3.55	0.64	0
0.62	0	0	1.12	3.64	0.99	0
0.55	0	0	0.74	1.91	1.44	0
0.34	0	0	0.67	1.47	2.67	0
0.12	0	0	0.67	1.08	18.99	0
*	*	*	*	*	*	16.71
*	*	*	*	*	*	7.68
*	*	*	*	*	*	2.88
8.93	**0.27**	**0**	**8.20**	**30.25**	**25.08**	**27.27**

S2 at Locality 94 [CBV-S-30] [Total sample weight: 199494 mg]

Grain diameter		Weight Fractions		Granulometric Analysis						
ϕ	mm	weight [mg]	Cumulative weight %	Φ_{84}	Φ_{84}	Φ_{16}	Φ_{50}	Md_Φ	σ_Φ	F2
-5.0	31.5	0	0	6.4	5.5	1.1	-1.9	4.2	2.35	57.68%
-4.5	22.4	0	0							
-4.0	16.0	0	0							
-3.5	11.2	0	0							
-3.0	8.0	5823	2.92							
-2.5	5.6	0	2.92							
-2.0	4.0	3579	4.71							
-1.5	2.8	2589	6.01							

Minor Lithic Counts		Abundance [volume %]	
SML	GCL	SML	GCL
n.a.	n.a.	n.a.	n.a.

-1.0	2.0	2499	7.26
-0.5	1.4	2863	8.70
0.0	1.0	3046	10.23
0.5	0.710	4092	12.28
1.0	0.500	6702	15.64
1.5	0.355	8776	20.04
2.0	0.250	10659	25.38
2.5	0.180	10722	30.75
3.0	0.125	12221	36.88
3.5	0.088	10845	42.32
4.0	0.063	12310	48.49
4.5	0.045	9668	53.33
5.0	0.032	40500	73.63
6.0	0.017	35940	91.65
7.0	0.008	16660	100.00

Counts:

ϕ	Wp	Gp	Bp	Xtal	Lithic	Glass	NA	total counts
-5.0	0	0	0	0	0	0	0	0
-4.5	0	0	0	0	0	0	0	0
-4.0	0	0	0	0	0	0	0	0
-3.5	0	0	0	0	0	0	0	0
-3.0	0	0	1	0	4	0	0	5
-2.5	0	0	0	0	0	0	0	0
-2.0	5	0	2	0	15	0	0	22
-1.5	12	6	0	0	37	0	0	55
-1.0	95	16	0	0	82	0	0	193
-0.5	498	0	0	0	252	0	0	750
0.0	397	0	0	2	351	0	0	750
0.5	416	0	0	19	315	0	0	750
1.0	299	0	0	21	425	5	0	750
1.5	234	2	0	34	429	51	0	750
2.0	164	0	0	65	422	99	0	750
2.5	81	0	0	87	329	253	0	750
3.0	39	0	0	128	242	341	0	750
3.5	16	0	0	113	25	403	0	557
4.0	8	0	0	108	33	399	0	548
4.5	0	0	0	132	28	369	0	529
5.0	*	*	*	*	*	*	*2531*	2531
6.0	*	*	*	*	*	*	*3267*	3267
7.0	*	*	*	*	*	*	*2381*	2381

Bulk Weight Percentages:

Wp	Gp	Bp	Xtal	Lithic	Glass	NA
0	0	0	0	0	0	0
0	0	0	0	0	0	0
0	0	0	0	0	0	0
0	0	0	0	0	0	0
0	0	0.62	0	2.30	0	0
0	0	0	0	0	0	0
0.20	0	0.14	0	1.46	0	0
0.08	0.01	0	0	1.21	0	0
0.41	0.10	0	0	0.75	0	0
0.77	0	0	0	0.67	0	0
0.62	0	0	0	0.90	0	0
0.84	0	0	0.07	1.15	0	0
0.81	0	0	0.10	2.14	0.02	0
0.76	0.02	0	0.24	3.07	0.31	0
0.46	0	0	0.55	3.58	0.75	0
0.27	0	0	0.68	2.58	1.84	0
0.18	0	0	1.12	2.11	2.72	0
0.15	0	0	1.32	0.29	3.68	0
0.08	0	0	1.44	0.44	4.21	0
0	0	0	1.42	0.30	3.13	0
*	*	*	*	*	*	20.30
*	*	*	*	*	*	18.01
*	*	*	*	*	*	8.35
5.90	**0.13**	**0.76**	**6.94**	**22.95**	**16.66**	**46.66**

S2 at Locality 99 [CBV-99-3] [Total sample weight: 35746.6 mg]

Grain diameter		Weight Fractions:		Granulometric Analysis						
ϕ	mm	weight [mg]	Cumulative weight %	ϕ_{05}	ϕ_{25}	ϕ_{10}	ϕ_{x}	Md_{ϕ}	σ_{ϕ}	F2
-5.0	31.5	0	0	5.5	4.4	-2.4	-3.2	1.9	2.99	30.44%
-4.5	22.4	0	0							
-4.0	16.0	0	0							
-3.5	11.2	0	0							
-3.0	8.0	2574.7	7.20							
-2.5	5.6	2262.8	13.53							
-2.0	4.0	2429.0	20.33							
-1.5	2.8	1475.9	24.46							

Minor Lithic Counts		Abundance [volume %]	
SML	GCL	SML	GCL
0	0	0	0
0	2	0	0.7
0	8	0	3.7
0	10	0	3.9
0	8	0	3.4
0	2	0	1.0
0	6	0	3.2
0	9	0	5.4
0	10	0	6.3

-1.0	2.0	1043.4	27.38
-0.5	1.4	1170.3	30.65
0.0	1.0	922.4	33.23
0.5	0.710	1310.4	36.90
1.0	0.500	1525.1	41.16
1.5	0.355	1746.5	46.05
2.0	0.250	1942.9	51.48
2.5	0.180	1948.6	56.93
3.0	0.125	2289.1	63.34
3.5	0.088	2225.3	69.56
4.0	0.063	2393.4	76.26
4.5	0.045	3682.5	86.56
5.0	0.032	2380	93.23
6.0	0.017	1535	97.52
7.0	0.008	890	100.00

Counts:

ϕ	Wp	Gp	Bp	Xtal	Lithic	Glass	NA	total counts
-5.0	0	0	0	0	0	0	*0*	0
-4.5	0	0	0	0	0	0	*0*	0
-4.0	0	0	0	0	0	0	*0*	0
-3.5	0	0	0	0	0	0	*0*	0
-3.0	1	0	0	0	2	0	*0*	3
-2.5	2	0	0	0	8	0	*0*	10
-2.0	4	1	1	0	16	0	*0*	22
-1.5	10	0	1	0	25	0	*0*	36
-1.0	31	3	5	0	46	0	*0*	85
-0.5	194	19	7	0	278	2	*0*	500
0.0	205	24	7	4	214	10	*0*	464
0.5	192	19	8	12	259	18	*0*	508
1.0	185	11	7	24	234	39	*0*	500
1.5	127	8	2	29	209	125	*0*	500
2.0	92	1	0	41	185	180	*0*	499
2.5	78	0	0	58	166	198	*0*	500
3.0	62	0	0	72	159	207	*0*	500
3.5	58	0	0	41	151	250	*0*	500
4.0	41	0	0	20	105	334	*0*	500
4.5	32	0	0	9	84	375	*0*	500
5.0	*	*	*	*	*	*	*1489*	1489
6.0	*	*	*	*	*	*	*1393*	1393
7.0	*	*	*	*	*	*	*1268*	1268

Bulk Weight Percentages:

Wp	Gp	Bp	Xtal	Lithic	Glass	NA
0	0	0	0	0	0	0
0	0	0	0	0	0	0
0	0	0	0	0	0	0
0	0	0	0	0	0	0
0.10	0	0	0	7.10	0	0
1.00	0	0	0	5.33	0	0
0.49	0.15	0.15	0	6.01	0	0
0.69	0	0.09	0	3.35	0	0
0.64	0.09	0.15	0	2.04	0	0
0.91	0.12	0.03	0	2.23	0.14	0
0.86	0.20	0.04	0.03	1.48	0.06	0
0.88	0.09	0.05	0.10	2.19	0.14	0
1.31	0.13	0.03	0.22	2.26	0.33	0
0.68	0.01	0	0.33	2.46	1.26	0
0.40	0	0	0.53	2.41	2.09	0
0.41	0	0	0.72	2.05	2.27	0
0.47	0	0	1.02	2.25	2.67	0
0.65	0	0	0.59	2.17	2.81	0
0.52	0	0	0.32	1.66	4.30	0
0	0	0	0.24	2.22	7.84	0
*	*	*	*	*	*	6.67
*	*	*	*	*	*	4.29
*	*	*	*	*	*	2.48
10.01	**0.79**	**0.54**	**4.10**	**47.21**	**23.91**	**13.44**

P3 at Locality 18 [13-38-1 (Lithic-rich base)] [Total sample weight: 1387830 mg]

Grain diameter		Weight Fractions		Granulometric Analysis						
ϕ	mm	weight [mg]	Cumulative weight %	ϕ_{5}	ϕ_{84}	ϕ_{16}	ϕ_{1}	Md_{ϕ}	σ_{ϕ}	F2
-5.0	31.5	16000	1.15	-0.6	-1.6	-4.2	-4.7	-2.9	1.29	0.00%
-4.5	22.4	113000	9.30							
-4.0	16.0	151000	20.18							
-3.5	11.2	187000	33.65							
-3.0	8.0	200000	48.06							
-2.5	5.6	193000	61.97							
-2.0	4.0	187830	75.50							
-1.5	2.8	121293.5	84.24							
-1.0	2.0	93506.7	90.98							
-0.5	1.4	64543.9	95.63							
0.0	1.0	31271.9	97.88							
0.5	0.710	14103.4	98.90							
1.0	0.500	5309.9	99.28							
1.5	0.355	2205.1	99.44							
2.0	0.250	1705.1	99.56							
2.5	0.180	6060	100.00							
3.0	0.125	0								
3.5	0.088	0								
4.0	0.063	0								
4.5	0.045	0								
5.0	0.032	0								
6.0	0.017	0								
7.0	0.008	0								

	Minor Lithic Counts		Abundance [volume %]	
	SMI.	GCI.	SMI.	GCI.
	6	2	3.2	1.1
	17	4	6.1	1.4
	28	8	7.5	2.1
	16	11	4.4	3.1
	8	10	2.3	2.9
	9	12	2.8	3.8
	8	11	2.7	3.8
	0	0	0	0
	0	0	0	0

Counts:

ϕ	Wp	Gp	Bp	Xtal	Lithic	Glass	NA	total counts
-5.0	3	0	n.a.	0	0	0	0	3
-4.5	14	4	n.a.	0	2	0	0	20
-4.0	25	23	n.a.	0	3	0	0	51
-3.5	59	24	n.a.	0	20	0	0	103
-3.0	321	59	n.a.	0	61	0	0	441
-2.5	986	144	n.a.	0	176	0	0	1308
-2.0	1987	206	n.a.	0	671	0	0	2866
-1.5	253	20	2	0	216	0	0	500
-1.0	277	21	2	0	190	0	0	500
-0.5	192	17	11	2	278	0	0	500
0.0	101	16	12	6	374	0	0	500
0.5	102	14	11	24	360	0	0	500
1.0	98	6	3	47	345	4	0	500
1.5	91	2	0	59	317	31	0	500
2.0	89	0	0	56	291	64	0	500
2.5	0	0	0	0	0	0	*	*
3.0	0	0	0	0	0	0	0	0
3.5	0	0	0	0	0	0	0	0
4.0	0	0	0	0	0	0	0	0
4.5	0	0	0	0	0	0	0	0
5.0	0	0	0	0	0	0	0	0
6.0	0	0	0	0	0	0	0	0
7.0	0	0	0	0	0	0	0	0

Bulk Weight Percentages:

Wp	Gp	Bp	Xtal	Lithic	Glass	NA
1.15	0	n.a.	0	0	0	0
4.05	1.21	n.a.	0	2.88	0	0
4.97	4.73	n.a.	0	1.18	0	0
7.48	1.44	n.a.	0	4.56	0	0
8.02	1.55	n.a.	0	4.85	0	0
7.72	1.49	n.a.	0	4.63	0	0
6.83	1.00	n.a.	0	5.59	0	0
3.21	0.35	0.07	0	4.31	0	0
2.55	0.28	0.01	0	3.75	0	0
1.27	0.12	0.23	0.02	3.17	0	0
0.30	0.06	0.16	0.03	1.85	0	0
0.13	0.04	0.08	0.05	0.80	0	0
0.60	0.0+	0.01	0.04	0.28	0.0+	0
0.10	0.0+	0	0.02	0.11	0.01	0
0.10	0	0	0.02	0.08	0.02	0
0	0	0	0	0	0	0.44
0	0	0	0	0	0	0
0	0	0	0	0	0	0
0	0	0	0	0	0	0
0	0	0	0	0	0	0
0	0	0	0	0	0	0
0	0	0	0	0	0	0
0	0	0	0	0	0	0
0	0	0	0	0	0	0
48.48	**12.27**	**0.56**	**0.18**	**38.04**	**0.03**	**0.44**

P3 at Locality 18 [13-38-2 (Coarse pumice level)] [Total sample weight: 9940000 mg]

Grain diameter		Weight Fractions:		Granulometric Analysis						
ϕ	mm	weight [mg]	Cumulative weight %	ϕ_{05}	ϕ_{50}	ϕ_{95}	ϕ_{5}	Md_{ϕ}	σ_{ϕ}	F2
-5.0	31.5	74000	7.44	-0.6	-1.8	-4.6	-5.2	-3.4	1.40	0.00%
-4.5	22.4	103000	17.81							
-4.0	16.0	153000	33.20							
-3.5	11.2	146000	47.89							
-3.0	8.0	125000	60.46							
-2.5	5.6	112000	71.73							
-2.0	4.0	100000	81.79							
-1.5	2.8	65044.9	88.33							
-1.0	2.0	48288.2	93.19							
-0.5	1.4	31739.9	96.39							
0.0	1.0	17576.1	98.15							
0.5	0.710	8593.1	99.02							
1.0	0.500	3612.4	99.38							
1.5	0.355	1899.0	99.57							
2.0	0.250	1642.0	99.74							
2.5	0.180	2405	100.00							
3.0	0.125	0								
3.5	0.088	0								
4.0	0.063	0								
4.5	0.045	0								
5.0	0.032	0								
6.0	0.017	0								
7.0	0.008	0								

Minor Lithic Counts		Abundance [volume %]	
SML	GCL	SML	GCL
12	1	7.7	0.6
12	8	4.9	3.3
11	10	3.1	2.8
10	14	3.1	4.3
9	26	2.8	8.0
11	22	3.4	6.9
8	21	2.7	7.1
0	0	0	0
0	0	0	0

Counts:

ϕ	Wp	Gp	Bp	Xtal	Lithic	Glass	NA	total counts
-5.0	4	0	n.a.	0	1	0	0	5
-4.5	10	15	n.a.	0	0	0	0	25
-4.0	30	13	n.a.	0	5	0	0	48
-3.5	56	22	n.a.	0	10	0	0	88
-3.0	239	44	n.a.	0	24	0	0	307
-2.5	678	96	n.a.	0	64	0	0	838
-2.0	3	21	n.a.	0	1	0	0	25
-1.5	334	21	19	0	126	0	0	500
-1.0	315	10	19	0	156	0	0	500
-0.5	315	12	11	2	246	0	0	500
0.0	229	10	6	7	358	0	0	500
0.5	119	7	4	59	326	0	0	500
1.0	83	3	0	84	327	3	0	500
1.5	72	2	0	92	320	14	0	500
2.0	58	0	0	121	294	27	0	500
2.5	0	0	0	0	0	0	*	*
3.0	0	0	0	0	0	0	0	0
3.5	0	0	0	0	0	0	0	0
4.0	0	0	0	0	0	0	0	0
4.5	0	0	0	0	0	0	0	0
5.0	0	0	0	0	0	0	0	0
6.0	0	0	0	0	0	0	0	0
7.0	0	0	0	0	0	0	0	0

Bulk Weight Percentages:

ϕ	Wp	Gp	Bp	Xtal	Lithic	Glass	NA
-5.0	1.94	0	n.a.	0	5.51	0	0
-4.5	4.04	6.32	n.a.	0	0	0	0
-4.0	8.65	3.88	n.a.	0	2.86	0	0
-3.5	9.75	1.81	n.a.	0	3.13	0	0
-3.0	8.31	1.61	n.a.	0	2.66	0	0
-2.5	7.49	1.41	n.a.	0	2.38	0	0
-2.0	0.86	8.50	n.a.	0	0.70	0	0
-1.5	3.52	0.30	0.33	0	2.39	0	0
-1.0	2.21	0.10	0.19	0	2.35	0	0
-0.5	1.08	0.06	0.05	0.02	1.96	0	0
0.0	0.29	0.03	0.02	0.03	1.41	0	0
0.5	0.13	0.02	0.0-	0.11	0.61	0	0
1.0	0.05	0	0	0.06	0.25	0.0-	0
1.5	0.01	0	0	0.04	0.13	0.01	0
2.0	0.01	0	0	0.04	0.11	0.01	0
2.5	0	0	0	0	0	0	0.26
3.0	0	0	0	0	0	0	0
3.5	0	0	0	0	0	0	0
4.0	0	0	0	0	0	0	0
4.5	0	0	0	0	0	0	0
5.0	0	0	0	0	0	0	0
6.0	0	0	0	0	0	0	0
7.0	0	0	0	0	0	0	0
	48.34	**24.04**	**0.59**	**0.30**	**26.45**	**0.02**	**0.26**

S3 at Locality 1[CBV-1-2] [Total sample weight 455835 mg]

Grain diameter		Weight Fractions		Granulometric Analysis						
ϕ	mm	weight [mg]	Cumulative weight %	ϕ_{05}	ϕ_{x}	ϕ_{16}	ϕ_{x}	Md_{ϕ}	σ_{ϕ}	F2
-5.0	31.5	0	0	5.9	4.9	0.4	-1.4	3.6	2.24	50.90%
-4.5	22.4	0	0							
-4.0	16.0	3700	0.81							
-3.5	11.2	0	0.81							
-3.0	8.0	1900	1.23							
-2.5	5.6	2400	1.76							
-2.0	4.0	4900	2.83							
-1.5	2.8	7100	4.89							
-1.0	2.0	16000	7.9							
-0.5	1.4	1600	8.25							
0.0	1.0	18600	12.33							
0.5	0.710	27900	18.45							
1.0	0.500	21700	23.21							
1.5	0.355	23900	28.45							
2.0	0.250	27100	34.40							
2.5	0.180	22600	39.36							
3.0	0.125	20700	43.90							
3.5	0.088	23700	49.10							
4.0	0.063	27500	55.13							
4.5	0.045	80585	72.81							
5.0	0.032	64225	86.90							
6.0	0.017	41315	95.96							
7.0	0.008	18410	100.00							

Minor Lithic Counts		Abundance [volume %]	
SMI.	GCI	SMI	GCI
n.a	n.a	n.a	n.a

Counts:

ϕ	Wp	Gp	Bp	Xtal	Lithic	Glass	NA	total counts
-5.0	0	0	0	0	0	0	*0*	0
-4.5	0	0	0	0	0	0	*0*	0
-4.0	0	1	0	0	0	0	*0*	1
-3.5	0	0	0	0	0	0	*0*	0
-3.0	0	1	0	0	2	0	*0*	3
-2.5	0	3	1	0	4	0	*0*	8
-2.0	0	12	3	0	19	10	*0*	44
-1.5	3	0	6	0	110	54	*0*	173
-1.0	3	0	0	1	165	331	*0*	500
-0.5	0	0	0	24	214	262	*0*	500
0.0	0	0	0	15	261	224	*0*	500
0.5	0	0	0	24	242	234	*0*	500
1.0	0	0	0	33	227	240	*0*	500
1.5	0	0	0	41	228	231	*0*	500
2.0	0	0	0	83	229	188	*0*	500
2.5	0	0	0	92	224	184	*0*	500
3.0	0	0	0	88	216	196	*0*	500
3.5	0	0	0	81	211	208	*0*	500
4.0	0	0	0	29	201	270	*0*	500
4.5	0	0	0	11	184	305	*0*	500
5.0	*	*	*	*	*	*	*401*	401
6.0	*	*	*	*	*	*	*376*	376
7.0	*	*	*	*	*	*	*263*	263

Bulk Weight Percentages:

Wp	Gp	Bp	Xtal	Lithic	Glass	NA
0	0	0	0	0	0	0
0	0	0	0	0	0	0
0	0.81	0	0	0	0	0
0	0	0	0	0	0	0
0	0.05	0	0	0.42	0	0
0	0.12	0.01	0	0.41	0	0
0	0.21	0.05	0	0.82	0.01	0
0.03	0	0.07	0	1.46	0.21	0
0.01	0	0	0.01	1.34	2.16	0
0	0	0	0.02	0.17	0.16	0
0	0	0	0.12	2.22	1.74	0
0	0	0	0.29	3.08	2.74	0
0	0	0	0.32	2.29	2.15	0
0	0	0	0.45	2.57	2.22	0
0	0	0	1.03	2.84	2.07	0
0	0	0	0.94	2.00	1.74	0
0	0	0	0.83	2.03	1.68	0
0	0	0	0.93	2.41	1.86	0
0	0	0	0.39	2.73	2.91	0
0	0	0	0.45	7.46	9.77	0
*	*	*	*	*	*	14.09
*	*	*	*	*	*	9.06
*	*	*	*	*	*	4.04
0.04	**1.19**	**0.13**	**5.78**	**34.25**	**31.42**	**27.19**

S3 at Locality 6 [CBV-6-2] | Total sample weight: 631782 mg]

Grain diameter		Weight Fractions		Granulometric Analysis						
ϕ	mm	weight [mg]	Cumulative weight %	ϕ_{05}	ϕ_{84}	ϕ_{16}	ϕ_{κ}	Md$_{\phi}$	σ_{ϕ}	F2
-5.0	31.5	0	0	5.9	4.8	-1.7	-3.4	2.1	3.02	39.92%
-4.5	22.4	0	0							
-4.0	16.0	15653.9	2.48							
-3.5	11.2	14254.8	4.73							
-3.0	8.0	7647.8	5.94							
-2.5	5.6	17530.6	8.72							
-2.0	4.0	19718.1	11.84							
-1.5	2.8	27474.4	16.19							
-1.0	2.0	34529.1	21.65							
-0.5	1.4	39307.6	27.88							
0.0	1.0	36229.6	33.61							
0.5	0.710	32209.6	38.71							
1.0	0.500	27520.2	43.06							
1.5	0.355	22982.4	46.70							
2.0	0.250	19658.8	49.81							
2.5	0.180	18109.9	52.68							
3.0	0.125	24684.6	56.11							
3.5	0.088	25038.0	60.08							
4.0	0.063	22887.2	63.70							
4.5	0.045	84170.0	77.02							
5.0	0.032	72015	88.42							
6.0	0.017	46330	95.75							
7.0	0.008	26830	100.00							

Minor Lithic Counts:		Abundance [volume %]	
SML	GCL	SML	GCL
10	0	3.0	0
9	0	2.8	0
8	0	2.5	0
3	0	1.1	0
2	0	1.0	0
3	0	1.5	0
3	0	1.5	0
1	0	0.5	0
0	0	0	0

Counts:

ϕ	Wp	Gp	Bp	Xtal	Lithic	Glass	NA	total counts
-5.0	0	0	0	0	0	0	*0*	0
-4.5	0	0	0	0	0	0	*0*	0
-4.0	0	0	0	0	2	0	*0*	2
-3.5	3	0	2	0	4	0	*0*	9
-3.0	9	0	1	0	3	0	*0*	13
-2.5	13	6	0	0	36	0	*0*	55
-2.0	30	3	0	0	109	16	*0*	158
-1.5	72	3	0	0	317	108	*0*	500
-1.0	33	5	0	0	332	130	*0*	500
-0.5	27	2	0	0	327	144	*0*	500
0.0	16	1	0	4	323	156	*0*	500
0.5	17	0	0	12	268	203	*0*	500
1.0	15	1	0	28	202	254	*0*	500
1.5	0	0	0	51	201	248	*0*	500
2.0	0	0	0	53	204	243	*0*	500
2.5	0	0	0	58	201	241	*0*	500
3.0	0	0	0	60	198	242	*0*	500
3.5	0	0	0	84	178	239	*0*	500
4.0	0	0	0	96	165	239	*0*	500
4.5	0	0	0	91	168	241	*0*	500
5.0	*	*	*	*	*	*	*451*	451
6.0	*	*	*	*	*	*	*421*	421
7.0	*	*	*	*	*	*	*384*	384

Bulk Weight Percentages:

ϕ	Wp	Gp	Bp	Xtal	Lithic	Glass	NA
-5.0	0	0	0	0	0	0	0
-4.5	0	0	0	0	0	0	0
-4.0	0	0	0	0	2.48	0	0
-3.5	0.59	0	0.40	0	1.27	0	0
-3.0	0.53	0	0.06	0	0.61	0	0
-2.5	0.22	0.11	0	0	2.44	0	0
-2.0	0.23	0.03	0	0	2.57	0.29	0
-1.5	0.20	0.03	0	0	2.69	1.43	0
-1.0	0.18	0.04	0	0	3.98	1.26	0
-0.5	0.25	0.02	0	0	4.45	1.54	0
0.0	0.12	0.01	0	0.05	3.86	1.70	0
0.5	0.10	0	0	0.12	2.87	2.00	0
1.0	0.10	0.01	0	0.25	1.89	2.10	0
1.5	0	0	0	0.39	1.58	1.67	0
2.0	0	0	0	0.35	1.34	1.42	0
2.5	0	0	0	0.34	1.19	1.33	0
3.0	0	0	0	0.43	1.42	1.58	0
3.5	0	0	0	0.74	1.57	1.65	0
4.0	0	0	0	0.77	1.33	1.52	0
4.5	0	0	0	2.70	4.98	5.64	0
5.0	*	*	*	*	*	*	11.40
6.0	*	*	*	*	*	*	7.33
7.0	*	*	*	*	*	*	4.25
	2.52	**0.25**	**0.46**	**6.14**	**42.52**	**25.13**	**22.98**

S3 at Locality 12 [CBV-12-7b] [Total sample weight: 73189.4 mg]

Grain diameter		Weight Fractions:		Granulometric Analysis						
ϕ	mm	weight [mg]	Cumulative weight %	ϕ_{05}	ϕ_{01}	ϕ_{10}	ϕ_5	Md$_\phi$	σ_ϕ	Fz
-5.0	31.5	0	0	4.8	3.7	-1.2	-1.7	0.7	2.20	19.38%
-4.5	22.4	0	0							
-4.0	16.0	0	0							
-3.5	11.2	0	0							
-3.0	8.0	0	0							
-2.5	5.6	1184.3	1.62							
-2.0	4.0	1356.6	3.47							
-1.5	2.8	3439.9	8.17							
-1.0	2.0	6787.3	17.45							
-0.5	1.4	8634.2	29.24							
0.0	1.0	7459.4	39.43							
0.5	0.710	6778.6	48.70							
1.0	0.500	5787.7	56.60							
1.5	0.355	4258.8	62.42							
2.0	0.250	3437.4	67.12							
2.5	0.180	3005.9	71.23							
3.0	0.125	3191.6	75.59							
3.5	0.088	3681.2	80.62							
4.0	0.063	4818.5	87.20							
4.5	0.045	3682.5	92.23							
5.0	0.032	2820	96.09							
6.0	0.017	1815	98.56							
7.0	0.008	1050	100.00							

Minor Lithic Counts		Abundance [volume %]	
SMI.	GCI	SMI.	GCI
7	3	2.5	1.1
7	3	2.5	1.1
8	2	2.6	0.6
10	3	3.4	1.0
14	3	5.3	1.1
12	4	4.1	1.4
15	2	5.2	0.7
10	4	3.5	1.4
7	4	2.3	1.3

Counts:

ϕ	Wp	Gp	Bp	Xtal	Lithic	Glass	NA	total counts
-5.0	0	0	0	0	0	0	*0*	0
-4.5	0	0	0	0	0	0	*0*	0
-4.0	0	0	0	0	0	0	*0*	0
-3.5	0	0	0	0	0	0	*0*	0
-3.0	0	0	0	0	0	0	*0*	0
-2.5	0	0	0	0	4	0	*0*	4
-2.0	2	0	1	0	11	0	*0*	14
-1.5	18	0	1	0	61	0	*0*	80
-1.0	74	6	7	4	276	0	*0*	367
-0.5	125	12	12	2	279	0	*0*	430
0.0	138	18	13	6	312	0	*0*	487
0.5	153	4	8	13	292	0	*0*	470
1.0	179	9	5	22	266	0	*0*	481
1.5	148	11	9	35	295	0	*0*	500
2.0	131	12	12	59	286	0	*0*	500
2.5	119	9	7	68	288	9	*0*	500
3.0	94	6	4	54	304	38	*0*	500
3.5	71	0	0	39	205	71	*0*	386
4.0	45	0	0	41	205	68	*0*	359
4.5	0	0	0	36	201	59	*0*	296
5.0	*	*	*	*	*	*	*1762*	1762
6.0	*	*	*	*	*	*	*1649*	1649
7.0	*	*	*	*	*	*	*1501*	1501

Bulk Weight Percentages:

ϕ	Wp	Gp	Bp	Xtal	Lithic	Glass	NA
-5.0	0	0	0	0	0	0	0
-4.5	0	0	0	0	0	0	0
-4.0	0	0	0	0	0	0	0
-3.5	0	0	0	0	0	0	0
-3.0	0	0	0	0	0	0	0
-2.5	0	0	0	0	1.62	0	0
-2.0	0.10	0	0.06	0	1.69	0	0
-1.5	0.61	0	0.05	0	4.04	0	0
-1.0	0.99	0.12	0.14	0.10	7.93	0	0
-0.5	2.33	0.23	0.23	0.06	8.94	0	0
0.0	2.02	0.30	0.22	0.14	7.51	0	0
0.5	1.88	0.12	0.11	0.29	6.86	0	0
1.0	2.41	0.13	0.17	0.39	4.90	0	0
1.5	0.92	0.21	0.06	0.49	4.03	0	0
2.0	0.51	0.06	0.03	0.70	3.37	0	0
2.5	0.49	0.04	0.02	0.66	2.79	0.08	0
3.0	0.49	0.03	0	0.53	2.96	0.34	0
3.5	0.79	0	0	0.55	2.90	0.79	0
4.0	0.78	0	0	0.80	4.02	1.06	0
4.5	0	0	0	0.64	3.57	0.83	0
5.0	*	*	*	*	*	*	3.85
6.0	*	*	*	*	*	*	2.48
7.0	*	*	*	*	*	*	1.44
	14.32	**1.24**	**1.09**	**5.35**	**67.13**	**3.10**	**7.77**

S3 at Locality 99 [CBV-99-1] [Total sample weight 1816710 mg]

Grain diameter		Weight fractions		Granulometric Analysis						
ϕ	mm	weight [mg]	Cumulative weight %	ϕ_{05}	ϕ_{25}	ϕ_{50}	ϕ_{75}	Md$_\phi$	σ_ϕ	Fz
-5.0	31.5	0	0	4.9	3.9	-2.7	-4.1	0.6	3.00	20.07%
-4.5	22.4	26500	1.46							
-4.0	16.0	69000	5.26							
-3.5	11.2	80700	9.70							
-3.0	8.0	72100	13.67							
-2.5	5.6	68900	17.46							
-2.0	4.0	74200	21.54							
-1.5	2.8	83800	26.16							
-1.0	2.0	89100	31.06							
-0.5	1.4	107700	36.99							
0.0	1.0	97500	42.36							
0.5	0.710	105700	48.17							
1.0	0.500	106900	54.06							
1.5	0.355	105100	59.84							
2.0	0.250	90900	64.85							
2.5	0.180	91500	69.88							
3.0	0.125	101300	75.46							
3.5	0.088	81200	79.93							
4.0	0.063	76200	84.12							
4.5	0.045	113640	90.38							
5.0	0.032	90560	95.36							
6.0	0.017	58260	98.57							
7.0	0.008	25960	100.00							

Minor Lithic Counts		Abundance [volume %]	
SML	GCL	SML	GCL
n.a.	n.a.	n.a.	n.a.

Counts:

ϕ	Wp	Gp	Bp	Xtal	Lithic	Glass	NA	total counts
-5.0	0	0	0	0	0	0	0	0
-4.5	0	0	0	0	1	0	0	1
-4.0	0	0	0	0	8	0	0	8
-3.5	8	0	0	0	24	0	0	32
-3.0	20	2	4	0	64	0	0	90
-2.5	58	6	19	0	163	0	0	246
-2.0	243	18	32	0	207	0	0	500
-1.5	188	16	28	0	268	0	0	500
-1.0	137	12	20	0	331	0	0	500
-0.5	106	17	0	2	368	0	0	500
0.0	71	25	0	9	395	0	0	500
0.5	76	29	0	13	381	0	0	500
1.0	61	32	0	27	378	0	0	500
1.5	75	27	0	36	356	0	0	500
2.0	86	21	0	49	305	30	0	500
2.5	71	14	0	83	283	43	0	500
3.0	78	9	0	111	210	90	0	500
3.5	63	0	0	134	199	104	0	500
4.0	41	0	0	129	183	147	0	500
4.5	0	0	0	121	178	201	0	500
5.0	*	*	*	*	*	*	566	566
6.0	*	*	*	*	*	*	529	529
7.0	*	*	*	*	*	*	371	371

Bulk Weight Percentages:

ϕ	Wp	Gp	Bp	Xtal	Lithic	Glass	NA
-5.0	0	0	0	0	0	0	0
-4.5	0	0	0	0	1.46	0	0
-4.0	0	0	0	0	3.80	0	0
-3.5	0	0	0	0	4.18	0	0
-3.0	0.26	0.03	0.07	0	3.55	0	0
-2.5	0.32	0.04	0.13	0	3.33	0	0
-2.0	0.30	0.07	0.13	0	3.44	0	0
-1.5	0.44	0.13	0.13	0	3.57	0	0
-1.0	0.79	0.10	0.16	0	3.90	0	0
-0.5	0.75	0.14	0.06	0.03	4.89	0	0
0.0	0.82	0.20	0	0.10	4.57	0	0
0.5	0.50	0.45	0.01	0.15	4.70	0	0
1.0	0.51	0.32	0.02	0.32	4.67	0	0
1.5	0.55	0.45	0.09	0.43	4.38	0	0
2.0	0.42	0.10	0.04	0.58	3.62	0.32	0
2.5	0.34	0.08	0.03	0.94	3.19	0.45	0
3.0	0.34	0.06	0.01	1.37	2.60	1.02	0
3.5	0.52	0	0	1.29	1.92	0.78	0
4.0	0.48	0	0	1.17	1.66	1.06	0
4.5	0.30	0	0	1.65	2.43	2.17	0
5.0	*	*	*	*	*	*	4.98
6.0	*	*	*	*	*	*	3.21
7.0	*	*	*	*	*	*	1.43
	7.64	**2.17**	**0.88**	**8.03**	**65.86**	**5.80**	**9.62**

P4 at Locality 18 [13-38-3 (Coarse pumice base)] [Total sample weight: 1027000 mg]

Grain diameter		Weight Fractions		Granulometric Analysis						
ϕ	mm	weight [mg]	Cumulative weight %	ϕ_{05}	ϕ_{25}	ϕ_{50}	ϕ_{75}	Md$_\phi$	σ_ϕ	F2
-5.0	31.5	17000	1.66	-0.4	-1.7	-4.3	-4.7	-3.3	1.30	0.00%
-4.5	22.4	74000	8.86							
-4.0	16.0	189000	27.26							
-3.5	11.2	175000	44.30							
-3.0	8.0	130000	56.96							
-2.5	5.6	115000	68.16							
-2.0	4.0	113000	79.16							
-1.5	2.8	74529.1	86.42							
-1.0	2.0	50440.7	91.33							
-0.5	1.4	35052.0	94.74							
0.0	1.0	17580.9	96.46							
0.5	0.710	13886.4	97.81							
1.0	0.500	7444.5	98.53							
1.5	0.355	5865.9	99.10							
2.0	0.250	3832.4	99.48							
2.5	0.180	5368	100.00							
3.0	0.125	0								
3.5	0.088	0								
4.0	0.063	0								
4.5	0.045	0								
5.0	0.032	0								
6.0	0.017	0								
7.0	0.008	0								

	Minor Lithic Counts		Abundance [volume %]	
	SML	GCL	SML	GCL
	11	0	4.6	0
	14	2	5.1	0.7
	15	2	4.7	0.6
	14	5	4.6	1.7
	12	4	4.1	1.4
	12	3	4.4	1.1
	11	3	4.2	1.2
	0	0	0	0
	0	0	0	0

Counts:

ϕ	Wp	Gp	Bp	Xtal	Lithic	Glass	NA	total counts
-5.0	4	0	n.a.	0	0	0	0	4
-4.5	9	3	n.a.	0	1	0	0	13
-4.0	57	9	n.a.	0	0	0	0	66
-3.5	70	11	n.a.	0	14	0	0	95
-3.0	264	19	n.a.	0	29	0	0	312
-2.5	724	41	n.a.	0	78	0	0	848
-2.0	328	16	n.a.	0	148	0	0	500
-1.5	247	13	5	0	232	0	0	500
-1.0	254	3	8	0	241	0	0	500
-0.5	209	14	8	2	273	0	0	500
0.0	152	20	2	11	317	0	0	500
0.5	171	12	2	15	302	0	0	500
1.0	182	3	0	19	292	4	0	500
1.5	133	2	0	62	274	29	0	500
2.0	130	0	0	87	259	24	0	500
2.5	0	0	0	0	0	0	*	*
3.0	0	0	0	0	0	0	0	0
3.5	0	0	0	0	0	0	0	0
4.0	0	0	0	0	0	0	0	0
4.5	0	0	0	0	0	0	0	0
5.0	0	0	0	0	0	0	0	0
6.0	0	0	0	0	0	0	0	0
7.0	0	0	0	0	0	0	0	0

Bulk Weight Percentages:

Wp	Gp	Bp	Xtal	Lithic	Glass	NA
1.66	0	n.a.	0	0	0	0
3.79	1.32	n.a.	0	2.10	0	0
15.82	2.58	n.a.	0	0	0	0
11.89	0.88	n.a.	0	4.27	0	0
8.88	0.67	n.a.	0	3.10	0	0
7.64	0.57	n.a.	0	2.77	0	0
4.98	0.57	n.a.	0	4.99	0	0
2.57	0.34	0.22	0	4.36	0	0
1.60	0.19	0.15	0	3.26	0	0
1.02	0.03	0.14	0.02	2.29	0	0
0.36	0.07	0.02	0.04	1.25	0	0
0.28	0.05	0.01	0.05	0.97	0	0
0.21	0.05	0	0.03	0.47	0.01	0
0.08	0.05	0	0.08	0.37	0.03	0
0.04	0	0	0.08	0.24	0.02	0
0	0	0	0	0	0	0.52
0	0	0	0	0	0	0
0	0	0	0	0	0	0
0	0	0	0	0	0	0
0	0	0	0	0	0	0
0	0	0	0	0	0	0
0	0	0	0	0	0	0
0	0	0	0	0	0	0
0	0	0	0	0	0	0
60.82	**7.32**	**0.54**	**0.30**	**30.44**	**0.06**	**0.52**

P4 at Locality 18 [13-38-4 (Lithic-rich top)] [Total sample weight 1296000 mg]

Grain diameter		Weight Fractions		Granulometric Analysis						
ϕ	mm	weight [mg]	Cumulative weight %	ϕ_{5}	ϕ_{16}	ϕ_{50}	ϕ_{84}	Md.	σ_{ϕ}	Fz
-5.0	31.5	0	0	-0.8	-1.6	-4.4	-4.6	-2.9	1.28	0.00%
-4.5	22.4	196000	15.12							
-4.0	16.0	73000	20.76							
-3.5	11.2	135000	31.17							
-3.0	8.0	221000	48.23							
-2.5	5.6	214000	64.74							
-2.0	4.0	160000	77.08							
-1.5	2.8	138424	87.76							
-1.0	2.0	73741	93.45							
-0.5	1.4	46717	97.06							
0.0	1.0	22559	98.80							
0.5	0.710	10154	99.58							
1.0	0.500	2643	99.79							
1.5	0.355	1083	99.87							
2.0	0.250	981	99.95							
2.5	0.180	670	100.00							
3.0	0.125	0								
3.5	0.088	0								
4.0	0.063	0								
4.5	0.045	0								
5.0	0.032	0								
6.0	0.017	0								
7.0	0.008	0								

Minor Lithic Counts		Abundance [volume %]	
SML	GCL	SML	GCL
24	0	6.9	0
25	0	6.7	0
21	9	6.2	2.7
19	14	5.1	3.7
15	27	3.8	6.9
19	26	5.3	7.2
25	24	8.0	7.7
0	0	0	0
0	0	0	0

Counts:

ϕ	Wp	Gp	Bp	Xtal	Lithic	Glass	NA	total counts
-5.0	0	0	n.a.	0	0	0	0	0
-4.5	8	11	n.a.	0	6	0	0	25
-4.0	5	15	n.a.	0	3	0	0	23
-3.5	22	33	n.a.	0	23	0	0	78
-3.0	181	121	n.a.	0	104	0	0	406
-2.5	543	286	14	0	303	0	0	1146
-2.0	328	38	42	0	326	0	0	734
-1.5	79	30	59	0	322	0	0	500
-1.0	84	31	36	0	349	0	0	500
-0.5	81	36	11	0	372	0	0	500
0.0	111	38	22	1	338	0	0	500
0.5	73	21	14	16	375	1	0	500
1.0	48	9	0	48	393	2	0	500
1.5	78	6	0	54	360	2	0	500
2.0	116	4	0	66	312	2	0	500
2.5	0	0	0	0	0	0	*	*
3.0	0	0	0	0	0	0	0	0
3.5	0	0	0	0	0	0	0	0
4.0	0	0	0	0	0	0	0	0
4.5	0	0	0	0	0	0	0	0
5.0	0	0	0	0	0	0	0	0
6.0	0	0	0	0	0	0	0	0
7.0	0	0	0	0	0	0	0	0

Bulk Weight Percentages:

ϕ	Wp	Gp	Bp	Xtal	Lithic	Glass	NA
-5.0	0	0	n.a.	0	0	0	0
-4.5	2.45	3.51	n.a.	0	9.16	0	0
-4.0	1.06	3.30	n.a.	0	1.27	0	0
-3.5	2.91	2.06	n.a.	0	5.45	0	0
-3.0	4.83	3.40	n.a.	0	8.83	0	0
-2.5	4.49	3.13	0.48	0	8.41	0	0
-2.0	3.27	0.54	0.51	0	8.02	0	0
-1.5	1.03	0.54	1.29	0	7.82	0	0
-1.0	0.51	0.27	0.32	0	4.58	0	0
-0.5	0.38	0.17	0.05	0	3.00	0	0
0.0	0.27	0.08	0.06	0.02	1.35	0	0
0.5	0.10	0.04	0.01	0.02	0.60	0.0+	0
1.0	0.01	0	0	0.01	0.17	0.0+	0
1.5	0.01	0	0	0.01	0.07	0.0+	0
2.0	0.01	0	0	0.0+	0.06	0.0+	0
2.5	0	0	0	0	0	0	0.05
3.0	0	0	0	0	0	0	0
3.5	0	0	0	0	0	0	0
4.0	0	0	0	0	0	0	0
4.5	0	0	0	0	0	0	0
5.0	0	0	0	0	0	0	0
6.0	0	0	0	0	0	0	0
7.0	0	0	0	0	0	0	0
	21.33	**17.04**	**2.72**	**0.06**	**58.79**	**0.01**	**0.05**

F2 at Locality 12 [CBV-12-3] [Total sample weight 1458621 mg]

Grain diameter		Weight Fractions		Granulometric Analysis						
ϕ	mm	weight [mg]	Cumulative weight %	ϕ_5	ϕ_{16}	ϕ_{50}	ϕ_{84}	Md	σ_ϕ	F2
-5.0	31.5	48387	3.32	5.5	4.3	-3.4	-4.7	0.2	3.47	22.00%
-4.5	22.4	76104	8.53							
-4.0	16.0	42493	11.45							
-3.5	11.2	64214	15.85							
-3.0	8.0	61710	20.08							
-2.5	5.6	66246	24.62							
-2.0	4.0	65291	29.10							
-1.5	2.8	78011	34.45							
-1.0	2.0	70234	39.26							
-0.5	1.4	69287	44.04							
0.0	1.0	69899	48.32							
0.5	0.710	69340	53.08							
1.0	0.500	66773	57.66							
1.5	0.355	70264	62.47							
2.0	0.250	63096	66.80							
2.5	0.180	59719	70.89							
3.0	0.125	58169	74.88							
3.5	0.088	45443	78.00							
4.0	0.063	43176	80.96							
4.5	0.045	101940	87.95							
5.0	0.032	87220	93.93							
6.0	0.017	56110	97.77							
7.0	0.008	32500	100.00							

Minor Lithic Counts		Abundance [volume %]	
SMI	GCI	SMI	GCI
14	0	4.8	0
14	5	4.3	1.5
13	10	3.6	2.8
10	16	2.7	4.3
9	24	2.5	6.8
15	16	4.3	4.6
19	14	6.1	4.5
20	15	6.7	5.1
18	16	6.2	5.5

Counts:

ϕ	Wp	Gp	Bp	Xtal	Lithic	Glass	NA	total counts
-5.0	0	0	0	0	1	0	*0*	1
-4.5	0	2	0	0	3	0	*0*	5
-4.0	0	2	4	0	4	0	*0*	10
-3.5	2	3	4	0	15	0	*0*	24
-3.0	17	5	12	0	41	0	*0*	75
-2.5	76	9	17	0	121	0	*0*	223
-2.0	329	58	48	0	293	0	*0*	728
-1.5	186	11	11	0	292	0	*0*	500
-1.0	179	21	6	0	294	0	*0*	500
-0.5	139	34	2	0	325	0	*0*	500
0.0	79	48	0	9	361	6	*0*	500
0.5	71	39	0	11	372	7	*0*	500
1.0	65	35	0	31	354	15	*0*	500
1.5	74	28	0	39	345	14	*0*	500
2.0	92	21	0	64	311	12	*0*	500
2.5	61	19	0	92	297	31	*0*	500
3.0	24	11	0	133	290	42	*0*	500
3.5	0	0	0	112	304	84	*0*	500
4.0	0	0	0	98	297	105	*0*	500
4.5	0	0	0	64	300	136	*0*	500
5.0	*	*	*	*	*	*	*5451*	5451
6.0	*	*	*	*	*	*	*5108*	5108
7.0	*	*	*	*	*	*	*4642*	4642

Bulk Weight Percentages:

Wp	Gp	Bp	Xtal	Lithic	Glass	NA
0	0	0	0	3.32	0	0
0	1.38	0	0	3.83	0	0
0	0.31	0	0	2.60	0	0
0.21	0.13	0.24	0	3.82	0	0
0.39	0.09	0.03	0	3.72	0	0
0.56	0.07	0.27	0	3.63	0	0
1.07	0.23	0.20	0	2.98	0	0
1.25	0.06	0.40	0	3.63	0	0
1.02	0.17	0.05	0	3.58	0	0
0.90	0.23	0.01	0	3.61	0	0
0.46	0.32	0	0.05	3.43	0.05	0
0.45	0.48	0	0.10	3.66	0.06	0
0.46	0.27	0	0.29	3.43	0.13	0
0.35	0.39	0	0.39	3.56	0.12	0
0.31	0.09	0	0.65	3.17	0.11	0
0.24	0.09	0	0.83	2.68	0.26	0
0.11	0.05	0	1.10	2.41	0.32	0
0	0	0	0.72	1.97	0.43	0
0	0	0	0.61	1.84	0.52	0
0	0	0	0.95	4.45	1.59	0
*	*	*	*	*	*	5.98
*	*	*	*	*	*	3.85
*	*	*	*	*	*	2.23
7.78	**4.36**	**1.20**	**5.69**	**65.32**	**3.59**	**12.06**

F3 Pumice Lens at Locality 12 [CBV-12-4] [Total sample weight: 711947.6 mg]

Grain diameter		Weight Fractions		Granulometric Analysis						
ϕ	mm	weight [mg]	Cumulative weight %	ϕ_{05}	ϕ_{84}	ϕ_{16}	ϕ_{50}	Md$_\phi$	σ_ϕ	F2
-5.0	31.5	151936.1	21.34	2.2	-1.2	-5.0	-5.0	-2.9	2.20	4.07%
-4.5	22.4	111282	22.90							
-4.0	16.0	27751	26.81							
-3.5	11.2	58147.1	34.97							
-3.0	8.0	83892.3	46.76							
-2.5	5.6	83463.7	58.48							
-2.0	4.0	76259.0	69.19							
-1.5	2.8	64135.7	78.20							
-1.0	2.0	49473.7	85.15							
-0.5	1.4	38962.9	90.62							
0.0	1.0	17173.8	93.03							
0.5	0.710	7802.2	94.13							
1.0	0.500	1508.1	94.34							
1.5	0.355	2281.2	94.66							
2.0	0.250	2288.4	94.98							
2.5	0.180	2065.4	95.27							
3.0	0.125	2463.5	95.62							
3.5	0.088	2186.3	95.93							
4.0	0.063	2587.9	96.29							
4.5	0.045	9761.7	97.66							
5.0	0.032	8970	98.92							
6.0	0.017	5315	99.67							
7.0	0.008	2370	100.00							

Minor Lithic Counts		Abundance [volume %]	
SML	GCL	SML	GCL
17	0	3.8	0
28	0	5.9	0
20	0	4.4	0
27	0	6.1	0
30	6	6.9	1.4
28	38	6.7	9.1
25	76	6.4	19.3
31	71	8.5	19.6
38	67	13.2	23.3

Counts:

ϕ	Wp	Gp	Bp	Xtal	Lithic	Glass	NA	total counts
-5.0	0	0	0	0	1	0	*0*	1
-4.5	0	1	1	0	0	0	*0*	2
-4.0	0	1	1	0	3	0	*0*	5
-3.5	0	5	6	0	14	0	*0*	25
-3.0	5	13	10	0	61	0	*0*	89
-2.5	10	34	7	0	196	0	*0*	247
-2.0	10	8	3	0	374	0	*0*	395
-1.5	39	35	5	0	421	0	*0*	500
-1.0	30	24	0	0	446	0	*0*	500
-0.5	7	16	0	3	474	0	*0*	500
0.0	11	25	2	3	459	0	*0*	500
0.5	19	23	0	16	442	0	*0*	500
1.0	32	6	0	28	434	0	*0*	500
1.5	26	4	0	52	416	2	*0*	500
2.0	26	3	0	70	393	8	*0*	500
2.5	21	5	0	93	363	18	*0*	500
3.0	24	8	0	148	288	32	*0*	500
3.5	0	0	0	161	290	49	*0*	500
4.0	0	0	0	107	314	79	*0*	500
4.5	0	0	0	92	304	104	*0*	500
5.0	*	*	*	*	*	*	*560*	560
6.0	*	*	*	*	*	*	*483*	483
7.0	*	*	*	*	*	*	*338*	338

Bulk Weight Percentages:

Wp	Gp	Bp	Xtal	Lithic	Glass	NA
0	0	0	0	21.34	0	0
0	1.59	0	0	0	0	0
0	0.31	0	0	3.59	0	0
0	0.58	1.46	0	6.13	0	0
0.26	0.72	0.53	0	10.27	0	0
0.16	0.71	0.46	0	10.39	0	0
0.11	0.13	0.04	0	10.43	0	0
0.41	0.50	0.09	0	8.00	0	0
0.20	0.24	0	0	6.51	0	0
0.05	0.11	0	0.03	5.29	0	0
0.03	0.09	0.01	0.01	2.27	0	0
0.01	0.06	0	0.03	0.98	0	0
0.01	0	0	0.01	0.19	0	0
0.01	0	0	0.03	0.27	0.00	0
0.01	0	0	0.05	0.26	0.00	0
0.01	0	0	0.06	0.22	0.01	0
0.01	0	0	0.11	0.21	0.02	0
0	0	0	0.10	0.18	0.02	0
0	0	0	0.08	0.24	0.05	0
0	0	0	0.26	0.87	0.24	0
*	*	*	*	*	*	1.26
*	*	*	*	*	*	0.75
*	*	*	*	*	*	0.33
1.28	**5.04**	**2.59**	**0.77**	**87.64**	**0.34**	**2.34**

F3 at Locality 12 [CBV-12-5] [Total sample weight 165438.5 mg]

Grain diameter		Weight Fractions:		Granulometric Analysis						
ϕ	mm	weight [mg]	Cumulative weight %	ϕ_{05}	ϕ_{25}	ϕ_{50}	ϕ_{75}	Md$_\phi$	σ_ϕ	F2
-5.0	31.5	0	0	4.4	1.7	-4.7	-4.9	-2.7	2.98	8.81%
-4.5	22.4	44103	26.66							
-4.0	16.0	10225	32.84							
-3.5	11.2	15614	42.28							
-3.0	8.0	11049	48.96							
-2.5	5.6	8455	54.07							
-2.0	4.0	6144	57.78							
-1.5	2.8	8589	62.97							
-1.0	2.0	7678	67.61							
-0.5	1.4	6675	71.65							
0.0	1.0	5627	75.05							
0.5	0.710	5325	78.27							
1.0	0.500	4934	81.25							
1.5	0.355	4183	83.78							
2.0	0.250	3836	86.10							
2.5	0.180	2933	87.87							
3.0	0.125	3118	89.75							
3.5	0.088	2378	91.19							
4.0	0.063	2405	92.65							
4.5	0.045	4823	95.56							
5.0	0.032	3800	97.86							
6.0	0.017	2450	99.34							
7.0	0.008	1090	100.00							

Minor Lithic Counts:		Abundance [volume %]	
SML	GCL	SML	GCL
5	0	1.7	0
17	4	5.4	1.3
25	10	7.1	2.8
23	11	6.6	3.2
25	6	7.3	1.7
28	5	8.3	1.5
30	2	9.2	0.6
33	7	11.0	2.3
38	4	13.9	1.5

Counts:

ϕ	Wp	Gp	Bp	Xtal	Lithic	Glass	NA	total counts
-5.0	0	0	0	0	0	0	*0*	0
-4.5	0	0	0	0	2	0	*0*	2
-4.0	1	0	0	0	1	0	*0*	2
-3.5	0	1	0	0	5	0	*0*	6
-3.0	4	1	0	0	9	0	*0*	14
-2.5	12	6	0	0	18	0	*0*	36
-2.0	28	14	0	0	34	0	*0*	76
-1.5	73	34	8	0	113	0	*0*	228
-1.0	181	26	7	0	286	0	*0*	500
-0.5	162	14	12	0	312	0	*0*	500
0.0	106	15	0	19	354	6	*0*	500
0.5	109	16	0	24	349	2	*0*	500
1.0	107	11	5	23	344	10	*0*	500
1.5	98	5	6	42	337	12	*0*	500
2.0	92	4	1	56	327	20	*0*	500
2.5	61	6	0	92	299	42	*0*	500
3.0	28	0	0	125	273	74	*0*	500
3.5	0	0	0	112	297	91	*0*	500
4.0	0	0	0	103	279	118	*0*	500
4.5	0	0	0	51	204	245	*0*	500
5.0	*	*	*	*	*	*	*237*	237
6.0	*	*	*	*	*	*	*222*	222
7.0	*	*	*	*	*	*	*159*	159

Bulk Weight Percentages:

Wp	Gp	Bp	Xtal	Lithic	Glass	NA
0	0	0	0	0	0	0
0	0	0	0	24.90	0	0
1.58	0	0	0	4.60	0	0
0	0	0	0	9.44	0	0
0.74	1.13	0	0	4.81	0	0
0.78	0.41	0	0	3.92	0	0
0.81	0.50	0	0	2.41	0	0
0.96	0.35	0.17	0	3.71	0	0
1.00	0.21	0.06	0	3.38	0	0
0.90	0.08	0.07	0	2.98	0	0
0.48	0.08	0.0	0.14	2.66	0.04	0
0.43	0.14	0.0	0.16	2.47	0.01	0
0.50	0.06	0.03	0.14	2.20	0.06	0
0.25	0.04	0.05	0.23	1.90	0.06	0
0.16	0.01	0	0.30	1.75	0.10	0
0.10	0.01	0	0.36	1.15	0.15	0
0.06	0	0	0.49	1.07	0.27	0
0	0	0	0.34	0.89	0.21	0
0	0	0	0.31	0.85	0.29	0
0	0	0	0.33	1.33	1.26	0
*	*	*	*	*	*	2.37
*	*	*	*	*	*	2.22
*	*	*	*	*	*	1.59
8.75	**3.02**	**0.38**	**2.80**	**76.42**	**2.45**	**6.18**

F4 at Locality 12 [CBV-12-8] [Total sample weight 1761364.4 mg]

Grain diameter		Weight Fractions		Granulometric Analysis						
ϕ	mm	weight [mg]	Cumulative weight %	ϕ_{05}	ϕ_{16}	ϕ_{50}	ϕ_{84}	Md$_\phi$	σ_ϕ	F2
-5.0	31.5	36998	2.10	4.9	3.9	-3.7	-4.7	-1.4	3.35	17.10%
-4.5	22.4	64198	5.75							
-4.0	16.0	141479	13.78							
-3.5	11.2	100013	19.46							
-3.0	8.0	122981	26.44							
-2.5	5.6	127079	33.65							
-2.0	4.0	121268	40.54							
-1.5	2.8	130560	47.95							
-1.0	2.0	105973	53.97							
-0.5	1.4	90569	59.11							
0.0	1.0	68939	63.02							
0.5	0.710	61962	66.54							
1.0	0.500	62216	70.07							
1.5	0.355	51528	73.00							
2.0	0.250	45877	75.60							
2.5	0.180	44827	78.15							
3.0	0.125	46629	80.80							
3.5	0.088	37039	82.90							
4.0	0.063	35581	84.92							
4.5	0.045	98163	90.49							
5.0	0.032	90225	95.61							
6.0	0.017	53450	98.65							
7.0	0.008	23810	100.00							

Minor Lithic Counts		Abundance [volume %]	
SMI	GCI	SMI	GCI
11	2	3.0	0.5
19	4	5.1	1.1
37	10	9.6	2.6
39	9	10.3	2.4
40	11	10.9	3.0
34	8	9.5	2.2
26	2	7.6	0.6
34	5	10.9	1.6
32	6	12.2	2.3

Counts:

ϕ	Wp	Gp	Bp	Xtal	Lithic	Glass	NA	total counts
-5.0	1	0	0	0	1	0	*0*	2
-4.5	3	0	0	0	2	0	*0*	5
-4.0	38	4	0	0	33	0	*0*	75
-3.5	71	1	1	0	9	0	*0*	82
-3.0	84	1	0	0	9	0	*0*	94
-2.5	268	9	0	0	24	0	*0*	301
-2.0	91	39	0	0	82	0	*0*	212
-1.5	104	12	0	0	129	0	*0*	245
-1.0	129	4	0	0	367	0	*0*	500
-0.5	111	12	0	2	371	4	*0*	500
0.0	89	14	0	10	384	3	*0*	500
0.5	78	9	0	24	380	9	*0*	500
1.0	74	4	0	43	367	12	*0*	500
1.5	62	8	0	62	357	11	*0*	500
2.0	50	10	0	91	340	9	*0*	500
2.5	48	11	0	101	311	29	*0*	500
3.0	42	12	0	119	262	65	*0*	500
3.5	0	0	0	129	243	128	*0*	500
4.0	0	0	0	113	228	159	*0*	500
4.5	0	0	0	78	173	249	*0*	500
5.0	*	*	*	*	*	*	*5639*	5639
6.0	*	*	*	*	*	*	*4859*	4859
7.0	*	*	*	*	*	*	*3402*	3402

Bulk Weight Percentages:

ϕ	Wp	Gp	Bp	Xtal	Lithic	Glass	NA
-5.0	0.28	0	0	0	1.82	0	0
-4.5	0.69	0	0	0	2.96	0	0
-4.0	4.02	0	0	0	4.01	0	0
-3.5	5.14	0	0.20	0	0.34	0	0
-3.0	5.05	0.37	0	0	1.57	0	0
-2.5	5.40	0.19	0	0	1.62	0	0
-2.0	1.84	0.97	0	0	4.08	0	0
-1.5	1.05	0.14	0	0	5.75	0	0
-1.0	0.84	0.04	0	0	5.14	0	0
-0.5	0.74	0.08	0	0.02	4.26	0.04	0
0.0	0.46	0.08	0	0.08	3.27	0.02	0
0.5	0.38	0.08	0	0.17	2.82	0.06	0
1.0	0.40	0.02	0	0.31	2.72	0.08	0
1.5	0.18	0.07	0	0.38	2.24	0.06	0
2.0	0.09	0.02	0	0.52	1.93	0.05	0
2.5	0.11	0.03	0	0.55	1.70	0.15	0
3.0	0.13	0.04	0	0.67	1.48	0.34	0
3.5	0	0	0	0.57	1.08	0.45	0
4.0	0	0	0	0.49	0.99	0.55	0
4.5	0	0	0	0.97	2.15	2.45	0
5.0	*	*	*	*	*	*	5.12
6.0	*	*	*	*	*	*	3.03
7.0	*	*	*	*	*	*	1.35
	27.26	**2.13**	**0.20**	**4.73**	**51.93**	**4.25**	**9.50**

NF deposit at Locality 18 [CBV-S-3] [Total sample weight: 200308.3 mg]

Grain diameter		Weight Fractions		Granulometric Analysis						
ϕ	mm	weight [mg]	Cumulative weight %	ϕ_{05}	ϕ_{50}	ϕ_{10}	ϕ_5	Md_ϕ	σ_ϕ	F2
-5.0	31.5	0	0	5.7	4.6	-0.2	-1.8	2.4	2.34	33.60%
-4.5	22.4	0	0							
-4.0	16.0	0	0							
-3.5	11.2	2429.9	1.21							
-3.0	8.0	302.1	1.36							
-2.5	5.6	3090.6	2.91							
-2.0	4.0	2841.4	4.33							
-1.5	2.8	4393.6	6.52							

				Minor Lithic Counts		Abundance [volume %]	
				SML	GCL	SML	GCL
-1.0	2.0	5412.7	9.22	8	1	7.6	1.0
-0.5	1.4	7991.5	13.21	13	3	11.0	2.5
0.0	1.0	8266.1	17.34	14	2	10.7	1.5
0.5	0.710	10756.7	22.71	15	2	8.8	1.2
1.0	0.500	13392.7	29.39	14	2	7.0	1.0
1.5	0.355	14174.2	36.47	13	2	6.8	1.0
2.0	0.250	15334.7	44.13	13	2	8.1	1.2
2.5	0.180	14143.6	51.19	12	2	8.2	1.4
3.0	0.125	16171.5	59.26	13	3	9.4	2.2
3.5	0.088	14300.2	66.40				
4.0	0.063	13553.5	73.16				
4.5	0.045	19863.0	83.08				
5.0	0.032	18255	92.20				
6.0	0.017	10815	97.59				
7.0	0.008	4815	100.00				

Counts:

ϕ	Wp	Gp	Bp	Xtal	Lithic	Glass	NA	total counts
-5.0	0	0	0	0	0	0	*0*	0
-4.5	0	0	0	0	0	0	*0*	0
-4.0	0	0	0	0	0	0	*0*	0
-3.5	0	0	1	0	1	0	*0*	2
-3.0	1	0	0	0	0	0	*0*	1
-2.5	6	0	2	0	6	0	*0*	14
-2.0	33	4	12	0	8	0	*0*	57
-1.5	165	12	22	0	31	0	*0*	230
-1.0	354	14	27	0	105	0	*0*	500
-0.5	343	13	26	0	118	0	*0*	500
0.0	328	13	24	4	131	0	*0*	500
0.5	290	15	13	11	171	0	*0*	500
1.0	264	16	5	15	200	0	*0*	500
1.5	268	12	3	23	192	2	*0*	500
2.0	273	4	0	48	161	14	*0*	500
2.5	229	0	0	72	147	52	*0*	500
3.0	153	0	0	137	138	72	*0*	500
3.5	0	0	0	159	121	220	*0*	500
4.0	0	0	0	198	119	183	*0*	500
4.5	0	0	0	89	108	303	*0*	500
5.0	*	*	*	*	*	*	*1141*	1141
6.0	*	*	*	*	*	*	*983*	983
7.0	*	*	*	*	*	*	*688*	688

Bulk Weight Percentages:

Wp	Gp	Bp	Xtal	Lithic	Glass	NA
0	0	0	0	0	0	0
0	0	0	0	0	0	0
0	0	0	0	0	0	0
0	0	0.43	0	0.78	0	0
0.15	0	0	0	0	0	0
0.27	0	0.37	0	0.90	0	0
0.64	0.11	0.29	0	0.38	0	0
1.32	0.13	0.29	0	0.45	0	0
1.50	0.09	0.17	0	0.95	0	0
2.33	0.09	0.18	0	1.38	0	0
2.29	0.10	0.19	0.04	1.50	0	0
2.56	0.25	0.10	0.14	2.31	0	0
3.07	0.20	0.06	0.23	3.15	0	0
2.41	0.32	0.08	0.44	3.79	0.03	0
2.22	0.04	0	1.17	3.92	0.30	0
1.90	0	0	1.39	2.84	0.93	0
1.56	0	0	2.62	2.64	1.26	0
0	0	0	2.51	1.91	2.72	0
0	0	0	2.90	1.74	2.13	0
0	0	0	2.02	2.46	5.44	0
*	*	*	*	*	*	9.11
*	*	*	*	*	*	5.40
*	*	*	*	*	*	2.41
22.22	**1.33**	**2.16**	**13.46**	**31.10**	**12.81**	**16.92**

P.F. deposit at Locality 29 [CBV-29-2] [Total sample weight: 202458.4 mg]

Grain diameter		Weight Fractions		Granulometric Analysis						
ϕ	mm	weight [mg]	Cumulative weight %	ϕ_{5}	ϕ_{50}	ϕ_{25}	ϕ_{75}	Md_{ϕ}	σ_{ϕ}	Fz
-5.0	31.5	0	0	5.7	4.9	-2.1	-3.6	2.6	2.34	39.77%
-4.5	22.4	0	0							
-4.0	16.0	7579.9	3.74							
-3.5	11.2	3822.9	5.63							
-3.0	8.0	7172.8	9.18							
-2.5	5.6	6363.8	12.32							
-2.0	4.0	10651.7	17.58							
-1.5	2.8	12812.2	23.91							
-1.0	2.0	11337.4	29.51							
-0.5	1.4	7476.2	33.20							
0.0	1.0	4545.8	35.45							
0.5	0.710	4849.5	37.84							
1.0	0.500	5024.9	40.32							
1.5	0.355	4196.9	42.40							
2.0	0.250	6199.5	45.46							
2.5	0.180	7802.2	49.31							
3.0	0.125	8946.2	53.73							
3.5	0.088	13149.7	60.23							
4.0	0.063	17465.9	68.85							
4.5	0.045	15251.6	76.39							
5.0	0.032	18980	85.76							
6.0	0.017	16300	93.81							
7.0	0.008	12525	100.00							

Minor Lithic Counts		Abundance [volume %]	
SML	GCL	SML	GCL
n.a.	n.a.	n.a.	n.a.

Counts:

ϕ	Wp	Gp	Bp	Xtal	Lithic	Glass	NA	total counts
-5.0	0	0	0	0	0	0	0	0
-4.5	0	0	0	0	0	0	0	0
-4.0	2	1	0	0	0	0	0	3
-3.5	2	3	0	0	0	0	0	5
-3.0	8	6	0	0	0	0	0	14
-2.5	21	7	0	0	1	0	0	29
-2.0	48	12	0	0	36	0	0	96
-1.5	116	26	0	0	109	0	0	251
-1.0	202	30	3	0	265	0	0	500
-0.5	207	30	1	0	262	0	0	500
0.0	191	33	1	1	258	6	0	490
0.5	186	26	2	2	279	5	0	500
1.0	171	22	0	7	283	17	0	500
1.5	162	24	0	14	280	10	0	490
2.0	162	27	0	26	257	28	0	500
2.5	159	19	0	36	212	74	0	500
3.0	151	3	0	48	166	132	0	500
3.5	0	0	0	51	104	245	0	400
4.0	0	0	0	42	76	382	0	500
4.5	0	0	0	19	41	440	0	500
5.0	*	*	*	*	*	*	*1186*	1186
6.0	*	*	*	*	*	*	*1482*	1482
7.0	*	*	*	*	*	*	*1789*	1789

Bulk Weight Percentages:

Wp	Gp	Bp	Xtal	Lithic	Glass	NA
0	0	0	0	0	0	0
0	0	0	0	0	0	0
1.58	2.16	0	0	0	0	0
0.65	1.24	0	0	0	0	0
1.98	1.56	0	0	0	0	0
1.96	0.87	0	0	0.31	0	0
1.64	0.58	0	0	3.04	0	0
2.11	0.65	0	0	3.57	0	0
1.38	0.30	0.03	0	3.89	0	0
1.11	0.17	0.03	0	2.41	0	0
0.61	0.13	0	0.01	1.43	0.03	0
0.62	0.18	0.03	0.01	1.55	0.03	0
0.69	0.10	0	0.04	1.57	0.08	0
0.37	0.17	0	0.07	1.42	0.04	0
0.44	0.09	0	0.21	2.11	0.20	0
0.67	0.09	0	0.35	2.07	0.67	0
0.86	0.02	0	0.51	1.76	1.28	0
0	0	0	0.96	1.95	3.59	0
0	0	0	0.86	1.56	6.21	0
0	0	0	0.35	0.76	6.42	0
*	*	*	*	*	*	9.37
*	*	*	*	*	*	8.05
*	*	*	*	*	*	6.19
16.67	**8.31**	**0.09**	**3.37**	**29.40**	**18.55**	**23.61**

Marquesado flow (lag breccia) base deposit at Locality 53 [CBV-M-1] [Total sample weight: 837635 mg]

Grain diameter		Weight Fractions:		Granulometric Analysis						
ϕ	mm	weight [mg]	Cumulative weight %	ϕ_{05}	ϕ_{84}	ϕ_{16}	ϕ_{x}	Md_{ϕ}	σ_{ϕ}	F2
-5.0	31.5	0	0	5.4	4.2	-2.8	-4.1	0.5	3.19	23.47%
-4.5	22.4	24000	2.87							
-4.0	16.0	24000	5.73							
-3.5	11.2	24000	8.60							
-3.0	8.0	42000	13.61							
-2.5	5.6	38000	18.15							
-2.0	4.0	46000	23.64							
-1.5	2.8	22950	26.34							
-1.0	2.0	52267	32.62							
-0.5	1.4	52303	38.86							
0.0	1.0	48769	44.68							
0.5	0.710	45125	50.07							
1.0	0.500	43774	55.30							
1.5	0.355	39948	60.07							
2.0	0.250	36805	64.46							
2.5	0.180	33318	68.44							
3.0	0.125	36326	72.77							
3.5	0.088	31477	76.53							
4.0	0.063	31747	80.29							
4.5	0.045	89327	90.95							
5.0	0.032	29095	94.43							
6.0	0.017	25840	97.51							
7.0	0.008	20835	100.00							

Minor Lithic Counts		Abundance [volume %]	
SML	GCL	SML	GCL
2	0	0.7	0
5	0	0.7	0
9	0	1.4	0
11	0	1.8	0
14	0	2.6	0
12	0	2.3	0
16	1	4.1	0.3
14	0	4.4	0
12	1	4.2	0.2

Counts:

ϕ	Wp	Gp	Bp	Xtal	Lithic	Glass	NA	total counts
-5.0	0	0	0	0	0	0	*0*	0
-4.5	2	0	0	0	1	0	*0*	3
-4.0	8	0	0	0	4	0	*0*	12
-3.5	11	0	0	0	9	0	*0*	20
-3.0	13	1	0	0	84	0	*0*	98
-2.5	61	2	1	0	129	0	*0*	193
-2.0	119	4	6	0	315	0	*0*	444
-1.5	144	3	7	0	1121	0	*0*	1275
-1.0	88	5	9	0	271	0	*0*	373
-0.5	70	3	0	1	676	0	*0*	750
0.0	74	7	0	10	659	0	*0*	750
0.5	54	2	0	46	614	34	*0*	750
1.0	31	16	0	76	537	90	*0*	750
1.5	37	15	0	146	511	41	*0*	750
2.0	88	22	0	213	390	37	*0*	750
2.5	129	19	0	239	317	46	*0*	750
3.0	130	6	0	280	283	51	*0*	750
3.5	173	0	0	464	82	31	*0*	750
4.0	0	0	0	458	45	247	*0*	750
4.5	0	0	0	405	7	338	*0*	750
5.0	*	*	*	*	*	*	*1818*	1818
6.0	*	*	*	*	*	*	*2349*	2349
7.0	*	*	*	*	*	*	*2977*	2977

Bulk Weight Percentages:

Wp	Gp	Bp	Xtal	Lithic	Glass	NA
0	0	0	0	0	0	0
0.82	0	0	0	2.04	0	0
1.14	0	0	0	1.73	0	0
1.16	0	0	0	1.70	0	0
0.23	0.02	0	0	4.76	0	0
0.55	0.02	0.04	0	3.92	0	0
0.72	0.03	0.04	0	4.69	0	0
0.18	0.01	0.01	0	2.54	0	0
0.80	0.07	0.12	0	5.26	0	0
0.35	0.02	0	0.01	5.87	0	0
0.36	0.04	0	0.08	5.34	0	0
0.31	0.02	0	0.32	4.50	0.23	0
0.16	0.09	0	0.53	3.87	0.57	0
0.11	0.13	0	0.93	3.36	0.23	0
0.19	0.06	0	1.39	2.54	0.21	0
0.33	0.06	0	1.43	1.95	0.26	0
0.44	0.02	0	1.78	1.80	0.30	0
0.72	0	0	2.47	0.44	0.13	0
0	0	0	2.46	0.24	1.05	0
0	0	0	6.36	0.11	4.19	0
*	*	*	*	*	*	3.47
*	*	*	*	*	*	3.08
*	*	*	*	*	*	2.49
8.57	**0.59**	**0.21**	**17.76**	**56.66**	**7.17**	**9.04**

NF deposit at Locality 77 [CBV-F-2] [Total sample weight: 552918.9 mg]

Grain diameter		Weight Fractions		Granulometric Analysis						
ϕ	mm	weight [mg]	Cumulative weight %	ϕ_{05}	ϕ_{25}	ϕ_{50}	ϕ_{75}	Md_ϕ	σ_ϕ	F2
-5.0	31.5	0	0	4.9	4.1	-2.4	-3.4	-0.6	2.88	17.46%
-4.5	22.4	0	0.85							
-4.0	16.0	11126.7	2.98							
-3.5	11.2	9233.4	6.66							
-3.0	8.0	18289.4	12.06							
-2.5	5.6	38371.3	19.38							
-2.0	4.0	40820.8	27.67							
-1.5	2.8	50495.1	37.05							
-1.0	2.0	55573.9	47.70							
-0.5	1.4	55502.9	57.41							
0.0	1.0	49633.1	64.10							
0.5	0.710	35796.9	70.26							
1.0	0.500	25093.1	73.98							
1.5	0.355	16720.7	76.57							
2.0	0.250	12747.9	78.93							
2.5	0.180	9853.5	80.50							
3.0	0.125	11943.7	82.05							
3.5	0.088	15157.7	83.30							
4.0	0.063	6078.0	84.90							
4.5	0.045	33434.7	90.48							
5.0	0.032	30730	95.61							
6.0	0.017	18205	98.65							
7.0	0.008	8110	100.00							

Minor Lithic Counts		Abundance [volume %]	
SML	GCL	SML	GCL
22	0	6.7	0
16	0	4.8	0
14	0	4.1	0
16	3	4.8	0.9
13	12	3.9	3.6
10	3	3.5	1.1
9	2	3.4	0.8
8	0	3.3	0
12	0	4.9	0

Counts:

ϕ	Wp	Gp	Bp	Xtal	Lithic	Glass	NA	total counts
-5.0	0	0	0	0	0	0	*0*	0
-4.5	0	0	0	0	0	0	*0*	0
-4.0	3	0	0	0	1	0	*0*	4
-3.5	6	0	0	0	2	0	*0*	8
-3.0	20	0	3	0	12	0	*0*	35
-2.5	53	0	0	0	81	0	*0*	134
-2.0	187	3	0	0	195	0	*0*	385
-1.5	266	2	1	0	230	1	*0*	500
-1.0	112	3	0	2	326	1	*0*	444
-0.5	149	6	0	7	336	2	*0*	500
0.0	144	1	0	9	341	2	*0*	497
0.5	139	2	0	28	331	2	*0*	502
1.0	125	3	0	35	333	4	*0*	500
1.5	158	2	0	41	284	15	*0*	500
2.0	166	0	0	55	262	17	*0*	500
2.5	154	0	0	73	244	29	*0*	500
3.0	103	0	0	94	247	56	*0*	500
3.5	98	0	0	82	241	79	*0*	500
4.0	102	0	0	79	210	109	*0*	500
4.5	0	0	0	71	173	256	*0*	500
5.0	*	*	*	*	*	*	*1920*	1920
6.0	*	*	*	*	*	*	*1655*	1655
7.0	*	*	*	*	*	*	*1158*	1158

Bulk Weight Percentages:

Wp	Gp	Bp	Xtal	Lithic	Glass	NA
0	0	0	0	0	0	0
0	0	0	0	0	0	0
1.0	0	0	0	1.01	0	0
1.04	0	0	0	0.63	0	0
1.08	0	0.16	0	2.06	0	0
1.13	0	0	0	5.81	0	0
2.06	0.04	0	0	5.29	0	0
3.54	0.04	0.02	0	5.51	0.03	0
1.37	0.05	0	0.05	8.56	0.02	0
2.0	0.08	0	0.15	7.76	0.04	0
1.79	0.01	0	0.18	6.96	0.04	0
1.21	0.04	0	0.39	4.81	0.03	0
0.89	0.02	0	0.33	3.26	0.03	0
0.53	0.02	0	0.29	2.09	0.09	0
0.33	0	0	0.33	1.56	0.09	0
0.29	0	0	0.32	1.06	0.12	0
0.27	0	0	0.45	1.19	0.25	0
0.46	0	0	0.49	1.43	0.37	0
0.19	0	0	0.19	0.51	0.21	0
0	0	0	0.96	2.33	2.74	0
*	*	*	*	*	*	5.56
*	*	*	*	*	*	3.29
*	*	*	*	*	*	1.47
19.18	**0.30**	**0.18**	**4.13**	**61.83**	**4.06**	**10.32**

Marquesado flow deposit at Locality 52 [CBV-52-2a] [Total sample weight 215393.1 mg]

Grain diameter		Weight Fractions		Granulometric Analysis						
ϕ	mm	weight [mg]	Cumulative weight %	$\phi_{5\%}$	ϕ_{84}	ϕ_{16}	ϕ_{50}	Md_ϕ	σ_ϕ	F2
-5.0	31.5	0	0	5.3	4.2	-0.2	-1.9	-0.6	1.57	25.32%
-4.5	22.4	0	0							
-4.0	16.0	0	0							
-3.5	11.2	3301.0	1.53							
-3.0	8.0	2247.7	2.58							
-2.5	5.6	3741	2.75							
-2.0	4.0	2051.5	3.70							
-1.5	2.8	4303.4	5.70							
-1.0	2.0	6749.6	8.83							
-0.5	1.4	9438.2	13.22							
0.0	1.0	8941.6	17.37							
0.5	0.710	14456.9	24.08							
1.0	0.500	14432.2	30.78							
1.5	0.355	17573.6	38.94							
2.0	0.250	20049.7	48.25							
2.5	0.180	21555.4	58.25							
3.0	0.125	18853.9	67.01							
3.5	0.088	16529.5	74.68							
4.0	0.063	14159.5	81.26							
4.5	0.045	15907.9	88.64							
5.0	0.032	12680	94.53							
6.0	0.017	8155	98.31							
7.0	0.008	3630	100.00							

Minor Lithic Counts		Abundance [volume %]	
SML	GCL	SML	GCL
25	2	9.0	0.7
32	4	6.6	0.8
47	10	9.9	2.1
44	8	9.4	1.7
40	10	8.7	2.2
24	9	6.9	2.6
13	6	4.1	1.9
12	3	4.1	1.0
9	0	3.4	0

Counts:

ϕ	Wp	Gp	Bp	Xtal	Lithic	Glass	NA	total counts
-5.0	0	0	0	0	0	0	0	0
-4.5	0	0	0	0	0	0	0	0
-4.0	0	0	0	0	0	0	0	0
-3.5	0	0	0	0	1	0	0	1
-3.0	0	0	0	0	2	0	0	2
-2.5	0	0	0	0	1	0	0	1
-2.0	0	0	0	0	13	0	0	13
-1.5	3	0	0	0	77	2	0	82
-1.0	8	0	0	0	277	4	0	289
-0.5	11	0	0	0	484	5	0	500
0.0	14	1	0	1	476	8	0	500
0.5	13	0	0	12	469	6	0	500
1.0	8	0	0	32	458	2	0	500
1.5	8	0	0	124	349	19	0	500
2.0	11	0	0	146	319	24	0	500
2.5	12	0	0	163	290	35	0	500
3.0	8	0	0	183	263	46	0	500
3.5	6	0	0	211	231	52	0	500
4.0	0	0	0	184	179	137	0	500
4.5	0	0	0	59	122	319	0	500
5.0	*	*	*	*	*	*	792	792
6.0	*	*	*	*	*	*	741	741
7.0	*	*	*	*	*	*	519	519

Bulk Weight Percentages:

Wp	Gp	Bp	Xtal	Lithic	Glass	NA
0	0	0	0	0	0	0
0	0	0	0	0	0	0
0	0	0	0	0	0	0
0	0	0	0	1.53	0	0
0	0	0	0	1.04	0	0
0	0	0	0	0.17	0	0
0	0	0	0	0.95	0	0
0.04	0	0	0	1.92	0.04	0
0.04	0	0	0	3.06	0.04	0
0.06	0	0	0	4.29	0.03	0
0.07	0.01	0	0.01	4.00	0.06	0
0.11	0	0	0.16	6.37	0.08	0
0.08	0	0	0.42	6.18	0.02	0
0.06	0	0	2.01	5.82	0.27	0
0.07	0	0	2.77	6.06	0.41	0
0.10	0	0	3.32	5.92	0.66	0
0.08	0	0	3.25	4.68	0.75	0
0.07	0	0	3.32	3.64	0.64	0
0	0	0	2.56	2.49	1.51	0
0	0	0	1.01	2.08	4.30	0
*	*	*	*	*	*	5.89
*	*	*	*	*	*	3.79
*	*	*	*	*	*	1.69
0.78	**0.01**	**0**	**18.83**	**60.20**	**8.81**	**11.37**

Marquesado flow deposit at Locality 52 (CBV-52-2b) (Total sample weight 329249.8 mg)

Grain diameter		Weight Fractions		Granulometric Analysis						
ϕ	mm	weight [mg]	Cumulative weight %	ϕ_{05}	ϕ_{25}	ϕ_{10}	ϕ_{5}	Md_{ϕ}	σ_{ϕ}	F2
-5.0	31.5	0	0	5.8	4.7	0.1	-2.1	2.8	2.33	38.79%
-4.5	22.4	0	0							
-4.0	16.0	9309.9	2.83							
-3.5	11.2	0	2.83							
-3.0	8.0	124.6	2.87							
-2.5	5.6	1917.3	3.45							
-2.0	4.0	5558.9	5.14							
-1.5	2.8	7137.4	7.30							
-1.0	2.0	7996.9	9.73							
-0.5	1.4	9795.9	12.71							
0.0	1.0	10181.4	15.80							
0.5	0.710	12584.8	19.62							
1.0	0.500	16670.9	24.69							
1.5	0.355	21896.1	31.34							
2.0	0.250	21630.2	37.91							
2.5	0.180	24690.3	45.40							
3.0	0.125	27671.1	53.81							
3.5	0.088	24365.7	61.21							
4.0	0.063	25556.3	68.97							
4.5	0.045	40251.9	81.20							
5.0	0.032	32080	90.94							
6.0	0.017	20635	97.21							
7.0	0.008	9195	100.00							

Minor Lithic Counts		Abundance (volume %)	
SML	GCL	SML	GCL
37	0	9.2	0
38	0	8.7	0
37	25	8.9	6.0
34	19	8.5	4.8
36	16	10.8	4.8
21	14	6.8	4.5
22	18	7.6	6.2
21	2	7.4	0.7
18	0	6.5	0

Counts:

ϕ	Wp	Gp	Bp	Xtal	Lithic	Glass	NA	total counts
-5.0	0	0	0	0	0	0	*0*	0
-4.5	0	0	0	0	0	0	*0*	0
-4.0	0	0	0	0	1	0	*0*	1
-3.5	0	0	0	0	0	0	*0*	0
-3.0	1	0	0	0	6	0	*0*	7
-2.5	0	0	0	0	26	0	*0*	26
-2.0	4	0	0	0	111	0	*0*	115
-1.5	7	0	0	0	297	24	*0*	328
-1.0	23	0	0	0	404	73	*0*	500
-0.5	25	0	0	0	435	40	*0*	500
0.0	26	2	0	5	418	49	*0*	500
0.5	19	0	0	29	399	53	*0*	500
1.0	14	0	0	50	334	102	*0*	500
1.5	8	0	0	119	311	62	*0*	500
2.0	6	0	0	139	291	64	*0*	500
2.5	7	0	0	146	285	62	*0*	500
3.0	6	0	0	161	279	54	*0*	500
3.5	0	0	0	189	246	65	*0*	500
4.0	0	0	0	184	218	98	*0*	500
4.5	0	0	0	61	184	255	*0*	500
5.0	*	*	*	*	*	*	*2004*	2004
6.0	*	*	*	*	*	*	*1876*	1876
7.0	*	*	*	*	*	*	*1314*	1314

Bulk Weight Percentages:

Wp	Gp	Bp	Xtal	Lithic	Glass	NA
0	0	0	0	0	0	0
0	0	0	0	0	0	0
0	0	0	0	2.83	0	0
0	0	0	0	0	0	0
0	0	0	0	0.04	0	0
0	0	0	0	0.58	0	0
0.02	0	0	0	1.67	0	0
0.02	0	0	0	2.01	0.14	0
0.06	0	0	0	2.07	0.30	0
0.09	0	0	0	2.69	0.19	0
0.10	0.01	0	0.03	2.67	0.29	0
0.12	0	0	0.22	3.11	0.38	0
0.11	0	0	0.50	3.50	0.95	0
0.05	0	0	1.59	4.28	0.73	0
0.03	0	0	1.87	3.91	0.76	0
0.05	0	0	2.23	4.35	0.88	0
0.05	0	0	2.75	4.76	0.84	0
0	0	0	2.88	3.75	0.77	0
0	0	0	2.98	3.53	1.26	0
0	0	0	1.67	5.02	5.51	0
*	*	*	*	*	*	9.74
*	*	*	*	*	*	6.27
*	*	*	*	*	*	2.79
0.70	**0.01**	**0**	**16.72**	**5.77**	**13.00**	**18.80**

Marquesado flow deposit at Locality 52 [CBV-52-2c] [Total sample weight: 261518.8 mg]

Grain diameter		Weight Fractions		Granulometric Analysis						
ϕ	mm	weight [mg]	Cumulative weight %	ϕ_{05}	ϕ_{25}	ϕ_{50}	ϕ_{75}	Md_ϕ	σ_ϕ	F2
-5.0	31.5	0	0	5.9	4.9	2.2	0.5	4.2	1.51	64.03%
-4.5	22.4	0	0							
-4.0	16.0	0	0							
-3.5	11.2	0	0							
-3.0	8.0	0	0							
-2.5	5.6	642.5	0.25							
-2.0	4.0	149.2	0.30							
-1.5	2.8	689.2	0.57							

	Minor Lithic Counts		Abundance [volume %]	
	SML	GCL	SML	GCL
-1.0	0	0	0	0
-0.5	12	0	7.4	0
0.0	16	0	7.2	0
0.5	22	5	7.7	1.8
1.0	31	11	9.5	3.4
1.5	22	6	7.6	2.1
2.0	15	5	6.8	2.3
2.5	12	3	8.0	2.0
3.0	11	0	7.1	0

3.5	0.088	21268.8	35.97
4.0	0.063	25092.0	45.57
4.5	0.045	56084.3	67.02
5.0	0.032	44700	84.11
6.0	0.017	28755	95.10
7.0	0.008	12810	100.00

Counts:

ϕ	Wp	Gp	Bp	Xtal	Lithic	Glass	NA	total counts
-5.0	0	0	0	0	0	0	*0*	0
-4.5	0	0	0	0	0	0	*0*	0
-4.0	0	0	0	0	0	0	*0*	0
-3.5	0	0	0	0	0	0	*0*	0
-3.0	0	0	0	0	0	0	*0*	0
-2.5	2	0	0	0	1	0	*0*	3
-2.0	3	0	0	0	1	0	*0*	4
-1.5	4	1	0	0	4	12	*0*	21
-1.0	9	1	0	0	47	84	*0*	141
-0.5	44	4	0	0	162	290	*0*	500
0.0	8	0	0	3	223	265	*0*	499
0.5	16	0	0	19	284	181	*0*	500
1.0	20	0	0	45	327	108	*0*	500
1.5	16	0	0	72	289	121	*0*	500
2.0	12	0	0	125	220	139	*0*	500
2.5	8	0	0	164	150	174	*0*	500
3.0	0	0	0	156	155	181	*0*	500
3.5	0	0	0	131	161	208	*0*	500
4.0	0	0	0	49	149	302	*0*	500
4.5	0	0	0	26	134	340	*0*	500
5.0	*	*	*	*	*	*	*2794*	2794
6.0	*	*	*	*	*	*	*2614*	2614
7.0	*	*	*	*	*	*	*1830*	1830

Bulk Weight Percentages:

ϕ	Wp	Gp	Bp	Xtal	Lithic	Glass	NA
-5.0	0	0	0	0	0	0	0
-4.5	0	0	0	0	0	0	0
-4.0	0	0	0	0	0	0	0
-3.5	0	0	0	0	0	0	0
-3.0	0	0	0	0	0	0	0
-2.5	0.10	0	0	0	0.15	0	0
-2.0	0.03	0	0	0	0.03	0	0
-1.5	0.03	0.01	0	0	0.06	0.16	0
-1.0	0.03	0.01	0	0	0.29	0.42	0
-0.5	0.06	0.01	0	0	0.41	0.57	0
0.0	0.01	0	0	0.01	0.49	0.53	0
0.5	0.02	0	0	0.07	1.02	0.60	0
1.0	0.06	0	0	0.18	1.36	0.40	0
1.5	0.05	0	0	0.45	1.85	0.66	0
2.0	0.05	0	0	1.24	2.18	1.22	0
2.5	0.06	0	0	2.04	1.86	2.01	0
3.0	0.06	0	0	2.30	2.28	2.44	0
3.5	0	0	0	2.34	2.86	2.91	0
4.0	0	0	0	1.07	3.27	5.25	0
4.5	0	0	0	1.30	6.71	13.44	0
5.0	*	*	*	*	*	*	17.09
6.0	*	*	*	*	*	*	10.99
7.0	*	*	*	*	*	*	4.90
	0.57	**0.02**	**0**	**11.00**	**24.82**	**30.61**	**32.98**

Marquesado flow (lag breccia) base deposit at Locality 53 [CBV-M-1] [Total sample weight: 837635 mg]

Grain diameter		Weight Fractions		Granulometric Analysis						
ϕ	mm	weight [mg]	Cumulative weight %	ϕ_{5}	ϕ_{50}	ϕ_{16}	$\phi_{\bar{x}}$	Md$_{\phi}$	σ_{ϕ}	F2
-5.0	31.5	0	0	5.4	4.2	-2.8	-4.1	0.5	3.19	23.47%
-4.5	22.4	24000	2.87							
-4.0	16.0	24000	5.73							
-3.5	11.2	24000	8.60							
-3.0	8.0	42000	13.61							
-2.5	5.6	38000	18.15							
-2.0	4.0	46000	23.64							
-1.5	2.8	22950	26.34							
-1.0	2.0	52267	32.62							
-0.5	1.4	52303	38.86							
0.0	1.0	48769	44.68							
0.5	0.710	45125	50.07							
1.0	0.500	43774	55.30							
1.5	0.355	39948	60.07							
2.0	0.250	36805	64.46							
2.5	0.180	33318	68.44							
3.0	0.125	36326	72.77							
3.5	0.088	31477	76.53							
4.0	0.063	31747	80.29							
4.5	0.045	89327	90.95							
5.0	0.032	29095	94.43							
6.0	0.017	25840	97.51							
7.0	0.008	20835	100.00							

Minor Lithic Counts		Abundance [volume %]	
SML	GCL	SML	GCL
2	0	0.7	0
5	0	0.7	0
9	0	1.4	0
11	0	1.8	0
14	0	2.6	0
12	0	2.3	0
16	1	4.1	0.3
14	0	4.4	0
12	1	4.2	0.2

Counts:

ϕ	Wp	Gp	Bp	Xtal	Lithic	Glass	NA	total counts
-5.0	0	0	0	0	0	0	0	0
-4.5	2	0	0	0	1	0	0	3
-4.0	8	0	0	0	4	0	0	12
-3.5	11	0	0	0	9	0	0	20
-3.0	13	1	0	0	84	0	0	98
-2.5	61	2	1	0	129	0	0	193
-2.0	119	4	6	0	315	0	0	444
-1.5	144	3	7	0	1121	0	0	1275
-1.0	88	5	9	0	271	0	0	373
-0.5	70	3	0	1	676	0	0	750
0.0	74	7	0	10	659	0	0	750
0.5	54	2	0	46	614	34	0	750
1.0	31	16	0	76	537	90	0	750
1.5	37	15	0	146	511	41	0	750
2.0	88	22	0	213	390	37	0	750
2.5	129	19	0	239	317	46	0	750
3.0	130	6	0	280	283	51	0	750
3.5	173	0	0	464	82	31	0	750
4.0	0	0	0	458	45	247	0	750
4.5	0	0	0	405	7	338	0	750
5.0	*	*	*	*	*	*	*1818*	1818
6.0	*	*	*	*	*	*	*2349*	2349
7.0	*	*	*	*	*	*	*2977*	2977

Bulk Weight Percentages:

ϕ	Wp	Gp	Bp	Xtal	Lithic	Glass	NA
-5.0	0	0	0	0	0	0	0
-4.5	0.82	0	0	0	2.04	0	0
-4.0	1.14	0	0	0	1.73	0	0
-3.5	1.16	0	0	0	1.70	0	0
-3.0	0.23	0.02	0	0	4.76	0	0
-2.5	0.55	0.02	0.04	0	3.92	0	0
-2.0	0.72	0.03	0.04	0	4.69	0	0
-1.5	0.18	0.01	0.01	0	2.54	0	0
-1.0	0.80	0.07	0.12	0	5.26	0	0
-0.5	0.35	0.02	0	0.01	5.87	0	0
0.0	0.36	0.04	0	0.08	5.34	0	0
0.5	0.31	0.02	0	0.32	4.50	0.23	0
1.0	0.16	0.09	0	0.53	3.87	0.57	0
1.5	0.11	0.13	0	0.93	3.36	0.23	0
2.0	0.19	0.06	0	1.39	2.54	0.21	0
2.5	0.33	0.06	0	1.43	1.95	0.26	0
3.0	0.44	0.02	0	1.78	1.80	0.30	0
3.5	0.72	0	0	2.47	0.44	0.13	0
4.0	0	0	0	2.46	0.24	1.05	0
4.5	0	0	0	6.36	0.11	4.19	0
5.0	*	*	*	*	*	*	3.47
6.0	*	*	*	*	*	*	3.08
7.0	*	*	*	*	*	*	2.49
	8.57	**0.59**	**0.21**	**17.76**	**56.66**	**7.17**	**9.04**

Marquesado flow (body) middle deposit at Locality 53 [CBV-M-2] [Total sample weight: 1578086 mg]

Grain diameter		Weight Fractions		Granulometric Analysis						
ϕ	mm	weight [mg]	Cumulative weight %	ϕ_{05}	ϕ_{25}	ϕ_{16}	ϕ_{84}	Md_ϕ	σ_ϕ	F2
-5.0	31.5	154800	9.81	4.2	3.1	-4.6	-5.2	-0.6	3.35	11.73%
-4.5	22.4	101250	16.23							
-4.0	16.0	101250	22.64							
-3.5	11.2	75200	27.41							
-3.0	8.0	55100	30.90							
-2.5	5.6	56900	34.50							
-2.0	4.0	47900	37.54							
-1.5	2.8	57700	41.20							
-1.0	2.0	71610	45.73							
-0.5	1.4	73960	50.42							
0.0	1.0	74880	55.16							
0.5	0.710	74090	59.86							
1.0	0.500	80530	64.96							
1.5	0.355	75570	69.75							
2.0	0.250	59330	73.51							
2.5	0.180	67350	77.78							
3.0	0.125	86660	83.27							
3.5	0.088	78820	88.27							
4.0	0.063	78820	93.26							
4.5	0.045	89326	98.92							
5.0	0.032	6545	99.33							
6.0	0.017	5810	99.70							
7.0	0.008	4685	100.00							

Minor Lithic Counts		Abundance [volume %]	
SML	GCL	SML	GCL
15	0	2.2	0
16	0	2.3	0
18	0	2.5	0
19	0	3.3	0
20	0	3.8	0
21	0	4.5	0
23	0	5.1	0
22	0	5.6	0
20	3	7.2	0.5

Counts:

ϕ	Wp	Gp	Bp	Xtal	Lithic	Glass	NA	total counts
-5.0	0	0	0	0	2	0	*0*	2
-4.5	0	0	0	0	10	0	*0*	10
-4.0	2	0	0	0	21	0	*0*	23
-3.5	5	0	0	0	56	0	*0*	61
-3.0	6	1	0	0	124	0	*0*	131
-2.5	29	0	0	0	229	0	*0*	258
-2.0	73	0	0	0	412	0	*0*	485
-1.5	101	0	14	0	635	0	*0*	750
-1.0	57	8	1	0	684	0	*0*	750
-0.5	54	6	1	0	689	0	*0*	750
0.0	25	9	0	0	716	0	*0*	750
0.5	64	13	0	84	584	5	*0*	750
1.0	65	13	0	118	527	27	*0*	750
1.5	56	14	0	190	471	19	*0*	750
2.0	52	19	0	203	452	24	*0*	750
2.5	48	16	0	237	396	59	*0*	750
3.0	59	13	0	331	277	70	*0*	750
3.5	0	0	0	104	73	573	*0*	750
4.0	0	0	0	57	25	668	*0*	750
4.5	0	0	0	69	22	659	*0*	750
5.0	*	*	*	*	*	*	*409*	409
6.0	*	*	*	*	*	*	*528*	528
7.0	*	*	*	*	*	*	*669*	669

Bulk Weight Percentages:

Wp	Gp	Bp	Xtal	Lithic	Glass	NA
0	0	0	0	9.81	0	0
0	0	0	0	6.42	0	0
0.20	0	0	0	6.22	0	0
0.23	0	0	0	4.54	0	0
0.05	0.01	0	0	3.43	0	0
0.13	0	0	0	3.47	0	0
0.20	0	0	0	2.83	0	0
0.29	0	0.07	0	3.30	0	0
0.17	0.03	0.0+	0	4.33	0	0
0.20	0.02	0.0+	0	4.46	0	0
0.10	0.04	0	0	4.61	0	0
0.10	0.11	0	0.54	3.92	0.03	0
0.34	0.07	0	0.80	3.72	0.17	0
0.17	0.13	0	1.24	3.15	0.11	0
0.09	0.04	0	1.09	2.42	0.11	0
0.12	0.03	0	1.42	2.37	0.33	0
0.24	0.05	0	2.56	2.14	0.49	0
0	0	0	0.83	0.58	3.58	0
0	0	0	0.47	0.21	4.33	0
0	0	0	0.64	0.20	4.82	0
*	*	*	*	*	*	0.41
*	*	*	*	*	*	0.37
*	*	*	*	*	*	0.30
2.63	**0.53**	**0.07**	**9.59**	**72.13**	**13.97**	**1.08**

Marquesado flow (body) top deposit at Locality 53 [CBV-M-3] [Total sample weight: 874016 mg]

Grain diameter		Weight Fractions		Granulometric Analysis						
ϕ	mm	weight [mg]	Cumulative weight %	ϕ_{05}	ϕ_{84}	ϕ_{16}	ϕ_{5}	Md_{ϕ}	σ_{ϕ}	F2
-5.0	31.5	0	0	5.3	3.3	-3.2	-4.4	-0.4	3.07	15.68%
-4.5	22.4	40600	4.65							
-4.0	16.0	40600	9.29							
-3.5	11.2	30400	12.77							
-3.0	8.0	45300	17.95							
-2.5	5.6	52700	23.95							
-2.0	4.0	44500	29.07							
-1.5	2.8	50100	34.80							
-1.0	2.0	50654	40.60							
-0.5	1.4	60848	47.56							
0.0	1.0	49162	53.19							
0.5	0.710	49079	58.80							
1.0	0.500	48857	64.39							
1.5	0.355	40656	69.04							
2.0	0.250	37984	73.39							
2.5	0.180	27994	76.59							
3.0	0.125	36863	80.81							
3.5	0.088	30639	84.32							
4.0	0.063	30639	87.82							
4.5	0.045	26148	90.81							
5.0	0.032	30830	94.34							
6.0	0.017	27380	97.47							
7.0	0.008	22080	100.00							

Minor Lithic Counts		Abundance [volume %]	
SML	GCL	SML	GCL
19	0	2.6	0
26	0	3.6	0
28	0	4.0	0
26	0	3.7	0
29	0	4.4	0
31	0	5.1	0
21	0	3.1	0
28	0	3.3	0
26	0	3.1	0

Counts:

ϕ	Wp	Cp	Bp	Xtal	Lithic	Glass	NA	total counts
-5.0	0	0	0	0	0	0	*0*	0
-4.5	0	0	0	0	4	0	*0*	4
-4.0	0	0	0	0	3	0	*0*	3
-3.5	0	0	0	0	9	0	*0*	9
-3.0	2	1	0	0	84	0	*0*	86
-2.5	0	0	0	0	241	0	*0*	241
-2.0	0	0	0	0	312	0	*0*	312
-1.5	44	0	0	0	468	0	*0*	512
-1.0	32	0	0	0	718	0	*0*	750
-0.5	35	0	0	0	715	0	*0*	750
0.0	40	1	0	2	707	0	*0*	750
0.5	23	6	0	14	703	4	*0*	750
1.0	30	9	0	33	660	18	*0*	750
1.5	29	0	0	51	610	60	*0*	750
2.0	41	0	0	159	449	101	*0*	750
2.5	72	7	0	228	385	58	*0*	750
3.0	76	0	0	259	367	48	*0*	750
3.5	0	0	0	127	99	524	*0*	750
4.0	0	0	0	138	92	520	*0*	750
4.5	0	0	0	107	112	531	*0*	750
5.0	*	*	*	*	*	*	*1927*	1927
6.0	*	*	*	*	*	*	*2489*	2489
7.0	*	*	*	*	*	*	*3154*	3154

Bulk Weight Percentages:

Wp	Cp	Bp	Xtal	Lithic	Glass	NA
0	0	0	0	0	0	0
0	0	0	0	4.65	0	0
0	0	0	0	4.65	0	0
0	0	0	0	3.48	0	0
0.04	0.01	0	0	5.14	0	0
0	0	0	0	6.03	0	0
0	0	0	0	5.09	0	0
0.28	0	0	0	5.41	0	0
0.12	0	0	0	5.68	0	0
0.19	0	0	0	6.77	0	0
0.19	0.01	0	0.01	5.42	0	0
0.17	0.06	0	0.10	5.26	0.03	0
0.17	0.06	0	0.24	5.01	0.12	0
0.08	0	0	0.32	3.92	0.33	0
0.08	0	0	0.97	2.74	0.55	0
0.14	0.02	0	1.04	1.76	0.25	0
0.24	0	0	1.54	2.18	0.26	0
0	0	0	0.70	0.55	2.26	0
0	0	0	0.75	0.50	2.25	0
0	0	0	0.50	0.53	1.97	0
*	*	*	*	*	*	3.53
*	*	*	*	*	*	3.13
*	*	*	*	*	*	2.53
1.70	**0.15**	**0**	**6.17**	**74.44**	**8.02**	**9.19**

Marquesado flow (lag breccia) top deposit at Locality 54 [CBV-M-5] [Total sample weight 615799 mg]

Grain diameter		Weight Fractions:		Granulometric Analysis						
ϕ	mm	weight [mg]	Cumulative weight %	ϕ_{05}	ϕ_{25}	ϕ_{50}	ϕ_{x}	Md_{ϕ}	σ_{ϕ}	F2
-5.0	31.5	78947	12.82	4.9	2.7	-4.4	-5.2	-1.4	3.29	10.93%
-4.5	22.4	17379	15.64							
-4.0	16.0	22600	19.31							
-3.5	11.2	42136	26.15							
-3.0	8.0	30615	31.13							
-2.5	5.6	28909	35.82							
-2.0	4.0	30451	40.77							
-1.5	2.8	39227	47.14							
-1.0	2.0	40071	53.64							
-0.5	1.4	39253	60.02							
0.0	1.0	30769	65.01							
0.5	0.710	29338	69.78							
1.0	0.500	27169	74.16							
1.5	0.355	22447	77.84							
2.0	0.250	22222	81.44							
2.5	0.180	14793	83.85							
3.0	0.125	18616	86.87							
3.5	0.088	13579	89.07							
4.0	0.063	14154	91.37							
4.5	0.045	10193	93.03							
5.0	0.032	16485	95.71							
6.0	0.017	14640	98.08							
7.0	0.008	11805	100.00							

Minor Lithic Counts		Abundance [volume %]	
SMI.	GCI.	SMI.	GCI.
2	0	0.4	0
0	0	0	0
6	0	1.4	0
40	0	9.5	0
29	0	6.9	0
24	0	6.5	0
26	0	7.0	0
24	0	7.5	0
21	0	7.6	0

Counts:

ϕ	Wp	Gp	Bp	Xtal	Lithic	Glass	NA	total counts
-5.0	0	0	0	0	1	0	*0*	1
-4.5	0	0	0	0	1	0	*0*	1
-4.0	0	0	0	0	15	0	*0*	15
-3.5	0	0	0	0	2	0	*0*	2
-3.0	2	0	0	0	24	0	*0*	26
-2.5	6	0	0	0	63	0	*0*	69
-2.0	20	1	0	0	175	0	*0*	196
-1.5	33	0	1	0	486	0	*0*	520
-1.0	53	0	1	0	452	0	*0*	506
-0.5	39	0	0	0	449	0	*0*	488
0.0	22	0	0	0	435	2	*0*	459
0.5	21	0	0	0	422	4	*0*	447
1.0	14	0	0	3	419	19	*0*	455
1.5	19	0	0	12	368	11	*0*	410
2.0	9	0	0	41	374	19	*0*	443
2.5	0	0	0	94	320	22	*0*	436
3.0	0	0	0	168	278	49	*0*	495
3.5	0	0	0	218	264	62	*0*	544
4.0	0	0	0	239	198	79	*0*	516
4.5	0	0	0	95	191	108	*0*	394
5.0	*	*	*	*	*	*	*1030*	1030
6.0	*	*	*	*	*	*	*1330*	1330
7.0	*	*	*	*	*	*	*1686*	1686

Bulk Weight Percentages:

Wp	Gp	Bp	Xtal	Lithic	Glass	NA
0	0	0	0	12.82	0	0
0	0	0	0	2.82	0	0
0	0	0	0	3.67	0	0
0	0	0	0	6.84	0	0
0.13	0	0	0	4.84	0	0
0.13	0	0	0	4.57	0	0
0.22	0.02	0	0	4.71	0	0
0.23	0	0.01	0	6.13	0	0
0.34	0	0.01	0	6.16	0	0
0.31	0	0	0	6.07	0	0
0.15	0	0	0	4.83	0.02	0
0.14	0	0	0	4.59	0.04	0
0.10	0	0	0.03	4.12	0.17	0
0.08	0	0	0.11	3.37	0.09	0
0.02	0	0	0.34	3.10	0.14	0
0	0	0	0.52	1.77	0.11	0
0	0	0	1.03	1.71	0.28	0
0	0	0	0.91	1.10	0.20	0
0	0	0	1.10	0.91	0.29	0
0	0	0	0.42	0.82	0.38	0
*	*	*	*	*	*	2.68
*	*	*	*	*	*	2.38
*	*	*	*	*	*	1.92
1.85	**0.02**	**0.02**	**4.46**	**84.95**	**1.72**	**6.98**

Marquesado flow (pumice lens) deposit at Locality 78 [CBV-M-4] [Total sample weight: 614085 mg]

Grain diameter		Weight Fractions		Granulometric Analysis						
ϕ	mm	weight [mg]	Cumulative weight %	$\phi_{5\%}$	ϕ_{84}	ϕ_{16}	ϕ_{5}	Md$_\phi$	σ_ϕ	F2
-5.0	31.5	25800	4.20	4.7	2.9	-3.9	-4.8	-0.4	3.13	12.64%
-4.5	22.4	29100	8.94							
-4.0	16.0	29100	13.68							
-3.5	11.2	29200	18.43							
-3.0	8.0	20800	21.82							
-2.5	5.6	22200	25.44							
-2.0	4.0	27300	29.88							
-1.5	2.8	29400	34.67							
-1.0	2.0	38963	41.01							
-0.5	1.4	42083	47.87							
0.0	1.0	37671	54.00							
0.5	0.710	37687	60.14							
1.0	0.500	39601	66.59							
1.5	0.355	32131	71.82							
2.0	0.250	27980	76.38							
2.5	0.180	25094	80.46							
3.0	0.125	24160	84.40							
3.5	0.088	18210	87.36							
4.0	0.063	21344	90.84							
4.5	0.045	19340	93.99							
5.0	0.032	14175	96.30							
6.0	0.017	12590	98.35							
7.0	0.008	10150	100.00							

Minor Lithic Counts		Abundance [volume %]	
SML	GCL	SML	GCL
15	0	3.1	0
22	0	5.1	0
21	0	4.5	0
25	0	5.9	0
29	0	6.7	0
24	5	6.5	1.2
29	26	6.9	6.1
28	14	8.1	4.2
34	13	12.9	5.1

Counts:

ϕ	Wp	Gp	Bp	Xtal	Lithic	Glass	NA	total counts
-5.0	6	0	0	0	0	0	*0*	6
-4.5	8	0	0	0	0	0	*0*	8
-4.0	10	0	0	0	0	0	*0*	10
-3.5	17	0	0	0	9	0	*0*	26
-3.0	89	13	47	0	23	0	*0*	172
-2.5	270	18	22	0	65	0	*0*	375
-2.0	595	32	72	0	195	0	*0*	894
-1.5	451	64	77	0	544	0	*0*	1136
-1.0	303	19	0	0	428	0	*0*	750
-0.5	227	16	0	0	533	0	*0*	750
0.0	98	34	0	2	487	0	*0*	750
0.5	158	18	0	38	596	0	*0*	750
1.0	158	39	0	33	520	0	*0*	750
1.5	104	33	0	44	569	0	*0*	750
2.0	80	55	0	225	140	250	*0*	750
2.5	125	83	0	195	97	250	*0*	750
3.0	76	32	0	348	86	208	*0*	750
3.5	0	45	0	532	105	68	*0*	750
4.0	0	0	0	298	79	373	*0*	750
4.5	0	0	0	171	58	521	*0*	750
5.0	*	*	*	*	*	*	*886*	886
6.0	*	*	*	*	*	*	*1144*	1144
7.0	*	*	*	*	*	*	*1454*	1454

Bulk Weight Percentages:

Wp	Gp	Bp	Xtal	Lithic	Glass	NA
4.20	0	0	0	0	0	0
4.74	0	0	0	0	0	0
4.74	0	0	0	0	0	0
2.44	0	0	0	3.32	0	0
1.35	0.21	0.71	0	1.11	0	0
1.61	0.14	0.55	0	1.31	0	0
2.19	0.17	0.33	0	1.77	0	0
1.31	0.25	0.37	0	2.85	0	0
1.54	0.14	0	0	4.66	0	0
1.22	0.10	0	0	4.55	0	0
1.30	0.22	0	0.02	4.59	0	0
1.03	0.18	0	0.28	4.65	0	0
1.07	0.29	0	0.29	4.80	0	0
0.35	0.33	0	0.32	4.23	0	0
0.19	0.16	0	1.61	1.00	1.59	0
0.35	0.27	0	1.29	0.64	1.53	0
0.23	0.10	0	2.01	0.50	1.10	0
0	0.14	0	2.17	0.43	0.22	0
0	0	0	1.54	0.41	1.53	0
0	0	0	0.84	0.29	2.02	0
*	*	*	*	*	*	2.31
*	*	*	*	*	*	2.05
*	*	*	*	*	*	1.65
29.86	**2.70**	**1.96**	**10.37**	**41.11**	**7.99**	**6.01**

Marquesado flow (lag breccia) base deposit at Locality 79 [CBV-M-6] [Total sample weight: 804144 mg]

Grain diameter		Weight Fractions		Granulometric Analysis						
ϕ	mm	weight [mg]	Cumulative weight %	ϕ_{05}	ϕ_{25}	ϕ_{50}	ϕ_{75}	Md_ϕ	σ_ϕ	F2
-5.0	31.5	0	0	5.4	4.8	-2.7	-4.5	0.9	3.35	26.22%
-4.5	22.4	40750	5.07							
-4.0	16.0	40750	10.14							
-3.5	11.2	17500	12.31							
-3.0	8.0	21200	14.95							
-2.5	5.6	21900	17.67							
-2.0	4.0	27500	21.09							
-1.5	2.8	28400	24.62							
-1.0	2.0	31163	28.50							
-0.5	1.4	64953	36.58							
0.0	1.0	34129	40.82							
0.5	0.710	37445	45.48							
1.0	0.500	38525	50.27							
1.5	0.355	38271	55.03							
2.0	0.250	37429	59.68							
2.5	0.180	31389	63.58							
3.0	0.125	42986	68.93							
3.5	0.088	38973	73.78							
4.0	0.063	38973	78.62							
4.5	0.045	91393	89.99							
5.0	0.032	30920	93.83							
6.0	0.017	27460	97.25							
7.0	0.008	22140	100.00							

Minor Lithic Counts		Abundance [volume %]	
SML	GCL	SML	GCL
0	0	0	0
2	0	0.3	0
4	0	0.6	0
6	0	0.9	0
7	0	1.1	0
5	0	0.8	0
6	0	1.1	0
5	0	0.8	0
5	0	1.1	0

Counts:

ϕ	Wp	Gp	Bp	Xtal	Lithic	Glass	NA	total counts
-5.0	0	0	0	0	0	0	*0*	0
-4.5	0	0	0	0	3	0	*0*	3
-4.0	12	0	0	0	4	0	*0*	16
-3.5	16	0	0	0	16	0	*0*	32
-3.0	29	1	0	0	29	0	*0*	59
-2.5	34	0	0	0	35	0	*0*	69
-2.0	46	0	0	0	214	0	*0*	260
-1.5	283	24	0	0	443	0	*0*	750
-1.0	69	12	0	0	669	0	*0*	750
-0.5	101	11	0	0	638	0	*0*	750
0.0	35	17	0	0	698	0	*0*	750
0.5	33	10	0	13	690	4	*0*	750
1.0	47	5	0	23	657	18	*0*	750
1.5	33	5	0	63	589	60	*0*	750
2.0	43	0	0	77	559	71	*0*	750
2.5	83	0	0	188	431	48	*0*	750
3.0	80	0	0	196	403	71	*0*	750
3.5	98	0	0	139	319	114	*0*	670
4.0	114	0	0	127	241	149	*0*	631
4.5	198	0	0	24	203	204	*0*	629
5.0	*	*	*	*	*	*	*1932*	1932
6.0	*	*	*	*	*	*	*2496*	2496
7.0	*	*	*	*	*	*	*3202*	3202

Bulk Weight Percentages:

ϕ	Wp	Gp	Bp	Xtal	Lithic	Glass	NA
-5.0	0	0	0	0	0	0	0
-4.5	0	0	0	0	5.07	0	0
-4.0	2.52	0	0	0	2.55	0	0
-3.5	0.78	0	0	0	1.40	0	0
-3.0	0.62	0.02	0	0	1.99	0	0
-2.5	0.61	0	0	0	2.11	0	0
-2.0	0.27	0	0	0	3.15	0	0
-1.5	0.90	0.10	0	0	2.53	0	0
-1.0	0.18	0.04	0	0	3.66	0	0
-0.5	0.36	0.08	0	0	7.33	0	0
0.0	0.12	0.07	0	0	4.05	0	0
0.5	0.13	0.08	0	0.08	4.35	0.02	0
1.0	0.22	0.03	0	0.14	4.29	0.10	0
1.5	0.10	0.04	0	0.40	3.88	0.34	0
2.0	0.09	0	0	0.50	3.65	0.41	0
2.5	0.20	0	0	1.05	2.02	0.25	0
3.0	0.32	0	0	1.48	3.05	0.49	0
3.5	0.60	0	0	1.08	2.48	0.69	0
4.0	0.76	0	0	1.07	2.03	0.99	0
4.5	0.71	0	0	0.70	5.95	4.72	0
5.0	*	*	*	*	*	*	3.84
6.0	*	*	*	*	*	*	3.41
7.0	*	*	*	*	*	*	2.75
	9.49	**0.46**	**0**	**6.50**	**65.54**	**8.01**	**10.00**

Marquesado flow (body) middle deposit at Locality 79 [CBV-M-7] [Total sample weight 548150 mg]

Grain diameter		Weight Fractions		Granulometric Analysis						
ϕ	mm	weight [mg]	Cumulative weight %	ϕ_{05}	ϕ_{84}	ϕ_{10}	ϕ_{x}	Md_{ϕ}	σ_{ϕ}	F2
-5.0	31.5	0	0	4.4	3.8	-2.6	-4.1	0.3	2.88	19.16%
-4.5	22.4	0	0							
-4.0	16.0	36300	6.62							
-3.5	11.2	11900	8.79							
-3.0	8.0	26600	13.65							
-2.5	5.6	17800	16.89							
-2.0	4.0	20800	20.69							
-1.5	2.8	25100	25.27							
-1.0	2.0	28468	30.46							
-0.5	1.4	32245	36.34							
0.0	1.0	30097	41.83							
0.5	0.710	30651	47.43							
1.0	0.500	31714	53.21							
1.5	0.355	29669	58.62							
2.0	0.250	27218	63.59							
2.5	0.180	24621	68.08							
3.0	0.125	38355	75.08							
3.5	0.088	31582	80.84							
4.0	0.063	39785	88.10							
4.5	0.045	41521	95.67							
5.0	0.032	9110	97.33							
6.0	0.017	8090	98.81							
7.0	0.008	6525	100.00							

Minor Lithic Counts:		Abundance [volume %]	
SML	GCL	SML	GCL
0	0	0	0
0	0	0	0
0	0	0	0
0	0	0	0
0	0	0	0
0	0	0	0
0	0	0	0
0	0	0	0
0	0	0	0

Counts:

ϕ	Wp	Gp	Bp	Xtal	Lithic	Glass	NA	total counts
-5.0	0	0	0	0	0	0	0	0
-4.5	0	0	0	0	0	0	0	0
-4.0	0	0	0	0	4	0	0	4
-3.5	0	0	0	0	3	0	0	3
-3.0	3	1	2	0	21	0	0	27
-2.5	19	0	0	0	35	0	0	54
-2.0	41	0	0	0	161	0	0	202
-1.5	49	13	32	0	551	0	0	645
-1.0	60	1	2	0	669	0	0	732
-0.5	72	17	8	0	638	0	0	735
0.0	105	23	15	1	698	0	0	842
0.5	70	0	0	15	690	4	0	779
1.0	40	0	0	75	657	18	0	790
1.5	54	0	0	112	589	60	0	815
2.0	64	0	0	192	559	71	0	886
2.5	41	0	0	195	431	48	0	715
3.0	28	0	0	289	403	71	0	791
3.5	0	0	0	149	319	114	0	582
4.0	0	0	0	112	241	149	0	502
4.5	0	0	0	49	203	204	0	456
5.0	*	*	*	*	*	*	569	569
6.0	*	*	*	*	*	*	735	735
7.0	*	*	*	*	*	*	932	932

Bulk Weight Percentages:

Wp	Gp	Bp	Xtal	Lithic	Glass	NA
0	0	0	0	0	0	0
0	0	0	0	0	0	0
0	0	0	0	6.62	0	0
0	0	0	0	2.17	0	0
0.20	0.07	0.13	0	4.45	0	0
0.45	0	0	0	2.80	0	0
0.36	0	0	0	3.44	0	0
0.20	0.07	0.22	0	4.08	0	0
0.21	0.01	0.01	0	4.97	0	0
0.35	0.09	0.04	0	5.40	0	0
0.44	0.11	0.07	0.01	4.86	0	0
0.44	0	0	0.10	5.02	0.03	0
0.22	0	0	0.54	4.91	0.12	0
0.10	0	0	0.76	4.12	0.36	0
0.13	0	0	1.14	3.32	0.38	0
0.11	0	0	1.27	2.81	0.29	0
0.14	0	0	2.62	3.65	0.59	0
0	0	0	1.54	3.37	0.92	0
0	0	0	1.73	3.71	1.82	0
0	0	0	0.90	3.72	2.95	0
*	*	*	*	*	*	1.66
*	*	*	*	*	*	1.48
*	*	*	*	*	*	1.19
3.35	**0.35**	**0.47**	**10.62**	**73.42**	**7.46**	**4.33**

Marquesado flow (lag breccia) middle deposit at Locality 79 [CBV-M-8] [Total sample weight: 407721 mg]

Grain diameter		Weight Fractions:		Granulometric Analysis						
ϕ	mm	weight [mg]	Cumulative weight %	ϕ_{05}	ϕ_{50}	ϕ_{95}	ϕ_5	Md$_\phi$	σ_ϕ	F2
-5.0	31.5	0	0	5.5	4.3	-3.1	-4.1	1.5	3.29	25.36%
-4.5	22.4	0	0							
-4.0	16.0	34100	8.36							
-3.5	11.2	19500	13.15							
-3.0	8.0	13400	16.43							
-2.5	5.6	11200	19.18							
-2.0	4.0	12100	22.15							
-1.5	2.8	13300	25.41							
-1.0	2.0	14322	28.92							
-0.5	1.4	16879	33.06							
0.0	1.0	16027	33.99							
0.5	0.710	17149	41.20							
1.0	0.500	18566	45.75							
1.5	0.355	19239	50.47							
2.0	0.250	20754	55.56							
2.5	0.180	22387	61.05							
3.0	0.125	28806	68.12							
3.5	0.088	26959	74.64							
4.0	0.063	26959	81.16							
4.5	0.045	28340	88.13							
5.0	0.032	18585	92.69							
6.0	0.017	16500	96.74							
7.0	0.008	13310	100.00							

Minor Lithic Counts		Abundance [volume %]	
SML	GCL	SML	GCL
0	0	0	0
5	0	0.8	0
6	0	0.9	0
5	0	0.8	0
7	0	1.2	0
12	0	2.0	0
14	0	2.9	0
15	0	3.9	0
18	0	4.5	0

Counts:

ϕ	Wp	Gp	Bp	Xtal	Lithic	Glass	NA	total counts
-5.0	0	0	0	0	0	0	*0*	0
-4.5	0	0	0	0	0	0	*0*	0
-4.0	0	0	0	0	3	0	*0*	3
-3.5	0	0	0	0	6	0	*0*	6
-3.0	0	0	0	0	12	0	*0*	12
-2.5	6	0	0	0	28	0	*0*	34
-2.0	11	0	0	0	98	0	*0*	109
-1.5	14	8	4	0	316	0	*0*	342
-1.0	67	11	1	0	669	0	*0*	748
-0.5	43	19	0	0	638	0	*0*	700
0.0	35	10	0	11	694	0	*0*	750
0.5	38	24	0	35	653	0	*0*	750
1.0	37	25	0	109	579	0	*0*	750
1.5	23	14	0	114	589	10	*0*	750
2.0	39	13	0	198	481	19	*0*	750
2.5	41	3	0	275	382	49	*0*	750
3.0	21	0	0	208	403	81	*0*	713
3.5	0	0	0	113	319	98	*0*	530
4.0	0	0	0	84	241	129	*0*	454
4.5	0	0	0	39	203	188	*0*	430
5.0	*	*	*	*	*	*	*1162*	1162
6.0	*	*	*	*	*	*	*1502*	1502
7.0	*	*	*	*	*	*	*1902*	1902

Bulk Weight Percentages:

ϕ	Wp	Gp	Bp	Xtal	Lithic	Glass	NA
-5.0	0	0	0	0	0	0	0
-4.5	0	0	0	0	0	0	0
-4.0	0	0	0	0	8.36	0	0
-3.5	0	0	0	0	4.78	0	0
-3.0	0	0	0	0	3.29	0	0
-2.5	0.16	0	0	0	2.58	0	0
-2.0	0.13	0	0	0	2.84	0	0
-1.5	0.08	0.06	0.04	0	3.09	0	0
-1.0	0.16	0.04	0.0+	0	3.32	0	0
-0.5	0.15	0.07	0	0	3.92	0	0
0.0	0.11	0.04	0	0.06	3.72	0	0
0.5	0.12	0.17	0	0.19	3.73	0	0
1.0	0.17	0.13	0	0.65	3.61	0	0
1.5	0.07	0.12	0	0.71	3.77	0.05	0
2.0	0.09	0.04	0	1.41	3.43	0.12	0
2.5	0.13	0.01	0	2.09	2.91	0.35	0
3.0	0.12	0	0	2.11	4.09	0.75	0
3.5	0	0	0	1.45	4.09	0.98	0
4.0	0	0	0	1.28	3.68	1.56	0
4.5	0	0	0	0.70	3.62	2.65	0
5.0	*	*	*	*	*	*	4.56
6.0	*	*	*	*	*	*	4.05
7.0	*	*	*	*	*	*	3.26
	1.48	**0.68**	**0.04**	**10.65**	**68.83**	**6.46**	**11.87**

Marquesado flow (body) top deposit at Locality 79 [CBV-M-9] [Total sample weight 567990 mg]

Grain diameter		Weight Fractions		Granulometric Analysis						
ϕ	mm	weight [mg]	Cumulative weight %	ϕ_{05}	ϕ_{84}	ϕ_{16}	$\phi_{\bar{x}}$	Md$_\phi$	σ_ϕ	F2
-5.0	31.5	0	0	6.4	5.0	-1.2	-3.2	2.9	2.99	40.55%
-4.5	22.4	0	0							
-4.0	16.0	14300	2.52							
-3.5	11.2	8400	4.00							
-3.0	8.0	11900	6.09							
-2.5	5.6	11500	8.12							
-2.0	4.0	16300	10.99							
-1.5	2.8	18600	14.26							
-1.0	2.0	18366	17.49							
-0.5	1.4	19796	20.98							
0.0	1.0	20534	24.59							
0.5	0.710	22430	28.54							
1.0	0.500	25570	33.05							
1.5	0.355	23149	37.12							
2.0	0.250	25016	41.53							
2.5	0.180	13789	43.95							
3.0	0.125	43924	51.69							
3.5	0.088	44105	59.45							
4.0	0.063	44105	67.22							
4.5	0.045	44203	75.00							
5.0	0.032	54530	57.60							
6.0	0.017	48425	93.12							
7.0	0.008	39050	100.00							

Minor Lithic Counts		Abundance [volume %]	
SMI.	GCI.	SMI.	GCI.
8	0	1.2	0
26	0	4.1	0
32	0	4.6	0
28	0	4.3	0
25	0	4.3	0
24	0	4.1	0
27	0	5.6	0
19	0	5.0	0
20	0	5.0	0

Counts:

ϕ	Wp	Gp	Bp	Xtal	Lithic	Glass	NA	total counts
-5.0	0	0	0	0	0	0	*0*	0
-4.5	0	0	0	0	0	0	*0*	0
-4.0	2	0	0	0	1	0	*0*	3
-3.5	3	0	0	0	1	0	*0*	1
-3.0	0	0	3	0	9	0	*0*	12
-2.5	6	0	0	0	29	0	*0*	35
-2.0	8	0	0	0	131	0	*0*	139
-1.5	9	6	5	0	316	0	*0*	336
-1.0	45	6	0	0	669	0	*0*	720
-0.5	34	12	0	5	638	0	*0*	689
0.0	20	13	0	8	694	0	*0*	735
0.5	14	8	0	39	653	0	*0*	714
1.0	9	5	0	77	579	0	*0*	670
1.5	13	4	0	91	589	9	*0*	706
2.0	20	2	0	102	481	20	*0*	625
2.5	0	0	0	216	382	42	*0*	640
3.0	0	0	0	198	403	63	*0*	664
3.5	0	0	0	73	319	115	*0*	507
4.0	0	0	0	64	241	225	*0*	530
4.5	0	0	0	38	203	345	*0*	589
5.0	*	*	*	*	*	*	*3408*	3408
6.0	*	*	*	*	*	*	*4402*	4402
7.0	*	*	*	*	*	*	*5579*	5579

Bulk Weight Percentages:

ϕ	Wp	Gp	Bp	Xtal	Lithic	Glass	NA
-5.0	0	0	0	0	0	0	0
-4.5	0	0	0	0	0	0	0
-4.0	1.00	0	0	0	1.52	0	0
-3.5	0.93	0	0	0	0.55	0	0
-3.0	0	0	0.20	0	1.90	0	0
-2.5	0.12	0	0	0	1.91	0	0
-2.0	0.07	0	0	0	2.80	0	0
-1.5	0.05	0.05	0.05	0	3.13	0	0
-1.0	0.10	0.02	0	0	3.12	0	0
-0.5	0.10	0.04	0	0.02	3.32	0	0
0.0	0.06	0.05	0	0.04	3.47	0	0
0.5	0.06	0.06	0	0.21	3.62	0	0
1.0	0.04	0.03	0	0.50	3.93	0	0
1.5	0.03	0.03	0	0.52	3.45	0.04	0
2.0	0.05	0.01	0	0.74	3.48	0.13	0
2.5	0	0	0	0.82	1.46	0.15	0
3.0	0	0	0	2.33	4.73	0.68	0
3.5	0	0	0	1.18	5.14	1.45	0
4.0	0	0	0	1.03	3.87	2.87	0
4.5	0	0	0	0.58	3.02	4.13	0
5.0	*	*	*	*	*	*	9.60
6.0	*	*	*	*	*	*	8.53
7.0	*	*	*	*	*	*	6.88
	2.61	**0.29**	**0.25**	**7.97**	**54.42**	**9.45**	**25.01**

Marquesado flow distal deposit at Locality 80 [CBV-M-10] [Total sample weight: 340429 mg]

Grain diameter		Weight Fractions		Granulometric Analysis						
ϕ	mm	weight [mg]	Cumulative weight %	ϕ_{95}	ϕ_{84}	ϕ_{16}	ϕ_5	Md_ϕ	σ_ϕ	F2
-5.0	31.5	0	0	6.4	5.4	0.9	-0.6	3.4	2.20	49.28%
-4.5	22.4	0	0							
-4.0	16.0	0	0							
-3.5	11.2	0	0							
-3.0	8.0	249	0.08							
-2.5	5.6	627	0.26							
-2.0	4.0	1253	0.63							
-1.5	2.8	2670	1.41							
-1.0	2.0	4474	2.72							
-0.5	1.4	8331	5.17							
0.0	1.0	9558	7.98							
0.5	0.710	14863	12.34							
1.0	0.500	16403	17.16							
1.5	0.355	18556	22.61							
2.0	0.250	21267	28.86							
2.5	0.180	23028	35.63							
3.0	0.125	30197	44.50							
3.5	0.088	21182	50.72							
4.0	0.063	30098	59.56							
4.5	0.045	36984	70.42							
5.0	0.032	38665	81.78							
6.0	0.017	34335	91.87							
7.0	0.008	27690	100.00							

Minor Lithic Counts:		Abundance [volume %]	
SMI:	GCI:	SMI	GCI
7	0	4.7	0
16	0	5.3	0
230	0	8.3	0
18	0	6.0	0
15	0	4.3	0
17	0	5.5	0
19	0	7.4	0
21	0	9.1	0
14	0	6.7	0

Counts:

ϕ	Wp	Gp	Bp	Xtal	Lithic	Glass	NA	total counts
-5.0	0	0	0	0	0	0	*0*	0
-4.5	0	0	0	0	0	0	*0*	0
-4.0	0	0	0	0	0	0	*0*	0
-3.5	0	0	0	0	0	0	*0*	0
-3.0	1.2	0	0	0	0	0	*0*	1
-2.5	16	0	1	0	0	0	*0*	3
-2.0	139	7	0	0	0	0	*0*	23
-1.5	175	14	9	0	41	0	*0*	203
-1.0	166	24	19	0	150	0	*0*	368
-0.5	241	27	3	0	304	0	*0*	500
0.0	153	8	4	1	241	2	*0*	500
0.5	81	12	2	13	298	22	*0*	500
1.0	96	11	11	19	346	29	*0*	500
1.5	119	12	2	45	308	37	*0*	500
2.0	134	13	2	62	257	47	*0*	500
2.5	129	9	4	71	231	51	*0*	500
3.0	121	4	3	99	209	56	*0*	500
3.5	0	0	0	103	79	197	*0*	500
4.0	0	0	0	64	61	375	*0*	500
4.5	0	0	0	34	48	418	*0*	500
5.0	*	*	*	*	*	*	*2417*	2417
6.0	*	*	*	*	*	*	*3121*	3121
7.0	*	*	*	*	*	*	*3955*	3955

Bulk Weight Percentages:

ϕ	Wp	Gp	Bp	Xtal	Lithic	Glass	NA
-5.0	0	0	0	0	0	0	0
-4.5	0	0	0	0	0	0	0
-4.0	0	0	0	0	0	0	0
-3.5	0	0	0	0	0	0	0
-3.0	0.07	0	0	0	0	0	0
-2.5	0.06	0	0.12	0	0	0	0
-2.0	0.23	0.14	0	0	0	0	0
-1.5	0.44	0.06	0.05	0	0.23	0	0
-1.0	0.41	0.08	0.06	0	0.73	0	0
-0.5	0.56	0.09	0.01	0	1.89	0	0
0.0	1.06	0.04	0.03	0.01	1.69	0.01	0
0.5	1.25	0.13	0.01	0.11	2.67	0.18	0
1.0	0.61	0.09	0.09	0.19	3.58	0.26	0
1.5	0.53	0.20	0.03	0.53	3.76	0.39	0
2.0	0.61	0.08	0.01	0.95	3.95	0.61	0
2.5	0.94	0.07	0.03	1.16	3.75	0.78	0
3.0	1.42	0.04	0.03	2.03	4.29	1.05	0
3.5	1.37	0	0	1.49	1.14	2.23	0
4.0	0	0	0	1.34	1.28	6.22	0
4.5	0	0	0	0.90	1.27	8.70	0
5.0	*	*	*	*	*	*	11.36
6.0	*	*	*	*	*	*	10.09
7.0	*	*	*	*	*	*	8.13
	9.56	**1.02**	**0.47**	**8.71**	**30.23**	**20.43**	**29.58**

Marquesado flow (body) base deposit at Locality 81 [CBV-M-13] [Total sample weight: 720345 mg]

Grain diameter		Weight Fractions:		Granulometric Analysis						
ϕ	mm	weight [mg]	Cumulative weight %	ϕ_{05}	ϕ_{84}	ϕ_{16}	ϕ_z	Md_ϕ	σ_ϕ	F2
-5.0	31.5	78300	10.87	5.0	3.7	-4.2	-5.2	-0.7	3.49	17.68%
-4.5	22.4	0	10.87							
-4.0	16.0	42300	16.74							
-3.5	11.2	22200	19.82							
-3.0	8.0	28100	23.72							
-2.5	5.6	34800	28.56							
-2.0	4.0	35100	33.43							
-1.5	2.8	42200	39.29							
-1.0	2.0	45671	45.63							
-0.5	1.4	43409	51.65							
0.0	1.0	38370	56.98							
0.5	0.710	37464	62.18							
1.0	0.500	64707	67.00							
1.5	0.355	30035	71.17							
2.0	0.250	24886	74.62							
2.5	0.180	20989	77.54							
3.0	0.125	17233	79.93							
3.5	0.088	17233	82.32							
4.0	0.063	31112	86.64							
4.5	0.045	44203	92.78							
5.0	0.032	19980	95.55							
6.0	0.017	17745	98.01							
7.0	0.008	14310	100.00							

Minor Lithic Counts		Abundance [volume %]	
SML	GCL	SML	GCL
6	0	0.9	0
9	0	1.4	0
14	0	2.0	0
18	0	2.8	0
19	0	3.3	0
14	0	2.4	0
9	0	1.9	0
11	0	2.9	0
6	0	1.5	0

Counts:

ϕ	Wp	Gp	Bp	Xtal	Lithic	Glass	NA	total counts
-5.0	0	0	0	0	1	0	*0*	1
-4.5	0	0	0	0	0	0	*0*	0
-4.0	0	0	0	0	4	0	*0*	4
-3.5	0	0	0	0	2	0	*0*	2
-3.0	0	0	0	0	19	0	*0*	19
-2.5	5	2	5	0	57	0	*0*	96
-2.0	23	0	8	0	271	0	*0*	302
-1.5	49	9	6	0	954	0	*0*	1018
-1.0	87	18	5	2	669	0	*0*	781
-0.5	82	20	5	2	638	0	*0*	747
0.0	158	41	12	2	694	0	*0*	907
0.5	77	18	4	12	653	0	*0*	764
1.0	71	12	1	29	579	0	*0*	692
1.5	72	14	0	68	589	9	*0*	752
2.0	74	14	0	101	481	20	*0*	960
2.5	52	11	0	124	382	42	*0*	611
3.0	43	8	0	119	403	63	*0*	636
3.5	0	0	0	89	319	115	*0*	523
4.0	0	0	0	61	241	225	*0*	527
4.5	0	0	0	42	203	345	*0*	590
5.0	*	*	*	*	*	*	*1249*	1249
6.0	*	*	*	*	*	*	*1613*	1613
7.0	*	*	*	*	*	*	*2044*	2044

Bulk Weight Percentages:

ϕ	Wp	Gp	Bp	Xtal	Lithic	Glass	NA
-5.0	0	0	0	0	10.87	0	0
-4.5	0	0	0	0	0	0	0
-4.0	0	0	0	0	5.87	0	0
-3.5	0	0	0	0	3.08	0	0
-3.0	0	0	0	0	3.90	0	0
-2.5	0.08	0.04	0.33	0	4.39	0	0
-2.0	0.16	0	0.07	0	4.64	0	0
-1.5	0.16	0.04	0.03	0	5.62	0	0
-1.0	0.35	0.11	0.03	0.02	5.84	0	0
-0.5	0.41	0.10	0.03	0.02	5.47	0	0
0.0	0.62	0.18	0.05	0.01	4.46	0	0
0.5	0.61	0.15	0.02	0.08	4.35	0	0
1.0	0.37	0.07	0.01	0.20	4.17	0	0
1.5	0.19	0.11	0	0.39	3.44	0.04	0
2.0	0.14	0.03	0	0.55	2.64	0.10	0
2.5	0.11	0.03	0	0.63	1.94	0.20	0
3.0	0.09	0.02	0	0.47	1.59	0.23	0
3.5	0	0	0	0.43	1.51	0.43	0
4.0	0	0	0	0.55	2.17	1.60	0
4.5	0	0	0	0.50	2.41	3.23	0
5.0	*	*	*	*	*	*	2.77
6.0	*	*	*	*	*	*	2.46
7.0	*	*	*	*	*	*	1.99
	3.29	**0.88**	**0.57**	**3.85**	**78.36**	**5.83**	**7.22**

Marquesado flow (body) middle deposit at Locality 81 [CBV-M-14] [Total sample weight: 1125559 mg]

Grain diameter		Weight Fractions		Granulometric Analysis						
ϕ	mm	weight [mg]	Cumulative weight %	ϕ_{95}	ϕ_{84}	ϕ_{16}	ϕ_5	Md$_\phi$	σ_ϕ	F2
-5.0	31.5	51000	4.53	4.7	3.0	-3.4	-5.2	-0.5	3.06	11.75%
-4.5	22.4	0	4.53							
-4.0	16.0	65900	10.39							
-3.5	11.2	45000	14.38							
-3.0	8.0	46900	18.55							
-2.5	5.6	62202	24.08							
-2.0	4.0	63851	29.75							
-1.5	2.8	68250	35.81							
-1.0	2.0	70219	42.05							
-0.5	1.4	75806	48.79							
0.0	1.0	59660	54.09							
0.5	0.710	72497	60.53							
1.0	0.500	68588	66.62							
1.5	0.355	64884	72.39							
2.0	0.250	53191	77.11							
2.5	0.180	43199	80.95							
3.0	0.125	45379	84.98							
3.5	0.088	36801	88.25							
4.0	0.063	35619	91.42							
4.5	0.045	35089	94.53							
5.0	0.032	23625	96.63							
6.0	0.017	20980	98.50							
7.0	0.008	16920	100.00							

Minor Lithic Counts		Abundance [volume %]	
SML	GCL	SML	GCL
25	0	5.3	0
16	0	3.5	0
20	0	4.2	0
23	0	5.3	0
22	0	5.5	0
22	0	5.8	0
25	0	6.7	0
26	0	7.2	0
23	0	6.7	0

Counts:

ϕ	Wp	Gp	Bp	Xtal	Lithic	Glass	NA	total counts
-5.0	0	0	0	0	1	0	0	1
-4.5	0	0	0	0	0	0	0	0
-4.0	0	0	0	0	4	0	0	4
-3.5	0	0	0	0	12	0	0	12
-3.0	0	0	0	0	41	0	0	41
-2.5	4	0	1	0	121	0	0	126
-2.0	46	0	16	0	460	0	0	522
-1.5	34	0	8	0	471	0	0	513
-1.0	23	1	0	2	474	0	0	500
-0.5	28	7	3	4	458	0	0	500
0.0	19	10	1	1	471	0	0	500
0.5	24	9	0	32	435	0	0	500
1.0	32	8	0	51	397	12	0	500
1.5	29	1	0	88	380	2	0	500
2.0	22	0	0	101	371	6	0	500
2.5	19	0	0	112	359	10	0	500
3.0	11	0	0	139	343	7	0	500
3.5	0	0	0	118	298	84	0	500
4.0	0	0	0	79	211	210	0	500
4.5	0	0	0	51	173	276	0	500
5.0	*	*	*	*	*	*	1477	1477
6.0	*	*	*	*	*	*	1907	1907
7.0	*	*	*	*	*	*	2417	2417

Bulk Weight Percentages:

Wp	Gp	Bp	Xtal	Lithic	Glass	NA
0	0	0	0	4.53	0	0
0	0	0	0	0	0	0
0	0	0	0	5.85	0	0
0	0	0	0	4.00	0	0
0	0	0	0	4.17	0	0
0.05	0	0.06	0	5.42	0	0
0.22	0	0.09	0	5.36	0	0
0.23	0	0.09	0	5.74	0	0
0.14	0.01	0	0.02	6.07	0	0
0.23	0.06	0.03	0.05	6.37	0	0
0.11	0.08	0.01	0.01	5.10	0	0
0.13	0.15	0	0.41	5.76	0	0
0.29	0.08	0	0.61	4.97	0.13	0
0.16	0.02	0	1.02	4.55	0.02	0
0.07	0	0	0.98	3.62	0.05	0
0.06	0	0	0.88	2.82	0.07	0
0.05	0	0	1.13	2.80	0.05	0
0	0	0	0.80	2.02	0.45	0
0	0	0	0.55	1.46	1.15	0
0	0	0	0.36	1.22	1.54	0
*	*	*	*	*	*	1.74
*	*	*	*	*	*	2.34
*	*	*	*	*	*	1.39
1.74	**0.40**	**0.28**	**6.82**	**81.83**	**3.46**	**5.47**

Marquesado flow (body) top deposit at Locality 81 [CBV-M-16] [Total sample weight 589376 mg]

Grain diameter		Weight Fractions		Granulometric Analysis						
ϕ	mm	weight [mg]	Cumulative weight %	ϕ_{05}	ϕ_{84}	ϕ_{16}	ϕ_{50}	Md$_\phi$	σ_ϕ	F:
-5.0	31.5	22400	3.80	5.3	3.9	-3.4	-4.5	0.6	3.31	19.78%
-4.5	22.4	7200	5.02							
-4.0	16.0	18420	8.15							
-3.5	11.2	42700	15.39							
-3.0	8.0	32300	20.87							
-2.5	5.6	30300	26.01							
-2.0	4.0	24500	30.17							
-1.5	2.8	20016	33.51							
-1.0	2.0	17280	36.50							
-0.5	1.4	20138	39.92							
0.0	1.0	22961	43.81							
0.5	0.710	25562	48.15							
1.0	0.500	29199	53.10							
1.5	0.355	28971	58.02							
2.0	0.250	27201	62.63							
2.5	0.180	27483	67.30							
3.0	0.125	39281	73.96							
3.5	0.088	36910	80.22							
4.0	0.063	33057	85.83							
4.5	0.045	31651	91.20							
5.0	0.032	19910	84.58							
6.0	0.017	17680	97.58							
7.0	0.008	14260	100.00							

Minor Lithic Counts		Abundance [volume %]	
SML	GCL	SML	GCL
4	0	6.7	0
10	0	6.2	0
14	0	5.6	0
11	0	3.9	0
8	0	2.7	0
12	0	4.0	0
13	0	4.4	0
12	0	4.2	0
11	0	4.3	0

Counts:

ϕ	Wp	Gp	Bp	Xtal	Lithic	Glass	NA	total counts
-5.0	1	0	0	0	0	0	0	1
-4.5	1	0	0	0	0	0	0	1
-4.0	6	0	4	0	0	0	0	10
-3.5	49	3	3	0	2	0	0	57
-3.0	82	1	13	0	4	0	0	103
-2.5	196	17	36	0	3	0	0	252
-2.0	364	36	32	0	21	0	0	453
-1.5	417	11	42	0	30	0	0	500
-1.0	379	42	19	0	60	0	0	500
-0.5	297	29	12	0	162	0	0	500
0.0	228	16	7	1	248	0	0	500
0.5	191	12	2	13	280	2	0	500
1.0	172	3	0	19	297	9	0	500
1.5	142	4	0	45	298	11	0	500
2.0	130	4	0	62	296	8	0	500
2.5	129	0	0	71	288	12	0	500
3.0	127	0	0	99	257	17	0	500
3.5	117	0	0	103	228	52	0	500
4.0	0	0	0	64	201	235	0	500
4.5	0	0	0	34	184	282	0	500
5.0	*	*	*	*	*	*	*1244*	1244
6.0	*	*	*	*	*	*	*1607*	1607
7.0	*	*	*	*	*	*	*2037*	2037

Bulk Weight Percentages:

Wp	Gp	Bp	Xtal	Lithic	Glass	NA
3.80	0	0	0	0	0	0
1.22	0	0	0	0	0	0
2.22	0	0.91	0	0	0	0
6.23	0.18	0.38	0	0.46	0	0
4.07	0.21	0.64	0	0.62	0	0
2.65	0.31	2.04	0	0.14	0	0
2.99	0.42	0.32	0	0.43	0	0
2.55	0.09	0.43	0	0.33	0	0
3.18	0.30	0.14	0	0.63	0	0
1.64	0.17	0.07	0	1.54	0	0
1.34	0.11	0.05	0.01	2.39	0	0
1.29	0.15	0.01	0.12	2.74	0.02	0
1.38	0.03	0	0.20	3.26	0.09	0
0.75	0.06	0	0.51	3.48	0.11	0
0.49	0.02	0	0.70	3.33	0.08	0
0.61	0	0	0.78	3.16	0.12	0
1.03	0	0	1.50	3.90	0.24	0
1.24	0	0	1.39	3.08	0.55	0
0	0	0	0.80	2.50	2.32	0
0	0	0	0.41	0.83	2.71	0
*	*	*	*	*	*	3.38
*	*	*	*	*	*	3.00
*	*	*	*	*	*	2.42
38.68	**2.05**	**4.99**	**6.42**	**32.82**	**6.24**	**8.80**

el at Locality 65 [CBV-65-1] [Total sample weight 41289.5 mg]

Grain diameter		Weight Fractions		Granulometric Analysis						
ϕ	mm	weight [mg]	Cumulative weight %	ϕ_{05}	ϕ_{25}	ϕ_{50}	ϕ_{75}	Md_ϕ	σ_ϕ	F2
-5.0	31.5	0	0	5.4	4.6	-0.8	-1.8	2.4	2.43	32.71%
-4.5	22.4	0	0							
-4.0	16.0	0	0							
-3.5	11.2	0	0							
-3.0	8.0	203.8	0.49							
-2.5	5.6	264.7	1.13							
-2.0	4.0	495.0	2.33							
-1.5	2.8	2364.8	8.06							
-1.0	2.0	2342	13.73							
-0.5	1.4	3447	22.08							
0.0	1.0	3696	31.03							
0.5	0.710	2614	37.36							
1.0	0.500	1493	40.98							
1.5	0.355	1607	44.87							
2.0	0.250	1018	47.34							
2.5	0.180	1289	50.46							
3.0	0.125	1941	55.16							
3.5	0.088	5008	67.29							
4.0	0.063	2617	73.63							
4.5	0.045	4181	83.75							
5.0	0.032	3710	92.75							
6.0	0.017	2285	98.29							
7.0	0.008	710	100.00							

Minor Lithic Counts		Abundance [volume %]	
SML	GCL	SML	GCL
11	0	36.7	0
4	0	1.3	0
5	0	0.9	0
6	0	1.4	0
6	0	1.3	0
5	0	1.1	0
1	0	0.3	0
0	0	0	0
0	0	0	0

Counts:

ϕ	Wp	Gp	Bp	Xtal	Lithic	Glass	NA	total counts
-5.0	0	0	0	0	0	0	0	0
-4.5	0	0	0	0	0	0	0	0
-4.0	0	0	0	0	0	0	0	0
-3.5	0	0	0	0	0	0	0	0
-3.0	1	0	0	0	0	0	0	1
-2.5	2	0	0	0	0	0	0	2
-2.0	10	0	0	0	0	0	0	10
-1.5	51	39	19	0	14	0	0	123
-1.0	78	76	53	0	30	0	0	237
-0.5	221	211	17	1	300	0	0	750
0.0	136	75	4	2	533	0	0	750
0.5	234	59	4	22	431	0	0	750
1.0	153	42	4	27	477	47	0	750
1.5	55	43	0	117	452	83	0	750
2.0	97	23	0	145	349	136	0	750
2.5	61	7	0	143	359	180	0	750
3.0	30	2	0	238	376	104	0	750
3.5	0	0	0	111	84	375	0	570
4.0	0	0	0	84	25	393	0	502
4.5	0	0	0	123	34	422	0	579
5.0	*	*	*	*	*	*	2321	2321
6.0	*	*	*	*	*	*	2079	2079
7.0	*	*	*	*	*	*	1011	1011

Bulk Weight Percentages:

Wp	Gp	Bp	Xtal	Lithic	Glass	NA
0	0	0	0	0	0	0
0	0	0	0	0	0	0
0	0	0	0	0	0	0
0	0	0	0	0	0	0
0.49	0	0	0	0	0	0
0.64	0	0	0	0	0	0
1.20	0	0	0	0	0	0
1.81	1.89	1.13	0	0.90	0	0
1.35	1.90	1.32	0	1.11	0	0
1.90	1.87	0.15	0.01	4.42	0	0
1.10	0.69	0.04	0.03	7.09	0	0
0.82	0.77	0.02	0.22	4.50	0	0
0.58	0.18	0.02	0.14	2.49	0.22	0
0.14	0.32	0	0.61	2.44	0.38	0
0.12	0.03	0	0.54	1.31	0.45	0
0.12	0.02	0	0.64	1.60	0.75	0
0.10	0.01	0	1.54	2.43	0.62	0
0	0	0	2.76	2.09	7.29	0
0	0	0	1.27	0.38	4.70	0
0	0	0	2.52	0.70	6.88	0
*	*	*	*	*	*	8.99
*	*	*	*	*	*	5.54
*	*	*	*	*	*	1.71
10.37	**7.68**	**2.68**	**10.28**	**31.46**	**21.29**	**16.24**

c1 at Locality 67 [CBV-67-1] [Total sample weight 136046.1 mg]

Grain diameter		Weight Fractions		Granulometric Analysis						
ϕ	mm	weight [mg]	Cumulative weight %	ϕ_{05}	ϕ_{25}	ϕ_{50}	ϕ_{75}	Md$_\phi$	σ_ϕ	F2
-5.0	31.5	0	0	5.8	4.9	-0.6	-1.6	2.9	2.5	42.22%
-4.5	22.4	0	0							
-4.0	16.0	0	0							
-3.5	11.2	0	0							
-3.0	8.0	1279.6	0.94							
-2.5	5.6	1879.5	2.32							
-2.0	4.0	2287.6	4.00							
-1.5	2.8	2022.3	5.49							

				Minor Lithic Counts		Abundance [volume %]	
				SML	GCL	SML	GCL
-1.0	2.0	6608.7	10.35	15	0	8.7	0
-0.5	1.4	8941.0	16.92	36	0	11.0	0
0.0	1.0	7791.5	22.65	28	0	9.6	0
0.5	0.710	6027.3	27.08	26	0	9.2	0
1.0	0.500	4610.9	30.47	24	0	8.7	0
1.5	0.355	5304.7	34.37	21	0	7.6	0
2.0	0.250	6386.7	39.06	18	0	6.8	0
2.5	0.180	7658.3	44.69	0	0	0	0
3.0	0.125	8726.9	51.10	0	0	0	0
3.5	0.088	9088.7	57.78				
4.0	0.063	7831.6	63.54				
4.5	0.045	10046.7	77.54				
5.0	0.032	16915	89.97				
6.0	0.017	10415	97.63				
7.0	0.008	3225	100.00				

Counts:

ϕ	Wp	Gp	Bp	Xtal	Lithic	Glass	NA	total counts
-5.0	0	0	0	0	0	0	*0*	0
-4.5	0	0	0	0	0	0	*0*	0
-4.0	0	0	0	0	0	0	*0*	0
-3.5	0	0	0	0	0	0	*0*	0
-3.0	4	0	1	0	0	0	*0*	5
-2.5	7	4	1	0	0	0	*0*	12
-2.0	25	3	8	0	0	0	*0*	36
-1.5	157	6	5	0	28	0	*0*	196
-1.0	209	37	0	0	173	0	*0*	419
-0.5	137	29	2	4	327	0	*0*	499
0.0	49	18	0	48	292	91	*0*	498
0.5	42	12	0	53	284	109	*0*	500
1.0	38	9	0	66	275	112	*0*	500
1.5	28	11	0	67	276	118	*0*	500
2.0	23	12	0	72	264	129	*0*	500
2.5	0	0	0	106	241	153	*0*	500
3.0	0	0	0	103	224	173	*0*	500
3.5	0	0	0	84	208	208	*0*	500
4.0	0	0	0	51	181	268	*0*	500
4.5	0	0	0	31	179	290	*0*	500
5.0	*	*	*	*	*	*	*1057*	1057
6.0	*	*	*	*	*	*	*947*	947
7.0	*	*	*	*	*	*	*460*	460

Bulk Weight Percentages:

Wp	Gp	Bp	Xtal	Lithic	Glass	NA
0	0	0	0	0	0	0
0	0	0	0	0	0	0
0	0	0	0	0	0	0
0	0	0	0	0	0	0
0.75	0	0.19	0	0	0	0
0.59	0.44	0.35	0	0	0	0
1.08	0.18	0.42	0	0	0	0
1.04	0.05	0.06	0	0.33	0	0
1.60	0.41	0	0	2.84	0	0
1.22	0.27	0.02	0.06	5.01	0	0
0.37	0.15	0	0.57	3.61	1.03	0
0.26	0.14	0	0.47	2.63	0.93	0
0.20	0.05	0	0.46	1.97	0.71	0
0.11	0.12	0	0.54	2.29	0.84	0
0.08	0.05	0	0.73	2.68	1.16	0
0	0	0	1.22	2.77	1.64	0
0	0	0	1.36	2.96	2.09	0
0	0	0	1.23	3.06	2.39	0
0	0	0	0.66	2.34	2.75	0
0	0	0	0.51	2.31	3.01	0
*	*	*	*	*	*	12.43
*	*	*	*	*	*	11.19
*	*	*	*	*	*	7.02
7.30	**1.86**	**1.04**	**7.81**	**34.80**	**16.55**	**30.64**

c1 at Locality 68 [CBV-68-2] [Total sample weight: 149962.4 mg]

Grain diameter		Weight Fractions		Granulometric Analysis						
ϕ	mm	weight [mg]	Cumulative weight %	ϕ_{05}	ϕ_{25}	ϕ_{50}	ϕ_{75}	Md_ϕ	σ_ϕ	F2
-5.0	31.5	0	0	5.8	4.9	-0.3	-1.5	3.2	2.41	47.47%
-4.5	22.4	0	0							
-4.0	16.0	0	0							
-3.5	11.2	1693.8	1.13							
-3.0	8.0	342.1	1.36							
-2.5	5.6	508.2	1.70							
-2.0	4.0	1585.2	2.75							
-1.5	2.8	3668.7	5.20							
-1.0	2.0	4795.2	8.40							
-0.5	1.4	8302.7	13.93							
0.0	1.0	7033.8	18.62							
0.5	0.710	7344.9	23.52							
1.0	0.500	8050.1	28.89							
1.5	0.355	8926.2	34.84							
2.0	0.250	6867.3	39.42							
2.5	0.180	6103.3	43.49							
3.0	0.125	6733.3	47.98							
3.5	0.088	6822.3	52.53							
4.0	0.063	13359.2	61.44							
4.5	0.045	22205.2	76.25							
5.0	0.032	19720	89.40							
6.0	0.017	12140	97.49							
7.0	0.008	3760	100.00							

Minor Lithic Counts		Abundance [volume %]	
SML	GCL	SML	GCL
4	0	2.8	0
7	0	2.4	0
8	2	2.6	0.7
9	0	4.9	0
5	0	3.6	0
6	0	5.6	0
11	0	14.3	0
0	0	0	0
0	0	0	0

Counts:

ϕ	Wp	Gp	Bp	Xtal	Lithic	Glass	NA	total counts
-5.0	0	0	0	0	0	0	0	0
-4.5	0	0	0	0	0	0	0	0
-4.0	0	0	0	0	0	0	0	0
-3.5	0	0	1	0	0	0	0	1
-3.0	0	0	1	0	0	0	0	1
-2.5	2	1	1	0	0	0	0	4
-2.0	21	1	1	0	4	0	0	27
-1.5	85	7	3	0	35	0	0	130
-1.0	228	7	3	0	145	0	0	383
-0.5	161	6	2	0	289	42	0	500
0.0	58	5	0	3	307	127	0	500
0.5	21	2	0	9	185	283	0	500
1.0	4	0	0	13	139	344	0	500
1.5	2	0	0	29	108	361	0	500
2.0	2	0	0	32	77	389	0	500
2.5	0	0	0	49	51	400	0	500
3.0	0	0	0	76	39	385	0	500
3.5	0	0	0	71	35	394	0	500
4.0	0	0	0	49	36	415	0	500
4.5	0	0	0	51	34	415	0	500
5.0	*	*	*	*	*	*	*1232*	1232
6.0	*	*	*	*	*	*	*1104*	1104
7.0	*	*	*	*	*	*	*536*	536

Bulk Weight Percentages:

ϕ	Wp	Gp	Bp	Xtal	Lithic	Glass	NA
-5.0	0	0	0	0	0	0	0
-4.5	0	0	0	0	0	0	0
-4.0	0	0	0	0	0	0	0
-3.5	0	0	1.13	0	0	0	0
-3.0	0	0	0.23	0	0	0	0
-2.5	0.09	0.06	0.19	0	0	0	0
-2.0	0.66	0.04	0.04	0	0	0	0
-1.5	1.28	0.14	0.08	0	0.31	0	0
-1.0	1.32	0.06	0.03	0	0.95	0	0
-0.5	1.23	0.05	0.02	0	1.80	0.43	0
0.0	0.36	0.04	0	0.03	3.81	1.17	0
0.5	0.34	0.02	0	0.09	3.10	2.60	0
1.0	0.03	0	0	0.15	1.85	3.56	0
1.5	0.01	0	0	0.38	1.63	4.12	0
2.0	0.01	0	0	0.32	1.44	4.48	0
2.5	0	0	0	0.42	0.77	4.31	0
3.0	0	0	0	0.73	0.44	4.48	0
3.5	0	0	0	0.78	0.38	3.78	0
4.0	0	0	0	1.05	0.77	7.08	0
4.5	0	0	0	1.04	0.79	9.84	0
5.0	*	*	*	*	*	*	13.15
6.0	*	*	*	*	*	*	8.10
7.0	*	*	*	*	*	*	2.51
				5.33	**0.41**	**1.72**	**4.99**	**18.04**	**45.75**	**23.76**

c2 at Locality 65 [CBV-65-2] [Total sample weight 41034.4 mg]

Grain diameter		Weight Fractions		Granulometric Analysis						
ϕ	mm	weight [mg]	Cumulative weight %	ϕ_{05}	ϕ_{84}	ϕ_{50}	ϕ_{σ}	Md$_{\phi}$	σ_{ϕ}	F2
-5.0	31.5	0	0	5.4	4.4	0.1	-0.8	1.4	2.01	28.00%
-4.5	22.4	0	0							
-4.0	16.0	0	0							
-3.5	11.2	0	0							
-3.0	8.0	538.5	1.31							
-2.5	5.6	64.3	1.47							
-2.0	4.0	247.1	2.07							
-1.5	2.8	202.3	2.56							
-1.0	2.0	567.6	3.95							
-0.5	1.4	1694.5	8.08							
0.0	1.0	2969.9	15.31							
0.5	0.710	5604.9	28.97							
1.0	0.500	6592.1	45.04							
1.5	0.355	3579.1	53.76							
2.0	0.250	2194.4	59.11							
2.5	0.180	1856.3	63.63							
3.0	0.125	1742.6	67.88							
3.5	0.088	1690.5	72.00							
4.0	0.063	1546.6	75.77							
4.5	0.045	3818.5	85.07							
5.0	0.032	3390	93.34							
6.0	0.017	2090	98.42							
7.0	0.008	645	100.00							

Minor Lithic Counts		Abundance [volume %]	
SML	GCL	SML	GCL
1	0	3.6	0
0	0	0	0
5	0	1.1	0
5	0	1.1	0
3	0	0.7	0
6	2	1.4	0.5
5	2	1.2	0.5
4	0	1.1	0
0	0	0	0

Counts:

ϕ	Wp	Gp	Bp	Xtal	Lithic	Glass	NA	total counts
-5.0	0	0	0	0	0	0	*0*	0
-4.5	0	0	0	0	0	0	*0*	0
-4.0	0	0	0	0	0	0	*0*	0
-3.5	0	0	0	0	0	0	*0*	0
-3.0	0	1	2	0	0	0	*0*	3
-2.5	0	1	0	0	0	0	*0*	1
-2.0	0	4	1	0	0	0	*0*	5
-1.5	0	7	0	0	2	0	*0*	9
-1.0	4	1	0	0	28	0	*0*	33
-0.5	17	15	0	3	184	0	*0*	219
0.0	36	16	0	6	442	0	*0*	500
0.5	24	12	0	8	445	11	*0*	500
1.0	17	8	0	8	436	31	*0*	500
1.5	21	11	0	24	425	19	*0*	500
2.0	22	10	0	57	402	9	*0*	500
2.5	28	12	0	73	376	11	*0*	500
3.0	33	11	0	111	318	27	*0*	500
3.5	0	0	0	158	284	58	*0*	500
4.0	0	0	0	91	228	181	*0*	500
4.5	0	0	0	98	221	181	*0*	500
5.0	*	*	*	*	*	*	*2110*	2110
6.0	*	*	*	*	*	*	*1898*	1898
7.0	*	*	*	*	*	*	*923*	923

Bulk Weight Percentages:

Wp	Gp	Bp	Xtal	Lithic	Glass	NA
0	0	0	0	0	0	0
0	0	0	0	0	0	0
0	0	0	0	0	0	0
0	0	0	0	0	0	0
0	0.45	0.86	0	0	0	0
0	0.16	0	0	0	0	0
0	0.49	0.11	0	0	0	0
0	0.36	0	0	0.13	0	0
0.08	0.03	0	0	1.27	0	0
0.20	0.18	0	0	3.69	0.28	0
0.33	0.17	0	0.06	6.65	0.90	0
0.57	0.41	0	0.09	12.19	0.29	0
0.41	0.21	0	0.21	14.29	0.09	0
0.17	0.27	0	0.25	7.58	0.10	0
0.08	0.04	0	0.42	4.49	0.22	0
0.11	0.06	0	0.64	3.56	0.38	0
0.16	0.05	0	0.69	2.83	1.17	0
0	0	0	0.99	2.40	1.17	0
0	0	0	1.34	1.86	3.59	0
0	0	0	1.36	1.84	2.09	0
*	*	*	*	*	*	8.26
*	*	*	*	*	*	5.09
*	*	*	*	*	*	1.58
2.11	**2.88**	**0.97**	**6.05**	**62.78**	**10.28**	**14.93**

c2, at Locality 67 [CBV-67-2] [Total sample weight 128433.9 mg]

Grain diameter		Weight Fractions		Granulometric Analysis						
ϕ	mm	weight [mg]	Cumulative weight %	ϕ_{05}	ϕ_{25}	ϕ_{50}	ϕ_{75}	Md_ϕ	σ_ϕ	F2
-5.0	31.5	0	0	4.6	2.1	-1.1	-1.8	-0.1	1.74	10.95%
-4.5	22.4	0	0							
-4.0	16.0	0	0							
-3.5	11.2	0	0							
-3.0	8.0	575.3	0.45							
-2.5	5.6	516.5	0.85							
-2.0	4.0	2973.0	3.16							
-1.5	2.8	4818.2	6.92							
-1.0	2.0	12632.0	16.75							
-0.5	1.4	21628.1	33.59							
0.0	1.0	22458.4	51.08							
0.5	0.710	20771.2	67.25							
1.0	0.500	12407.3	76.91							
1.5	0.355	5876.0	81.49							
2.0	0.250	2853.1	83.71							
2.5	0.180	2117.7	85.36							
3.0	0.125	2267.1	87.12							
3.5	0.088	2481.7	89.05							
4.0	0.063	3009.4	91.40							
4.5	0.045	4242.8	94.70							
5.0	0.032	3767.7	97.63							
6.0	0.017	2320.3	99.44							
7.0	0.008	718.2	100.00							

Minor Lithic Counts:		Abundance [volume %]	
SML	GCL	SML	GCL
4	0	1.8	0
9	0	2.3	0
12	0	3.0	0
12	2	3.0	0.5
10	0	2.5	0
12	0	3.1	0
11	0	3.1	0
0	0	0	0
0	0	0	0

Counts:

ϕ	Wp	Gp	Bp	Xtal	Lithic	Glass	NA	total counts
-5.0	0	0	0	0	0	0	*0*	0
-4.5	0	0	0	0	0	0	*0*	0
-4.0	0	0	0	0	0	0	*0*	0
-3.5	0	0	0	0	0	0	*0*	0
-3.0	2	0	0	0	0	0	*0*	2
-2.5	4	0	1	0	0	0	*0*	5
-2.0	11	3	2	0	12	0	*0*	28
-1.5	47	5	0	0	81	0	*0*	133
-1.0	158	2	2	0	228	0	*0*	390
-0.5	98	3	2	2	383	12	*0*	500
0.0	32	0	0	17	403	48	*0*	500
0.5	14	0	0	29	403	54	*0*	500
1.0	1	0	0	35	405	59	*0*	500
1.5	0	0	0	52	384	64	*0*	500
2.0	0	0	0	72	356	72	*0*	500
2.5	0	0	0	99	331	70	*0*	500
3.0	0	0	0	109	309	82	*0*	500
3.5	0	0	0	79	278	143	*0*	500
4.0	0	0	0	53	203	244	*0*	500
4.5	0	0	0	51	199	250	*0*	500
5.0	*	*	*	*	*	*	*2354*	2354
6.0	*	*	*	*	*	*	*2108*	2108
7.0	*	*	*	*	*	*	*1026*	1026

Bulk Weight Percentages:

Wp	Gp	Bp	Xtal	Lithic	Glass	NA
0	0	0	0	0	0	0
0	0	0	0	0	0	0
0	0	0	0	0	0	0
0	0	0	0	0	0	0
0.45	0	0	0	0	0	0
0.20	0	0.21	0	0	0	0
0.54	0.21	0.12	0	1.45	0	0
0.88	0.12	0	0	2.74	0	0
2.38	0	0.04	0	7.37	0	0
2.11	0.04	0.04	0.07	14.20	0.35	0
0.71	0.04	0	0.59	14.60	1.59	0
0.60	0	0	0.90	13.06	1.61	0
0.01	0	0	0.66	7.96	1.03	0
0	0	0	0.47	3.59	0.51	0
0	0	0	0.33	1.61	0.29	0
0	0	0	0.33	1.44	0.22	0
0	0	0	0.39	1.11	0.27	0
0	0	0	0.33	1.15	0.46	0
0	0	0	0.28	1.06	1.01	0
0	0	0	0.21	1.02	2.07	0
*	*	*	*	*	*	2.93
*	*	*	*	*	*	1.81
*	*	*	*	*	*	0.56
7.88	**0.41**	**0.41**	**4.23**	**72.36**	**9.41**	**5.30**

c3 at Locality 65 [CBV-65-3] [Total sample weight: 148369.1 mg]

Grain diameter		Weight Fractions		Granulometric Analysis						
ϕ	mm	weight [mg]	Cumulative weight %	ϕ_{05}	ϕ_{84}	ϕ_{16}	ϕ_{50}	Md_ϕ	σ_ϕ	F2
-5.0	31.5	0	0	4.5	1.7	-0.7	-1.1	0.4	1.41	8.32%
-4.5	22.4	0	0							
-4.0	16.0	0	0							
-3.5	11.2	0	0							
-3.0	8.0	0	0							
-2.5	5.6	0	0							
-2.0	4.0	452.8	0.31							
-1.5	2.8	1915.5	1.60							
-1.0	2.0	5832.2	5.53							
-0.5	1.4	17686.5	17.45							
0.0	1.0	25023.2	34.31							
0.5	0.710	33697.3	57.03							
1.0	0.500	23774.3	73.05							
1.5	0.355	13701.1	82.28							
2.0	0.250	7175.3	87.12							
2.5	0.180	3500.8	89.48							
3.0	0.125	1848.1	90.72							
3.5	0.088	1416.8	91.68							
4.0	0.063	2401.1	93.30							
4.5	0.045	3818.5	95.87							
5.0	0.032	3390	98.16							
6.0	0.017	2090	99.56							
7.0	0.008	645	100.00							

Minor Lithic Counts		Abundance [volume %]	
SML	GCL	SML	GCL
2	0	0.7	0
5	0	1.1	0
9	0	2.0	0
6	0	1.3	0
4	0	0.9	0
5	0	1.2	0
3	0	0.8	0
2	0	0.5	0
0	0	0	0

Counts:

ϕ	Wp	Gp	Bp	Xtal	Lithic	Glass	NA	total counts
-5.0	0	0	0	0	0	0	*0*	0
-4.5	0	0	0	0	0	0	*0*	0
-4.0	0	0	0	0	0	0	*0*	0
-3.5	0	0	0	0	0	0	*0*	0
-3.0	0	0	0	0	0	0	*0*	0
-2.5	0	0	0	0	0	0	*0*	0
-2.0	0	4	1	0	0	0	*0*	5
-1.5	0	19	0	0	33	0	*0*	52
-1.0	16	35	0	0	287	0	*0*	338
-0.5	15	35	0	3	447	0	*0*	500
0.0	19	17	0	13	451	0	*0*	500
0.5	8	12	0	28	452	0	*0*	500
1.0	3	1	0	57	437	2	*0*	500
1.5	5	0	0	72	419	4	*0*	500
2.0	6	0	0	93	396	5	*0*	500
2.5	6	0	0	102	380	12	*0*	500
3.0	5	0	0	113	363	19	*0*	500
3.5	0	0	0	124	318	58	*0*	500
4.0	0	0	0	84	219	197	*0*	500
4.5	0	0	0	85	221	194	*0*	500
5.0	*	*	*	*	*	*	*2119*	2119
6.0	*	*	*	*	*	*	*1898*	1808
7.0	*	*	*	*	*	*	*923*	923

Bulk Weight Percentages:

ϕ	Wp	Gp	Bp	Xtal	Lithic	Glass	NA
-5.0	0	0	0	0	0	0	0
-4.5	0	0	0	0	0	0	0
-4.0	0	0	0	0	0	0	0
-3.5	0	0	0	0	0	0	0
-3.0	0	0	0	0	0	0	0
-2.5	0	0	0	0	0	0	0
-2.0	0	0.25	0.05	0	0	0	0
-1.5	0	0.39	0	0	0.90	0	0
-1.0	0.09	0.29	0	0	3.55	0	0
-0.5	0.22	0.52	0	0.07	11.11	0	0
0.0	0.40	0.41	0	0.43	15.62	0	0
0.5	0.49	0.67	0	1.21	20.33	0	0
1.0	0.07	0.03	0	1.77	14.10	0.06	0
1.5	0.04	0	0	1.31	7.82	0.06	0
2.0	0.02	0	0	0.91	3.87	0.04	0
2.5	0.01	0	0	0.49	1.81	0.05	0
3.0	0.01	0	0	0.28	0.91	0.04	0
3.5	0	0	0	0.24	0.62	0.09	0
4.0	0	0	0	0.30	0.77	0.55	0
4.5	0	0	0	0.30	0.28	1.49	0
5.0	*	*	*	*	*	*	2.29
6.0	*	*	*	*	*	*	1.41
7.0	*	*	*	*	*	*	0.44
	1.35	**3.08**	**0.05**	**7.31**	**81.69**	**2.38**	**4.14**

Lithic Fall at Locality 109 [LL CBV-109-2] [Total sample weight 2084050 mg]

Grain diameter		Weight Fractions		Granulometric Analysis						
ϕ	mm	weight [mg]	Cumulative weight %	ϕ_{05}	ϕ_{25}	ϕ_{50}	ϕ_{75}	Md_ϕ	σ_ϕ	F2
-5.0	31.5	150881	7.24	4.7	2.7	-4.1	-4.2	-4.1	3.03	11.83%
-4.5	22.4	107326	12.39							
-4.0	16.0	92057	16.81							
-3.5	11.2	112481	22.20							
-3.0	8.0	120922	28.01							
-2.5	5.6	116356	33.59							
-2.0	4.0	110067	38.87							
-1.5	2.8	112912	44.29							
-1.0	2.0	123046	50.19							
-0.5	1.4	119687	55.93							
0.0	1.0	105513	61.00							
0.5	0.710	113417	66.44							
1.0	0.500	109254	71.68							
1.5	0.355	93799	76.18							
2.0	0.250	82149	80.12							
2.5	0.180	68564	83.41							
3.0	0.125	49549	85.79							
3.5	0.088	49639	88.17							
4.0	0.063	43605	90.27							
4.5	0.045	77895	94.00							
5.0	0.032	69175	97.32							
6.0	0.017	42600	99.37							
7.0	0.008	13185	100.00							

Minor Lithic Counts		Abundance [volume %]	
SML	GCL	SML	GCL
33	0	7.1	0
37	0	7.8	0
22	0	5.0	0
21	0	5.3	0
19	0	5.0	0
20	0	5.5	0
18	0	5.0	0
18	8	5.0	2.2
19	10	5.6	2.9

Counts:

ϕ	Wp	Gp	Bp	Xtal	Lithic	Glass	NA	total counts
-5.0	0	0	0	0	3	0	0	0
-4.5	0	0	0	0	7	0	0	0
-4.0	0	0	0	0	12	0	0	0
-3.5	0	3	0	0	32	0	0	0
-3.0	0	3	0	0	111	0	0	2
-2.5	0	24	0	0	656	0	0	10
-2.0	15	34	0	0	451	0	0	30
-1.5	6	43	0	0	451	0	0	500
-1.0	9	23	0	6	462	0	0	448
-0.5	0	12	0	16	472	0	0	500
0.0	40	1	0	23	436	0	0	500
0.5	21	24	0	51	400	4	0	500
1.0	9	20	0	65	380	26	0	500
1.5	6	22	0	72	362	38	0	500
2.0	3	2	0	91	362	42	0	500
2.5	2	10	0	87	357	44	0	500
3.0	4	15	0	92	342	47	0	500
3.5	0	0	0	118	338	44	0	500
4.0	0	0	0	91	321	48	0	500
4.5	*	*	*	*	*	*	*	*
5.0	*	*	*	*	*	*	*	*
6.0	*	*	*	*	*	*	*	*
7.0	*	*	*	*	*	*	*	*

Bulk Weight Percentages:

Wp	Gp	Bp	Xtal	Lithic	Glass	NA
0	0	0	0	7.24	0	0
0	0	0	0	5.15	0	0
0	0	0	0	4.42	0	0
0	0.13	0	0	5.27	0	0
0	0.05	0	0	5.75	0	0
0	0.08	0	0	5.50	0	0
0.07	0.22	0	0	5.00	0	0
0.04	0.38	0	0	5.02	0	0
0.05	0.19	0	0.06	5.60	0	0
0	0.08	0	0.18	5.48	0	0
0.25	0.01	0	0.23	4.57	0	0
0.25	0.32	0	0.53	4.30	0.04	0
0.07	0.17	0	0.67	4.08	0.25	0
0.02	0.27	0	0.63	3.28	0.29	0
0.01	0.01	0	0.73	2.90	0.30	0
0.01	0.03	0	0.58	2.39	0.27	0
0.01	0.04	0	0.45	1.67	0.21	0
0	0	0	0.57	1.64	0.17	0
0	0	0	0.40	1.39	0.30	0
*	*	*	*	*	*	3.74
*	*	*	*	*	*	3.32
*	*	*	*	*	*	2.04
*	*	*	*	*	*	0.63
0.78	**1.98**	**0**	**5.03**	**80.65**	**1.83**	**9.73**

Lithic Fall at Locality 112 [L2_CBV-112-1] [Total sample weight 918050 mg]

Grain diameter		Weight Fractions		Granulometric Analysis						
ϕ	mm	weight [mg]	Cumulative weight %	ϕ_{05}	ϕ_{84}	ϕ_{16}	ϕ_{50}	Md$_\phi$	σ_ϕ	F2
-5.0	31.5	0	0	0.6	-0.6	-3.5	-4.1	-2.2	1.42	1.41%
-4.5	22.4	0	0							
-4.0	16.0	57286	6.24							
-3.5	11.2	89294	15.97							
-3.0	8.0	93823	26.19							
-2.5	5.6	147059	42.20							
-2.0	4.0	114828	54.71							
-1.5	2.8	116172	67.37							
-1.0	2.0	90761	77.25							
-0.5	1.4	84854	86.50							
0.0	1.0	47043	91.62							
0.5	0.710	28110	94.68							
1.0	0.500	14680	96.28							
1.5	0.355	6774	97.02							
2.0	0.250	3652	97.42							
2.5	0.180	3657	97.81							
3.0	0.125	3701	98.22							
3.5	0.088	3369	98.59							
4.0	0.063	3331	98.95							
4.5	0.045	3709	99.35							
5.0	0.032	3295	99.71							
6.0	0.017	2030	99.93							
7.0	0.008	625	100.00							

Minor Lithic Counts		Abundance [volume %]	
SML	GCL	SML	GCL
57	0	12.6	0
46	0	10.0	0
60	0	13.3	0
63	2	14.0	0.4
66	4	14.9	0.9
64	29	15.5	7.0
51	34	13.3	8.9
58	39	16.3	11.0
56	42	16.7	12.5

Counts:

ϕ	Wp	Gp	Bp	Xtal	Lithic	Glass	NA	total counts
-5.0	0	0	0	0	0	0	*0*	0
-4.5	0	0	0	0	0	0	*0*	0
-4.0	0	1	0	0	6	0	*0*	0
-3.5	0	2	0	0	32	0	*0*	0
-3.0	2	5	0	0	95	0	*0*	2
-2.5	9	28	0	0	421	0	*0*	10
-2.0	16	65	0	0	537	0	*0*	30
-1.5	12	42	0	0	446	0	*0*	500
-1.0	6	39	0	2	453	0	*0*	448
-0.5	13	25	0	2	460	0	*0*	500
0.0	15	16	0	18	450	1	*0*	500
0.5	12	15	0	24	449	0	*0*	500
1.0	11	7	0	31	443	8	*0*	500
1.5	16	13	0	45	414	12	*0*	500
2.0	22	15	0	63	383	17	*0*	500
2.5	19	17	0	79	356	29	*0*	500
3.0	16	15	0	92	335	42	*0*	500
3.5	0	0	0	126	318	56	*0*	500
4.0	0	0	0	76	298	126	*0*	500
4.5	*	*	*	*	*	*	*168*	168
5.0	*	*	*	*	*	*	*206*	206
6.0	*	*	*	*	*	*	*184*	184
7.0	*	*	*	*	*	*	*90*	90

Bulk Weight Percentages:

Wp	Gp	Bp	Xtal	Lithic	Glass	NA
0	0	0	0	0	0	0
0	0	0	0	0	0	0
0	0.50	0	0	5.74	0	0
0	0.16	0	0	9.57	0	0
0.07	0.17	0	0	9.98	0	0
0.10	0.41	0	0	15.51	0	0
0.14	0.80	0	0	11.56	0	0
0.17	0.83	0	0	11.65	0	0
0.06	0.54	0	0.04	9.26	0	0
0.14	0.29	0	0.04	8.78	0	0
0.10	0.12	0	0.18	4.72	0.01	0
0.05	0.11	0	0.14	2.75	0	0
0.03	0.02	0	0.10	1.44	0.02	0
0.01	0.03	0	0.07	0.62	0.02	0
0.01	0.01	0	0.05	0.32	0.01	0
0.01	0.01	0	0.07	0.30	0.02	0
0.01	0.01	0	0.08	0.23	0.03	0
0	0	0	0.09	0.24	0.03	0
0	0	0	0.06	0.23	0.08	0
*	*	*	*	*	*	0.40
*	*	*	*	*	*	0.36
*	*	*	*	*	*	0.22
*	*	*	*	*	*	0.07
0.90	**4.01**	**0**	**0.92**	**92.90**	**0.22**	**1.05**

Lithic Fall ash bed at Locality 12 [L2: CBV-12e-3] [Total sample weight: 637000 mg]

Grain diameter		Weight Fractions		Granulometric Analysis						
ϕ	mm	weight [mg]	Cumulative weight %	ϕ_{05}	ϕ_{84}	ϕ_{10}	ϕ_{5}	Md_{ϕ}	σ_{ϕ}	F2
-5.0	31.5	0	0	4.9	4.0	0.2	-0.8	1.9	1.83	20.90%
-4.5	22.4	0	0							
-4.0	16.0	0	0							
-3.5	11.2	0	0							
-3.0	8.0	0	0							
-2.5	5.6	0	0							
-2.0	4.0	0	0							
-1.5	2.8	11915.5	1.87							
-1.0	2.0	11812.3	3.72							
-0.5	1.4	21892.3	7.16							
0.0	1.0	30460.7	11.94							
0.5	0.710	61907.4	21.66							
1.0	0.500	66408.0	32.09							
1.5	0.355	73127.5	43.57							
2.0	0.250	71140.3	54.73							
2.5	0.180	67309.3	65.30							
3.0	0.125	51265.0	73.35							
3.5	0.088	36661.9	79.10							
4.0	0.063	31717.6	84.08							
4.5	0.045	38936.5	90.19							
5.0	0.032	34570	95.62							
6.0	0.017	21290	98.97							
7.0	0.008	6590	100.00							

Minor Lithic Counts		Abundance [volume %]	
SML	GCL	SML	GCL
47	4	9.8	0.8
40	0	8.4	0
41	0	8.6	0
39	0	8.7	0
35	0	8.8	0
36	0	9.3	0
34	0	9.1	0
36	0	9.8	0
41	0	11.2	0

Counts:

ϕ	Wp	Gp	Bp	Xtal	Lithic	Glass	NA	total counts
-5.0	0	0	0	0	0	0	*0*	0
-4.5	0	0	0	0	0	0	*0*	0
-4.0	0	0	0	0	0	0	*0*	0
-3.5	0	0	0	0	0	0	*0*	0
-3.0	0	0	0	0	0	0	*0*	0
-2.5	0	0	0	0	0	0	*0*	0
-2.0	0	0	0	0	0	0	*0*	0
-1.5	5	5	2	0	151	0	*0*	163
-1.0	65	13	0	3	478	0	*0*	500
-0.5	4	3	2	13	478	0	*0*	500
0.0	3	7	0	16	474	0	*0*	502
0.5	5	6	0	42	447	0	*0*	500
1.0	6	3	0	92	399	0	*0*	500
1.5	7	5	0	101	387	0	*0*	500
2.0	5	4	0	117	374	0	*0*	500
2.5	2	6	0	124	368	0	*0*	500
3.0	1	12	0	121	366	0	*0*	500
3.5	0	0	0	119	349	32	*0*	500
4.0	0	0	0	109	331	60	*0*	500
4.5	*	*	*	*	*	*	*1560*	1560
5.0	*	*	*	*	*	*	*2160*	2160
6.0	*	*	*	*	*	*	*1910*	1910
7.0	*	*	*	*	*	*	*940*	940

Bulk Weight Percentages:

Wp	Gp	Bp	Xtal	Lithic	Glass	NA
0	0	0	0	0	0	0
0	0	0	0	0	0	0
0	0	0	0	0	0	0
0	0	0	0	0	0	0
0	0	0	0	0	0	0
0	0	0	0	0	0	0
0	0	0	0	0	0	0
0.03	0.04	0.02	0	1.77	0	0
0.01	0.03	0	0.01	1.80	0	0
0.02	0.01	0.02	0.09	3.31	0	0
0.02	0.05	0.01	0.15	4.56	0	0
0.03	0.15	0	0.79	8.75	0	0
0.09	0.05	0	1.87	8.42	0	0
0.07	0.16	0	2.28	8.97	0	0
0.04	0.04	0	2.64	8.45	0	0
0.02	0.06	0	2.64	7.84	0	0
0.01	0.10	0	1.97	5.96	0	0
0	0	0	1.39	4.07	0.29	0
0	0	0	1.11	3.38	0.49	0
*	*	*	*	*	*	6.11
*	*	*	*	*	*	5.43
*	*	*	*	*	*	3.34
*	*	*	*	*	*	1.03
0.35	**0.69**	**0.05**	**14.94**	**67.28**	**0.78**	**15.91**

Lithic Fall at Locality 12 [L2 CBV-12e-2] [Total sample weight 203400 mg]

Grain diameter		Weight Fractions		Granulometric Analysis						
ϕ	mm	weight [mg]	Cumulative weight %	ϕ_{05}	ϕ_{25}	ϕ_{10}	ϕ_{5}	Md$_\phi$	σ_ϕ	Fz
-5.0	31.5	0	0	2.9	-1.2	-4.2	-4.8	-3.2	1.93	4.12%
-4.5	22.4	181333	8.92							
-4.0	16.0	185203	18.02							
-3.5	11.2	518948	45.53							
-3.0	8.0	362062	61.34							
-2.5	5.6	223721	72.33							
-2.0	4.0	141428	79.29							
-1.5	2.8	76173	83.03							
-1.0	2.0	54428	85.71							
-0.5	1.4	40971	87.72							
0.0	1.0	27925	89.10							
0.5	0.710	28215	90.48							
1.0	0.500	23679	91.65							
1.5	0.355	21108	92.68							
2.0	0.250	18820	93.61							
2.5	0.180	17191	94.46							
3.0	0.125	16849	95.28							
3.5	0.088	12142	95.88							
4.0	0.063	13876	96.56							
4.5	0.045	26846	97.88							
5.0	0.032	23840	99.05							
6.0	0.017	14680	99.78							
7.0	0.008	4550	100.00							

Minor Lithic Counts		Abundance [volume %]	
SML	GCL	SML	GCL
27	4	17.3	0.9
99	0	22.5	0
55	0	12.8	0
52	0	12.3	0
46	0	10.9	0
38	0	8.1	0
31	0	6.5	0
29	8	6.1	1.7
34	10	7.4	2.2

Counts:

ϕ	Wp	Gp	Bp	Xtal	Lithic	Glass	NA	total counts
-5.0	0	0	0	0	0	0	0	0
-4.5	0	0	0	0	8	0	0	8
-4.0	0	5	1	0	17	0	0	23
-3.5	0	5	4	0	38	0	0	47
-3.0	0	5	12	0	41	0	0	58
-2.5	1	12	8	0	64	0	0	85
-2.0	4	14	6	0	576	0	0	600
-1.5	16	19	6	0	553	0	0	594
-1.0	29	18	0	0	446	0	0	493
-0.5	33	17	0	10	440	0	0	500
0.0	21	18	2	30	429	0	0	500
0.5	26	12	0	42	423	0	0	503
1.0	31	9	0	50	422	5	0	515
1.5	30	6	0	67	469	27	0	600
2.0	0	0	0	89	480	1	0	600
2.5	0	0	0	107	478	15	0	600
3.0	0	0	0	124	461	15	0	600
3.5	0	0	0	91	429	80	0	600
4.0	0	0	0	44	416	40	0	500
4.5	*	*	*	*	*	*	*	*
5.0	*	*	*	*	*	*	*	*
6.0	*	*	*	*	*	*	*	*
7.0	*	*	*	*	*	*	*	*

Bulk Weight Percentages:

ϕ	Wp	Gp	Bp	Xtal	Lithic	Glass	NA
-5.0	0	0	0	0	0	0	0
-4.5	0	0	0	0	8.92	0	0
-4.0	0	1.19	0.14	0	7.77	0	0
-3.5	0	0.81	1.37	0	23.34	0	0
-3.0	0	0.63	1.45	0	15.72	0	0
-2.5	0.04	0.66	1.39	0	8.91	0	0
-2.0	0.02	0.10	0.04	0	6.80	0	0
-1.5	0.06	0.09	0.04	0	3.56	0	0
-1.0	0.08	0.07	0	0	2.53	0	0
-0.5	0.08	0.04	0	0.04	1.85	0	0
0.0	0.04	0.04	0	0.08	1.22	0	0
0.5	0.03	0.04	0.0+	0.11	1.20	0	0
1.0	0.05	0.02	0	0.11	0.98	0.01	0
1.5	0.03	0.01	0	0.12	0.84	0.04	0
2.0	0.02	0	0	0.16	0.77	0.0+	0
2.5	0	0	0	0.15	0.67	0.02	0
3.0	0	0	0	0.17	0.64	0.02	0
3.5	0	0	0	0.09	0.44	0.06	0
4.0	0	0	0	0.06	0.55	0.04	0
4.5	*	*	*	*	*	*	1.32
5.0	*	*	*	*	*	*	1.17
6.0	*	*	*	*	*	*	0.72
7.0	*	*	*	*	*	*	0.22
	0.45	**3.70**	**4.43**	**1.09**	**86.71**	**0.19**	**3.43**

Lithic Fall ash bed at Locality 58 [L3_CBV-B-1a] [Total sample weight: 336300 mg]

Grain diameter		Weight Fractions		Granulometric Analysis						
ϕ	mm	weight [mg]	Cumulative weight %	ϕ_{05}	ϕ_{50}	ϕ_{95}	ϕ_{σ}	Md$_{\phi}$	σ_{ϕ}	F2
-5.0	31.5	0	0	4.9	3.9	-0.8	-2.5	2.8	2.29	25.54%
-4.5	22.4	0	0							
-4.0	16.0	0	0							
-3.5	11.2	0	0							
-3.0	8.0	8796	2.62							
-2.5	5.6	7926	4.97							
-2.0	4.0	6739	6.98							
-1.5	2.8	8732	9.57							

Minor Lithic Counts		Abundance [volume %]	
SML	GCL	SML	GCL
14	0	3.4	0
30	0	6.3	0
26	0	5.4	0
22	0	4.9	0
16	0	4.2	0
18	0	5.2	0
17	0	5.6	0
16	0	5.1	0
15	0	4.8	0

-1.0	2.0	13608	13.62
-0.5	1.4	15356	18.19
0.0	1.0	15593	22.82
0.5	0.710	15038	27.29
1.0	0.500	16239	32.12
1.5	0.355	16689	37.08
2.0	0.250	22486	43.77
2.5	0.180	28017	52.10
3.0	0.125	38574	63.57
3.5	0.088	36613	74.46
4.0	0.063	43777	87.48
4.5	0.045	16173	92.29
5.0	0.032	14360	96.56
6.0	0.017	8845	99.19
7.0	0.008	2735	100.00

Counts:

ϕ	Wp	Gp	Bp	Xtal	Lithic	Glass	NA	total counts
-5.0	0	0	0	0	0	0	0	0
-4.5	0	0	0	0	0	0	0	0
-4.0	0	0	0	0	0	0	0	0
-3.5	0	0	0	0	0	0	0	0
-3.0	0	0	0	0	2	0	0	2
-2.5	0	1	0	0	9	0	0	10
-2.0	0	2	1	0	27	0	0	30
-1.5	0	16	0	0	484	0	0	500
-1.0	3	31	0	0	414	0	0	448
-0.5	2	23	0	2	473	0	0	500
0.0	2	16	0	4	478	0	0	500
0.5	0	24	0	12	445	19	0	500
1.0	2	27	0	40	382	49	0	500
1.5	0	25	0	74	349	52	0	500
2.0	2	24	0	115	306	53	0	500
2.5	1	24	0	98	315	62	0	500
3.0	0	22	0	87	312	79	0	500
3.5	0	0	0	61	308	131	0	500
4.0	0	0	0	39	298	163	0	500
4.5	*	*	*	*	*	*	*735*	735
5.0	*	*	*	*	*	*	*898*	898
6.0	*	*	*	*	*	*	*805*	805
7.0	*	*	*	*	*	*	*390*	390

Bulk Weight Percentages:

Wp	Gp	Bp	Xtal	Lithic	Glass	NA
0	0	0	0	0	0	0
0	0	0	0	0	0	0
0	0	0	0	0	0	0
0	0	0	0	0	0	0
0	0	0	0	2.61	0	0
0	0.10	0	0	2.26	0	0
0	0.08	0.03	0	1.89	0	0
0	0.06	0	0	2.53	0	0
0.01	0.19	0	0	3.84	0	0
0.01	0.13	0	0.02	4.41	0	0
0.01	0.12	0	0.04	4.48	0	0
0	0.27	0	0.10	3.94	0.15	0
0.01	0.22	0	0.38	3.79	0.43	0
0	0.34	0	0.72	3.47	0.44	0
0.01	0.13	0	1.61	4.28	0.66	0
0.01	0.21	0	1.69	5.43	0.99	0
0	0.28	0	2.07	7.41	1.71	0
0	0	0	1.41	7.11	2.37	0
0	0	0	1.09	8.32	3.61	0
*	*	*	*	*	*	4.81
*	*	*	*	*	*	4.27
*	*	*	*	*	*	2.63
*	*	*	*	*	*	0.81
0.06	**2.13**	**0.03**	**9.13**	**65.77**	**10.36**	**12.52**

Lithic Fall at Locality 58 [L3 CBV-B-1c] [Total sample weight: 1366860 mg]

Grain diameter		Weight Fractions		Granulometric Analysis						
ϕ	mm	weight [mg]	Cumulative weight %	ϕ_{16}	ϕ_{84}	ϕ_{05}	ϕ_{95}	Md_ϕ	σ_ϕ	F2
-5.0	31.5	27510	2.01	0.3	-0.8	-3.6	-4.4	-2.3	1.41	0.71%
-4.5	22.4	19715	3.45							
-4.0	16.0	60807	7.90							
-3.5	11.2	152593	19.07							
-3.0	8.0	163025	30.99							
-2.5	5.6	185207	44.54							
-2.0	4.0	183119	57.94							
-1.5	2.8	179244	71.05							
-1.0	2.0	131645	80.69							
-0.5	1.4	103542	88.26							
0.0	1.0	66402	93.12							
0.5	0.710	42569	96.23							
1.0	0.500	18897	97.62							
1.5	0.355	7710	98.18							
2.0	0.250	5349	98.57							
2.5	0.180	3922	98.86							
3.0	0.125	3491	99.11							
3.5	0.088	2471	99.29							
4.0	0.063	2536	99.48							
4.5	0.045	2324	99.65							
5.0	0.032	2650	99.84							
6.0	0.017	1360	99.96							
7.0	0.008	505	100.00							

Minor Lithic Counts		Abundance [volume %]	
SML	GCL	SML	GCL
45	0	12.2	0
43	0	10.5	0
57	0	13.3	0
51	6	11.7	1.4
46	12	10.4	2.7
63	15	15.5	3.7
72	17	19.0	4.5
0	0	0	0
0	0	0	0

Counts:

ϕ	Wp	Gp	Bp	Xtal	Lithic	Glass	NA	total counts
-5.0	0	0	0	0	1	0	0	0
-4.5	0	2	0	0	0	0	0	0
-4.0	0	10	4	0	7	0	0	0
-3.5	2	62	6	0	31	0	0	0
-3.0	12	104	13	0	98	0	0	0
-2.5	78	15	11	0	122	0	0	0
-2.0	81	16	12	0	312	0	0	0
-1.5	96	17	9	0	332	0	0	163
-1.0	102	24	6	0	368	0	0	500
-0.5	71	9	4	5	411	0	0	500
0.0	24	13	4	30	429	0	0	502
0.5	23	8	3	29	437	0	0	500
1.0	20	3	2	32	443	0	0	500
1.5	19	0	0	64	406	11	0	500
2.0	17	0	0	89	379	15	0	500
2.5	0	0	0	90	348	62	0	500
3.0	0	0	0	97	324	79	0	500
3.5	0	0	0	61	341	98	0	500
4.0	0	0	0	31	372	97	0	500
4.5	*	*	*	*	*	*	*	*
5.0	*	*	*	*	*	*	*	*
6.0	*	*	*	*	*	*	*	*
7.0	*	*	*	*	*	*	*	*

Bulk Weight Percentages:

Wp	Gp	Bp	Xtal	Lithic	Glass	NA
0	0	0	0	2.01	0	0
0	1.47	0	0	0	0	0
0	1.72	0.41	0	2.31	0	0
0.24	3.52	0.72	0	6.69	0	0
0.32	2.92	0.35	0	8.33	0	0
1.91	0.49	1.13	0	10.03	0	0
1.22	0.34	0.22	0	11.61	0	0
1.72	0.42	0.27	0	10.71	0	0
1.05	0.36	0.09	0	8.13	0	0
0.67	0.09	0.04	0.08	6.70	0	0
0.15	0.09	0.03	0.29	4.30	0	0
0.09	0.06	0.01	0.18	2.77	0	0
0.04	0.01	0	0.09	1.24	0	0
0.01	0	0	0.07	0.47	0.01	0
0.0+	0	0	0.07	0.30	0.01	0
0	0	0	0.05	0.20	0.03	0
0	0	0	0.05	0.17	0.04	0
0	0	0	0.02	0.13	0.03	0
0	0	0	0.01	0.14	0.03	0
*	*	*	*	*	*	0.17
*	*	*	*	*	*	0.19
*	*	*	*	*	*	0.12
*	*	*	*	*	*	0.04
7.42	**11.49**	**3.27**	**0.91**	**76.24**	**0.15**	**0.52**